Oregon International Port of Coos Bay

Proposed Section 204(f)/408 Channel Modification Project

Sub Appendix 3

Estuarine Dynamics

February 2024 Draft

EXECUTIVE SUMMARY

The Oregon International Port of Coos Bay (OIPCB or Port) proposes a Pacific Coast Intermodal Port (PCIP) project at Coos Bay, Oregon. The PCIP consists of integrated elements that would link freight arriving by container ship to the Port to Class 1 rail networks in Oregon. The in-water component of the project includes the deepening and widening of the existing Federal Navigation Channel (FNC) for deep-draft container vessels.

The Port proposes navigation channel improvements to the FNC. The Proposed Alteration (PA) generally consists of widening the channel from 300 feet (ft) to 450 ft and deepening it from a depth of 47 ft to 57 ft Mean Lower Low Water (MLLW) from RM -1.0 to RM 0.0 and deepening it from a depth of 37 ft to 45 ft MLLW from RM 0.0 through approximately RM 8.2. To accommodate the Post Panamax Generation 3 (PPX3) containership, a turning basin was added at the container facility around RM 5.0. The PPX3 turning basin's design bottom elevation is at -45 ft MLLW, the same as the main channel. In addition, a Capesize turning basin was added at RM 8.0. Because the Capesize turning basin will be used by inbound empty vessels, the turning basin's design bottom elevation is only at -37 ft MLLW. In this study, all these in-water components are referred to as the 2023 Proposed Alteration (2023 PA).

This Sub-Appendix 3 describes an evaluation of estuarine processes (hydrodynamics, sediment transport, salinity mixing, residence time, water age, dissolved oxygen, as well as ship-generated wakes) within Coos Bay (also referred to as Coos Bay estuary). The purpose of this study is to evaluate possible changes in each of these processes resulting from the 2023 PA relative to the Existing Conditions[1]. Analysis methodology for each process was defined in coordination with the U.S. Army Corps of Engineers (USACE). A brief description of study methodology and findings on possible changes in each process is summarized below.

HYDRODYNAMICS

Hydrodynamic circulation within estuaries is driven primarily by ocean tides and freshwater runoff. The tidal exchange is often quantified by tidal prism, which is the volume of water being exchanged between an estuary (enclosed bay) and the open sea over a complete tidal cycle. This analysis refers to the mean tidal prism (estuary storage volume between mean high tide and mean low tide). The tidal prism volume can be expressed by the relationship: $Prism = h_b \cdot A_b$, where h_b is the average tidal range and A_b is the average surface area of the basin between mean high tide and mean low tide. For the 2023 PA, the channel deepening and widening are both sub-tidal, i.e., all dredging occurs well below the low tide elevation. Hence, the area A_b does not change. Therefore, changes to tidal amplitude can be used to estimate changes to tidal prism.

Tidal amplitude in an estuary is affected by the inlet channel dimensions (width, depth, and length), energy loss through the inlet channel due to friction, and inertia. Friction has the effect of restricting the conveyance of water through the channel, dampening the tides upstream. The effect of inertia causes water to move in the direction opposite to the slope of water surface (i.e., water moves from the ocean into the bay even though the bay has a higher water level elevation),

[1] This report mainly focuses on the areas above RM 2.5, Charleston Channel, and South Slough. The geophysical conditions and the federal projects downstream of RM 2.5 (the channel entrance and offshore of the channel entrance) are described in detail in the Sub-Appendix 4 (Offshore and Ocean Entrance Dynamics Report). Ocean wave propagation into the estuary is also described in Sub-Appendix 4.

effectively amplifying the tidal amplitude upstream and creating a system in which the currents lag the tides. Inertia is more pronounced in estuary systems with a relatively long and hydraulically efficient inlet channel such as Coos Bay. Comparison of tidal measurements from the gauge at Charleston, OR (Station ID 9432780, used as the offshore boundary) and at North Bend (located at approximately RM 11) show that the tidal range is 7% higher at North Bend than that at Charleston. This tidal amplification indicates that Coos Bay is a hydraulically efficient estuary system, frictional effects are not strong, and that inertia influences the hydrodynamics of Coos Bay. Generally, channel widening and deepening has the effect of reducing friction. Because frictional effects are already limited within Coos Bay, channel widening and deepening are not expected to significantly change the effect of friction within the system.

A state-of-the-art numerical modeling system (MIKE) developed by the Danish Hydraulic Institute (DHI) was used to simulate hydrodynamics within the Coos Bay estuary. The three-dimensional MIKE-3 Hydrodynamic (HD) model with flexible mesh and unstructured (triangular) elements allows varying resolution throughout the modeling domain. The modeling domain encompassed the entire estuary from offshore depths of up to 300 ft to freshwater streams including the South Slough, Coos River, Isthmus Slough, Kentuck & Willanch Sloughs, and Haynes Inlet. The model was calibrated against measured water levels and depth-averaged currents at two locations, as well as measured discharge along three transects. The model was then used to investigate any changes in estuary hydrodynamics resulting from the 2023 PA.

The MIKE-3 HD model results show that the mean tidal range (e.g., the difference in height between mean high water and mean low water) generally increases starting at the mouth and moving upstream. The 2023 PA results in a slight increase (less than 0.1 ft) of mean tidal range, with the maximum of 0.1 feet, the mean of 0.04 feet, and the mode of 0.05 feet throughout the estuary. In the South Slough, the increase in mean tidal range does not exceed 0.04 ft. In the Isthmus Slough, the Coos River, and the Haynes Inlet, the increase in mean tidal range does not exceed 0.06 ft. The maximum increase occurs in the FNC, where the mean tidal range increases by 0.09 ft (corresponding to a 1.6% increase in mean tidal range). These slight increases in mean tidal range are consistent with the expected response of this hydraulically efficient estuary system to the proposed channel improvements.

Except at RM 5 and RM 8, the HD model of the 2023 PA predicts an increase of current velocity of generally less than 0.25 ft/s in the estuary and tributaries. The maximum increase occurs along the channel alignment at RM 2, where the ebb current velocity increases by 0.55 ft/s. This probably results from the proposed change in channel alignment here, i.e., the 2023 PA alignment directs more flow towards the channel centerline. In contrast, modeled velocities at RM 5 and RM 8 indicate a reduction in current velocity for the 2023 PA, because the flow cross-sectional area is increased by deepening and widening the turning basins while the tidal prism increases by less than 1.6%. As roughly the same volume of water passes through a larger cross-section, it is expected to lower the current velocity.

Based on more detailed analysis of the morphology and hydrodynamics between RM 1.0 and RM 3.0, the 2023 PA is not expected to cause adverse impacts on channel morphology or the morphology or stability of adjacent structures and river features. It should be noted that the channel and estuary bathymetry will be monitored post-construction of the channel improvements as part of the Adaptive Risk Management Plan.

SALINITY MIXING

The MIKE-3 FM modeling suite has the capability to simulate salinity mixing. Salinity modeling was built on the hydrodynamic modeling and used the same model grids. The model was calibrated against two measured salinity profiles along the main navigation channel. Model validation was conducted using time histories of measured salinity at five off-channel stations, including three stations in the South Slough. The comparison shows that the modeled and measured salinity are in agreement and the metrics in terms of salinity model performance achieved in this study are consistent with recent and similar modeling studies conducted by ERDC or approved by USACE. The model was then used to study possible changes in salinity as a result of the 2023 PA.

Salinity modeling was performed for three simulation periods: a summer period, and two winter periods (one corresponding to a spring tide and one corresponding to a neap tide). The freshwater discharge for winter simulations corresponded to approximately a 2-year storm event.

For the winter simulations, the results of the salinity modeling generally show an increase in mean salinity; the deeper, wider channel allows the salt wedge to propagate further upstream, increasing salinity throughout. The largest absolute increase in mean salinity between the 2023 PA and the Existing Conditions is 0.82 psu (i.e., 4.4%) in Haynes Inlet. The largest percent increase of 7% occurs in Coos River, where the baseline salinity is low (i.e., 2.25 psu).

ESTUARINE FLUSHING

Residence time and water age are two metrics that are commonly used to determine the flushing characteristics within an estuary system. Residence time is a measure of the amount of time it takes for the water within an area or water body to be replaced by the water from another area or water body. In this investigation, residence time was calculated to estimate water exchange rates between different parts of the estuary, not between the entire estuary and the ocean. Residence time can also be interpreted as how quickly an area flushes.

Model results show that residence times increase of 11 hours within the Lower Bay as a result of the increased volume capacity of this area compared to the small increase in tidal prism. However, residence time in the Lower Bay is still less than 1.5 days for the 2023 PA, indicating highly flushed conditions with no concern of impact to water quality parameters. In addition, residence times as a result of the 2023 PA change from the Existing Conditions by less than 1.2 hours in the Upper Bay and the tributaries, indicating little change to flushing here. Except at the Upper Isthmus Slough, residence times are generally less than 3 days throughout the Coos Bay estuary, which indicate good flushing.

Water age is a measure of the duration that water within a computational cell has resided within the modeling domain. These metrics are calculated using tracers within the hydrodynamic model. Water age was calculated to estimate exchange rates between different parts of the estuary and the ocean, which is different from residence time assessing water exchange rates between different parts of the estuary.

The water age calculation shows that water particles reside for more time within the entire Coos Bay under the 2023 PA than under the Existing Conditions. The largest increases in water age occur in the Upper Lower Bay, which results from the increase in water volume in this area as a result of the new turning basins in the 2023 PA. Overall, the mean water age increase is less than 1.85 days.

Dissolved oxygen (DO) concentrations within Coos Bay are a function of physical (salinity, temperature, and estuarine mixing) as well as biological processes. Changes to DO resulting from the 2023 PA were estimated based on an analytical assessment that estimated the rate of DO uptake and water age. Assessment results showed that average expected changes to the DO in the tributaries are expected to be less than 0.26 mg/L and in the Upper Upper Bay less than 0.4 mg/L. The greatest reduction in average summer DO (i.e., 0.85 mg/L) occurs at the Upper Lower Bay as a result of the greatest increase in water age. However, the existing DO at this location is relatively high, with the median summer DO above 7 mg/L. In the Lower Isthmus Slough, where the existing DO is low, the expected reduction in DO is 0.26 mg/L under the 2023 PA (approximately a 5% change). All changes to median DO under the 2023 PA are within 11% of the existing median DO concentrations. It should be noted that these DO concentrations reflect the bottom DO in summer (i.e., the worst case) and are always above the water quality standard.

SEDIMENT TRANSPORT

Estuarine sediment transport modeling was performed to evaluate changes to maintenance dredging resulting from the 2023 PA for the channel from RM 2.5 upstream to RM 15 and in the Charleston Channel. Maintenance dredging in the ocean entrance is addressed in Sub-Appendix 4, *Offshore and Ocean Entrance Dynamics*. Therefore, the downstream extent of applicability for this sediment transport modeling is at RM 2.5.

Sediment transport modeling was conducted using the two-dimensional (2D) MIKE-21 FM model suite with coupled hydrodynamics and non-cohesive sediment (sand) transport modules. The modeling domain, model grids, and boundary conditions were the same as that used for hydrodynamic modeling. The model was calibrated against annual average dredging records for various reaches of the FNC. Simulations quantified annual shoaling volume upstream of RM 2.5. Model results indicate that shoaling volume as a result of the 2023 PA would increase by about 57,000 cubic yards per year (CY/yr) over the Existing Conditions; this represents an increase of 36% relative to the existing O&M of 160,000 CY/yr.

The model results also indicate that erosion or deposition as a result of the 2023 PA occurs mainly between RM 5 and RM 8, as a result of the increased cross-sectional area due to the proposed turning basins and corresponding decrease in water velocity. Outside of RM 5 to RM 8, the majority of the navigation channel and shallow-water habitat areas show either no changes or minor changes because these areas are further away from the proposed navigation channel improvements and hence the improvements have very little effect on the hydrodynamics at these locations.

VESSEL-GENERATED WAVES

Vessel-generated waves can influence shoreline stability. Analysis of ship-generated waves show an overall small reduction in the wake height generated by tugs and only small changes in drawdown height associated with larger vessels transiting under the 2023 PA as compared to the Existing Conditions. Compared to the Existing Conditions, impacts from container ships are newly introduced under the 2023 PA and drawdown height associated with container ships can reach up to 0.6 ft. For bulk ships, a 0.1-0.3 ft reduction in drawdown height are observed in most parts of the channel under the 2023 PA as compared to the Existing Conditions, and the ship sizes are larger and the frequency of larger bulk vessels will likely decrease under the 2023 PA compared to the Existing Condition, which will further reduce the wave impacts at the shorelines.

WAVES

Analysis of offshore wave penetration into the estuary – detailed in Sub-Appendix 4, *Offshore and Ocean Entrance Dynamics*, indicates a decrease in wave penetration into the estuary under the 2023 PA in comparison to the Existing Conditions. In addition, ebb current velocities away from the channel centerline are expected to be lower in the 2023 PA than in the Existing Conditions. Thus, with lower current velocities outside of the channel, the 2023 PA is not expected to cause increased erosion of channel edge areas. Therefore, shoreline erosion is not expected to increase within the Coos Bay estuary as a result of the 2023 PA.

RISK MANAGEMENT PLAN

Results of the investigations described in this Section 204(f)/408 Report, in the opinion of the OIPCB, show that all project effects on infrastructure and the natural environment have been managed and are minor and manageable. The Corps of Engineers, through their Section 408 and 404 reviews, will make the Federal determination whether the Proposed Alteration is environmentally acceptable and consistent with Federal policy. As is the case with the implementation of any navigation improvement project in such a dynamic physical environment and within an important and ecologically valuable estuary, there will be inherent residual risk and uncertainty associated project implementation. As such, Risk Management will be a critical element of the project. Throughout the development of the Section 204(f)/408 Report, potential areas of residual risk regarding the potential for impacts within the Coos Bay estuary have been identified. While these potential impacts will be further evaluated in the NEPA process, preliminary elements of risk identified as warranting quantitative risk management plan are summarized in Table ES-1.

The Risk Management Plan will be developed based on USACE Risk Management guidance.

Table ES-1
Risk Management Elements Related to Estuarine Dynamics Analyses

Issue or Concern	Primary Monitoring	Monitoring Tools	Frequency and Duration of Monitoring	Trigger(s) For Action	Possible Response Actions
Infrastructure Stability	Bathymetric surveys	Bathymetric surveys to establish baseline Existing Conditions variability	Annually – 5-year period post construction. Periodic following major storm events.	Erosion beyond predicted limits and / or in close proximity to jetty structure	Temporarily suspend dredging operations; Add or enhance rock apron or other protective measures
Estuary Water Quality	Monitor range of WQ parameters for which baseline Existing Condition data exists including salinity, temperature, DO, others	Utilize present monitoring programs but augment in potential areas of concern – important to establish baseline and reasonable variability for Existing conditions	Quarterly – using data retrieved from real time and periodic automated sampling stations for 5-year period.	Compare post construction WQ parameter data – trigger is exceedance of water quality standards **Temperature:** 0.5 ° Fahrenheit increase in Coos Bay waters **Dissolved Oxygen:** < 4.0 mg/L Minimum <6.5 mg/L 30 Day Mean Minimum	Adaptive mitigation and negotiated water quality enhancement projects (e.g. stormwater enhancement projects, riparian and estuary enhancement activities in basin)
Shallow Subtidal/Salt Marsh/Mudflat Habitats	Bathymetric surveys	Bathymetric surveys to determine extent of equilibration	Biennial for 10-year period	Equilibration that extends into these habitat types where none is currently modeled to occur	Adaptive mitigation – replacement of lost habitat function and value with restoration actions in the estuary

TABLE OF CONTENTS

Attachments

LIST OF TABLES

LIST OF FIGURES

ACRONYMS AND ABBREVIATIONS

2D	Two-dimensional
3D	Three-dimensional
3D HD	3D Hydrodynamic
ac	Acres
ADCP	Acoustic Doppler Current Profilers
AIS	Automatic identification system
AMD	Advanced Maintenance Dredging
ASA(CW)	Assistant Secretary of the Army for Civil Works
ATON	Aids to Navigation
BMPs	Best Management Practices
BOD	Biological Oxygen Demand
BOE	Basis of Estimate
BW	Boussinesq Wave
CBNS	Coos Bay North Spit
CDF	Confined Disposal Facility
CDIP	Coastal Data Information Program
CERF	Cape Fear River Estuary
CFD	Cumulative Frequency Distributions
CFR	Code of Federal Regulations
cfs	Cubic feet per second
CLBK	Coalbank Slough
CMOP	Coastal Margin Observation and Protection
CMS	Coastal Modeling System
CR-	Coos River Observation Point No.
CRA	Cost Risk Analysis
CSZ	Cascadia Subduction Zone
CTD	Conductivity, Temperature, and Depth
CWA	Clean Water Act
cy	Cubic yards
cy/yr	Cubic yards per year
CZMA	Coastal Zone Management Act
DBB	Design-Bid-Build
DDR	Design Documentation Report
DEA	David Evans and Associates, Inc.
DHI	Danish Hydraulic Institute
DMMP	Dredged Material Management Plan
DO	Dissolved Oxygen
DOC	Disolved Organic Carbon
DOGAMI	Oregon Department of Geology and Mineral Industries
DTM	Digital Terrain Model
EC	Engineering Circular
EIS	Environmental Impact Statement
ENSO	El Niño/Southern Oscillation
ER	Engineer Regulations
ERDC	Engineer Research and Development Center
ESA	Endangered Species Act
ESDE	Eastside Bridge
ETL	Engineer Technical Letter
FAA	Federal Aviation Administration
FERC	Federal Energy Regulatory Commission
FM	Flexible Mesh
FM HD	Flexible Mesh Hydrodynamic
FNC	Federal Navigation Channel
FNC-	Federal Navigation Channel Observation Point No.
FR	Federal Register

ACRONYMS AND ABBREVIATIONS

ft	Foot or feet
FY	Fiscal Year
gpm	Gallons per minute
GRI	Geotechnical Resources, Inc.
HCSS	Heavy Construction Systems Specialists
HI-	Haynes Inlet Observation Point No.
HOWL	Highest Observed Water Level
HRA	Habitat Restoration Area
HSE	Health, safety and environment
IG	Infragravity
ILS	Instrument Landing System
in.	Inches
IWP	Industrial Waste Pond
JCLNG	Jordan Cove LNG Export Facility
lf	Linear feet
JNSL	Joey Ney Slough
LiDAR	Light Detection And Ranging
LIS-	Lower Isthmus Slough Observation Point No.
LNG	Liquefied natural gas
LNGC	Liquefied natrual gas carrier
LOA	Length Overall
LSB	Log-spiral Bay
LSS-	Lower South Slough Observation Point No.
LST	Longshore Transport
LUB-	Lower Upper Bay Observation Point No.
M&N	Moffatt & Nichol
MAE	Mean Absolute Error
MCR	Mouth of the Columbia River
MCX	Mandatory Center of Expertise
mcy	Million cubic yards
MDFL	Mudflat
MHHW	Mean Higher High Water
MHW	Mean High Water
mi	Miles
MLLW	Mean Lower Low Water
MLW	Mean Low Water
mm	Millimeters
MMR	Major Maintenance Report
MOF	Material Offloading Facility
MPRSA	Marine Protection, Research, and Sanctuaries Act
MSL	Mean Sea Level
MTL	Mean Tide Level
MTO	Material takeoffs
NAIP	National Agricultural Imagery Program
NAVD88	North American Vertical Datum of 1988
NDBC	National Data Buoy Center
NED	National Economic Development
NEPA	National Environmental Policy Act
NERRS	National Estuarine Research Reserve System
NGDC	National Geodetic Data Center
NH_4-N	Nitrification of Ammonium Nitrogen
NM	Nautical Mile
NMFS	National Marine Fisheries Service
NOAA	National Oceanic and Atmospheric Administration
NOS	National Ocean Service

ACRONYMS AND ABBREVIATIONS

NRC	National Research Council
NTPro	Navi Trainer Pro 5000
NW	Northwest
O&M	Operations and Maintenance
OCMP	Oregon Coastal Management Program
ODEQ	Oregon Department of Environmental Quality
ODFW	Oregon Department of Fish and Wildlife
ODLCD	Oregon Department of Land Conservation and Development
ODMDS	Ocean Dredged Material Disposal Site
ODSL	Oregon Department of State Lands
OESA	Oregon Endangered Species Act
OGMT	Oregon Gateway Marine Terminal
OIPCB or Port	Oregon International Port of Coos Bay
OPC	Opinion of probable costs
OPRD	Oregon Parks and Recreation Department
ORDEQ	Oregon Department of Environmental Quality
OSU	Oregon State University
PA	Proposed Alteration
PCIP	Pacific Coast Intermodal Port
POC	Particulate Organic Carbon
POT	Peak-Over-Threshold
PPX3	Post Panamax Generation 3
PRG	Project Review Group
psi	pounds per square inch
PSU	Practical salinity unit
QC	Quality control
RAO	Response Amplitude Operators
RFP	Roseburg Forest Products
RM	River mile
RMS	Root-mean-square
RMSE	Root-mean-square Error
ROD	Record of Decision
SDPP	South Dunes Power Plant
SEF	Sediment Evaluation Framework
SELFE	Semi-implicit Eulerian-Lagrangian Finite Element
SHPO	Oregon State Historic Preservation Office
SL	Screening levels
SLC	Sea level change
SLR	Sea-level Rise
SMMP	Site Management/Monitoring Plan
SOD	Sediment Oxygen Demand
SOORC	Southern Oregon Ocean Resource Commission
ST	Sand Transport
SSC	Suspended Sediment Concentration
SSE	Safe Shutdown Earthquake
SSNERR	South Slough National Estuarine Research Reserve
SW	Spectral Wave
SWORA	Southwest Oregon Regional Airport
TCX	Technical expertise
the “Project”	Coos Bay Section 204(f) Channel Modification Project
TIN	Triangular irregular networks
TN	Total Nitrogen
TON	Total Organic Nitrogen
TOC	Total organic carbon
TSP	Tentatively Selected Plan

ACRONYMS AND ABBREVIATIONS

U.S.	United States
UIS-	Upper Isthmus Slough Observation Point No.
USS-	Upper South Slough Obssssservation Point No.
USACE	U.S. Army Corps of Engineers
USBLM	U.S. Bureau of Land Management
USC	United States Code
USCG	U.S. Coast Guard
USDA	U.S. Department of Agriculture
USEPA	U.S. Environmental Protection Agency
USFWS	U.S. Fish and Wildlife Service
USGS	U.S. Geological Survey
USGS	U.S. Geological Survey
UUB-	Upper Upper Bay Observation Point No.
VFR	Visual flight rules
WIIN	Water Infrastructure Improvements for the Nation
WNW	West-northwest
WOP	Without Project
WRDA	Water Resources Development Act
WRRDA	Water Resources Reform and Development Act
WSP	Western Snowy Plover
WSW	West-southwest
WY	Water Years

1. INTRODUCTION

The Oregon International Port of Coos Bay (OIPCB or Port) is home to the second largest deep-draft coastal harbor between San Francisco and the Puget Sound, based on the tonnage of cargo transported through the Port. Access to the Port's facilities is provided by the Coos Bay Federal Navigation Channel (FNC), a federal channel that was first dredged in the early 1900s. The channel was last improved in 1998, when the channel was deepened by 2 feet (ft) from 35 ft to 37 ft. Since 1998, vessels calling at the Port have substantially increased in size.

1.1 Overview

The OIPCB proposes a Pacific Coast Intermodal Port (PCIP) project at Coos Bay, Oregon. The PCIP consists of integrated elements that would link freight arriving by container ship to the Port to Class 1 rail networks in Oregon. The in-water component of the project includes the deepening and widening of the existing FNC for deep-draft container vessels. In support of that work, the Port is conducting economic, engineering, and environmental studies preparatory to improving the Federal navigation project. These investigations are being conducted under the authority granted by Section 204 of the Water Resources Development Act (WRDA), 1986, as modified by Section 1014 of the Water Resources Reform and Development Act (WRRDA), 2014. This action will require approval by the U.S. Army Corps of Engineers under Section 14 of the Rivers and Harbors Appropriation Act of 1899, 33 United States Code 408, to modify the Federal navigation project. The Section 204/408 Report and Environmental Impact Statement (EIS) will propose modifications to the Coos Bay Navigation Channel in Coos County, Oregon, to accommodate larger deep draft vessels and provide local, state, and federal economic benefits. The USACE, Portland District is presumed to be the lead federal agency for the EIS in cooperation with the U.S. Department of Transportation's Federal Rail Administration.

1.2 Study Area Description

Coos Bay is located in Coos County, Oregon, on the southern Oregon coast, about 200 miles (mi) south of the mouth of the Columbia River (MCR) and 445 mi north of San Francisco Bay. It is the navigational approach to Charleston, Empire, North Bend, Glasgow, Coos Bay, and Eastside (Figure 1-1 and Figure 1-2). The bay is formed by the junction of Isthmus Slough, Coos River, South Slough, Kentuck Slough, Haynes Slough, and Winchester Creek, and is located at the foot of the Coast Range. Deep-draft navigation is limited to the lower 15 mi of the estuary.

The surface area of the Coos Bay estuary is about 12,000 acres (ac) (about 19 square mi). Tidelands, located from River Mile (RM) 0 through 15, comprise 20 percent to 30 percent of the estuary area. The inlet to the estuary, referred to as the Entrance Channel, is fully exposed to waves.

The Coos Bay estuary drains directly into the Pacific Ocean. The nearshore zone adjacent to the Entrance Channel is composed of fine- to medium-grained sediments and intermittent rock outcroppings. The coastal shelf within 8 mi of the inlet has a roughly 100:1 (Horizontal: Vertical) slope. Cape Arago, a headland that limits sediment transport and marks the southern boundary of the littoral cell, is located 2.5 mi south of the inlet.

The topography of the lower Coos River area is a combination of rugged mountain terrain, extensive sand dunes adjacent to the ocean, and relatively flat pasture land along the river. The terrain of the area is quite rugged, because the mountains are relatively young, denoted by the

typical narrow, sinuous valleys and steep side slopes. Relief varies from sea level to just under 3,000 ft; however, most of the land lies between 500 ft and 1,500 ft in elevation.

Geotechnical investigations indicate the subsurface conditions in the channel typically vary from relatively clean sand to siltstone and sandstone sedimentary rock. The sedimentary rock is present near the mudline from about RM 2 to RM 6 and at Guano Rock from about RM 0.7 to RM 0.9.

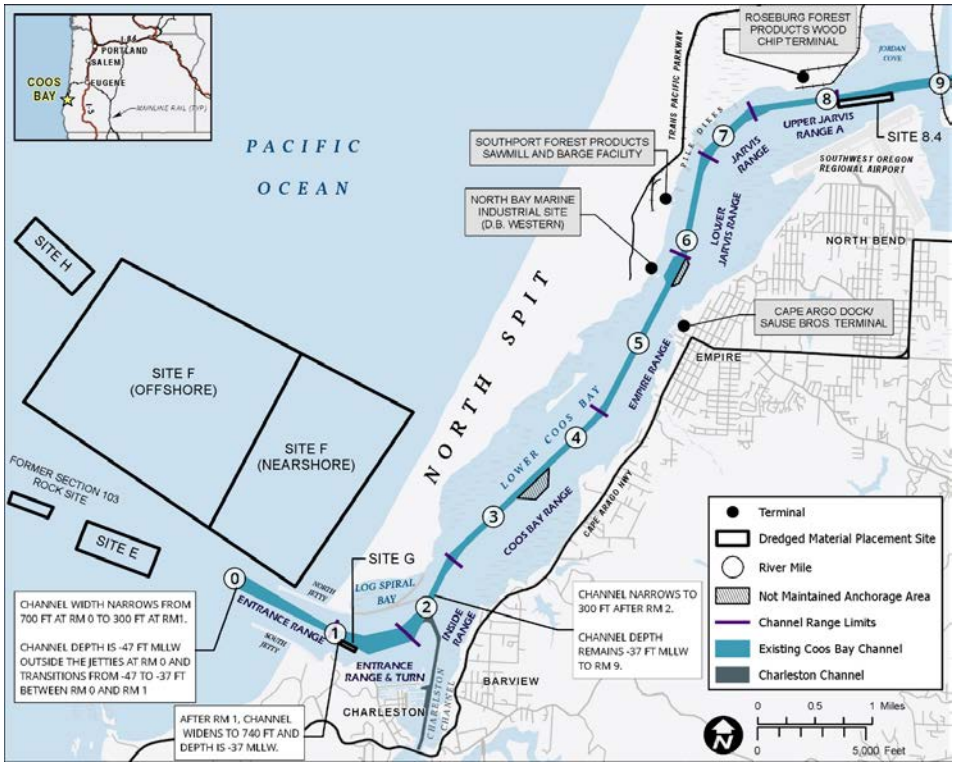

Figure 1-1
Coos Bay Project Vicinity Map, Lower Bay

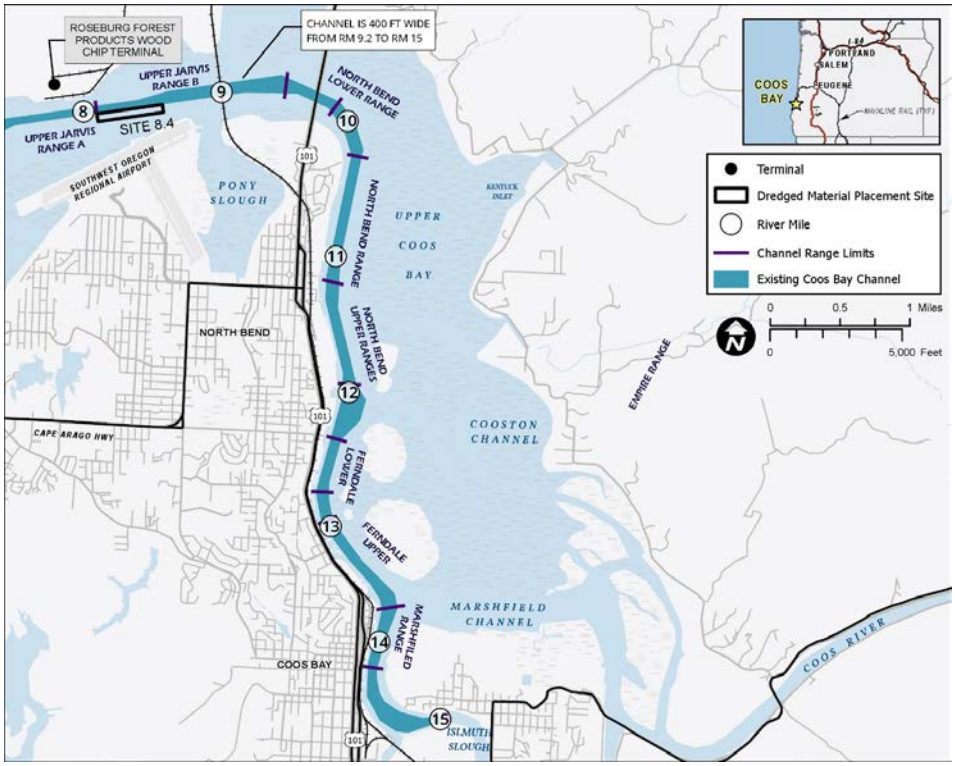

Figure 1-2
Coos Bay Project Vicinity Map, Upper Bay

1.3 Existing Navigation Channel

The Coos Bay Federal Navigation Project was first authorized by the Rivers and Harbors Appropriation Act of March 3, 1899, and has been subsequently modified in 1919, 1937, 1951, 1952, 1979, and 1998. The 1979 project represents the completion of the 1970 authorized which allowed the USACE to deepen and maintain the Entrance Channel at -45 ft Mean Lower Low Water (MLLW) and the inner channel to -35 ft MLLW. The most recent project modification was authorized in the fiscal year (FY) 1996 Energy and Water Development Appropriations Act, Public Law 104-46, which provided for deepening the channel by 2 ft to -47 ft MLLW from the ocean entrance to Guano Rock at RM 1, and to -37 ft MLLW from RM 1 to RM 15. Public Law 104-46 also provided for deepening the turning basin at RM 12 by 2 ft and expanding it by 100 ft, from 800 ft by 1,000 ft to 900 ft by 1,000 ft.

The U.S. Army Corps of Engineers (USACE) Federal Navigation Project consists of the following federally authorized elements:

- North Jetty (9,600 ft long) and South Jetty (3,900 ft long), located on either side of the Entrance Channel, including the two relic structures that extend from the root of the North Jetty, one of which extends into Log-spiral Bay (LSB) and the other of which extends into the estuary.
- An Entrance Channel with an authorized depth of -47 ft MLLW, which decreases from a width of 700 ft at RM 0 to a width of 300 ft at RM 1.
- An inner channel (from RM 1 to RM 15) that has an authorized depth of -37 ft MLLW, a width of 300 ft from RM 1 to RM 9, and a width of 400 ft from RM 9 to RM 15.
- Two (2) turning basins, both of which are 1,000 ft long. The first is located at RM 12, and has a width of 900 ft. The other, located at RM 14, has a width of 730 ft. Both have a depth of -37 ft MLLW, consistent with the channel depth.
- Five (5) pile dikes between RM 6.4 and RM 7.3 in the main channel.
- Continuation of the main channel beyond RM 15 (in the Isthmus Slough) with a width of 150 ft and a depth of -22 ft MLLW.
- A 150-ft-wide Charleston Access Channel that has a depth that varies from –17 to -14 ft MLLW.
- A breakwater and bulkhead at Charleston.
- Charleston Small Boat Basin (10 feet deep) constructed by USACE in 1956 and maintained by the OIPCB.
- Advanced maintenance dredging (AMD) of the channel extends offshore to RM -0.55, where the width of maintenance is 1,060 ft. Authorized AMD is 5 ft of depth in the Entrance Channel (RM 0.55 to RM 1) and 1 ft of depth upstream of RM 1.

The USACE maintains the above elements to provide navigational access to Coos Bay. USACE maintenance of the main navigation channel and jetty features provides ongoing deep-draft navigation access to Coos Bay.

1.4 Description of the 2023 Proposed Alteration (2023 PA)

To accommodate larger deep draft vessels and provide local, state, and federal economic benefits, the Port proposes navigation channel improvements to the Coos Bay Navigation Channel. These proposed channel improvements are hereinafter referred to as the 2023 Proposed Alteration (2023 PA) and they are summarized as follows:

- *Coos Bay Inside Range*: the channel from RM 1.3 to RM 2.8 on the red side of the channel was widened. The range heading of the Coos Bay Inside Range was changed by 1° from 28.0° - 208.0° to 27.0° - 207.0°.

- *Bend Widener at RM 4.0*: a bend widener was included in the 2023 PA to add an additional 50 ft on the green side in the turn from Coos Bay Range to Empire Range.

- *Post Panamax Generation 3 (PPX3) Containership Turning Basin at RM 5.0*: a larger turning basin at the container facility is needed to accommodate the PPX3 containership. Based on the vessel's dimension, the proposed turning basin is 2,000 feet long (parallel to the channel) and 1,600 feet wide. The turning basin's design bottom elevation is -45 ft MLLW, the same as the 2023 PA channel.

- *Capesize Turning Basin at RM 8.0*: a Capesize turning basin was added at RM 8.0 to replace the turning basin that was removed at RM 7.5. Operationally, this turning basin will be used by inbound empty vessels. Therefore, the turning basin's design bottom elevation is -37 ft MLLW. The deeper navigation channel (450-ft wide at -45 ft MLLW) continues through the length of the turning basin.

The above improvements are shown in Table 1-1 and Table 1-2; no dredging is proposed beyond the boundaries in these tables. The project vicinity is represented graphically in Figure 1-3. In this figure, the channel is labeled by RM. Figure 1-3 also shows the location of the adjacent federal infrastructure: the two jetties that run parallel to the channel from RM 0 to RM 1 and the pile dikes located along the north bank of the channel from RM 6.4 to RM 7.5.

Table 1-1

Channel Footprint for Existing Authorized Project and 2023 PA

Range(s) and RM	Existing Conditions	2023 PA
	Offshore Extent	
Offshore Limit including Advanced Maintenance Dredging	RM -0.55[1]	RM -1
Offshore Limit of Navigation Channel	RM 0[1]	RM -0.9
	Channel Width (ft)	
Offshore Inlet Offshore Limit of Navigation Channel to RM 0.3	700 narrowing to 550	1,280 narrowing to 600
Entrance Range RM 0.3 to 1.0	550 narrowing to 300	600
Entrance Range RM 1.0 to 2.0 and Turn	Varies up to 740	Varies up to 1,140
Inside Range RM 2.0 to 2.5	300	500
Coos Bay Range RM 2.5 to 4.3	300	450
Empire Range RM 4.3 to 5.9	300	450
Post Panamax Generation 3 Turning Basin RM 4.7 to 5.6	None	2,000 x 1,600
Lower Jarvis Range RM 5.9 to 6.8	300	450
Jarvis Turn RM 6.8 to 7.3	400	500

Range(s) and RM	Existing Conditions	2023 PA
Upper Jarvis Range RM 7.3 to 8.2	300	450
Capesize Turning Basin RM 7.6 to 8.0	None	2,000 × 1,100

Notes:

1. The authorized FNC starts at RM 0. However, advanced maintenance dredging (AMD) occurs further offshore, typically from the channel entrance to RM -0.55. The channel width at RM -0.55 is approximately 960 ft.

Table 1-2
Channel Depth for Existing Authorized Project and 2023 PA

	Navigation Bottom Elevation (ft, MLLW)		Advance Maintenance Dredging[1] (ft)	
Range(s) and RM	**Existing Conditions**	**2023 PA**	**Existing Conditions**	**2023 PA**
Offshore Inlet Offshore Limit of Navigation Channel to RM 0.3	-47	-57	5	6
Entrance Range RM 0.3 to 1.0	-47 decreasing to -37[2]	-57 decreasing to -45[3]	Varies 5 to 1[4]	Varies 1 or 6[5]
Entrance Range and Turn RM 1.0 to 2.0	-37	-45	1	1
Inside Range RM 2.0 to 2.5	-37	-45	1	1
Coos Bay Range RM 2.5 to 4.3	-37	-45	1	1
Empire Range RM 4.3 to 5.9	-37	-45	1	1
Post Panamax Generation 3 Turning Basin RM 4.7 to 5.6	None	-45	None	1
Lower Jarvis Range RM 5.9 to 6.8	-37	-45	1	1

Jarvis Turn RM 6.8 to 7.3	-37	-45	1	1
Upper Jarvis Range RM 7.3 to 8.2	-37	-45	1	1
Capesize Turning Basin RM 7.6 to 8.0	None[6]	-37[6]	None	1

Notes:

1. Capital dredging consists of the navigation depth plus AMD plus a rock buffer plus a portion of overdepth.
2. For the existing channel, the navigation depth decreases from a depth of -47 to 37 ft MLLW between RM 0.4 and RM 0.7. The channel is dredged farther offshore to obtain AMD depth.
3. For the 2023 PA, the navigation depth decreases by 12 ft between RM 0.3 (a depth of 57 ft MLLW) and RM 1.0 (a depth of 45 ft MLLW).
4. AMD of 5 ft starts at the offshore daylight line, approximately RM -0.6, and continues to RM 0.7.
5. AMD of 6 ft starts at the offshore daylight line. The AMD will be 1 ft in areas where Guano Rock is present (RM 0.7 to RM 1).
6. Under the Existing Conditions, there is no formal turning basin; vessels that visit Roseburg Forest Products turn in existing deeper water at this location. Under the 2023 PA, incoming vessels will enter the channel and turn under ballast load, so it is not necessary to dredge beyond a depth of 37 ft MLLW.

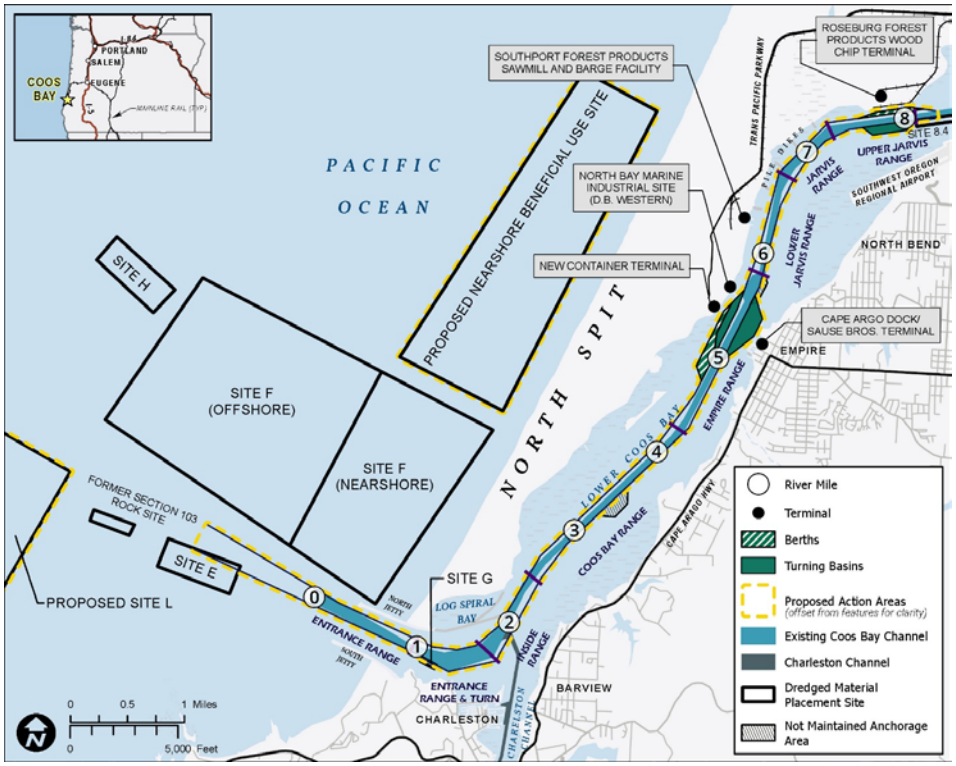

Figure 1-3
Summary of Proposed Alteration

1.5 Previous Coos Bay Channel Modification Studies

From 2016 to 2019, the Port evaluated alternatives for modifications to the Coos Bay Federal Navigation Project in support of a previous proposal. In support of that effort, M&N prepared 19 substantial works of engineering and design, economics, modeling, and construction planning. The USACE, Portland District comprehensively reviewed and evaluated the entirety of the Port's proposals as reflected in their Main Report and all appendices (OIPCB 2019).

1.6 Objective

This study supports the design of the Project by evaluating potential changes in the following estuarine processes throughout the entire Coos Bay estuary resulting from the 2023 PA with respect to the Existing Conditions:

- Tidal hydrodynamics: potential change in mean tidal ranges and maximum currents;
- Salinity mixing: potential change in salinity;
- Residence time, water age, and dissolved oxygen: potential change in water quality and tidal flushing;
- Sediment transport: potential change in deposition, transport, and erosion of sand under the action of tidal and riverine currents; and
- Ship-generated wakes: potential change in exposure of shoreline to ship-generated wakes

Hydrodynamics and salinity mixing were modeled using the three-dimensional (3D) MIKE-3 flexible mesh (FM) model, with coupled hydrodynamics and salinity modules. Sediment transport and deposition was modeled using the two-dimensional (2D) MIKE-21 FM model with coupled hydrodynamics and sand transport modules. Residence time and water age were evaluated using the ECO Lab module within the MIKE-3 FM model suite. The dissolved oxygen was evaluated with an analytical assessment based on salinity and water age results. Ship-generated wakes were assessed based on empirical formulations. A summary list of applied numerical models with descriptions is presented in Table 1-3.

Table 1-3
Summary of Numerical Models

Model Name	Model Description and Application
MIKE-3 model suites by the Danish Hydraulic Institute (DHI)	MIKE-3 is a computer program that simulates free surface flows, cohesive and non-cohesive sediment transport, water quality, and ecology in rivers, lakes, estuaries, bays, coastal areas and seas in three dimensions. MIKE-3 is used for assessment of hydrographic conditions for design, construction, EIS, and coastal and estuarine circulation studies. MIKE-3 includes a three-dimensional Flexible Mesh Hydrodynamic model (MIKE-3 FM HD), which simulates stratified density driven flows and circulation of salinity. The hydrodynamic model is coupled with MIKE ECO Lab module, also developed by DHI. The module is used in water quality assessment. Water quality assessment is focused on changes residence time. Capabilities of the ECO Lab module are used to evaluate residence time and water age parameters for selected areas within the

	estuary. The parameters are applied in assessment of dissolved oxygen using analytical methods with a spreadsheet model.
MIKE-21 model suites by the Danish Hydraulic Institute (DHI)	MIKE-21 is a computer program that simulates free surface flows, waves, cohesive and non-cohesive sediment transport, water quality, and ecology in rivers, lakes, estuaries, bays, coastal areas and seas in two dimensions.Wave propagation is computed by MIKE-21 Spectral Wave (SW) module. The Spectral Wave module is used to simulate wave propagation from offshore to the coast. Estuarine hydrodynamics is simulated using MIKE-21 Flexible Mesh Hydrodynamic model (MIKE-21 FM HD), a two-dimensional depth averaged hydrodynamic model. The hydrodynamic model is coupled with sediment transport (ST) model to evaluate sedimentation processes within the estuary. MIKE-21 Classical hydrodynamic model is a two-dimensional hydrodynamic model, which uses finite difference numerical solution over structured grid. The model is capable to accurately resolve flows over land under rapid flooding conditions. The model is used in the evaluation of propagation of a potential tsunami.

1.7 Report Organization

This report was prepared to document the data and methodology used, and results of the numerical modeling work for the Coos Bay estuary. This report mainly focuses on the area above RM 2.5 (plus Charleston Channel and South Slough). The geophysical conditions and the federal projects in the entrance and offshore of the entrance are described in detail in Sub-Appendix 4, *Offshore and Ocean Entrance Dynamics*. Below is a brief content description of each chapter:

- ***Section 2*** describes the geophysical conditions and summarizes the history of the federal projects.
- ***Section 3*** presents the development of the hydrodynamic (HD) model. The HD model is used to evaluate the effects on hydrodynamics as a result of the proposed channel improvements, and it is the basis for the subsequent salinity mixing and sediment transport analyses.
- ***Section 4*** presents the salinity mixing analysis and results and summarizes the effects as a result of the proposed channel improvements.
- ***Section 5*** presents the residence time, water age, and dissolved oxygen analysis and results and summarizes the effects as a result of the proposed channel improvements.
- ***Section 6*** presents the sediment transport analysis and summarizes the resulting effects from the proposed channel improvements.
- ***Section 7*** summarizes the ship-generated wake analysis for the Coos Bay navigation channel including any changes resulting from the proposed channel improvements.

2. COOS BAY ESTUARY, EXISTING AND HISTORICAL CONDITIONS

This chapter provides a brief description of the Coos Bay estuary in terms of the geophysical and meteorological setting and water quality conditions as well as history of changes in the estuary related to federal projects and infrastructure, focusing on the area above RM 2.5 (as well as Charleston Channel and South Slough). Analysis of the Entrance Channel and Entrance Turn (downstream of RM 2.5) can be found in Sub-Appendix 4, *Offshore and Ocean Entrance Dynamics*.

2.1 Physical Setting

2.1.1 Geology

The Coos Bay estuary is located in a drowned river valley. The region's geology is dominated by sand and old sedimentary rock deposits. Most of the sediment deposits in the estuary are fairly new, from the Holocene or Recent Epoch (10,000 years ago, to the present). To the north, the North Spit is primarily deflation plain and beach sand. To the east of the bay are old (40 to 55 million-year-old) deposits of sandstone, coal, and siltstone covered by sandy or silty loam. The south is composed of 2 million-year-old deposits of sand, silt, and gravel.

Approximately half of Coos Bay's 12,000 ac surface area are tidal flats consisting of mud, silt, sand, clay, and organic matter and are exposed to air during low tide.

The continental shelf off Coos Bay is approximately 14 mi wide. Regional offshore bathymetric contours generally run northeast to southwest, parallel to the coastline (USACE/USEPA 1986). Studies of the continental shelf sediments find that the movement of beach sand during lower sea levels was to the north, with a substantial fraction of the material on the beach sourced from the Klamath Mountains to the south rather than from the Oregon Coast Range (Komar 1997).

2.1.2 Hydrology

Coos Bay is an estuary formed at the junction of the Coos River with many smaller tributaries including South Slough, Isthmus Slough, Kentuck and Willanch Sloughs, Catching Slough, and Haynes Inlet. Coos Bay and the 30 tributaries that flow into the estuary lie within the U.S. Geological Survey (USGS) designated watershed, Coos Bay (USGS Cataloging Unit: 17100304). Among the tributaries, the South Fork Coos and Millicoma Rivers provide the largest source of freshwater to the estuary.

This report identifies a number of watersheds: South Slough, Isthmus Slough, Coos River (including the Millicoma River), Kentuck and Willanch Sloughs, and Haynes Inlet; these watersheds are illustrated in Figure 2-1. Hydrodynamic modeling combined a number of smaller inflows on the east side of the Upper Bay (reach upstream of RM 9.0) into a single source, labeled Kentuck and Willanch Sloughs. A number of other minor inflows, i.e., Pony Slough, agriculture drainage channels and urban runoff, contribute small quantities of freshwater to the watershed and are not directly included in the model.

The USGS had several gauges within the watershed, from which data is available from 1955-1996. Additionally, since 2003, the Coos Watershed Association (CWA) has been monitoring several streams (CWA 2018). The stream gauge locations (gauging stations) are illustrated as red circles

in Figure 2-2. Rain gauges, indicated in this figure as green crosses, have been present at Allegany (north gauge) since 1949 and at Millicoma (south gauge) since 2004.

Table 2-1 lists the stream gauge data inventory, excluding those gauges monitoring smaller or controlled drainage areas (Pony Slough and an unnamed tributary to Winchester Creek). Big Creek is not a tributary to Coos Bay—it flows directly into the Pacific Ocean. The gauged portion of the Coos Bay watershed is approximately 230,000 ac out of the total watershed area of approximately 360,000 ac. The average flow (per unit area of watershed) generally increases from south to north.

Table 2-1
Stream Gauge Data Availability

Gauge Number and Name	Drainage Area (sq. miles)	Data Availability (water year)
USGS Gauges		
14324500 West Fork Millicoma River	46.7	1955 – 1981
14323500 Tioga Creek near Tioga, OR	24.5	1983 – 1996
14324590 Big Creek near Charleston, OR	5.3	1983 – 1996
14324583 Winchester Creek near Charleston, OR	6.7	1992 – 1996
14324580 Pony Creek at Coos Bay, OR	4.1	1975 - 2008
Coos Watershed Association (CWA) Gauges		
14324100 East Fork Millicoma River	65.3	2003 – 2017
14324500 West Fork Millicoma River	46.7	2003 – 2017
14324300 Marlow Creek	6.0	2003 – 2017
14323600 South Fork Coos River	210.0	2003 – 2017
14324583 Winchester Creek near Charleston, OR	6.7	2010 – 2013

The Coos River represents approximately 90% of freshwater inflow to Coos Bay. Discharge in the Coos River was calculated as the sum of measurements from the gauges at the East Fork Millicoma River, West Fork Millicoma River, Marlow Creek, and South Fork Coos River. Discharges for water years from 2003 through 2017, as well as extreme value statistics are shown in Figure 2-3. This figure shows that the discharge can vary from below 20 cubic feet per second (cfs) to around 37,000 cfs. The freshwater inflow is highly seasonal, steeply rising at the time of the first major storm event, peaking around January, and decreasing to the summer dry condition.

The monthly average precipitation based on recorded data from water years 1949 to 2006 at Allegany (located approximately at Station 14324300 on Figure 2-2), is presented in Figure 2-4. Precipitation peaks in December at over 14 inches (in.) and drops to less than 1 in. in July. This data was used in the hydrodynamic modeling and is described in more detail in Section 3.4.2.

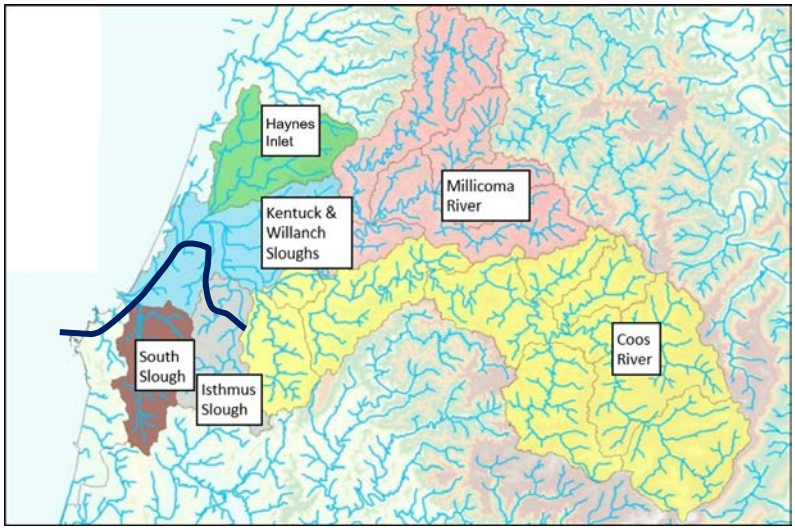

Figure 2-1
Watersheds Draining into Coos Bay

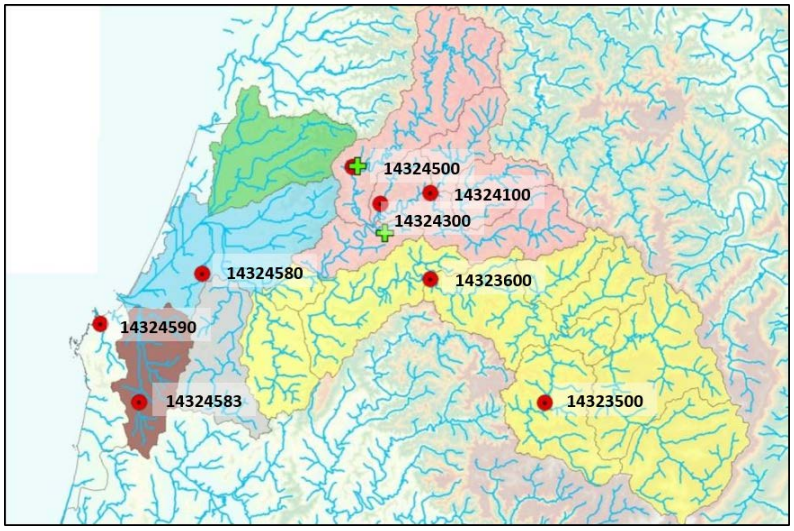

Figure 2-2
Stream (Red Circles, Labeled) and Rain (Green Crosses, Unlabeled) Gauges in Coos Bay Watershed

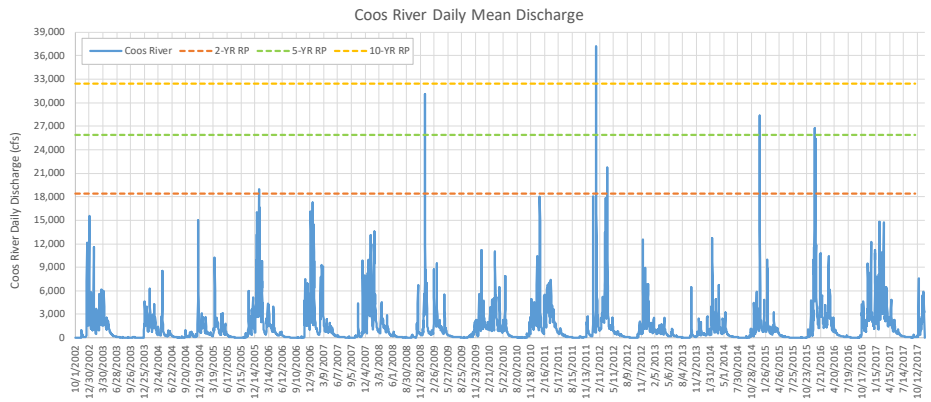

Figure 2-3
Measured Coos River Discharge

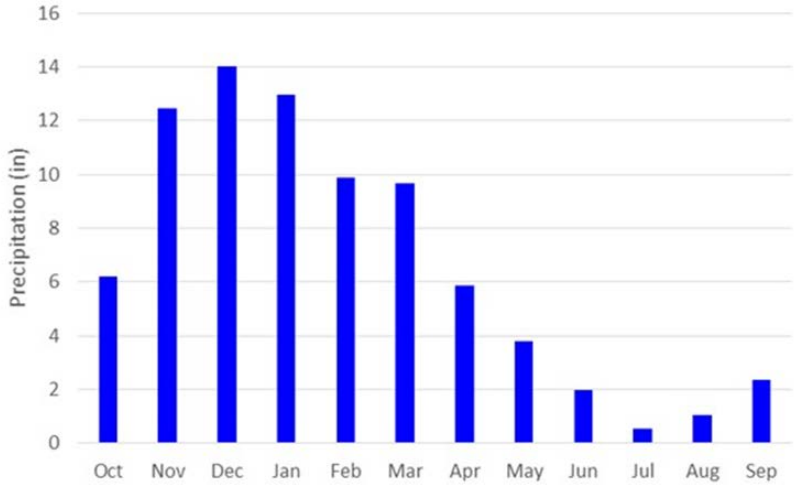

Figure 2-4
Average Monthly Precipitation at Allegany

Return period of extreme events for the Coos River were obtained using extreme value analysis based on 15 years of CWA records, see Table 2-2 and Figure 2-5. Because the period of record is limited, the 95% non-exceedance values were used for analysis and modeling. The 2012 peak discharge, which was approximately 37,000 cfs, corresponds to a 20-year return period storm.

Table 2-2
Statistics of Freshwater Inflow

Return period	Daily Mean Discharge (cfs)	
	Central Estimate	95% Non-Exceedance
2	15,900	18,400
5	20,900	25,900
10	24,700	32,400
25	29,700	41,000
50	33,400	47,600
100	37,200	54,200

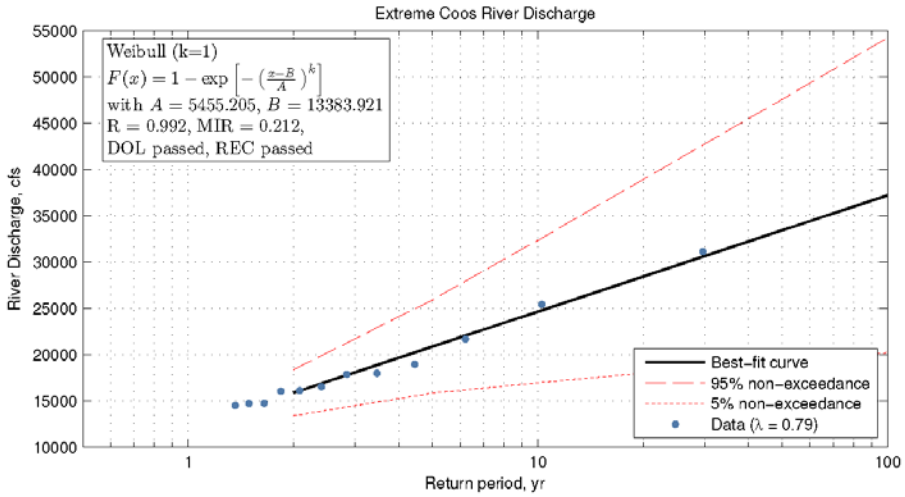

Figure 2-5
Extreme Value Analysis of Coos River Discharge

2.1.3 Tides and Water Levels

Tides in the Coos Bay estuary are mixed and follow a semidiurnal pattern with two unequal high tides and two unequal low tides per day. Diurnal range and mean range of tides are equal to 7.62 and 5.69 ft, respectively (NOAA 2017). Total water level consists of astronomical and meteorological tide components. Meteorological tides refer to changes in expected astronomical tides caused by local meteorological conditions. It is commonly called storm surge if the water surface is elevated due to the passage of a storm. Storm surge is more likely to occur during the winter months; therefore, its effect also causes an apparent seasonal variation in water levels.

Tide gauges throughout Coos Bay are shown in Figure 2-6 and Table 2-3. The National Oceanic and Atmospheric Administration (NOAA)/National Ocean Service (NOS) maintains a tide gauge (number 9432780) in Charleston near the mouth of Coos Bay. Hourly total water levels were measured since March 1970 (NOAA 2017). Tidal datums for analysis are based at Charleston, since it has the longest period of record and data from the current epoch (1983-2001). Comparing data from the various gauges reveals that the tidal range appears to increase upstream. Comparing tidal measurements from the gauge at Charleston, OR (Station ID 9432780, used as the offshore boundary) and at North Bend (located at approximately RM 11) show that the tidal range is 7% higher at North Bend than that at Charleston. This tidal amplification indicates that inertia does influence the hydrodynamics of Coos Bay (see Section 3.1).

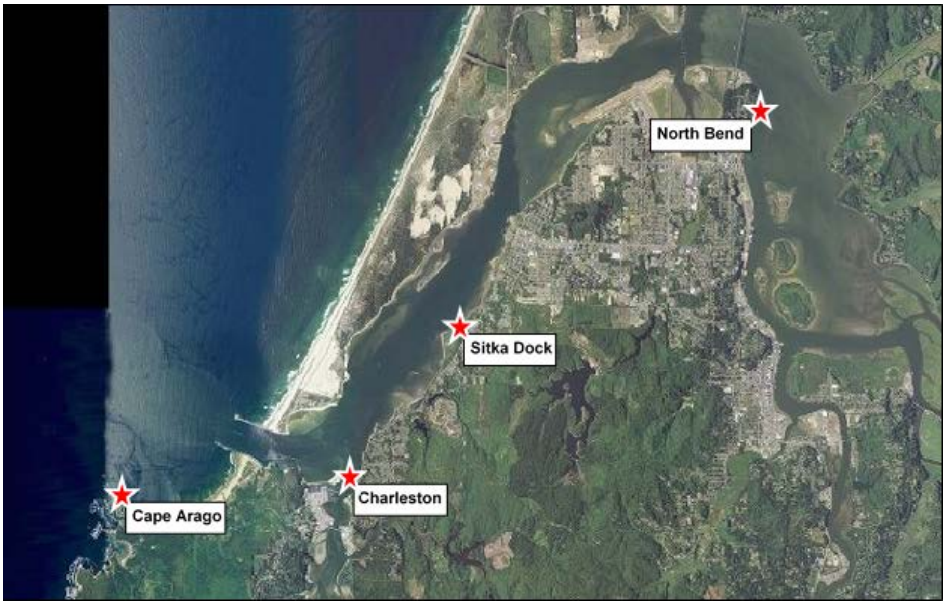

Figure 2-6
Location of Tide Gauges within Coos Bay

Table 2-3
Tidal Datums within Coos Bay

Datum	Charleston 4/1/1970 to 12/31/2018	Cape Arago 12/1/1976 to 12/31/1976	Sitka Dock 9/1/1982 to 9/30/1982	North Bend 9/1/1982 to 9/30/1982
Highest Observed Water Level (HOWL) (1/26/1983)	11.18	-	-	-
Mean Higher High Water (MHHW)	7.62	7.62	7.72	8.43
Mean High Water (MHW)	6.96	6.94	7.06	7.78
Mean Tide Level (MTL)	4.11	4.03	4.17	4.55
Mean Sea Level (MSL)	4.08	3.88	4.18	4.67
Mean Low Water (MLW)	1.27	1.12	1.28	1.33
North American Vertical Datum of 1988 (NAVD88)*	0.50*	-	0.49	0.97
Mean Lower Low Water (MLLW)	0.00	0.00	0.00	0.00
Lowest Observed Water Level (6/1/1973)	-3.08	-	-	-

Note:

*NAVD88 is a geodetic datum rather than a tidal datum.

2.1.4 Currents

Currents in Coos Bay are dominated by tidal action combined with freshwater flows from Coos River and other tributaries. Sutherland and O'Neill (2016) summarized that the extensive mud flats inside the estuary, in conjunction with a deep, dredged navigation channel, produce an ebb-dominant system where flood tides are dampened by friction with the mud flats and ebb tides rush out the channel. There can be a slight increase, relative to the overall range of velocities, in ebb current velocities in the winter due to high river runoff. Currents are at the highest in the lower bay (< RM 9.0) and generally decrease further upstream.

Field measurements of near-surface (at an approximate depth of 6.4 ft) and near-bottom (at an approximate depth of 25.6 ft) current velocities were conducted in lower estuary in 2013-2014 by South Slough National Estuarine Research Reserve (SSNERR). Current velocity was measured using an acoustic Doppler current profiler (ADCP). Highest near-surface and near-bottom current velocities of 3.5 and 2.3 knots, respectively, were reported (Partnership for Coastal Watersheds, 2018b).

2.1.5 Climate

Regional weather consists of cool, moist winters and mild summers. Weather is generally warm and dry from May through September with an average rainfall of less than 4 in. (10 cm). Cooler, wetter weather occurs from October through April, when average annual rainfall is about 56 in. (142.24 cm). In the Reserve and surrounding estuary, heavy winter precipitation results in large volumes of freshwater and sediment inputs during and after storms (Schrager et al. 2017).

Annual temperatures generally range between 40° and 75° F (4.5° - 24° C). In summer, high barometric pressure and northerly winds prevail, while in winter the wind is generally from the south and southwest. Winter storms are generally driven by southwesterly gales, which can exceed 75 mph (120 km/hr) (Rumrill 2006). Wind forcing was not included in the hydrodynamic modeling in this study as Elliott (1982) found that surface wind stresses do not create significant acceleration in shallow estuaries such as Coos Bay.

2.1.6 Waves

Radiation stresses generated by ocean waves affect hydrodynamics up to approximately RM 2 (Sub-Appendix 4. *Offshore and Ocean Entrance Dynamics*). Because this is outside of the area of interest of the hydrodynamic model for the estuary, wave forcing was not included in the hydrodynamic modeling. Ocean waves are analyzed in depth in Sub-Appendix 4, *Offshore and Ocean Entrance Dynamics*.

2.1.7 Seiche

A seiche is a standing wave that occurs in an enclosed or partially closed basin. When the frequency of the waves match that of the basin, the basin may resonate. Seiches have been observed in harbors, lakes, and bays. Forcing may include infragravity (IG) waves, wind events, moving low pressure systems, or tides. Additionally, the generated perturbation may result in a standing wave.

Seiching in Coos Bay has a low potential risk of occurrence. The bay has a complex shape with significant areas of shallow flats. These conditions would prevent a standing wave from forming and the shallows would dissipate wave energy quickly.

The natural period of the water body can be estimated by Merian's formula (Dean & Dalrymple 1984):

$$T = \frac{2l}{n\sqrt{gh}}$$

where l is the length of water body, g is the gravity acceleration, h is the average depth, and n is the mode. The lowest mode is usually more energetic than higher modes due to higher dissipation of the higher frequency waves.

Assuming the length of Coos Bay is approximately 65,000 ft and the average water depth under the existing channel configuration is about 12.5 ft (the value computed as volume divided by area), the lowest mode period is 1.8 hours. Under the PA channel configuration, the average water depth is about 14.4 ft, which results in the lowest mode period of 1.7 hours. The difference in the periods is insignificant and shall not trigger an increase in seiche potential. Additionally, considering that the period is in the order of 2 hours, only specific forcing, for example, associated with moving atmospheric systems, can trigger seiche. However, it is unknown to OIPCB of any reported conditions that caused seiche in Coos Bay.

2.2 Water Quality

Coos Bay estuary water quality data has been collected by various researchers and entities (Thom et al. 2003, Sigmon et al. 2006, ODEQ 2007, Brown & Folger 2009, SSNERR 2014, Sutherland & O'Neill 2016, among others). Currently, water quality in Coos Bay estuary is actively monitored

with a network of several continuously operating water quality monitoring stations (PCW 2018a). Monitoring began in 1995 and the network has expanded throughout the entire Coos Bay estuary since that time. The network is maintained by the Confederated Tribes of Coos, Lower Umpqua, and Siuslaw Indians (CTCLUSI) (two stations), the Coquille Indian Tribe (one station), Oregon Department of Environmental Quality (ODEQ) (four stations) and the SSNERR (four stations). These sensors are listed in Table 2-4 and mapped in Figure 2-7.

At each water quality station, measurements of water temperature, specific conductivity, salinity, DO, pH, turbidity, and depth are collected every 15 minutes. The network provides water quality data in the entire Coos Bay estuary. Analysis of this data can identify episodic, seasonal, and annual patterns in known areas of the bay that have temperature, turbidity, or hypoxia concerns.

Table 2-4
Water Quality Sensors within Coos Bay

Gauge (or ID)	Station Name	Source	Data Period
CTCNSWQ	BLM	CTCLUSI	4/2006- 1/2017
CTCEDWQ	EMP	CTCLUSI	8/2008- 1/2017
SOSCHWQ	Charleston Bridge	SSNERR	4/2002-3/2018
SOSECWQ	Sengstacken Arm (Elliot Creek)	SSNERR	7/2012- 3/2018
SOSVAWQ	Valino Island	SSNERR	6/1999-2/2018
SOSWIWQ	Winchester Arm	SSNERR	4/1995- 6/16/1997; 10/17/1997- 4/2/1998; 7/12/1998- 8/8/1998; 11/4/1998-3/2018
SOSNPWQ	North Point	ODEQ	10/21/2013-2/3/15
SOSISWQ	Isthmus Slough	ODEQ	10/21/2013- 7/2014; 11/2014 -9/13/2017
SOSCAWQ	Catching Slough	ODEQ	10/23/2013-7/2017; 11/2017-1/2018
SOSCRQQ	Coos River	ODEQ	12/19/2013- 5/23/2017
KoKwel Wharf	Upper Bay	Coquille Tribe	10/25/2016- 10/28/2016; 6/22/2017- 11/28/2018

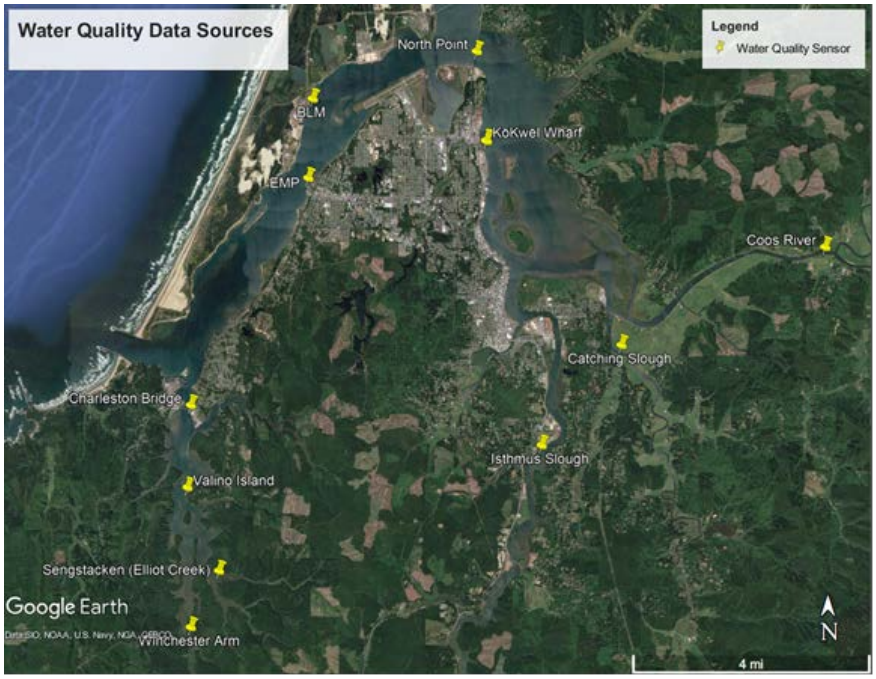

Figure 2-7
Water Quality Sensors within Coos Bay

2.2.1 Salinity

Salinity in Coos Bay estuary has strong seasonal variability. The estuary is vertically well-mixed in the summer and partially mixed in the fall. In the winter, the estuary is considered highly stratified: bottom waters, especially in the lower estuary, largely consist of a tidally-driven "salt wedge" separated from fresher surface waters (Hyde 2007, Sutherland & O'Neill 2016).

Salinity is consistently higher in the dry season than the wet season. Dry season salinities are less variable and markedly skewed towards higher values than in the winter months. As expected, stations further from the mouth of the Coos Bay estuary have lower median salinities and are more variable than sites closer to the ocean (Cornu et al. 2015, Sutherland & O'Neill 2016).

Salinity is based on water quality gauges throughout the estuary. Histograms of salinity at Charleston Bridge, Winchester Arm, EMP, North Point, Isthmus Slough, and Coos River are shown in Figure 2-8 through Figure 2-13, below. As these figures show, Charleston Bridge, EMP, and BLM maintain a salinity of over 20 psu over the entire year. At Winchester Arm, salinity varies throughout the year, with an average salinity of 6.7 psu during March to an average salinity of 21.4 psu during September. A similar trend is observed at the Isthmus Slough sensor, although it is slightly more saline. The Coos River stays relatively fresh throughout the entire year, due to the large freshwater inflow. The average salinity ranges from less than 0.1 psu in March to 17.2 psu in September.

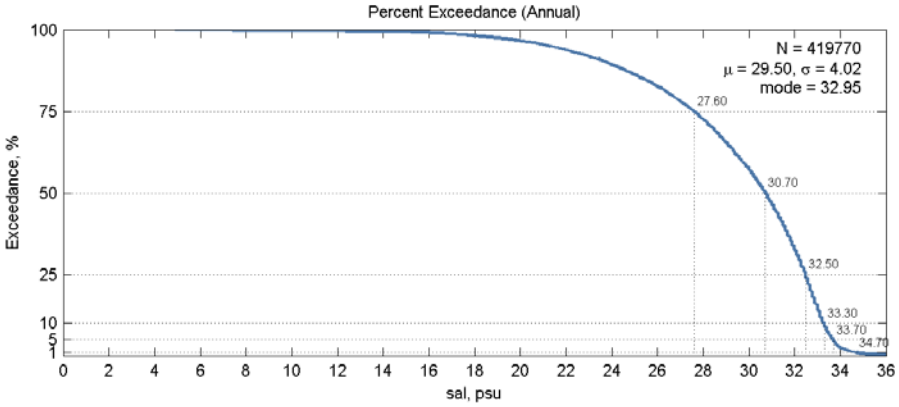

Figure 2-8
Exceedance Plot of Salinity at Charleston Bridge (SOSCHWQ)

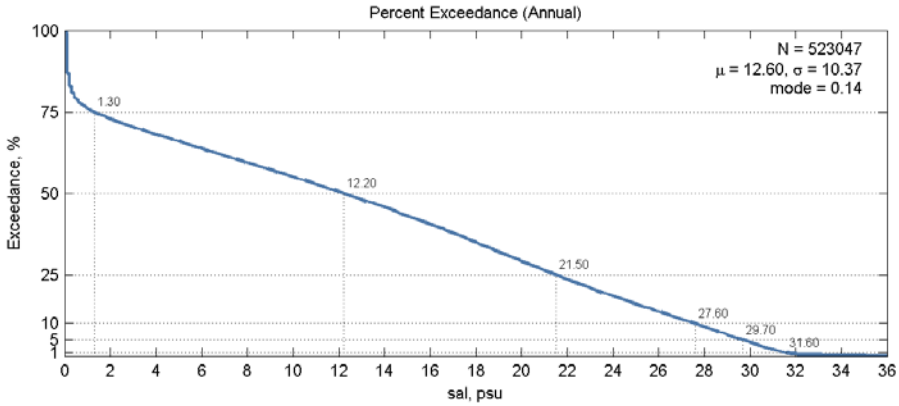

Figure 2-9
Exceedance Plot of Salinity at Winchester Arm (SOSWIWQ)

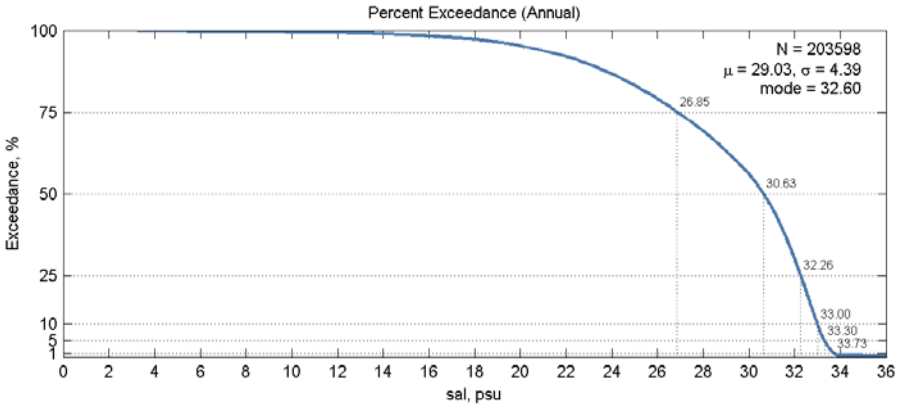

Figure 2-10
Exceedance Plot of Salinity at EMP (CTCEDWQ)

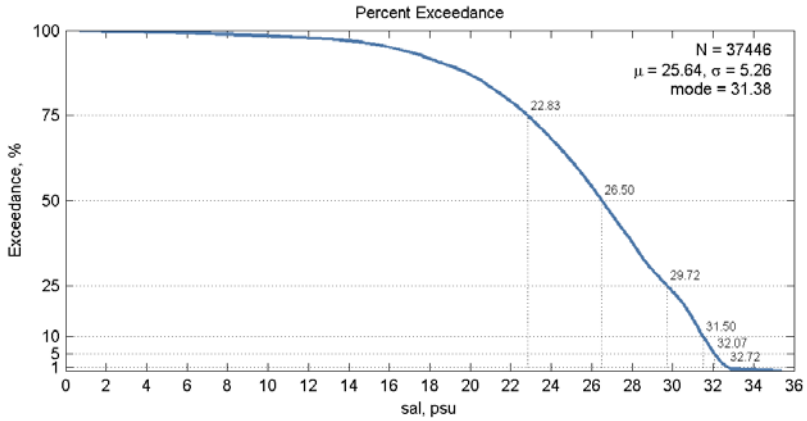

Figure 2-11
Exceedance Plot of Salinity at North Point (SOSNPWQ)

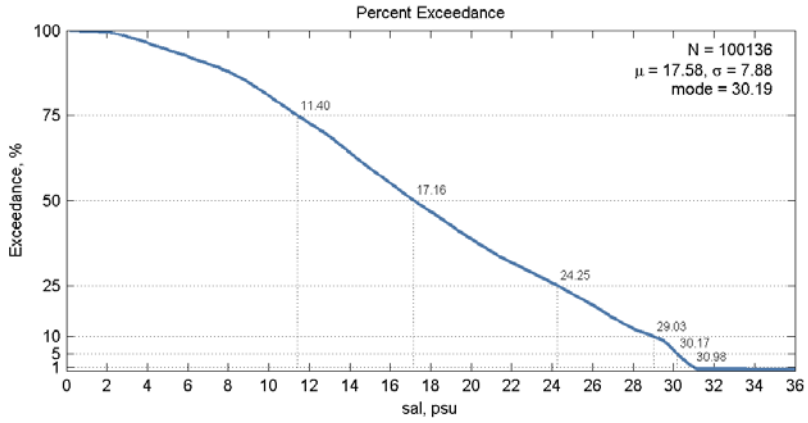

Figure 2-12
Exceedance Plot of Salinity at Isthmus Slough (SOSISWQ)

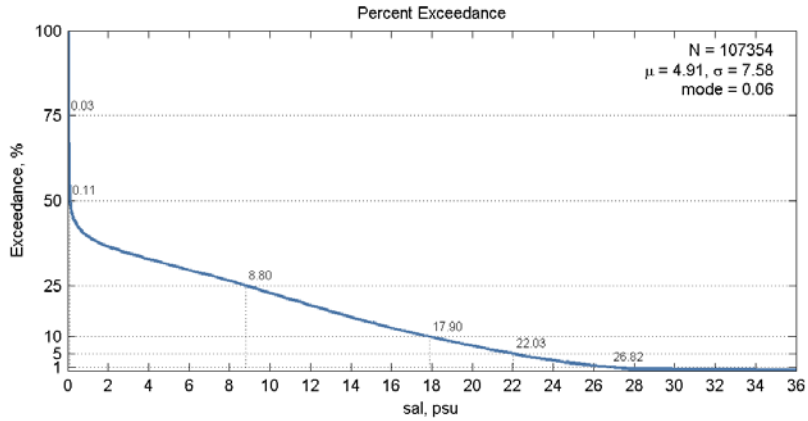

Figure 2-13
Exceedance Plot of Salinity at Coos River (SOSCRQQ)

2.2.2 Water Temperature

The temperature of Coos Bay estuary has both seasonal and diurnal fluctuations. Freshwater inflow and tidal currents are the main factors affecting temperature distribution in the estuary. Coastal upwelling causes offshore surface temperatures to be coldest during summer. River temperatures are coldest in winter and warmest during summer and fall. Seasonal temperature fluctuations are greater in the Upper Bay than near the mouth of the estuary, reflecting that fluctuations in tributary temperatures are more extreme than those of the ocean (Roye 1979).

The ODEQ defines healthy temperatures as below 64.4°F. The Partnership for Coastal Watersheds (2018b) reports that many stations within Coos Bay, including the South Slough, Haynes Inlet,

Upper Bay, Isthmus Slough, Catching Slough, and Coos River, show temperature exceedances. Exceedances occur during the summer months; for year-round, median temperatures, all stations met the ODEQ criteria for healthy waters. Temperatures increase over the summer with higher air temperature, warmer freshwater inflows, and greater solar irradiance. Warmer freshwater can overlay colder ocean water, but the estuary is usually well mixed vertically in summer. During the summer months, temperature is inversely proportional to residence time (i.e., increased tidal flushing is expected to decrease temperatures).

2.2.3 Dissolved Oxygen

Slow moving, higher temperature water tends to contain less DO than cool, fast flowing waters. In addition, transport and decay of organic materials carried into the estuary contribute to a high biological oxygen demand (BOD) and low levels of DO (hypoxia). Dry season DO levels often drop into unhealthy levels in upper regions of the estuary, especially in Isthmus Slough at a location approximately 32.1 mi (20 km) above the mouth (Rumrill 2006, Cornu et al. 2015).

Hypoxia was not observed in the main channel of Coos Bay during a 2-year data collection program in 2012-2013 and has not been observed for the past decade and possibly longer (Sutherland & O'Neill 2016). This contrasts with the other Pacific Northwest estuaries, including Columbia River and Hood Canal, which are deep fjord-like estuaries that experience intermittent hypoxia (Roegner et al. 2011). The absence of hypoxic waters in the main channel of Coos Bay is in part due to the well-mixed conditions in summer. Coos Bay does not have a strong enough summer freshwater inflow nor is it currently deep enough to cause stratification that prevents mixing of aerated surface waters with deeper, DO-depleted waters (Sutherland & O'Neill 2016).

The Partnership for Coastal Watersheds (2018a) provides an overview of DO, summarized as follows: The ODEQ standard for DO is 6.5 mg/L (30-day mean minimum) and 4.0 mg/L (instantaneous limit); this standard is met in the lower Coos Estuary (e.g., South Slough, Lower Bay, and Haynes Inlet), but this standard is often not met in the upper estuary during dry months. Isthmus Slough, Catching Slough, and Coos River stations show DO levels below 6.5 mg/L during parts of the May-October dry season. The lowest concentrations were measured at a station midway within Isthmus Slough, which had a mean August DO concentration of 3.9 mg/L in August 2001. Figure 2-14 shows the data summarized from Partnership for Coastal Watersheds (2018b), which again shows high DO levels in the lower estuary, with lower levels in the upper bay. Aquatic life studies found median lethal DO levels were ~0.75 mg/L for gastropods, ~1.75 mg/L for fish and bivalves, and ~2.0 mg/L for crustaceans. DO levels have not been observed below these standards.

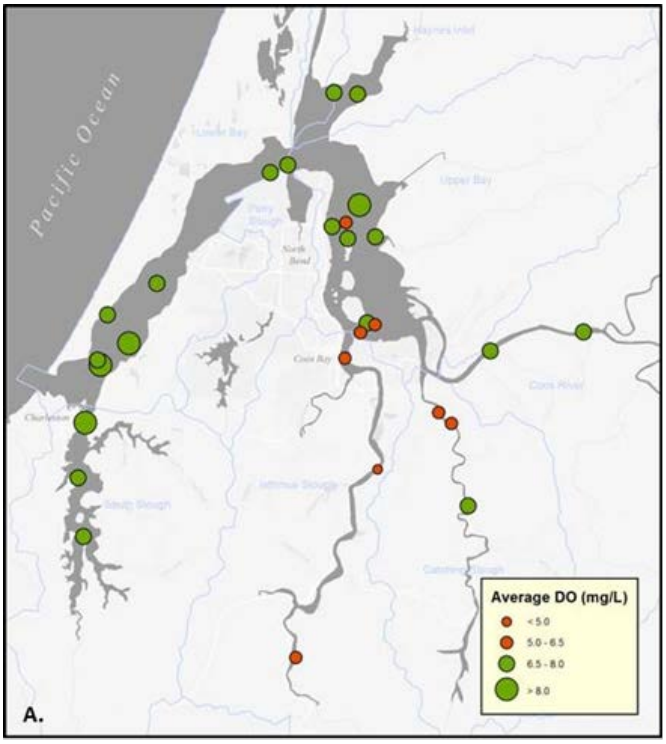

Figure 2-14
Compiled DO Data within Coos Bay (Partnership for Coastal Watersheds 2018b)

Sutherland & O'Neill (2016) examined occurrences of low DO within Coos Bay, relating observations to estuarine processes. They identified three "types" of low-DO events.

- Type 1 events occur during the late spring, with the lowest DO levels observed near the mouth of the estuary during high tides, and there is significant tidal fluctuation of DO. These low DO pulses are caused by the upwelled ocean waters into the channel. During these events, DO concentrations may reach as low as 5.5 mg/L during high tides, and return to above 7 mg/L during low tides.
- Type 2 events occur during the late summer, with the lowest DO levels observed in the upper estuary. DO levels show little tidal fluctuation and show a longer-term drawdown. During these events, DO concentrations under 5 mg/L are present for sustained periods of time.
- Type 3 events during the late summer show similar tidal variability as Type 1 events. These events are observed the least frequently, and DO seldom drops below 6 mg/L.

Sutherland & O'Neill (2016) noted that, "the lowest DO waters observed in the conductivity, temperature, and depth (CTD) transects along the main channel coincide with the warmest waters,

e.g., in September." These are Type 2 events. The transition from Type 1 to Type 2 events occurs from the spring to the fall, as "the location of the minima in DO levels along the estuary migrated from the mouth in the spring to the head of the estuary in the summer. This spatiotemporal shift is due to upwelled shelf water spending longer in the estuary. Increased residence times in Coos Bay in the dry season were facilitated by weakened residual flow resulting from diminished discharge lowering the buoyancy forcing to the estuary." It is concluded that, "the low DO observed in Coos Bay in late summer must occur due to local processes when waters spend more time in the estuary, and they are subjected to increased biologic respiration that draws down DO levels." Essentially, the instances of low DO observed in the upper estuary are very closely related to residence time. Biological processes are accelerated by slow turnover and warm waters. Reducing residence time would lead to colder waters and faster turnover, reducing biological activity and potentially increasing DO levels.

Rumrill's (2006) work indicates that the lowest DO concentrations in South Slough occur during low tides, when upstream water is being transported downstream. This indicates that DO minima are driven more so by upstream biological activity than by ocean water entering the estuary.

DO data for several of these sensors are plotted as exceedance curves in Figure 2-15 through Figure 2-22. These figures also include two standards posted by Oregon Department of Fish and Wildlife (ODFW); the 6.5 mg/L standard is the 30-day mean minimum and the 4.0 mg/L is the instantaneous minimum. Because the plots show instantaneous DO values, the instantaneous standard is more applicable. These plots focus on the summer months when DO tends to be lower. In the Main Channel, at BLM and North Point, DO levels are generally above 6.5 mg/L (approximately 98% of the time at BLM and more than 99% of the time at North Point). It is counter-intuitive that DO concentrations are higher at North Point than at BLM; it is likely due to the deeper location of the sensor, as there is less biological activity at the actual sensor location.

In South Slough, DO tends to decrease further upstream. The 1% exceedance level for DO is about 12 mg/L for each of the three stations, however the median and 99% exceedance level values decrease upstream. DO concentrations are lowest during July and August; for these months, DO can be less than the 6.5 mg/L ODFW threshold over 20% of the time at Valino Island and over 50% of the time at Winchester Arm. The 4.0 mg/L standard is exceeded for 5% of the time in August at Winchester Arm.

The annual exceedance curves for the upstream sensors (Catching Slough, Coos River, and Isthmus Slough) seem to show discontinuities as opposed to the smooth curves seen from elsewhere in Coos Bay, with inflexion points around the 50% and 80% exceedance levels. This indicates high DO during wet months and drastically lower DO levels during the dry months. Coos River has the highest DO, exceeding the Oregon Department of Fish and Wildlife (ODFW) 6.5 mg/L threshold over 90% of the time annually, likely due to sustained upstream inputs with relatively high DO levels. DO concentrations at Catching Slough are generally above the ODFW threshold (90% of the time), and show the lowest DO concentrations in July. DO concentrations at Isthmus Slough are lower, with the DO below the ODFW threshold 25% of the time annually and the concentration of DO below the threshold more than 90% of August and September. The 4.0 mg/L threshold is not exceeded in these areas.

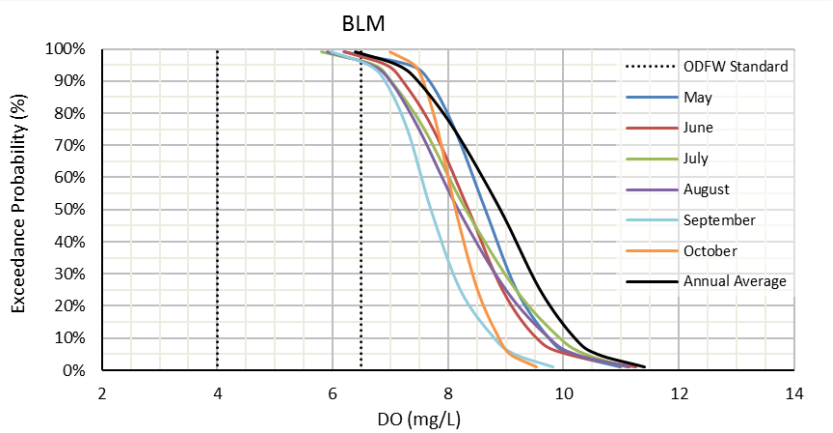

Figure 2-15
Observed DO at BLM Sensor

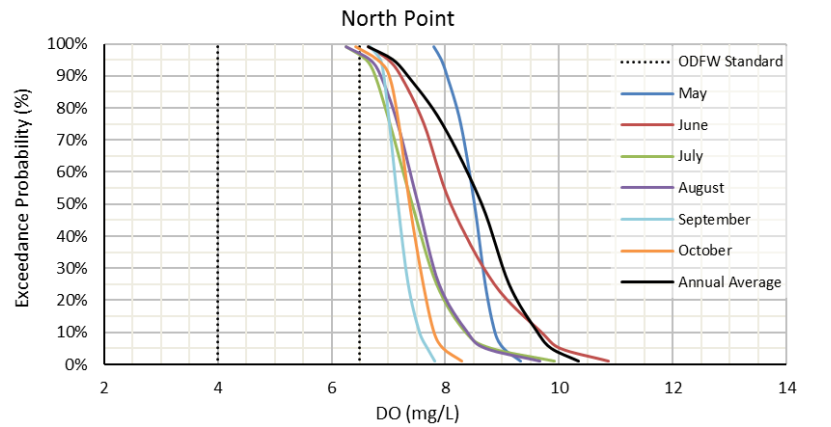

Figure 2-16
Observed DO at North Point Sensor

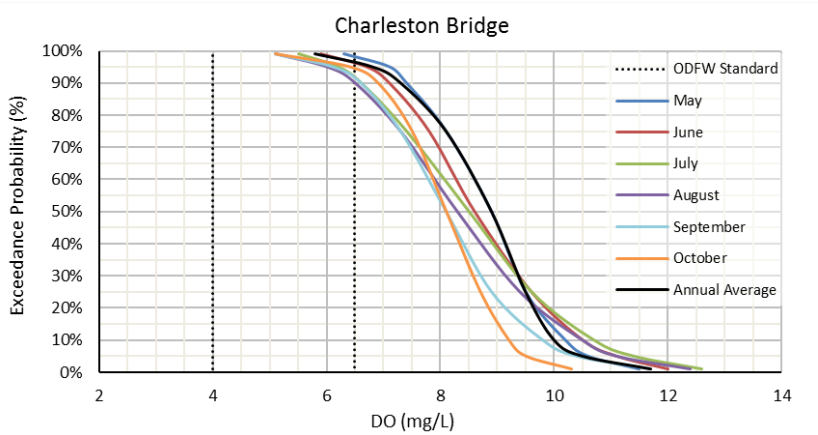

Figure 2-17
Observed DO at Charleston Bridge Sensor

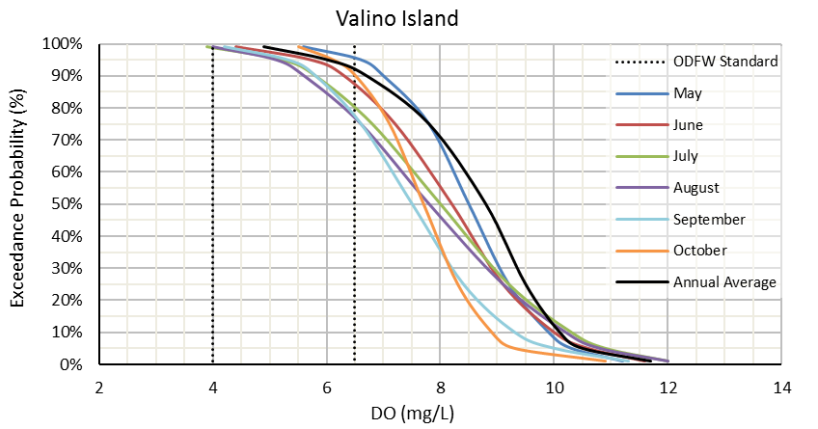

Figure 2-18
Observed DO at Valino Island Sensor

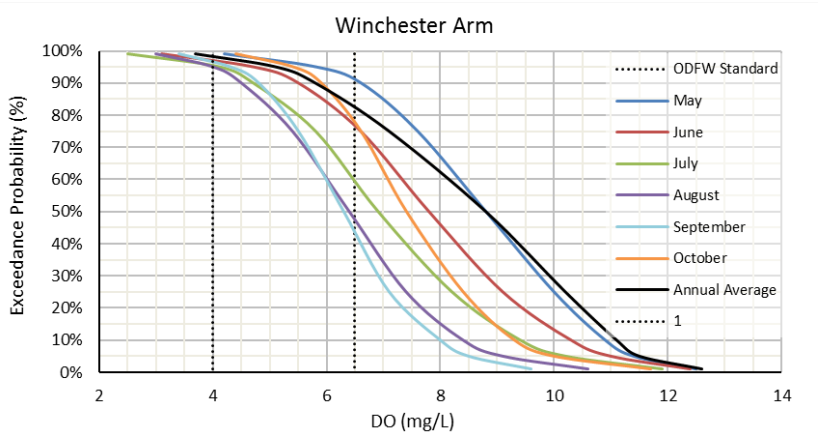

Figure 2-19
Observed DO at Winchester Arm Sensor

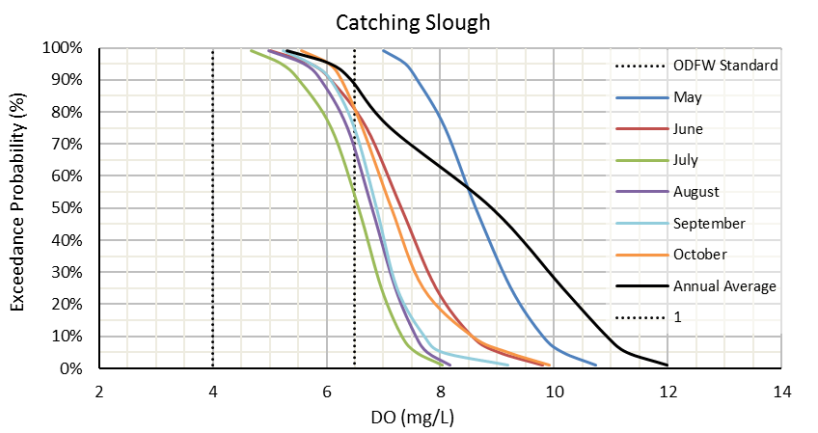

Figure 2-20
Observed DO at Catching Slough Sensor

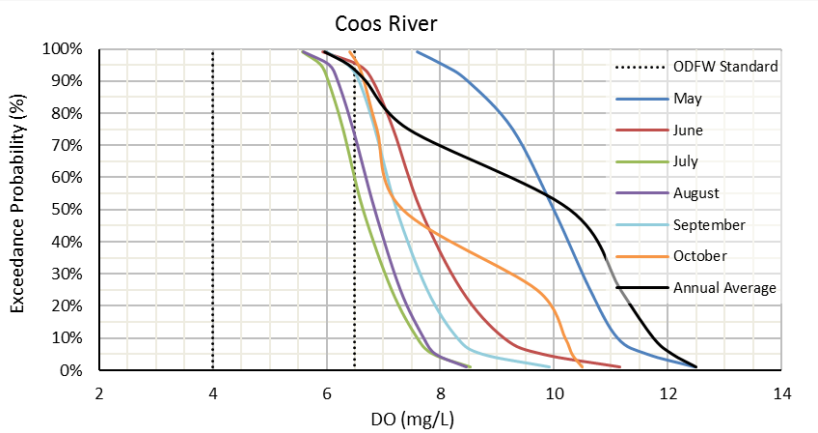

Figure 2-21
Observed DO at Coos River Sensor

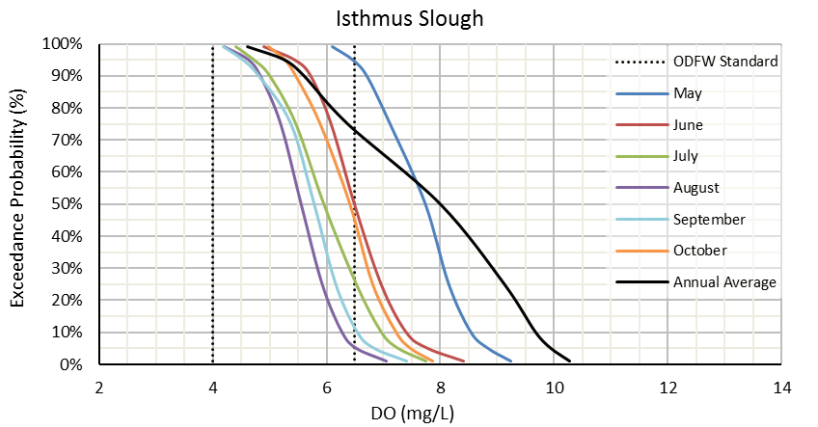

Figure 2-22
Observed DO at Isthmus Slough Sensor

2.3 History of Coos Bay estuary and Federal Infrastructure

Like many estuaries, Coos Bay has evolved since the turn of the 20th Century. Some changes in Coos Bay can be observed by comparison of historical and recent nautical charts. An example of such comparison for the area between RM 6 and RM 11 is shown in Figure 2-23 using nautical charts of 1892, 1948, 1974, and 2010. This figure highlights the following events:

- In 1892, Pony Slough had a wide-open mouth. Early dredging by the USACE removed material from the shoal at Pony Slough.

- By 1948, the airport, the railroad bridge, and the Highway 101 Bridge had been constructed. Dredge material was regularly placed near the mouth of Pony Slough.
- By 1974, the mouth of Pony Slough had been further constricted by the ongoing placement of dredge material from regular maintenance dredging of the channel. A causeway under the railroad bridge divides the slough into two distinct areas. The City of Coos Bay expanded into a newly filled area at the south end of Coos Bay.
- On the north side of the channel, Roseburg Lumber Co. had constructed its wharf and berth and the USACE had constructed pile dikes to protect against bank erosion. A portion of Jarvis Range, on its west bank, had been filled artificially or because of changed circulation in the area.
- By 2010, the airport had been expanded further into the Bay (the runway expansion occurred in 1989). In response to the Clean Water Act of 1974, the material from regular maintenance dredging were no longer placed in the bay, but were placed offshore in Ocean Dredged Material Disposal Site (ODMDS) F.

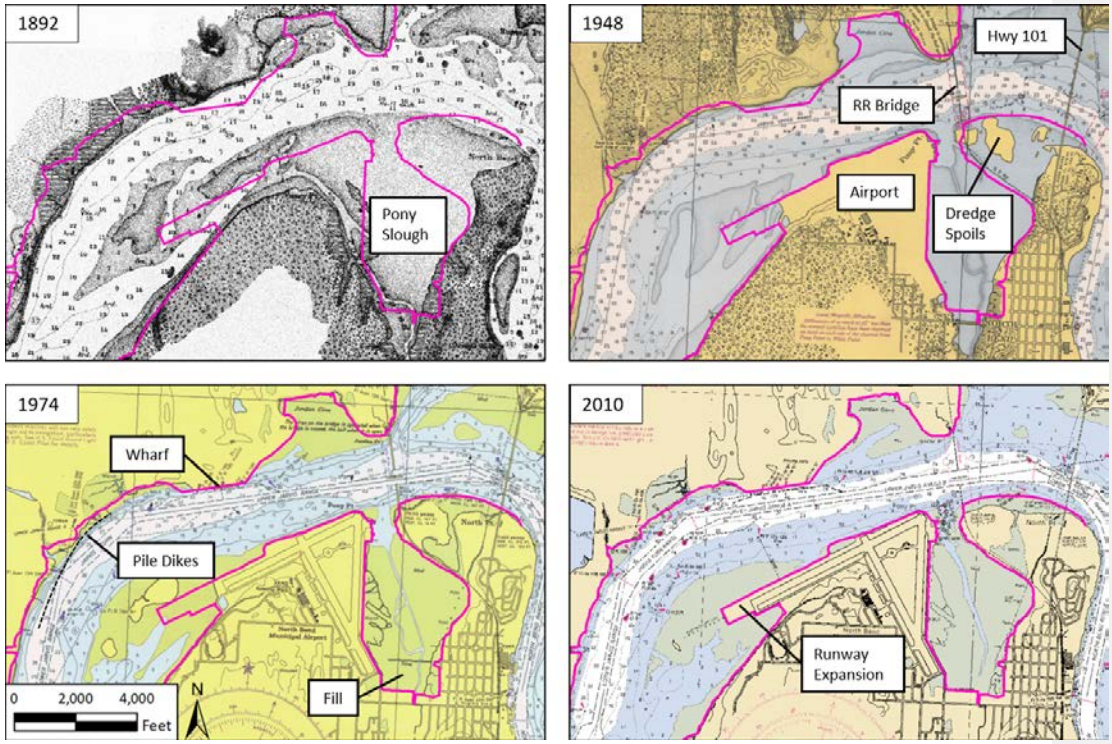

Figure 2-23
Conditions for the Area between RM 6 and 11 Reflected in Nautical Charts from 1892 to 2010 . Solid Magenta Line Represents the 2010 Shoreline as a Reference

2.3.1 Navigation Channel

The navigation channel has been deepened several times since its initial construction, as shown in Table 2-5.

Table 2-5
Authorized Depth at MLLW of Channel above Entrance

Date Authorized	Authorized Depth
1919	22 ft
1935	24 ft
1946	30 ft
1970	35 ft
1996	37 ft

2.3.2 Maintenance Dredging History

Table 2-6 provides the maintenance dredging quantities for the federally maintained channel below RM 12 from 1998 to 2018. This includes the full period since the most recent channel deepening project.

Table 2-6
Coos Bay Dredging History 1998 to 2018 (Below RM 12), Cubic Yards

Fiscal Year	Entrance RM -0.55 to 1+00	Coos Bay Ranges RM 1+00 to 3+20	Coos Bay Empire Ranges RM 3+20 to 5+35	Jarvis Ranges RM 5+35 to 8+05	North Bend Turn RM 8+05 to 10+10	North Bend Ranges RM 10+10 to 12+20	Charleston Channel	Total
1998	849,242	0	0	48,911	-	0	27,429	925,582
1999	697,217	0	0	71,405	83,094	818,915	51,522	1,722,153
2000	749,158	28,198	49,287	53,964	36,563	0	28,098	945,268
2001	569,128	16,783	16,425	99,701	27,581	0	53,446	783,064
2002	663,040	33,792	0	88,586	55,254	0	61,252	901,924
2003	634,039	1,226	28,954	30,408	13,667	0	37,026	745,320
2004	390,620	19,848	6,336	44,679	58,760	0	29,230	549,473
2005	442,828	0	0	51,485	36,793	35,159	44,352	610,617

Fiscal Year	Entrance RM -0.55 to 1+00	Coos Bay Ranges RM 1+00 to 3+20	Coos Bay Empire Ranges RM 3+20 to 5+35	Jarvis Ranges RM 5+35 to 8+05	North Bend Turn RM 8+05 to 10+10	North Bend Ranges RM 10+10 to 12+20	Charleston Channel	Total
2006	497,615	29,868	0	34,706	3,953	0	0	566,142
2007	955,967	3,922	8,804	81,063	48,651	1,004	34,072	1,133,483
2008	622,007	26,358	5,082	59,686	51,637	2,947	16,105	783,822
2009	777,472	45,171	17,336	44,681	13,198	2,028	15,243	915,129
2010	598,906	17,010	6,067	83,147	33,049	0	9,024	747,203
2011	645,847	0	0	115,427	10,837	0	55,804	827,915
2012	532,384	30,527	18,898	55,051	42,101	0	0	678,961
2013	364,343[2]	22,412	19,693	148,032	40,948	0	0	595,428
2014	428,327[2]	2,937	19,492	21,168	30,645	0	40,628	543,197
2015	589,258	0	0	59,614	21,993	0	0	670,865
2016	656,729	16,664	24,007	81,290	65,710	335,109	26,228	1,205,737
2017	732,884	14,024	0	79,580	27,089	0	0	853,577
2018	572,707	0	0	89,849	95,849	0	0	758,405
Average, CY	640,897	14,702	10,494	68,687	39,869	56,912	25,212	831,584
Standard Deviation	136,271	14,008	13,051	30,180	23,844	189,229	21,018	271,101

2.3.3 Pile Dikes

Five pile dikes are present along the north bank of the Jarvis Turn. These structures are important to include in the analysis as these structures impact the hydrodynamics and sedimentation in the vicinity of Jarvis Turn. This section presents the existing conditions of the structures.

Prior to construction of the pile dikes, the channel thalweg (deepest part of the river) was shifting northwest towards the North Spit, eroding the outer bank of the Jarvis Turn. This was likely caused by a change in the hydrodynamics of the turn, triggered by the construction of a runway in the bay

[2] In 2013 and 2014, USACE had less funding and issues with dredge capability (lost time due to repairs) so less material was dredged than was available - the full dredge prism was not dredged. This would skew the averages down so USACE requested that these years not be included in average cubic yard (cy) calculation.

(~1937) or ongoing channel improvement. Over a 20-year span (1937-1957), the banks near Jarvis Turn eroded between 200 to 500 ft (Figure 2-24).

In 1943 or earlier, rock was placed on the outer bank at RM 7 near the low water line. This rock was likely placed to prevent further erosion of the banks, but appears not to have been effective. The rock placement is still visible in bathymetric surveys.

In 1957, the pile dikes were constructed on the outer (northwestern) bank in the Jarvis Turn. Five pile dikes were constructed and named based on their approximate RM location: CB-6.4, CB-6.6, CB-6.8, CB-7.0, and CB-7.3. While the main purpose of the 1957 construction was to retard bank erosion, pile dikes also reduced maintenance dredging requirements and increased channel stability. The location of the five pile dikes can be seen in Figure 2-24.

Each dike consists of three major components: the pile dike, a pile dolphin, and a stone blanket. Figure 2-25 shows a typical stone distribution plan for a typical pile dike (USACE 1958). The piles are creosote treated and about 12 in. in diameter. The dike piles extend up to +10 ft MLLW, and the dolphin piles extend 6 ft higher to +16 ft MLLW and help mark the location of the structures. Typically, the shoreward-most piles are 18 ft long and embedded to -8 ft MLLW. As the structure extends further toward the channel, the length of piles and depth of embedment increases to 50 ft in length and 40 ft below MLLW. Each pile dike's pile driving plan varies according to local depths.

David Evans & Associates (DEA) conducted a detailed pile dike survey in 2016, detailed in Sub-Appendix 2, *Geophysical Report*. Figure 2-26 illustrates an example of the point cloud dataset and the corresponding photograph at RM 6.8.

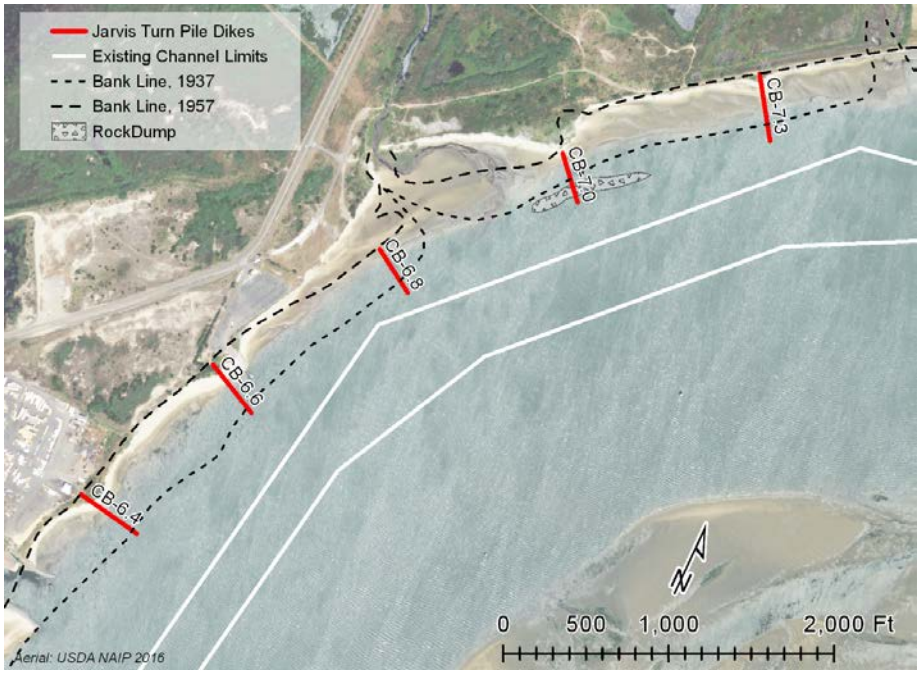

Figure 2-24
Location of Pile Dikes at Jarvis Turn and Indication of the Bank Erosion from 1937 to 1957

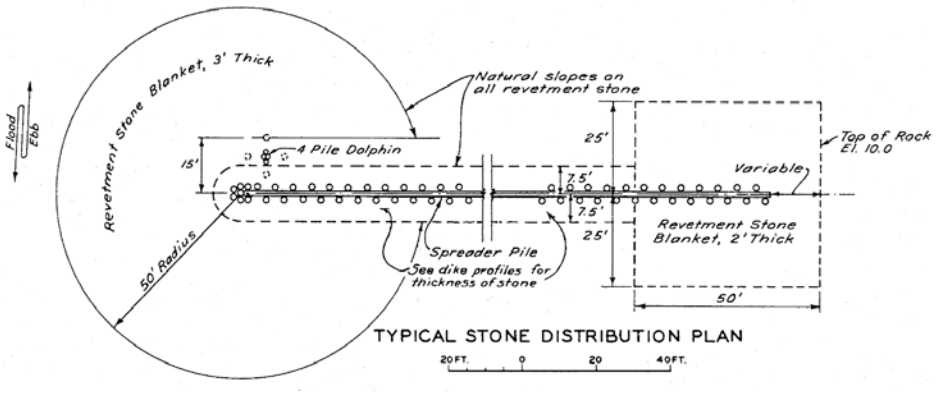

Figure 2-25
Typical Stone Distribution Plan for Pile Dike (Excerpted from USACE 1958)

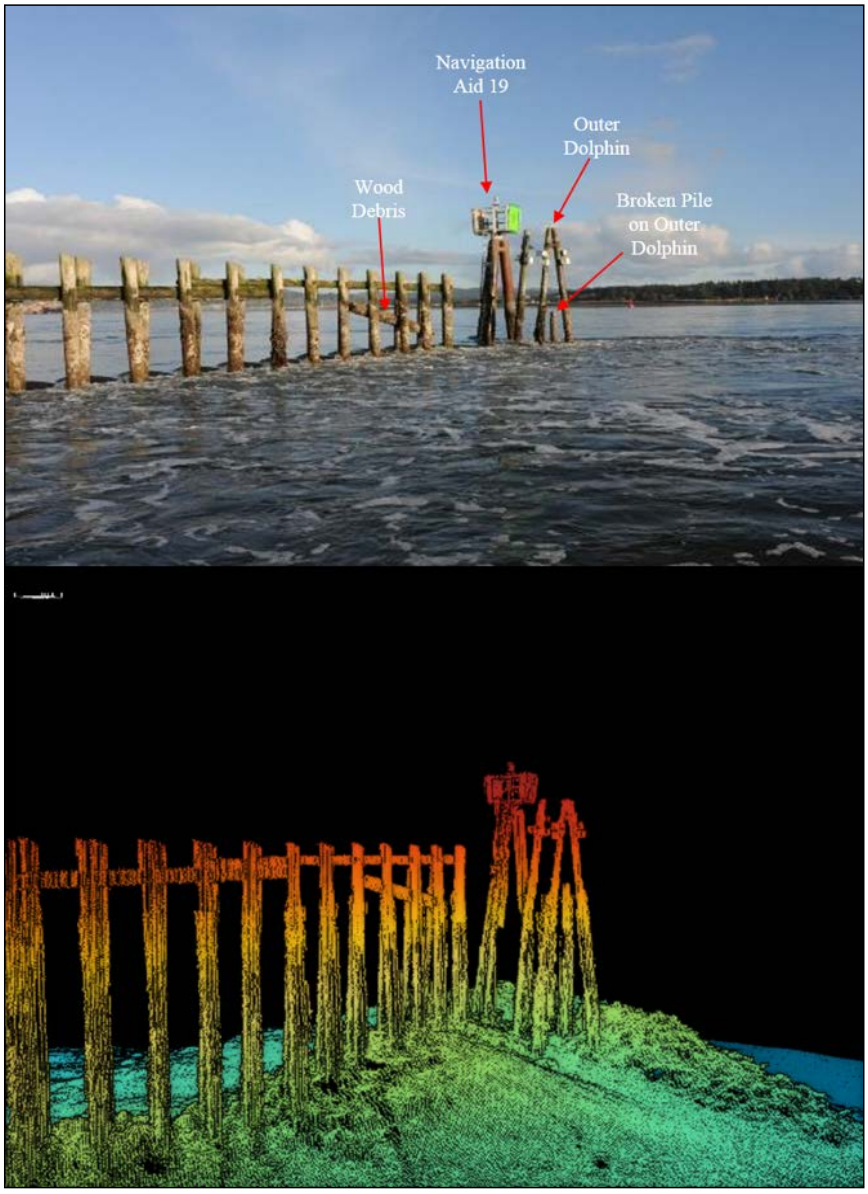

Figure 2-26
Example of Pile Dike Survey – Pile Dike 6.8 Viewed from Downstream Looking Riverward (Excerpted from OIPCB 2016e)

3. HYDRODYNAMIC MODELING

This chapter evaluates the possible changes in tidal range and depth-averaged current velocities as a result of the proposed channel improvements using the MIKE-3 hydrodynamic model. The hydrodynamic modeling domain encompasses the entire estuary from offshore depths of up to 300 ft to upstream freshwater streams.

Commented [JS1]: PDT A-3-2: Specify the downstream extent of applicability for estuary models, for both the circulation model and the sediment transport model.

Commented [JS2R1]: Added the downstream extent of hydrodynamic modeling.

Commented [TCF3R1]: Added.

3.1 Overview of Estuarine Processes in Coos Bay

Hydrodynamic circulation within estuaries is driven primarily by ocean tides and freshwater runoff. The tidal exchange is often quantified by tidal prism, which is the volume of water being exchanged between an estuary (enclosed bay) and the open sea over a complete tidal cycle. This analysis refers to the mean tidal prism (estuary storage volume between mean high tide and mean low tide). The tidal prism volume can be expressed by the relationship: $Prism = h_b \cdot A_b$, where *hb* is the average tidal range and A_b is the average surface area of the basin between mean high tide and mean low tide. For the proposed project improvements, the channel deepening and widening are both sub-tidal, i.e., all dredging occurs well below the low tide elevation. Hence, the area A_b does not change. Therefore, changes to tidal amplitude can be used to estimate changes to tidal prism.

Tidal amplitude in an estuary is affected by the inlet channel dimensions (width, depth, and length), energy loss through the inlet channel due to friction, and inertia. Friction has the effect of restricting the conveyance of water through the channel, dampening the tides upstream. The effect of inertia causes water to move in the direction opposite to the slope of water surface (i.e., water moves from the ocean into the bay even though the bay has a higher water level elevation), effectively amplifying the tidal amplitude upstream and creating a system in which the currents lag the tides. Inertia is more pronounced in estuary systems with a relatively long and hydraulically efficient inlet channel such as Coos Bay. For small or narrow inlets, friction tends to dominate and the tide amplitude in an estuary is dampened relative to the offshore tidal amplitude (i.e., tidal range in the bay is smaller than that in the ocean). In these friction-dominated, muted tidal estuaries, an increase in the inlet channel geometry efficiently reduces the friction loss, resulting in an increased tidal range and reduced phase lag between the ocean and bay. After the tidal range in the estuary reaches the full ocean tidal range, however, further increase in the channel geometry will no longer efficiently increase the tidal range in the estuary; however, it will continue to reduce the phase lag of tides in the bay.

Comparison of tidal measurements from the gauge at Charleston, OR (Station ID 9432780, used as the offshore boundary) and at North Bend (located at approximately RM 11) show that the tidal range is 7% higher at North Bend than that at Charleston. This tidal amplification indicates that Coos Bay is a hydraulically efficient estuary system, frictional effects are not strong, and that inertia influences the hydrodynamics of Coos Bay. Generally, channel widening and deepening has the effect of reducing friction. Because frictional effects are already limited within Coos Bay, channel widening and deepening are not expected to significantly change the effect of friction within the system.

3.2 Preliminary Desktop Analysis

In order to understand the major factors that influence the hydrodynamics of the Coos Bay estuary, a preliminary desktop analysis was performed to assess how physical changes in the channel

dimensions may affect the tidal prism and overall water circulation within the estuary. The analysis was performed for the 2023 PA. The 2023 PA includes modifications to the channel cross-section and therefore may have an effect on the bay hydraulics. Modifications under the 2023 PA increase the average cross-sectional area from the Existing Condition by approximately 14.5%, with 0.1% change in the wetted perimeter. The calculations were performed using the Existing Conditions and the 2023 PA bathymetric profiles at 0.5-mile increments along the Coos Bay from RM 0.5 to 8.0. The cross-section areas and wetted perimeters were computed for the entire width of the bay relative to MSL. The approach was based on the one-dimensional equation of motion that incorporates inlet cross-sectional area, bay surface area, ocean tide amplitude and period, length of the connecting inlet channel, and head loss coefficients. Two solutions of the equation are presented in *Coastal Engineering Manual* (CEM), one developed by Keulegan (1967) and one improved by King (1974). This conceptual approach investigates the effects of both friction and inertia. Both methods show that, under the Existing Conditions, tidal prism is not dampened by friction. The King method, which includes inertia (the Keulegan method only includes friction) predicts tidal amplification of 5% (similar to the 7% amplification observed). Neither method indicates any change to tidal prism under the 2023 PA relative to the Existing Conditions. Details of these desktop analyses are summarized in Attachment D.

3.3 Modeling System

A more detailed hydrodynamic assessment of the estuary was performed using the three-dimensional (3D) MIKE-3 modeling suite, developed by the Danish Hydraulic Institute (DHI 2017). The DHI MIKE-3 Hydrodynamic model uses flexible mesh (FM) with unstructured (triangular) elements. Use of an unstructured grid allows for having varying resolution (higher resolution within the estuary and lower resolution offshore) and higher computational efficiency. Use of the MIKE-3 FM suite for this study was approved by USACE (OIPCB 2016).

3.4 Model Setup

3.4.1 Model Grid and Elevation

The modeling domain encompasses the entire estuary from offshore depths of up to 300 ft to freshwater streams including the South Slough, Coos River, Isthmus Slough, Kentuck & Willanch (K&W) Sloughs, and Haynes Inlet.

The model grid consists of approximately 91,000 unstructured triangular elements size ranging from approximately 15 ft in the estuary to 2,400 ft at the offshore boundary. In the South Slough, the grid's resolution is 50 ft in the main channel and 80 ft in the overbanks. Figure 3-1 shows the modeling domain and Figure 3-2 illustrates the unstructured elements at the South Slough and Haynes Inlet, respectively.

Commented [SJ4]: A-3-6: Please incorporate Port comment into the report itself

Commented [TCF5R4]: Revised to 91,000 for A-3-6.

For vertical mapping, the model uses a hybrid sigma and z-level type with 15 sigma layers from the free surface up to a depth of 49 ft (15 m) referenced to the modeling datum of NAVD88 and 10 z-level layers below that when water depth is deeper than 49 ft NAVD88.

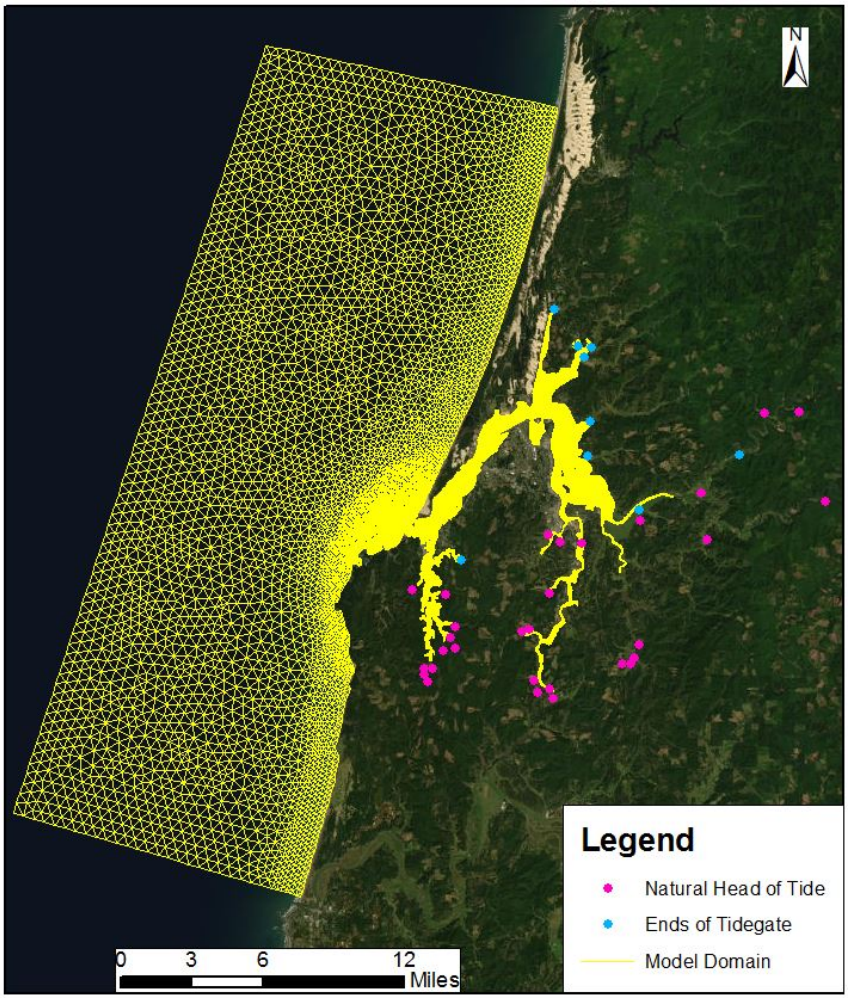

Figure 3-1
Hydrodynamic Modeling Domain and Triangular Elements with Varying Resolutions as well as Historical Locations of Head of Tides

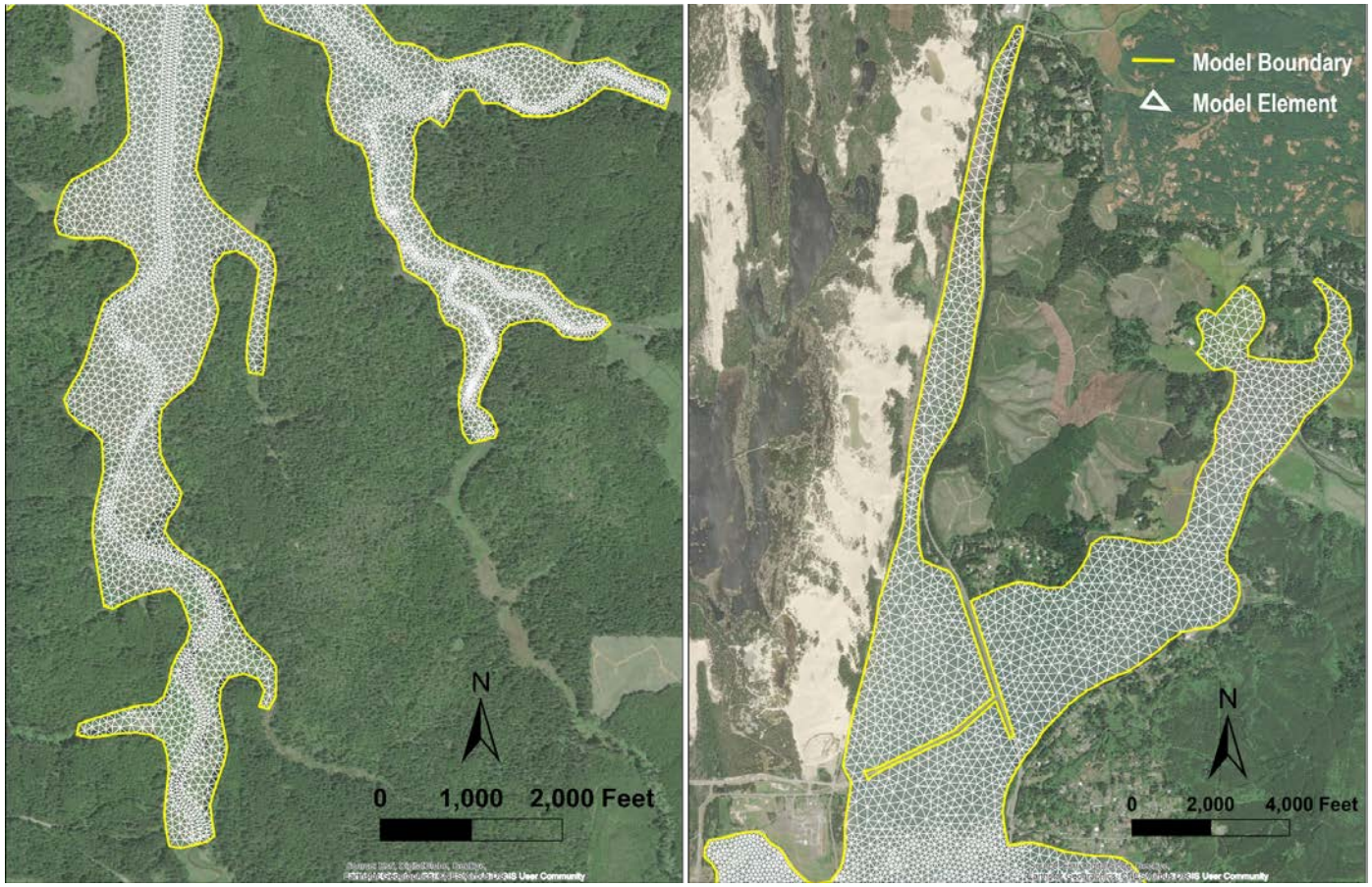

Figure 3-2
Hydrodynamic Modeling Domain and Unstructured Elements at: (a) South Slough; and (b) Haynes Inlet.

Commented [JS6]: A-3-8: Replace with larger maps that can adequately show the intent.

Commented [JS7R6]: Figures enlarged.

To represent the Existing Conditions, elevation data were combined from various datasets listed below with their spatial coverage shown in Figure 3-3. The datasets are listed in the order of increasing priority as datasets overlap in some areas. Details on these datasets are provided in Sub-Appendix 2, *Geophysical Report:*

- Existing Hydrodynamic Model mesh (M&N 2014) for offshore areas;
- USACE (2014) survey data for shallow parts and land coverage of the estuary;
- Existing Hydrodynamic Model mesh (M&N 2014) for regions upstream of RM 12.0;
- OSU's survey (Sutherland & O'Neill 2016) in March 2014 for regions around Haynes Inlet;
- DEA's compilation of digital terrain model (DTM) for shallow part of the navigation channel including, but are not limited to:
  - ✓ 2008 multibeam survey by DEA conducted in deep water located in and close to the Coos Bay navigation channel, inshore of the jetty tips;
  - ✓ 2010 jet-ski surveys by DEA within the Log-spiral Bay (LSB) - this is the only known survey data for the LSB bathymetry;
  - ✓ 2016 multibeam survey by DEA conducted around the jetties and near Guano Rock;
- NOAA (2007) bathymetry survey data for shallow parts of the navigation channel where DEA has no coverage;
- OSU's bathymetry survey (Sutherland & O'Neill 2016) in March 2014 for South Slough - this bathymetry was slightly modified to "channelize" the slough, based on comparison with aerial imagery;
- USACE (2011) Navigation Channel survey for navigation channel from Entrance to Coos River; and
- At the North Jetty, the design elevations from the Coos Bay North Jetty Repair Major Maintenance project (USACE 2021) were incorporated.

All datasets were converted to reference geographic coordinates (UTM-10 North). Vertical reference was converted to NAVD88 in meters using the NOAA VDatum software, which can convert data from different horizontal/vertical references into a common system, and account spatial variance.

The 2011 USACE Navigation Channel survey was only used for calibration and validation runs since it best represents the existing bathymetry during the periods of calibration and validation data measurements. For production runs, bathymetry data covering navigation channel was replaced by channel depths associated with the 2023 PA channel.

The survey coverage of the additional and more recent bathymetry data (Sutherland and O'Neil 2016) was reviewed and compared against high-resolution aerial images taken at low tide in shallow tributaries. Model elevation was updated with the more recent bathymetry data (Sutherland and O'Neil 2016) where more recent data provided a better spatial resolution/better representation of the tributaries (see Figure 3-4 for South Slough as an example). However for the specific areas mentioned and observation points (LUB-4, UUB-2, UUB-3, CR-4 in Figure 4-18), review of the additional bathymetry data (Sutherland and O'Neil 2016) indicated that the survey did not have adequate coverage and resolution to improve the model elevation.

Commented [JS8]: A-3-6 Incorporate port comment into the report itself.

Commented [JS9R8]: Moved from Section 4 footnote to this paragraph.

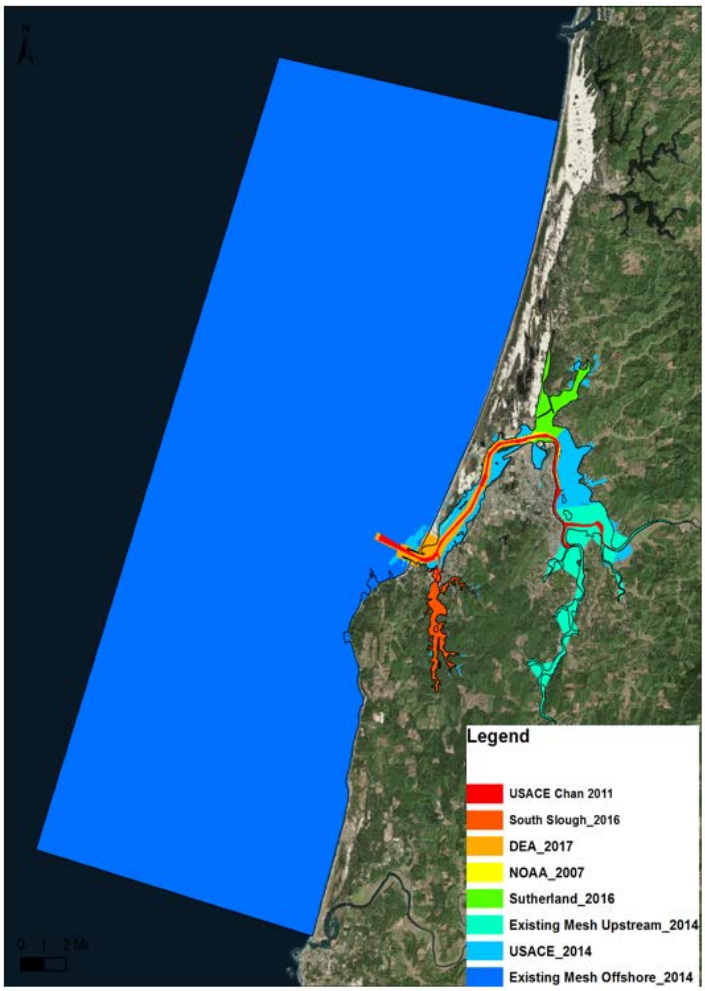

Figure 3-3
Coverage of Various Elevation Datasets

Commented [JS10]: A-3-17: Add port comment to report itself

Commented [JS11R10]: Added Port comment as a paragraph above the figure.

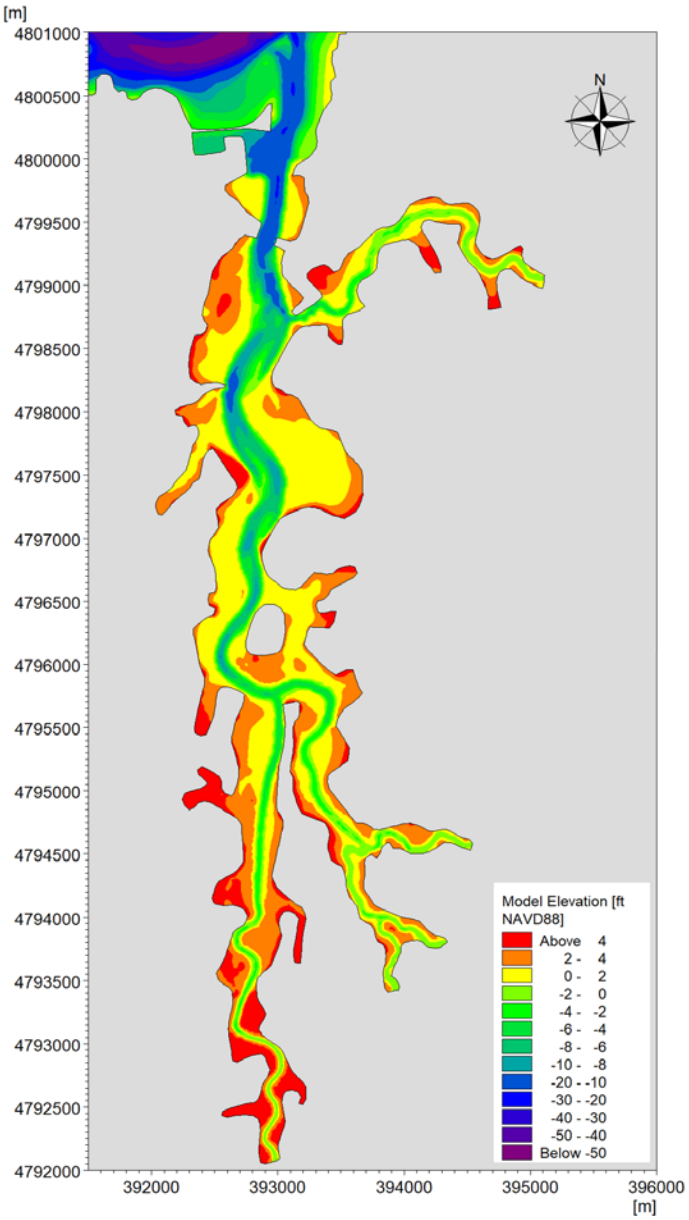

Figure 3-4
Model Elevation Zoom-in View for South Slough

Commented [TCF12]:

Commented [TCF13R12]: Figure revised. Moved from Section 4.

Two simulation scenarios were conducted in the study: the Existing Conditions and the 2023 PA. Table 3-1 lists the channel configurations and design features considered in each scenario. The model elevation and design features are shown in Figure 3-5 and Figure 3-6. A uniform advanced maintenance dredging (AMD) value of 1 ft was included in both scenarios to construct the model elevation for RM>1.0. It should be noted that the proposed AMD for the 2023 PA offshore of RM 1.0 is 6 ft. To represent typical conditions, an AMD value of 3 ft was included in development of the model elevation for the 2023 PA. The offshore area (RM<1.0) is the deepest stretch of the channel and it is not expected that increasing the depth to the full AMD (an increase of ~5%) would influence model results. A channel depth of 37 ft MLLW was used in the navigation channel from RM 9.0 to RM 15.0 for production runs to account for planned future dredging.

The side slopes used for the 2023 PA channel are based on *Constructed Condition* slopes from project drawings. Modeling for the 2023 PA scenario was performed for construction slopes (as was done for the 2017 PA) since these slopes provide the most conservative results with respect to currents and sediment transport, especially given the uncertainty associated with the future equilibrium side slopes. It also shows the immediate potential environmental impacts. These slopes are also summarized in Sub-Appendix 6 - *Channel Side Slope Analysis*.

Commented [JS14]: USACE 10462082: Use of construction slopes vs. equilibrium slopes.

Commented [JS15R14]: Explanation added to text

Table 3-1
Design Features Considered in Each Case

Case	Authorized Channel Upstream of RM 1.0		Included AMD (ft)		USACE North Jetty Repair	Container Turning Basin	Roseburg Turning Basin
	Elev (ft, MLLW)	Width (ft)	< RM 1.0	> RM 1.0			
Existing Conditions	-37	300	5	1	Yes	No	No
2023 PA	-45	450	3	1	Yes	Yes	Yes

In addition, the five pile dike structures present on the outer (northwestern) bank in the Jarvis Turn (see Figure 2-24) were included in the MIKE-3 HD model, because these structures would impact the hydrodynamics in the vicinity of Jarvis Turn by increasing flow resistance (e.g. current induced drag force) in the water column.

The pile dike structures were parameterized in the model to capture the increasing flow resistance (e.g. current induced drag force) in the water column. The model input included the pile location, type, dimension, and a streamline factor which takes into account the increased flow velocity due to the blocking of piles. According to the DHI User Manual (DHI 2017), the effective drag force is calculated using the following equation:

Commented [TCF16]: PDT A-3-1: Please change sentence "The pile dike structures were modeled as individual piles to capture the increasing flow resistance
(e.g. current induced drag force) in the water column." to "The pile dike structures were parameterized in the model to capture the increasing flow resistance (e.g. current induced drag force) in the water column." The model mesh does not appear to support the differentiation of individual piles.

Commented [TCF17R16]: Revised as suggested. Now moved to Section 3.4.1.

$$F = \frac{1}{2}\rho_w \gamma C_D A_e V^2$$

where ρ_w is the density of water, γ is the streamline factor, C_D is the drag coefficient, A_e is the effective area of pile exposed to current, and V is the current speed.

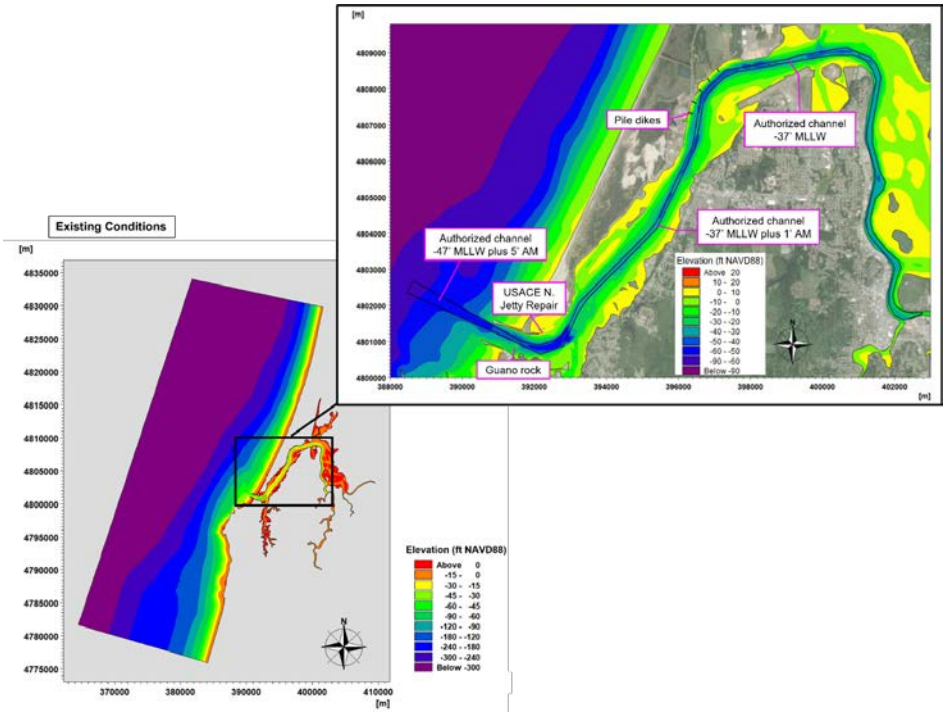

Figure 3-5
Model Elevation and Features for Existing Conditions

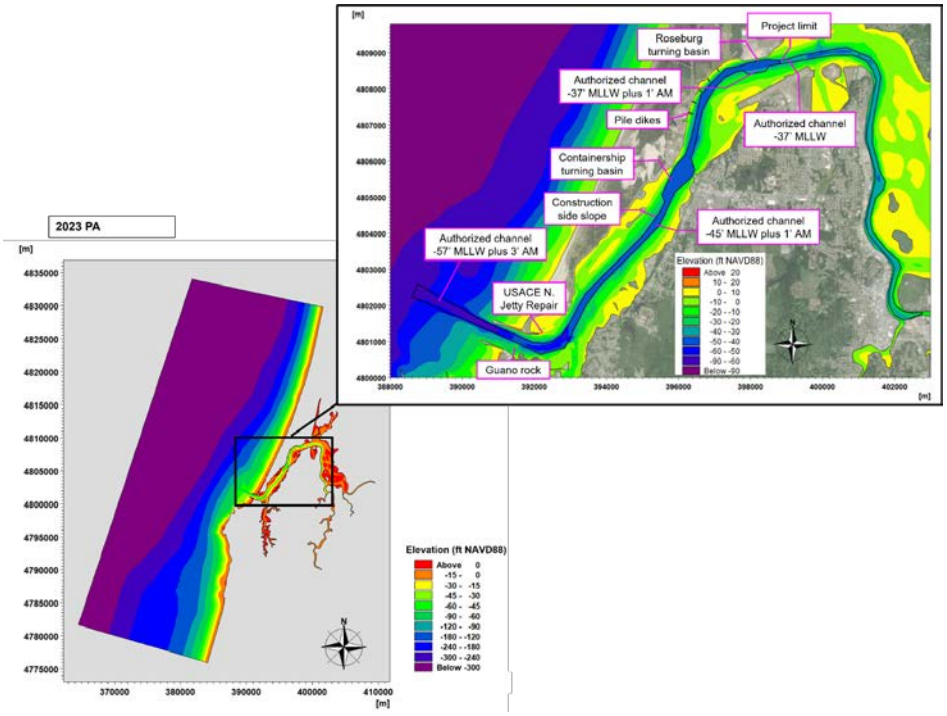

Figure 3-6
Model Elevation and Features for 2023 PA

3.4.2 Boundary Conditions

Hydrodynamic models compute water surface elevations and current velocities over an area of modeled water body. The water levels and currents respond to changes in water levels, bathymetry, roughness and inflows or outflows at the model boundaries. These variations are referred to as boundary conditions. These conditions may include ocean tides and currents, and freshwater inflows from surrounding rivers. A summary of boundary conditions for the Coos Bay model are presented in Table 3-2.

Table 3-2
Boundary Conditions for Hydrodynamic Modeling Runs

	Input	Source	Data & Period
Calibration Runs	Tides (Offshore boundary conditions)	Oregon State University (OSU) tidal database global solution, TPXO8 1/6 resolution with adjustments based on residuals at NOAA Charleston station	Hourly tidal levels and flow velocities along three offshore boundaries for 3/11/2010 to 4/18/2010
	Freshwater runoff (Upstream boundary conditions)	Freshwater discharge of Coos River: Based on measured daily discharge provided by the CWA Freshwater discharge of other (much smaller) tributaries: In lieu of measured discharge, daily discharge was estimated using rainfall-runoff analysis using monthly rainfall data	Daily freshwater inflow for 3/11/2010 to 4/18/2010 for Coos River and other tributaries shown in Figure 3-7
Production Runs	Tides (Offshore boundary conditions)	Same as calibration runs	Hourly tidal levels and flow velocities along three offshore boundaries for 12/21/2011 to 1/19/2012
	Freshwater runoff (Upstream boundary conditions)	Same as calibration runs	Daily freshwater inflow for 12/21/2011 to 1/19/2012

The offshore boundary conditions, both water levels and currents, were extracted from the OSU Tidal Data Inversion, specifically the TPXO8 global tidal solution with a resolution of 1/6° (Egbert & Erofeeva 2002). The OSU global model of astronomical tides was developed assimilating the TOPEX/Poseidon global altimeter data (satellite-measured ocean surface). Additionally, meteorological tides, which are changes in expected astronomical tides caused by local meteorological conditions, were determined from the Charleston gauge and superimposed at the offshore boundaries. Each offshore boundary was divided into 11 segments so that the phase difference was included.

The upstream freshwater boundary conditions included in the 3D hydrodynamic (3D HD) model are labeled in Figure 3-7. These include the Coos River, the Haynes Inlet, the Kentuck & Willanch (K&W) Sloughs, the Isthmus Slough, and the South Slough.

Coos River daily freshwater discharge for water years (WY) from 2003 through 2017, as well as estimated extreme value statistics are shown in Figure 2-3. The hydrodynamic model input boundary condition in terms of freshwater discharge for Coos River was based on daily discharge values for WY 2012 with a peak daily discharge corresponding to a 2-yr return period event.

For other tributaries, in lieu of daily freshwater inflow measurements, the runoff was estimated using a rainfall-runoff analysis based on average monthly precipitation (Black & Veatch 2006). The equation multiplies the area of the watershed by the precipitation and a scale factor based on land type. For these assessments, a land type corresponding to undeveloped wilderness was selected. This method was selected because runoff data was not available directly at these tributaries. Therefore, the model input boundary condition for freshwater tributaries other than Coos River was based on monthly-averaged estimations of discharge interpolated into a daily time series, see Figure 3-8 for WY 2012. It should be noted that discharge values from these tributaries are much (approximately one order of magnitude) smaller than typical winter and spring discharges from the Coos River; therefore, they do not drive the dynamics of the estuary and this is an acceptable approximation. The tributaries not included in the model contribute even less freshwater input.

For the hydrodynamic modeling, the daily discharge data for the South Slough was combined as one point source and this approach was considered reasonable. For the salinity mixing, a detailed analysis by delineating the sub-watersheds within South Slough was conducted to validate the three salinity stations in the South Slough watershed. The delineation of South Slough watershed is provided in Section 4.2.2.

There are a few tidal gates in the Coos Bay estuary sloughs, but not many of these structures are functional. Accordingly, there is continuous exchange between the Coos Bay estuary and the associated tributaries. If tide gates function properly, they can prevent intrusion of saltwater into the estuary and allow drainage of the tributary into the estuary at low tides. The tide gates typically do not change the total volume of freshwater that enters the estuary, but change the timing of the inflows (freshwater inflows can only occur at low tides). Tidal gates were not included in the model setup as a conservative assumption.

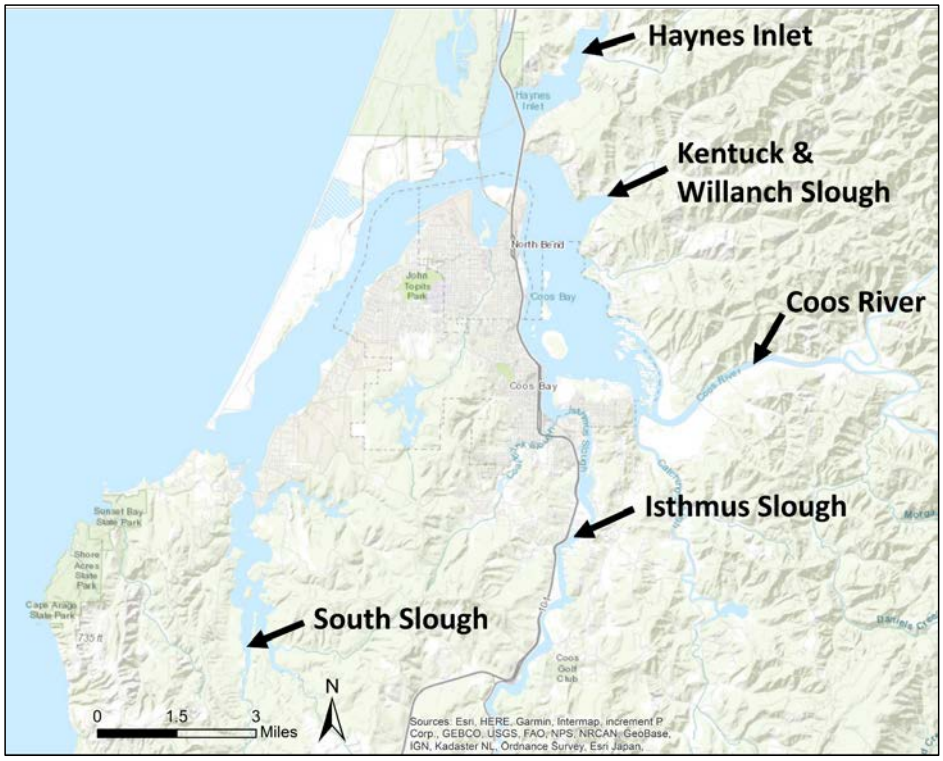

Figure 3-7
Upstream Freshwater Open Boundaries

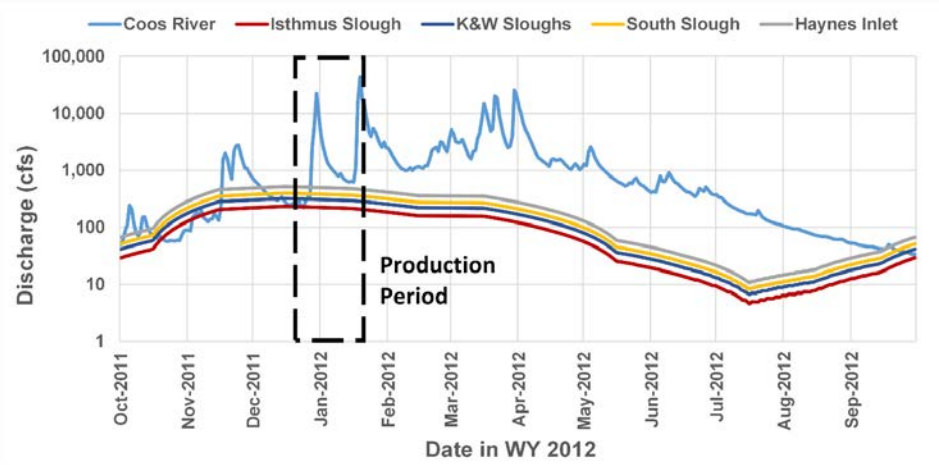

Figure 3-8
Estimated Daily Freshwater Discharge for Isthmus Slough, Kentuck & Willanch (K&W) Sloughs, South Slough, and Haynes Inlet as well as Measured Daily Discharge for Coos River for WY 2012

3.4.3 Model Assumptions and Input Parameters

Table 3-3 lists the primary parameters used in the 3D HD model. All parameters were determined through calibration, as opposed to direct measurement, and following the guidelines provided by the DHI User Manual. Manning's *n* quantifies bottom roughness and accounts for energy loss due to friction. Eddy viscosity quantifies turbulence and determines the rate at which momentum and constituents spread. The Smagorinsky coefficient of horizontal eddy viscosity ranges typically between 0 and 1, with 0 meaning no eddy viscosity. Default values were used for all empirical constants in the vertical k-epsilon turbulence formulation.

Table 3-3
Input Parameters for Hydrodynamic and Turbulence Modules

Parameter	Value	Comment
Roughness Height	A constant of 0.05 m	Typical range from 0.01 to 0.30 m
Horizontal Eddy Viscosity (Smagorinsky coefficient)	A constant of 0.24	Typical range from 0 to 1. Default value is 0.28
Vertical Eddy Viscosity	K-Epsilon formulation	Selected from four types: No eddy; Constant eddy formulation; Log law formulation; K-Epsilon formulation
K-Epsilon Turbulence	All constants	All default values

3.5 Model Calibration

The hydrodynamic model for the Existing Conditions was calibrated against observations of water levels and currents. Field measurements used for calibration of the model and metrics for goodness of fit are described in the following subsections.

3.5.1 Measured Water Levels and Currents for Model Calibration

Available water level and current measurements were compiled for the 3D HD model calibration. Location of measuring stations and transects in Coos Bay estuary is shown in Figure 3-9. Below is a list of data used for model calibration:

- NOAA has been recording water levels at Charleston, Oregon (Section 2.1.3) since 1970 and analyzed harmonic tidal constituents. This is the only active tide gauge in the Coos Bay estuary.
- DEA used Teledyne RD Instruments 600 kHz Workhorse bottom-mounted Acoustic Doppler Current Profilers (ADCP) and measured water level elevations and currents at three locations from March 28 to April 23, 2010 (OIPCB 2010). Two of these locations are inside the estuary, while the third is offshore. Each bin recorded horizontal currents (easting and northing components) within a depth of 1.15 ft (0.35 m).
- DEA also used vessel-mounted ADCP and measured velocity from bank-to-bank along three transects during ebb and flood tides (OIPCB 2010). Data is available on 3/18/2010 and 3/19/2010.

Table 3-4 includes specific calibration events.

Table 3-4
Calibration Events

Calibration Tests	Duration	Observation Data Used
Tested different schemes to solve shallow water equations (high scheme or low scheme).	3/27/2010 – 3/31/2010	1. Measured WLs at Charleston. 2. Measured WLs at ADCP M1. 3. Measured U, V velocity at ADCP M1. 4. Reported tidal constituents at Charleston. 5. Depth-averaged currents across 3 transects. 6. Current speed at various vertical layers.
Tested with winds from North Bend (KOTH) airport.		
Tested bed resistance.		
Tested vertical layer resolutions.		
Tested various vertical eddy options.		
Tested on wave radiation stress.	3/11/2010 – 4/18/2010	
Full period, with individual piles for pile dikes.		

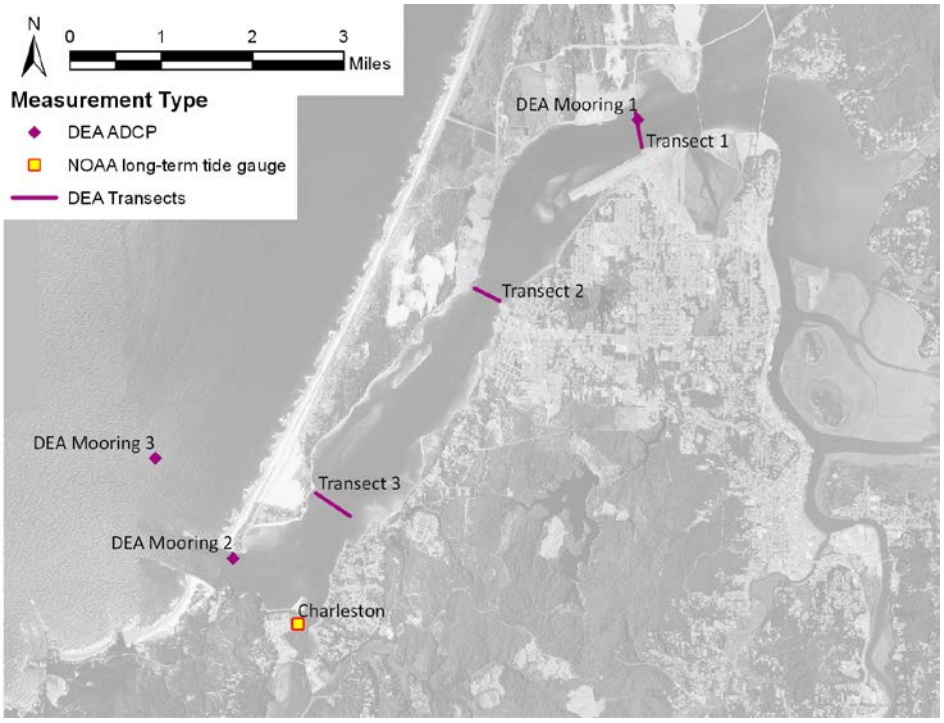

Figure 3-9
Location of Measuring Stations and Transects in the Project Vicinity

There are no specific standards for assessing goodness of fit between model predictions and measurements. The following statistical parameters, in addition to phase lag (ΔT), were used to evaluate and maximize the goodness of fit between model predictions and measurements by changing model input parameters.

- Root-Mean-Squared (RMS) Error: $\varepsilon_{RMS} = \sqrt{\overline{(x-y)^2}}$
- Mean Absolute Error (MAE): $MAE = \overline{|x-y|}$
- Index of Agreement (d): $d = 1 - \frac{\overline{(x-y)^2}}{\left(\overline{|x-\bar{x}|} + \overline{|y-\bar{x}|}\right)^2}$, $0 \le d \le 1$

Where x and y represent the calculated (model) and the measured data, respectively, and the $\bar{}$ symbol represents the mean value of a parameter.

RMS error is one of the most commonly used metrics to evaluate the accuracy of a fit. When a variable can be represented as a sum of its true value plus noise, RMS error represents an estimate of standard deviation of the noise (which assumes that the noise is normally distributed). In this

application, RMS error only represents the deviation between measurements and computed values, which is not necessarily the same as model accuracy. Firstly, measured quantities themselves can have error or noise within the measurements, and the RMS error is a combination of this noise plus the model error. Second, the measured and modeled quantities are dynamic and changing in time. A phase lag between the measured and modeled data can have an RMS error, even if the model accurately predicts the behavior of the system. This is evident from Figure 3-10, where the maximum residual corresponds to a time before the peaks and valleys of the data. Ultimately, using RMS error as a blanket statement for model accuracy is misleading.

Still, RMS error is often interpreted as model accuracy; a common interpretation is that it represents standard deviation around measurements. This means that the model results are within plus-or-minus the measured value 68% of the time. A RMS error that is higher than a difference between project conditions does not dismiss the difference between project conditions.

Comparison of model results against observations of hourly water levels at the NOAA Charleston tide gauge and the DEA ADCP1 location is shown in Figure 3-10. The period of comparison is between March 28 and April 18, 2010. The RMS errors for water levels is 0.4 ft at NOAA Charleston station and 0.5 ft at DEA ADCP1 location. To put these numbers in perspective, these RMS errors represent a maximum 6 percent of the great diurnal range (e.g., 7 ft at Charleston). In addition, the index of agreement of 0.99 was obtained at both locations.

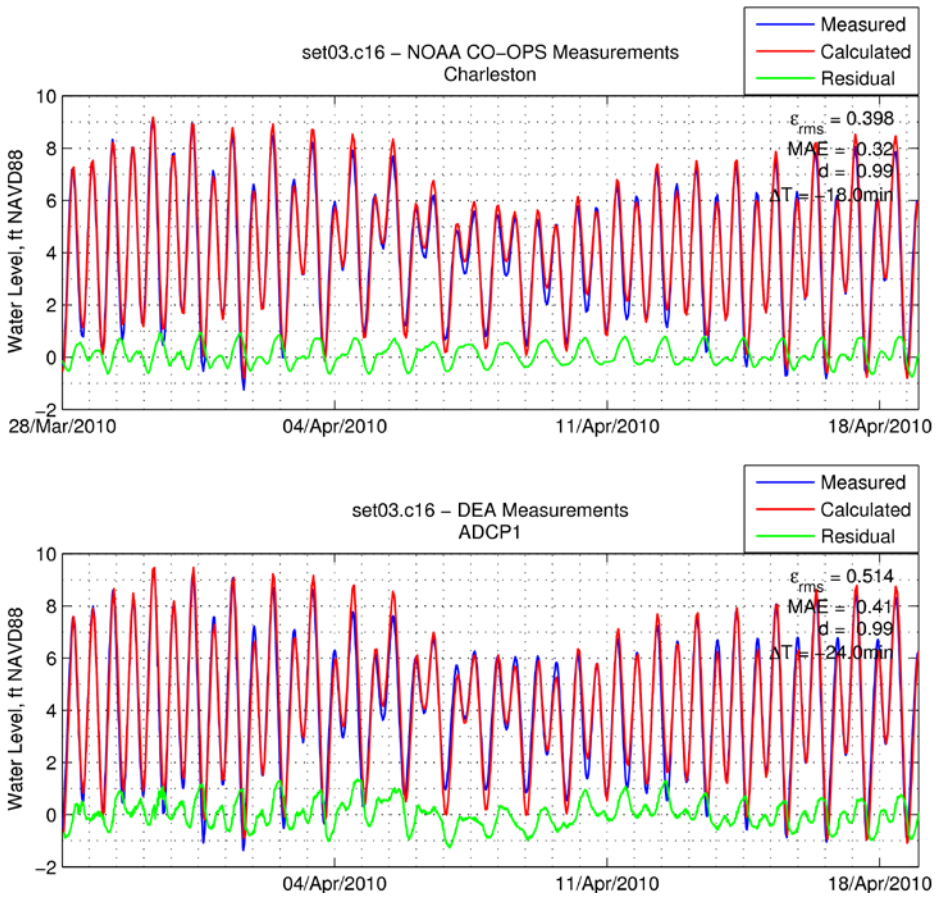

Figure 3-10
Comparison of Water Levels against Observations at: (Top) NOAA Charleston Station and (Bottom) DEA ADCP1 Location

Table 3-5 provides tidal datum comparison between the 3D HD model outputs (calculated) and recorded at the NOAA tide gauges and the DEA ADCP1 location for the same specified period. The model outputs are in good agreement with the measurements and capture the increase in tidal range moving up the estuary. The model-predicted great diurnal ranges are slightly higher than the recorded, while the mean tide ranges are slightly lower than the recorded. The differences in general are all less than 0.2 ft (about 3 percent relative to the mean tidal range) and can mainly be attributed to the uncertainty of computation of tidal datums based on results from a short-term simulation (22 days). Figure 3-11 shows a comparison of calculated and measured tidal constituents at the NOAA stations at Charleston, Sitka Dock, North Bend, and Isthmus Slough. Figure 3-12 shows a comparison of tidal constituents at the DEA ADCP1 location. It can be seen

that the major tidal constituents agree with the NOAA published values and computed from DEA measurements. The results indicate reasonable representation[3] of tidal water levels in the model.

Table 3-5
Comparison of Tidal Datums inside Coos Bay Estuary

Location	Charleston	Charleston	Sitka Dock	DEA ADCP1	North Bend	Isthmus Slough
NOAA CO-OPS ID	9432780	9432780	9432879	-	9432895	9432796
Period of Records Analyzed	1/1/2011 – 12/30/2011	3/28/2010 - 4/18/2010	9/1/1982 - 9/30/1982	3/28/2010 - 4/18/2010	9/1/1982 - 9/30/1982	9/1/1982 - 9/30/1982
Tidal Datums (ft, MSL)	Measured	Measured/ Calculated	Measured/ Calculated	Measured/ Calculated	Measured/ Calculated	Measured / Calculated
MHHW	3.52	3.25/3.35	3.38/3.38	3.54/3.57	3.58/3.74	3.67/3.87
MHW	2.82	2.79/2.73	2.79/2.76	2.95/2.94	2.99/3.09	3.07/3.18
MTL	0.02	0.03/0.06	-0.03/0.04	0.00/0.04	-0.13/0.03	-0.16/0.07
MSL	0.00	0.00/0.00	0.00/0.00	0.00/0.00	0.00/0.00	0.00/0.00
MLW	-2.77	-2.69/-2.61	-2.85/-2.67	-2.92/-2.86	-3.22/-3.03	-3.38/-3.04
MLLW	-4.03	-3.74/-3.82	-3.84/-3.88	-4.04 /-4.08	-4.20/-4.27	-4.39/-4.29
Mean Range of Tide (ft)	5.59	5.48/5.34	5.64/5.43	5.87/5.80	6.17/6.12	6.44/6.22
Great Diurnal Range (ft)	7.55	7.02/7.17	7.22/7.26	7.58/7.65	7.78/8.01	8.06/8.16

[3] Similar and recent Environmental Impact Statements (EIS) conducted by USACE/Engineer Research and Development Center (ERDC) were compiled to identify range of model-measurement agreement that is accepted and approved by USACE.

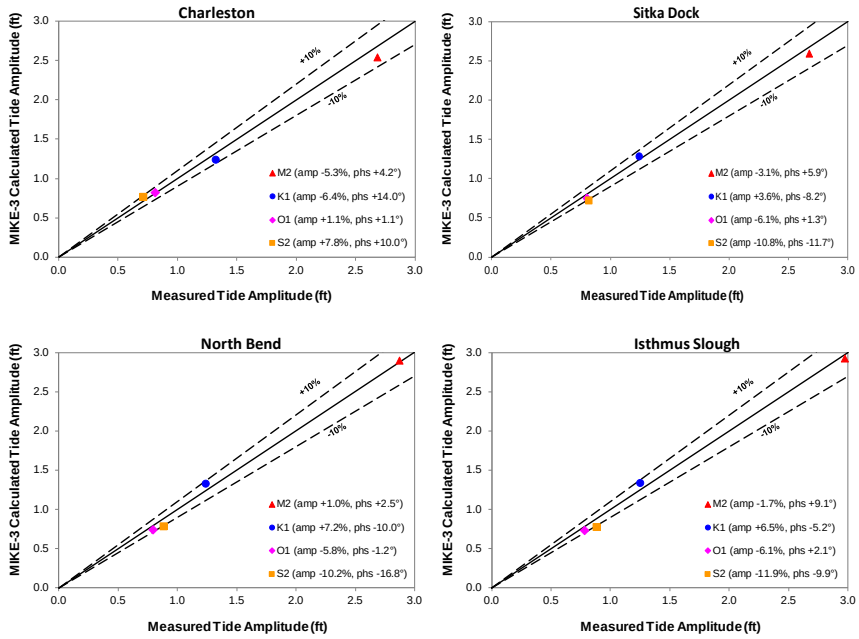

Figure 3-11
Comparison of Tidal Constituents at NOAA Stations

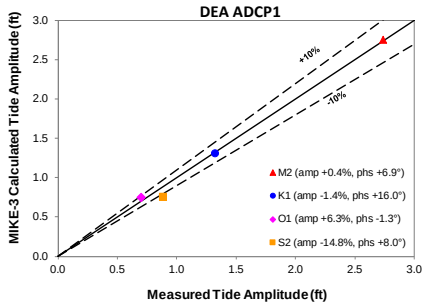

Figure 3-12
Comparison of Tidal Constituents at DEA Station ADCP1

DEA used vessel-mounted ADCPs and measured velocity from bank-to-bank along three transects during ebb and flood tides (OIPCB 2010). Table 3-6 provides the log of survey performed between March 18 and March 19, 2010.

Figure 3-13 through Figure 3-15 show the current speed comparison along the three DEA transects. As it can be seen, the measured currents show some variability along the transects. Ebb currents are usually higher than flood currents over the banks, while flood currents are higher than ebb currents in the deeper channel. The model replicates the same patterns. However, the model results are smoother along the transect lines compared to the measurements, which can be attributed to the limited representation of bathymetric features in the model compared to reality due to grid resolution. In general, the 3D HD model under-estimates the ebb currents over the shallower areas and over-estimates in the channel. Similarly, the model under-estimates flood currents in the channel and over-estimates flood currents over the banks. The total discharges during flood and ebb match well, which is important for modeling of salinity propagation.

Table 3-6
Log of DEA ADCP Transect Survey Periods

DEA Transect	Tide	Start Date/Time (LDT)	End Date/Time (LDT)
1	Flood	3/18/2010 11:41	3/18/2010 12:05
	Ebb	3/18/2010 16:49	3/18/2010 17:05
2	Flood	3/18/2010 12:21	3/18/2010 12:36
	Ebb	3/18/2010 17:35	3/18/2010 18:05
3	Flood	3/19/2010 12:14	3/19/2010 12:48
	Ebb	3/19/2010 18:32	3/19/2010 18:55

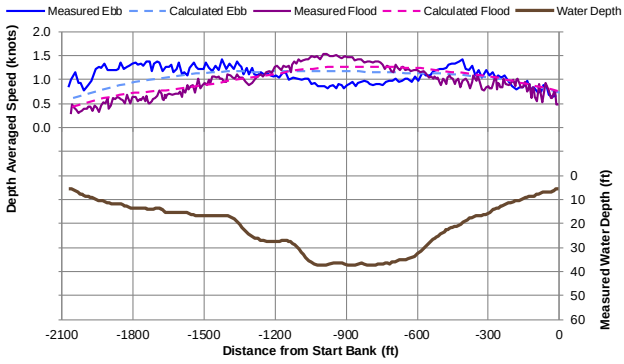

Figure 3-13
Ebb and Flood Current Speed along DEA Transect 1 (Looking Downstream)

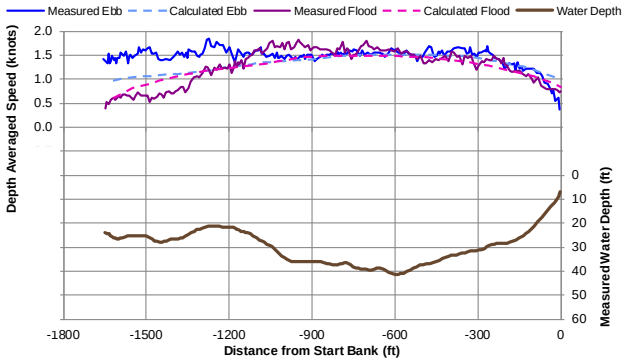

Figure 3-14
Ebb and Flood Current Speed along DEA Transect 2 (Looking Downstream)

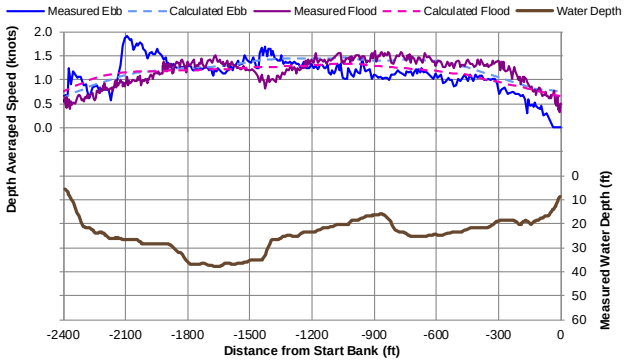

Figure 3-15
Ebb and Flood Current Speed along DEA Transect 3 (Looking Downstream)

DEA deployed bottom-mounted ADCPs and measured tidal currents from March 28 to April 23, 2010 (OIPCB 2010). Figure 3-16 illustrates selected bins in the water column at the ADCP1 location. Current velocities were collected and analyzed within each bin. The yellow lines represent MHHW and MLLW. Figure 3-17 shows longitudinal (along the channel) velocity component comparison between the 3D HD model outputs (calculated) and the DEA ADCP1 measurements (measured) at selected bins. The results show that the model slightly under-predicts currents along the channel at the location of DEA ADCP1 station (about 0.2-0.3 knots or about 10% of the range). A portion of the error can be attributed to the unstable flow patterns at the measurement location due to the ADCP1 location in Jarvis Turn, where local eddies are not replicated by the model. There is also variability in current predictions along the channel transects, as seen in Figure 3-13 through Figure 3-15, when currents can be over or under-predicted depending on a small error in the location of the measured current.

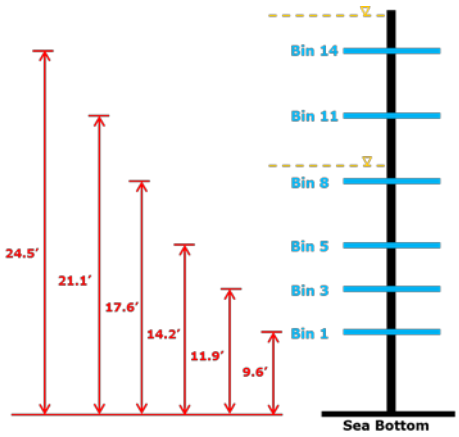

Figure 3-16
Location of Selected DEA ADCP1 Bins in the Water Column

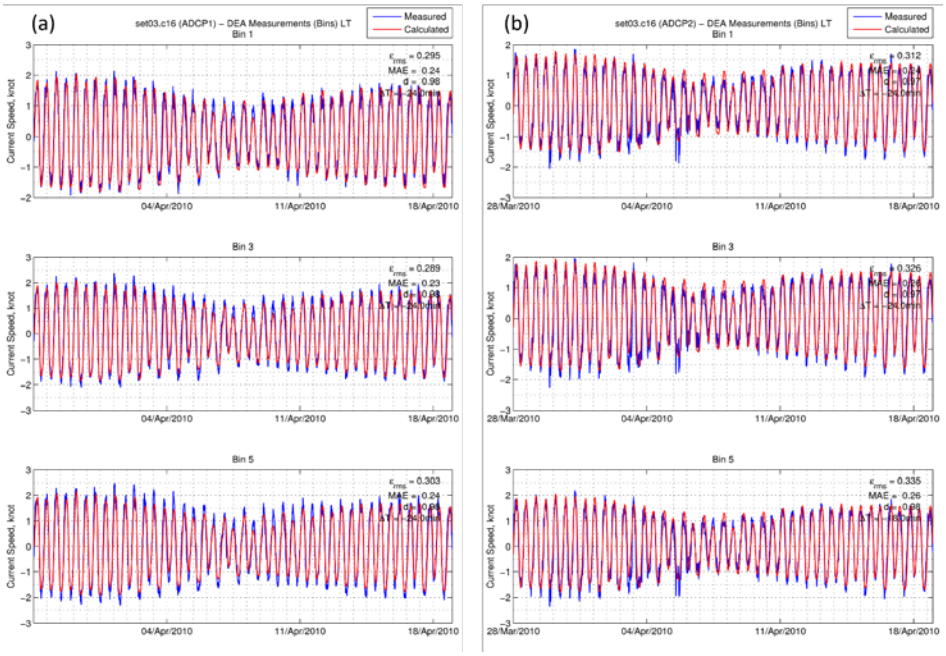

Figure 3-17
Comparison of Longitudinal Component of Current Speed at Selected Bins (No. 1, 3, and 5) for: (a) ADCP1 and (b) ADCP2.

3.5.2 Model Performance against Similar Projects

There are no specific codes or standards for assessing performance of numerical models in terms of simulation of observations. To assess the performance of this modeling study in representing the Existing Conditions and the 2023 PA, similar and recent studies conducted by ERDC or approved by USACE were compiled and reviewed. A list of these studies and metrics used to report and quantify goodness of fit for water levels and currents is listed in Table 3-7 and Table 3-8, respectively. The model's performance metrics are listed in the last row of these two tables. It can be observed that this study is consistent with recent and similar modeling studies conducted by ERDC or approved by USACE in terms of model performance.

Table 3-7
Descriptors and Metrics for Reporting Goodness of Fit for Hydrodynamic Modeling Results, in Terms of Water Levels, against Observations in Similar and Recent Modeling Studies Conducted by ERDC or Approved by USACE for Channel Modification Projects as well as This Project

Project (Source)	Visual Inspection	Max. Diff	RMSE	IOA	Phase Shift	Sensitivity Analysis	Description of Model Performance
Channel Deepening in Thimble Shoals (Zhang et al. 2017)	✓	1.3 ft*	x**	0.92 – 0.95	6°	x	"Sufficient Skill"
Seattle Harbor Deepening EIS (ERDC 2016)	✓	< 0.1 ft*	x	x	x	x	"Excellent comparison"
Redwood City Harbor Navigation Improvement EIS (HydroPlan 2015)	✓	0.2 ft*	x	0.99	x	x	"Very accurate"
Houston-Galveston Navigation Channel (ERDC 2014)	✓	0.3 ft*	3 - 4%	0.99	x	x	"Good agreement"
Matagorda Ship Channel Study (ERDC 2013)	✓	0.7 ft*	x	x	x	x	x
Savannah Harbor Expansion Project (Tetra Tech 2011)	✓	0.3 ft*	x	x	x	x	x
Grays Harbor Navigation Improvement EIS (ERDC 2010)	✓	3.0 ft*	x	x	x	x	"Very good"
This Study	✓	1.0 ft*	0.4 - 0.5 ft	0.99	8°	x	"In agreement"

* indicates that the value was not listed in the report and is based on interpretation of results

** symbol 'x' indicates that this parameter was not estimated/reported to quantify model performance

Table 3-8
Descriptors and Metrics for Reporting Goodness of Fit for Hydrodynamic Modeling Results, in Terms of Currents, against Observations in Similar Studies Conducted by ERDC or Approved by USACE for Channel Modification Projects as well as This Project

Project (Source)	Visual Inspection	Max. Diff	RMSE	IOA	Phase Shift	Sensitivity Analysis	Description of Model Performance
Channel Deepening in Thimble Shoals (Zhang et al. 2017)	✓	1 ft/s*	0.3 ft/s	> 0.7	x**	x	"Sufficient Skill"
Seattle Harbor Deepening EIS (ERDC 2016)	x	x	x	x	x	x	x
Redwood City Harbor Navigation Improvement EIS (HydroPlan 2015)	x	x	x	x	x	x	x
Houston-Galveston Navigation Channel (ERDC 2014)	✓	1.5 ft/s*	0.7 - 39%	x	x	x	"Good agreement"
Matagorda Ship Channel Study (ERDC 2013)	x	x	x	x	x	x	x
Savannah Harbor Expansion Project (Tetra Tech 2011)	✓	0.01 ft/s*	x	x	x	x	x
Grays Harbor Navigation Improvement EIS (ERDC 2010)	✓	3.0 ft/s*	x	x	x	x	"Reasonable"
This Study	✓	1.5 ft/s*	0.5 - 0.8 ft/s	0.87 - 0.98	x	x	"In agreement"

* indicates that the value was not listed in the report and is based on interpretation of results

** symbol 'x' indicates that this parameter was not estimated/reported to quantify model performance

3.6 Model Results

To assess possible changes as a result of the proposed navigation channel improvements, the general approach in this study was to explicitly model both simulation scenarios (the Existing Conditions and the 2023 PA) and to compare the results. The model inputs and constants for both scenarios were the same and the only difference was the model bathymetry for each scenario. Location of observation points used for reporting the HD model results is shown in Figure 3-18. The 3D HD model was used to simulate a 30-day period for a high-runoff winter period from December 21, 2011 to January 19, 2012.

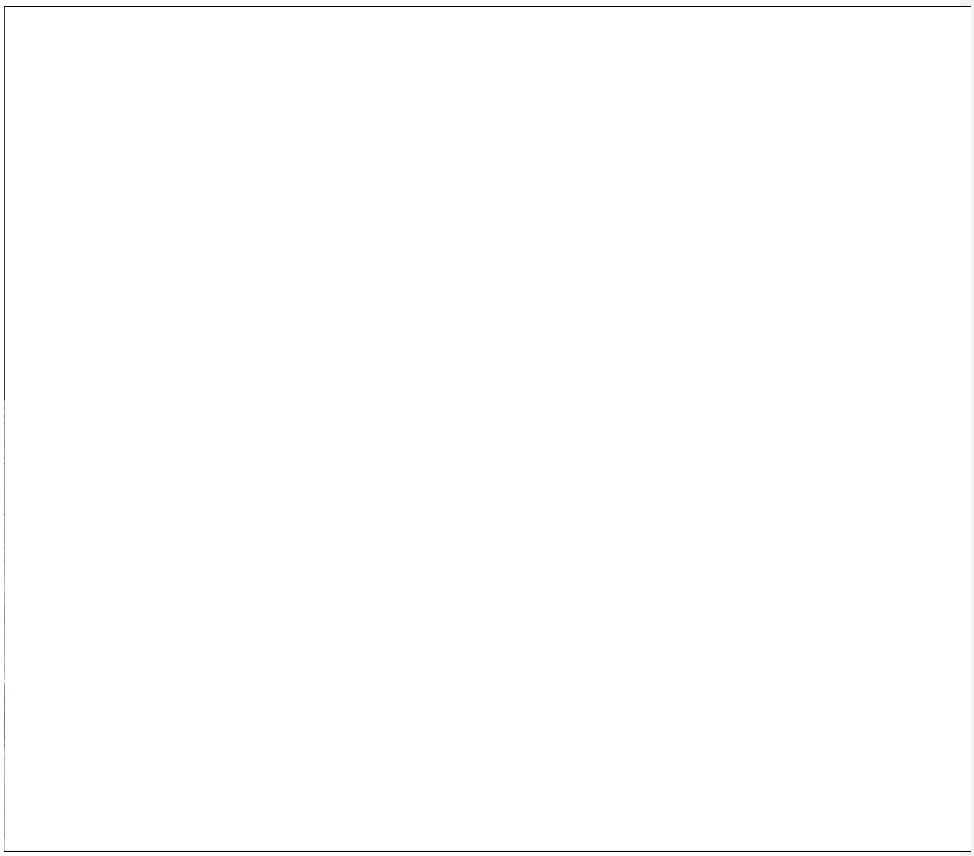

Figure 3-18
Locations Observation Points for Reporting HD Model Results

3.6.1 Water Levels

Model results in terms of time history of water levels were extracted at the observation points to calculate the mean tidal range (e.g., the difference in height between mean high water and mean

low water). Results of mean tidal range for both scenarios are listed in Table 3-9 and show that the mean tidal range generally increases starting at the mouth and moving upstream. The 2023 PA channel results in a slight increase (less than 0.1 ft) of mean tidal range throughout the estuary. In the South Slough, the increase in mean tidal range does not exceed 0.04 ft. In the Isthmus Slough, the Coos River, and the Haynes Inlet, the increase in mean tidal range does not exceed 0.06 ft. The maximum increase occurs in the FNC, where the mean tidal range increases by 0.09 ft (corresponding to a 1.6% increase in mean tidal range). To put this estimated change in perspective, the average mean tidal range in Coos Bay is approximately 5.7 ft.

As discussed in Section 3.1, the Coos Bay estuary is a hydraulically efficient estuary system, resulting in little change in upstream tide range due to an increase in the FNC channel dimensions.

Table 3-9
Mean Tidal Range under Existing Conditions and 2023 PA

Observation Point	Easting (OR State Plane South, ft)	Northing (OR State Plane South, ft)	RM / Slough	Mean Tidal Range in feet		
				Existing Conditions	2023 PA	2023 PA-Existing
1	3891988.6	643165.5	RM -1	5.51	5.51	0.00
2	3896627.9	640644.5	RM 0	5.49	5.49	0.00
3	3901267.1	638123.5	RM 1	5.39	5.44	0.05
4	3905474.5	639329.1	RM 2	5.42	5.45	0.03
5	3908566.0	643505.8	RM 3	5.45	5.51	0.06
6	3912387.2	647149.5	RM 4	5.51	5.58	0.07
7	3915256.9	651507.2	RM 5	5.56	5.64	0.08
8	3917486.8	656262.6	RM 6	5.62	5.71	0.09
9	3919189.8	661074.1	RM 7	5.69	5.76	0.07
10	3923954.0	662778.7	RM 8	5.80	5.86	0.06
11	3929182.0	663518.1	RM 9	5.95	6.00	0.05
12	3933959.7	662418.4	RM 10	6.09	6.13	0.04
13	3933508.2	657299.8	RM 11	6.19	6.23	0.04
14	3934003.3	652146.2	RM 12	6.26	6.31	0.05
15	3933308.9	647075.3	RM 13	6.31	6.37	0.06
16	3935153.5	642686.2	RM 14	6.35	6.41	0.06

Observation Point	Easting (OR State Plane South, ft)	Northing (OR State Plane South, ft)	RM / Slough	Mean Tidal Range in feet		
				Existing Conditions	2023 PA	2023 PA-Existing
17	3937460.3	639777.8	RM 15	6.39	6.46	0.07
18	3906315.9	636379.6	South	5.43	5.46	0.03
19	3905317.9	633516.7	South	5.43	5.47	0.04
20	3904771.1	630365.7	South	5.45	5.49	0.04
21	3904328.4	627579.2	South	5.47	5.51	0.04
22	3904432.5	624376.1	South	5.48	5.51	0.03
23	3907106.1	631164.3	South	5.29	5.31	0.02
24	3904618.1	619580.3	South	5.24	5.26	0.02
25	3905972.3	619736.6	South	5.33	5.35	0.02
26	3909305.6	633434.4	South	5.23	5.25	0.02
27	3904386.8	615430.6	South	5.30	5.32	0.02
28	3906730.5	617296.9	South	5.42	5.44	0.02
29	3939152.3	637262.1	Isthmus	6.24	6.30	0.06
30	3938718.3	634484.4	Isthmus	6.22	6.27	0.05
31	3937937.0	631836.8	Isthmus	6.20	6.25	0.05
32	3939325.9	629449.6	Isthmus	6.20	6.25	0.05
33	3937459.6	627279.5	Isthmus	6.21	6.26	0.05
34	3935853.7	625152.8	Isthmus	6.23	6.28	0.05
35	3936157.5	621810.8	Isthmus	6.25	6.30	0.05
36	3933900.6	618946.2	Isthmus	6.28	6.33	0.05
37	3932468.3	615213.6	Isthmus	6.32	6.37	0.05
38	3929560.3	612609.4	Isthmus	6.37	6.41	0.04
39	3937589.8	644119.8	Marshfield	6.30	6.36	0.06
40	3943362.4	644206.6	Marshfield	6.14	6.19	0.05

Observation Point	Easting (OR State Plane South, ft)	Northing (OR State Plane South, ft)	RM / Slough	Mean Tidal Range in feet		
				Existing Conditions	2023 PA	2023 PA-Existing
41	3944360.6	639779.5	Coos River	6.10	6.15	0.05
42	3948266.9	638694.4	Coos River	6.00	6.05	0.05
43	3951782.5	642079.8	Coos River	5.97	6.01	0.04
44	3955428.3	643989.5	Coos River	5.94	5.99	0.05
45	3945879.7	635265.6	Catching	6.13	6.18	0.05
46	3931339.8	666211.7	Haynes	5.93	5.97	0.04
47	3931122.8	671940.9	Haynes	5.17	5.20	0.03
48	3935029.1	671376.6	Haynes	6.03	6.08	0.05
49	3938935.3	674675.3	Haynes	6.02	6.08	0.06

3.6.2 Tidal Currents

Maximum[4] depth-averaged currents under the 2023 PA for ebb and flood currents are shown in Figure 3-19. It can be observed that ebb currents are stronger than flood currents throughout the estuary and indicates that Coos Bay estuary is ebb-dominant. The model results are consistent with the ebb-dominant characterization of Coos Bay (Baptista 1989 and 1994, Hyde 2007, and Sutherland & O'Neill 2016 among others). Maximum ebb currents of 5.0 ft/s can be observed vs. maximum flood currents of 3.4 ft/s at RM 1.0.

Difference in maximum depth-averaged currents between the Existing Conditions and the 2023 PA for both flood and ebb currents is shown in Figure 3-20. Maximum flood and ebb currents were extracted at observation points and are listed in Table 3-10 and Table 3-11, respectively.

Model results show a reduction in current velocity at RM 5 and RM 8. This reduction is most likely because the 2023 PA increases the flow cross-sectional area by deepening and widening the turning basins while the tidal prism increases by less than 1.6%. As roughly the same volume of water passes through a larger cross-section, it is expected to lower the current velocity.

Except at RM 5 and RM 8, the 2023 PA predicts an increase of current velocity of generally less than 0.25 ft/s in the estuary and tributaries. The maximum increase occurs along the channel alignment at RM 2, where the ebb current velocity increases by 0.55 ft/s. This probably results from the proposed change in channel alignment here, i.e., the 2023 PA alignment directs more flow towards the channel centerline.

Commented [JS18]: A-3-12: Reword sentence

Commented [JS19R18]: Text revised

[4] Maximum current speed was represented by the 99th percentile value. This value indicates that 99 percent of the current speeds are below this value.

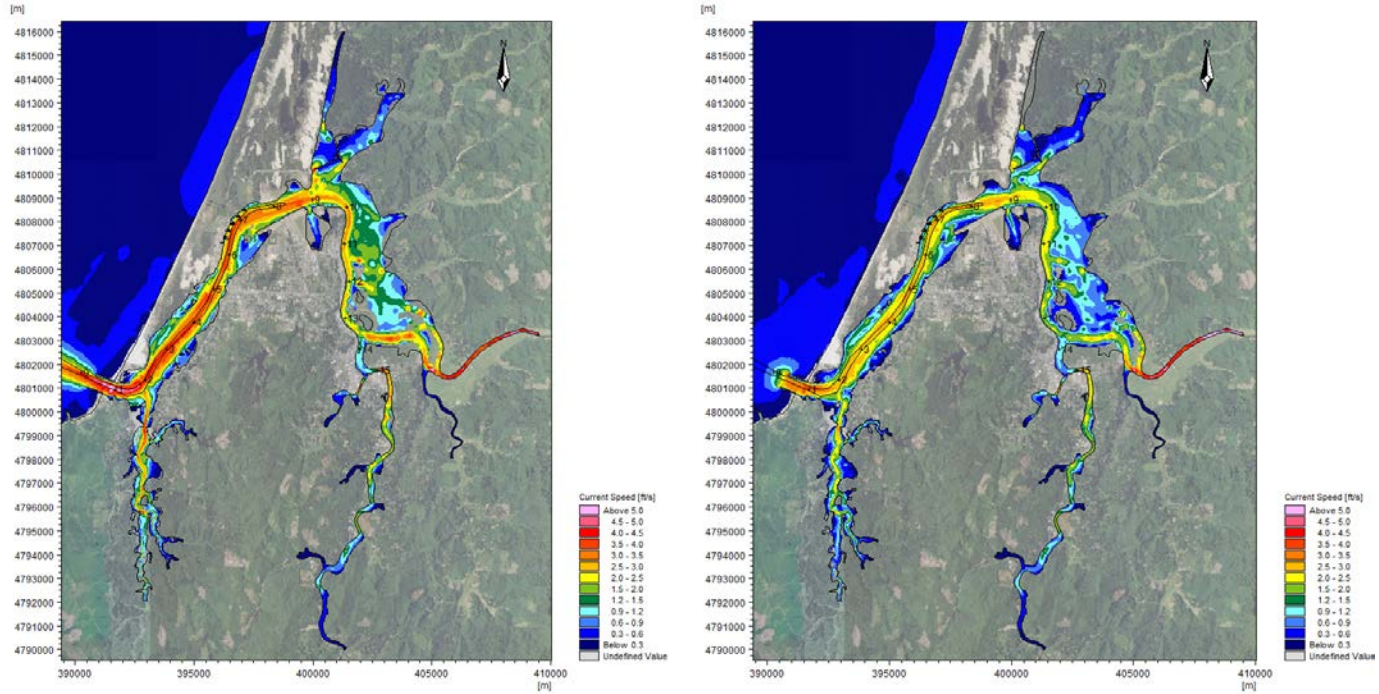

Figure 3-19
Maximum (99th Percentile) Depth-Averaged Currents at Coos Bay Estuary for 2023 PA: (Left Panel) Ebb Currents and (Right Panel) Flood Currents

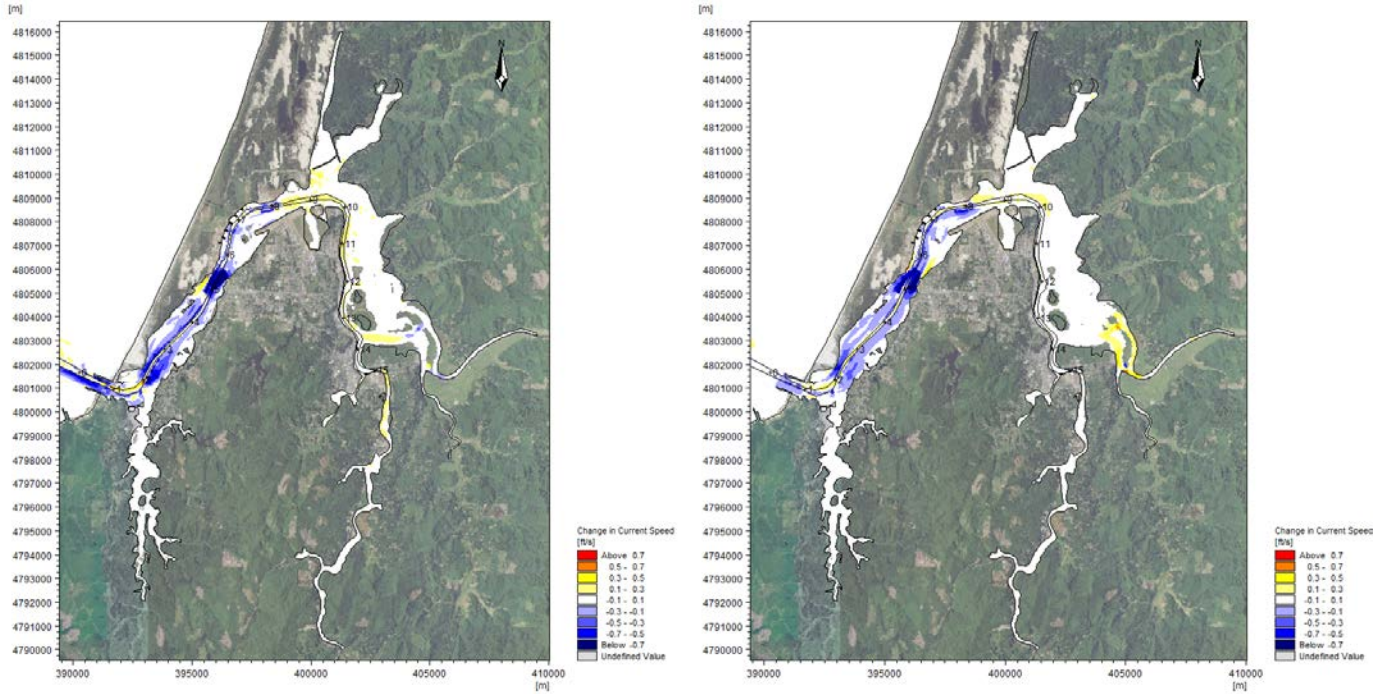

Figure 3-20
Difference in Maximum (99th Percentile) Currents at Coos Bay Estuary as a Result of the 2023 PA (2023 PA – Existing Conditions) for: (Left Panel) Ebb Currents and (Right Panel) Flood Currents

Table 3-10
Maximum Current Speed Calculated from All Flood Tides

Observation Point	Easting (OR State Plane South, ft)	Northing (OR State Plane South, ft)	RM/Slough	Maximum Current Speed in ft/sec		
				Existing Conditions	2023 PA	2023 PA-Existing
1	3891988.6	643165.5	RM -1	0.45	0.71	0.26
2	3896627.9	640644.5	RM 0	1.00	1.02	0.02
3	3901267.1	638123.5	RM 1	3.42	3.39	-0.04
4	3905474.5	639329.1	RM 2	2.58	2.71	0.13
5	3908566.0	643505.8	RM 3	2.54	2.54	0.01
6	3912387.2	647149.5	RM 4	2.75	2.83	0.08
7	3915256.9	651507.2	RM 5	3.30	3.15	-0.15
8	3917486.8	656262.6	RM 6	2.65	2.66	0.01
9	3919189.8	661074.1	RM 7	3.09	3.18	0.09
10	3923954.0	662778.7	RM 8	3.10	3.03	-0.07
11	3929182.0	663518.1	RM 9	2.19	2.23	0.04
12	3933959.7	662418.4	RM 10	2.28	2.37	0.08
13	3933508.2	657299.8	RM 11	2.31	2.37	0.06
14	3934003.3	652146.2	RM 12	1.97	1.99	0.02
15	3933308.9	647075.3	RM 13	1.87	1.92	0.05
16	3935153.5	642686.2	RM 14	1.06	1.09	0.02
17	3937460.3	639777.8	RM 15	1.66	1.70	0.04
18	3906315.9	636379.6	South	1.77	1.78	0.01
19	3905317.9	633516.7	South	2.51	2.53	0.02
20	3904771.1	630365.7	South	1.62	1.63	0.01
21	3904328.4	627579.2	South	2.17	2.17	0.00
22	3904432.5	624376.1	South	2.46	2.47	0.01

Observation Point	Easting (OR State Plane South, ft)	Northing (OR State Plane South, ft)	RM/Slough	Maximum Current Speed in ft/sec		
				Existing Conditions	2023 PA	2023 PA-Existing
23	3907106.1	631164.3	South	1.00	1.01	0.01
24	3904618.1	619580.3	South	0.76	0.76	0.00
25	3905972.3	619736.6	South	1.61	1.61	0.00
26	3909305.6	633434.4	South	1.25	1.25	0.00
27	3904386.8	615430.6	South	1.09	1.09	0.00
28	3906730.5	617296.9	South	1.60	1.60	0.00
29	3939152.3	637262.1	Isthmus	2.24	2.28	0.04
30	3938718.3	634484.4	Isthmus	1.70	1.73	0.04
31	3937937.0	631836.8	Isthmus	1.03	1.05	0.02
32	3939325.9	629449.6	Isthmus	1.50	1.55	0.04
33	3937459.6	627279.5	Isthmus	1.33	1.36	0.03
34	3935853.7	625152.8	Isthmus	2.02	2.04	0.03
35	3936157.5	621810.8	Isthmus	1.78	1.82	0.04
36	3933900.6	618946.2	Isthmus	1.65	1.69	0.04
37	3932468.3	615213.6	Isthmus	1.31	1.33	0.02
38	3929560.3	612609.4	Isthmus	0.50	0.52	0.01
39	3937589.8	644119.8	Marshfield	1.81	1.84	0.03
40	3943362.4	644206.6	Marshfield	1.60	1.66	0.06
41	3944360.6	639779.5	Coos River	2.36	2.50	0.15
42	3948266.9	638694.4	Coos River	4.88	4.87	-0.01
43	3951782.5	642079.8	Coos River	4.57	4.56	-0.01
44	3955428.3	643989.5	Coos River	5.62	5.62	0.00
45	3945879.7	635265.6	Catching	0.27	0.28	0.01
46	3931339.8	666211.7	Haynes	1.20	1.23	0.03

Observation Point	Easting (OR State Plane South, ft)	Northing (OR State Plane South, ft)	RM/Slough	Maximum Current Speed in ft/sec		
				Existing Conditions	2023 PA	2023 PA-Existing
47	3931122.8	671940.9	Haynes	0.70	0.74	0.04
48	3935029.1	671376.6	Haynes	0.47	0.46	-0.01
49	3938935.3	674675.3	Haynes	0.67	0.78	0.11

Table 3-11
Maximum Current Speed Calculated from All Ebb Tides

Observation Point	Easting (OR State Plane South, ft)	Northing (OR State Plane South, ft)	RM/Slough	Maximum Current Speed in ft/sec		
				Existing Conditions	2023 PA	2023 PA-Existing
1	3891988.6	643165.5	RM -1	2.18	2.28	0.10
2	3896627.9	640644.5	RM 0	3.95	4.07	0.12
3	3901267.1	638123.5	RM 1	4.75	4.98	0.23
4	3905474.5	639329.1	RM 2	4.09	4.64	0.55
5	3908566.0	643505.8	RM 3	4.03	4.15	0.12
6	3912387.2	647149.5	RM 4	3.91	4.16	0.25
7	3915256.9	651507.2	RM 5	4.23	3.56	-0.67
8	3917486.8	656262.6	RM 6	3.21	3.30	0.09
9	3919189.8	661074.1	RM 7	3.54	3.60	0.05
10	3923954.0	662778.7	RM 8	3.29	3.07	-0.22
11	3929182.0	663518.1	RM 9	3.04	3.17	0.13
12	3933959.7	662418.4	RM 10	3.17	3.27	0.10
13	3933508.2	657299.8	RM 11	2.82	2.99	0.17
14	3934003.3	652146.2	RM 12	2.41	2.48	0.07
15	3933308.9	647075.3	RM 13	2.31	2.40	0.09
16	3935153.5	642686.2	RM 14	1.23	1.22	0.00

Observation Point	Easting (OR State Plane South, ft)	Northing (OR State Plane South, ft)	RM/Slough	Maximum Current Speed in ft/sec		
				Existing Conditions	2023 PA	2023 PA-Existing
17	3937460.3	639777.8	RM 15	1.96	1.98	0.02
18	3906315.9	636379.6	South	1.28	1.29	0.01
19	3905317.9	633516.7	South	3.80	3.85	0.05
20	3904771.1	630365.7	South	3.20	3.24	0.05
21	3904328.4	627579.2	South	2.29	2.31	0.03
22	3904432.5	624376.1	South	3.46	3.47	0.01
23	3907106.1	631164.3	South	1.02	1.05	0.02
24	3904618.1	619580.3	South	1.08	1.09	0.01
25	3905972.3	619736.6	South	1.00	1.01	0.01
26	3909305.6	633434.4	South	0.87	0.87	0.00
27	3904386.8	615430.6	South	1.83	1.83	0.00
28	3906730.5	617296.9	South	1.09	1.08	-0.02
29	3939152.3	637262.1	Isthmus	2.57	2.71	0.13
30	3938718.3	634484.4	Isthmus	1.95	2.08	0.12
31	3937937.0	631836.8	Isthmus	1.17	1.26	0.09
32	3939325.9	629449.6	Isthmus	1.57	1.63	0.05
33	3937459.6	627279.5	Isthmus	1.55	1.63	0.07
34	3935853.7	625152.8	Isthmus	2.10	2.13	0.02
35	3936157.5	621810.8	Isthmus	1.85	1.91	0.05
36	3933900.6	618946.2	Isthmus	1.76	1.83	0.06
37	3932468.3	615213.6	Isthmus	1.27	1.33	0.06
38	3929560.3	612609.4	Isthmus	0.49	0.50	0.01
39	3937589.8	644119.8	Marshfield	2.83	3.01	0.18
40	3943362.4	644206.6	Marshfield	1.96	1.91	-0.04

Observation Point	Easting (OR State Plane South, ft)	Northing (OR State Plane South, ft)	RM/Slough	Maximum Current Speed in ft/sec		
				Existing Conditions	2023 PA	2023 PA-Existing
41	3944360.6	639779.5	Coos River	2.75	2.78	0.03
42	3948266.9	638694.4	Coos River	4.59	4.62	0.03
43	3951782.5	642079.8	Coos River	4.13	4.15	0.02
44	3955428.3	643989.5	Coos River	4.84	4.86	0.02
45	3945879.7	635265.6	Catching	0.26	0.27	0.01
46	3931339.8	666211.7	Haynes	1.63	1.73	0.10
47	3931122.8	671940.9	Haynes	0.52	0.53	0.01
48	3935029.1	671376.6	Haynes	0.53	0.53	0.00
49	3938935.3	674675.3	Haynes	1.20	1.23	0.03

3.6.3 Morphological and Hydrodynamic Processes (RM 1.0 to 3.0)

The focus of this subsection is on the FNC between RM 1.0 and RM 3.0. The area of interest is highlighted in yellow along the channel centerline in Figure 3-21. Representative cross-sections stations used in the discussion are highlighted with red lines.

3.6.3.1 Existing Conditions

As documented earlier in this section, the Coos Bay estuary is ebb-dominated. Figure 3-22 illustrates representative peak ebb and peak flood depth-averaged[5] current speeds in the estuary between RM 1.0 and RM 4.0. Peak ebb currents in the main channel are approximately 4.5 to 5.0 feet per second (ft/s) upstream of RM 1.0, increasing to greater than 5.0 ft/s downstream of RM 1.0 between the North Jetty and South Jetty. Peak flood currents are generally less than 3.5 ft/s, except immediately downstream of RM 1.0 where currents are accelerated locally as they pass through the jetties. In general, currents are trained by rubble mound structures and Guano Rock from the ocean entrance to RM 1.0. Upstream of RM 1.0, rubble structures continue on the northern and western sides of the channel, in the form of a rail spur and the North Jetty root that bounds Log Spiral Bay (LSB) up to approximately RM 2.2.

[5] Unless otherwise noted, all current speeds discussed herein are depth-averaged values.

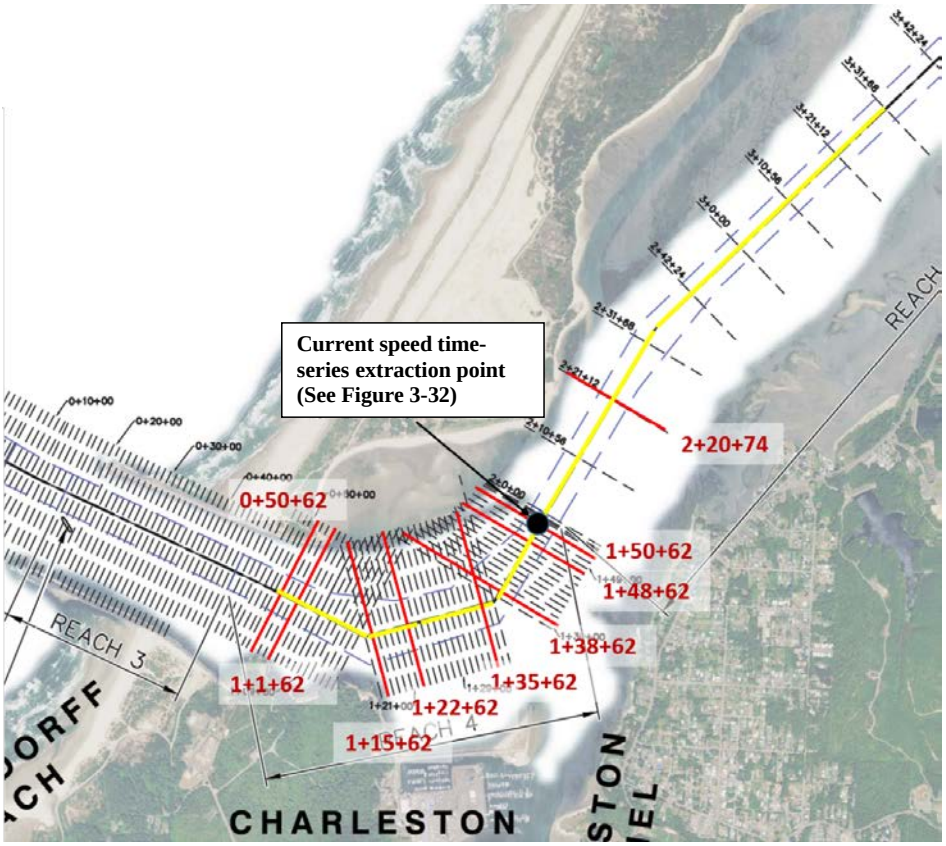

Figure 3-21
Location of Selected Cross-Sections

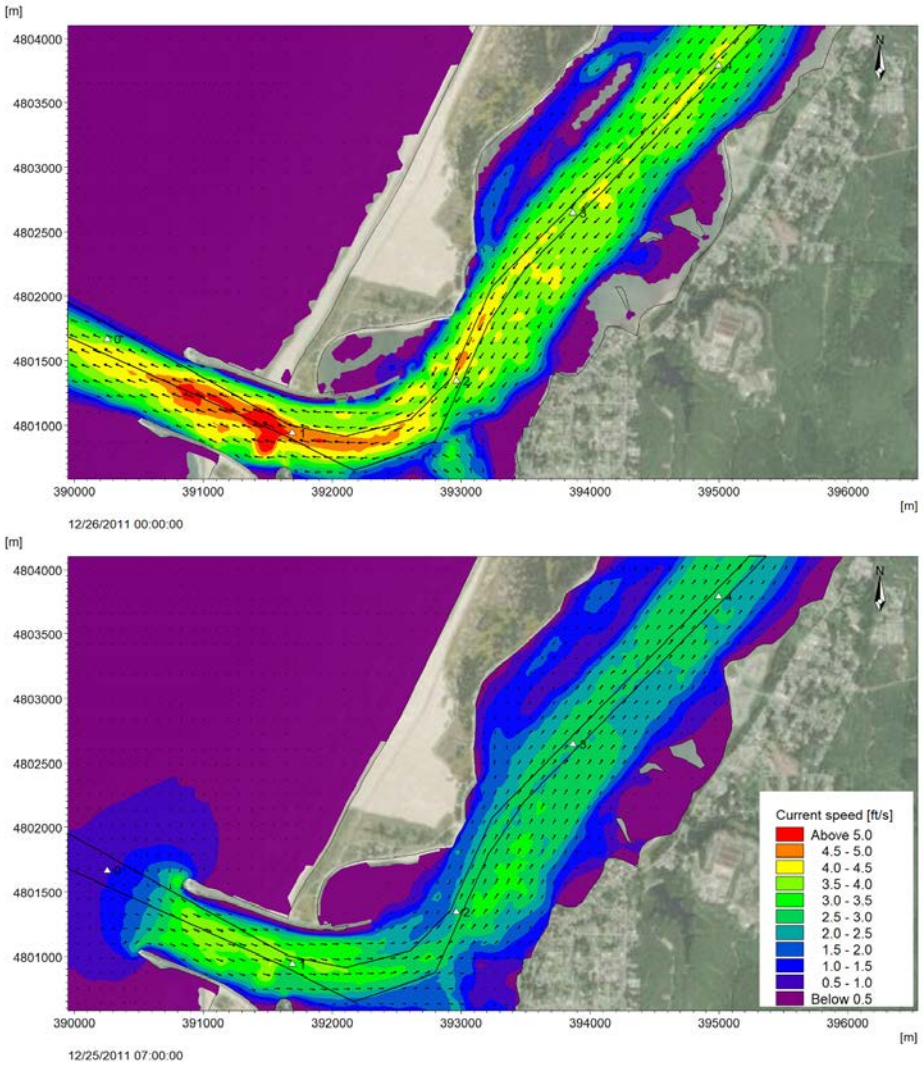

Figure 3-22
Peak Ebb (Top Panel) and Peak Flood (Bottom Panel) Current Speeds and Vectors Downstream of RM 4.0 for Existing Conditions

Figure 3-23 provides the channel bed morphological information for the area highlighted in Figure 3-21. The figure shows how the existing bathymetry deepens dramatically just downstream of RM 2.0, compared to the upstream bathymetry. This occurs as the channel bed changes from rock (above RM 2.0) to varying depths of sand over rock in the deeper area.

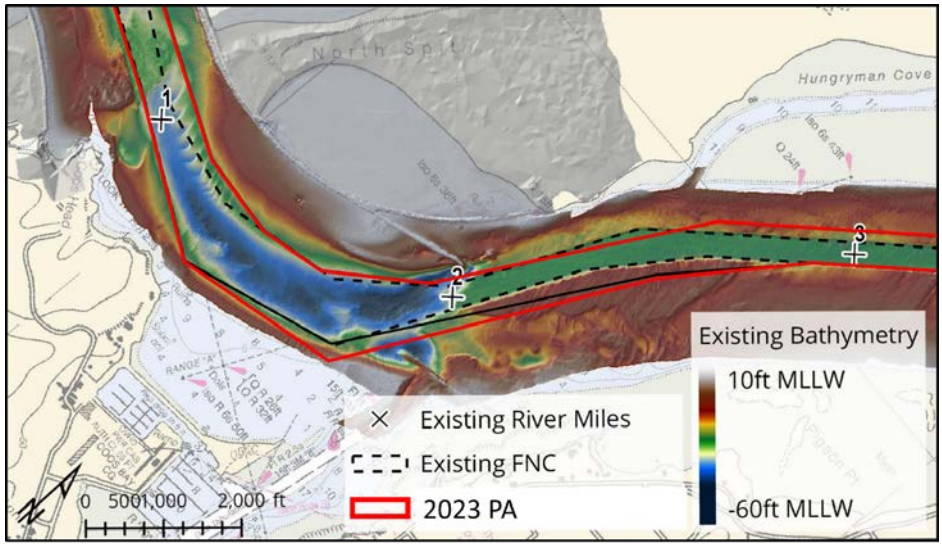

Figure 3-23
Channel Bed Morphology with Channel Outlines between RM 1.0 and RM 3.0

A complex arrangement of the existing rock structures and bed morphology exists in the vicinity of RM 2.0 (Figure 3-24). Log Spiral Bay (LSB) is largely separated from ebb and flood flows by the North Jetty root rubble structure. Between the North Jetty root and the main channel, the rail spur rubble structure projects off the North Jetty root at an oblique angle to the channel. The rail spur serves to concentrate flood flows more toward the main channel than would be the case without the structure. Ebb flows passing the tip of the rail spur cause eddies on the downstream side, and scour holes are evidenced in the bathymetry in this area. While the bed on the eastern side of the channel has a layer of sand over rock, the bed continues as exposed rock on the western/northern side of the channel adjacent to the rail spur.

These structures and the underlying rock layer, exposed on the western side of the channel, prevent the channel from migrating toward LSB.

Across the channel from LSB and slightly downstream (Figure 3-25), a relic jetty exists as a submerged feature to the east of the existing and proposed channel boundaries. The existing sandy bed appears to have been scoured around the submerged relic, and this may be related to the counterclockwise eddy in the ebb current vectors seen in the model results for that area as illustrated in Figure 3-22.

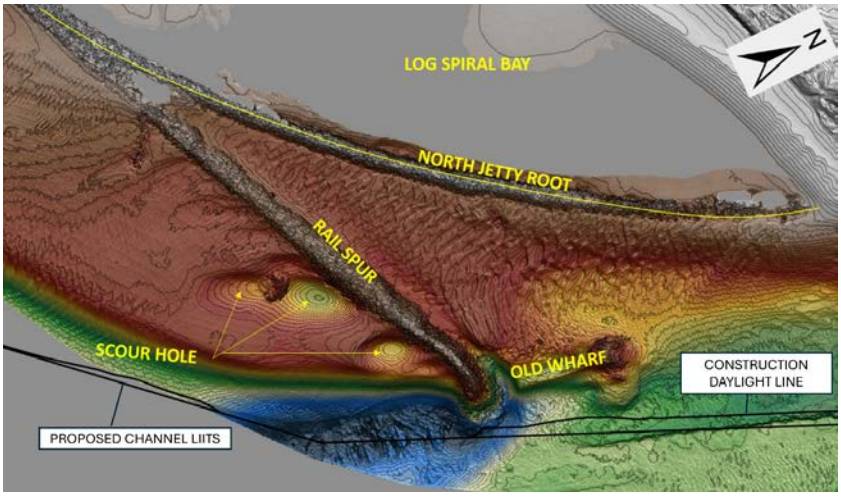

Figure 3-24
Channel Morphology and Structures on the Western Side of the FNC at RM 2.0

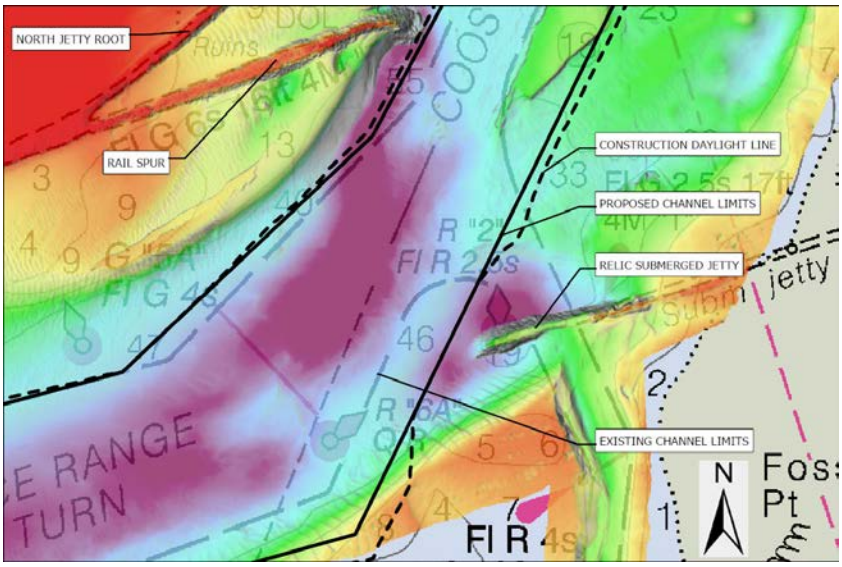

Figure 3-25
Channel Morphology and Structures on the Eastern Side of the FNC Downstream of RM 2.0

Commented [CT20]: PDT A-3-3: Provide legend to indicate what the red and green lines signify.

Commented [CT21R20]: Revised the figure and provided the legend.

Commented [TCF22]: PDT A-3-4: What is the green splotch area that abruptly begins along shallow morphology immediately south of the relic north jetty submerged rail spur? Ensure report clearly describes the figure.

Commented [TCF23R22]: The green areas immediately south of the relic rail spur are scour holes. They are noted in Figure 3-24 and the report.

3.6.3.2 Anticipated Effects of the 2023 PA

In addition to showing the existing bathymetry, Figure 3-23 also shows the outline of the existing and 2023 PA channels. The dogleg between RM 2.0 and RM 3.0 is shifted upstream under the 2023 PA. Therefore, it is expected that ebb currents would begin to shift away from the LSB further upstream under the 2023 PA. Model results support this assessment, see Figure 3-28 showing the change in 99th percentile ebb current speeds as a result of the 2023 PA. The effect of the 2023 PA channel is to direct more flow towards the channel centerline at RM 2, reducing currents in the vicinity of the North Jetty root/LSB and increasing currents within the channel.

Note that the 2023 PA channel used constructed side slopes. Modeling for the 2023 PA scenario was performed for constructed slopes since these slopes provide the most conservative results with respect to currents and sediment transport, especially given the uncertainty associated with the future equilibrium side slopes. It also shows the immediate potential environmental impacts.

Figure 3-30 and Figure 3-31 show the change in mean (average) current speeds as a result of the 2023 PA for ebb and flood currents, respectively. The mean current speeds in the 2023 PA are generally less than or equivalent to the Existing Conditions, except in the main channel where the 2023 PA is expected to increase average speed between 0.1 and 0.3 ft/sec.

The cross-section figures used in the discussion of channel morphology below contain peak ebb current speeds for both the Existing Conditions and the 2023 PA. The peak ebb current speeds were extracted at the same time step for both scenarios, and that representative peak ebb time step was determined through inspection of a time series at the point near RM 2 as marked in Figure 3-21. The time series is shown in Figure 3-32, and the peak ebb time step with the highest speed in the simulation period was at midnight on December 26, 2011.

The separate discussions by cross-section, below Figure 3-32, briefly describe the existing channel morphology and the expected effects of the 2023 PA channel geometry along several channel reaches. The reaches are denoted by RM positions, and the discussion is illustrated by one or two representative cross-sections in each reach. All of the cross-sections are looking downstream.

Commented [TCF24]: PDT A-3-5: It appears that the estuary model's FNC bathymetry was based on "constructed" side slopes for PA. What are the implications of realizing "equilibrated" side slopes for the PA in terms of model results based on "constructed" side slopes? Please add supplement of narrative to explain.

USACE 10462082: It would seem to me that what we really care about for the 2023 PA is not the construction slopes, but rather the long-term equilibrium side slopes, since that will be the channel/bathymetry/topography that the USACE will take on to manage and maintain after the project is done.

Commented [TCF25R24]: Added
"Modeling for the 2023 PA scenario was performed for constructed slopes since these slopes provide the most conservative results with respect to currents and sediment transport, especially given the uncertainty associated with the future equilibrium side slopes. It also shows the immediate potential environmental impacts."

Commented [SJ26R24]: Also USACE 1046082

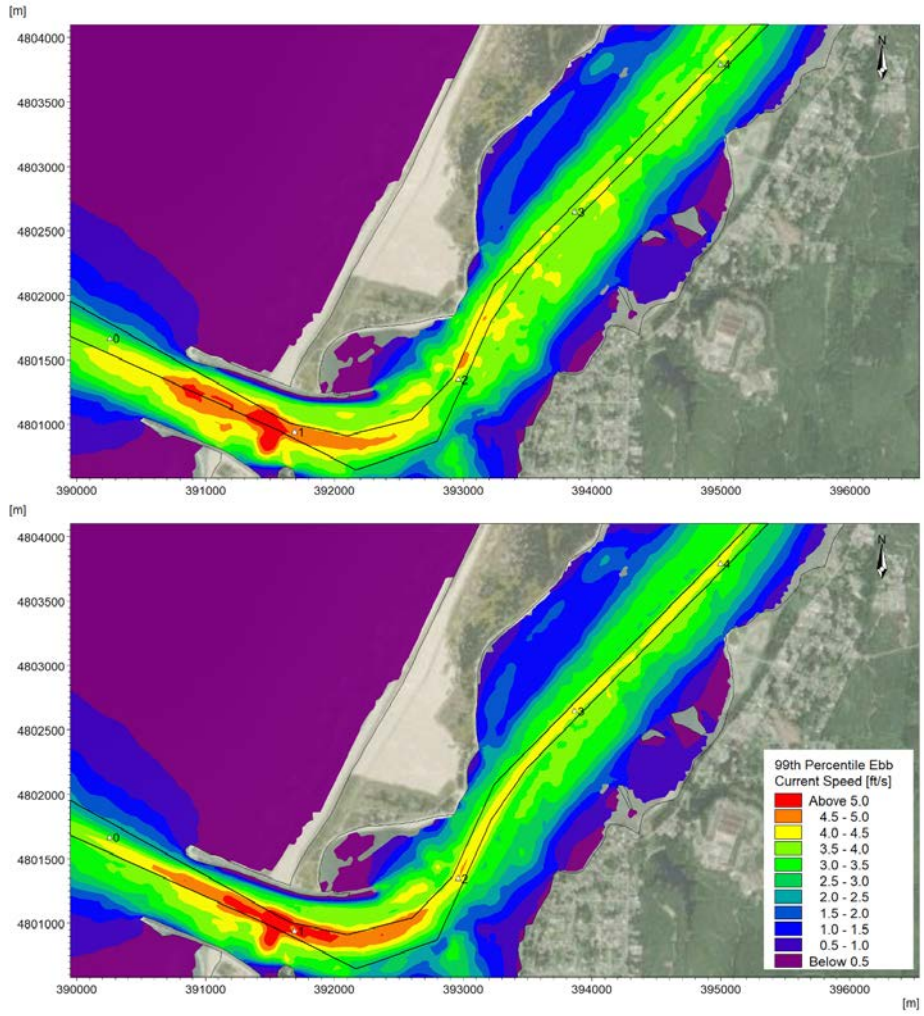

* Existing Channel Outline Shown in Black Line

Figure 3-26
99th Percentile Depth-Averaged Ebb Current Speeds from Existing Conditions (Top Panel) and 2023 PA (Bottom Panel) Simulations

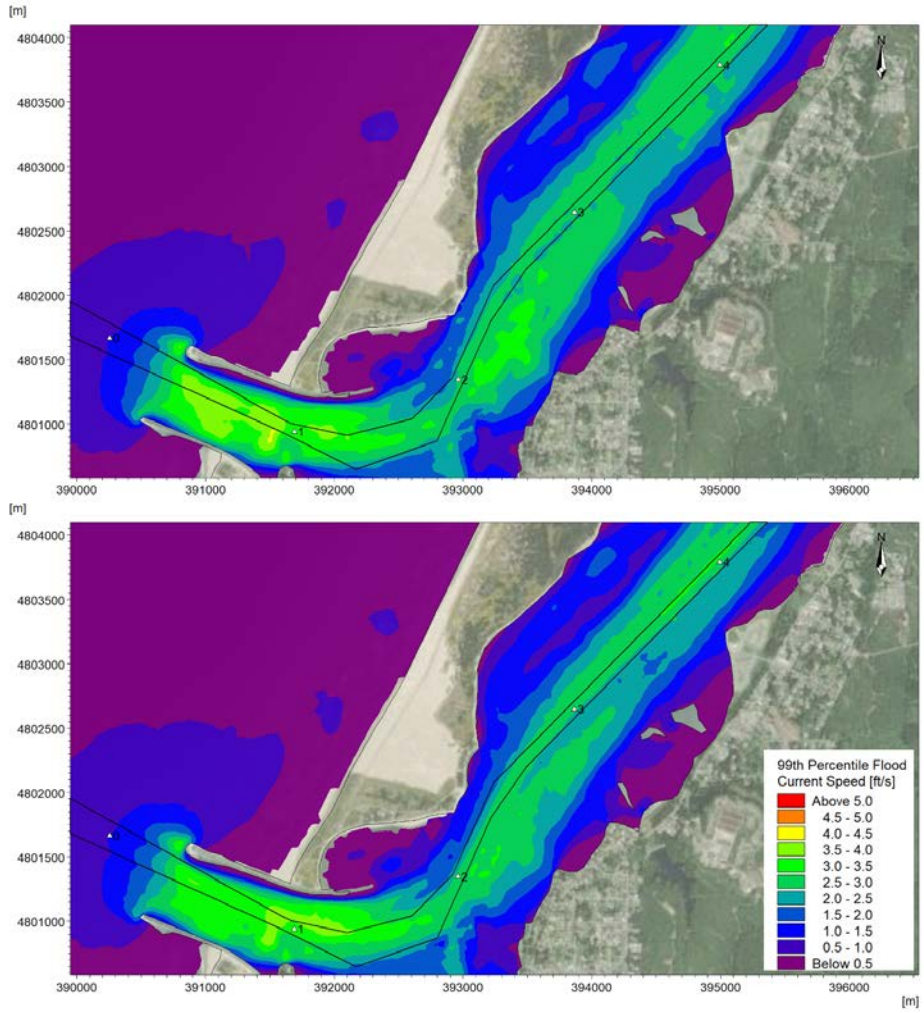

* Existing Channel Outline Shown in Black Line

Figure 3-27
99th Percentile Depth-Averaged Flood Current Speeds from Existing Conditions (Top Panel) and 2023 PA (Bottom Panel) Simulations

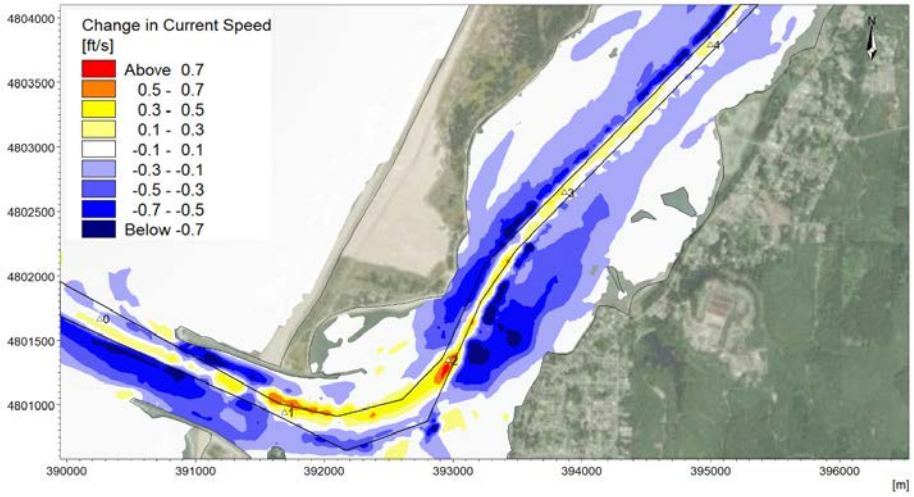

* Existing Channel Outline Shown in Black Line

Figure 3-28
Change in 99th Percentile Ebb Current Speeds between RM 1.0 and RM 4.0 as a Result of 2023 PA (2023 PA – Existing Conditions)

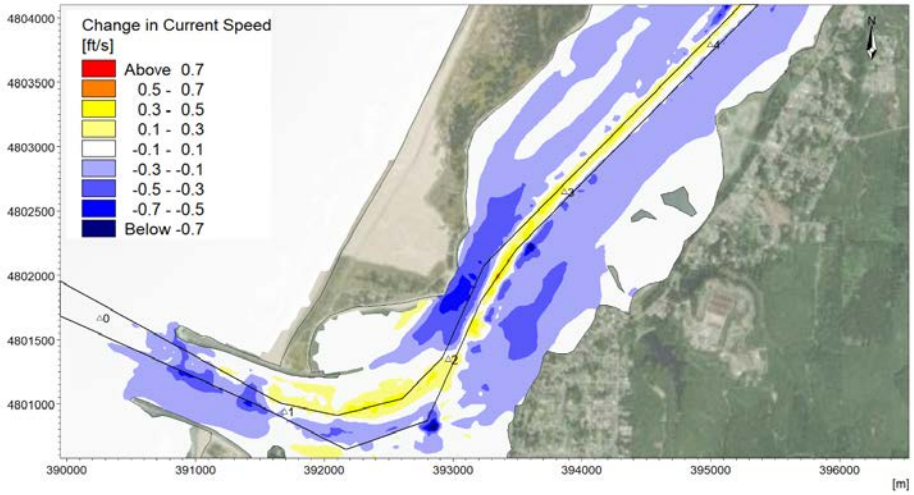

* Existing Channel Outline Shown in Black Line

Figure 3-29
Change in 99th Percentile Flood Current Speeds between RM 1.0 and RM 4.0 as a Result of 2023 PA (2023 PA – Existing Conditions)

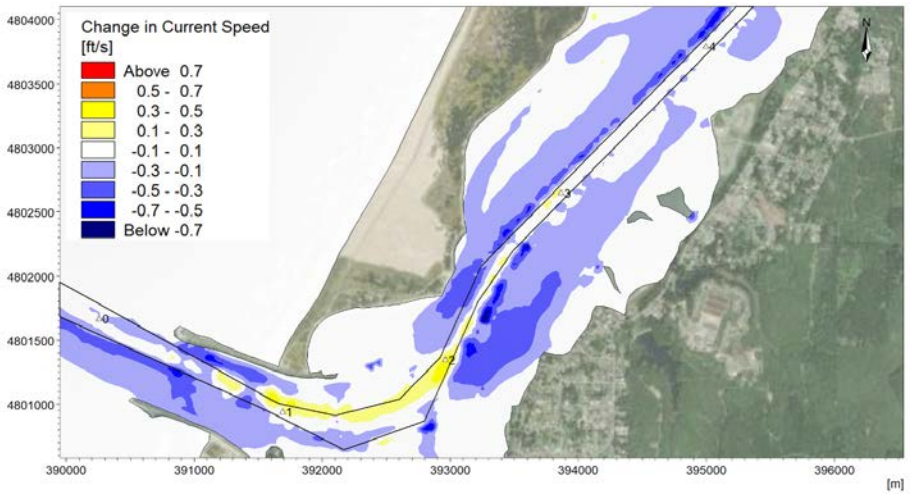

* Existing Channel Outline Shown in Black Line

Figure 3-30
Change in Mean Ebb Current Speeds between RM 1.0 and RM 4.0 as a Result of 2023 PA (2023 PA – Existing Conditions)

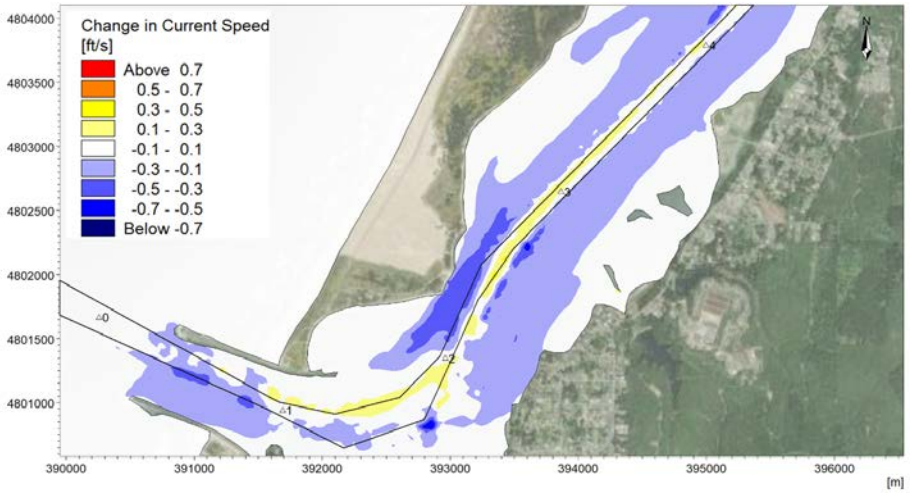

* Existing Channel Outline Shown in Black Line

Figure 3-31
Change in Mean Flood Current Speeds between RM 1.0 and RM 4.0 as a Result of 2023 PA (2023 PA – Existing Conditions)

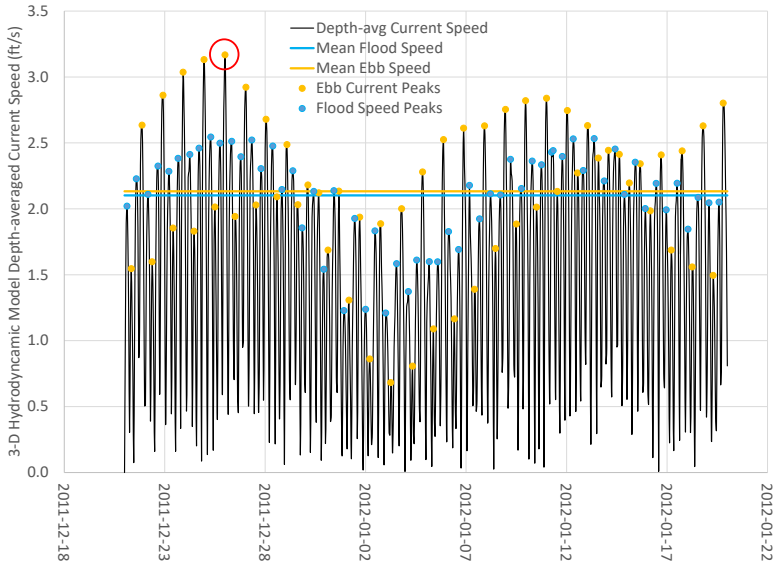

Figure 3-32
Time Series of Depth-Averaged Current Speeds near RM 2.0

RM 3.6 to RM 2.0

This reach has exposed rock in the channel bed and adjacent flow areas on both the left and right sides of the channel. Station 2+20+74 (RM 2.0 plus 2,074 feet) was used to represent the typical cross-section in this reach. Figure 3-33 shows the existing bathymetry, existing rock surface, and the 2023 PA channel geometry, taken from Sub-Appendix 13 cross-sections. The figure also includes curves representing the peak ebb current speeds from the MIKE-3 HD model (for the high ebb time step discussed above) for both the 2023 PA (green line) and the Existing Conditions (blue line).

The proposed 2023 PA channel would cut into the existing rock, but would not expand into areas with exposed sediment beds. The maximum vertical cut into the rock on the eastern side of the channel would be approximately 25 to 27 feet below the existing grade. The higher ebb current speeds are expected to shift toward the left (east) as the 2023 PA expands the channel to the east. While the absolute peak ebb speed is shown to increase slightly above the Existing Conditions at the channel centerline, ebb current speeds away from the centerline are expected to be lower in the 2023 PA than in the Existing Conditions. Thus, the 2023 PA current speeds within the channel are sufficient to prevent sedimentation in the rock channel; and, with lower speeds than the Existing Conditions outside of the channel, the 2023 PA is not expected to cause increased erosion of channel side areas.

An area of increased peak ebb currents in the 2023 PA is seen in Figure 3-28 at RM 2. As described, the effect of the 2023 PA channel is to direct more flow towards the channel centerline at RM 2, reducing currents in the vicinity of the North Jetty root/LSB and increasing currents within the channel.

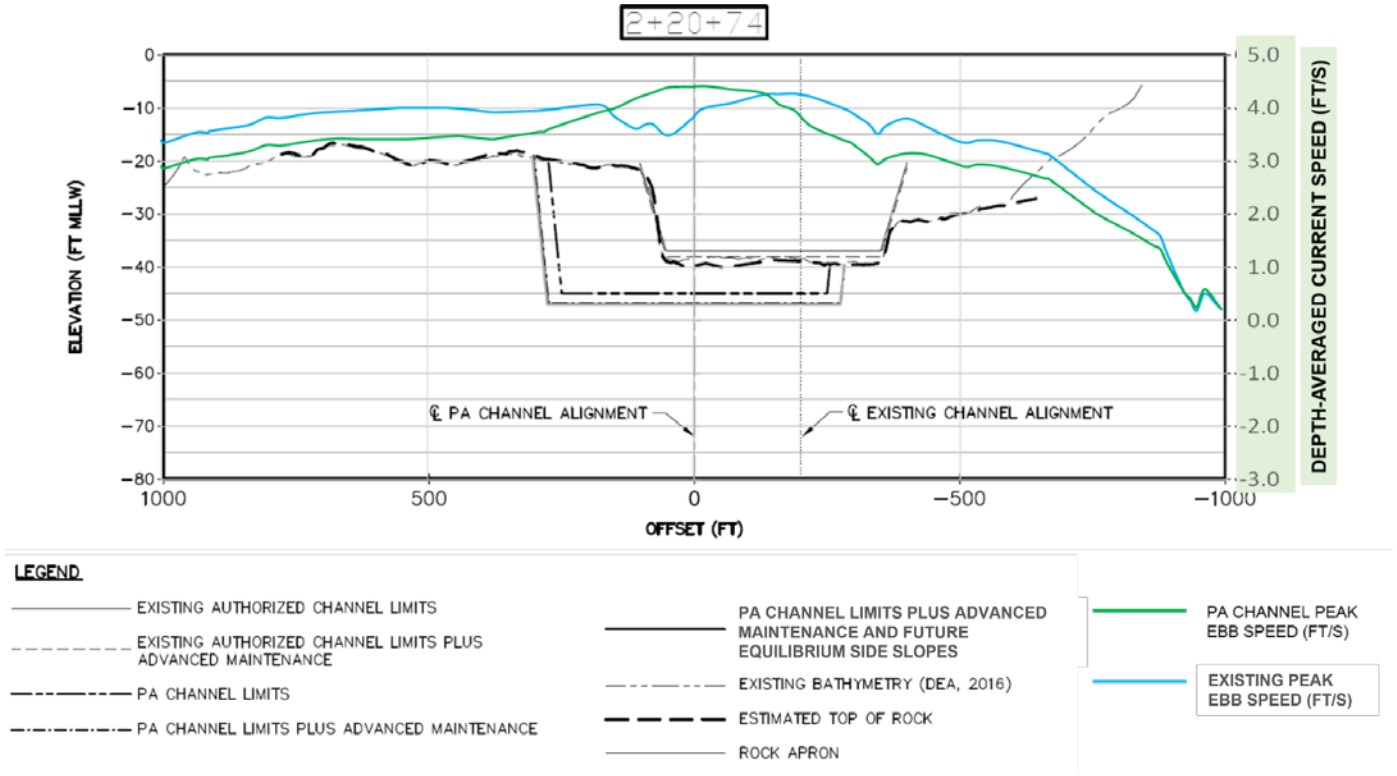

Figure 3-33
Cross-section at 2+20+74 Representing RM 3.6 to RM 2.0 (Looking Downstream)

Immediately downstream of RM 2.0

In the vicinity of RM 2.0, the channel bed changes from exposed rock to exposed sand (of varying layer thickness) across most of the cross-section. Stations 1+50+62 and 1+48+62 were used to represent the typical cross-sections in this reach (Figure 3-34 and Figure 3-35, respectively). The existing bed deepens to a maximum depth of 55 to 65 feet below MLLW. Data on the presence and depth of rock is limited outside of the main channel area.

In this reach, the proposed 2023 PA channel would cut up to approximately 10 feet (vertical) and into the rock layer on the east side of the channel. No cut would be needed on the west side of the channel, as illustrated. The MIKE-3 HD model results indicate that the peak ebb speeds in the center of the channel would be higher in the 2023 PA than in the Existing Conditions, and the position of the peak speed would shift to the left (with expansion of the channel to the east). East of the channel, the HD model results show peak ebb speeds being lower in the 2023 PA than in the Existing Conditions. Thus, the 2023 PA channel is not expected to cause increased erosion of the (potentially) sandy bed areas east of the channel.

West of the channel, toward the rubble rail spur structure and LSB, peak ebb speeds are expected to be slightly lower in the 2023 PA than in the Existing Conditions. Thus, the 2023 PA channel is not expected to cause adverse morphological developments at the rail spur or in the vicinity of LSB in this reach.

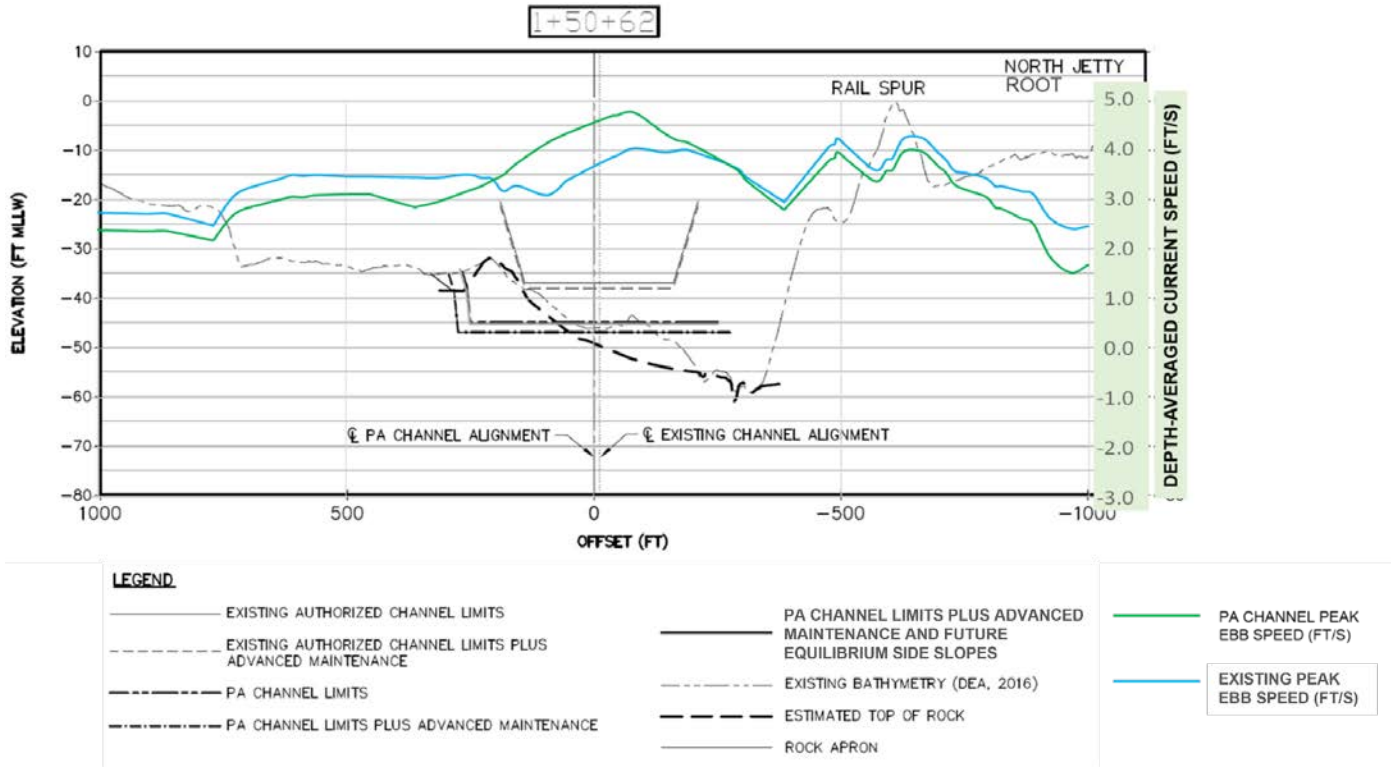

Figure 3-34
Cross-section at 1+50+62 Representing the Transition Area at RM 2.0 (Looking Downstream)

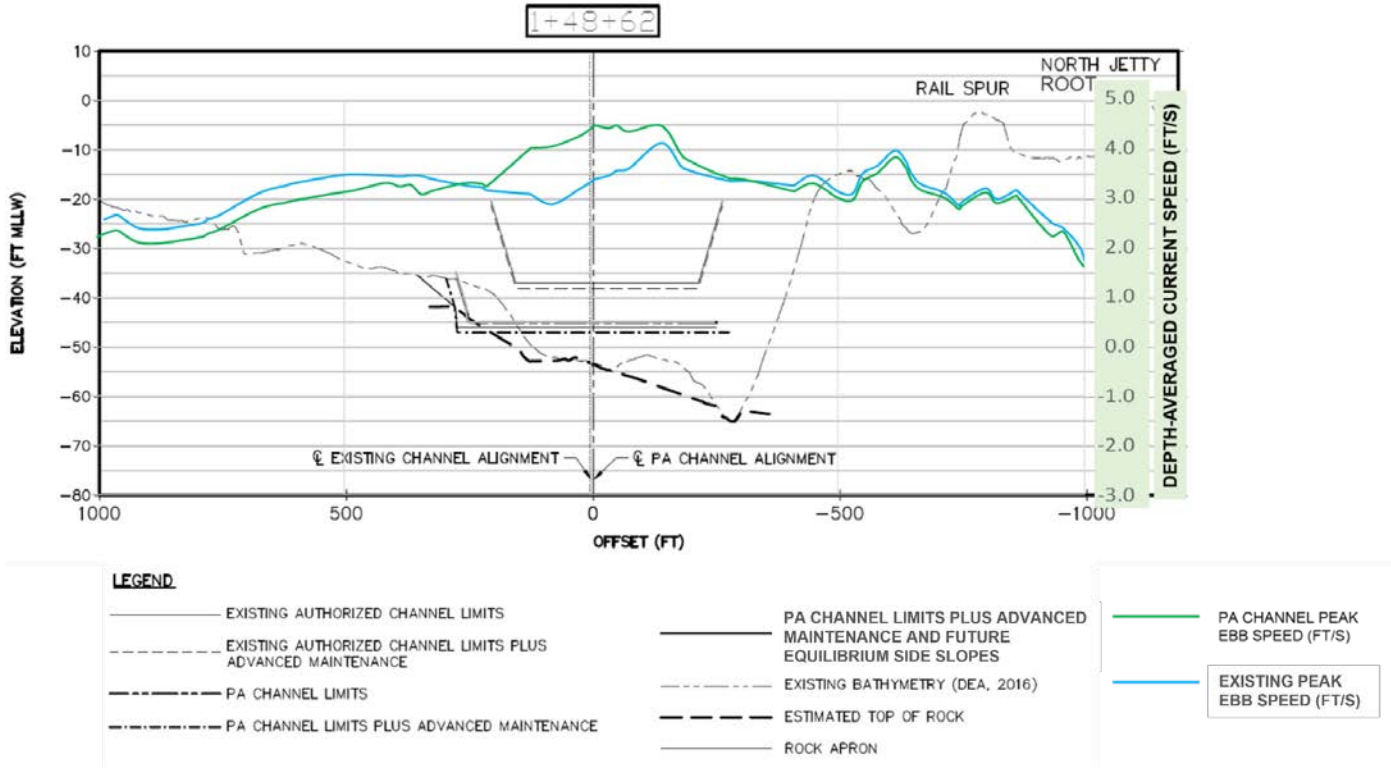

Figure 3-35
Cross-section at 1+48+62 Representing the Transition Area at RM 2.0 (Looking Downstream)

RM 1.9 to RM 1.4

In this reach, as the river begins to turn west toward the ocean entrance, the existing river bed is (in general) deeper than the proposed 2023 PA channel depth. The existing bed is sand, and the elevation of the underlying rock layer is much deeper than at the reaches upstream (described above).

At the upstream end of this reach (shown at station 1+38+62 in Figure 3-36), the rock layer is more than 20 feet below the existing bed elevation. The North Jetty rubble structure is separated from the main channel by more than 500 feet of very flat and relatively shallow (10 feet below MLLW) bathymetry. The proposed 2023 PA channel would cut approximately 5 feet (vertical) into sand over a relatively short lateral distance east of the centerline. The MIKE-3 HD model results indicate that the 2023 PA channel would slightly decrease peak ebb current speeds east of the centerline and increase speeds (by less than 0.5 ft/s) over about 700 feet west of the centerline, before again becoming similar to the Existing Conditions. The increase in speed is attributed more to the increase in conveyance upstream of this location, causing more volume to flow through a relatively unchanged cross-section (at 1+38+62). Given the relatively small increase in current speed and the thickness of the sand layer in this reach, any increased potential for bed erosion due to the current speed increase would be expected to equilibrate by slightly deepening the channel bed approximately 500-feet from the centerline area. While this effect is expected to be contained within the channel, it is a factor that would be considered within the project's risk management framework.

The station 1+38+62 is close to the submerged relic jetty feature. The model results indicate very little change associated with the 2023 PA channel in the 99th percentile and mean current speeds outside of the navigation channel. Thus, it is not expected that the 2023 PA channel would adversely impact the submerged relic jetty; however, the monitoring of this feature can be included in the project's risk management framework.

The station 1+35+62 (Figure 3-37) is similar to station 1+38+62, with two exceptions:

- West of the centerline, the 2023 PA channel would cut into an existing sand side slope (with the future equilibrium side slope projected up and west toward the existing rail spur rubble structure as shown).

- East of the centerline, the 2023 PA channel would cut slightly into the existing channel side slope. The compound future equilibrium side slope shown in the figure is described in Sub-Appendix 6 *Channel Side Slope Analysis*.

At the station 1+35+62, the MIKE-3 HD model results also indicate that the 2023 PA channel would slightly decrease peak ebb current speeds east of the centerline and increase speeds west of the centerline, as compared to the Existing Conditions. The speed increase in the western part of the channel is expected to be less than 0.5 ft/s; however, this is a factor that would be considered within the project's risk management framework.

At the station 1+22+62 (Figure 3-38), the underlying rock layer is closer to the sand surface, with a sand thickness of approximately five feet in the center of the channel. The MIKE-3 HD model results are similar as the other two cross-sections in this reach. The 2023 PA channel would increase peak ebb current speeds west of the centerline. Therefore, the expected future equilibrium side slopes are shown.

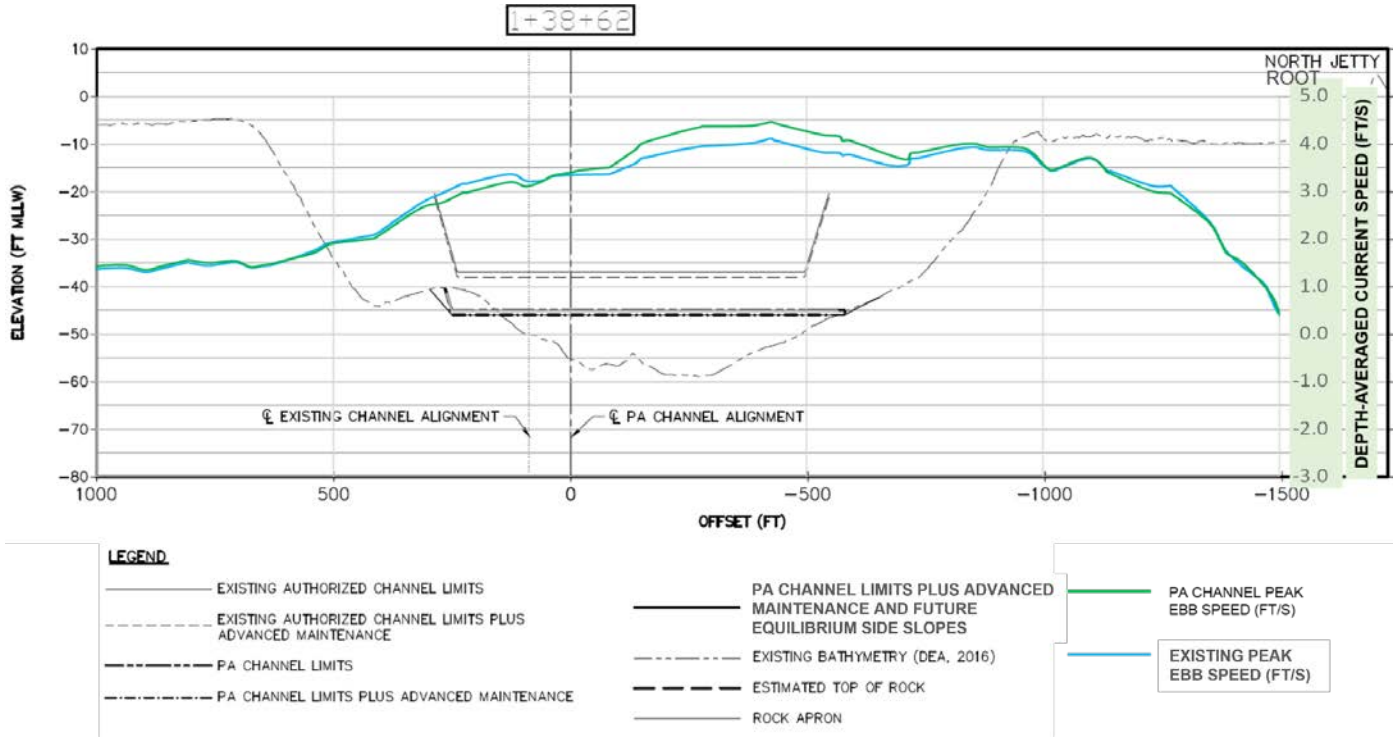

Figure 3-36
Cross-section at 1+38+62 Representing RM 1.9 to RM 1.4 (Looking Downstream)

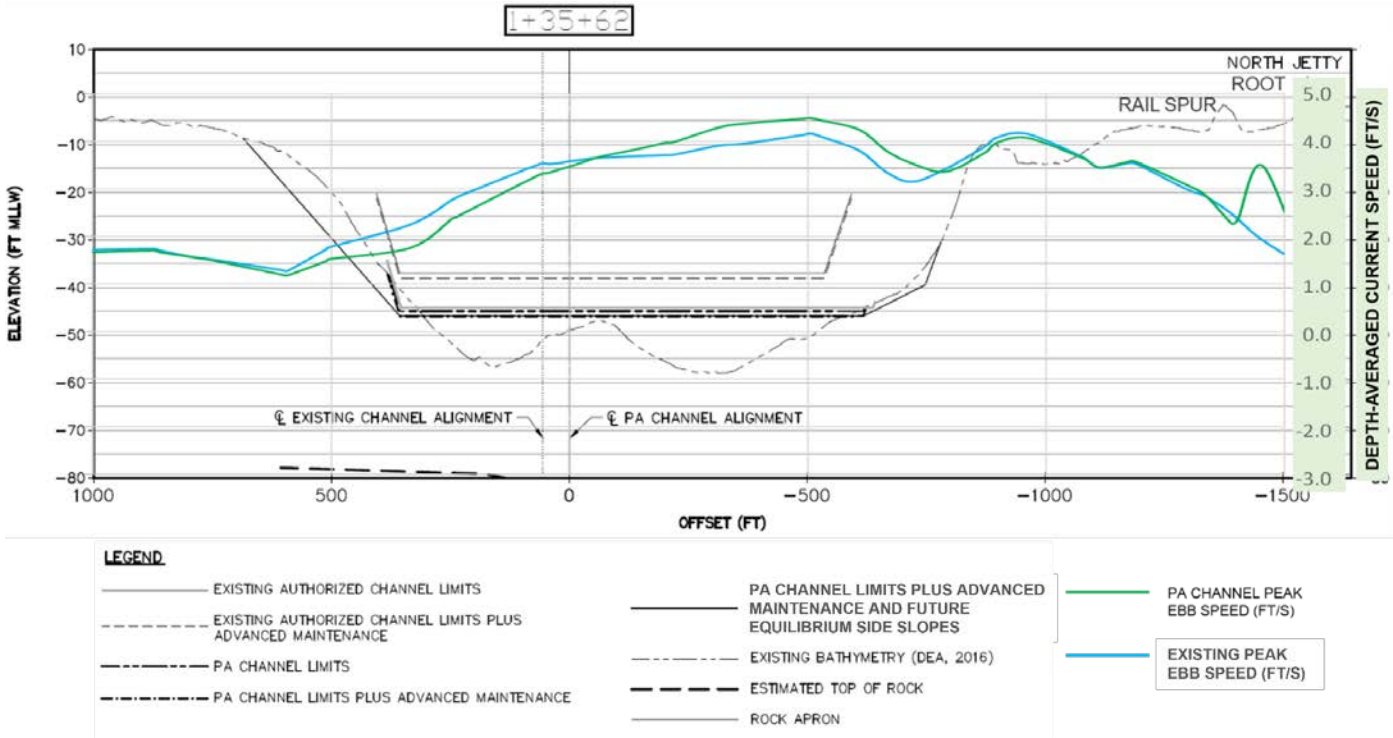

Figure 3-37
Cross-section at 1+35+62 Representing RM 1.9 to RM 1.4 (Looking Downstream)

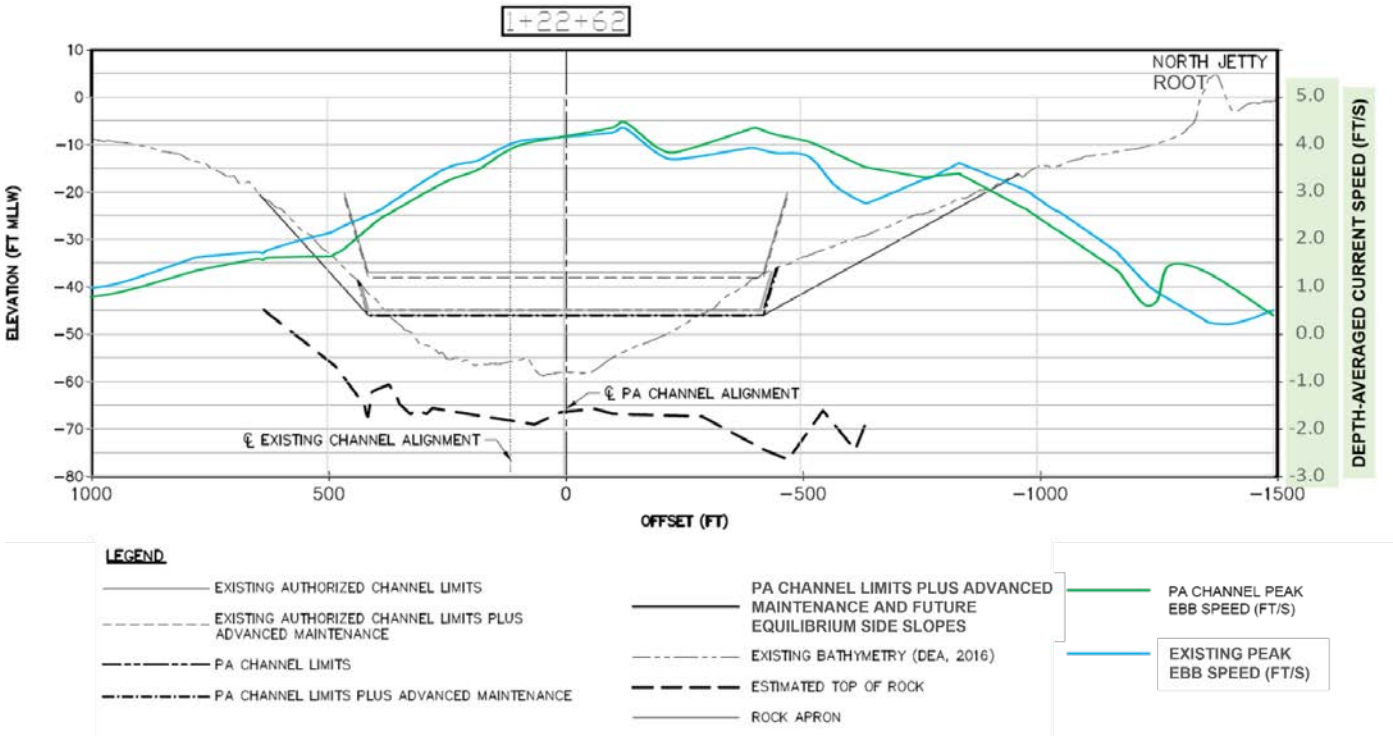

Figure 3-38
Cross-section at 1+22+62 Representing RM 1.9 to RM 1.4 (Looking Downstream)

Commented [TCF27]: PDT A-3-6: Figure 3-38 and similar figures: Replace the word "Evaluated" Side Slopes with appropriate term (constructed, equilibrated, etc).

Commented [CT28R27]: Changed to equilibrium side slopes.

RM 1.4 to RM 1.3

Just before its final turn toward the ocean, the channel passes through a reach with exposed rock at the southeastern side slope and 10 to 20 feet of sand over rock in the main channel. The station 1+15+62 (Figure 3-39) represents this reach. The 2023 PA channel would cut into the southeastern rock side slope and would also cut into the northwestern sand side slope.

The MIKE-3 HD model results indicate that the 2023 PA channel would increase peak ebb current speeds between approximately 400 and 600 feet northwest of the centerline (toward North Jetty), and the increased speeds would be contained within the 2023 PA channel outline. As noted above for other locations, this potential increased current speed is a factor that would be considered within the project's risk management framework. The sandy bed and side slopes may adjust to be in equilibrium with the increased current speed, and it is expected that these bed adjustments would be contained within the limits of the future equilibrium side slope. Elsewhere, the 2023 PA channel is expected to have lower current speeds than the Existing Conditions.

RM 1.3 to RM 0.9

In this reach between the turn and RM 1, the channel is characterized by exposed rock on the far left (south) side slope, highly varying thickness of sand over rock in the main channel, and sand on the right (north) side slope up to the toe of the North Jetty rubble structure. Stations 1+1+62 and 0+50+62 (Figure 3-40 and Figure 3-41) were used to represent typical cross-sections in this reach.

The MIKE-3 HD model results indicate that the 2023 PA channel would increase peak ebb current speeds within approximately 400 feet north of the channel centerline, as the increased conveyance due to the channel cut would allow greater flow volumes through the main channel. Further toward the sandy side slope, the 2023 PA channel peak ebb current speeds are expected to be less than the Existing Conditions. It is expected that bed adjustments to equilibrate with this increased peak ebb current speeds would be contained within the limits of the future equilibrium side slope.

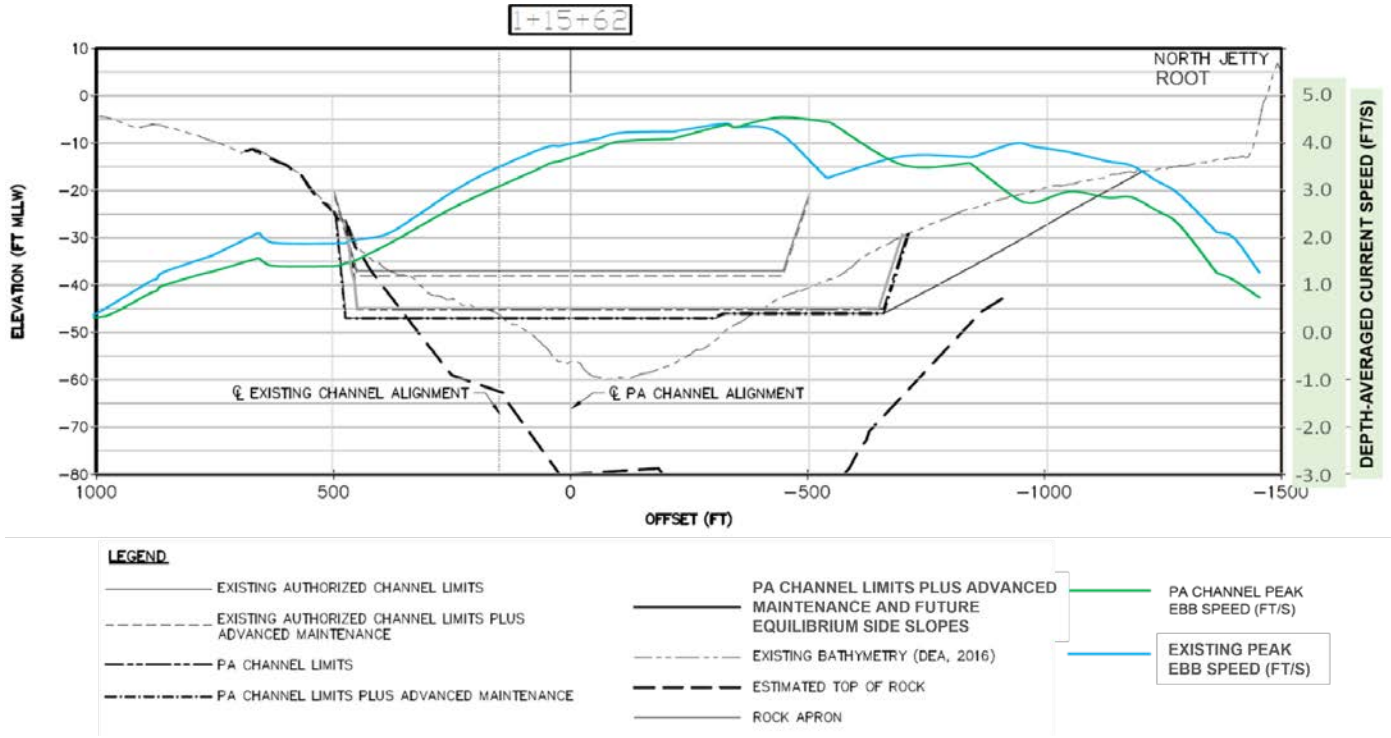

Figure 3-39
Cross-section at 1+15+62 Representing RM 1.4 to RM 1.3 (Looking Downstream)

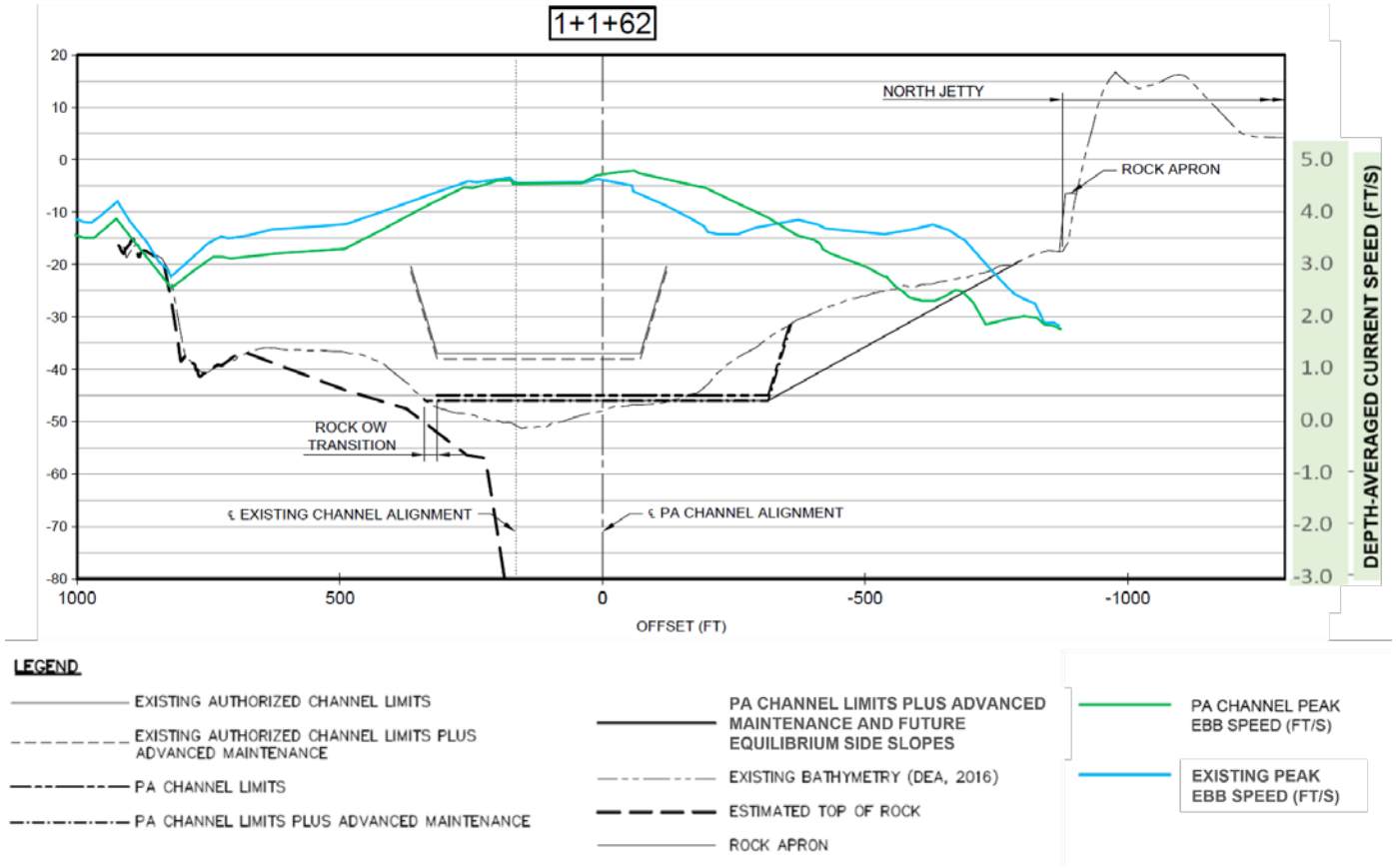

Figure 3-40
Cross-section at 1+1+62 Representing RM 1.3 to RM 0.9 (Looking Downstream)

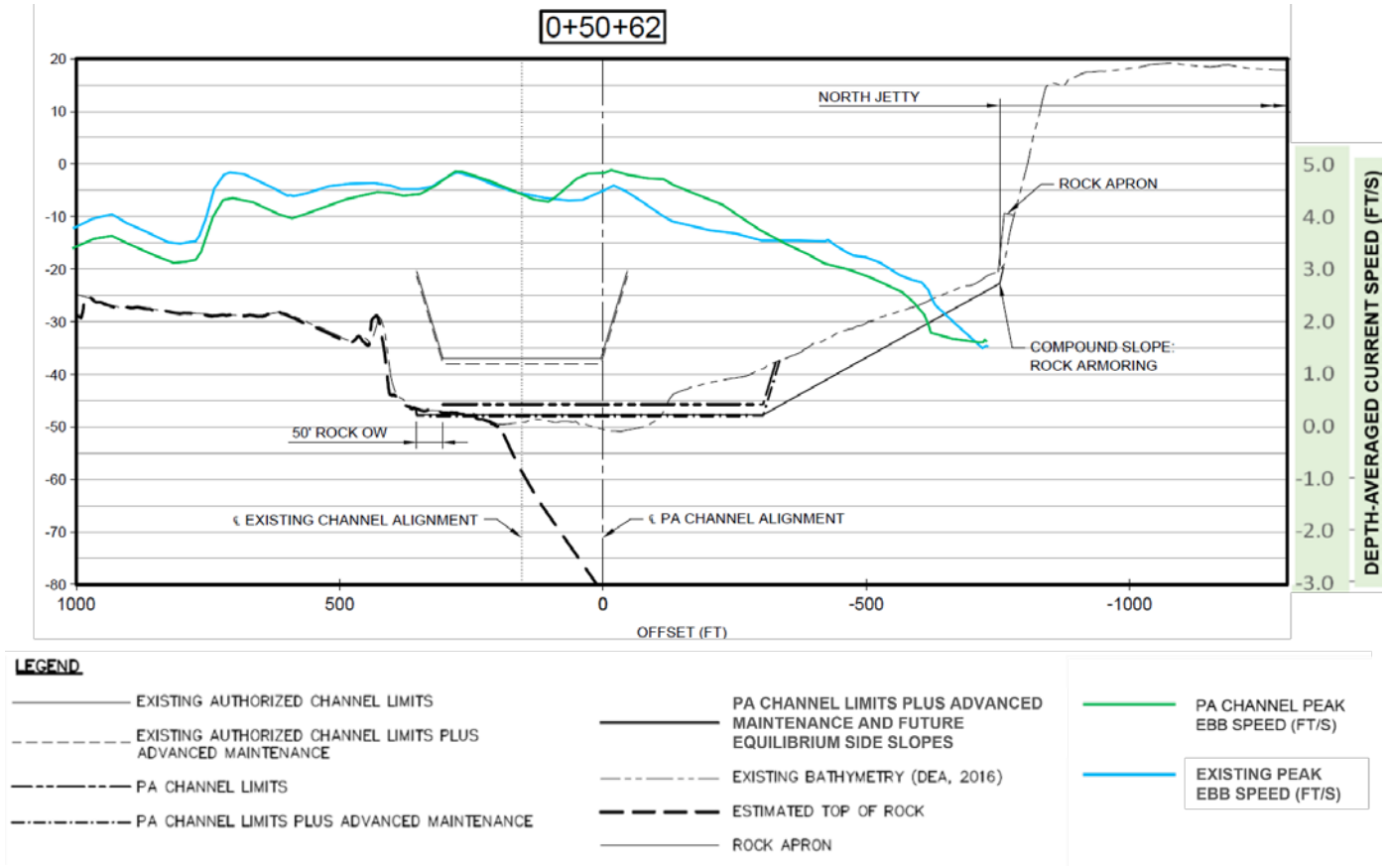

Figure 3-41
Cross-section at 0+50+62 Representing RM 1.3 to RM 0.9 (Looking Downstream)

3.7 Conclusions

To assess possible changes as a result of the proposed navigation channel improvements, the general approach in this study was to explicitly model both the Existing Conditions and the 2023 PA scenarios and to compare the results. The model inputs and constants for both scenarios were the same and the only difference was the model bathymetry for each scenario.

The MIKE-3 HD model results show that the mean tidal range (e.g., the difference in height between mean high water and mean low water) generally increases starting at the mouth and moving upstream. The 2023 PA channel results in a slight increase (less than 0.1 ft) of mean tidal range, with the maximum of 0.1 feet, the mean of 0.04 feet, and the mode of 0.05 feet throughout the estuary. In the South Slough, the increase in mean tidal range does not exceed 0.04 ft. In the Isthmus Slough, the Coos River, and the Haynes Inlet, the increase in mean tidal range does not exceed 0.06 ft. The maximum increase occurs in the FNC, where the mean tidal range increases by 0.09 ft (corresponding to a 1.6% increase in mean tidal range). These slight increases in mean tidal range are consistent with the expected response of this hydraulically efficient estuary system to the proposed channel improvements.

The HD model results further indicate a reduction in current velocity at RM 5 and RM 8 for the 2023 PA, because it increases the flow cross-sectional area by deepening and widening the turning basins while the tidal prism increases by less than 1.6%. As roughly the same volume of water passes through a larger cross-section, it is expected to lower the current velocity.

Except at RM 5 and RM 8, the 2023 PA predicts an increase of current velocity of generally less than 0.25 ft/s in the estuary and tributaries. The maximum increase occurs along the channel alignment at RM 2, where the ebb current velocity increases by 0.55 ft/s. This probably results from the proposed change in channel alignment here, i.e., the 2023 PA alignment directs more flow towards the channel centerline.

Based on more detailed analysis of the morphology and hydrodynamics between RM 1.0 and RM 3.0, the 2023 PA is not expected to cause adverse impacts on channel morphology or the morphology or stability of adjacent structures and river features. It should be noted that the channel and estuary bathymetry will be monitored post-construction of the channel improvements as part of the Adaptive Risk Management Plan.

Commented [CT29]: PDT A-3-7: Add sentence describing what the increase in max current magnitude was for the areas of interest discussed in the part of the report for results summarized in Section 3.6.1.

Commented [CT30R29]: Added max. ebb current velocity increases by 0.55 fps.

4. SALINITY MIXING MODELING

The salinity regime in Coos Bay is strongly seasonal resulting from the highly variable freshwater inflow mixing with saltwater from the ocean. This estuary can be well-mixed to highly stratified, depending on the intensity of freshwater inflow. Field measurements of salinity profiles throughout a year showed that the estuary is well-mixed for low river discharge (less than 1,100 cfs), shows salt-wedge characteristics for high river discharge (greater than 5,300 cfs), and is partially-mixed for river discharges between these thresholds; see Sutherland & O'Neill (2016) for further details.

The salinity model builds upon the MIKE-3 HD model presented in Section 3. This section presents the changes in salinity under the 2023 PA relative to the Existing Conditions. Evaluation of salinity changes was performed for three simulation periods to capture a range of tidal and inflow conditions. The following three scenarios with different combinations of freshwater inflow and tide scenarios were used for production runs:

- A summer period (1-month including spring tide and neap tide) with constant low freshwater inflow from 07/01/2011 to 08/01/2011.
- A winter period with spring tide and freshwater inflow from 01/11/2011 to 01/31/2011.
- A winter period with neap tide and freshwater inflow from 01/11/2011 to 01/31/2011.

4.1 Modeling System

Numerical simulation of salinity mixing was conducted also using the MIKE-3 FM suite with coupled hydrodynamic and salinity modules, see DHI 2017 for a detailed description of the modeling system. A three-dimensional numerical scheme was used so that the strongly seasonal salinity variations in the estuary can be resolved. Estuary hydrodynamics and salinity are mutually affected because water density varies with salinity and temperature. Horizontal gradients in water density and buoyancy cause density-driven flows such as freshwater flow over seawater and propagation of seawater further into the estuary.

As noted in Section 3.3, USACE approved the use of the MIKE-3 FM suite for this application.

4.2 Model Setup

4.2.1 Model Grid and Elevation

The same model grids and sources of elevation information as described in Section 3.4.1 were used for salinity mixing modeling and therefore are not reiterated here.

4.2.2 Boundary Conditions

The sources and the methodology used in preparation of offshore tides and upstream freshwater boundary conditions are the same as described in Section 3.4.2.

For the salinity boundary conditions, a constant value of 33 psu was assumed at the offshore boundaries, and a constant value of 0 psu was assumed at the upstream boundaries (shown in Figure 3-7) following salinity measurements by Moore et al. (2000). Both values were selected to represent typical seawater and freshwater conditions (even though these can vary) and were applied as constants for all simulation cases.

Table 4-1 provides an overview of the boundary conditions for the salinity model. Details of tides and freshwater inflows are provided in each corresponding subsection, for the model calibration, validation, and production runs, respectively.

Table 4-1
Boundary Conditions for Salinity Mixing Modeling Runs

	Input	Source	Data & Period
Calibration/ Validation Runs	Tides (Offshore boundary conditions)	OSU tidal database global solution, TPXO8 1/6 resolution with adjustments based on residuals at NOAA Charleston station	Calibration period: 3-month from 10/10/2012 – 01/20/2013 Validation period: 1-month from 12/17/2011 – 01/16/2012
	Freshwater runoff (Upstream boundary conditions)	Freshwater discharge of Coos River: Based on measured daily discharge provided by the CWA Freshwater discharge of other (much smaller) tributaries: daily discharge was estimated using rainfall-runoff analysis based on monthly rainfall data and drainage area	
	Salinity	Moore et al. (2000) measurements	A constant value of 33 psu at the offshore boundaries, and 0 psu at all upstream boundaries
Production Runs	Tides (Offshore boundary conditions)	Same as calibration runs	(1) A summer period (1-month including spring tide and neap tide) from 07/01/2011 – 08/01/2011 (2) A winter period with spring tide from 01/11/2011 to 01/31/2011 (3) A winter period with neap tide from 01/11/2011 to 01/31/2011
	Freshwater runoff (Upstream boundary conditions)	Same as calibration runs	
	Salinity	Same as calibration runs	Same as calibration runs

For the salinity mixing purposes, a detailed analysis was performed to capture salinity variations from the three salinity stations spreading out in the South Slough watershed. This analysis consisted of delineating the sub-watersheds within South Slough, calculating the area for each, and estimating the corresponding discharge based on these areas. The location map of the sub-watersheds and the assumed source water is shown in Figure 4-1. In lieu of field measurements at these points, discharge from the un-gauged watersheds was estimated based on gauged watershed at Winchester Creek gauge using Equation (1) below – which relates the discharge to the drainage

area for each sub-watershed. The drainage area for Winchester Creek gauge is approximately 6.7 square miles (see Table 2-1). Table 4-2 lists the estimated drainage area for each sub-watershed.

$$Q_{ungaged} = Q_{gaged} \times \frac{A_{ungaged}}{A_{gaged}}$$

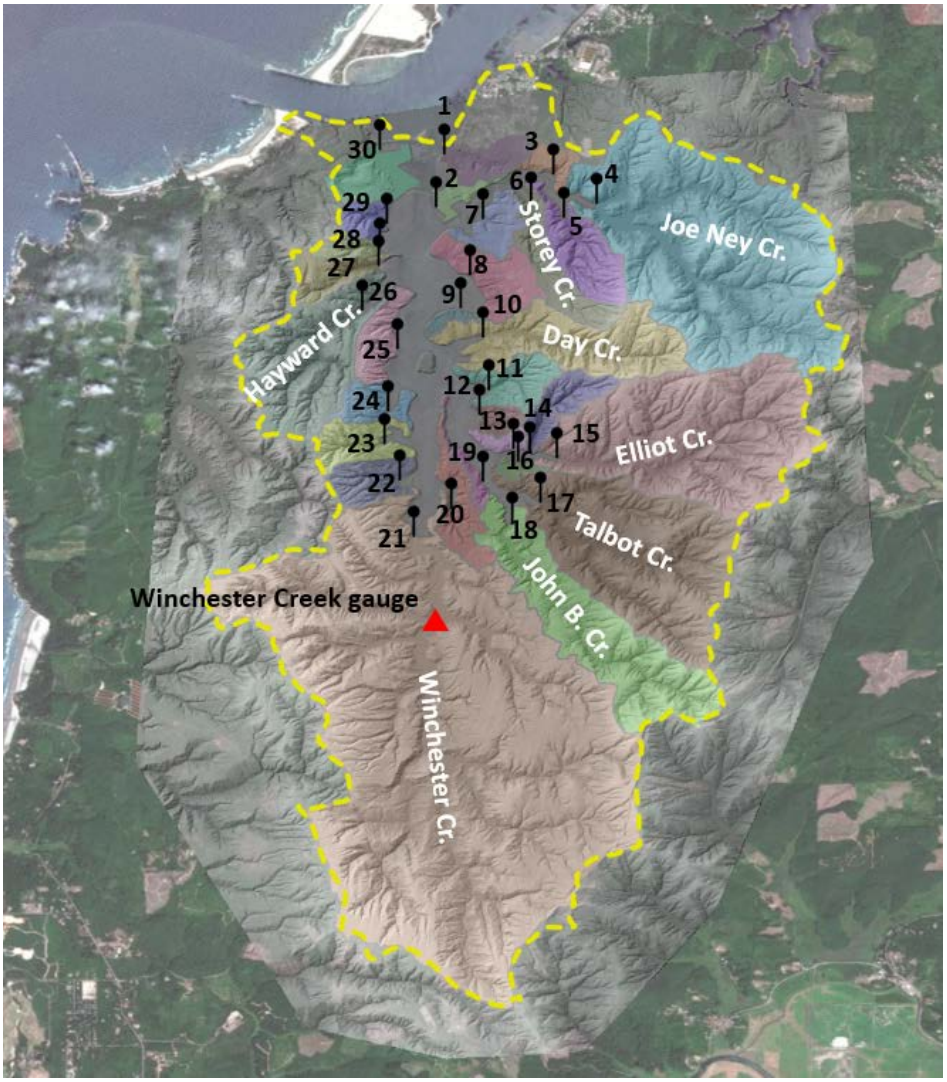

Figure 4-1
Map of Discharge Points and Corresponding Sub-watersheds in South Slough

Table 4-2
Drainage Area for Sub-watersheds in South Slough

Sub-watershed	Drainage Area (mi^2)	Sub-watershed	Drainage Area (mi^2)	Sub-watershed	Drainage Area (mi^2)
Point1	0.25	Point11	0.31	Point21	10.59
Point2	0.12	Point12	0.11	Point22	0.28
Point3	0.13	Point13	0.08	Point23	0.31
Point4	3.83	Point14	0.29	Point24	0.22
Point5	0.48	Point15	2.62	Point25	0.26
Point6	0.39	Point16	0.06	Point26	1.22
Point7	0.24	Point17	2.28	Point27	0.24
Point8	0.42	Point18	1.57	Point28	0.12
Point9	0.07	Point19	0.10	Point29	0.15
Point10	1.07	Point20	0.33	Point30	0.34

4.3 Model Calibration

4.3.1 Calibration Data

Model calibration was conducted against field measurements by O'Neill (2014). O'Neill performed a series of along-channel salinity sampling during a 21-month period from November 3, 2012 to July 24, 2014. Figure 4-2 shows the sampling transects.

Field measurements by O'Neill (2014) were used for calibration because they captured both well-mixed and stratified conditions, which are critical for assessing the model's ability to capture the estuarine recovery after storms from stratified to well-mixed. It should be noted that O'Neill's data is limited to salinity measurements along the channel.

Two additional off-channel (away from the channel) field measurements were used to demonstrate the model's ability to simulate off-channel processes for the calibration period.

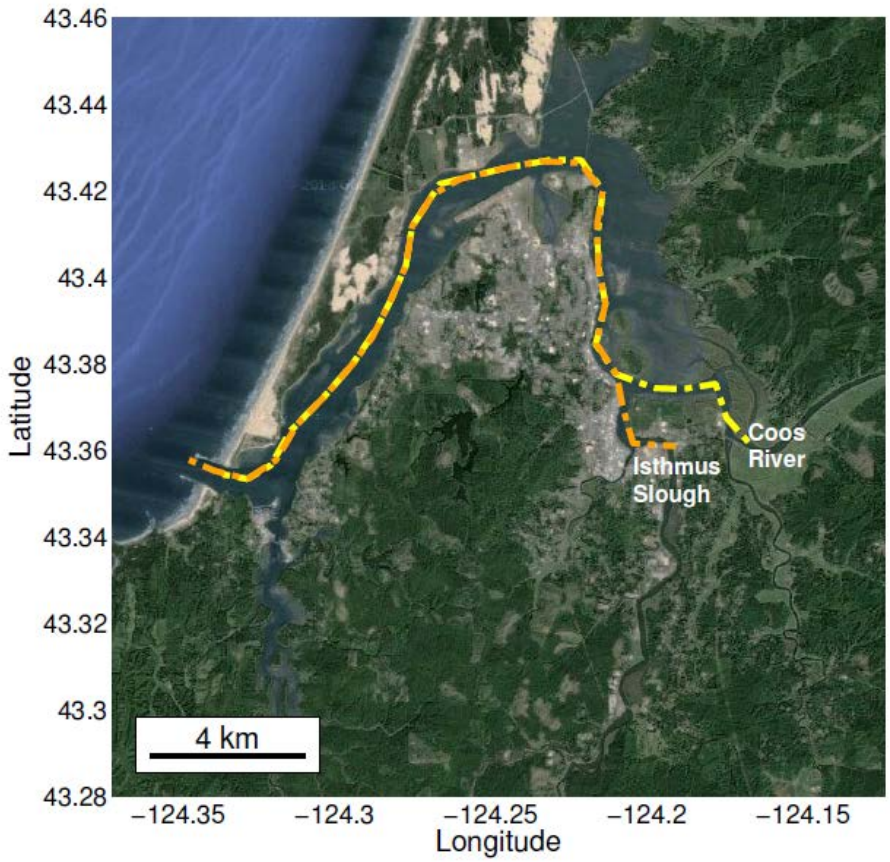

Figure 4-2
Transects for Salinity Sampling Conducted on November 3, 2012 and January 19, 2013 (O'Neill 2014)

4.3.2 Boundary Conditions for Calibration Runs

The calibration period was selected to include both the well-mixed and stratified conditions that occur within Coos Bay. Model calibration was conducted for a 3-month period, covering two salinity measurements on November 3, 2012 and January 19, 2013 (O'Neill 2014). Figure 4-3 provides the real-time daily discharge in the Coos River during this period. This data was used as the upstream freshwater boundary conditions for Coos River in the calibration runs.

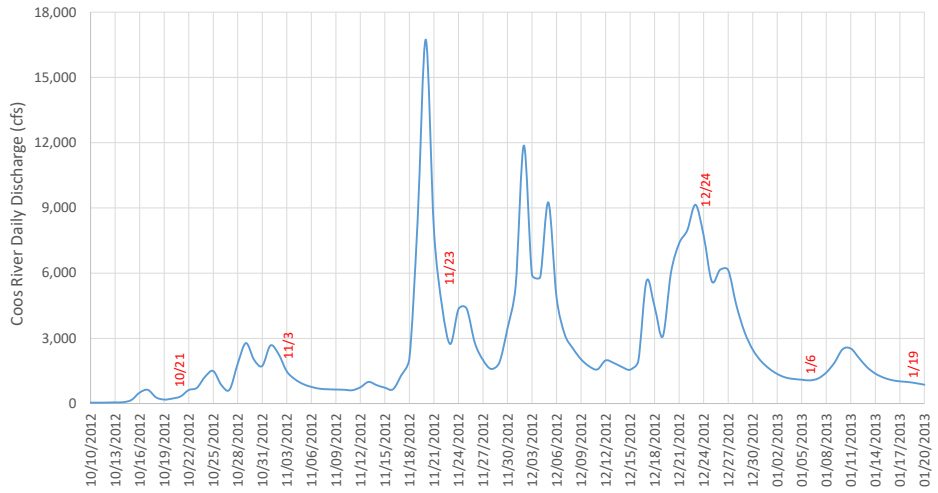

Figure 4-3
Time Series of Coos River Daily Discharge for Salinity Calibration Period

4.3.3 Calibration Results

The salinity model results along the channel for three instantaneous "snapshots" during the calibration period are shown in Figure 4-4. The first snapshot (i.e., October 21, 2012) illustrates a well-mixed salinity condition inside the estuary due to a preceding long, low river flow period. The middle snapshot (i.e., December 24, 2012) illustrates a highly-stratified condition after peak river flow events. The last snapshot (i.e., January 6, 2013) illustrates a partially-mixed condition, which is typical of estuarine recovery from a large storm event when river flow recedes. The results show that the model can capture all salinity regimes as responses to different river flows.

The model results were compared against salinity profiles along the main channel as documented by O'Neill (2014). The main target was the measured salt wedge (> 28 psu) location along the channel. The primary calibration parameter used was the scaled eddy viscosity for horizontal and vertical dispersion.

Vertical and longitudinal salinity distributions were compared between the field measurements and the model results in Figure 4-5 and Figure 4-6 for 11/3/2012 and 1/19/2013, respectively. The November 3, 2012 comparison shows that the salt wedge is approximately at RM 8.7 in both the modeled and measured profiles. The January 19, 2013 comparison shows that the salt wedge is approximately at RM 7.0 in both the modeled and measured profiles. Comparison of the model results against measurements demonstrate the model's ability to simulate salinity mixing regimes and to estimate the location of salt wedge within the estuary.

It should be noted that the measured and modeled salinity profiles are inherently different: measured salinity profiles, as shown in Figure 4-5 top panel and Figure 4-6 top panel, were developed based on salinity samples taken along the transects over a 1-day period (not concurrently). However, modeled salinity profiles from the model outputs, as shown in Figure 4-5

bottom panel and Figure 4-6 bottom panel, are instantaneous. In addition, the input discharge used in the model was daily-averaged values since more detailed hourly data was not available.

The salinity model results were further compared to the measured salinity at the BLM and EMP water quality stations (locations see Figure 4-8) for the calibration period. Comparison of the model results against measured salinity time histories at these two locations during the calibration period is shown in Figure 4-7. This comparison shows that the modeled and measured salinity are in agreement. The salinity model performance is discussed in the following subsection.

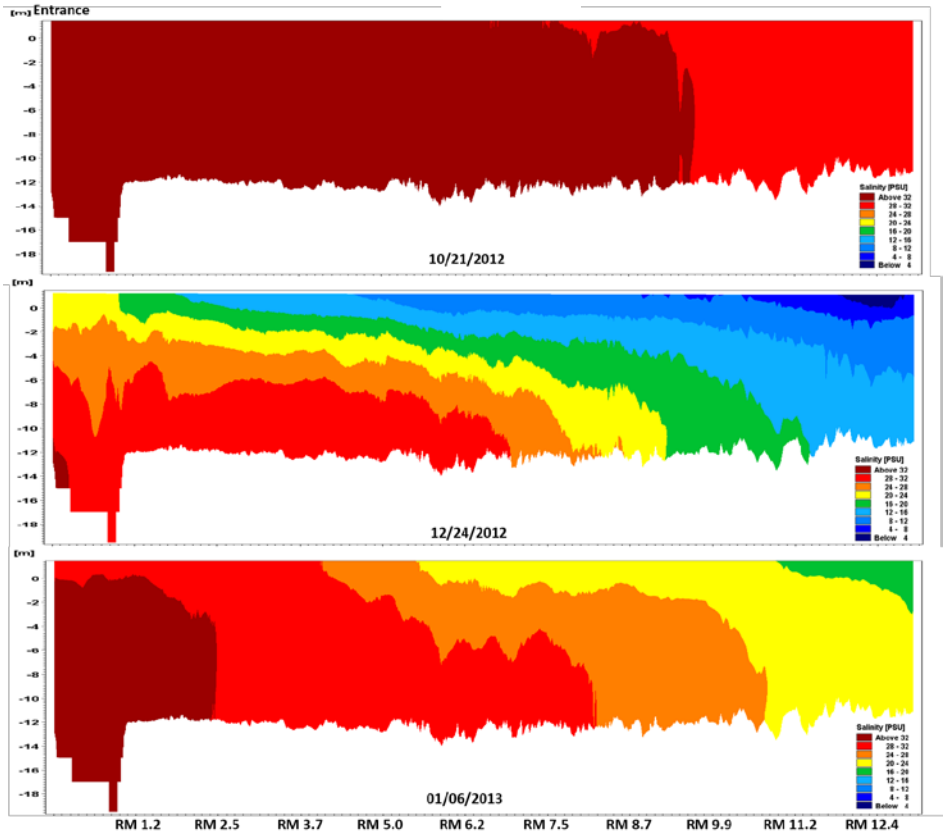

Figure 4-4
Snapshots of Salinity Model Results Representing Three Salinity Regimes on 10/21/2012, 12/24/2012, and 1/6/2013.

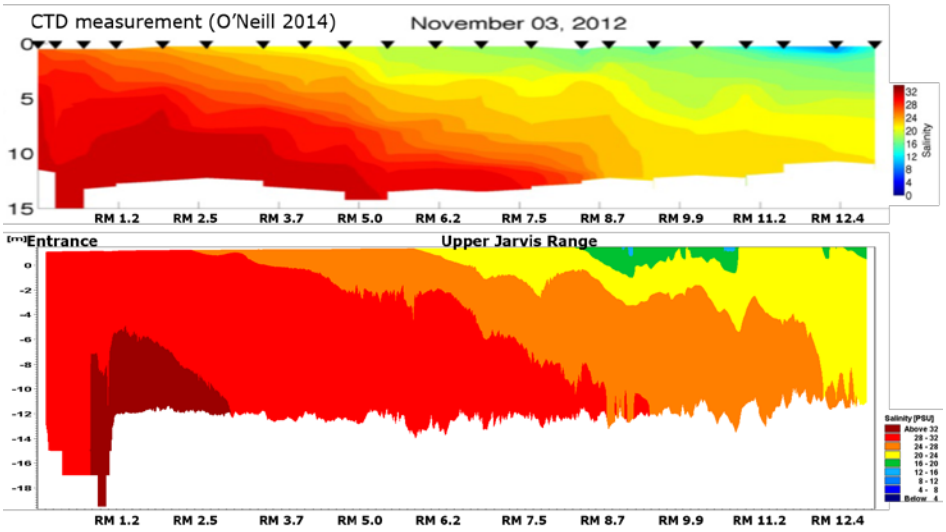

Figure 4-5
Comparison of Salinity Profile on 11/3/2012 between: (Top Panel) Field Measurements by O'Neill (2014) and (Bottom Panel) Salinity Model Results

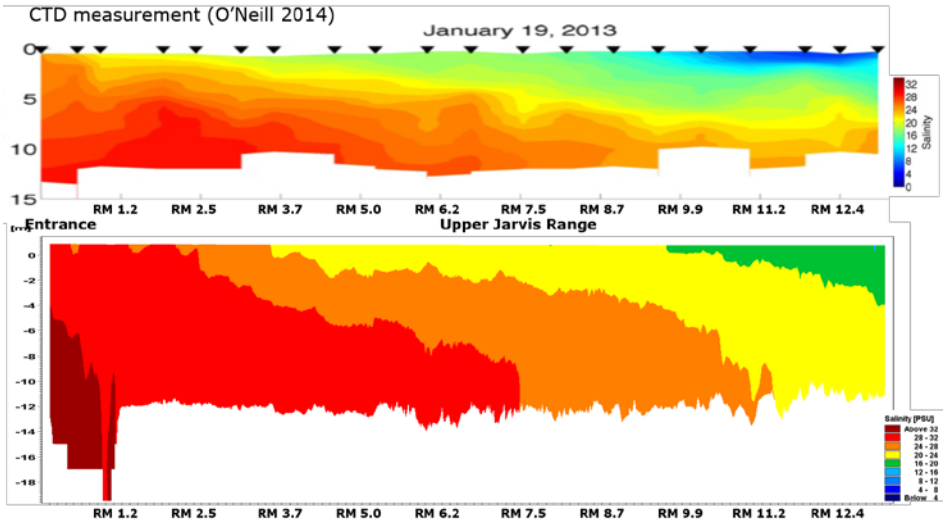

Figure 4-6
Comparison of Salinity Profile on 1/19/2013 between: (Top Panel) Field Measurements by O'Neill (2014) and (Bottom Panel) Salinity Model Results

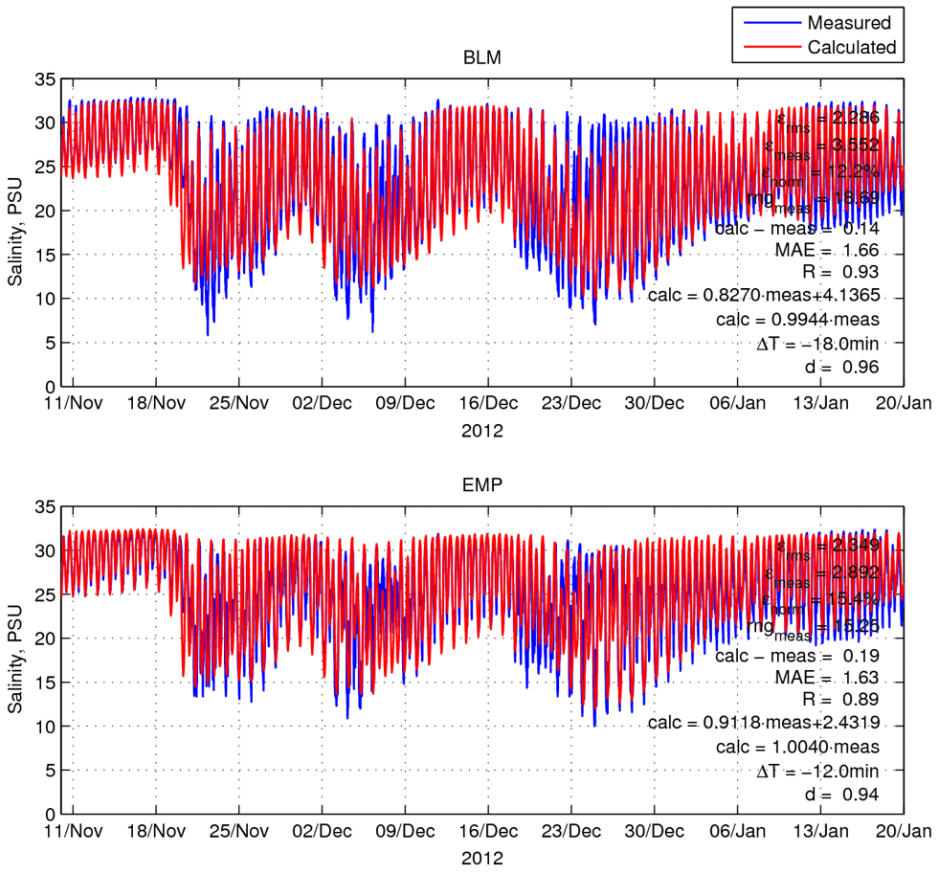

Figure 4-7
Comparison of Modeled vs. Measured Salinity at BLM and EMP Stations during Calibration Period

4.3.4 Model Performance against Similar Projects

There are no specific codes or standards for assessing the performance of salinity models. To assess the performance of this modeling study in representing the Existing Conditions and the 2023 PA, similar and recent studies conducted by ERDC or approved by USACE were compiled and reviewed. A list of these studies and metrics used to report and quantify goodness of fit for time history of salinity at a specific location and stratification regime is summarized in Table 4-3. This study's salinity model performance metrics are provided in the last two rows of the table. It can be seen that this study is consistent with recent and similar modeling studies conducted by ERDC or approved by USACE in terms of salinity model performance.

Table 4-3
Descriptors and Metrics for Reporting Goodness of Fit for Salinity Modeling Results, in Terms of Time History of Salinity at a Specific Location and Stratification Regime, against Observations in Similar and Recent Modeling Studies Conducted by ERDC or Approved by USACE for Channel Modification Projects as well as This Project

Project (Source)	Visual Inspection	Max. Diff	RMSE	IOA	Phase Shift	Sensitivity Analysis	Description of Model Performance
Channel Deepening in Thimble Shoals (Zhang et al. 2017)	✓	10 psu	2 psu	×	×	×	"Sufficient Skill"
Seattle Harbor Deepening EIS (ERDC 2016)	✓	12 psu	×	×	×	×	"Correctly representing"
Redwood City Harbor Navigation Improvement EIS (HydroPlan 2015)	✓	×	×	×	×	×	"Accurate"
Houston-Galveston Navigation Channel (ERDC 2014)	✓	6 ppt*	×	×	×	×	"Acceptable"
Matagorda Ship Channel Study (ERDC 2013)	✓	×	×	×	×	×	×
Savannah Harbor Expansion Project (Tetra Tech 2011)	✓	×	×	×	×	×	×
Grays Harbor Navigation Improvement EIS (ERDC 2010)	✓	×	×	×	×	×	×
This Study (EMP)	✓	6 psu	2 psu	×	×	×	"In agreement"
This Study (BLM)	✓	5 psu	2 psu	×	×	×	"In agreement"

*This value is based on interpretation of results

4.4 Model Validation

The purpose of model validation is to demonstrate that the model simulates the physics of the system for different conditions than those encountered during calibration. Therefore, the calibrated model is re-run during a period other than that used for model calibration, and modeled results are compared against field measurements for the model validation period. An additional goal of validation was to compare model performance with measured data from off-channel field measurements of salinity, since calibration was primarily focused on along-the-channel data.

The criteria for selecting a validation period was defined in coordination with the USACE reviewers as follows:

1. The validation period should be different from the calibration period;
2. Measured flow data must be available for all tributaries;
3. A winter period, preferable with flow above a 1-year return period, should be selected; and
4. The period should maximize the number of water quality sensors with salinity measurements available to validate model performance.

Achieving the validation period criteria was challenging due to limited availability of concurrent measured flow data and measured salinity. As Table 2-1 shows, flow data from the Winchester Creek gauge is not available after 2013. However, as Table 2-4 indicates, many of the upstream water quality stations (North Point, Coos River, Isthmus Slough, and Catching Slough) were not operational until 2013. Ultimately, the period from 12/17/2011 to 01/16/2012 was selected, since (1) it had flow data available from all gauged tributaries and a peak flow above 18,000 cfs, which corresponds to approximately a 2-year flow (see Table 2-2); and (2) this period maximized the number of water quality stations (five stations) with available salinity measurements concurrent with measured flow data.

4.4.1 Validation Data

Model validation was conducted using field measurements from five water quality stations. Period of record as well as the source for each station is listed in Table 4-4. Their location is shown in Figure 4-8.

Table 4-4
Salinity Measurement Stations

Station	Source	Start date	End date	Frequency (min)	Censor Elevation (ft, NAVD88)
BLM	CTCLUSI	02/04/2009	01/11/2017	15	-12.47
EMP	CTCLUSI	06/01/2010	01/11/2017	15	-15.78
Charleston Bridge	NERR	04/20/2002	01/01/2018	15	-4.04
Valino Island	NERR	06/04/1999	01/01/2018	15	-2.56
Winchester Arm	NERR	04/04/1995	01/01/2018	15	0.16

Figure 4-8
Map of Water Quality Stations with Salinity Measurements Used for Model Validation

4.4.2 Boundary Conditions for Validation Runs

The offshore boundary conditions, including water levels and currents, are consistent with those used in the hydrodynamic model described in Section 3.4.2. The measured water levels at Charleston, Oregon during the validation period are shown in Figure 4-9.

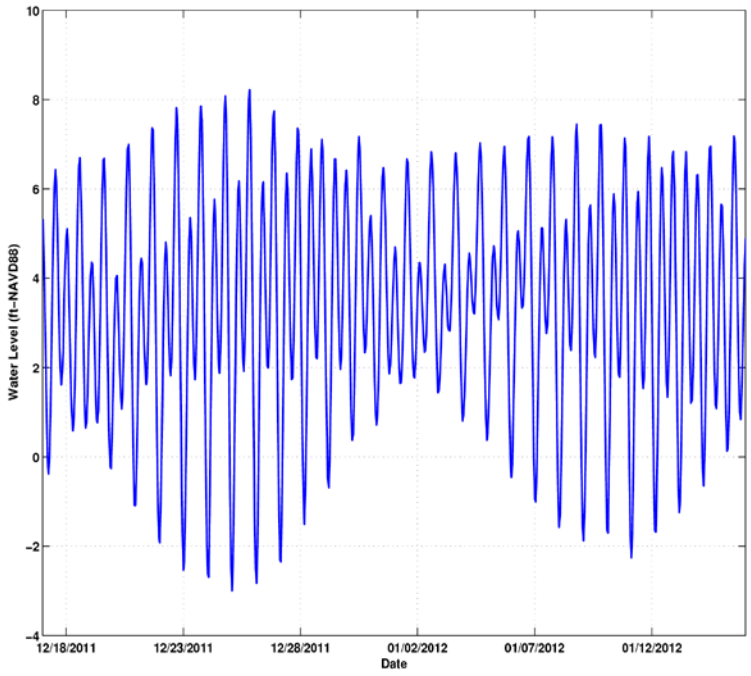

Figure 4-9
Measured Water Levels at Charleston, OR for Salinity Validation Period

Figure 4-10 and Figure 4-11 show the upstream freshwater boundary conditions for the validation period. Their locations are presented in Figure 3-7 and Figure 4-1, respectively.

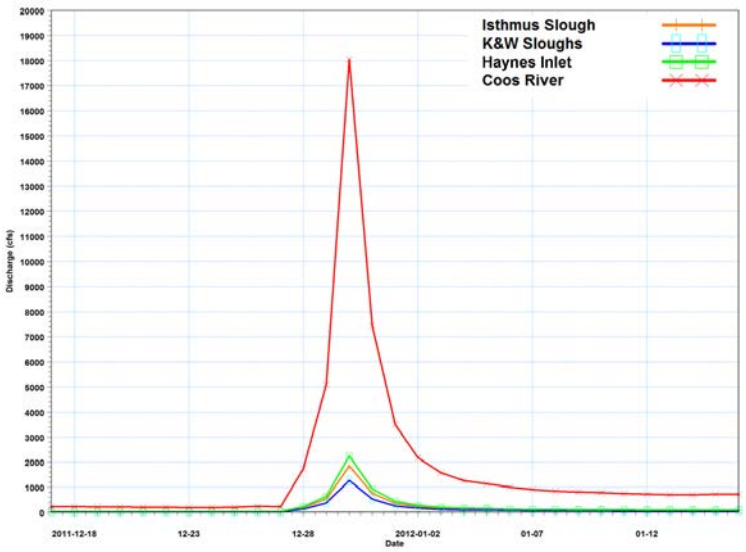

Figure 4-10
Time Series of Daily Discharge Used as Upper Bay Boundary Conditions for Salinity Validation Period

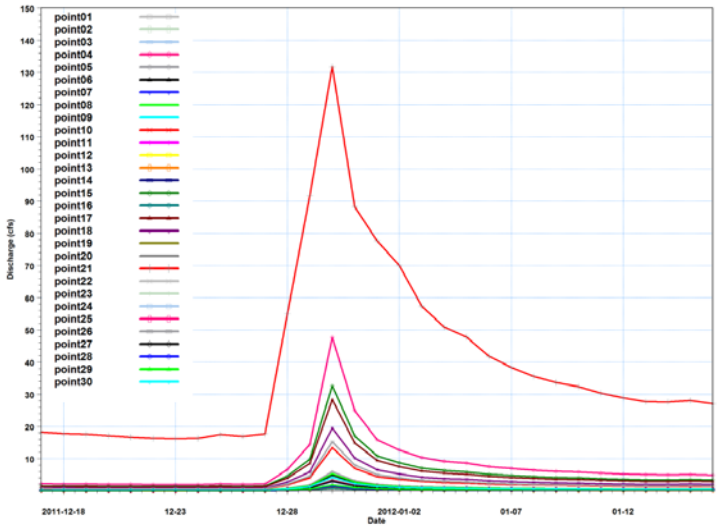

Figure 4-11
Time Series of Daily Discharge Used as South Slough Boundary Conditions for Salinity Validation Period

4.4.3 Validation Results

Modeled salinity was compared against field measurements available at the five water quality stations shown in Figure 4-8. Comparison of salinity time series at all five stations is shown in Figure 4-12 and Figure 4-13. The results show that the model is in agreement with measured salinity at BLM, EMP, Charleston Bridge, and Valino Island in terms of phase and captures local maxima/minima. During the storm period, modeled salinity tends to decrease 1 to 2 tidal cycles before measured salinity. At station Winchester Arm (Figure 4-13), the model can capture only half of the daily salinity variations. Two potential sources of error could be bathymetry (the spacing of the bathymetry was sometimes too sparse to define the main channel) or discharge data (this data was daily-averaged, which cannot represent the variance during the tide cycle). Ultimately, the validation run produced a max difference between 0.8 and 4.4 psu, and a root-mean-square error (RMSE) of 1.1 to 6.2 psu. It should be noted that all stations except for the Winchester Arm had a RMSE less than 2.2 psu.

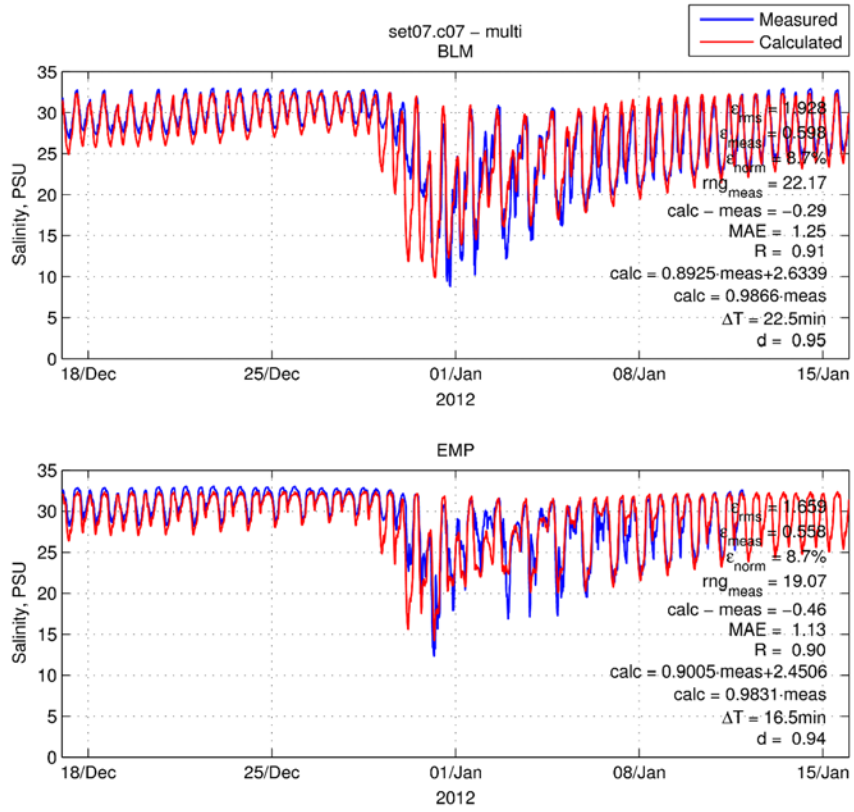

Figure 4-12
Comparison of Model Results to Salinity Measurements at Upper Bay

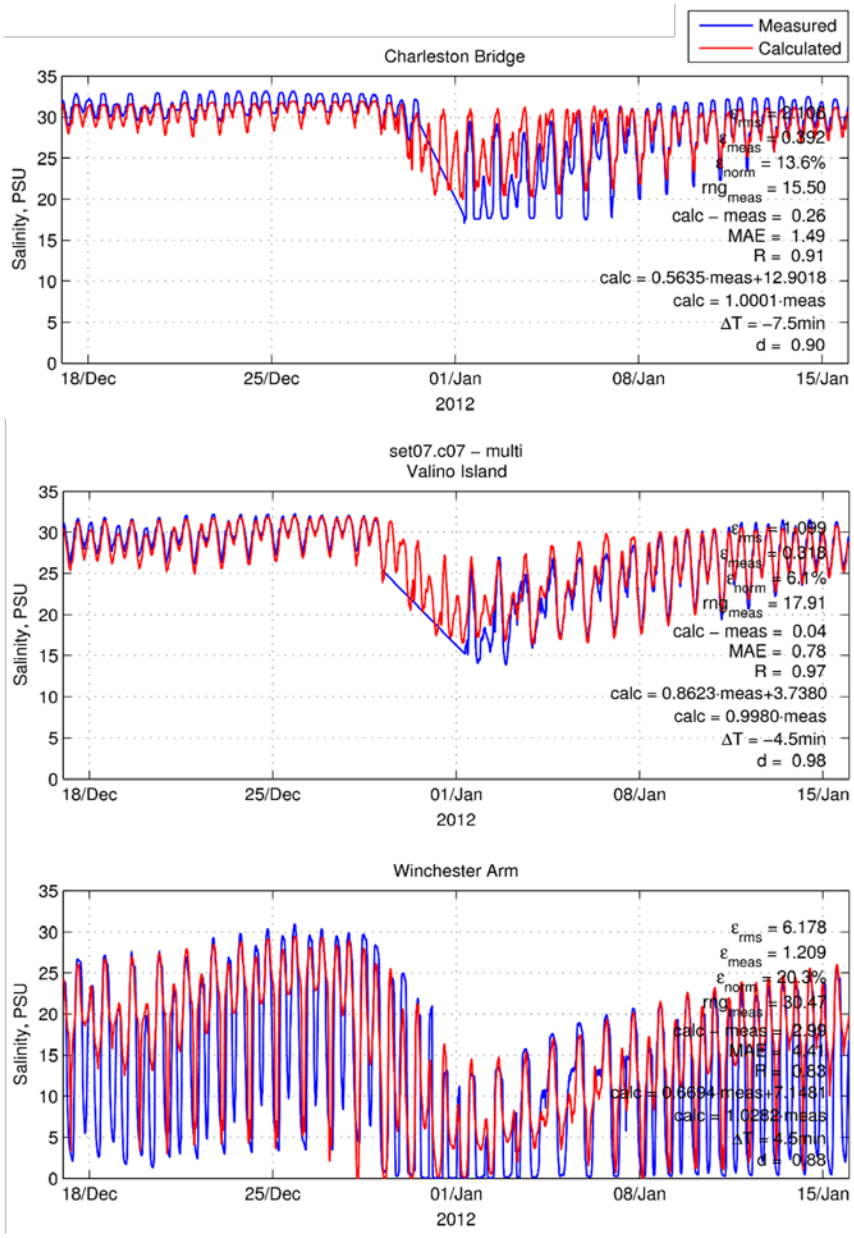

Figure 4-13
Comparison of Model Results to Salinity Measurements at South Slough

4.5 Production Runs

Three production runs with different combinations of freshwater inflows and tides were selected:

- A summer period (1-month including spring tide and neap tide) with constant low freshwater inflow from 07/01/2011 to 08/01/2011.
- A winter period with spring tide and freshwater inflow from 01/11/2011 to 01/31/2011.
- A winter period with neap tide and freshwater inflow from 01/11/2011 to 01/31/2011.

The summer period includes both a spring and a neap tidal cycle and, therefore, the full tidal variability is included in just one simulation. The winter period from 01/11/2011 to 01/31/2011 was selected because it coincided with data availability from the streamflow gauges throughout Coos Bay and contained a peak inflow that corresponded to approximately a 2-year return period storm event followed by a low-flow recovery period. A 2-year return period storm event represents a flow that is sufficiently large to cause stratification throughout the estuary and is also fairly common, occurring every other year on average. This period was simulated so that the peak flow corresponded with both a spring and a neap tidal cycle to explore the full range of flow variability.

4.5.1 Boundary Conditions

4.5.1.1 Summer Period

Upstream freshwater boundary conditions for the summer period were selected based on typical summer low flow rates. The measured water levels at Charleston, OR for the summer period are shown in Figure 4-14, and the freshwater inflows are presented in Table 4-5 and Table 4-6.

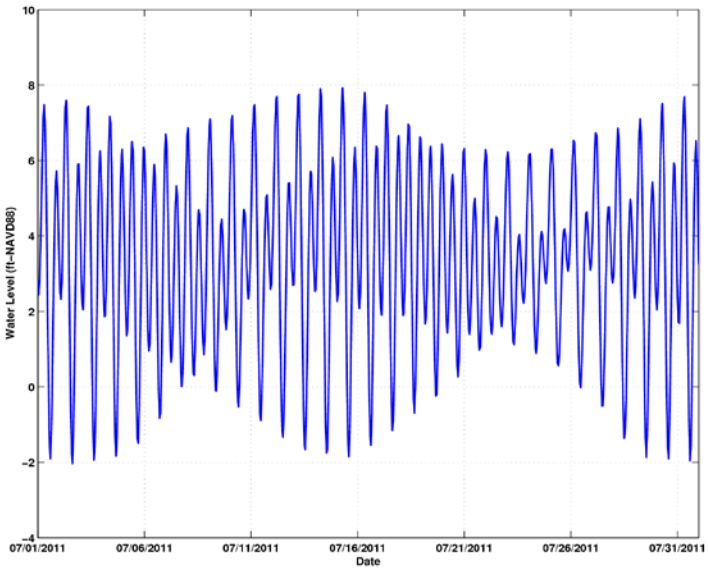

Figure 4-14
Measured Water levels at Charleston, OR for Summer Period

Table 4-5
Freshwater Inflows as Upper Bay Boundary Conditions, Summer Period

Upstream Boundary	Isthmus Slough	K&W Sloughs	Haynes Inlet	Coos River
Discharge (cfs)	8.8	12.5	20.4	70.1

Table 4-6
Freshwater Inflows for South Slough Sub-watersheds, Summer Period

Sub-watershed	Discharge (cfs)	Sub-watershed	Discharge (cfs)	Sub-watershed	Discharge (cfs)
Point1	0.12	Point11	0.15	Point21	5.25
Point2	0.06	Point12	0.06	Point22	0.14
Point3	0.07	Point13	0.04	Point23	0.16
Point4	1.90	Point14	0.14	Point24	0.11
Point5	0.24	Point15	1.30	Point25	0.13
Point6	0.19	Point16	0.03	Point26	0.61
Point7	0.12	Point17	1.13	Point27	0.12
Point8	0.21	Point18	0.78	Point28	0.06
Point9	0.03	Point19	0.05	Point29	0.07
Point10	0.53	Point20	0.16	Point30	0.17

4.5.1.2 Winter Period

The measured water levels at Charleston, OR for the winter period are shown in Figure 4-15. It should be noted that the neap tide for the winter period was actually extracted from 02/23/2011 to 03/15/2011 with a time shift to match the simulation period from 01/11/2011 to 01/31/2011, so that the freshwater inflows will be the same between spring tide and neap tide for the winter period.

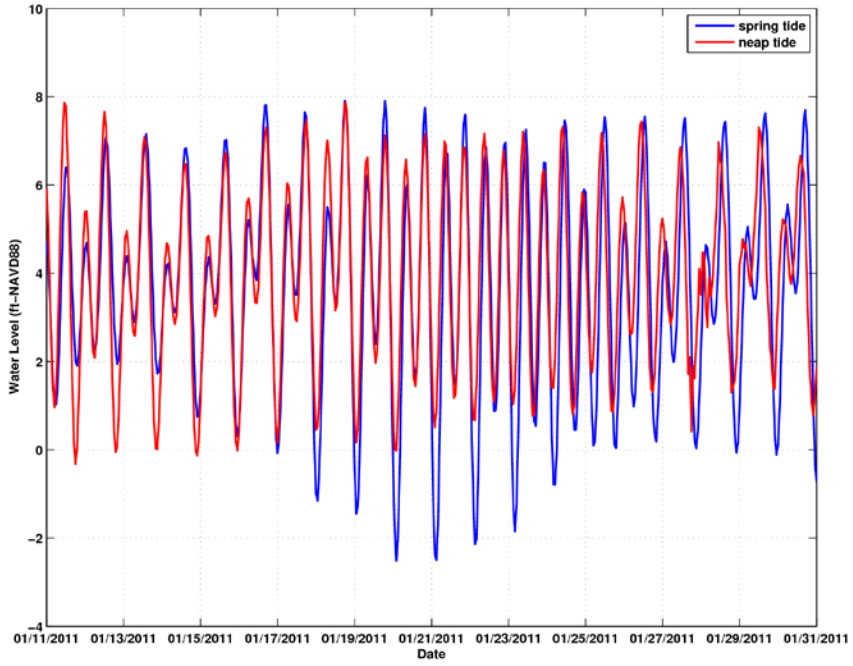

Figure 4-15
Measured Water Levels of Spring and Neap Tide at Charleston, OR for Winter Period

The freshwater inflows used as the Upper Bay boundary conditions for the winter period are shown in Figure 4-16. The peak flow, which occurred on the 6th day of the simulation, is approximately 18,000 cfs in Coos River. The freshwater inflows for the South Slough sub-watersheds are presented in Figure 4-17.

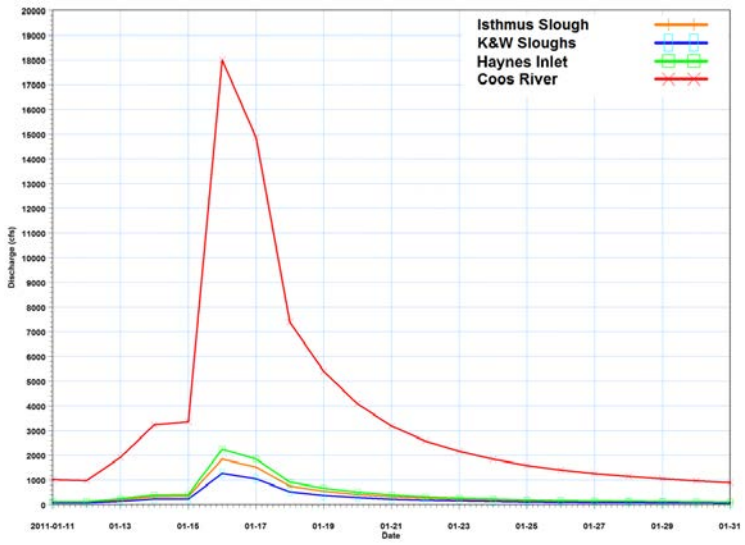

Figure 4-16
Time Series of Daily Discharge Used as Upper Bay Boundary Conditions for Winter Period

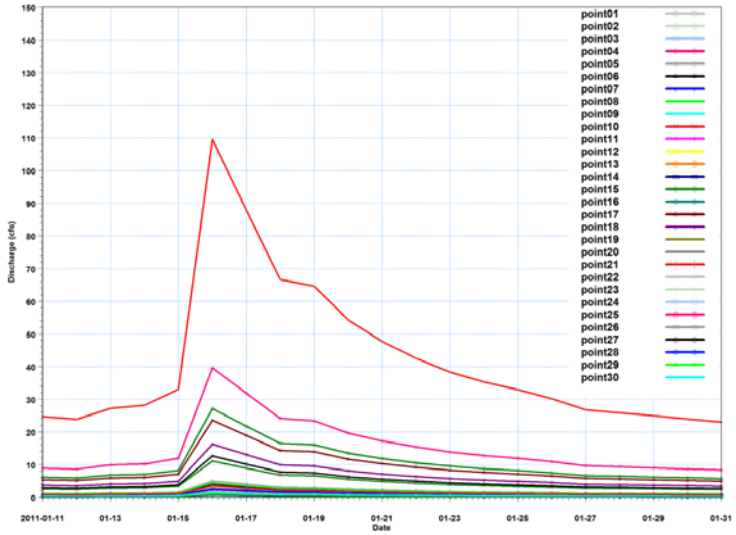

Figure 4-17
Time Series of Daily Discharge Used as South Slough Boundary Conditions for Winter Period

4.5.2 Production Results

The production results consist of summary statistics and time series plots extracted at the observation points shown in Figure 4-18 for the surface, middle, and bottom layer. These points were selected to represent salinity changes throughout the estuary within the main channel, the tributaries, and the shallow water areas.

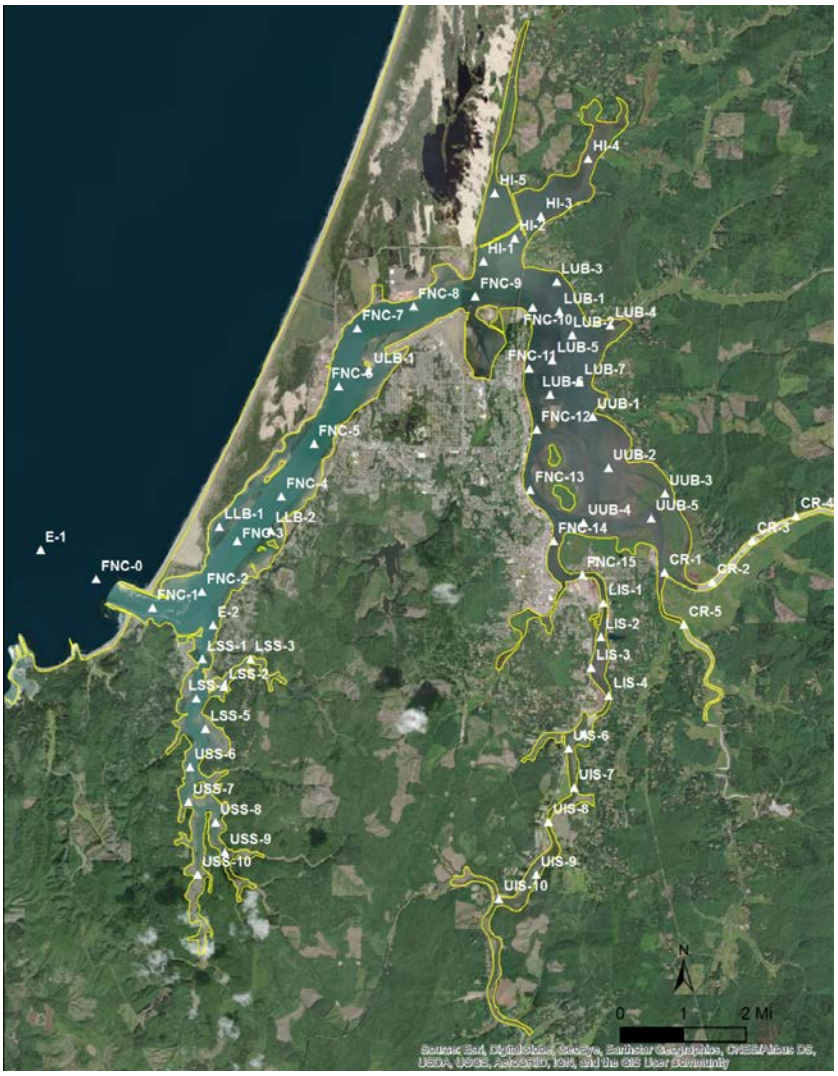

Figure 4-18
Observation Points for Presenting Salinity Model Results

4.5.2.1 Summer Period

The summary statistics including the minimum, mean, and maximum salinity for the summer period and the percent change of mean salinity between the Existing Conditions and the 2023 PA for the surface, middle, and bottom layer are provided in Table 4-7 through Table 4-9. The time series plots are provided in Attachment A.

Under the summer low flow condition, the entire estuary is well-mixed with high salinity. In general, the changes in mean salinity resulting from the 2023 PA are either reduced or unchanged and are between -0.3% and 0.1% (i.e., a negative value indicates a decrease in salinity). The difference in mean salinity does not exceed 0.1 psu.

Table 4-7
Salinity Statistics for Summer Period – Surface Layer

Location	RM/ Slough	Minimum Salinity		Mean Salinity		Maximum Salinity		% Change of Mean
		Existing	2023PA	Existing	2023PA	Existing	2023PA	2023 PA-Existing
E-1	RM -1	32.45	32.51	32.86	32.86	32.96	32.95	0.0%
FNC-0	RM 0	32.29	32.40	32.83	32.85	32.97	32.97	0.0%
FNC-1	RM 1	32.13	32.09	32.79	32.78	32.96	32.96	0.0%
FNC-2	RM 2	31.65	31.92	32.75	32.74	32.96	32.96	0.0%
FNC-3	RM 3	31.71	31.72	32.67	32.65	32.94	32.95	-0.1%
FNC-4	RM 4	30.85	31.17	32.57	32.54	32.94	32.94	-0.1%
FNC-5	RM 5	31.33	29.74	32.46	32.42	32.94	32.94	-0.1%
FNC-6	RM 6	30.02	31.10	32.37	32.29	32.94	32.91	-0.2%
FNC-7	RM 7	30.76	30.78	32.13	32.05	32.92	32.89	-0.3%
FNC-8	RM 8	30.62	30.62	31.98	31.89	32.91	32.88	-0.3%
FNC-9	RM 9	28.93	27.33	31.86	31.80	32.84	32.77	-0.2%
FNC-10	RM 10	30.02	29.78	31.53	31.49	32.66	32.56	-0.1%
FNC-11	RM 11	29.76	29.73	31.31	31.28	32.47	32.45	-0.1%
FNC-12	RM 12	29.29	29.28	31.11	31.08	32.35	32.28	-0.1%
FNC-13	RM 13	28.84	28.84	30.75	30.72	32.12	32.03	-0.1%
FNC-14	RM 14	28.71	28.69	30.49	30.47	31.75	31.72	0.0%
FNC-15	RM 15	29.01	29.03	30.19	30.18	31.25	31.25	0.0%
LLB-1	Lower Bay	22.92	23.20	32.77	32.74	32.96	32.96	-0.1%
LLB-2	Lower Bay	30.75	30.35	32.72	32.69	32.94	32.94	-0.1%
ULB-1	Lower Bay	12.40	12.43	32.35	32.29	32.90	32.83	-0.2%
LUB-1	Upper Bay	26.57	26.69	31.12	31.08	32.70	32.60	-0.1%
LUB-2	Upper Bay	29.41	29.38	31.19	31.16	32.55	32.45	-0.1%
LUB-3	Upper Bay	28.65	28.61	30.77	30.76	32.35	32.26	0.0%
LUB-4	Upper Bay	0.05	0.05	23.50	23.42	30.80	30.78	-0.3%

Commented [JS31]: A-3-21: present data geographically A-3-22: Provide data to EIS team

Commented [JS32R31]: Re-organized the location list based on approximate distance from the entrance and apply to all the following tables. Data will be provided to EIS team as requested.

LUB-5	Upper Bay	30.05	30.02	31.18	31.15	32.65	32.54	-0.1%
LUB-6	Upper Bay	29.78	29.75	31.01	30.99	32.32	32.24	-0.1%
LUB-7	Upper Bay	29.62	29.60	30.71	30.70	31.94	31.90	0.0%
UUB-1	Upper Bay	29.27	29.21	30.39	30.37	31.27	31.26	0.0%
UUB-2	Upper Bay	28.19	28.16	30.09	30.07	31.28	31.30	-0.1%
UUB-3	Upper Bay	18.79	18.79	28.65	28.64	30.36	30.35	-0.1%
UUB-4	Upper Bay	27.81	27.80	30.27	30.25	31.81	31.76	-0.1%
UUB-5	Upper Bay	26.02	26.01	29.20	29.18	31.02	31.01	-0.1%
E-2	South	28.84	28.84	32.66	32.67	32.95	32.95	0.0%
LSS-1	South	27.85	27.85	32.48	32.49	32.94	32.94	0.0%
LSS-2	South	7.26	7.35	32.27	32.28	32.90	32.90	0.0%
LSS-3	South	9.63	9.58	31.19	31.21	32.67	32.67	0.1%
LSS-4	South	26.96	26.97	32.36	32.36	32.92	32.92	0.0%
LSS-5	South	1.61	1.54	32.38	32.39	32.92	32.93	0.0%
USS-6	South	27.14	27.15	32.22	32.23	32.90	32.90	0.0%
USS-7	South	23.13	23.10	31.51	31.52	32.90	32.90	0.0%
USS-8	South	23.41	23.41	31.03	31.05	32.75	32.75	0.0%
USS-9	South	12.41	12.45	30.27	30.29	32.35	32.38	0.0%
USS-10	South	9.83	9.83	29.63	29.64	32.70	32.71	0.0%
LIS-1	Isthmus	28.29	28.10	30.14	30.13	31.12	31.15	0.0%
LIS-2	Isthmus	24.49	23.92	30.10	30.09	31.03	31.02	0.0%
LIS-3	Isthmus	27.96	27.95	30.05	30.04	30.83	30.82	0.0%
LIS-4	Isthmus	29.20	29.27	29.98	29.98	30.62	30.62	0.0%
LIS-5	Isthmus	29.41	29.42	29.93	29.93	30.45	30.45	0.0%
UIS-6	Isthmus	29.19	29.19	29.88	29.88	30.46	30.46	0.0%
UIS-7	Isthmus	28.98	28.98	29.81	29.81	30.46	30.46	0.0%
UIS-8	Isthmus	28.59	28.62	29.74	29.74	30.47	30.47	0.0%

UIS-9	Isthmus	28.75	28.73	29.67	29.67	30.47	30.47	0.0%
UIS-10	Isthmus	27.68	27.68	29.11	29.11	30.41	30.41	0.0%
CR-1	Coos River	23.48	23.48	27.41	27.39	30.45	30.44	-0.1%
CR-2	Coos River	20.24	20.15	23.86	23.80	29.74	29.74	-0.2%
CR-3	Coos River	17.55	17.49	20.81	20.76	28.74	28.73	-0.2%
CR-4	Coos River	15.50	15.64	18.42	18.38	21.50	21.56	-0.2%
CR-5	Coos River	26.72	26.71	27.98	27.96	28.82	28.81	0.0%
HI-1	Haynes	12.98	12.98	31.44	31.41	32.61	32.48	-0.1%
HI-2	Haynes	29.18	29.14	31.22	31.20	32.58	32.42	-0.1%
HI-3	Haynes	19.66	19.67	30.44	30.41	32.04	32.02	-0.1%
HI-4	Haynes	7.16	7.35	28.00	27.98	30.93	30.92	-0.1%
HI-5	Haynes	29.29	29.30	31.32	31.31	32.19	32.21	0.0%

Table 4-8
Salinity Statistics for Summer Period – Middle Layer

Location	RM/ Slough	Minimum Salinity		Mean Salinity		Maximum Salinity		% Change of Mean
		Existing	2023PA	Existing	2023PA	Existing	2023PA	2023 PA-Existing
E-1	RM -1	32.72	32.72	32.90	32.90	32.97	32.95	0.0%
FNC-0	RM 0	32.51	32.58	32.90	32.90	32.97	32.97	0.0%
FNC-1	RM 1	32.30	32.37	32.86	32.86	32.96	32.97	0.0%
FNC-2	RM 2	32.12	32.26	32.82	32.83	32.96	32.96	0.0%
FNC-3	RM 3	31.97	32.09	32.76	32.77	32.95	32.95	0.0%
FNC-4	RM 4	31.92	31.95	32.71	32.71	32.94	32.94	0.0%
FNC-5	RM 5	31.58	31.61	32.61	32.61	32.94	32.94	0.0%
FNC-6	RM 6	31.35	31.44	32.51	32.48	32.95	32.94	-0.1%
FNC-7	RM 7	31.09	31.11	32.36	32.32	32.93	32.92	-0.1%
FNC-8	RM 8	30.97	30.96	32.20	32.15	32.92	32.89	-0.2%
FNC-9	RM 9	30.78	30.78	32.09	32.03	32.87	32.83	-0.2%
FNC-10	RM 10	30.62	30.58	31.87	31.83	32.78	32.73	-0.1%
FNC-11	RM 11	30.34	30.31	31.65	31.62	32.67	32.58	-0.1%
FNC-12	RM 12	29.85	29.77	31.44	31.41	32.44	32.37	-0.1%
FNC-13	RM 13	29.59	29.59	31.12	31.10	32.17	32.10	-0.1%
FNC-14	RM 14	29.55	29.53	30.74	30.73	31.75	31.72	0.0%
FNC-15	RM 15	29.56	29.56	30.34	30.34	31.41	31.40	0.0%
LLB-1	Lower Bay	31.91	31.84	32.81	32.79	32.96	32.96	-0.1%
LLB-2	Lower Bay	31.28	30.73	32.74	32.72	32.94	32.94	-0.1%
ULB-1	Lower Bay	29.40	28.99	32.42	32.37	32.90	32.83	-0.2%
LUB-1	Upper Bay	28.86	28.83	31.25	31.21	32.69	32.59	-0.1%
LUB-2	Upper Bay	29.78	29.72	31.22	31.19	32.53	32.43	-0.1%
LUB-3	Upper Bay	29.31	29.27	31.17	31.15	32.40	32.30	-0.1%
LUB-4	Upper Bay	17.63	17.29	29.85	29.82	31.24	31.21	-0.1%

LUB-5	Upper Bay	30.05	30.03	31.19	31.16	32.64	32.53	-0.1%
LUB-6	Upper Bay	29.78	29.76	31.11	31.08	32.31	32.22	-0.1%
LUB-7	Upper Bay	29.95	29.92	30.76	30.75	31.92	31.88	0.0%
UUB-1	Upper Bay	29.54	29.51	30.51	30.49	31.33	31.31	-0.1%
UUB-2	Upper Bay	28.83	28.78	30.26	30.25	31.37	31.37	-0.1%
UUB-3	Upper Bay	27.92	27.89	29.38	29.36	30.65	30.62	-0.1%
UUB-4	Upper Bay	28.32	28.30	30.59	30.57	31.84	31.80	-0.1%
UUB-5	Upper Bay	27.81	27.89	29.96	29.94	31.33	31.32	-0.1%
E-2	South	29.16	29.16	32.72	32.72	32.95	32.95	0.0%
LSS-1	South	29.11	29.09	32.64	32.64	32.94	32.95	0.0%
LSS-2	South	27.72	27.74	32.43	32.44	32.91	32.91	0.0%
LSS-3	South	26.33	26.27	31.79	31.80	32.74	32.75	0.0%
LSS-4	South	27.31	27.36	32.44	32.44	32.93	32.93	0.0%
LSS-5	South	22.88	22.80	32.50	32.51	32.92	32.92	0.0%
USS-6	South	27.12	27.13	32.28	32.28	32.90	32.90	0.0%
USS-7	South	25.24	25.25	31.73	31.74	32.90	32.90	0.0%
USS-8	South	25.34	25.33	31.36	31.37	32.76	32.76	0.0%
USS-9	South	23.94	23.46	30.88	30.89	32.37	32.40	0.0%
USS-10	South	19.87	19.81	30.14	30.15	32.70	32.71	0.0%
LIS-1	Isthmus	29.52	29.51	30.24	30.24	31.22	31.21	0.0%
LIS-2	Isthmus	29.50	29.48	30.16	30.15	31.04	31.04	0.0%
LIS-3	Isthmus	29.49	29.48	30.09	30.08	30.85	30.85	0.0%
LIS-4	Isthmus	29.44	29.43	30.00	30.00	30.64	30.64	0.0%
LIS-5	Isthmus	29.41	29.42	29.93	29.93	30.44	30.44	0.0%
UIS-6	Isthmus	29.27	29.27	29.90	29.90	30.47	30.47	0.0%
UIS-7	Isthmus	29.20	29.20	29.86	29.86	30.48	30.48	0.0%
UIS-8	Isthmus	28.84	28.85	29.79	29.79	30.47	30.47	0.0%

UIS-9	Isthmus	28.81	28.78	29.70	29.70	30.47	30.47	0.0%
UIS-10	Isthmus	28.40	28.41	29.37	29.37	30.41	30.41	0.0%
CR-1	Coos River	28.26	28.24	29.52	29.50	30.56	30.55	-0.1%
CR-2	Coos River	28.20	28.23	28.98	28.97	29.78	29.78	0.0%
CR-3	Coos River	28.41	28.41	28.73	28.72	29.18	29.18	0.0%
CR-4	Coos River	28.13	28.13	28.57	28.57	28.90	28.92	0.0%
CR-5	Coos River	28.63	28.60	29.12	29.11	29.60	29.61	0.0%
HI-1	Haynes	28.92	28.97	31.71	31.67	32.63	32.55	-0.1%
HI-2	Haynes	29.54	29.63	31.50	31.47	32.58	32.41	-0.1%
HI-3	Haynes	28.20	28.22	31.23	31.19	32.31	32.26	-0.1%
HI-4	Haynes	24.92	24.77	29.71	29.69	31.13	31.11	-0.1%
HI-5	Haynes	29.29	29.30	31.32	31.31	32.18	32.19	0.0%

Table 4-9
Salinity Statistics for Summer Period – Bottom Layer

Location	RM/ Slough	Minimum Salinity		Mean Salinity		Maximum Salinity		% Change of Mean
		Existing	2023PA	Existing	2023PA	Existing	2023PA	2023 PA-Existing
E-1	RM -1	32.79	32.87	32.93	32.93	32.98	32.97	0.0%
FNC-0	RM 0	32.60	32.69	32.92	32.92	32.98	32.97	0.0%
FNC-1	RM 1	32.46	32.52	32.88	32.88	32.97	32.97	0.0%
FNC-2	RM 2	32.19	32.37	32.84	32.85	32.96	32.96	0.0%
FNC-3	RM 3	32.15	32.27	32.80	32.81	32.95	32.95	0.0%
FNC-4	RM 4	32.17	32.21	32.76	32.77	32.95	32.95	0.0%
FNC-5	RM 5	31.79	32.14	32.69	32.72	32.94	32.94	0.1%
FNC-6	RM 6	31.54	31.60	32.57	32.57	32.94	32.94	0.0%
FNC-7	RM 7	31.24	31.20	32.45	32.42	32.93	32.93	-0.1%
FNC-8	RM 8	31.11	31.07	32.29	32.24	32.91	32.89	-0.1%
FNC-9	RM 9	31.07	31.04	32.14	32.09	32.88	32.81	-0.2%
FNC-10	RM 10	30.76	30.73	31.94	31.90	32.77	32.72	-0.1%
FNC-11	RM 11	30.75	30.74	31.77	31.74	32.66	32.57	-0.1%
FNC-12	RM 12	30.22	30.19	31.55	31.52	32.44	32.38	-0.1%
FNC-13	RM 13	29.95	29.93	31.27	31.25	32.14	32.07	-0.1%
FNC-14	RM 14	29.68	29.68	30.89	30.87	31.74	31.73	-0.1%
FNC-15	RM 15	29.56	29.56	30.39	30.38	31.39	31.37	0.0%
LLB-1	Lower Bay	32.07	32.14	32.83	32.81	32.96	32.96	-0.1%
LLB-2	Lower Bay	31.70	31.44	32.75	32.73	32.94	32.94	-0.1%
ULB-1	Lower Bay	30.64	29.53	32.50	32.44	32.88	32.83	-0.2%
LUB-1	Upper Bay	28.87	28.84	31.27	31.23	32.67	32.57	-0.1%
LUB-2	Upper Bay	29.76	29.70	31.22	31.20	32.51	32.41	-0.1%
LUB-3	Upper Bay	30.12	30.11	31.30	31.27	32.42	32.31	-0.1%
LUB-4	Upper Bay	21.57	21.12	30.44	30.43	31.27	31.26	-0.1%

LUB-5	Upper Bay	30.06	30.03	31.20	31.17	32.61	32.50	-0.1%
LUB-6	Upper Bay	29.79	29.76	31.16	31.13	32.29	32.20	-0.1%
LUB-7	Upper Bay	29.95	29.92	30.78	30.76	31.90	31.86	0.0%
UUB-1	Upper Bay	29.55	29.51	30.55	30.53	31.39	31.35	-0.1%
UUB-2	Upper Bay	28.95	28.91	30.34	30.32	31.41	31.40	-0.1%
UUB-3	Upper Bay	28.55	28.50	29.77	29.75	30.87	30.85	-0.1%
UUB-4	Upper Bay	28.38	28.36	30.67	30.65	31.83	31.79	-0.1%
UUB-5	Upper Bay	28.22	28.17	30.10	30.08	31.39	31.38	-0.1%
E-2	South	29.58	29.60	32.77	32.77	32.95	32.95	0.0%
LSS-1	South	29.85	29.84	32.70	32.70	32.95	32.95	0.0%
LSS-2	South	28.08	28.06	32.47	32.48	32.91	32.92	0.0%
LSS-3	South	27.19	26.98	31.92	31.93	32.74	32.75	0.0%
LSS-4	South	27.50	27.54	32.48	32.48	32.94	32.93	0.0%
LSS-5	South	23.69	23.56	32.51	32.52	32.92	32.92	0.0%
USS-6	South	27.10	27.11	32.29	32.30	32.90	32.90	0.0%
USS-7	South	25.28	25.28	31.79	31.80	32.89	32.89	0.0%
USS-8	South	25.30	25.29	31.40	31.41	32.75	32.75	0.0%
USS-9	South	25.51	25.51	31.03	31.05	32.39	32.42	0.0%
USS-10	South	21.06	20.99	30.26	30.27	32.68	32.70	0.0%
LIS-1	Isthmus	29.55	29.56	30.27	30.26	31.19	31.19	0.0%
LIS-2	Isthmus	29.54	29.54	30.18	30.17	31.02	31.02	0.0%
LIS-3	Isthmus	29.52	29.51	30.10	30.09	30.84	30.84	0.0%
LIS-4	Isthmus	29.47	29.47	30.00	30.00	30.61	30.61	0.0%
LIS-5	Isthmus	29.41	29.41	29.93	29.93	30.42	30.42	0.0%
UIS-6	Isthmus	29.31	29.30	29.91	29.91	30.47	30.47	0.0%
UIS-7	Isthmus	29.28	29.28	29.89	29.89	30.48	30.48	0.0%
UIS-8	Isthmus	28.93	28.94	29.81	29.81	30.48	30.48	0.0%

UIS-9	Isthmus	28.82	28.82	29.71	29.71	30.47	30.47	0.0%
UIS-10	Isthmus	28.60	28.59	29.49	29.49	30.40	30.40	0.0%
CR-1	Coos River	28.28	28.25	29.74	29.72	30.59	30.58	0.0%
CR-2	Coos River	28.40	28.38	29.25	29.23	29.79	29.79	0.0%
CR-3	Coos River	28.73	28.72	28.91	28.91	29.27	29.28	0.0%
CR-4	Coos River	28.72	28.72	28.86	28.86	29.16	29.16	0.0%
CR-5	Coos River	29.32	29.32	29.51	29.50	29.83	29.83	0.0%
HI-1	Haynes	28.97	29.03	31.80	31.76	32.64	32.56	-0.1%
HI-2	Haynes	29.74	29.73	31.60	31.56	32.59	32.44	-0.1%
HI-3	Haynes	28.55	28.59	31.40	31.37	32.41	32.35	-0.1%
HI-4	Haynes	26.25	26.34	29.96	29.94	31.10	31.08	-0.1%
HI-5	Haynes	29.28	29.30	31.31	31.31	32.16	32.17	0.0%

4.5.2.2 Winter Period with Spring Tide

The summary statistics for the winter period with spring tide are presented in Table 4-10 through Table 4-12 for the surface, middle, and bottom layer, respectively. The time series plots are provided in Attachment B. The changes in salinity resulting from the 2023 PA are more pronounced during the winter as compared to the summer period because of higher salinity variability in the winter when the estuary undergoes stratification and subsequent recovery with strong river flows. The results generally show an increase in mean salinity; the deeper, wider channel allows the salt wedge to propagate further upstream, increasing salinity throughout.

For these simulations, the largest percent increases do not correspond to the largest absolute increases, because the largest percentage increases tend to occur where the baseline salinity is lowest (i.e., in Coos River). Overall, the most significant absolute increases in salinity occur upstream of RM 9.0 of the FNC. This phenomenon is a factor of the bathymetry of this reach. The reach upstream of RM 9.0 (also referred to as Upper Bay) has a wide cross-section, with only a relatively narrow portion dredged for the channel. Saltwater tends to concentrate in the deeper, dredged area and, therefore, the salt wedge is most noticeable here. In the Lower Bay (RM < 9.0), by contrast, a larger portion of the cross-section is channelized and the saline water is distributed throughout the channel bottom. The observation points in the Lower Bay (i.e., LLB-1, LLB-2, and ULB-1) generally show a decrease in salinity due to their geographic position in shallow water. These points are located on the shallow banks of the channel; as more saltwater propagates within the deeper main channel, the proportion of freshwater on these shallow banks increases. The difference in mean salinity does not exceed 1 psu.

Larger salinity changes occur at the surface layer than at the middle and the bottom layer. This occurs because salinity levels are generally more variable on the surface than at the bottom, as the bottom layer remains relatively saline.

Table 4-10
Salinity Statistics for Winter Period with Spring Tide – Surface Layer

Location	RM/ Slough	Minimum Salinity		Mean Salinity		Maximum Salinity		% Change of Mean
		Existing	2023PA	Existing	2023PA	Existing	2023PA	2023 PA-Existing
E-1	RM -1	15.50	17.47	27.66	27.72	30.96	30.99	0.2%
FNC-0	RM 0	8.72	10.10	26.74	26.72	32.22	32.40	-0.1%
FNC-1	RM 1	5.62	6.50	25.45	25.34	31.67	31.47	-0.4%
FNC-2	RM 2	4.57	5.50	24.13	24.06	32.56	32.65	-0.3%
FNC-3	RM 3	4.16	4.86	22.95	23.05	31.67	31.29	0.5%
FNC-4	RM 4	3.70	4.24	21.21	21.26	30.91	30.67	0.3%
FNC-5	RM 5	3.02	3.35	19.51	19.38	30.78	30.66	-0.7%
FNC-6	RM 6	2.66	2.67	17.96	18.24	30.95	30.16	1.5%
FNC-7	RM 7	1.93	2.18	16.71	17.01	30.75	29.42	1.8%
FNC-8	RM 8	1.38	1.50	15.37	15.78	29.04	27.26	2.7%
FNC-9	RM 9	1.45	1.51	14.65	14.92	27.50	27.12	1.8%
FNC-10	RM 10	1.10	1.18	13.58	13.95	26.98	27.33	2.8%
FNC-11	RM 11	0.64	0.69	12.93	13.29	25.69	26.34	2.7%
FNC-12	RM 12	0.38	0.41	12.75	13.11	24.54	25.07	2.8%
FNC-13	RM 13	0.14	0.14	11.76	12.08	24.02	24.43	2.8%
FNC-14	RM 14	0.12	0.12	11.96	12.20	22.64	23.15	2.0%
FNC-15	RM 15	0.33	0.33	10.87	11.08	21.92	22.32	1.9%
LLB-1	Lower Bay	3.87	4.66	22.45	21.97	32.88	32.83	-2.1%
LLB-2	Lower Bay	4.19	4.76	20.06	19.95	31.08	30.70	-0.5%
ULB-1	Lower Bay	3.87	3.73	17.70	17.69	29.16	28.19	-0.1%
LUB-1	Upper Bay	0.04	0.03	11.31	11.56	26.11	26.23	2.3%
LUB-2	Upper Bay	0.05	0.05	10.51	10.71	24.32	24.97	1.9%
LUB-3	Upper Bay	0.08	0.12	10.28	10.53	23.05	23.83	2.5%
LUB-4	Upper Bay	0.00	0.00	2.54	2.60	14.50	14.82	2.6%

LUB-5	Upper Bay	0.01	0.01	11.19	11.44	25.11	25.78	2.2%
LUB-6	Upper Bay	0.26	0.16	10.98	11.22	23.16	23.67	2.1%
LUB-7	Upper Bay	0.00	0.00	9.33	9.49	20.45	21.00	1.7%
UUB-1	Upper Bay	0.01	0.01	8.43	8.57	20.07	20.72	1.7%
UUB-2	Upper Bay	0.00	0.00	6.68	6.77	19.60	20.06	1.4%
UUB-3	Upper Bay	0.00	0.00	2.54	2.57	12.02	12.29	1.3%
UUB-4	Upper Bay	0.01	0.01	8.06	8.17	22.49	22.72	1.3%
UUB-5	Upper Bay	0.00	0.00	4.53	4.56	20.19	20.46	0.5%
E-2	South	5.56	6.24	23.06	23.21	30.19	30.16	0.7%
LSS-1	South	6.20	6.89	22.52	22.67	30.15	30.14	0.6%
LSS-2	South	11.82	11.41	21.62	21.69	28.56	28.71	0.3%
LSS-3	South	8.58	8.42	18.60	18.64	26.42	26.81	0.2%
LSS-4	South	7.29	7.75	21.81	21.95	30.17	30.12	0.6%
LSS-5	South	8.73	8.89	21.60	21.72	29.14	29.27	0.6%
USS-6	South	11.45	12.01	21.25	21.36	28.64	28.85	0.5%
USS-7	South	8.14	7.84	19.34	19.43	27.60	27.90	0.5%
USS-8	South	9.89	9.59	18.21	18.30	25.94	26.29	0.4%
USS-9	South	8.20	7.99	16.62	16.69	23.90	24.17	0.5%
USS-10	South	3.45	3.31	14.81	14.88	25.55	25.83	0.4%
LIS-1	Isthmus	0.41	0.41	10.32	10.50	21.71	22.19	1.7%
LIS-2	Isthmus	0.68	0.68	10.33	10.50	21.81	22.27	1.6%
LIS-3	Isthmus	0.79	0.78	9.71	9.86	21.70	22.13	1.5%
LIS-4	Isthmus	1.04	1.03	9.10	9.24	21.16	21.68	1.5%
LIS-5	Isthmus	1.56	1.55	9.24	9.38	20.70	21.15	1.4%
UIS-6	Isthmus	0.83	0.84	7.65	7.73	17.97	18.35	1.1%
UIS-7	Isthmus	0.49	0.50	6.54	6.59	17.27	17.68	0.7%
UIS-8	Isthmus	0.17	0.17	5.03	5.08	14.79	15.01	1.0%

UIS-9	Isthmus	0.09	0.09	4.47	4.48	13.75	14.02	0.4%
UIS-10	Isthmus	0.01	0.01	2.79	2.80	11.44	11.58	0.6%
CR-1	Coos River	0.00	0.00	1.65	1.65	16.28	16.59	-0.3%
CR-2	Coos River	0.00	0.00	0.23	0.24	3.36	3.46	4.7%
CR-3	Coos River	0.00	0.00	0.16	0.17	2.88	2.97	5.3%
CR-4	Coos River	0.00	0.00	0.10	0.11	2.48	2.57	6.3%
CR-5	Coos River	0.00	0.00	3.29	3.38	13.38	13.74	2.9%
HI-1	Haynes	1.03	1.04	12.96	13.36	25.23	25.71	3.1%
HI-2	Haynes	0.80	0.72	11.82	12.09	23.81	25.34	2.3%
HI-3	Haynes	0.05	0.05	9.42	9.64	20.95	21.69	2.4%
HI-4	Haynes	0.00	0.00	5.52	5.64	18.56	18.96	2.2%
HI-5	Haynes	2.40	2.12	13.94	14.40	24.57	25.23	3.3%

Table 4-11
Salinity Statistics for Winter Period with Spring Tide – Middle Layer

Location	RM/ Slough	Minimum Salinity		Mean Salinity		Maximum Salinity		% Change of Mean
		Existing	2023PA	Existing	2023PA	Existing	2023PA	2023 PA-Existing
E-1	RM -1	31.43	30.88	32.60	32.57	32.82	32.83	-0.1%
FNC-0	RM 0	30.10	30.34	32.66	32.63	32.92	32.92	-0.1%
FNC-1	RM 1	20.51	22.13	31.81	31.90	32.90	32.90	0.3%
FNC-2	RM 2	17.15	19.62	31.56	31.60	32.89	32.90	0.1%
FNC-3	RM 3	19.34	20.44	31.54	31.57	32.84	32.86	0.1%
FNC-4	RM 4	20.75	20.40	31.28	31.09	32.78	32.81	-0.6%
FNC-5	RM 5	18.98	18.97	30.47	29.61	32.71	32.65	-2.8%
FNC-6	RM 6	17.59	16.81	29.53	29.31	32.68	32.68	-0.7%
FNC-7	RM 7	11.50	12.23	27.33	27.44	32.52	32.49	0.4%
FNC-8	RM 8	12.98	14.57	27.77	27.83	32.35	32.40	0.2%
FNC-9	RM 9	12.98	13.64	25.97	26.06	31.96	31.77	0.3%
FNC-10	RM 10	13.44	13.85	25.33	25.52	31.40	31.30	0.7%
FNC-11	RM 11	11.42	11.67	23.74	24.05	30.34	30.43	1.3%
FNC-12	RM 12	8.27	8.51	22.96	23.31	29.70	29.78	1.5%
FNC-13	RM 13	6.88	7.04	21.49	21.86	28.84	28.99	1.7%
FNC-14	RM 14	5.00	4.96	19.48	19.85	27.52	27.73	1.9%
FNC-15	RM 15	5.33	5.46	18.08	18.44	26.95	27.08	2.0%
LLB-1	Lower Bay	11.85	13.26	28.56	27.89	32.90	32.88	-2.4%
LLB-2	Lower Bay	4.79	5.38	24.43	24.09	32.51	32.43	-1.4%
ULB-1	Lower Bay	4.13	3.98	21.12	20.66	31.43	30.61	-2.2%
LUB-1	Upper Bay	0.09	0.09	15.37	15.80	26.96	27.19	2.8%
LUB-2	Upper Bay	0.06	0.05	14.06	14.47	25.77	26.05	2.9%
LUB-3	Upper Bay	0.40	0.41	13.13	13.50	26.29	26.39	2.8%
LUB-4	Upper Bay	0.00	0.00	10.47	10.89	23.08	23.51	3.9%

LUB-5	Upper Bay	0.97	1.02	14.14	14.58	26.34	26.78	3.1%
LUB-6	Upper Bay	0.80	0.85	16.21	16.67	26.06	26.58	2.8%
LUB-7	Upper Bay	0.47	0.67	12.53	12.87	23.93	24.25	2.7%
UUB-1	Upper Bay	0.13	0.13	13.03	13.39	23.25	23.51	2.7%
UUB-2	Upper Bay	0.00	0.00	12.10	12.41	23.20	23.63	2.5%
UUB-3	Upper Bay	0.00	0.00	6.83	6.93	18.94	19.17	1.4%
UUB-4	Upper Bay	0.06	0.06	16.58	16.90	26.80	27.23	1.9%
UUB-5	Upper Bay	0.00	0.00	10.25	10.43	23.59	23.86	1.7%
E-2	South	6.16	7.26	25.76	25.76	31.30	31.46	0.0%
LSS-1	South	17.23	16.44	27.95	27.97	32.20	32.13	0.1%
LSS-2	South	12.66	12.50	25.46	25.47	30.72	30.86	0.0%
LSS-3	South	15.00	14.40	22.23	22.25	28.52	28.67	0.1%
LSS-4	South	14.41	13.89	25.72	25.72	31.21	31.41	0.0%
LSS-5	South	12.61	12.47	23.86	23.90	30.09	30.33	0.2%
USS-6	South	12.98	12.59	22.72	22.78	30.10	30.15	0.3%
USS-7	South	11.82	11.47	22.08	22.10	29.51	29.50	0.1%
USS-8	South	11.14	10.70	20.50	20.55	28.22	28.51	0.3%
USS-9	South	10.44	10.00	19.05	19.13	25.69	26.18	0.4%
USS-10	South	3.56	3.44	17.68	17.76	26.89	27.34	0.4%
LIS-1	Isthmus	4.71	4.95	16.60	16.90	26.67	26.81	1.8%
LIS-2	Isthmus	4.16	4.24	15.56	15.84	25.50	25.55	1.8%
LIS-3	Isthmus	3.95	4.03	14.96	15.25	24.87	25.13	1.9%
LIS-4	Isthmus	3.36	3.54	14.08	14.38	24.52	24.73	2.1%
LIS-5	Isthmus	2.72	2.82	11.43	11.61	22.14	22.59	1.6%
UIS-6	Isthmus	2.18	2.30	11.46	11.66	21.14	21.47	1.8%
UIS-7	Isthmus	2.03	2.08	10.51	10.72	20.27	20.67	2.0%
UIS-8	Isthmus	1.30	1.37	9.47	9.66	19.28	19.74	2.0%

UIS-9	Isthmus	0.34	0.31	6.31	6.37	16.27	16.65	1.1%
UIS-10	Isthmus	0.33	0.34	6.06	6.19	15.26	15.65	2.1%
CR-1	Coos River	0.00	0.00	9.15	9.36	20.58	20.89	2.2%
CR-2	Coos River	0.00	0.00	4.95	5.03	17.51	17.86	1.7%
CR-3	Coos River	0.00	0.00	4.28	4.40	16.08	16.39	2.9%
CR-4	Coos River	0.00	0.00	4.18	4.35	17.08	17.51	4.0%
CR-5	Coos River	0.43	0.44	10.16	10.42	19.74	20.19	2.6%
HI-1	Haynes	2.92	3.59	18.34	18.96	29.30	29.47	3.4%
HI-2	Haynes	1.14	1.20	15.62	15.97	26.87	26.97	2.3%
HI-3	Haynes	1.34	1.77	15.37	15.92	25.12	25.45	3.5%
HI-4	Haynes	0.00	0.00	10.19	10.52	20.39	20.93	3.2%
HI-5	Haynes	5.48	5.76	14.58	15.09	24.63	25.33	3.5%

Table 4-12
Salinity Statistics for Winter Period with Spring Tide – Bottom Layer

Location	RM/ Slough	Minimum Salinity		Mean Salinity		Maximum Salinity		% Change of Mean
		Existing	2023PA	Existing	2023PA	Existing	2023PA	2023 PA-Existing
E-1	RM -1	32.76	32.76	32.89	32.89	32.95	32.94	0.0%
FNC-0	RM 0	32.25	32.53	32.86	32.86	32.95	32.94	0.0%
FNC-1	RM 1	28.94	29.37	32.51	32.59	32.94	32.93	0.2%
FNC-2	RM 2	27.45	29.68	32.41	32.63	32.91	32.91	0.7%
FNC-3	RM 3	28.54	29.71	32.41	32.56	32.90	32.90	0.5%
FNC-4	RM 4	28.43	29.06	32.28	32.44	32.86	32.88	0.5%
FNC-5	RM 5	28.02	28.09	32.01	32.13	32.80	32.82	0.4%
FNC-6	RM 6	27.68	28.12	31.71	31.79	32.75	32.77	0.2%
FNC-7	RM 7	26.62	26.67	31.31	31.21	32.64	32.68	-0.3%
FNC-8	RM 8	25.76	25.86	31.01	30.92	32.53	32.59	-0.3%
FNC-9	RM 9	24.56	24.16	30.24	29.96	32.39	32.29	-0.9%
FNC-10	RM 10	21.32	21.03	29.19	28.98	32.14	32.06	-0.7%
FNC-11	RM 11	20.13	20.01	27.87	27.88	31.52	31.41	0.0%
FNC-12	RM 12	18.39	18.27	26.59	26.74	30.56	30.52	0.6%
FNC-13	RM 13	14.43	14.18	25.21	25.43	29.73	29.68	0.9%
FNC-14	RM 14	10.66	10.54	22.69	23.02	28.73	28.76	1.5%
FNC-15	RM 15	6.13	6.67	20.49	20.87	27.73	27.83	1.9%
LLB-1	Lower Bay	20.82	20.64	31.31	30.94	32.91	32.90	-1.2%
LLB-2	Lower Bay	5.61	6.14	26.77	26.54	32.61	32.59	-0.9%
ULB-1	Lower Bay	4.27	4.15	22.65	22.11	31.76	31.41	-2.4%
LUB-1	Upper Bay	0.11	0.12	17.26	17.79	27.44	27.75	3.0%
LUB-2	Upper Bay	0.06	0.06	15.10	15.58	26.51	26.88	3.1%
LUB-3	Upper Bay	0.53	0.55	14.33	14.67	26.64	26.59	2.4%
LUB-4	Upper Bay	0.00	0.00	12.73	13.25	24.44	24.81	4.1%

LUB-5	Upper Bay	0.99	1.03	15.54	16.02	26.79	27.09	3.1%
LUB-6	Upper Bay	0.86	0.91	18.93	19.44	28.56	28.96	2.7%
LUB-7	Upper Bay	0.71	0.75	14.09	14.52	25.58	26.01	3.1%
UUB-1	Upper Bay	0.52	0.61	15.28	15.74	25.55	26.28	3.0%
UUB-2	Upper Bay	0.00	0.00	14.42	14.79	24.15	24.45	2.5%
UUB-3	Upper Bay	0.00	0.00	9.90	10.04	21.23	21.46	1.4%
UUB-4	Upper Bay	0.06	0.06	19.56	19.91	27.61	27.86	1.8%
UUB-5	Upper Bay	0.00	0.00	14.73	15.08	24.95	25.21	2.3%
E-2	South	7.74	8.41	27.07	27.09	32.08	32.19	0.1%
LSS-1	South	18.68	17.69	29.59	29.69	32.40	32.33	0.3%
LSS-2	South	12.50	12.40	27.30	27.31	31.50	31.47	0.1%
LSS-3	South	15.42	14.92	23.97	23.95	30.06	29.97	-0.1%
LSS-4	South	14.86	14.28	27.22	27.27	31.99	31.73	0.2%
LSS-5	South	14.91	14.66	25.31	25.33	30.58	30.70	0.1%
USS-6	South	12.98	12.59	23.55	23.58	30.37	30.43	0.1%
USS-7	South	12.49	12.13	23.11	23.11	29.61	29.61	0.0%
USS-8	South	11.22	10.81	21.14	21.18	28.65	28.81	0.2%
USS-9	South	10.50	10.04	19.77	19.84	26.87	27.27	0.4%
USS-10	South	3.76	3.63	18.30	18.38	27.05	27.47	0.4%
LIS-1	Isthmus	5.28	5.53	18.55	18.91	26.74	26.90	2.0%
LIS-2	Isthmus	4.98	5.28	17.40	17.75	26.30	26.50	2.0%
LIS-3	Isthmus	5.03	5.30	17.20	17.56	26.05	26.26	2.1%
LIS-4	Isthmus	4.25	4.38	15.79	16.13	25.34	25.58	2.2%
LIS-5	Isthmus	2.71	2.79	12.38	12.61	22.41	22.87	1.8%
UIS-6	Isthmus	2.43	2.56	13.44	13.72	22.39	22.87	2.1%
UIS-7	Isthmus	2.35	2.48	12.76	13.04	20.65	21.12	2.3%
UIS-8	Isthmus	1.62	1.74	11.33	11.60	19.76	20.20	2.4%

UIS-9	Isthmus	0.39	0.43	7.49	7.61	17.71	18.06	1.6%
UIS-10	Isthmus	1.09	1.17	8.36	8.57	16.22	16.67	2.5%
CR-1	Coos River	0.02	0.02	12.63	12.96	22.95	23.47	2.6%
CR-2	Coos River	0.00	0.00	9.04	9.27	20.84	21.28	2.6%
CR-3	Coos River	0.00	0.00	7.30	7.49	18.75	19.19	2.7%
CR-4	Coos River	0.00	0.00	5.96	6.17	17.93	18.37	3.4%
CR-5	Coos River	11.04	11.35	16.42	16.71	21.55	22.02	1.8%
HI-1	Haynes	3.70	4.90	22.05	22.33	31.19	30.87	1.3%
HI-2	Haynes	1.67	1.88	17.03	17.41	27.11	27.27	2.2%
HI-3	Haynes	2.23	2.83	17.54	18.10	25.58	25.87	3.2%
HI-4	Haynes	0.00	0.00	11.30	11.73	20.84	21.55	3.8%
HI-5	Haynes	5.52	5.80	14.97	15.50	24.67	25.34	3.5%

4.5.2.3 Winter Period with Neap Tide

The summary statistics for the winter period with neap tide are presented in Table 4-13 through Table 4-15 for the surface, middle, and bottom layer, respectively. The time series plots are provided in Attachment C. The results of the neap tide simulations are similar to the patterns/trends of the results for the spring tide simulations, with slightly different values and spatial variations.

Similar to the results presented in Section 4.5.2.2, implementation of the wider, deeper navigation channel generally results in an increase in mean salinity upstream. The largest changes in salinity occur in the portion of the FNC located within the Upper Bay. Again, the points LLB-1, LLB-2, and ULB-1 generally show a decrease in salinity. The difference in mean salinity does not exceed 1 psu.

Table 4-13
Salinity Statistics for Winter Period with Neap Tide – Surface Layer

Location	RM/ Slough	Minimum Salinity		Mean Salinity		Maximum Salinity		% Change of Mean
		Existing	2023PA	Existing	2023PA	Existing	2023PA	2023 PA-Existing
E-1	RM -1	17.01	18.56	28.15	28.25	32.33	31.98	0.4%
FNC-0	RM 0	9.57	10.82	27.28	27.27	32.25	32.32	0.0%
FNC-1	RM 1	6.12	7.02	26.06	25.95	31.99	31.76	-0.4%
FNC-2	RM 2	5.02	6.04	24.82	24.82	32.35	32.49	0.0%
FNC-3	RM 3	4.48	5.41	23.70	23.89	32.26	32.19	0.8%
FNC-4	RM 4	4.04	4.67	21.87	21.79	32.17	32.08	-0.4%
FNC-5	RM 5	3.45	3.77	19.98	19.43	32.26	31.60	-2.8%
FNC-6	RM 6	3.01	3.04	18.14	18.47	30.73	29.91	1.8%
FNC-7	RM 7	2.18	2.43	16.81	17.34	30.17	28.81	3.1%
FNC-8	RM 8	1.63	1.74	15.61	16.13	27.23	26.39	3.3%
FNC-9	RM 9	1.56	1.66	14.88	15.29	25.82	26.75	2.7%
FNC-10	RM 10	1.16	1.23	13.71	14.22	25.24	25.38	3.7%
FNC-11	RM 11	0.67	0.74	13.12	13.54	23.76	23.97	3.2%
FNC-12	RM 12	0.40	0.44	13.06	13.47	22.70	23.30	3.1%
FNC-13	RM 13	0.14	0.15	12.52	12.89	22.69	23.19	3.0%
FNC-14	RM 14	0.13	0.13	12.82	13.14	21.93	22.26	2.4%
FNC-15	RM 15	0.41	0.42	11.89	12.17	21.80	22.19	2.4%
LLB-1	Lower Bay	4.26	5.12	23.16	22.33	32.72	32.60	-3.6%
LLB-2	Lower Bay	4.40	5.00	20.11	20.05	31.26	30.98	-0.3%
ULB-1	Lower Bay	4.03	3.98	17.93	18.06	28.24	27.30	0.7%
LUB-1	Upper Bay	0.04	0.04	11.86	12.21	23.12	23.49	3.0%
LUB-2	Upper Bay	0.02	0.02	11.05	11.31	20.61	21.46	2.4%
LUB-3	Upper Bay	0.14	0.16	10.33	10.57	20.62	21.52	2.3%
LUB-4	Upper Bay	0.00	0.00	2.82	2.94	11.94	12.33	4.4%

LUB-5	Upper Bay	0.03	0.02	11.47	11.77	21.90	22.90	2.6%
LUB-6	Upper Bay	0.41	0.41	10.95	11.17	20.72	21.27	2.1%
LUB-7	Upper Bay	0.02	0.01	9.70	9.87	18.10	18.61	1.8%
UUB-1	Upper Bay	0.01	0.01	8.77	8.94	17.61	18.05	1.9%
UUB-2	Upper Bay	0.00	0.00	6.81	6.94	17.06	17.43	1.9%
UUB-3	Upper Bay	0.00	0.00	2.62	2.67	10.05	10.30	2.0%
UUB-4	Upper Bay	0.01	0.02	8.61	8.75	20.89	21.53	1.7%
UUB-5	Upper Bay	26.00	25.99	29.39	29.39	31.26	31.29	0.0%
E-2	South	6.30	7.00	23.96	24.18	31.38	31.42	0.9%
LSS-1	South	6.61	7.29	23.30	23.55	30.73	30.78	1.1%
LSS-2	South	12.67	12.47	22.08	22.25	28.96	28.85	0.8%
LSS-3	South	10.72	10.53	19.44	19.57	26.84	27.07	0.7%
LSS-4	South	7.70	8.35	22.52	22.79	30.91	30.89	1.2%
LSS-5	South	8.86	9.11	22.00	22.28	29.27	29.54	1.3%
USS-6	South	12.95	12.93	21.84	22.08	29.28	29.68	1.1%
USS-7	South	11.09	11.03	20.34	20.57	28.43	28.34	1.1%
USS-8	South	11.52	11.44	19.24	19.44	27.92	27.84	1.1%
USS-9	South	10.34	10.24	17.73	17.91	26.43	26.33	1.0%
USS-10	South	4.84	4.90	16.18	16.35	26.92	27.02	1.0%
LIS-1	Isthmus	0.54	0.53	11.42	11.69	21.08	21.91	2.4%
LIS-2	Isthmus	0.91	0.90	11.57	11.83	21.39	21.79	2.2%
LIS-3	Isthmus	1.05	1.01	10.95	11.18	20.70	21.27	2.1%
LIS-4	Isthmus	1.36	1.32	10.30	10.50	19.31	19.97	2.0%
LIS-5	Isthmus	1.84	1.78	10.27	10.44	18.99	19.52	1.6%
UIS-6	Isthmus	0.96	0.97	8.86	9.00	17.57	18.02	1.5%
UIS-7	Isthmus	0.56	0.58	7.57	7.64	15.52	15.63	0.9%
UIS-8	Isthmus	0.21	0.22	6.07	6.15	14.13	14.13	1.4%

UIS-9	Isthmus	0.10	0.10	5.25	5.29	13.59	13.55	0.9%
UIS-10	Isthmus	0.01	0.01	3.42	3.47	11.06	10.90	1.6%
CR-1	Coos River	0.00	0.00	1.37	1.39	11.73	12.05	1.4%
CR-2	Coos River	0.00	0.00	0.27	0.28	3.31	3.41	5.7%
CR-3	Coos River	0.00	0.00	0.20	0.21	2.73	2.82	6.2%
CR-4	Coos River	0.00	0.00	0.13	0.14	2.25	2.34	7.0%
CR-5	Coos River	0.00	0.00	3.93	4.02	14.09	14.31	2.3%
HI-1	Haynes	0.98	0.99	13.33	13.87	22.26	22.97	4.0%
HI-2	Haynes	0.59	0.67	11.93	12.28	22.09	22.77	2.9%
HI-3	Haynes	0.07	0.08	9.73	10.04	17.26	17.95	3.2%
HI-4	Haynes	0.00	0.00	5.62	5.82	14.84	15.39	3.5%
HI-5	Haynes	2.62	2.39	14.86	15.39	23.93	23.92	3.6%

Table 4-14
Salinity Statistics for Winter Period with Neap Tide – Middle Layer

Location	RM/ Slough	Minimum Salinity		Mean Salinity		Maximum Salinity		% Change of Mean
		Existing	2023PA	Existing	2023PA	Existing	2023PA	2023 PA-Existing
E-1	RM -1	31.00	30.72	32.56	32.54	32.84	32.83	-0.1%
FNC-0	RM 0	30.75	30.94	32.62	32.59	32.92	32.92	-0.1%
FNC-1	RM 1	21.17	22.23	31.83	31.91	32.91	32.90	0.3%
FNC-2	RM 2	18.49	20.39	31.57	31.65	32.90	32.91	0.2%
FNC-3	RM 3	20.34	21.20	31.61	31.62	32.85	32.88	0.0%
FNC-4	RM 4	21.50	21.25	31.36	31.15	32.79	32.81	-0.7%
FNC-5	RM 5	20.01	19.51	30.61	29.71	32.66	32.70	-2.9%
FNC-6	RM 6	18.04	17.73	29.54	29.33	32.60	32.62	-0.7%
FNC-7	RM 7	12.32	13.27	27.17	27.36	32.44	32.19	0.7%
FNC-8	RM 8	14.24	15.42	27.79	27.96	32.26	32.02	0.6%
FNC-9	RM 9	13.65	14.27	25.77	26.00	32.04	31.89	0.9%
FNC-10	RM 10	13.61	14.26	25.37	25.63	31.42	31.34	1.0%
FNC-11	RM 11	11.37	11.85	23.72	24.15	30.24	30.40	1.8%
FNC-12	RM 12	8.42	8.78	23.08	23.52	29.99	30.03	1.9%
FNC-13	RM 13	7.06	7.35	21.82	22.27	29.10	29.21	2.1%
FNC-14	RM 14	5.59	5.84	20.00	20.44	27.98	28.12	2.2%
FNC-15	RM 15	5.68	5.74	18.86	19.30	27.37	27.54	2.3%
LLB-1	Lower Bay	12.18	13.38	29.12	28.73	32.88	32.85	-1.4%
LLB-2	Lower Bay	5.22	5.79	25.13	24.92	32.48	32.31	-0.8%
ULB-1	Lower Bay	4.49	4.64	21.63	21.10	31.70	31.30	-2.4%
LUB-1	Upper Bay	0.16	0.18	16.05	16.66	25.82	26.73	3.8%
LUB-2	Upper Bay	0.17	0.19	14.82	15.33	24.84	25.51	3.5%
LUB-3	Upper Bay	0.55	0.55	13.17	13.57	24.43	24.91	3.0%
LUB-4	Upper Bay	0.00	0.00	11.78	12.35	22.30	22.95	4.8%

LUB-5	Upper Bay	1.08	1.14	14.57	15.12	26.01	26.79	3.8%
LUB-6	Upper Bay	0.87	0.92	16.40	16.95	25.06	25.65	3.3%
LUB-7	Upper Bay	0.75	0.79	13.04	13.41	22.44	22.96	2.8%
UUB-1	Upper Bay	0.12	0.13	13.49	13.89	22.19	22.88	3.0%
UUB-2	Upper Bay	0.00	0.00	12.92	13.30	21.45	21.98	2.9%
UUB-3	Upper Bay	0.00	0.00	7.31	7.43	17.55	17.92	1.6%
UUB-4	Upper Bay	0.07	0.06	17.63	18.03	26.44	26.78	2.3%
UUB-5	Upper Bay	0.03	0.03	11.32	11.54	22.96	23.26	1.9%
E-2	South	6.65	8.26	26.54	26.68	31.84	31.55	0.5%
LSS-1	South	18.30	18.15	28.36	28.47	32.12	32.10	0.4%
LSS-2	South	15.84	15.78	26.14	26.21	31.05	31.07	0.3%
LSS-3	South	16.70	16.61	22.96	23.10	27.96	28.09	0.6%
LSS-4	South	15.45	14.83	26.31	26.45	31.43	31.44	0.5%
LSS-5	South	12.05	11.77	24.53	24.71	30.96	31.02	0.7%
USS-6	South	14.36	14.30	23.33	23.51	30.70	30.80	0.8%
USS-7	South	13.80	13.85	22.77	22.93	30.05	30.26	0.7%
USS-8	South	13.33	13.31	21.43	21.62	28.75	28.75	0.9%
USS-9	South	12.90	12.81	20.10	20.31	27.08	27.08	1.0%
USS-10	South	8.00	8.00	19.02	19.23	28.11	28.11	1.1%
LIS-1	Isthmus	5.90	5.95	17.77	18.15	27.05	27.30	2.1%
LIS-2	Isthmus	5.11	5.12	16.92	17.29	26.78	27.07	2.2%
LIS-3	Isthmus	4.92	5.21	16.32	16.68	25.69	26.07	2.2%
LIS-4	Isthmus	4.42	4.79	15.23	15.57	25.28	25.66	2.2%
LIS-5	Isthmus	2.67	2.76	12.73	12.97	22.22	22.58	1.9%
UIS-6	Isthmus	2.95	3.09	13.04	13.32	21.49	21.75	2.1%
UIS-7	Isthmus	2.30	2.30	12.13	12.41	21.38	21.68	2.3%
UIS-8	Isthmus	2.00	2.08	11.26	11.52	19.90	20.23	2.3%

UIS-9	Isthmus	0.33	0.31	7.67	7.77	16.21	16.23	1.4%
UIS-10	Isthmus	0.53	0.57	7.88	8.08	16.16	16.53	2.6%
CR-1	Coos River	0.00	0.00	10.06	10.33	21.45	21.88	2.7%
CR-2	Coos River	0.00	0.00	5.51	5.64	17.87	18.25	2.4%
CR-3	Coos River	0.00	0.00	5.03	5.19	17.89	18.18	3.2%
CR-4	Coos River	0.00	0.00	5.09	5.25	18.41	18.76	3.2%
CR-5	Coos River	0.32	0.32	11.20	11.54	21.15	21.53	3.0%
HI-1	Haynes	3.83	4.08	18.64	19.46	28.40	29.47	4.4%
HI-2	Haynes	1.23	1.32	15.93	16.47	25.29	25.14	3.4%
HI-3	Haynes	2.89	3.53	16.05	16.77	23.13	23.68	4.5%
HI-4	Haynes	0.00	0.00	11.02	11.46	18.90	19.53	4.0%
HI-5	Haynes	6.60	6.69	15.45	16.03	23.92	23.91	3.8%

Table 4-15
Salinity Statistics for Winter Period with Neap Tide – Bottom Layer

Location	RM/ Slough	Minimum Salinity		Mean Salinity		Maximum Salinity		% Change of Mean
		Existing	2023PA	Existing	2023PA	Existing	2023PA	2023 PA-Existing
E-1	RM -1	32.80	32.70	32.90	32.90	32.90	32.90	0.0%
FNC-0	RM 0	32.20	32.20	32.90	32.80	32.90	32.90	0.0%
FNC-1	RM 1	30.30	30.70	32.50	32.60	32.90	32.90	0.2%
FNC-2	RM 2	28.70	30.30	32.50	32.60	32.90	32.90	0.5%
FNC-3	RM 3	29.80	30.30	32.50	32.50	32.90	32.90	0.3%
FNC-4	RM 4	29.60	29.50	32.30	32.50	32.90	32.90	0.4%
FNC-5	RM 5	29.30	28.80	32.10	32.10	32.80	32.90	0.2%
FNC-6	RM 6	28.70	28.50	31.80	31.80	32.80	32.70	0.2%
FNC-7	RM 7	27.60	27.60	31.30	31.20	32.70	32.70	-0.4%
FNC-8	RM 8	26.80	27.40	31.00	30.90	32.60	32.70	-0.2%
FNC-9	RM 9	25.80	25.60	30.10	29.90	32.50	32.40	-0.8%
FNC-10	RM 10	25.10	24.60	29.10	29.00	31.90	31.90	-0.4%
FNC-11	RM 11	22.30	22.80	27.80	27.90	31.40	31.30	0.5%
FNC-12	RM 12	19.90	20.30	26.50	26.80	30.60	30.50	1.0%
FNC-13	RM 13	17.00	17.60	25.30	25.60	29.90	29.80	1.2%
FNC-14	RM 14	13.90	14.00	23.00	23.40	28.80	28.90	1.8%
FNC-15	RM 15	8.50	9.60	21.30	21.80	27.80	28.00	2.1%
LLB-1	Lower Bay	23.60	23.40	31.70	31.60	32.90	32.90	-0.3%
LLB-2	Lower Bay	6.50	7.00	27.60	27.30	32.60	32.60	-1.0%
ULB-1	Lower Bay	4.60	4.70	23.30	22.60	32.00	31.70	-3.0%
LUB-1	Upper Bay	0.60	0.60	17.60	18.30	28.00	28.50	4.0%
LUB-2	Upper Bay	0.20	0.20	15.70	16.30	26.70	27.20	3.7%
LUB-3	Upper Bay	0.70	0.70	14.40	14.80	25.40	26.10	2.9%
LUB-4	Upper Bay	0.00	0.00	13.70	14.40	24.20	24.80	4.8%

LUB-5	Upper Bay	1.10	1.20	15.90	16.40	27.20	27.70	3.6%
LUB-6	Upper Bay	0.90	1.00	19.30	19.90	28.00	28.50	3.2%
LUB-7	Upper Bay	0.80	0.80	14.50	14.90	24.60	25.20	3.2%
UUB-1	Upper Bay	0.80	0.90	15.70	16.30	24.50	24.90	3.3%
UUB-2	Upper Bay	0.00	0.00	15.30	15.80	22.70	23.20	2.7%
UUB-3	Upper Bay	0.00	0.00	10.40	10.60	19.40	19.70	1.4%
UUB-4	Upper Bay	0.10	0.10	20.50	21.00	28.00	28.20	2.2%
UUB-5	Upper Bay	0.00	0.00	16.00	16.40	25.60	25.80	2.5%
E-2	South	8.50	9.60	27.60	27.70	32.40	32.20	0.3%
LSS-1	South	20.90	20.70	29.80	29.90	32.50	32.40	0.4%
LSS-2	South	15.80	15.70	27.80	27.80	31.80	31.60	0.3%
LSS-3	South	17.50	17.30	24.50	24.60	29.20	29.20	0.4%
LSS-4	South	16.50	16.50	27.60	27.80	32.10	31.90	0.5%
LSS-5	South	14.60	14.20	26.10	26.30	31.20	31.20	0.6%
USS-6	South	14.40	14.40	24.10	24.20	31.00	31.10	0.7%
USS-7	South	14.20	14.20	23.60	23.70	30.30	30.40	0.7%
USS-8	South	13.40	13.40	22.00	22.20	28.90	28.90	0.8%
USS-9	South	13.00	12.90	20.70	20.90	27.70	27.70	1.0%
USS-10	South	8.20	8.20	19.70	19.90	28.40	28.40	1.1%
LIS-1	Isthmus	7.00	7.80	19.50	20.00	27.30	27.60	2.4%
LIS-2	Isthmus	6.10	6.10	18.60	19.00	26.80	27.10	2.4%
LIS-3	Isthmus	6.30	6.60	18.50	18.90	26.50	26.80	2.5%
LIS-4	Isthmus	5.80	5.90	17.00	17.40	25.80	26.20	2.4%
LIS-5	Isthmus	3.30	3.40	13.70	14.00	23.30	23.80	2.0%
UIS-6	Isthmus	4.20	4.50	15.10	15.40	23.20	23.60	2.3%
UIS-7	Isthmus	3.40	3.60	14.20	14.60	22.60	22.90	2.5%
UIS-8	Isthmus	3.10	3.50	13.00	13.30	20.50	20.70	2.6%

UIS-9	Isthmus	0.40	0.40	9.30	9.50	17.30	17.70	1.9%
UIS-10	Isthmus	2.30	2.50	10.40	10.60	17.90	18.30	2.8%
CR-1	Coos River	0.00	0.00	13.70	14.10	24.40	24.80	3.0%
CR-2	Coos River	0.00	0.00	10.10	10.40	22.40	22.80	2.9%
CR-3	Coos River	0.00	0.00	8.50	8.80	21.30	21.60	3.4%
CR-4	Coos River	0.00	0.00	7.20	7.40	20.30	20.70	3.4%
CR-5	Coos River	10.90	11.30	16.80	17.20	23.20	23.60	2.0%
HI-1	Haynes	8.90	9.50	22.50	22.90	30.80	30.80	1.9%
HI-2	Haynes	1.70	2.30	17.40	18.00	26.20	25.80	3.6%
HI-3	Haynes	5.20	6.50	18.00	18.80	24.00	24.60	4.2%
HI-4	Haynes	0.00	0.00	12.40	12.90	19.90	20.70	4.5%
HI-5	Haynes	6.80	7.30	15.90	16.60	23.90	23.90	3.8%

4.6 Conclusions

The MIKE-3 FM suite with coupled hydrodynamic and salinity modules was calibrated against two salinity profiles measured along the main channel and was validated against time histories of salinity measurements available at the five off-channel water quality stations. The model validation analyses at four of the five stations exhibited an RMSE less than 2.2 psu. Overall, the comparison shows that the modeled and measured salinity are in agreement and the metrics in terms of salinity model performance achieved in this study are consistent with recent and similar modeling studies conducted by ERDC or approved by USACE.

For the winter simulations, the results of the salinity modeling generally show an increase in mean salinity; the deeper, wider channel allows the salt wedge to propagate further upstream, increasing salinity throughout. The changes in mean salinity between the 2023 PA and the Existing Conditions typically do not exceed 1 psu. The largest percent increases occur at the observation points in Coos River, where the baseline salinity is lowest. Besides Coos River, the change in salinity resulting from the 2023 PA with respect to the Existing Conditions is less than 5%.

5. RESIDENCE TIME AND ESTUARINE FLUSHING

In estuaries such as Coos Bay, understanding the hydrodynamic processes that exchange water and its constituents between the estuary and the ocean can be critical to quantifying the physical effects associated with an alteration to the system. A first-order description of this exchange is expressed as *residence time*, which is a measure of the amount of time it takes for the water within an area or water body to be replaced by the water from another area or water body. It is commonly referred to as "flushing time" as it represents the rate at which waters in a hydraulic system are renewed. In physical terms, the introduction of a tracer into a water body of interest could represent discharge of a pollutant, and the amount of time to replace that water with clean ocean water is represented by residence time.

In addition to residence time, another useful parameter to quantify water exchange is *water age*, which is a measure of the length of time that water within a computational cell has resided within the model domain. It is frequently referred to as "water renewal time," as used in Shen et al. (2017).

Residence time is often used as a first-order indicator of changes to water quality and the model results are presented in this section. Changes to water age was used as the basis for a mass balance analysis of changes to DO within Coos Bay, as discussed in Section 5.3. Residence times and water ages were calculated for each of the 11 polygons shown in Figure 5-1 (i.e., Entrance, Lower Lower Bay, Upper Lower Bay, Lower Upper Bay, Upper Upper Bay, Lower South Slough, Upper South Slough, Haynes Inlet, Lower Isthmus Slough, Upper Isthmus Slough, and Coos River).

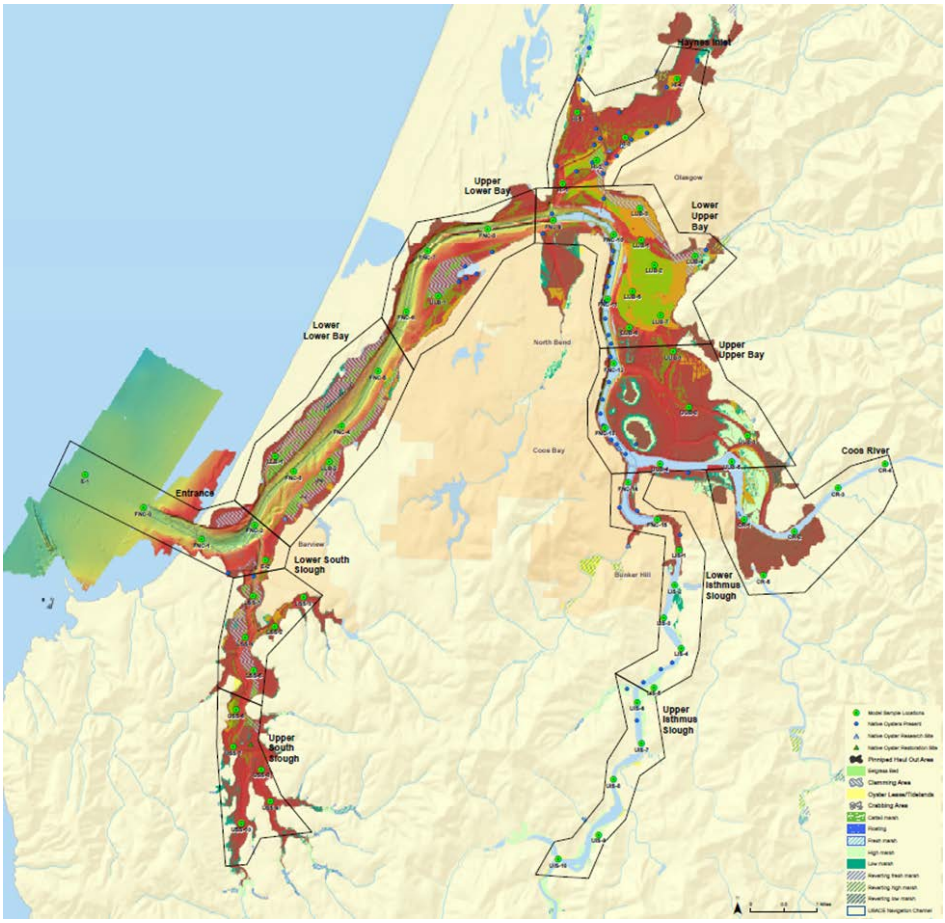

Figure 5-1
Residence Time/Water Age Polygons

5.1 Methodology

The ECO Lab module within the MIKE model suite was used to calculate residence times, based on the salinity modeling production runs described in Section 4.5. This particular application of ECO Lab uses conservative tracers. A description of the residence time and water age calculations are provided below. The conservative tracer is a numerical, non-decaying property of water, which is used to trace flows and exchanges within the modeled water body. The conservative tracer is a numerical analog to physical tracers such as dye. In a numerical model, the conservative tracer is defined with its concentration, which changes due to advection, when the tracer moves with the flow, and dispersion, when water with different tracer concentrations mixes together. The tracers do not affect the hydrodynamics and are neutrally buoyant. The computations of the residence time

and water age were performed with a time step of 15 minutes. The simulation periods are the same as the salinity modeling production runs:

- A summer period (1-month including spring tide and neap tide) with constant low freshwater inflow from 07/01/2011 to 08/01/2011.
- A winter period with spring tide and freshwater inflow from 01/11/2011 to 01/31/2011.
- A winter period with neap tide and freshwater inflow from 01/11/2011 to 01/31/2011.

Commented [JS33]: A-3-26: Describe the Simulation period in the text.

Commented [JS34R33]: Text describing the simulation periods added.

5.1.1 Residence Time

The general procedure of computing residence times for different parts of a tidal embayment is as follows:

- Assign an initial conservative tracer concentration of 1 over the entire embayment element mesh and a value of 0 at the open water boundaries to simulate an instantaneous release of a new constituent into an embayment.
- Run the numerical model for an adequate number of tidal cycles until substantial reduction of constituent concentrations have occurred due to tidal flushing at the locations of interest.
- Analyze the computed concentration results and find the time step when the relative concentration dropping below 1/e (Fisher et al. 1979).

To perform this analysis, the model run is commenced until the water levels and current velocities replicate physical conditions of the estuary (sometimes referred to as model "spin-up"). At this point, the model is initialized with introduction of a conservative tracer with a concentration of 1 (e.g. 100%). Each of the residence time polygons is initialized with a different "color" tracer. Conservative tracers will follow the movement of water and their concentration will change during the simulation (note that the tracers do not affect the movement of water). Tracer concentration within its original area of interest will be plotted as a time series, from which an estimation of the residence time will be computed in each area of interest. The residence time is defined as the time until the concentration drops below 37% (1/e) of the initial concentration (residence times are measured in days).

It is important to note that this analysis computes residence time for each individual polygon and includes flushing caused by water exchanges between neighboring polygons as well as by mixing with the "new water" from ocean or river inflows. That is, when the water within a particular polygon is replaced by water from another polygon, the tracer concentration in both polygons is reduced even if the two polygons exchange waters with similar water quality properties. Therefore, the residence times computed from the tracer concentrations do not provide a measure of how quickly the polygons are flushed by riverine/ocean waters (the water age analysis does this) but any water in the bay. This analysis therefore informs the flushing response to water quality changes within specific areas of the estuary and is specifically important if water quality issues are localized (for example, if low DO is observed in one area such as Isthmus Slough).

5.1.2 Water Age

Water age is calculated by tracking an "age" to tracers as they remain within a particular area. The water age throughout the domain is set to 0 initially. A unitless growth rate of 1.0 is applied to water within the estuary during each time step, while inflow from the offshore boundary continues

to have an age of 0. As the simulation progresses, water parcels become older unless flushed by water of lesser age, such as inflowing water. Thus, at any time over the simulation, the water age can be viewed for all computational cells throughout the domain. The water age simulations are run for a one-month period to drive the water ages towards dynamic equilibrium.

Dynamic equilibrium is when the tides reach repetitive, cyclic conditions, assuming the tides are repeated, such as monthly spring-neap tides. If repeating tidal conditions are imposed along with a constant freshwater flow; water age will grow over time until approaching a constant, maximum age within each cell. Converging to a constant age is caused by local flushing with younger water, which can only occur with dynamic equilibrium flow conditions for a tidal system. Once the dynamic steady-state is reached, the water age will continue to fluctuate a little from the tides.

The summer one-month period covers both spring and neap cycles; moreover, results indicated that the system reaches dynamic equilibrium within this time period. A month was considered long enough for the water age analysis since any longer would require seasonal flow changes as well as sea level fluctuations affecting tides.

Commented [BR35]: A-3-27 (Dr. Checks # 8071912)

Commented [WA36R35]: Added Port comment to the report

Because the summer low flow condition is usually the most detrimental to water quality, the difference in water age ($\Delta\tau$) under the summer low flow condition throughout the entire domain was calculated for the 2023 PA minus the Existing Conditions. The final product was a cumulative distribution of water age changes for each polygon. It should be noted that decreases in water age were assigned a change of 0, since these changes would correspond to an increase in DO.

5.2 Results

5.2.1 Residence Time

Residence time is calculated by plotting the reduction in tracer concentrations against time. Figure 5-2 shows a sample plot for the Existing Conditions. This plot represents the summer low flow condition and contains the actual tracer concentration (blue lines), the trend line (red line), and the point where the trend line intersects 37% (1/e – technically 36.79%) of the tracer remaining (red circle). Residence time is, therefore, determined by identifying the duration of time the concentration is reduced to 37% of its initial concentration, by definition. As the plot shows, the tracer moves in and out of the polygon with the tides. Over many tidal cycles, the tracer disperses so that less tracer returns to the polygon for subsequent tidal cycles. Under this example, the residence time is approximately 1.53 days in the Lower Isthmus Slough polygon.

One thing to note about this plot is that it indicates the initial concentration of tracer is less than 100%. This is because the initial concentration is based on the trend line. Moreover, the precise tracer concentration at which 37% of the tracer remains varies since it is based on 37% of the initial concentration. For instance, the trend line shows an initial concentration of 83.05%; the residence time corresponds to the amount of time after which 37% of this 83.05% remains (so, the residence time corresponds to a trend line tracer concentration of 30.55%).

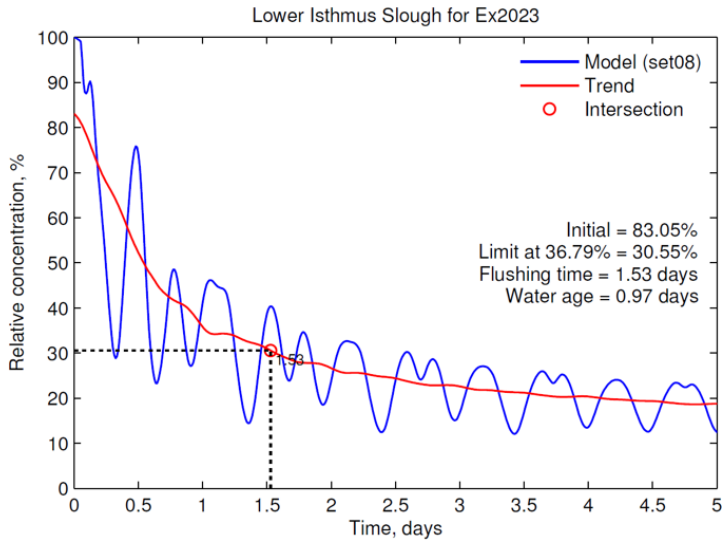

Figure 5-2
Residence Time Tracer Concentrations in the Lower Isthmus Slough Polygon, Existing Conditions

Residence time for the summer low flow, winter spring tide, and winter neap tide simulations are presented in Table 5-1 through Table 5-3, respectively. Each table includes the estimated residence time for the selected polygons under the Existing Conditions and the 2023 PA, as well as percent differences for the 2023 PA relative to the Existing Conditions.

Model results show that residence times increase within the Lower Bay as a result of the increased volume capacity of this area compared to the small increase in tidal prism. However, residence times in the Lower Bay for both the Existing Conditions and the 2023 PA are less than 1.5 days, indicating highly flushed conditions with no concern of impact to water quality parameters. In addition, residence times as a result of the 2023 PA change by less than 1.2 hours in the Upper Bay and the tributaries, indicating little change to flushing here.

Overall, residence times are on the order of 3 days or smaller, which indicate good flushing. The high residence time in the Upper Isthmus Slough is due to the polygon's position between the model boundary and the Lower Isthmus Slough. Tracers from the Upper Isthmus Slough move back and forth between Upper and Lower Isthmus slough polygons without mixing throughout the estuary.

5.2.1.1 Summer Period

For the summer low flow condition (Table 5-1) residence times appear to increase within the Lower Bay and increase into the Haynes Inlet. The increase in the Lower Bay may be a result of the increased volume capacity of this area compared to the small increase in tidal prism, which also results in a reduction in current speeds. Slightly reduced residence times (i.e., 0.2 hours) in the Upper Bay and the surrounding tributaries are likely a result of the slight increase in tidal range.

Overall, all changes to residence times are small, within 1.2 hours (except for in the Upper Lower Bay). In the Upper Lower Bay, the increased residence time is due to the shape of the trend line and a slightly different threshold concentration. Figure 5-3 and Figure 5-4 show that the actual tracer concentrations are similar. Furthermore, the Upper Lower Bay residence times for both the Existing Conditions and the 2023 PA are less than 1.5 days, indicating highly flushed conditions with no concern of impact to water quality parameters. Finally, residence times change by less than 1.2 hours in the Upper Bay and the tributaries, indicating little change to flushing here.

Table 5-1
Calculated Residence Time: Summer Low Flow Condition

Area	Residence Time, Existing Conditions (days)	Residence Time, 2023 PA (days)	Residence Time Change (hours), 2023 PA – Existing	Percent Change, 2023 PA vs Existing
Entrance	0.44	0.44	0	0%
Lower Lower Bay	0.55	0.59	+1.0	7%
Upper Lower Bay	1.03	1.49	+11.0	45%
Haynes Inlet	1.51	1.53	+0.5	1%
Lower Upper Bay	1.60	1.60	0	0%
Upper Upper Bay	2.63	2.62	-0.2	0%
Coos River	3.05	3.04	-0.2	0%
Lower Isthmus Slough	1.53	1.52	-0.2	-1%
Upper Isthmus Slough	29.02	29.07	+1.2	0%
Lower South Slough	0.67	0.67	0	0%
Upper South Slough	2.26	2.27	+0.2	0%

Commented [JS37]: A-3-28: Provide % change column. Provide data to EIS Team.

Commented [JS38R37]: Added the % change to tables. Data will be provided to EIS team as requested.

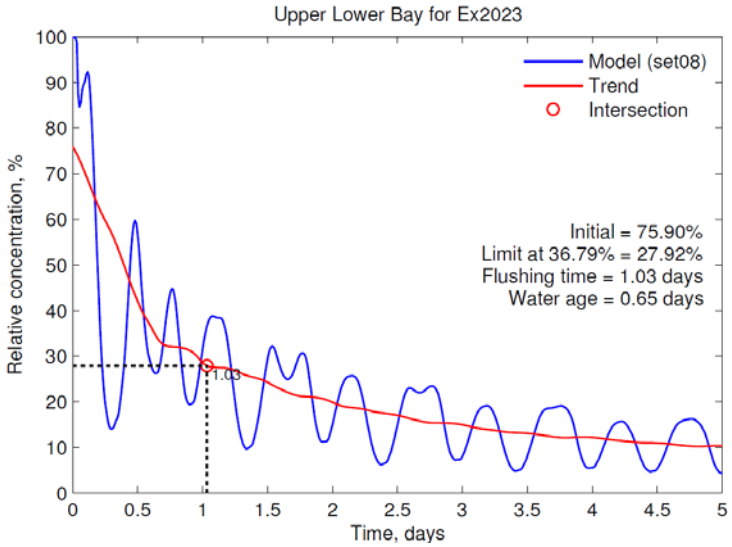

Figure 5-3
Residence Time Tracer Concentrations in the Upper Lower Bay Polygon, Existing Conditions under Summer Low Flow

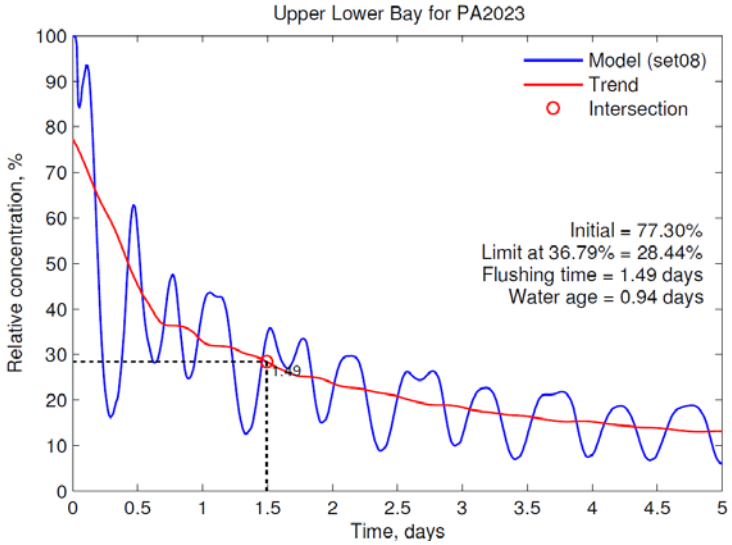

Figure 5-4
Residence Time Tracer Concentrations in the Upper Lower Bay Polygon, 2023 PA under Summer Low Flow

5.2.1.2 Winter Period with Spring Tide

For the winter spring tide condition (Table 5-2), residence times decrease relative to the summer simulation (Table 5-1) for most of the areas. The reason for the increased residence times in the Upper South Slough and Haynes Inlet is that both are relatively low flow areas before day 5 of the simulation and residence times are driven by tidal flushing. Comparing Figure 4-14 and Figure 4-15 shows that the initial tidal range of the summer simulation is larger than the winter simulation, resulting in faster flushing of these areas. In other locations throughout the estuary, the decrease in residence times is a result of enhanced runoff promoting flushing. The change is particularly evident in the Upper Isthmus Slough, where the onset of the peak discharge flushes this polygon (see Figure 5-5 and Figure 5-6).

Table 5-2
Calculated Residence Time: Winter Spring Tide Condition

Area	Residence Time, Existing Conditions (days)	Residence Time, 2023 PA (days)	Residence Time Change (hours), 2023 PA – Existing	Percent Change, 2023 PA vs Existing
Entrance	0.39	0.39	0	0%
Lower Lower Bay	0.55	0.58	+0.7	5%
Upper Lower Bay	0.89	0.97	+1.9	9%
Haynes Inlet	1.58	1.56	-0.5	-1%
Lower Upper Bay	0.90	0.86	-1.0	-4%
Upper Upper Bay	1.02	1.02	0	0%
Coos River	0.94	0.94	0	0%
Lower Isthmus Slough	1.20	1.19	-0.2	-1%
Upper Isthmus Slough	5.15	5.15	0	0%
Lower South Slough	0.64	0.65	+0.2	2%
Upper South Slough	2.92	2.96	+1.0	1%

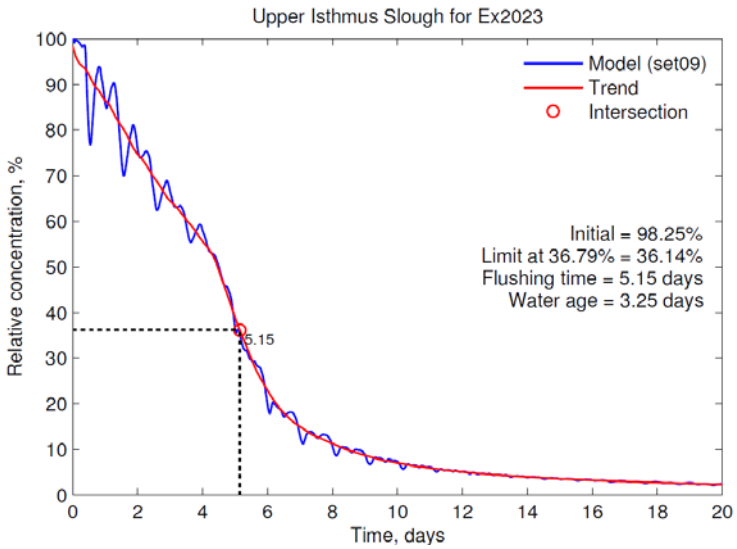

Figure 5-5
Residence Time Tracer Concentrations in the Upper Isthmus Slough Polygon, Existing Conditions under Winter Spring Tide

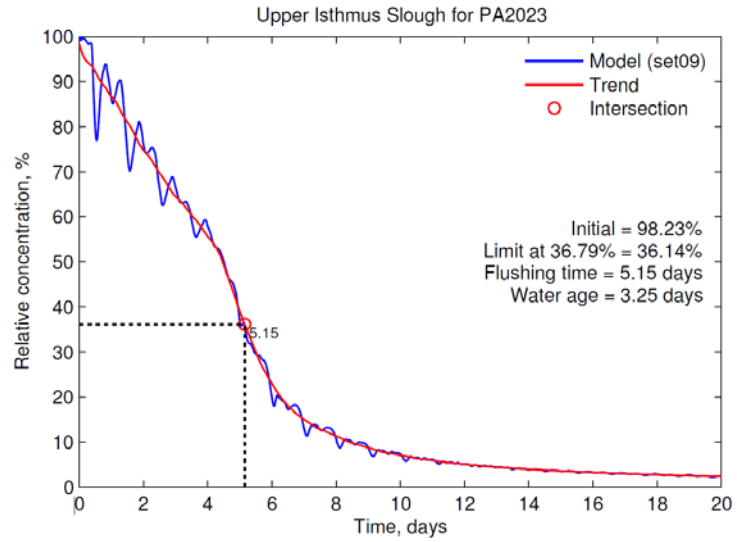

Figure 5-6
Residence Time Tracer Concentrations in the Upper Isthmus Slough Polygon, 2023 PA under Winter Spring Tide

5.2.1.3 Winter Period with Neap Tide

For the winter neap tide condition (Table 5-3), residence times further decrease relative to the winter spring tide simulation. The reason for the decrease is that, during the initial portions of the simulation (before the peak discharge), the neap tides have a wider range than the spring tides (since the spring tides were meant to correspond to the peak, see Figure 4-15).

Figure 5-7 and Figure 5-8 illustrate that the largest increase of residence time (i.e., 5.5 hours) as a result of 2023 PA occurs at the Upper Lower Bay.

Table 5-3
Calculated Residence Time: Winter Neap Tide Condition

Area	Residence Time, Existing Conditions (days)	Residence Time, 2023 PA (days)	Residence Time Change (hours), 2023 PA – Existing	Percent Change, 2023 PA vs Existing
Entrance	0.37	0.37	0	0%
Lower Lower Bay	0.45	0.47	+0.5	4%
Upper Lower Bay	0.59	0.82	+5.5	39%
Haynes Inlet	1.19	1.19	0	0%
Lower Upper Bay	0.90	0.84	-1.4	-7%
Upper Upper Bay	1.01	0.99	-0.5	-2%
Coos River	0.82	0.82	0	0%
Lower Isthmus Slough	0.95	0.93	-0.5	-2%
Upper Isthmus Slough	5.23	5.23	0	0%
Lower South Slough	0.53	0.54	+0.2	2%
Upper South Slough	2.72	2.71	-0.2	0%

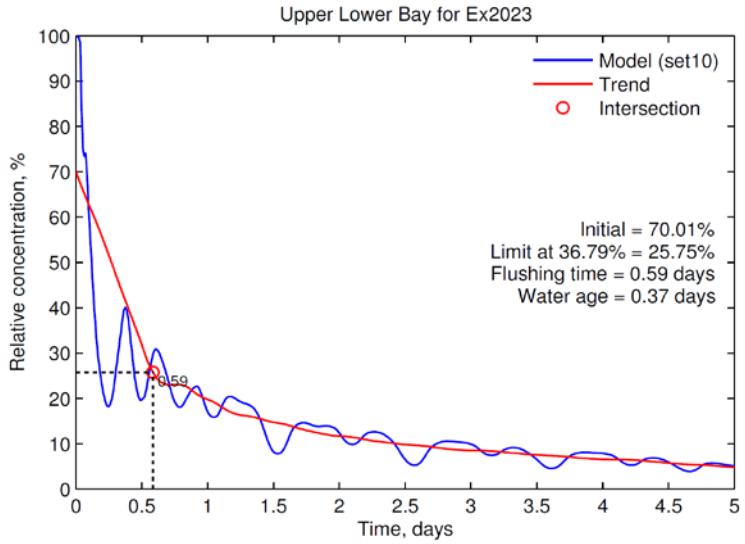

Figure 5-7
Residence Time Tracer Concentrations in the Upper Lower Bay Polygon, Existing Conditions under Winter Neap Tide

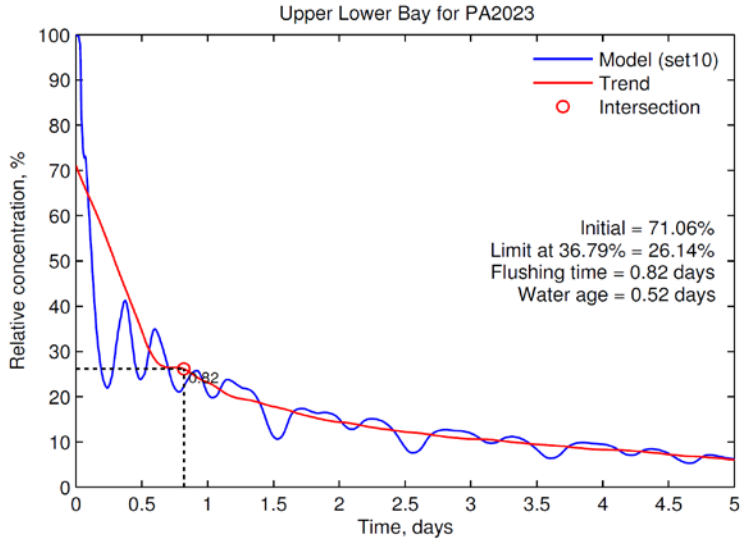

Figure 5-8
Residence Time Tracer Concentrations in the Upper Lower Bay Polygon, Existing Conditions under Winter Neap Tide

5.2.2 Water Age

The ECO Lab water age simulation was run for the summer low flow condition under the Existing Conditions and the 2023 PA. The water ages were saved for all computational cells at the end of the simulation (day 31). The values for $\Delta\tau$ were computed (with the 2023 PA minus the Existing Conditions) for all cells; these values were then averaged over each column of cells with each residence time polygon, producing depth-averaged $\Delta\tau$ for all cells within each polygon. The depth-averaged $\Delta\tau$ were ranked in order of increasing value for determining the cumulative frequency distribution (CFD) of $\Delta\tau$ for each polygon. The depth-averaged $\Delta\tau$ CFD and statistics for the 2023 PA are shown in Table 5-4. The depth-averaged $\Delta\tau$ at the end of summer simulation is illustrated to show how $\Delta\tau$ varies spatially throughout Coos Bay for the 2023 PA in Figure 5-9.

Water ages are expected to increase throughout the estuary under the 2023 PA. Ultimately, these results show that the increase in volume of the estuary is more substantial than the increase in tidal flushing, and that water particles are expected to reside in Coos Bay for more time, on average. These results appear to differ from the residence time calculation because of how the polygon boundaries are applied. The residence time calculation shows that water particles spend less time, on average, in the upstream individual polygons under the 2023 PA. The water age calculation shows that water particles reside for more time within the entire Coos Bay system under the 2023 PA (similarly, summing the individual residence times would yield a net increase in residence time). The largest increases in water age occur within the Upper Lower Bay, which results from the increase in water volume in this area. The mean water age increase is less than 1.85 days.

Table 5-4
Non-exceedance CFD (percent less than value) and Statistics for Depth-averaged Δτ (days) for 2023 PA

Area	1%	5%	10%	25%	50%	75%	90%	95%	99%	Mean
Entrance	-1.12	-0.54	-0.15	-0.01	0.05	0.27	0.50	0.60	1.73	0.12
Lower Lower Bay	-1.24	-0.74	-0.37	0.14	0.47	0.78	1.24	1.51	1.84	0.45
Upper Lower Bay	0.36	0.65	1.03	1.57	1.88	2.28	2.54	2.66	2.88	1.85
Haynes Inlet	0.51	0.62	0.67	0.79	1.06	1.37	1.60	1.69	1.79	1.09
Lower Upper Bay	0.50	0.80	0.88	1.02	1.33	1.75	1.97	2.07	2.20	1.38
Upper Upper Bay	0.37	0.42	0.50	0.63	0.79	1.13	1.24	1.34	1.67	0.86
Coos River	-0.68	-0.32	-0.02	0.15	0.35	0.42	0.48	0.52	0.58	0.25
Lower Isthmus Slough	0.30	0.45	0.53	0.57	0.63	0.84	0.95	0.97	0.98	0.68
Upper Isthmus Slough	-0.24	-0.02	0.07	0.10	0.17	0.30	0.48	0.70	0.88	0.22
Lower South Slough	-0.34	-0.12	-0.11	-0.08	-0.04	0	0.04	0.07	0.23	-0.04
Upper South Slough	-0.10	-0.09	-0.09	-0.08	-0.05	-0.02	0	0.01	0.04	-0.05

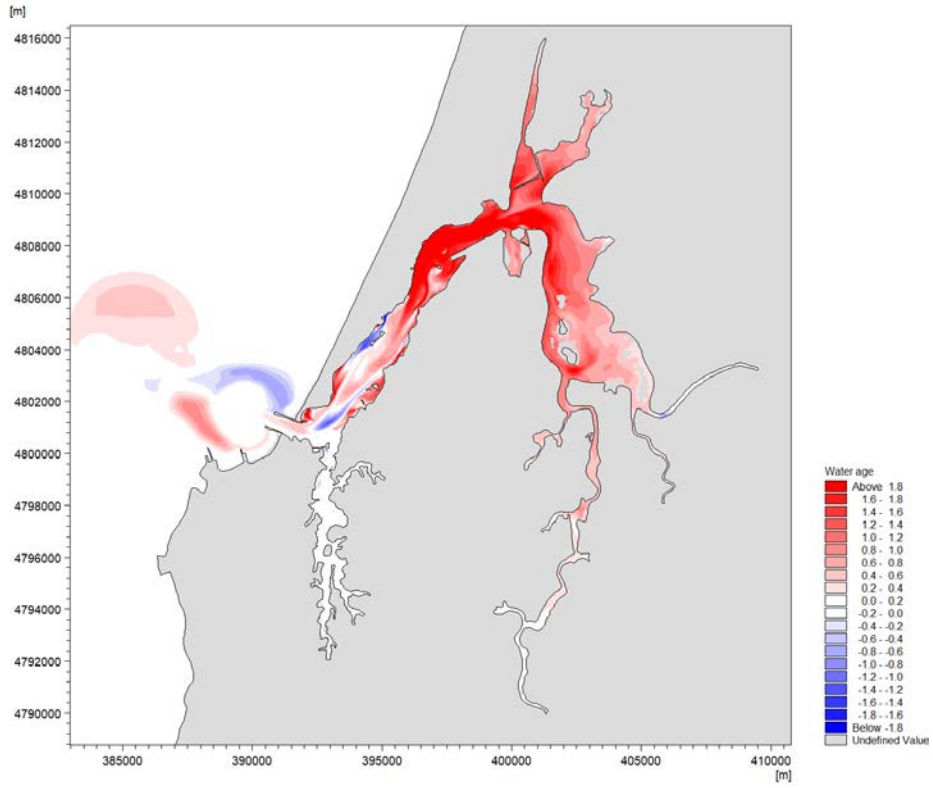

Figure 5-9
Contour Plot of Depth-averaged Δτ (days) at the End of the 31-day Summer Simulation for 2023 PA Minus Existing Conditions

The implications for the change in water ages is presented in the DO analysis below.

5.3 Dissolved Oxygen Analysis

Navigation channel widening and deepening can alter water age and salinity. The results show an increase in salinity (see Section 4.5.2) and in water age (see Section 5.2.2). Concurrent with increased salinity, there can be greater vertical stratification in salinity, which causes increased density stratification that can result in reduced vertical mixing. Increased water age and reduced vertical mixing can potentially cause lower DO during periods of higher DO demand (i.e., periods of increased biological activity) in the water column and within benthic sediments.

5.3.1 Other Studies

There are numerous examples of the use of numerical hydrodynamic models coupled with tracer and flushing models of various types to predict flushing metrics, which in turn were used to infer

impacts of water quality. Recent examples of such models include Norfolk Harbor and the Elizabeth River (Shen et al. 2017), Mobile Bay (USACE 2018), Cape Fear (Bowen et al. 2009), and Charleston Harbor (USACE 2015a). The need for discrete water quality modeling was driven by the existing conditions, sediment characteristics, or project features.

In Mobile Bay, water quality modeling was required because of the existing stratification and elevated temperatures that cause existing water quality impairments. Moreover, the project proposed in-bay disposal of dredged organic sediment, which may contain organics. The Cape Fear estuary has existing DO impairments due to high levels of organics from upstream sources. Therefore, it was necessary to understand how changes to the estuary could affect the flushing of organics and resultant changes to DO. Charleston Harbor had similar high organic loads from adjacent marshes, and existing DO impairments. At Norfolk Harbor, dredging has the potential to suspend organics from the existing sediment.

Channel deepening on the West Coast includes Grays Harbor (USACE 2014), Redwood City Harbor (USACE 2015b), and Seattle Harbor USACE (2016). These projects cited high existing DO levels, lack of fine-grain or organic sediment, and offshore disposal as not warranting DO modeling for these projects, although short-term impacts may result from dredging activities. The Coos Bay estuary has similar characteristics; DO concentrations remain above the ODFW standard of 4.0 mg/L (for an instantaneous value) throughout the year, sediment is medium-to-coarse sand without organics, and offshore disposal is proposed. Therefore, discrete water quality modeling was not proposed. Instead, changes to DO have been evaluated based on a limited-scope DO model similar to that used for the Inner Harbor Navigation Channel associated with hurricane surge barriers to protect New Orleans (Dortch and Martin 2008).

5.3.2 Methodology

This ΔDO analysis is based on the conservation of DO mass over the water column at a planar geospatial point location and as affected by three DO uptake mechanisms that include, mineralization of dissolved organic carbon (DOC), nitrification of ammonium nitrogen (NH_4-N), and benthic SOD. The single source of oxygen in the mass balance is surface reaeration. The reactions noted above represent a rate of change of DO. Therefore, increasing water age allows these processes to occur for a longer time within a particular area, increasing the amount of DO uptake and reducing DO concentrations.

The DO mass balance is mathematically stated as,

$$\frac{d\,DO}{dt} = -2.67\,K_d\,DOC - 4.57\,K_n\,NH_4 - \frac{SOD}{H} + \frac{K_r}{H}\left(DO_s - DO\right) \qquad (1)$$

where K_d is the decay or mineralization rate (day^{-1}) for DOC (g/m^3), K_n is the nitrification rate (day^{-1}) of NH_4 (g/m^3), H is local water depth (m), K_r is oxygen mass transfer coefficient (m/day), DO_s (mg/L) is the saturation value of DO, and dt is the change in time (day). The local water depth is used for SOD ($g\ O_2/m^2/day$) exertion and reaeration since the CBE is vertically well mixed in the summer. After recognizing that the left side of Equation (1) can be stated as $\Delta DO / \Delta\tau$, Equation (1) has the simple analytical solution,

$$\Delta\,DO = S\,\Delta\tau \qquad (2)$$

where

$$S = -2.67\,K_d\,DOC - 4.57\,K_n\,NH_4 - \frac{SOD}{H} + \frac{K_r}{H}\left(DO_s - DO\right) \qquad (3)$$

The *DO* parameter in Equations (1) and (3) is the local value of DO for the Existing Conditions. The factors 2.67 and 4.57 are the stoichiometric conversions for DOC to oxygen and NH_4 nitrogen to oxygen, respectively. Equations (2) and (3) assume that DOC, NH_4, and SOD are constant over time, whereas in reality, DOC and NH_4 can decrease over time as decay and nitrification occur.

The variable *S* in Equation (3) is the DO depletion rate (mg/L/day). A negative value of *S* indicates that DO is being reduced over time. If $\Delta\tau$ from Equation (2) is positive (i.e., water age increases), and *S* is negative, ΔDO is negative and DO decreases by the amount calculated. If the change in water age is negative (i.e., water age decreases), and *S* is negative, the change in DO is positive, and DO increases. Similarly, a negative $\Delta\tau$ and positive *S* results in reduction in DO. This limited-scope DO model is considered conservative for predicting DO decreases (i.e., the model produces potentially greater than expected DO decreases) since it assumes constant DOC and NH_4. Realistically, DOC and NH_4 concentrations would decrease with the activity consuming DO. Moreover, predicted increases in DO can be greater than expected since the model assumes constant DOC and NH_4.

The saturation value of DO (DO_s) is computed from

$$\ln DO_s = \ln DO_{sf} - Sal\left(1.7674x10^{-2} - \frac{10.754}{T_a} + \frac{2140.7}{T_a^2}\right) \qquad (4)$$

where *Sal* is the local salinity in parts per thousand (ppt), and T_a is the local water temperature in degrees Kelvin ($T_a = T + 273$). The parameter DO_{sf} is computed from

$$\ln DO_{sf} = -139.3441 + \frac{1.575701x10^5}{T_a} - \frac{6.642308x10^7}{T_a^2} + \frac{1.2438x10^{10}}{T_a^3} - \frac{8.621949x10^{11}}{T_a^4} \qquad (5)$$

The Banks and Herrera (1977) equation is used to estimate the oxygen mass transfer coefficient at 20 deg C, $K_r(20)$ (m/day) for wind reaeration of standing water,

$$K_r\left(20\right) = 0.728U_w^{0.5} - 0.317U_w + 0.0372U_w^2 \qquad (6)$$

where U_w (m/sec) is the wind speed measured 10 m above the water surface. The wind speed is a model input that can be varied.

The rate coefficients and SOD in Equations (1) and (3) depend on local water temperature. Values for the three rate coefficients and SOD are entered for 20 degrees Celsius (C) and corrected for the local water temperature *T* (deg C) using the formula,

$$K\left(T\right) = K\left(20\right)\theta^{(T-20)} \qquad (7)$$

where *T* is the local water temperature (degrees C), *K(T)* is the coefficient or SOD at temperature *T*, *K(20)* is the coefficient or SOD value entered for 20 degrees C, and θ is the temperature correction parameter for a particular rate coefficient or SOD. Values typically used for θ are 1.047, 1.085, 1.024, and 1.065 for the parameters K_d, K_n, K_r, and SOD, respectively (Thomann and

Mueller 1987). Values for the three rate parameters, DOC, NH_4, and SOD are discussed in Section 5.3.3.

Water depth *H* is the average water depth averaged over time for the month-long simulation and averaged for both projects scenarios (Existing Conditions and 2023 PA). Local water temperatures and DO were estimated for each polygon based on measured data from measured summer water temperature and DO data, as discussed in Section 5.3.3. Salinity was provided by the salinity modeling outputs as discussed in Section 4.5.2.

The DO model was applied within an Excel® spreadsheet for each polygon using the changes in water age from Table 5-4 to provide a CFD of changes to DO under the 2023 PA.

5.3.3 Model Input

5.3.3.1 Parameters

Inputs for the DO model include various parameters; spatially and summer averaged values of temperature, salinity, DO, and water depth; wind speed; and the CFD and statistics for $\Delta\tau$ for each polygon at the end of the summer simulation. Each of these inputs is discussed below.

The model required estimates of DOC and NH_4-N concentrations. The most recent available nutrient data (CTCLUSI 2016) reveals that NH_4-N concentrations at the three Empire sampling stations ranged from 0.025 to 0.079 mg/L on June 16 and October 5, 2016. Concentrations of total nitrogen (TN) at the same stations and dates ranged from 0.14 to 0.74 mg/L. Ammonium nitrogen concentrations on the order of 0.1 mg/L are common in moderately productive estuaries; thus, the upper bound at the Empire station of 0.079 mg/L appears quite reasonable, and this value was rounded up to 0.1 mg/L for model input to provide a conservatively high concentration that contributes to a conservatively greater DO depletion.

The Partnership for Coastal Watershed (2018b) reports total organic carbon (TOC) concentrations for Coalbank Slough mouth (CLBK) and Isthmus Sough at Eastside Bridge (ESDE) averaging between 2.0 mg/L (24 observations) and 1.8 mg/L (26 observations), respectively, between April 2006 and March 2007. These are two of four stations closest to the main bay open water. Two other stations closest to main bay open water, Joey Ney Slough at mudflat (MDFL) east of boatyard and Coos Bay South Slough near Joey Ney Slough (JNSL), had concentrations of 0.5 and 2.0 mg/L, respectively, in April 1998. Thus, TOC of 2.0 mg/L appears to be a reasonable value for the estuary. Using Redfield stoichiometry of C/N = 5.68, using the upper bound of TN of 0.74 mg/L, and assuming a reasonable ratio of total organic nitrogen (TON) to TN of 0.6, yields TOC = 2.52 mg/L (i.e., 5.68 x 0.6 x 0.74 = 2.52). A value for TOC of 2.5 mg/L appears to be a reasonable, yet conservatively high value to use for modeling DO in Coos Bay. However, DOC is required for the model since the normal practice is to assume DOC mineralization with oxygen utilization with particulate organic carbon (POC) hydrolyzing to DOC without consuming oxygen. Unfortunately, no DOC data could be found for Coos Bay; thus, the ratio of DOC/TOC was assumed. Cerco and Noel (2017) reported the ratio of particulate carbon to total carbon for the main eight tributaries entering Chesapeake Bay, with an average for the eight tributaries of 0.29, resulting in an estimate for DOC/TOC of 0.71. Using this ratio and a TOC concentration of 2.5 mg/L, results in an estimated DOC concentration of 1.77 mg/L for input to the DO model. This value was rounded up to 1.8 mg/L for the model.

No measured SOD values were found for Coos Bay. The SOD of estuarine mud averages about 1.5 g O_2/m^2/day, whereas sandy benthic sediments average about 0.5 g/m^2/day (Thomann and

Mueller 1987). Measurements of SOD in the Cape Fear River Estuary (CFRE), North Carolina, ranged from 0.25 to 0.67 g O_2/m^2/day at 20 degrees C (Bowen et al. 2009). Portions of the CFRE are listed on the North Carolina Section 303(d) list required by the Federal Clean Water Act for waters not meeting water quality standards or which are not meeting their designated use. Thus, SOD values of the CFRE are most likely higher than those in Coos Bay. Cowan and Boynton (1996) reported that measured average SOD rates along the longitudinal axis of Chesapeake Bay ranged from 0.05 to 0.86 g O_2/m^2/day. Chesapeake Bay is a highly productive estuary that receives rather large quantities of allochthonous loadings, experiences regular seasonal hypoxia, and has received a high level of study related to its eutrophication status. Thus, the SOD values within Coos Bay are expected to be lower than those of Chesapeake Bay. Given the above information, a reasonable and conservatively high value of 0.5 g O_2/m^2/day at 20 degrees C was assigned for the model SOD input.

Calibration values of the nitrification rate, K_n (per day), are reported to range from 0.025 to 0.2 day^{-1} (Bowie et al. 1985). Nitrification rates can be higher for shallow streams receiving waste loads. The highest value used for recent modeling of Chesapeake Bay was equivalent to 0.125 day^{-1} (Cerco and Noel 2017). Based on these values, a reasonable value of K_n to use for Coos Bay is 0.125 day^{-1} at 20 degrees C.

The rate of organic carbon mineralization, K_d (per day), is generally around 0.1 day^{-1} at 20 degrees C. This value was used for the water quality model of the CFRE (Bowen et al. 2009). The highest value used in the recent Chesapeake Bay model (Cerco and Noel 2017) was 0.075 day^{-1}. Thus, a K_d value of 0.1 day^{-1} at 20 degrees C was selected for the present model as a conservatively high but reasonable value. A summary of the recommended parameter input values for the Coos Bay DO model are provided in Table 5-5.

Table 5-5
Parameter Inputs for the Coos Bay DO Model

Input parameter	Units	Value
NH_4-N	mg/L	0.1
DOC	mg/L	1.8
SOD	g O_2/m^2/day	0.5
K_n	day^{-1}	0.125
K_d	day^{-1}	0.1

5.3.3.2 Temperature

Temperature data were estimated for each polygon based on data available from the Partnership for Coastal Watersheds (2018b). Table 5-6 shows the estimated summer average temperature assigned to each polygon and the data source/rationale behind each estimate.

Table 5-6
Assumed Temperature for Each Polygon

Area	Temperature (C)	Rationale
Entrance	14.6	Based on the average dry season 2009-2014 temperature measured at Charleston Bridge. The average was selected as opposed to a higher percentile because the Entrance Polygon is likely cooler than Charleston Bridge, which receives warm upstream waters.
Lower Lower Bay	15.3	Based on the estimated 75th percentile of summer 2006-2013 at Empire Station.
Upper Lower Bay	15.8	Based on the estimated 75th percentile of summer 2006-2013 at BLM Station.
Haynes Inlet	17.0	Based on 2006 and 2007 summer measurements of a tributary to Haynes Inlet. The average was used here because the Haynes Inlet polygon is deeper, and likely has cooler waters than the tributary.
Lower Upper Bay	17.0	Based on the estimated 75th percentile of summer 2014 at North Point Station.
Upper Upper Bay	17.3	No sensors are available here, but due its location upstream of Lower Upper Bay, likely has slightly warmer temperatures.
Coos River	19.0	Upstream Coos River had an August 2006 temperature of 21°C. The polygon is downstream, and likely cooler.
Lower Isthmus Slough	19.0	Based on the estimated 75th percentile temperature at ESDE during summer 2006.
Upper Isthmus Slough	20.0	Based on the estimated 75th percentile temperature at Summer Bridge during summer 2006.
Lower South Slough	16.1	Based on the 75th percentile dry season 2009-2014 temperature measured at Valino Island. The 75th percentile was selected as it is on the warmer end of annually occurring temperatures.
Upper South Slough	18.1	Based on the 75th percentile dry season 2009-2014 temperature measured at Winchester Arm. The 75th percentile was selected as it is on the warmer end of annually occurring temperatures.

5.3.3.3 Salinity

Salinity results for the summer low flow condition were averaged from the Existing Conditions and the 2023 PA over time and over the entire water depth to produce the average salinity required for calculating saturation DO, DO_s. The assigned salinity values are shown in Table 5-7.

Table 5-7
Assigned Salinity for Each Polygon

Area	Salinity (ppt)
Entrance	32.80
Lower Lower Bay	32.66
Upper Lower Bay	32.21
Haynes Inlet	30.54
Lower Upper Bay	31.36
Upper Upper Bay	30.55
Coos River	28.45
Lower Isthmus Slough	30.27
Upper Isthmus Slough	29.48
Lower South Slough	32.23
Upper South Slough	30.62

5.3.3.4 Dissolved Oxygen

Existing average DO concentrations were estimated based on the in-bay sensor data described in Section 2.2.3. The model uses the median DO for the lowest month from the closest sensor. For polygons in which no sensor is present, nearby values were adjusted. Table 5-8 shows the estimated summer average DO values and the data source/rationale behind each estimate.

Table 5-8
Assigned DO for Each Polygon

Area	DO (mg/L)	Rationale
Entrance	8.1	September median (Charleston Bridge sensor)
Lower Lower Bay	7.9	Entrance/Upper Lower Bay average
Upper Lower Bay	7.7	September median (BLM sensor)
Haynes Inlet	6.7	0.5 mg/L less than Lower Upper Bay
Lower Upper Bay	7.2	September median (North Point sensor)
Upper Upper Bay	6.6	Same as Coos River value

Coos River	6.6	July median (Coos River sensor)
Lower Isthmus Slough	5.7	August median (Isthmus Slough sensor)*
Upper Isthmus Slough	5.3	August median (Isthmus Slough sensor)*
Lower South Slough	7.5	September median (Valino Island sensor)
Upper South Slough	6.3	September median (Winchester Arm sensor)

** The sensor is on the border between these two polygons, and is 5.5 mg/L*

5.3.3.5 Water Depth

Average water depth of each polygon was obtained from the hydrodynamic model bathymetry input. The depths were averaged from the Existing Conditions and the 2023 PA to provide an overall average water depth for use in the DO model. Averaging from both scenarios was necessary since the DO model is based on $\Delta\tau$ for the 2023 PA minus the Existing Conditions.

5.3.3.6 Wind Speed

Wind speed data was obtained from the NOAA meteorological station CHAO3 - 9432780 - Charleston, OR. The period May 2014 – November 2018 was used for determining wind speed statistics. Years prior to 2014 were available, but the data were sparse. The lowest summer winds occur in August. The August mean wind speed for the analysis period is 2.05 m/sec, so this value was used in the model.

5.3.3.7 Difference in Water Age

The final model input consists of the change in water age ($\Delta\tau$) for each polygon resulting from the 2023 PA compared to the Existing Conditions (see Table 5-4).

5.3.4 Results

The computed cumulative frequency distribution (CFD) for changes in DO during the summer were computed for the 2023 PA and are listed in Table 5-9. In this table, a negative value indicates a decrease in DO.

Average expected changes (mean values in the table) to the DO in the tributaries, based on projected changes in temperature and salinity, are expected to be less than 0.26 mg/L and in the Upper Upper Bay less than 0.4 mg/L. The greatest reduction in average summer DO (i.e., 0.85 mg/L) occurs at the Upper Lower Bay as a result of the greatest increase in water age. However, the existing DO at this location is relatively high, with the median summer DO above 7 mg/L (see Figure 2-15). In the Lower Isthmus Slough, where the existing DO is low, the expected reduction in DO is 0.26 mg/L under the 2023 PA (approximately a 5% change), with the maximum predicted change being 0.37 mg/L at the 99th percentile. All changes to median DO under the 2023 PA are within 11% of the existing median DO concentrations.

As noted above, this limited-scope DO model is considered conservative for predicting DO decreases (i.e., the model produces potentially greater than expected DO decreases) since it assumes constant DOC and NH_4.

Table 5-9
Non-exceedance CFD (percent less than value) for summer ΔDO (mg/L) for 2023 PA

Area	1%	5%	10%	25%	50%	75%	90%	95%	99%	Mean
Entrance	0.50	0.24	0.07	0.00	-0.02	-0.12	-0.22	-0.27	-0.77	-0.05
Lower Lower Bay	0.57	0.34	0.17	-0.06	-0.22	-0.36	-0.57	-0.69	-0.84	-0.21
Upper Lower Bay	-0.16	-0.30	-0.47	-0.72	-0.86	-1.04	-1.16	-1.22	-1.32	-0.85
Haynes Inlet	-0.14	-0.17	-0.18	-0.22	-0.29	-0.37	-0.44	-0.46	-0.49	-0.30
Lower Upper Bay	-0.23	-0.37	-0.40	-0.47	-0.61	-0.80	-0.91	-0.95	-1.01	-0.63
Upper Upper Bay	-0.16	-0.18	-0.21	-0.27	-0.34	-0.48	-0.53	-0.57	-0.71	-0.37
Coos River	0.28	0.13	0.01	-0.06	-0.14	-0.17	-0.20	-0.21	-0.24	-0.10
Lower Isthmus Slough	-0.11	-0.17	-0.20	-0.21	-0.24	-0.32	-0.36	-0.37	-0.37	-0.26
Upper Isthmus Slough	0.05	0.00	-0.01	-0.02	-0.03	-0.06	-0.09	-0.13	-0.17	-0.04
Lower South Slough	0.16	0.06	0.05	0.04	0.02	0.00	-0.02	-0.03	-0.11	0.02
Upper South Slough	0.02	0.02	0.02	0.02	0.01	0.00	0.00	0.00	-0.01	0.01

The above analytical method predicts changes to DO. The distribution of DO can be estimated by adding the changes to the measured median DO (see Figure 2-15 through Figure 2-22). Figure 5-10 through Figure 5-17 take the worst-case month of the year from the measured median data, and apply DO changes under the 2023 PA. These figures also include two standards posted by Oregon Department of Fish and Wildlife (ODFW); the 6.5 mg/L standard is the 30-day mean minimum and the 4.0 mg/L is the instantaneous minimum.

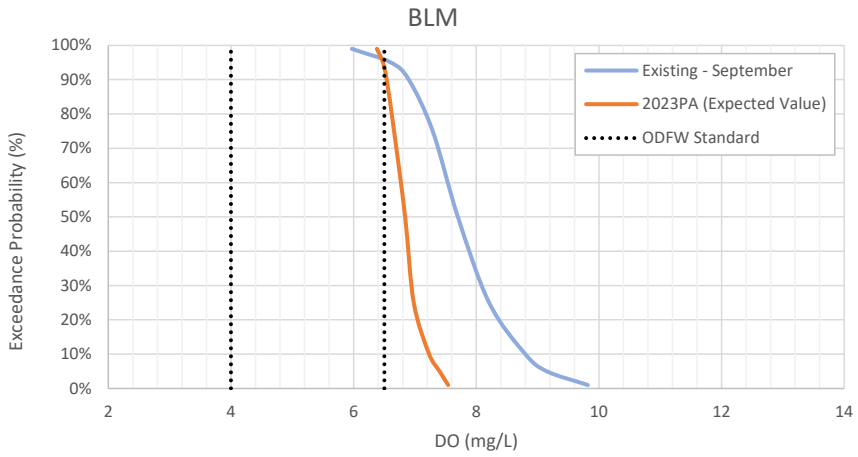

Figure 5-10
DO under 2023 PA, BLM sensor

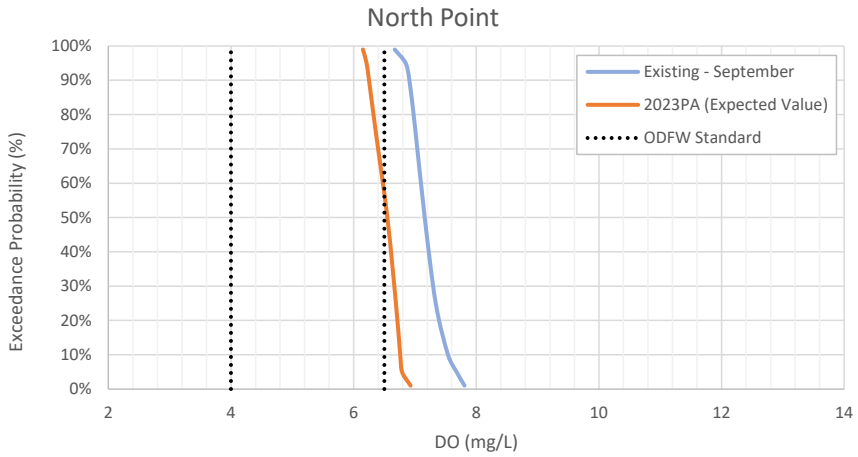

Figure 5-11
DO under 2023 PA, North Point sensor

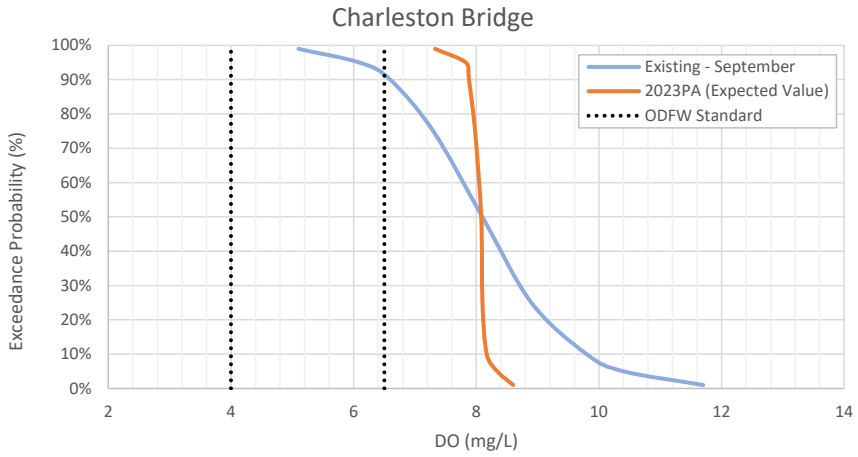

Figure 5-12
DO under 2023 PA, Charleston Bridge sensor

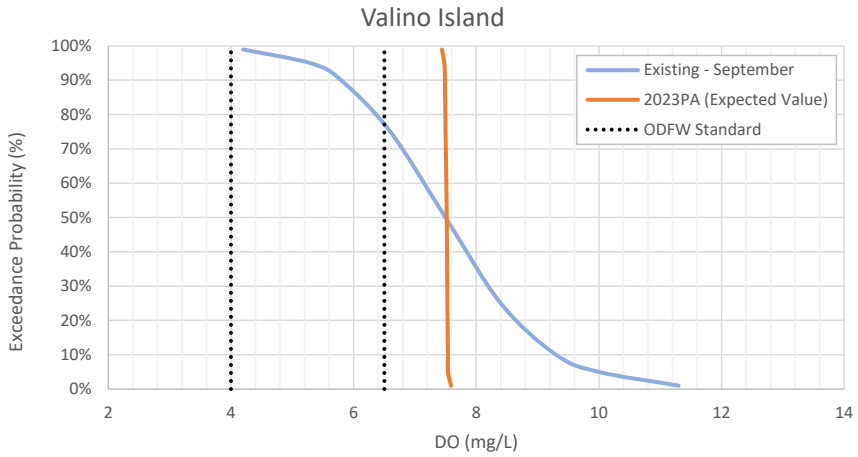

Figure 5-13
DO under 2023 PA, Valino Island sensor

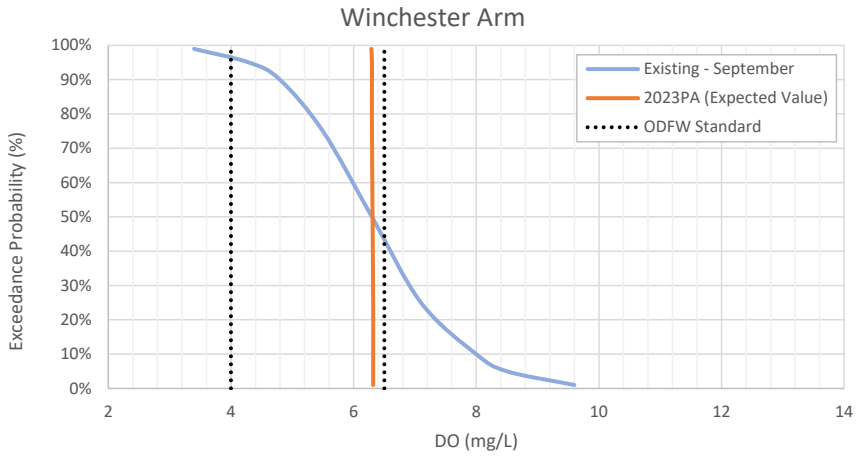

Figure 5-14
DO under 2023 PA, Winchester Arm sensor

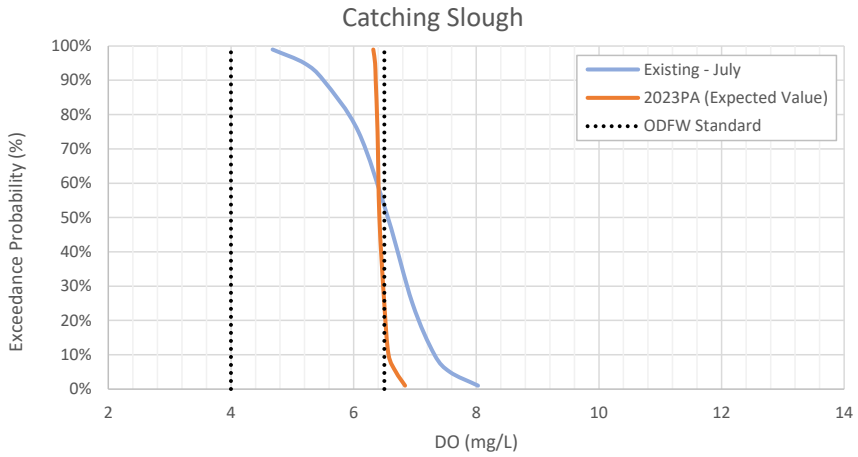

Figure 5-15
DO under 2023 PA, Catching Slough sensor

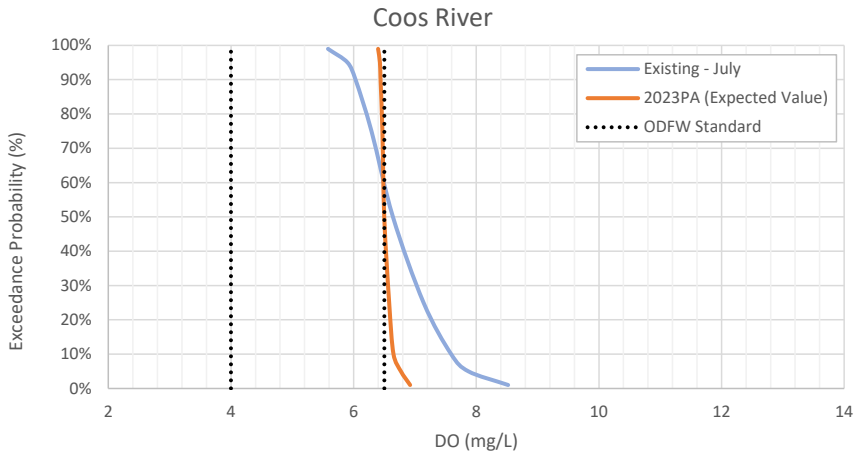

Figure 5-16
DO under 2023 PA, Coos River sensor

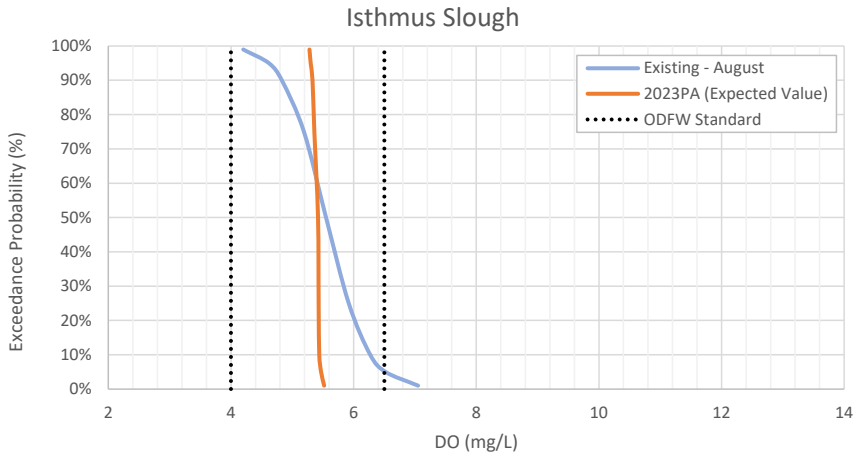

Figure 5-17
DO under 2023 PA, Isthmus Slough sensor

5.4 Conclusions

Model results show that residence times increase within the Lower Bay as a result of the increased volume capacity of this area compared to the small increase in tidal prism. However, residence time in the Lower Bay is still less than 1.5 days for the 2023 PA, indicating highly flushed conditions with no concern of impact to water quality parameters. In addition, residence times as a result of the 2023 PA change by less than 1.2 hours in the Upper Bay and the tributaries, indicating little change to flushing here. Except at the Upper Isthmus Slough, residence times are generally less than 3 days throughout the Coos Bay estuary.

The water age calculation shows that water particles reside for more time within the entire Coos Bay system under the 2023 PA. The largest increases in water age occur within the Upper Lower Bay, which results from the increase in water volume in this area. The mean water age increase is less than 1.85 days.

Commented [SJ39]: A-3-31: Clearly define residence time results.

Commented [SJ40R39]: Text added for results.

Average expected changes to the DO in the tributaries are expected to be less than 0.26 mg/L and in the Upper Upper Bay less than 0.4 mg/L. The greatest reduction in average summer DO (i.e., 0.85 mg/L) occurs at the Upper Lower Bay as a result of the greatest increase in water age. However, the existing DO at this location is relatively high, with the median summer DO above 7 mg/L. In the Lower Isthmus Slough, where the existing DO is low, the expected reduction in DO is 0.26 mg/L under the 2023 PA (approximately a 5% change). All changes to median DO under the 2023 PA are within 11% of the existing median DO concentrations.

6. SEDIMENT TRANSPORT MODELING

This chapter evaluates sediment transport and changes to maintenance dredging resulting from proposed navigation channel improvements for the channel from RM 2.5 upstream to RM 15 and in the Charleston Channel. Maintenance dredging in the ocean entrance is addressed in Sub-Appendix 4, *Offshore and Ocean Entrance Dynamics*. Therefore, the downstream extent of applicability for the sediment transport modeling is at RM 2.5.

Commented [CT41]: PDT A-3-2: Specify the downstream extent of applicability for estuary models, for both the circulation model and the sediment transport model.

Commented [CT42R41]: Added the downstream extent of sediment transport modeling.

Sediment dredged from the Coos Bay channel between RM 2.5 and RM 12 is typically of silt or sand sized (USACE/USEPA 1986). Table 2-6 summarizes complete maintenance dredging quantities from 1998 to 2014 for the federally maintained channel below RM 12. A sieve analysis conducted by SHN Consulting Engineers and Geologists, Inc. in 2006 also showed that the fine, well-sorted sand is the primary sediment in the channel (Black & Veatch 2006). The finer sediments that are sourced from the Coos River and other tributaries settle out above RM 12. At present, the area above RM 12 is not regularly maintained by the USACE. It should be noted that this study only considered sand-sized sediments.

6.1 Model Setup

Sediment transport and deposition was modeled using the 2D MIKE-21 FM model suite, with coupled hydrodynamic and non-cohesive sand transport (ST) modules[6]. The modeling domain and boundary conditions (in terms of water levels and discharge) were the same as that used for hydrodynamics. Deposition, transport, and erosion of sand under the action of currents was taken into account by the sand transport module. Use of MIKE-21 model for this application was accepted by USACE (OIPCB 2016).

Both 2D and 3D models use the same sand transport module which can include bed load and suspended load. The only difference between the two configurations is the ability to use bed shear stresses computed from the bottom layer in 3D, while both configurations include depth averaged velocity forcing option. The module allows to adjust bottom roughness for sand transport separately from flow computation, which gives the sand module similar abilities in either 2D or 3D configuration. As a result, the primary reason for using 2D model was the computational time as the production runs for sediment transport were conducted for one full year and 3D simulations would substantially increase the computational time.

6.1.1 Boundary Conditions

The sediment transport modeling was conducted for the full year of 2011, with offshore tides and upstream freshwater inflows being applied as the hydrodynamic boundary conditions. Details about hydrodynamic boundary conditions are described in Section 3.4.2. Figure 6-1 presents the measured water levels at Charleston, OR for the full year of 2011 and Figure 6-2 presents the upstream freshwater inflows.

Equilibrium sediment transport boundary conditions were assumed at all boundaries, including offshore and upstream. Such boundary conditions imply that sediment inflow is in equilibrium with local current velocity and therefore allows the model to account for sediment fluxes at model

[6] The model does not capture transport, sedimentation, and erosion of fine sediments that typically settle out above RM 12.0 and on the mud flats.

boundaries. This assumption allows the model to simulate sediment transport under a changed condition with different velocities at boundaries, as calculated from the hydrodynamic module.

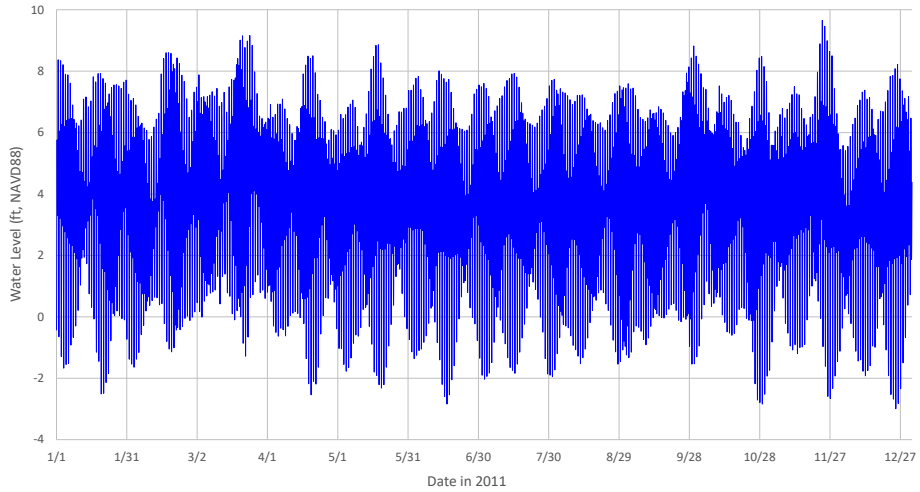

Figure 6-1
Measured Water levels at Charleston, OR for Sediment Transport Modeling

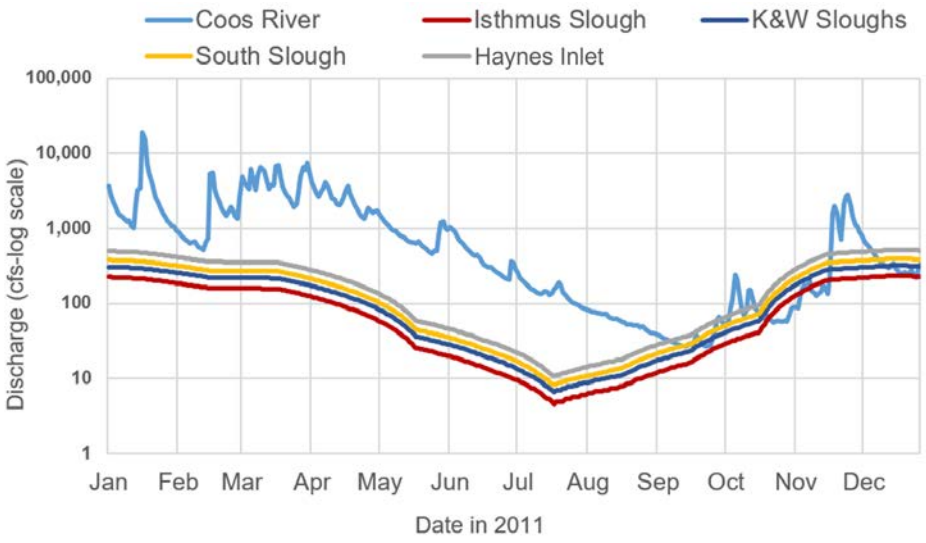

Figure 6-2
Freshwater Inflows as Upstream Boundary Conditions for Sediment Transport Modeling

6.1.2 Grain Size Measurements

Information regarding grain size within the Coos Bay estuary is available from these sources: USACE (2005 & 2009), SHN Consulting Engineers & Geologists (2006), and Geotechnical Resources, Inc. (2010 & 2011). These data are described in Sub-Appendix 5. Figure 6-3 through Figure 6-6 and Table 6-1 show the median grain size and percent of fines and sand compiled from these sources.

The measurements generally show a mixture of coarser grain sizes in the channel and finer grain sizes that may be in the channel or in shallow water areas. The coarser grain sizes between 0.35 and 0.45 mm reflect channel bottom conditions from the entrance to RM 9, and grain size decreases to 0.2 mm between RM 10 and RM 11. There is a mixture of grain sizes around 0.25 mm in this area. The southern part of the Upper Bay, above RM 12, is characterized by much finer sediments with a typical grain size of 0.04 mm.

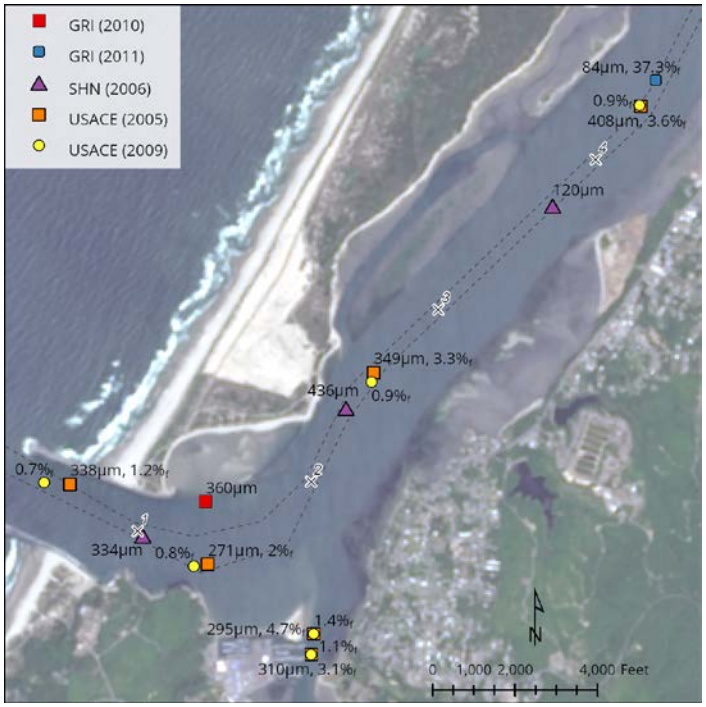

Figure 6-3
Measured Channel Bed Grain Size (D_{50} in µm, % of fines) in Lower Bay

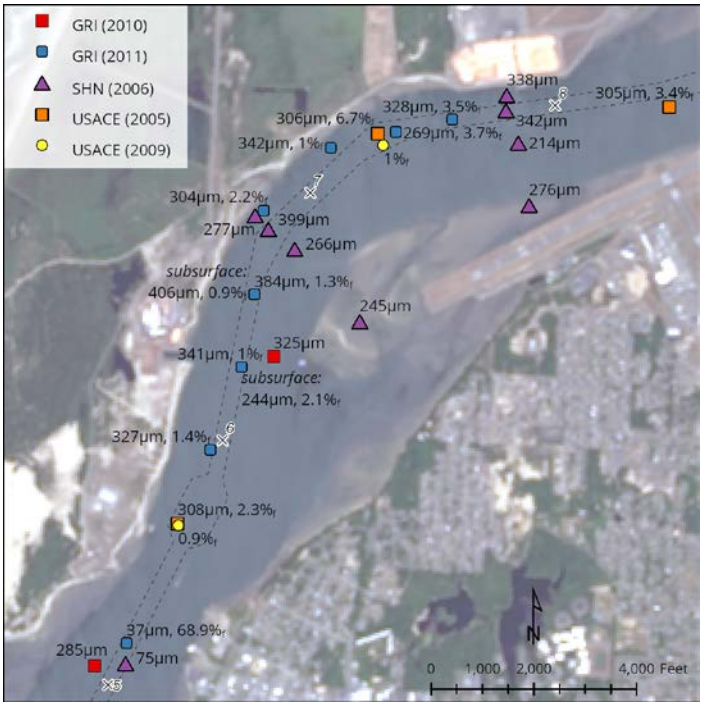

Figure 6-4
Measured Channel Bed Grain Size (D_{50} in µm, % of fines) in Jarvis Ranges

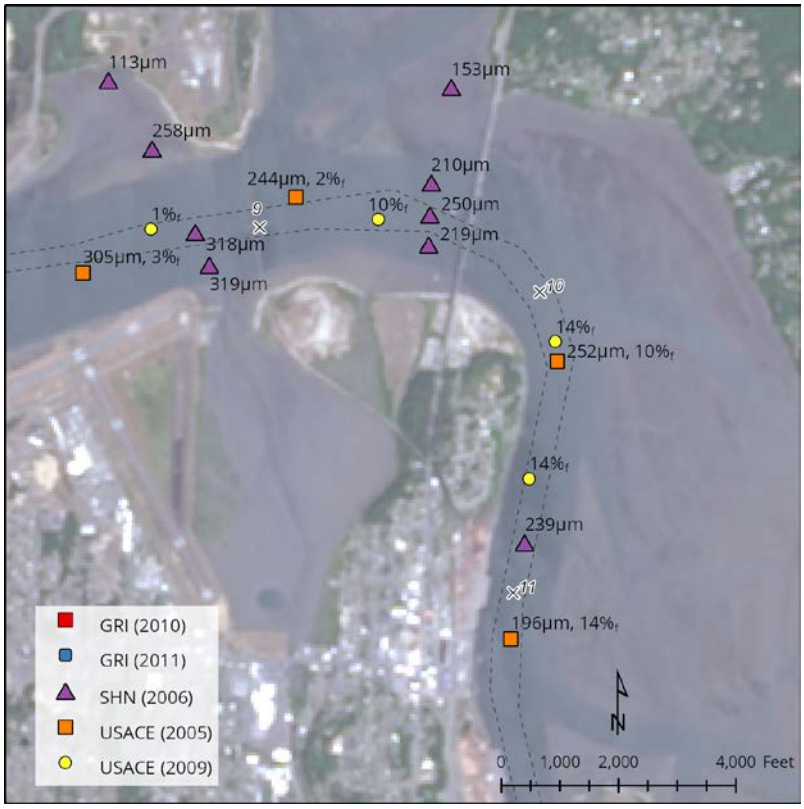

Figure 6-5
Measured Channel Bed Grain Size (D_{50} in µm, % of fines) in North Bend Ranges

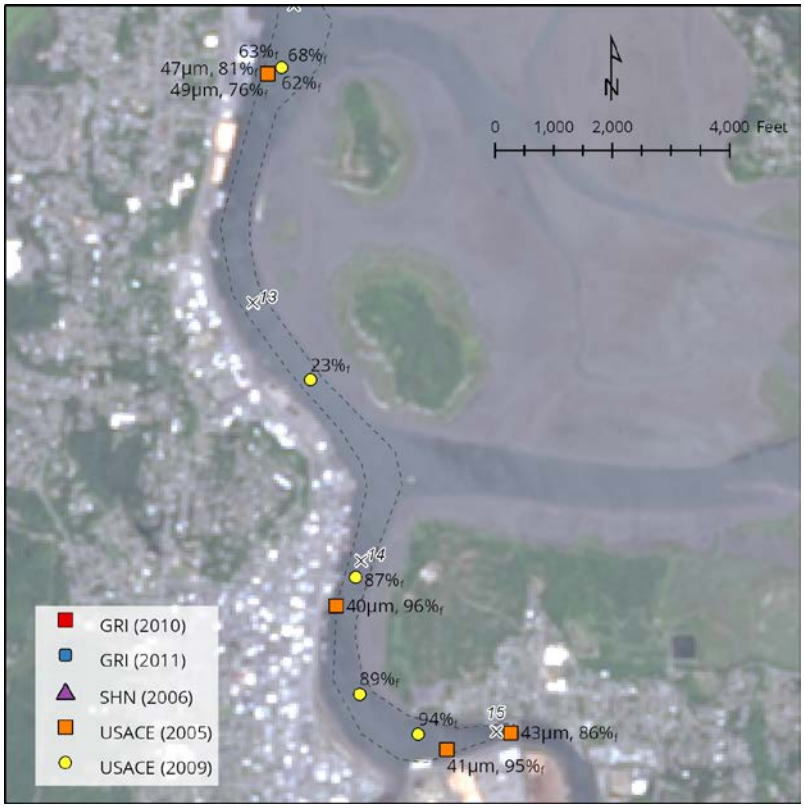

Figure 6-6
Measured Channel Bed Grain Size (D_{50} in µm, % of fines) in Upper Bay

Table 6-1
Measured Channel Bed Grain Size

Sample ID	Latitude	Longitude	Depth, ft	D50, mm	% Fines	% Sand	Source
S-3	43.3851	-124.291	44	0.083929	37.3	61.8	GRI2011
S-4	43.3942	-124.285	45	0.036824	68.9	29.4	GRI2011
S-5	43.4047	-124.28	39	0.326757	1.4	98.2	GRI2011
S-6	43.4092	-124.278	46	0.341127	1	98.9	GRI2011
6-Z	43.4092	-124.278	51	0.244397	2.1	97.9	GRI2011
S-7	43.4131	-124.277	42	0.383904	1.3	98.1	GRI2011
7-Z	43.4131	-124.277	51	0.406211	0.9	98.7	GRI2011
S-8	43.4176	-124.276	37	0.304417	2.2	97.6	GRI2011
S-9	43.4211	-124.272	33	0.341571	1	98.4	GRI2011

Sample ID	Latitude	Longitude	Depth, ft	D50, mm	% Fines	% Sand	Source
S-10	43.4221	-124.267	45	0.268877	3.7	96.3	GRI2011
S-11	43.4229	-124.263	46	0.328095	3.5	96.2	GRI2011
0915CB-GC-01	43.36247	-124.2		0.043	86.4	13.6	USACE2005
0915CB-GC-02	43.36156	-124.204		0.041	94.6	5.4	USACE2005
0915CB-GC-03	43.36803	-124.211		0.04	96	4	USACE2005
0915CB-GC-04	43.39272	-124.217		0.049	75.9	23.4	USACE2005
0915CB-BC-05	43.39272	-124.217		0.047	80.9	19.1	USACE2005
0915CB-BC-06	43.40789	-124.219		0.196	13.5	80.9	USACE2005
0915CB-BC-07	43.42094	-124.216		0.252	10	80	USACE2005
0915CB-BC-08	43.42806	-124.234		0.244	2.3	97.6	USACE2005
0915CB-BC-09	43.42408	-124.247		0.305	3.4	88.6	USACE2005
0915CB-BC-10	43.42197	-124.268		0.306	6.7	92.9	USACE2005
0915CB-BC-11	43.40069	-124.282		0.308	2.3	97.7	USACE2005
0915CB-BC-12	43.38331	-124.292		0.408	3.6	94.4	USACE2005
0915CB-BC-13	43.36478	-124.316		0.349	3.3	96.3	USACE2005
0915CB-BC-14	43.35153	-124.33		0.271	2	97.6	USACE2005
0915CB-BC-15	43.35642	-124.343		0.338	1.2	98.8	USACE2005
0915CB-BC-16	43.34722	-124.32		0.295	4.7	95.3	USACE2005
0915CB-BC-17	43.34583	-124.32		0.31	3.1	96.9	USACE2005
JCEP-1	43.3532	-124.336		0.334		99	SHN2006
JCEP-2	43.3623	-124.318		0.436		99.2	SHN2006
JCEP-3	43.3764	-124.3		0.12		62	SHN2006
JCEP-4	43.3931	-124.285		0.075		50	SHN2006
JCEP-5	43.4173	-124.277		0.277		97.1	SHN2006
JCEP-6	43.4166	-124.276		0.399		99.2	SHN2006
JCEP-7	43.4156	-124.274		0.266		99	SHN2006
JCEP-8	43.4119	-124.269		0.245		98.6	SHN2006
JCEP-9	43.4243	-124.259		0.338		95.5	SHN2006
JCEP-10	43.4235	-124.259		0.342		72	SHN2006
JCEP-11	43.4218	-124.258		0.214			SHN2006
JCEP-12	43.4185	-124.257		0.276			SHN2006
JCEP-13	43.4331	-124.246		0.113			SHN2006
JCEP-14	43.43	-124.243		0.258			SHN2006
JCEP-15	43.4262	-124.24		0.318			SHN2006
JCEP-16	43.4247	-124.239		0.319			SHN2006
JCEP-17	43.4335	-124.224		0.153			SHN2006
JCEP-18	43.429	-124.225		0.21			SHN2006
JCEP-19	43.4275	-124.225		0.25			SHN2006

Sample ID	Latitude	Longitude	Depth, ft	D50, mm	% Fines	% Sand	Source
JCEP-20	43.4261	-124.225		0.219			SHN2006
JCEP-21	43.4124	-124.218		0.239			SHN2006
POCB-B2	43.40983	-124.275		0.325			GRI2010
POCB-B4A	43.39292	-124.287		0.285			GRI2010
POCB-B9	43.35569	-124.33		0.36			GRI2010
091609CB-BC-1	43.34583	-124.32			1.1	98.9	USACE2009
091609CB-BC-2	43.34722	-124.32			1.4	98.6	USACE2009
091609CB-BC-3	43.35647	-124.345			0.7	99	USACE2009
091609CB-BC-4	43.35133	-124.331			0.8	99.2	USACE2009
091609CB-BC-5	43.36414	-124.316			0.9	99.1	USACE2009
091609CB-BC-6	43.38336	-124.292			0.9	99	USACE2009
091609CB-BC-7	43.40061	-124.282			0.9	99	USACE2009
091609CB-BC-8	43.42136	-124.268			1	99	USACE2009
091609CB-BC-9	43.42628	-124.243			1	98.9	USACE2009
091609CB-BC-10	43.42719	-124.228			10.13	89.89	USACE2009
091609CB-BC-11	43.42186	-124.217			14.15	73.08	USACE2009
091609CB-BC-12	43.41542	-124.218			13.68	86.21	USACE2009
091609CB-BC-13	43.39303	-124.216			68.42	31.49	USACE2009
091609CB-GC-13A	43.39303	-124.216			62.24	37.76	USACE2009
091609CB-GC-13Z	43.39303	-124.216			62.87	37.11	USACE2009
091609C8-GC-14	43.37853	-124.214			23.38	76	USACE2009
091609CB-BC-15	43.36942	-124.21			87.18	12.81	USACE2009
091609CB-BC-16	43.36397	-124.21			88.86	11.13	USACE2009
091609CB-BC-17	43.36222	-124.206			94.43	5.57	USACE2009

Figure 6-7 shows the grain size map used for sediment transport modeling. This map assumes a grain size of 0.36 mm in the deeper water areas from the entrance to RM 9, with smaller grain sizes in the shallower areas and in the South Slough. At the Upper Bay, the grain size decreases further. The grain sizes were limited to 0.04 mm as finer sediments were observed upstream of RM 12.

The grain size mapping follows the standard of practice for modeling sediment transport, which is to look at the general trend of grain size distribution. This method is used because there is always limited data available on measured grain size over a large area like an estuary. A complete distribution of grain size is rarely available and, quite often, there are a few samples that contradict the general pattern. Therefore, it may appear that some individual data points were ignored during the development of the grain size map because the general pattern (decreasing grain size with increasing river mile) was identified and simulated. For instance, two data samples from the SHN (2006) between RM 3 and RM 5 (i.e., JCEP-3 and JCEP-4) show the presence of fine material in the FNC, but the grab samples mostly consisted of dissolved sandstone, not loose sediments.

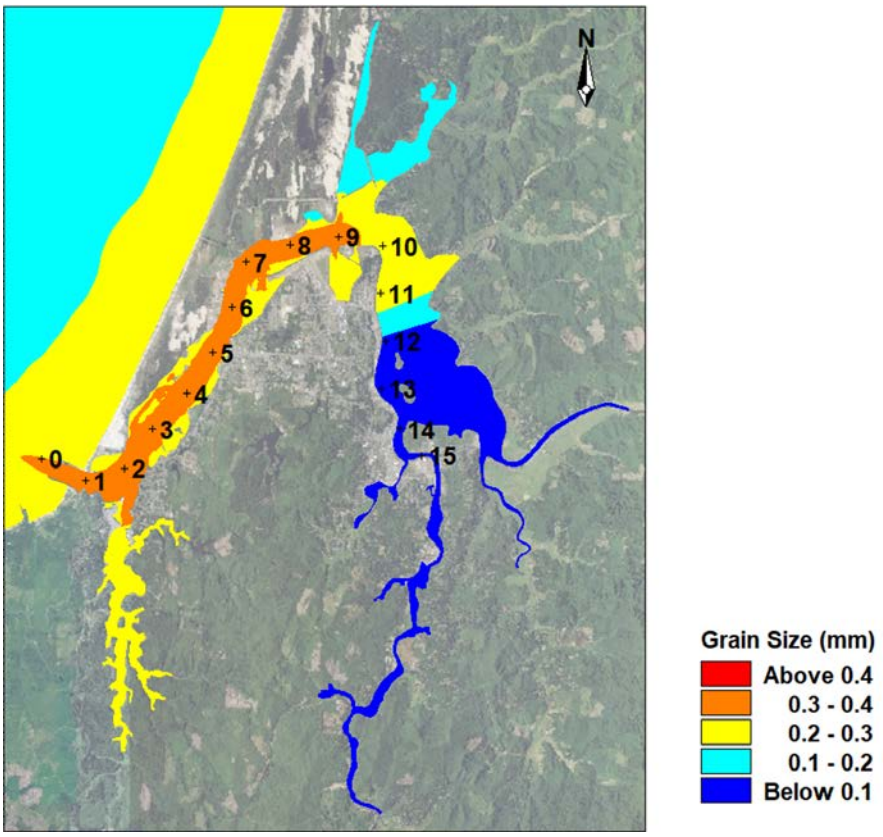

Figure 6-7
Grain Size Map for Sediment Transport Modeling

6.1.3 Geophysical Investigations

Shallow rock underlies much of the navigation channel, from the ocean entrance to approximately RM 6. When this underlying rock is close to the surface, it limits the potential for erosion. Figure 6-8 shows the sand layer thickness used for sediment transport modeling. This sand layer thickness was developed based on the depth to the rock layer measured by various DEA surveys described in Sub-Appendix 2, *Geophysical Report*. Outside the navigation channel, areas of shallow rock were estimated based on bathymetric features. To simulate armored reaches of the shoreline that are not susceptible to erosion, shallow rock was included – that is, the sand layer was assumed to be thin – along the hardened reaches of the shoreline at RFP, part of the airport runway, and the shoreline close to the navigation channel in the Upper Bay. It should be noted that the map of sand layer thickness only covers RM 2.5 and upstream as this is the focus area for the estuarine sediment transport modeling.

Commented [NY43]: A-3-34 (Dr. Checks # 8071912)

Commented [SJ44R43]: Also A-3-53

Commented [CT45R43]: Added explanation in the above paragraph. Also note that we now revised the grain size map to reflect 0.04 mm size above RM 12 and used it in the model.

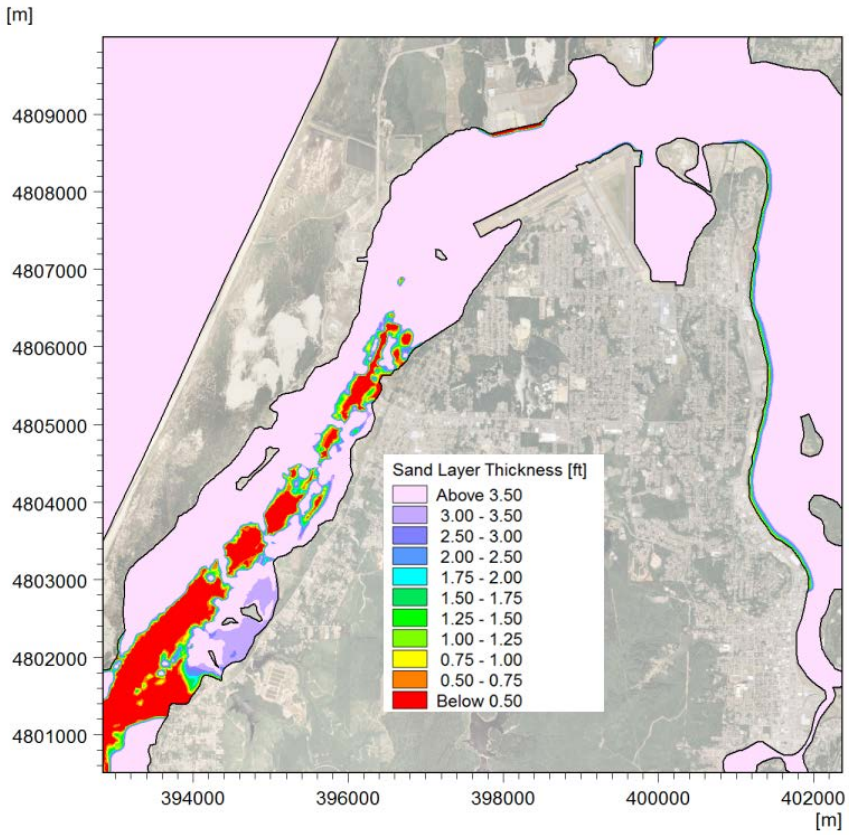

Figure 6-8
Thickness of Sand Layer above Rock

6.1.4 Model Assumptions and Input Parameters

Model input parameters used in the sand transport module are listed in Table 6-2. All parameters were selected within typical ranges through calibration efforts.

During the calibration, three out of four sediment theories were tested. Both the "Engelund & Fredsoe" and the "Engelund & Hansen" theory predicted higher shoaling rate in the Coos & Empire Ranges than the Jarvis Ranges, which is the reverse trend from that observed in the dredging records. Only the "Van Rijn" theory predicted the same trend.

Table 6-2
Input Parameters for Sand Transport Module

Parameter	Value	Comment
Bedload Formula	Van Rijn	Selected from four bedload formulae available in MIKE-21 ST: Engelund & Fredsøe Engelund & Hansen Van Rijn Meyer-Peter and Müller
Suspended Load Formula	Van Rijn	Selected from three formulae available in MIKE-21 ST: Engelund & Fredsøe Engelund & Hansen Van Rijn
Bedload to Suspended Load Ratio	1:1.7	Selected based on model calibration
Model description	Non-Equilibrium	Uses advection-dispersion module to track suspended load
Porosity	0.4	Default value
Relative Sediment Density	2.65	Default value
Scaling Factor for Eddy Viscosity	1.0	Default value: dispersion follows hydrodynamic model
Bed Resistance	Resistance from HD module (i.e., used value determined during HD simulation)	Selected from four bed resistance: Chezy number Manning number Alluvial resistance Resistance from HD simulation

6.2 Model Calibration

The calibration for sediment transport modeling within the Coos Bay estuary was based on existing bathymetry and the annual average quantity of maintenance dredging listed in Table 2-6. Because the compiled model elevation is a composite of surveys after 2006, the existing bathymetry best represents an estuary condition after 2006. Therefore, the dredging quantities were also processed after 2006 accordingly. Figure 6-9 shows the channel ranges as defined in Table 2-6. The model's predicted annual sedimentation volumes in these ranges were compared to annual dredging volumes in the corresponding range.

Over an extended period of time, dredging records reasonably well corroborate the average annual sedimentation rate. Although the frequency and magnitude of annual dredging is dependent on budget and capability, the amount of sediment removed depends on the sedimentation levels and is limited by the authorized depths. The removed volume was deposited over the time between two consecutive dredging events, from which a rate can be derived. The only uncertainty in this method

is the exact surface area being dredged. However, the surface is limited by the authorized dimensions. Therefore, over several dredging cycles, all deposited material within critical areas of the channel would be removed.

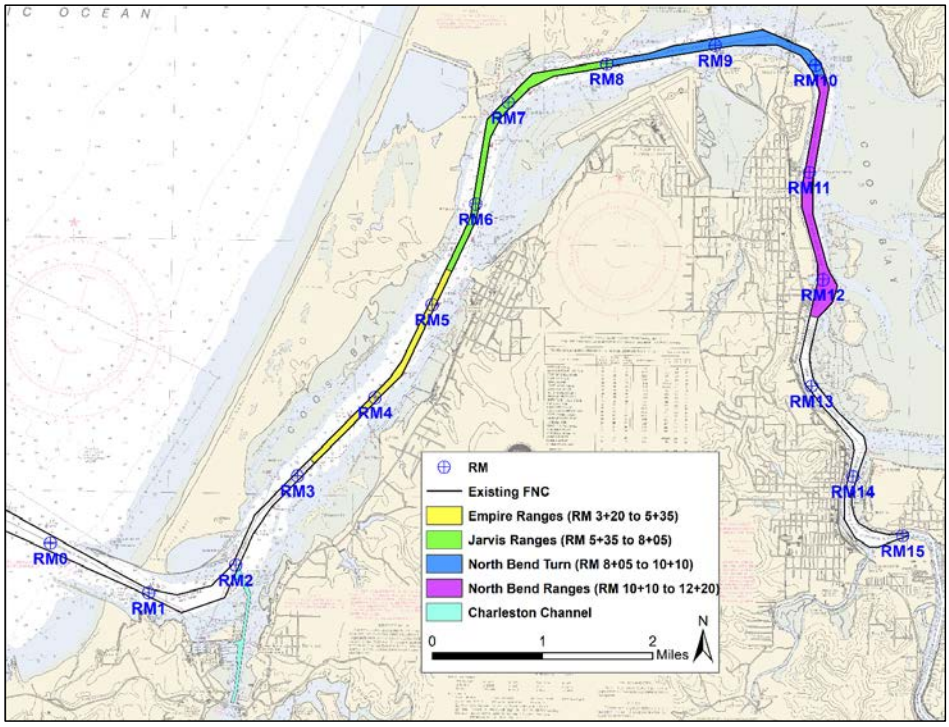

Figure 6-9
Channel Ranges Used for Sediment Transport Modeling Calibration

Table 6-3 and Figure 6-10 show that the model over-predicted the annual dredging volume at the North Bend Turn, and under-predicted the dredge volumes everywhere else. The simulated volume is generally within 10 percent of the average annual dredging volume, except in the Charleston Channel. In addition, the simulated total sediment volume is within 5 percent of the total annual dredging volume. This represents good overall calibration given the typical uncertainty of sediment transport modeling.

The main discrepancy between the simulated and actual maintenance dredging volumes is the location of where the deposition occurs. Nevertheless, the difference between total predicted volume and actual volume is less than 5 percent. Review of recent[7] modeling studies confirmed

[7] Williams & Esteves (2017) stated that "a model predicting the dredged volumes to within 50% of the measured rates is normally deemed to be satisfactory for most practical applications".

that performance of the sediment transport modeling is within the standard of practice to quantitatively compare alternatives. Sediment transport model results should be interpreted with an understanding of model calibration and skill in representing existing average dredge volumes.

Table 6-3
Sedimentation Calibration Results

Reach	Average Dredge Volume, CY/yr	Simulated Volume, CY/yr	Ratio simulated / actual volume
Empire Ranges RM 3+20 to 5+35	9,000	8,000	0.9
Jarvis Ranges RM 5+35 to 8+05	73,000	67,000	0.9
North Bend Turn RM 8+05 to 10+10	37,000	41,000	1.1
North Bend Ranges RM 10+10 to 12+20	26,000	24,000	0.9
Charleston Channel	15,000	12,000	0.8
Total Federal	160,000	152,000	0.95

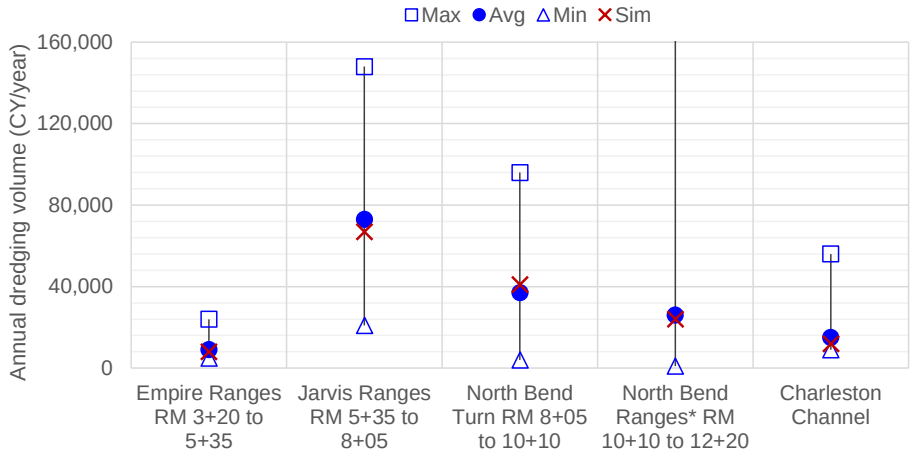

** The maximum annual dredging volume for North Bend Ranges is 335,000 and is not shown for clarity.*

Figure 6-10
Range of Annual Dredging Volume

The results in terms of 1-year bed level change for the Existing Conditions for the entire estuary and a zoomed-in view of the FNC are shown in Figure 6-11 and Figure 6-12, respectively. Within each tidal cycle, sand moves upstream and downstream with flood and ebb currents, respectively, but the net sediment transport direction is downstream.

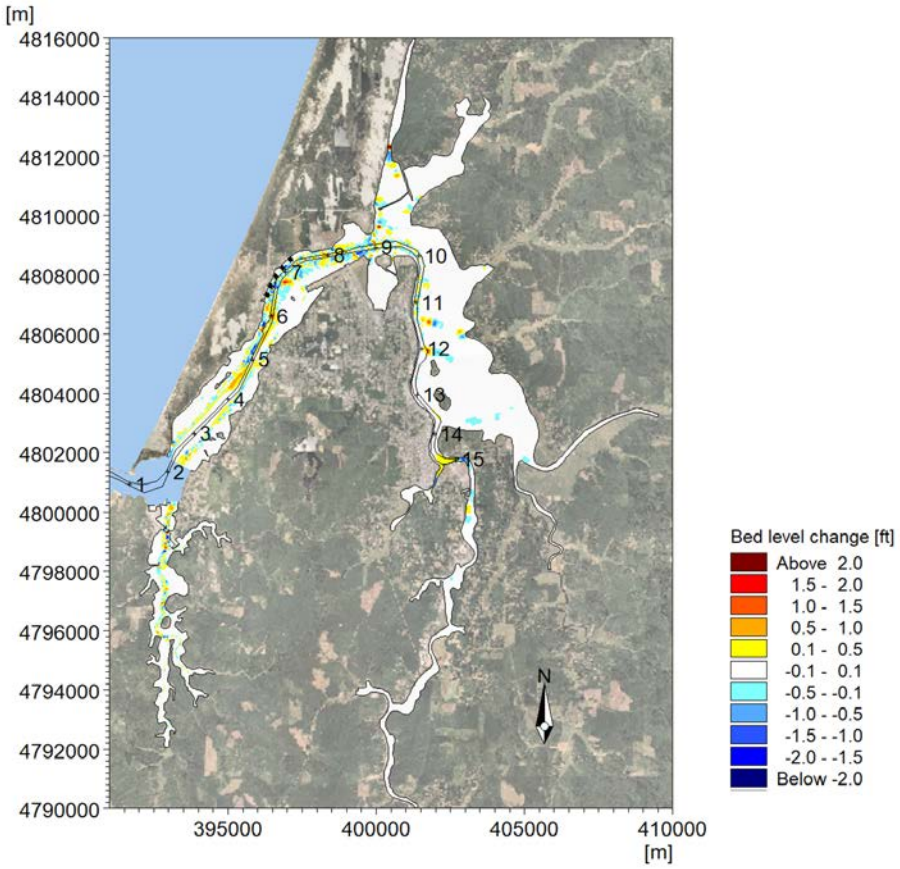

** Results downstream of RM 2.5 see Sub-Appendix 4 Offshore and Ocean Entrance Dynamics.*

Figure 6-11
One Year Bed Level Changes in Coos Bay Estuary: Existing Conditions

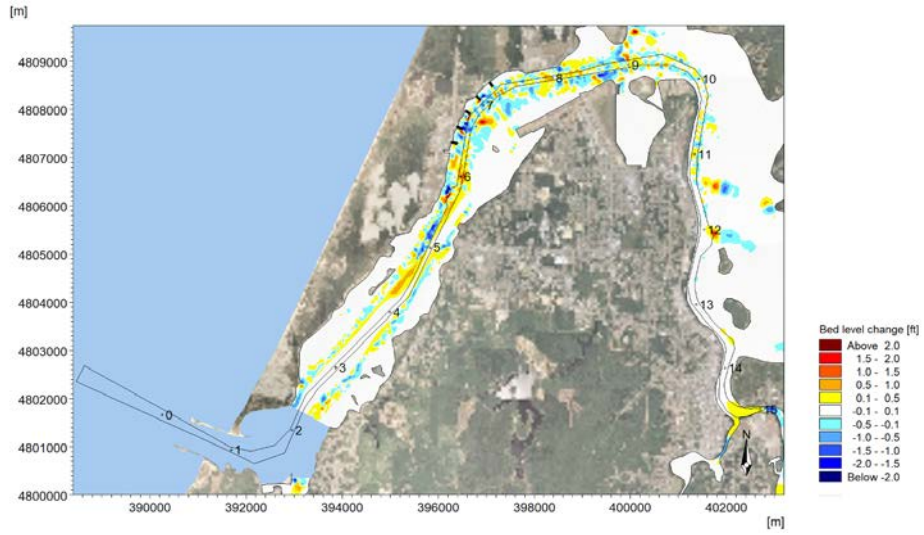

** Results downstream of RM 2.5 see Sub-Appendix 4 Offshore and Ocean Entrance Dynamics.*

Figure 6-12
One Year Bed Level Changes in Coos Bay FNC: Existing Conditions

6.2.1 Model Performance and Similar Projects

There are no specific codes or standards for assessing the performance of sediment transport models. To assess the performance of this modeling study in representing the Existing Conditions and the 2023 PA, similar and recent studies conducted by ERDC or approved by USACE were compiled and reviewed. A list of these studies and metrics they used to report and quantify goodness of fit for suspended sediment concentration and sedimentation rate is listed in Table 6-4. The model's performance metrics is listed in the last row of this table. It can be observed that this study is consistent with recent and similar modeling studies conducted by ERDC or approved by USACE in terms of model performance.

Table 6-4
Descriptors and Metrics for Reporting Goodness of Fit for Sediment Transport Modeling Results, in terms of Suspended Sediment Concentration or Sedimentation Rate, against Observations in Similar and Recent Modeling Studies Conducted by ERDC or Approved by USACE for Channel Modification Projects as well as This Project

Project (Source)	Visual Inspection	Max. Diff	RMSE	IOA	Phase Shift	Sensitivity Analysis	Description of Model Performance
Channel Deepening in Thimble Shoals (Zhang et al. 2017)	N/A	N/A	N/A	N/A	N/A	N/A	N/A
Seattle Harbor Deepening EIS (ERDC 2016)	N/A	N/A	N/A	N/A	N/A	N/A	N/A
Redwood City Harbor Navigation Improvement EIS (HydroPlan 2015)	✓	350 mg/L*	×	×	×	✓	"Sufficiently accurate"
Houston-Galveston Navigation Channel (ERDC 2014)	✓	20 mg/L*#	×	×	×	✓	×
Matagorda Ship Channel Study (ERDC 2013)	✓	×	×	×	×	×	"Agree"
Savannah Harbor Expansion Project (Tetra Tech 2011)	N/A	N/A	N/A	N/A	N/A	N/A	N/A
Grays Harbor Navigation Improvement EIS (ERDC 2010)	✓	3000 mg/L*#	×	×	×	×	×
This Study Total Volume	✓	5%	×	×	×	×	"Good"

* indicates that the value was not listed in the report and is based on interpretation of results
# indicates suspended sediment concentration (SSC) values

6.3 Model Results

To assess possible changes as a result of proposed navigation channel improvements, the general approach in this study was to explicitly model both simulation scenarios (the Existing Conditions and the 2023 PA) and to compare the results. The model inputs and constants for both scenarios were the same and the only difference was the model bathymetry for each scenario. Figure 6-13 depicts the observation areas used to calculate the quantities of sediment settling in the channel. It should be noted that the proposed turning basins at RM 5 and RM 8 are included in the Empire Ranges and the Jarvis Ranges, respectively.

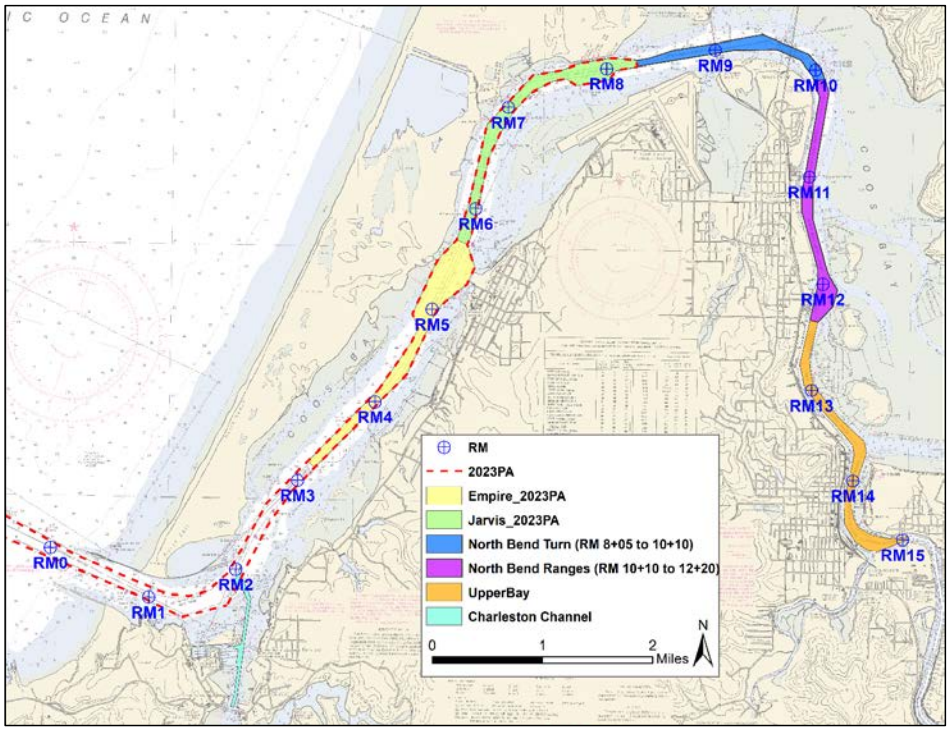

Figure 6-13
Observation Areas for Presenting Sediment Transport Modeling Results

Model results in terms of difference in bed level change over 1-year (i.e., full year of 2011) as a result of the 2023 PA are shown in multiple zoomed-in views from Figure 6-14 to Figure 6-17. The model results indicate that erosion or deposition as a result of the 2023 PA occurs mainly between RM 5 and RM 8. Outside of RM 5 to RM 8, the majority of the navigation channel and shallow-water habitat areas show either no changes or minor changes because these areas are further away from the proposed navigation channel improvements and hence the improvements have very little effect on the hydrodynamics at these locations. Figure 6-18 shows a zoom-in difference plot at the pile dikes, which indicates that erosion at these structures is expected to be

reduced under the 2023 PA relative to the Existing Conditions. The reduced erosion is likely a result of reduced current velocities here.

The sedimentation volume as a result of the 2023 PA is expected to increase by about 57,000 cubic yard (cy) annually. The predicted future O&M of 217,000 CY annually is calculated by combining the modeled increases in shoaling with the existing O&M. The increases and final volumes are provided in Table 6-5.

Table 6-5
Estimated Change in Shoaling (in brackets) and Future O&M Dredging

Location	Estimated O&M in CY/yr	
	Existing	**2023 PA**
Empire Ranges RM 3+20 to 5+35	9,000	[+30,000] 39,000
Jarvis Ranges RM 5+35 to 8+05	73,000	[+19,000] 92,000
North Bend Turn RM 8+05 to 10+10	37,000	[+5,000] 42,000
North Bend Ranges RM 10+10 to 12+20	26,000	[+2,000] 28,000
Upper Bay RM 12+20 to 15+00	0	[+1,000] 1,000
Charleston Channel	15,000	[+0] 15,000
Total Federal	160,000	[+57,000] 217,000

Commented [CT46]: Comment 10462089: USACE has started to implement period maintenance dredging for FNC areas upstream of RM12. The re-initiation of O&M dredging US of RM 12 has been in coordination with OIPCB. Supplement the modeling report accordingly and consider including areas US of RM12 within the sediment transport conditions for this modelling effort. Revised grain size map as needed to portray fine grain sediments above RM 12.

Commented [CT47R46]: Included the Upper Bay above RM 12 in the output estimate. The grain size map has been updated with finer sediments above RM 12.

A further investigation of the model results assessed evolution of bed level change with time to determine whether the observed erosional/depositional patterns were consistent (i.e., the actual bed level change) or alternating (i.e., merely depict the movement of sand waves). The results showed that these patterns form early on and while magnitude of erosion/deposition increases with time, the patterns stays consistent.

Commented [CT48]: A-3-39: Revise document to integrate explanation within the text.

Commented [CT49R48]: Added this paragraph from Port response.

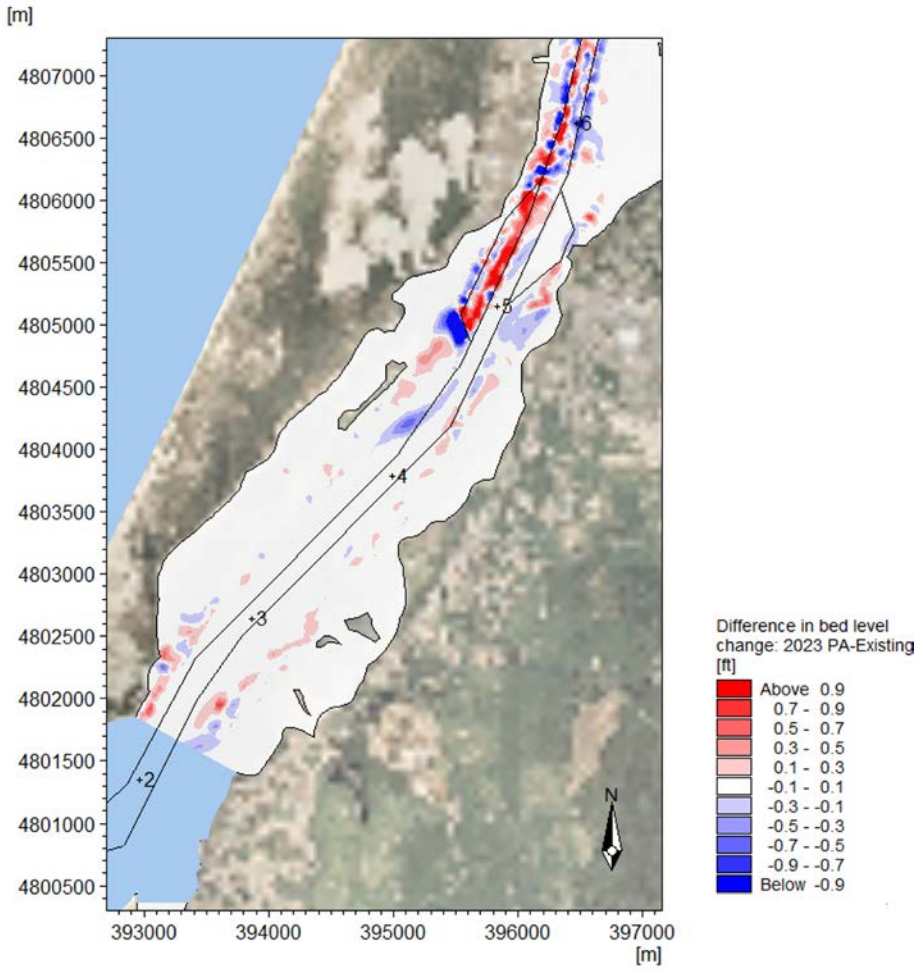

** Results downstream of RM 2.5 see Sub-Appendix 4 Offshore and Ocean Entrance Dynamics.*

Figure 6-14
Difference in Bed Level Change as a Result of 2023 PA (2023 PA – Existing Conditions), a Zoomed-In View of RM 2.5 – RM 6

Commented [CT50]: A-3-38: There appears to be a gap between RM 1.5 and 2.5. See Figures 6-14 in SA 3 and Figure 5-44 in the SA 4.

Commented [CT51R50]: The Sub-Appx 4 has extended the result coverage to RM 2.5.

Commented [CT52]: A-3-37: Please indicate raster pixel/cell size, e.g. "map shows 1 m^2 data".

Commented [CT53R52]: The resolution of the model result varies based on model elements. The finest resolution is approximately 10 m2.

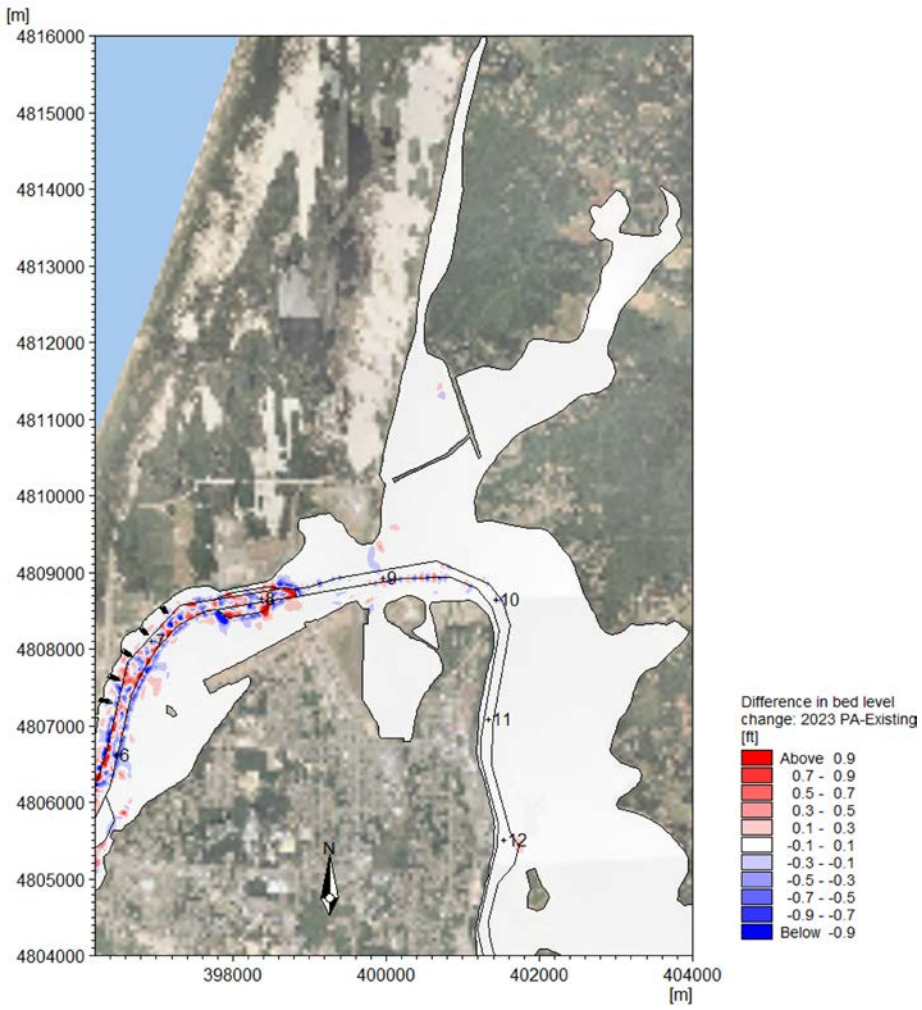

Figure 6-15
Difference in Bed Level Change as a Result of 2023 PA (2023 PA – Existing Conditions), a Zoomed-In View of RM 6 – RM 12

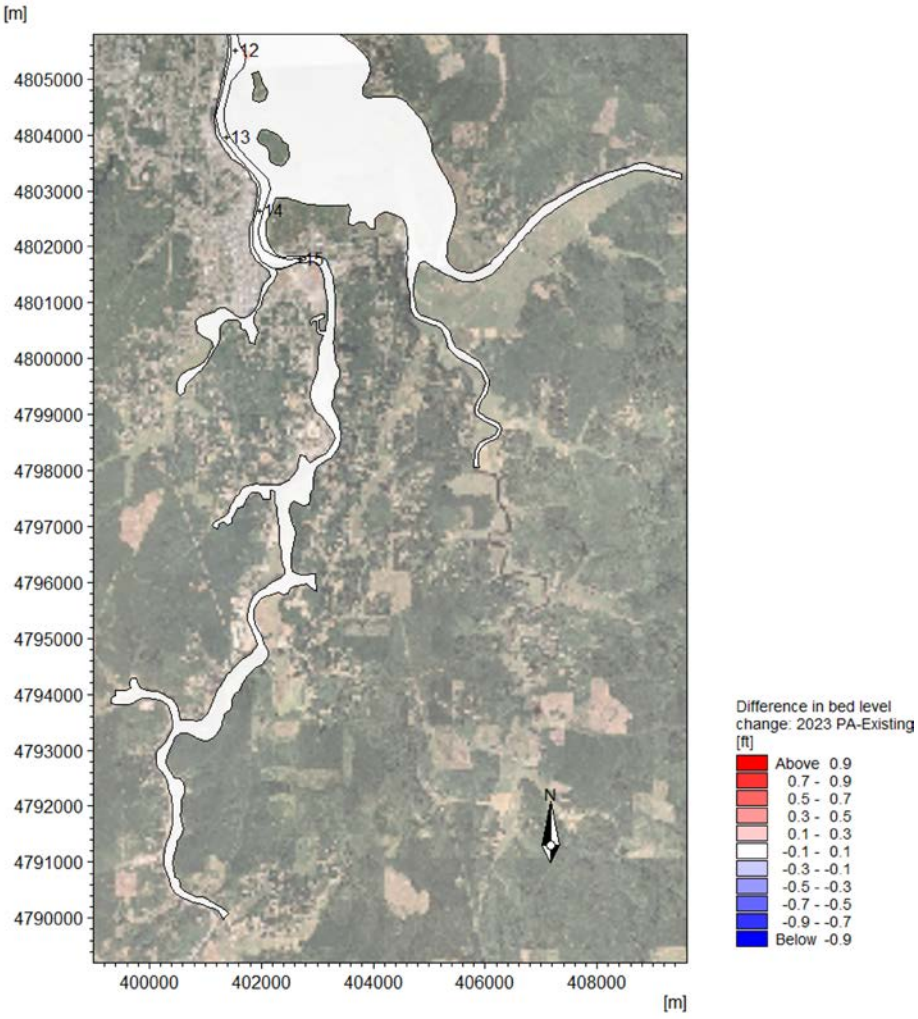

Figure 6-16
Difference in Bed Level Change as a Result of 2023 PA (2023 PA – Existing Conditions), a Zoomed-In View of RM 12 and Upstream

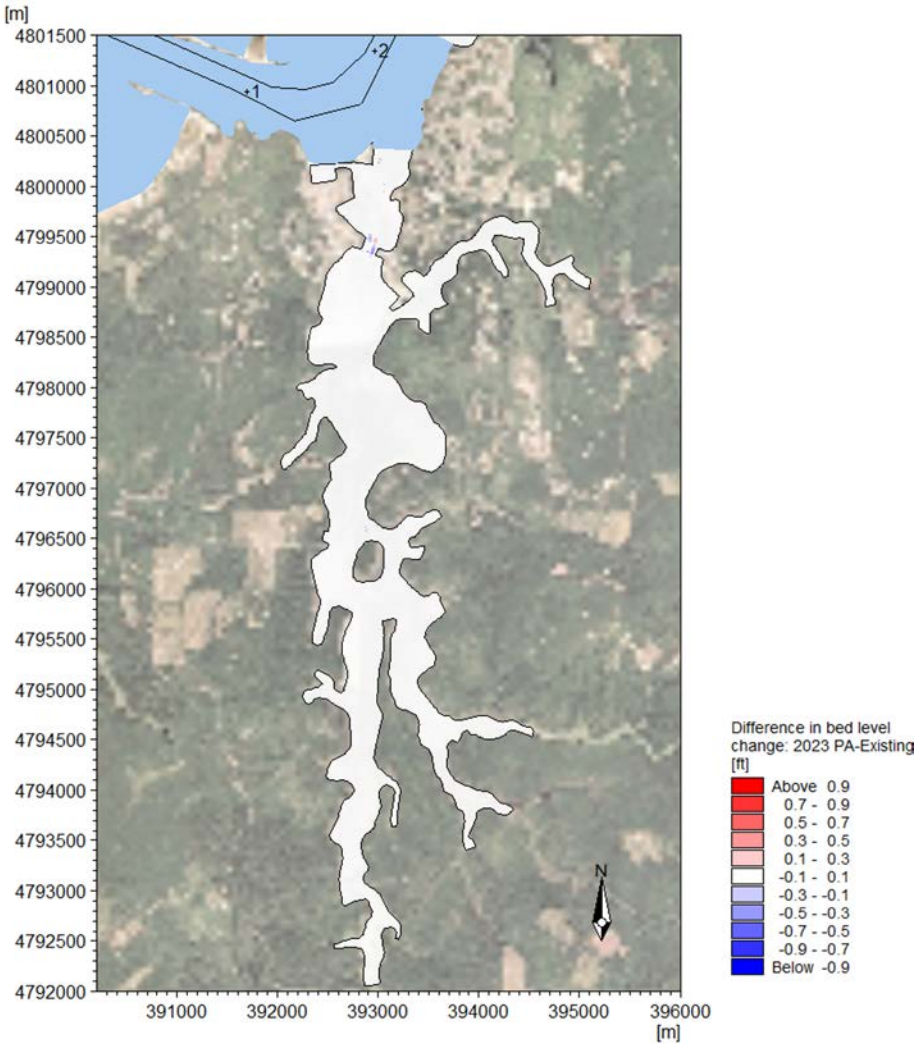

** Results downstream of RM 2.5 see Sub-Appendix 4 Offshore and Ocean Entrance Dynamics.*

Figure 6-17
Difference in Bed Level Change as a Result of 2023 PA (2023 PA – Existing Conditions), a Zoomed-In View of South Slough

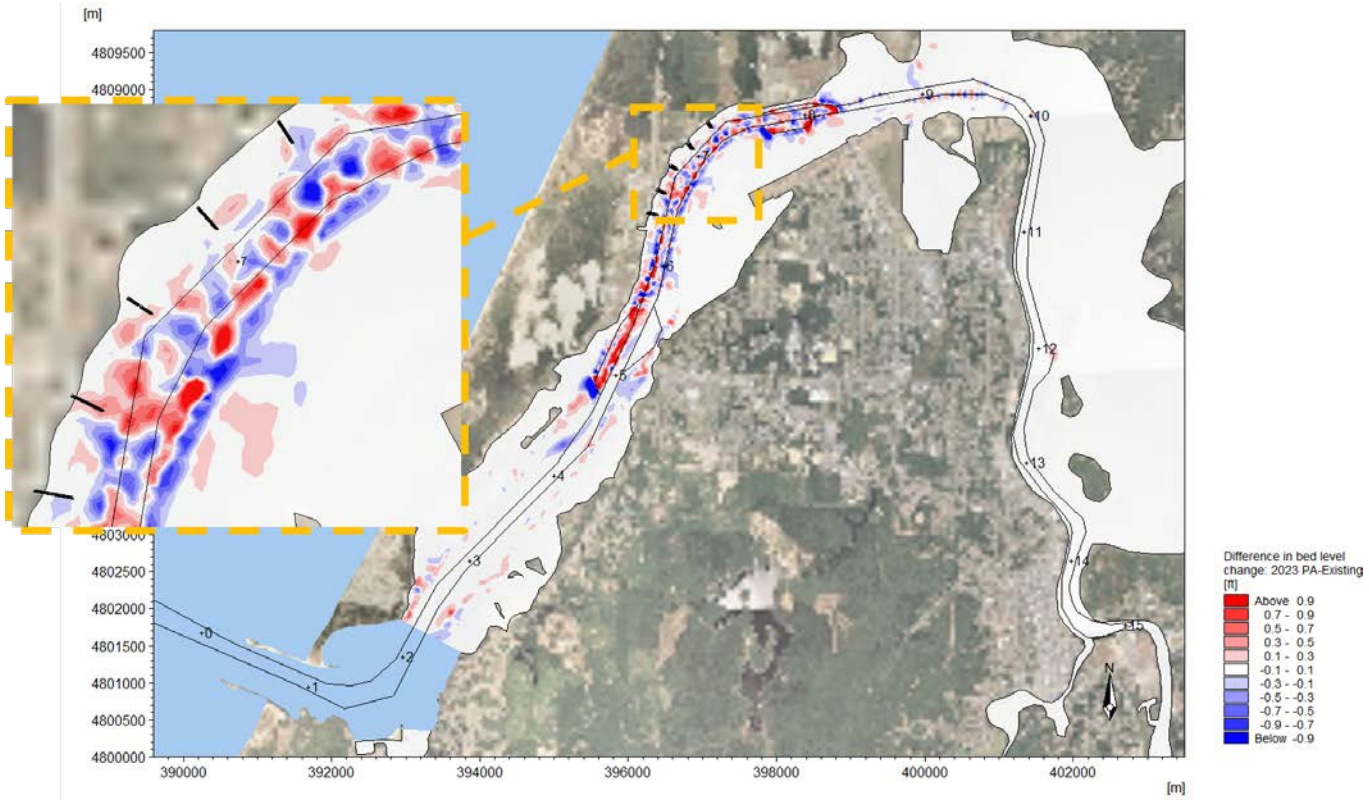

** Results downstream of RM 2.5 see Sub-Appendix 4 Offshore and Ocean Entrance Dynamics.*

Figure 6-18
Difference in Bed Level Change as a Result of 2023 PA (2023 PA – Existing Conditions), a Zoomed-In View at Pile Dikes

6.4 Conclusions

Estuarine sediment transport modeling was performed to evaluate changes to maintenance dredging resulting from proposed navigation channel improvements for the channel from RM 2.5 upstream to RM 15 and in the Charleston Channel. Maintenance dredging in the ocean entrance is addressed in Sub-Appendix 4, *Offshore and Ocean Entrance Dynamics*. Therefore, the downstream extent of applicability for this sediment transport modeling is at RM 2.5.

The model was calibrated against annual average dredging records for various reaches of the FNC. Simulations quantified annual shoaling volume upstream of RM 2.5. Model results indicate that shoaling volume as a result of 2023 PA would increase by about 57,000 cubic yards per year (CY/yr); this represents a percent increase of 36% relative to the existing O&M of 160,000 CY/yr.

The model results also indicate that erosion or deposition as a result of the 2023 PA occurs mainly between RM 5 and RM 8. Outside of RM 5 to RM 8, the majority of the navigation channel and shallow-water habitat areas show either no changes or minor changes because these areas are further away from the proposed navigation channel improvements and hence the improvements have very little effect on the hydrodynamics at these locations.

7. VESSEL-GENERATED WAVES

Commented [CL54]: Dr. Checks # 10502390

Commented [CL55R54]: Noted - More simulations will be implemented to address specific impacts on fisheries.

Commented [JS56R54]: These additional simulations will be included in the EIS

This chapter presents the vessel-generated wave analysis for the Coos Bay navigation channel. The purpose of this analysis is to estimate the magnitude of ship-generated waves in the navigation channel under two configurations: Existing Condition and PA. This analysis shows how proposed channel modifications may affect the Coos Bay shoreline. The ship-generated wave study area spans from the channel ocean entrance to RM 8.2 (Figure 7-1).

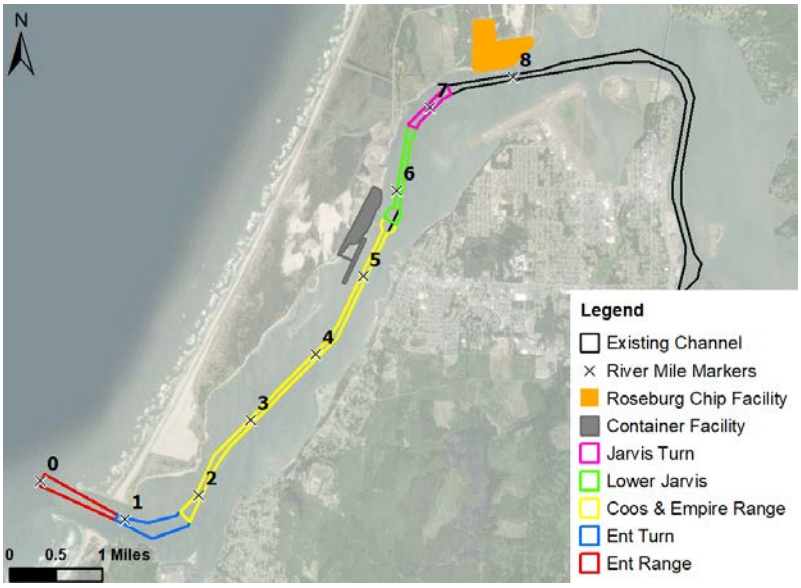

Figure 7-1
Ship-Generated Wave Modeling Domain

7.1 Literature Review

Vessels in the Coos Bay navigation channel may produce both a primary wave and a secondary wave that have the potential to affect shoreline conditions. The following paragraphs, adapted from several sources including Permanent International Association of Navigation Congresses (PIANC 1987), Sorensen (1997), and Schiereck (2001), describe the characteristics of ship-generated waves in confined channels.

7.1.1 Primary Wave (Drawdown)

From a hydrodynamic point of view, flow around a moving ship is similar to flow around a fixed body, such as a bridge abutment. As the ship transits the channel, water flows past the vessel hull opposite the direction of transit, known as the return current. The velocity head associated with the return current must be counteracted by a local drop in water level along the vessel's length to maintain the total head constant. This water level depression is referred to as *primary wave* (see Figure 7-2).

The water surface immediately ahead of the vessel is elevated by the approaching ship. The transition between this elevated water surface and the water level depression takes the form of a sloping water surface referred to as the front wave. The transversal stern wave is the transition between the water level depression and the normal water level behind the ship.

The combination of water level depression, front wave and transversal stern wave, will hereafter be referred to as *drawdown*. Drawdown behaves like a solitary wave with a wavelength on the order of the ship's length. Drawdown is generally not easily observed in the field, other than in the case of relatively large vessels transiting in confined channels. Typically, drawdown does not "break" at the shoreline as "normal" waves do. It is more like a tidal "pulse," slowly rising and falling as the vessel passes.

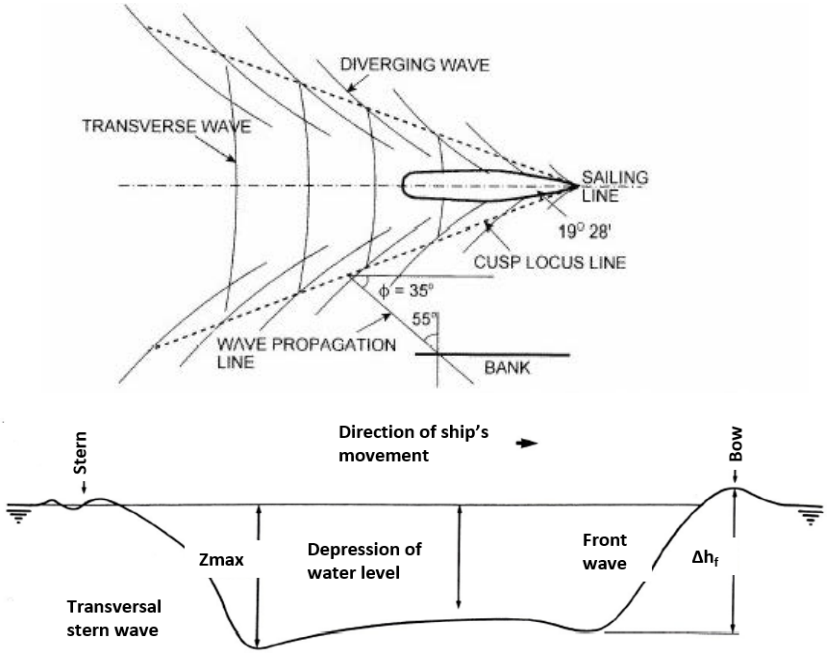

Figure 7-2
Components of Ship Induced Water Motions – Top Plot: Plan view (Excerpted from Schiereck 2001); Bottom Plot: Profile view (Excerpted from PIANC 1987)

Based on laboratory and field observations, investigators have developed empirical equations for predicting drawdown based on channel and vessel parameters. After calculating the maximum drawdown in the vicinity of a ship, a decay term is added to calculate the drawdown for the entire flow field in the channel. The equations used in this study for estimating the drawdown at a given distance from sailing line are given by Bhowmik et al. (1981) for Equation (10) and the USACE (1980) for Equation (11).

$$h = 0.478 * Y'\left(F_{Y'}\right)^{0.5}\left(\frac{A_s}{A_c}\right)^{0.81} * \left(\frac{L}{y - B/2}\right)^{0.26} \quad (10)$$

$$h = 0.0448 * V^2\left(\frac{D}{L}\right)^{0.5}\left(1 - \frac{BD}{A_c}\right)^{-2.5} * \left(\frac{L}{y - B/2}\right)^{0.26} \quad (11)$$

Where:

h = drawdown

V = vessel speed

B = ship beam

D = ship draft

Y' = d - D

d = channel depth

L = ship length

A_c = cross-section area of the channel

A_s = the submerged cross-sectional area of the vessel

y = distance from sailing line, for y > B/2

$$F_{Y'} = \frac{V}{\sqrt{gY'}}$$

Equation (10) is used to calculate the drawdown for tugs and Equation (11) is used to calculate drawdown for larger vessels, such as bulk and container ship. As shown in both equations, the drawdown is a function of vessel speed, distance from sailing line, water depth and width of the channel, and basic hull geometry.

7.1.2 Secondary Wave (Wake)

In response to the sharp rise and fall in the water surface at the bow and stern, inertia causes the water surface to oscillate after the transiting vessel has passed. This, in turn, produces the pattern of free surface waves called secondary waves that propagate from the vessel (Figure 7-2 top plot). Diffraction causes the waves to spread from the vessel, decreasing in amplitude. The pattern consists of symmetrical sets of diverging waves that move obliquely out from the sailing line and a single set of transverse waves that move in the direction of the sailing line. The transverse and diverging waves interact to form cusps, also called interference peaks, located along a pair of lines that form an angle of 19.5 degrees with the sailing line. The highest waves in the pattern are found along this cusp locus line. These secondary waves are the ones that are generally observed in the field and even on aerial photographs. Secondary waves are relatively "short" and behave like "normal" waves, which means that the linear wave theory relations for wavelength, celerity etc. are valid. They also break as they approach the shoreline and breaking type (i.e., spilling, plunging, or surging) is dictated by the same slope and wavelength relationship as other "normal" waves.

Numerous empirical formulae for predicting secondary waves exist based on theoretical, laboratory and field investigations. For this study, the PIANC (1987) formulation is used to estimate secondary waves generated by vessels:

$$\frac{gH}{V^2} = F_d{}^2 \left(\frac{y - B/2}{d} \right)^{-1/3} \quad (12)$$

Where:

g = gravity constant

H = wave height

d = channel depth

F_d = Depth-based Froude number $= \frac{V}{\sqrt{gd}}$

All other variables are the same as the preceding equations. From Equation (12), wave height increases with increasing Froude number for a given vessel size and shape; and the Froude number increases with increasing vessel speed but decreases with increasing channel depth.

7.2 Ship-Generated Wave Model Setup

The following paragraphs focus on prediction and analysis of ship-generated primary wave (drawdown) and secondary waves (wake), for the Existing Condition and PA. The wave heights generated by vessels were calculated with the three empirical equations listed above, project-specific ship data, and channel configurations; shallow water effects, such as wave shoaling and breaking, were not taken into account in this simulation. However, the waves were modified to include decay from the sailing line. The computed wave fields were analyzed on a regular 5-m grid. The approach is further discussed in the following sections.

7.2.1 Ship Data

Vessel speeds and vessel tracks were obtained from the full bridge ship simulations (Sub-Appendix 7, *Full Ship Simulation*). Three types of vessels were used in the model: tug, bulk carrier and container ship; the dimensions of the design vessels vary according to the channel configuration. The vessels and their relevant characteristics are listed in Table 7-1. Vessel track data, including vessel position and speed derived from the full bridge ship simulations, were input at an interval of four seconds and over the arrival and departure ship route. An example of a bulk vessel track is presented in Figure 7-3.

For the tugs traveling by themselves, a vessel speed of 12 knots was observed from the ship simulations. However, a speed of 15 knots was also used for this analysis to understand the relationship between vessel speed and wake.

7.2.2 Bathymetry

Bathymetric data was extracted from the MIKE-3 Hydrodynamic Model, as described in detail in Section 3.4.1.

Figure 7-3
Example of Ship Track

Table 7-1
Modeled Case Information

Case	Condition	Channel Depth (ft,MLLW)	Tide (ft)	Arrival/ Departure	Vessel Speed (knots)	Draft (ft)	LOA (ft)	Beam (ft)	Type	Name
1	Existing	37	1	Arrival	Ent Range: 8 Ent Turn: 8 Coos Range: 7.5 Lower Jarvis: 6 Jarvis Turn: 4	31	655.9	105.6	Bulk	Glorious Lotus
2	PA	45	3.6	Arrival	6	34	837.5	141.1	Bulk	Carrier 19
3	Existing	37	7	Departure	Ent Range: 7 Ent Turn: 7 Coos Range: 6.5 Lower Jarvis: 5 Jarvis Turn: 4	36	655.9	105.6	Bulk	Glorious Lotus
4	PA	45	3.6	Departure	5	45	837.5	141.1	Bulk	Carrier 19
5	PA	45	4.5	Arrival	Ent Range: 9 Ent Turn: 5 Rest: 4.5	45	1200.8	168	Container	Kalina

Commented [CL57]: Dr. Checks # 10509154

Commented [CL58R57]: Unit "ft,MLLW" has been added to channel depth; "Tide Stage" has been replaced by "Arrival/Departure"

Case	Condition	Channel Depth (ft,MLLW)	Tide (ft)	Arrival/ Departure	Vessel Speed (knots)	Draft (ft)	LOA (ft)	Beam (ft)	Type	Name
6	PA	45	4.5	Departure	Ent Range: 10 Ent Turn: 5 Rest: 5	45	1200.8	168	Container	Kalina
7	Existing	37	2	Arrival	Ent Range: 7 Ent Turn: 7 Coos Range: 6.5 Lower Jarvis: 5 Jarvis Turn: 4	19	105	11.6	Tug	Conventional
8	PA	45	3.6	Bulk - Arrival	6	19	105	11.6	Tug	ASD
9	PA	45	4.5	Container - Departure	Ent Range: 5-6 Rest: 5	19	105	11.6	Tug	ASD
10	Existing	37	1.75	Departure	12	19	105	11.6	Tug	Conventional
11	Existing	37	7	Departure	15	19	105	11.6	Tug	Conventional
12	PA	45	7	Departure	12	19	105	11.6	Tug	ASD

7.2.3 Modeled Cases

Twelve cases covering the range of vessel types, navigation patterns and channel configurations were modeled in this study, as described in Table 7-1. For vessel speed distribution, five channel reaches are considered (Figure 7-1): Entrance Range, Entrance Turn, Coos Bay Range, Lower Jarvis, and Jarvis Turn. For some cases, vessel speed is a constant, and for other cases vessel speed varies by reach. For tugs traveling with either a bulk or container vessel, the worst-case scenario was determined by selecting either the arrival or departure case, based on the higher traveling speed.

7.3 Ship-Generated Wave Results

The procedures outlined in the above sections were used to compute the ship-generated wave field at every grid-cell on a 5-m resolution raster grid within the Coos Bay estuary. The MLLW tide condition was selected as it represents a conservative case for the wave field since the MLLW shoreline is closer to the sailing line than that of higher tides.

As described in the following sections, larger vessels tended to generate large primary waves and negligible secondary waves, while tugs with high traveling speeds tend to generate large secondary waves and negligible primary waves. As described in Section 7.1, these two types of waves behave very differently and an attempt to superimpose the significant wave heights from these two types of waves does not make sense from a technical perspective.

7.3.1 Primary Wave Prediction

The drawdown for all tug cases is very small (see Figure 7-4 through Figure 7-5 as examples). Therefore, the results for drawdown focus on the larger vessels. Figure 7-6 and Figure 7-7 show the drawdown for the bulk vessel during arrival under the Existing Condition and PA, respectively. Results indicate that the drawdown decreases in the deepened and widened channel conditions. Figure 7-8 and Figure 7-9 show the drawdown for the bulk vessel during departure. Similarly, the drawdown decreases in the deepened and widened channel conditions. Figure 7-10 and Figure 7-11 show the drawdown for the container ship during arrival and departure, respectively. There is no comparison case for container ships in the Existing Condition. Overall, the drawdown for container ships is < 0.4 ft in most parts of the channel except near the entrance between RM1 and RM2, where the maximum drawdown can reach 0.7 ft during the departure. This is due to a relatively high speed near the entrance where the container ship speed is transiting at 9 knots for arrival and 10 knots for departure.

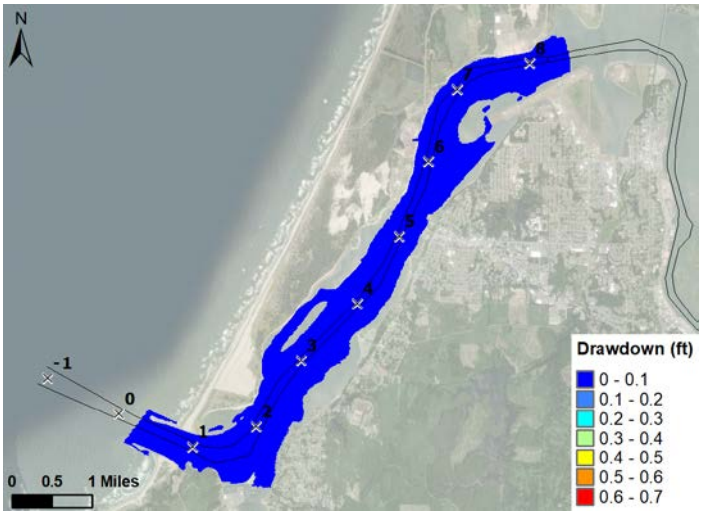

Figure 7-4
Drawdown of Case 10 – Conventional Tug Departure at 12 Knots, Existing Condition

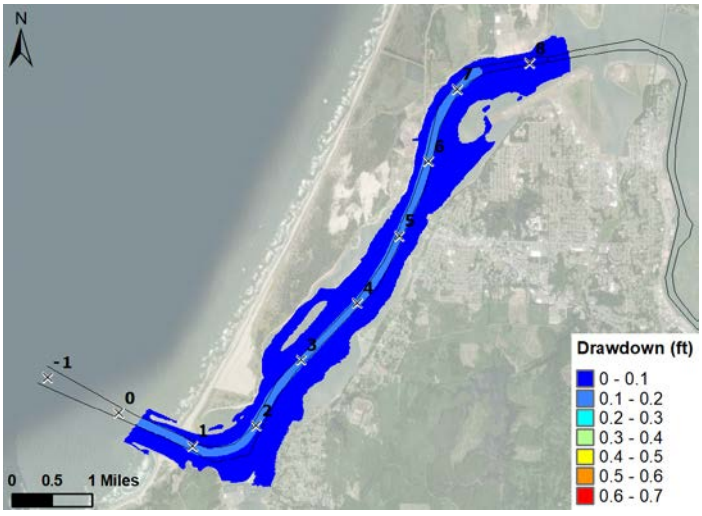

Figure 7-5
Drawdown of Case 12 – ASD Tug Departure at 12 Knots, PA

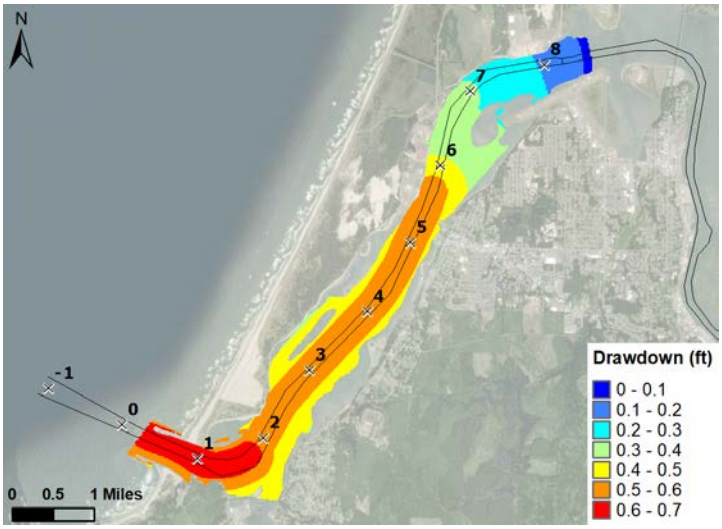

Figure 7-6
Drawdown of Case 01 - Bulk Arrival, Existing Condition

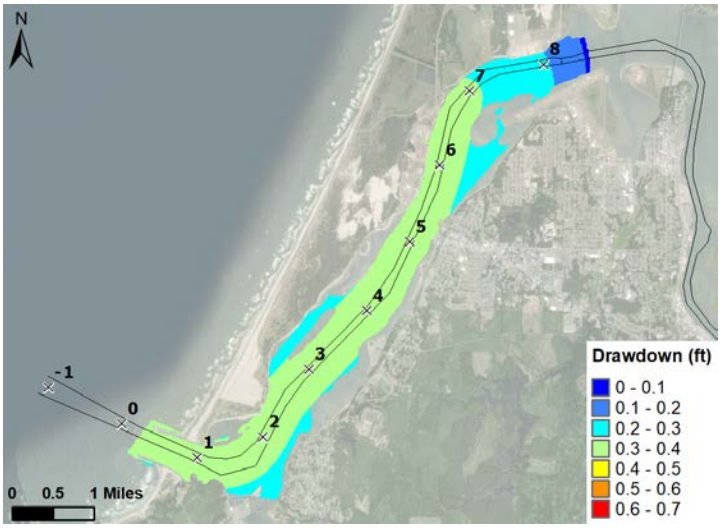

Figure 7-7
Drawdown of Case 02 - Bulk Arrival, PA

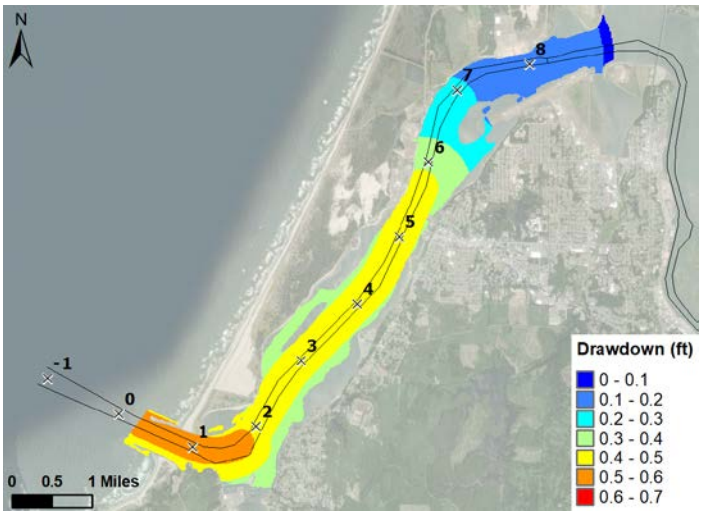

Figure 7-8
Drawdown of Case 03 - Bulk Departure, Existing Condition

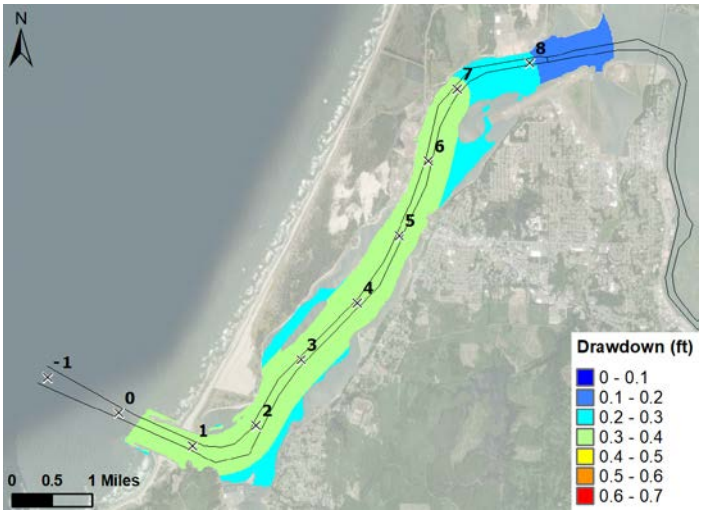

Figure 7-9
Drawdown of Case 04 - Bulk Departure, PA

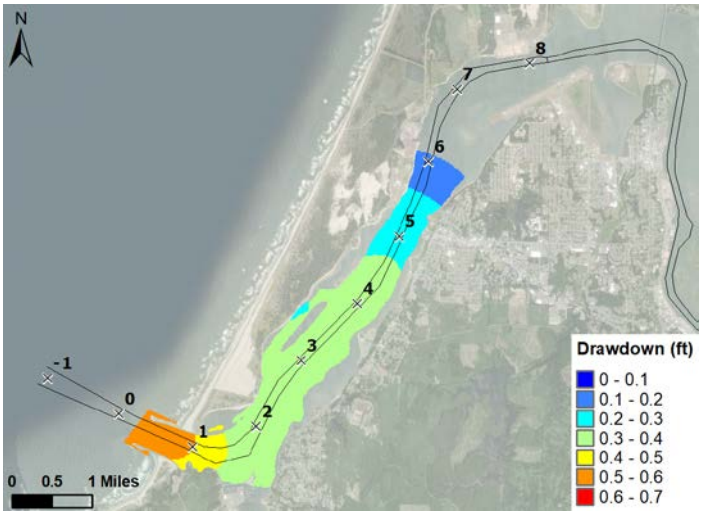

Figure 7-10
Drawdown of Case 05 – Container Ship Arrival, PA

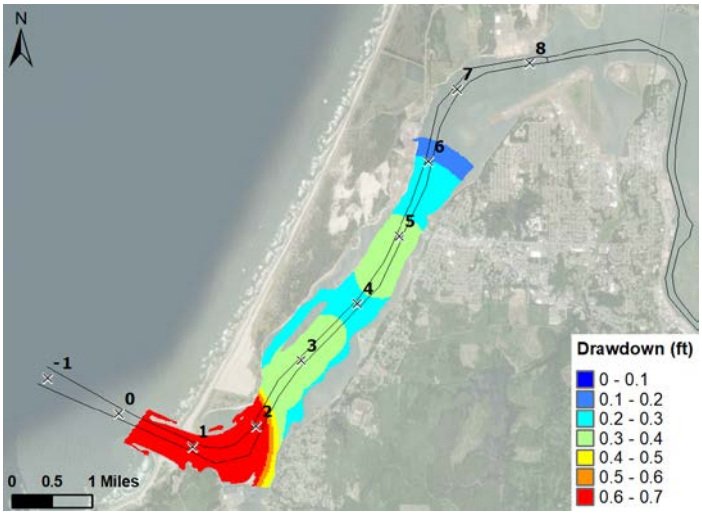

Figure 7-11
Drawdown of Case 06 - Container Ship Departure, PA

7.3.2 Secondary Wave Prediction

The wakes for the larger vessel cases (bulk carrier and container ship) are generally small due to their low transit speeds in the channel except for the container ship at the entrance (see Figure 7-12 and Figure 7-13 as examples). Therefore, the analysis of wakes primarily considers tugs.

Figure 7-14 through Figure 7-16 show the wake for the conventional tug in the existing channel at constant speeds of 12 knots, 15 knots, and at variable speeds while accompanying a larger vessel. Results indicate that vessel speed is an important factor for ship wake generation. Wake wave height increases linearly with the vessel speed. Similar results for the ASD tug in the PA condition are presented in Figure 7-17 and Figure 7-18.

Figure 7-14 and Figure 7-17 compare the wake from tugs transiting at the same speed of 12 knots under the Existing Condition and PA, respectively. At a constant speed, the wakes are almost identical between Existing Condition and PA with a slight decrease in the PA (deepened and widened channel conditions).

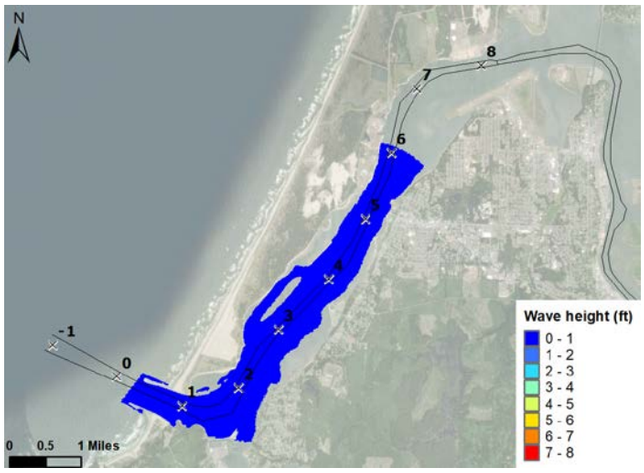

Figure 7-12
Wake of Case 05 – Container Ship Departure, PA Condition

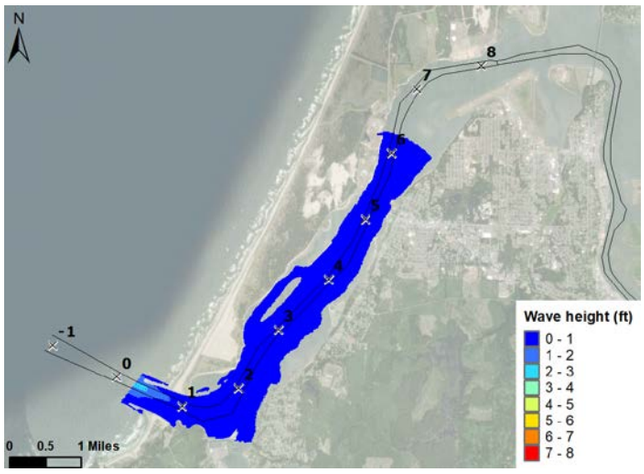

Figure 7-13
Wake of Case 06 – Container Ship Arrival, PA Condition

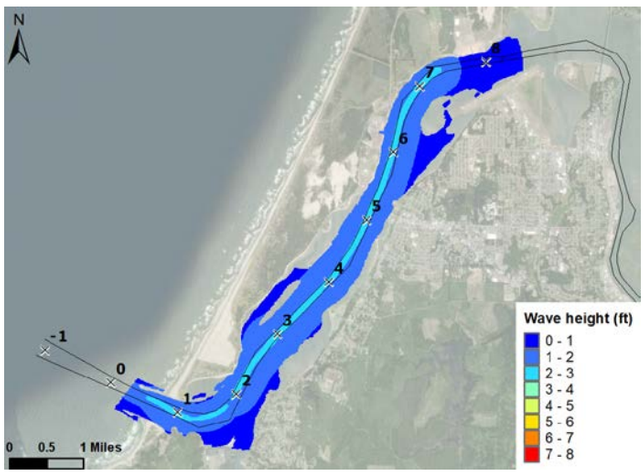

Figure 7-14
Wake of Case 10 – Conventional Tug Departure at 12 Knots, Existing Condition

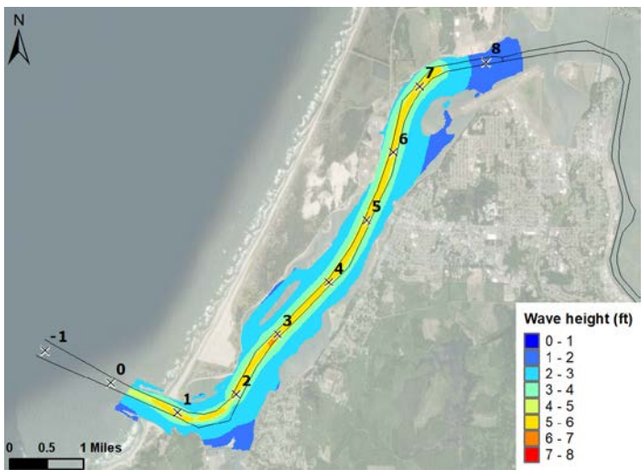

Figure 7-15
Wake of Case 11 - Conventional Tug Departure at 15 Knots, Existing Condition

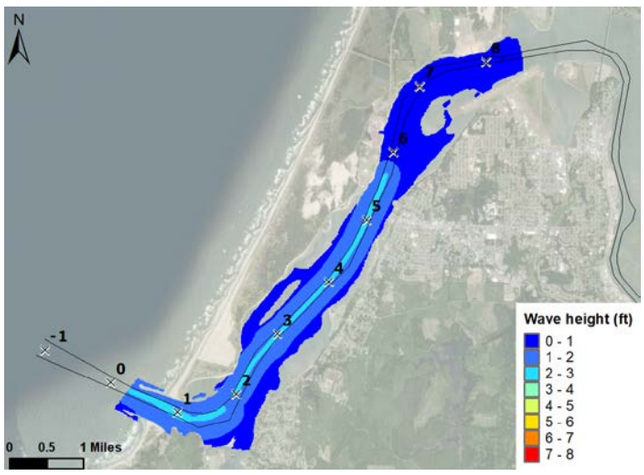

Figure 7-16
Wake of Case 07 – Conventional Tug Arrival while Accompanying Larger Vessels, Existing Condition

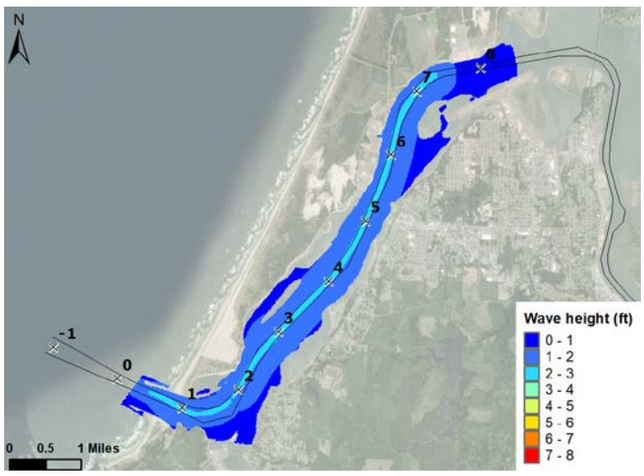

Figure 7-17
Wake of Case 12 – ASD Tug Departure at 12 Knots, PA Condition

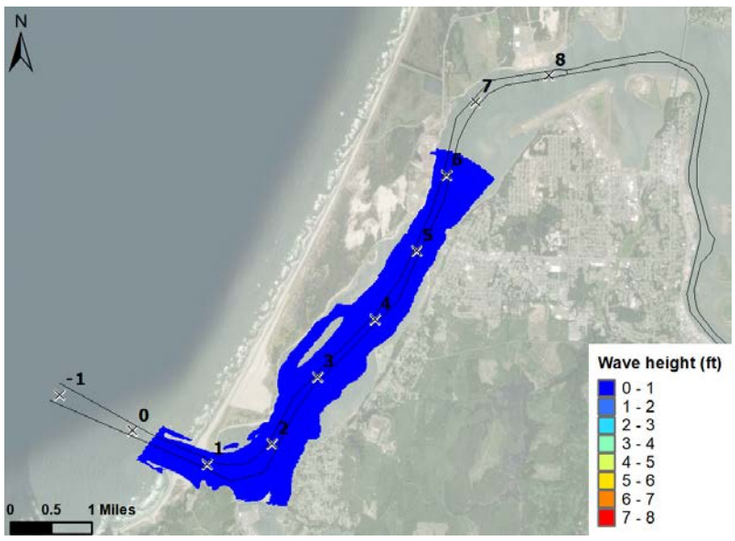

Figure 7-18
Wake of Case 09 – ASD Tug Arrival while Accompanying Larger Vessels, PA Condition

7.3.3 Wave Height at the Shoreline

Wave heights were extracted along the shoreline on both sides of the Coos Bay Channel (Figure 7-19) to compare the ship-generated wave heights between project configurations. The left and right banks are defined by the relative position when facing downstream. Five comparison sets are listed in Table 7-2. Figure 7-20 through Figure 7-24 present the comparisons.

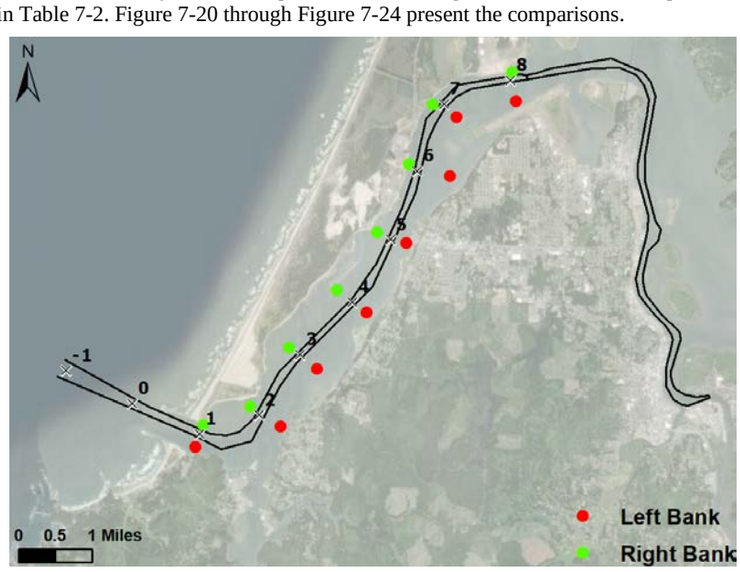

Figure 7-19
Location map of shoreline extraction points

Table 7-2
Comparison Sets of Wave Height

Set No.	Cases	Comparison
Set 01 (Figure 7-20)	Case 07, Case 10, Case 11	Conventional tug-generated wakes at different speeds
Set 02 (Figure 7-21)	Case 08, Case 09, Case 12	ASD tug-generated wakes at different speeds
Set 03 (Figure 7-22)	Case 10, Case 12	Tug-generated wake for various channel configurations
Set 04 (Figure 7-23)	Case 01, Case 02	Bulk carrier-generated drawdown for two channel configurations, during arrival
Set 05 (Figure 7-24)	Case 03, Case 04	Bulk carrier-generated drawdown for two channel configurations, during departure

Overall, the wave heights of wake and drawdown are larger along the right bank than those along the left bank (right and left banks are defined facing downstream). This is because the right bank is closer to the sailing line than the left bank (Figure 7-19), so the wave decay distance at the right bank is shorter.

Figure 7-20 through Figure 7-24 show the modeled wake wave heights at the shoreline. Figure 7-20 shows that the wake heights generated by the conventional tug at the shoreline will vary from about 0-0.1 ft when accompanying a larger vessel and traveling slowly (4-8 knots), to 2.0-3.5 ft when traveling at 15 knots. Similar wake height values can be seen in Figure 7-21 for the ASD tugs at different speeds. For both the conventional tug and the ASD tug, increasing vessel speed will cause larger wake heights at the shoreline. Figure 7-22 compares the tugs transiting at the same speed of 12 knots in the Existing Condition and PA. Wake heights are similar for tugs transiting at the same speed in the Existing Condition and the PA.

Figure 7-23 and Figure 7-24 show the modeled drawdown wave heights at the shoreline. Figure 7-23 shows that the wave heights generated by the bulk carrier at the shoreline will vary from 0.2-0.6 ft under the Existing Condition and will vary from 0.2-0.3 ft in the PA channel. For the Existing Condition the drawdown decreases upstream of RM 5 due to a significant decrease in vessel speed. Similar drawdown patterns can be observed from Figure 7-24. Downstream of RM 5, the drawdown under the PA is reduced by 25%-40% relative to the Existing Condition. Further upstream, the drawdown is similar under both conditions expect a 0.1 ft increase at RM7 for the PA condition.

For container ships operating under the PA condition, no comparative figures were plotted. The drawdown results at the shoreline are detailed in Table 7-3. Notably, RM1 and RM2 exhibit the highest drawdown during both container ship arrivals and departures among all channel sections with a wave height exceeding 0.5 ft. This is attributed to the relatively high speed of the vessels in this section. Moving upstream to RM2, the drawdown gradually decreases. Approaching RM5, near the proposed container ship terminal, the drawdown diminishes to 0.3 ft on both sides of the channel. On the right (west) bank, the construction of a riprap revetment as part of the terminal might introduce wave reflection on the shoreline, potentially resulting in a drawdown higher than 0.3 ft but less than 0.6 ft in real-world scenarios. Conversely, on the left (east) bank, no existing or planned structures for future construction implies that wave conditions will remain unaffected by structures. At RM6, the drawdown further diminishes to 0.0 – 0.2 ft on both the left and right banks due to the slower vessel speed near this section. Note that for Case 07, Case 08 and Case09, the tugs are modeled as if accompanying a large vessel. With two or three tugs pushing or towing a large vessel, the tugs will generate wake and the large vessel will generate drawdown, which will result in interaction of the respective ship-generated waves. However, wave heights cannot be simply added together because the drawdown propagates as a solitary wave and the wake propagates as a “normal’ wave train. The wave height comparison for the individual vessel transits remains the best measure of the potential shoreline effects. Over the course of a year, the effects to the shoreline will also depend on the frequency of vessel transits.

Commented [LC59]: Dr. Checks # 10508085

Commented [LC60R59]: Discussion has been included in the draft report to compare same vessel transits on PC and PA channels. And more information about the transit frequency will be collected.

Commented [JS61R59]: Transit frequency impacts will be addressed in the EIS

Commented [CL62]: Dr. Checks # 10508086

Commented [CL63R62]: Discussion added

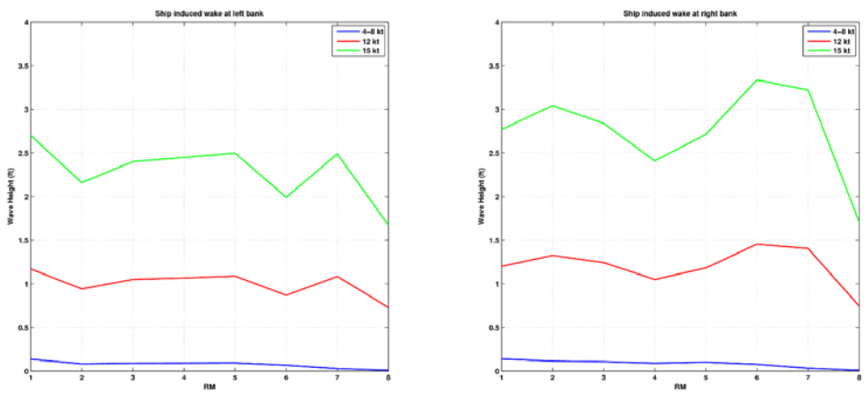

Figure 7-20
Wave Height Comparison for Set 01 - Conventional Tug-Generated Wakes at Different Speeds

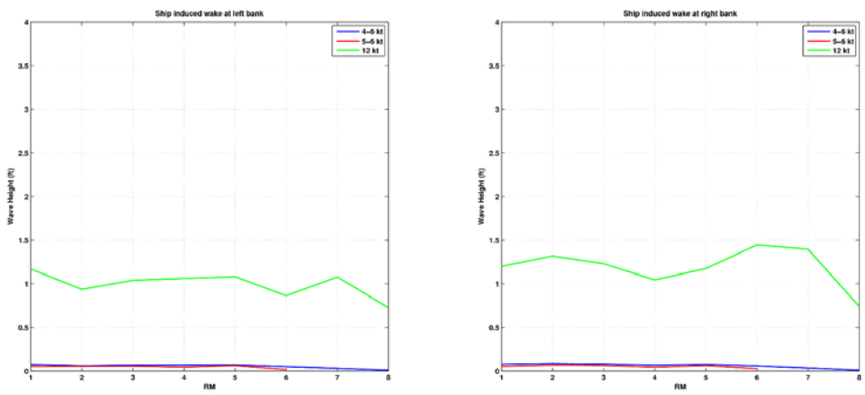

Figure 7-21
Wave Height Comparison for Set 02 - ASD Tug-Generated Wakes at Different Speeds

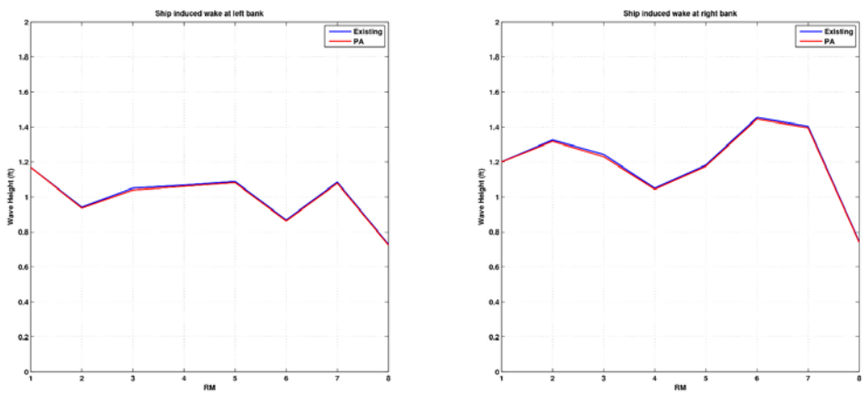

Figure 7-22
Wave Height Comparison for Set 03 - Tug-Generated Wake for Various Channels

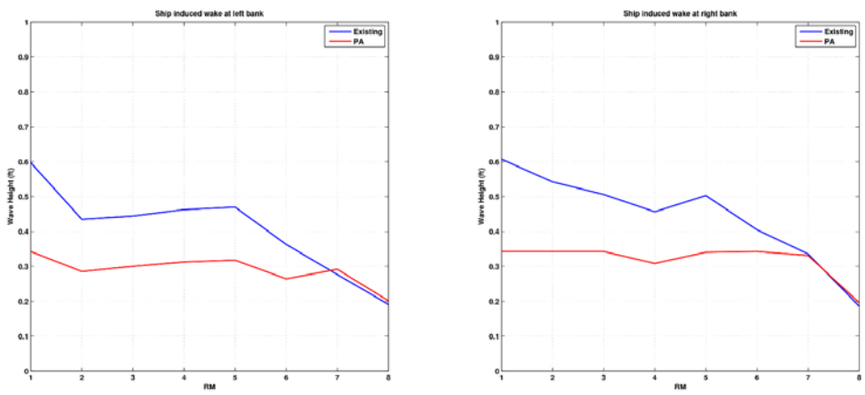

Figure 7-23
Wave Height Comparison for Set 04 – Bulk Carrier-Generated Drawdown during Arrival

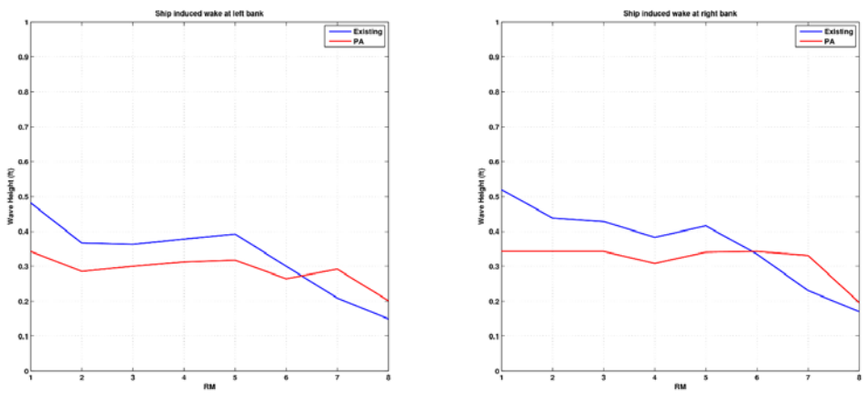

Figure 7-24
Wave Height Comparison for Set 05 - Bulk Carrier -Generated Drawdown during Departure

Table 7-3
Results of Vessel Drawdown (ft) at RMs 1 to 8 for Left (L) and Right (R) Bank.

	RM1		RM2		RM3		RM4		RM5		RM6		RM7		RM8	
Case/ Location	**L**	**R**	**L**	**R**	**L**	**R**	**L**	**R**	**L**	**R**	**L**	**R**	**L**	**R**	**L**	**R**
Case 01 Bulk Arrival (Existing)	0.6	0.6	0.4	0.5	0.4	0.5	0.5	0.5	0.5	0.5	0.4	0.4	0.3	0.3	0.2	0.2
Case 02 Bulk Arrival (PA)	0.3	0.3	0.3	0.3	0.3	0.3	0.3	0.3	0.3	0.3	0.3	0.3	0.3	0.3	0.3	0.2
Case 03 Bulk Depart (Existing)	0.5	0.5	0.4	0.4	0.4	0.4	0.4	0.4	0.4	0.4	0.3	0.3	0.2	0.2	0.2	0.2
Case 04 Bulk Depart (PA)	0.3	0.3	0.3	0.3	0.3	0.3	0.3	0.3	0.3	0.3	0.3	0.3	0.3	0.3	0.2	0.2
Case 05 Container Arrival (PA)	0.5	0.5	0.3	0.4	0.4	0.4	0.4	0.4	0.3	0.3	0.0	0.1	NA	NA	NA	NA
Case 06 Container Depart (PA)	1.1	1.1	0.3	0.9	0.3	0.3	0.3	0.3	0.3	0.3	0.1	0.2	NA	NA	NA	NA

Table 7-4
Results of Vessel Wake (ft) at RMs 1 to 8 for Left (L) and Right (R) Bank.

	RM1		RM2		RM3		RM4		RM5		RM6		RM7		RM8	
Case/ Location	**L**	**R**	**L**	**R**	**L**	**R**	**L**	**R**	**L**	**R**	**L**	**R**	**L**	**R**	**L**	**R**
Case 07 Convent. Tug Arrival at 4-8 kt (Existing)	0.1	0.1	0.1	0.1	0.1	0.1	0.1	0.1	0.1	0.1	0.1	0.1	0.0	0.0	0.0	0.0
Case 08 ASD Tug Arrival at 4-6 kt (PA)	0.1	0.1	0.1	0.1	0.1	0.1	0.1	0.1	0.1	0.1	0.1	0.1	0.0	0.0	0.0	0.0
Case 09 ASD Tug Arrival at 5-6 kt (PA)	0.1	0.1	0.1	0.1	0.1	0.1	0.0	0.0	0.1	0.1	0.0	0.0	NA	NA	NA	NA
Case 10 Convent. Tug Arrival at 12 kt (Existing)	1.2	1.2	1.0	1.3	1.1	1.2	1.1	1.1	1.1	1.2	0.9	1.5	1.1	1.4	0.7	0.7
Case 11 Convent. Tug Arrival at 15 kt (Existing)	2.7	2.7	2.2	3.0	2.4	2.8	2.5	2.4	2.5	2.7	2.0	3.3	2.5	3.2	1.7	1.7
Case 12 ASD Tug Arrival at 12 kt (PA)	1.2	1.2	1.0	1.3	1.0	1.2	1.1	1.0	1.1	1.2	0.9	1.4	1.1	1.4	0.7	0.7

7.4 Project Effects

The analysis of ship-generated waves in the Coos Bay navigation channel yielded the following conclusions:

1) For tugs transiting the channel, drawdown is expected to be small and negligible, while wake can be up to 3.5 ft at the right bank for tugs traveling at high speed (12-15 knots). However, this is a relatively high speed for tugs, and is unlikely. The difference in wake generation between conventional tugs and ASD tugs is very little. Deepening and widening the channel under the PA condition will result in a slight reduction in wake height due to increased channel cross-section. Therefore, the effect of the project would be to lessen the wake energy at the shoreline.

2) For larger vessels, such as the bulk carrier and container ship in the channel, wake is expected to be small and negligible due to lower vessel speeds, but drawdown can produce wave heights up to 0.6 ft. Deepening and widening the channel will result in a 0.1-0.3 ft reduction in drawdown in most parts of the channel. One exception to this is in the Entrance Range and Entrance Turn where the simulated container ships under the PA transited at a relatively high speed (9-10 kt), corresponding to wake of 1-3 ft.

In summary, the model results show an overall small reduction in wake height generated by tugs and only small changes in drawdown height associated with larger vessels transiting between the Existing condition and the PA cases. Compared to the Existing condition, impacts from container ships are newly introduced under the PA condition. For bulk ships, the ship sizes are larger and the frequency of larger bulk vessels will likely decrease under the PA conditions compared to the Existing condition.

8. RISK MANAGEMENT PLAN

Results of the investigations described in this Section 204(f)/408 Report, in the opinion of the OIPCB, show that all project effects on infrastructure and the natural environment have been managed and are minor and manageable. The Corps of Engineers, through their Section 408 and 404 reviews, will make the Federal determination whether the Proposed Alteration is environmentally acceptable and consistent with Federal policy. As is the case with the implementation of any navigation improvement project in such a dynamic physical environment and within an important and ecologically valuable estuary, there will be inherent residual risk and uncertainty associated project implementation. As such, Risk management will be a critical element of the project.

This Sub-Appendix 3 describes an evaluation of estuarine processes (hydrodynamics, sediment transport, salinity mixing, residence time, dissolved oxygen, as well as ship-generated wakes) within Coos Bay (also referred to as Coos estuary). The purpose of this study is to evaluate possible changes in each of these processes resulting from the proposed modifications relative to the Existing Condition. Throughout the development of the Section 204(f)/408 Report, potential areas of residual risk regarding the potential for impacts within the Coos Bay Estuary have been identified. While these potential impacts will be further evaluated in the EIS process, preliminary elements of risk identified as warranting quantitative risk management plan are summarized in Table 8-1.

Table 8-1
Risk Management Elements Related to Estuarine Dynamics Analyses

Issue or Concern	Primary Monitoring	Monitoring Tools	Frequency and Duration of Monitoring	Trigger(s) For Action	Possible Response Actions
Infrastructure Stability	Bathymetric surveys	Bathymetric surveys to establish baseline Existing Conditions variability	Annually – 5-year period post construction. Periodic following major storm events.	Erosion beyond predicted limits and / or in close proximity to jetty structure	Temporarily suspend dredging operations; Add or enhance rock apron or other protective measures
Estuary Water Quality	Monitor range of WQ parameters for which baseline Existing Conditions data exists including salinity, temperature, DO, others	Utilize present monitoring programs but augment in potential areas of concern – important to establish baseline and reasonable variability for	Quarterly – using data retrieved from real time and periodic automated sampling stations for 5-year period.	Compare post construction WQ parameter data – trigger is exceedance of water quality standards **Temperature:** 0.5 ° Fahrenheit increase in	Adaptive mitigation and negotiated water quality enhancement projects (e.g. stormwater enhancement projects, riparian and estuary enhancement

Issue or Concern	Primary Monitoring	Monitoring Tools	Frequency and Duration of Monitoring	Trigger(s) For Action	Possible Response Actions
		Existing conditions		Coos Bay waters **Dissolved Oxygen:** < 4.0 mg/L Minimum <6.5 mg/L 30 Day Mean Minimum	activities in basin)
Shallow Subtidal/Salt Marsh/Mudflat Habitats	Bathymetric surveys	Bathymetric surveys to determine extent of equilibration	Biennial for 10-year period	Equilibration that extends into these habitat types where none is currently modeled to occur	Adaptive mitigation – replacement of lost habitat function and value with restoration actions in the estuary

The Risk Management Plan will be developed based on USACE Risk Management guidance.

9. REFERENCES

Banks, R.B., and F. F. Herrera. 1977. "Effect of Wind and Rain on Surface Reaeration," J. Envion. Engr. Div. ASCE, 103(EE3): 489-504.

Baptista, A.M. (1989). Salinity in Coos Bay, Oregon: review of historical data (1930- 1989). Report ESE-89- 001, U.S. Army Corps of Engineers, Portland, OR. 40 pp

Baptista, A.M. Coos Bay Navigational Improvements, Salinity Workshop, July 20, 1989. Charleston, Oregon. in USACE. 1994. Coos Bay, Oregon, Navigation Improvements, Final Feasibility Report and Environmental Impact Statement, Appendix H.

Bhowmik, N.G., Demissie, M., and Guo, C.Y. 1981. Waves and Drawdown Generated by River Traffic on the Illinois and Mississippi Rivers. SWS Contract Report 271.

Bowen, J.D., S. Negusse, J.M. Goodman, B. Duclaud, M. Robin, and J. Williams. 2009. "Development and use of a three-dimensional water quality model to predict dissolved oxygen concentrations in the lower Cape Fear River Estuary, North Carolina." University of North Carolina at Charlotte.

Bowie, G.L., W.B. Mills, D.B. Porcella, C.L. Campbell, J.R. Pagenkopf, G.L. Rupp, K.M. Johnson, P.W.H. Chan, S.A. Gherini. 1985. "Rates, Constants, and Kinetic Formulations in Surface Water Quality Modeling," EPA/600/3-85/040, Environmental Research Laboratory, U.S. Environmental Protection Agency, Athens, GA.

Brown, C. A. and C. L. Folger. 2009. Chapter 4: Water Quality Surveys in Seven Target Estuaries, in Lee II, H. and Brown, C.A. (eds.) Classification of Regional Patterns of Environmental Drivers and Benthic Habitats in Pacific Northwest Estuaries. U.S. EPA, Office of Research and Development, National Health and Environmental Effects Research Laboratory, Western Ecology Division.

Cerco, C.F. and Noel. M.R. 2017. The 2017 "Chesapeake Bay Water Quality and Sediment Transport Model." A Report to the US Environmental Protection Agency Chesapeake Bay Program. May 2017 Draft. US Army Engineer Research and Development Center, Vicksburg MS.

Chow, V.T. 1959. Open-Channel Hydraulics. McGraw-Hill.

Coos Watershed Association. 2018. Stream Data. http://www.cooswatershed.org/downloaddata/

Cornu, C. E., and J. Souder (eds). 2015. Communities, Lands & Waterways Data Source. Partnership for Coastal Watersheds, South Slough Natonal Estuarine Research Re-serve, and Coos Watershed Association. Coos Bay, OR.

Confederated Tribes of Coos, Lower Umpqua, and Siuslaw Indians (CTCLUSI). 2016. "Intermediate Water Quality Assessment Report for the Confederated Tribes of Coos, Lower Umpqua, and Siuslaw Indians," October 2015 – September 2016, Department of Culture and Natural Resources, Coos Bay, OR.

Cowan, J.L.W. and W.R. Boynton. 1996. "Sediment-Water Oxygen and Nutrient Exchanges Along the Longitudinal Axis of Chesapeake Bay: Seasonal Patterns, Controlling Factors and Ecological Significance," Estuaries, 19, 3, pp. 562 – 580.

Danish Hydraulic Institute (DHI). 2017. MIKE 3 Flow Model FM - Hydrodynamic Module User Guide. http://manuals.mikepoweredbydhi.help/2017/Coast_and_Sea/m3HD.pdf

Dortch, M.S., and S.K. Martin. 2008. "Estimating Bottom Water Dissolved Oxygen in the Mississippi River Gulf Outlet and Gulf Intracoastal Waterway Resulting from Proposed Structures," ERDC/EL TR-08-9, U.S. Army Engineer Research and Development Center, Vicksburg, MS.

Egbert, G.D. and Erofeeva, S.Y. 2002. Efficient Inverse Modeling of Barotropic Ocean Tides. Journal of Atmospheric and Oceanic Technology, Volume 19.

Elliott, A.J. 1982. Wind-Driven Flow in a Shallow Estuary. Oceanologica ACTA 1982 – Vol 5, No. 1.

Fischer, H.B., List, E.J., et. al., "Mixing in Inland and Coastal Waters", Academic Press, Inc., 1979.

GRI. 2011. Coos Bay Channel Modification Section 203 Feasibility Study / Environmental Impact Study. Geotechnical Data Report. Prepared for David Evans & Associates.

Hyde, N. 2007. Towards national estuarine modeling and characterization/classification systems a pilot study for Coos Bay. Oregon Health & Science University (OHSU), Master of Science Dissertation. Scholar Archive. 127.

HydroPlan LLC. 2015. Redwood City Harbor Navigation Improvement Feasibility Report and Integrated EIS/EIR. Prepared for U.S. Army Corps of Engineers, San Francisco District. Prepared in collaboration with GAIA and Moffatt and Nichol. Contract No. W912P7-11-D-0004, Task Order No. 0013. June 2015.

Komar, P.D. 1997, The Pacific Northwest Coast: Living with the Shores of Oregon and Washington. Duke University Press.

Moffatt & Nichol. 2012. "Dissolved Oxygen Modeling for Proposed Perquimans County Marine Industrial Park Marina." Report prepared for the North Carolina Department of Commerce.

___. 2014. "Circulation and Water Quality Study, San Rafael Rock Quarry – Reclamation Plan Project, M&N File No: 5487-03." Letter report submitted to sponsor.

___. 2015. "Smith Canal Gate Hydrodynamic Modeling Alignment and Gate Width Evaluation, Final Report," prepared for Peterson Brustad, Inc.

___. 2017. "Modeling and Initial Water Quality Evaluations Supporting the Federal Feasibility Study and NEPA Documentation – Broad Creek," prepared for the City of Norfolk, Department of Public Works.

___. 2017. "Modeling and Initial Water Quality Evaluations Supporting the Federal Feasibility Study and NEPA Documentation – Pretty Lake," prepared for the City of Norfolk, Department of Public Works.

Moore, J.W., K.D. Martin and M.E. Gray. 2000. Coos Bay Salinity Intrusion Study-the effects of deepening the shipping channel on striped bass and other fish populations. ODFW Contract Number W66QKZ01017672.

National Ocean and Atmospheric Administration (NOAA). 2014. Chart 18587, U. S. Department of Commerce, National Oceanic and Atmospheric Administration, National Ocean Service, Coast Survey. Last Correction 3/26/2014. http://www.charts.noaa.gov/OnLineViewer/18587.shtml

__. 2017. Extreme Water Levels: 9432780 Charleston, OR. Available online at: http://tidesandcurrents.noaa.gov/est/est_station.shtml?stnid=9432780

O'Neill, M.A. 2014. Seasonal Hydrography and Hypoxia of Coos Bay, Oregon. Master Thesis. Submitted to the Department of Geological Sciences, University of Oregon.

Oregon Department of Environmental Quality (ODEQ). 2007. 2007 Coos Basin Temperature Project. Unpublished raw data. Retrieved from: http://deq12.deq.state.or.us/lasar2/

Oregon Department of State Lands (ODSL). 2018. South Slough Reserve. https://www.oregon.gov/dsl/SS/Pages/About.aspx, accessed on July 29, 2018.

Oregon International Port of Coos Bay (OIPCB). 2010. Coos Bay Channel Modifications Project. Current and Wave Monitoring Survey Results. Prepared by David Evans & Associates (DEA): May.

___. 2015. Section 204/408 Report and Environmental Impact Statement. Tentatively Selected Plan Report. Prepared by DMA.

___. 2016. One-Time Authorization for Using MIKE-21 Modeling Suite. Memorandum for Record.

___. 2017. Coos Bay, OR Section 204(f) Channel Modification Project 60% Engineering Design Report. Prepared by Moffatt & Nichol.

___. 2019. Engineering Appendix A: Design Documentation Report. Oregon International Port of Coos Bay Proposed Section 204(f)/408 Channel Modification Project. October 2019.

Partnership for Coastal Watersheds (PCW). 2018a. Coos Estuary Water Quality Monitoring Network, https://www.partnershipforcoastalwatersheds.org/coos-bay-water-quality-monitoring-network/, accessed on July 29, 2018.

__. 2018b. Water Quality in the Coos Estuary and Lower Coos Watershed: Physical Factors. Lands & Waterways, Coos Bay Area. http://www.partnershipforcoastalwatersheds.org/water-quality-in-the-coos-estuary-and-lower-coos-watershed-physical-factors/, accessed on July 29, 2018.

Permanent International Association of Navigation Congress (PIANC). 1987. Guidelines for the Design and Construction of Flexible Revetments Incorporating Geotextiles for Inland Waterways. Report of Working Group 4 of the Permanent Technical Committee I. Supplement to Bulletin No.57.

Roegner, G.C., Needoba, J.A., Baptista, A.M. 2011. Coastal upwelling supplies oxygen-depleted water to the Columbia River estuary. PLoS ONE 6(4): e18672. https://doi.org/10.1371/journal.pone.0018672.

Roye, C. 1979. Natural Resources of Coos Bay Estuary, Estuary Inventory Report, Vol. 2, No. 6.

Rumrill, S.S. 2006. The Ecology of the South Slough Estuary: Site Profile of the South Slough National Estuarine Research Reserve. South Slough National Estuarine Research Reserve. Charleston, OR. 238 p.

Shen, J., R. Wang, and M. Sisson. 2017. "Assessment of Hydrodynamic and Water Quality Impacts for Channel Deepening in the Thimble Shoals, Norfolk Harbor, and Elizabeth River Channels, Final Report," Special Report No. 454, prepared for Virginia Port Authority, by Applied Marine Science and Ocean Engineering, Virginia Institute of Marine Science (VIMS), Gloucester Point, VA.

Schiereck, G.J. 2001. Introduction to Bed, Bank and Shore Protection. Delft University Press.

Schrager, H., Brag, J., Demarzo, A., Yednock, B., Schmitt, J., Helms, A., Tally, J., Rudd, D., Dean, E., Muse, R., Cooper, G., Cornu, C., Gaskill, T., Wilson, P. 2017. South Slough National Estuarine Research Reserve Management Plan 2017-2022, Coos County Oregon.

SHN. 2006. Sediment Sampling and Analysis Report, Oregon Marine Gateway Terminal, Coos Bay, Oregon. Prepared for The Port of Coos Bay and Jordan Cove Energy.

Shen, J., R. Wang, and M. Sisson. 2017. "Assessment of Hydrodynamic and Water Quality Impacts for Channel Deepening in the Thimble Shoals, Norfolk Harbor, and Elizabeth River Channels, Final Report," Special Report No. 454, prepared for Virginia Port Authority, by Applied Marine Science and Ocean Engineering, Virginia Institute of Marine Science (VIMS), Gloucester Point, VA.

Sigmon C.L.T., Caton L., Coffeen G., Miller S. 2006. Coastal Environmental Monitoring and Assessment Program. The Condition of Oregon's Estuaries in 1999, a Statistical Summary. Oregon Department of Environmental Quality, Laboratory.

Sorensen, R.M. 1997. Prediction of Vessel-Generated Waves with Reference to Vessels Common to the Upper Mississippi River System. Prepared for US Army Corps of Engineers.

South Slough National Estuarine Research Reserve (SSNERR). 2014. [Greater Coos Bay stations, 2013- 2014)]. Unpublished raw data.

Sutherland, D.A. and O'Neill, M.A. 2016. Hydrographic and Dissolved Oxygen Variability in a Seasonal Pacific Northwest Estuary. Journal of Estuarine, Coastal and Shelf Science, Volume 172.

Tetra Tech, Inc. 2011. Model Comparison Report in Support of the Savannah Harbor Expansion Project. Prepared for USACE – Savannah District. Contract No: W912HN-09-R-0081. July 29, 2011.

Thom, R. M., A. B. Borde, S. Rumrill, D. L. Woodruff, G. D. Williams, J. A. Southard, and S. L. Sargeant. 2003. Factors Influencing Spatial and Annual Variability in Eelgrass (Zostera marina L.) Meadows in Willapa Bay, Washington, and Coos Bay, Oregon, Estuaries. Estuaries. 26 (4): 1117-1129.

Thomann, R.V. and J.A. Mueller. 1987. Principles of Surface Water Quality Modeling and Control, Harper Collins Publishers, Inc., New York, NY.

U.S. Army Corps of Engineers (USACE). 1958. Coos Bay, Oregon: Construction of Pile Dikes. Drawing Number: CB-1-449. Revision 3. January 2.

___. 1980. Gallipolis Locks and Dam Replacement, Ohio River, Phase I, Advanced Engineering and Design Study. General Design Memorandum, Appendix J, Vol. 1, Environmental and Social Impact Analysis. Prepared by USACE, Huntington District.

___. 1994. Coos Bay, Oregon, Navigation Improvements. Final Feasibility Report and Environmental Impact Statement.

___. 2003. Columbia River Channel Improvement Project, Final Supplemental Integrated Feasibility Report and Environmental Impact Statement. January 2003.

___. 2005. Coos Bay Sediment Quality Evaluation Report. Prepared by Tim Sherman, Portland District Corps of Engineers, CENWP-EC-HR. March.

___. 2012. Coos Bay Jetties: Preliminary Major Maintenance Report. Prepared by M&N. July.

___. 2014. Grays Harbor, Washington. Navigation Improvement Project General Investigation Feasibility Study FINAL Limited Reevaluation Report. June 2014.

___. 2015a. Charleston Harbor Post 45 Final Integrated Feasibility Report and Environmental Impact Statement. June 2015.

___. 2015b. Draft Integrated Feasibility Report and Environmental Impact Statement/Environmental Impact Report Redwood City Harbor Navigation Improvement. June 2015.

___. 2016. Environmental Impact Statement: Seattle Harbor Navigation Improvement Project.

___. 2018. Mobile Harbor, Mobile, Alabama. Draft Integrated General Reevaluation Report with Supplemental Environmental Impact Statement.

___. 2021. Coos Bay North Jetty Repair Major Maintenance Design Drawings. July 26, 2021.

U.S. Army Corps of Engineers and U.S. Environmental Protection Agency (USACE/USEPA). 1986. Coos Bay, Oregon: Dredged Material Disposal Site Designation.

U.S. Army Engineer Research and Development Center (ERDC). 2010. Waves, Hydrodynamics and Sediment Transport Modeling at Grays Harbor, WA. ERDC/CHL TR-10-13. December 2010.

__. 2013. Regional Sediment Management Studies of Matagorda Ship Channel and Matagorda Bay System, Texas. ERDC/CHL TR-13-10. August 2013.

__. 2014. Houston-Galveston Navigation Channel Shoaling Study. ERDC/CHL TR-14-14. December 2014.

__. 2016. Salinity Transport Modeling in the Lower Duwamish Waterway Estuary. ERDC/EL Letter Report. August 2016.

Williams, J.J., and L.S. Esteves (2017) “Guidance on Setup, Calibration, and Validation of Hydrodynamic, Wave, and Sediment Models for Shelf Seas and Estuaries”, Advances in Civil Engineering, Volume 2017, Article ID 5251902, 25 pages, https://doi.org/ 10.1155/2017/5251902.

Willmott, C.J., Ackleson, S.G., Davis, R.E., Feddema, J.J., Klink, K.M., Legates, D.R., O'Donnell, J., and Rowe, C.M. 1985. Statistics for the evaluation and comparison of models. Journal of Geophysical Research 90.C5 (1985): 8995-9005.

Zhang, J., Wang, H., Ye, F., & Wang, Z. (2017) Assessment of Hydrodynamic and Water Quality Impacts for Channel Deepening in the Timble Shoals, Norfolk Harbor, and Elizabeth River Channels : Final report on the “hydrodynamic modeling”. Special report in applied marine science and ocean engineering ; no. 455.. Virginia Institute of Marine Science, College of William and Mary. https://doi.org/10.21220/V5MF0F

Attachment A

Salinity Results for Summer Period

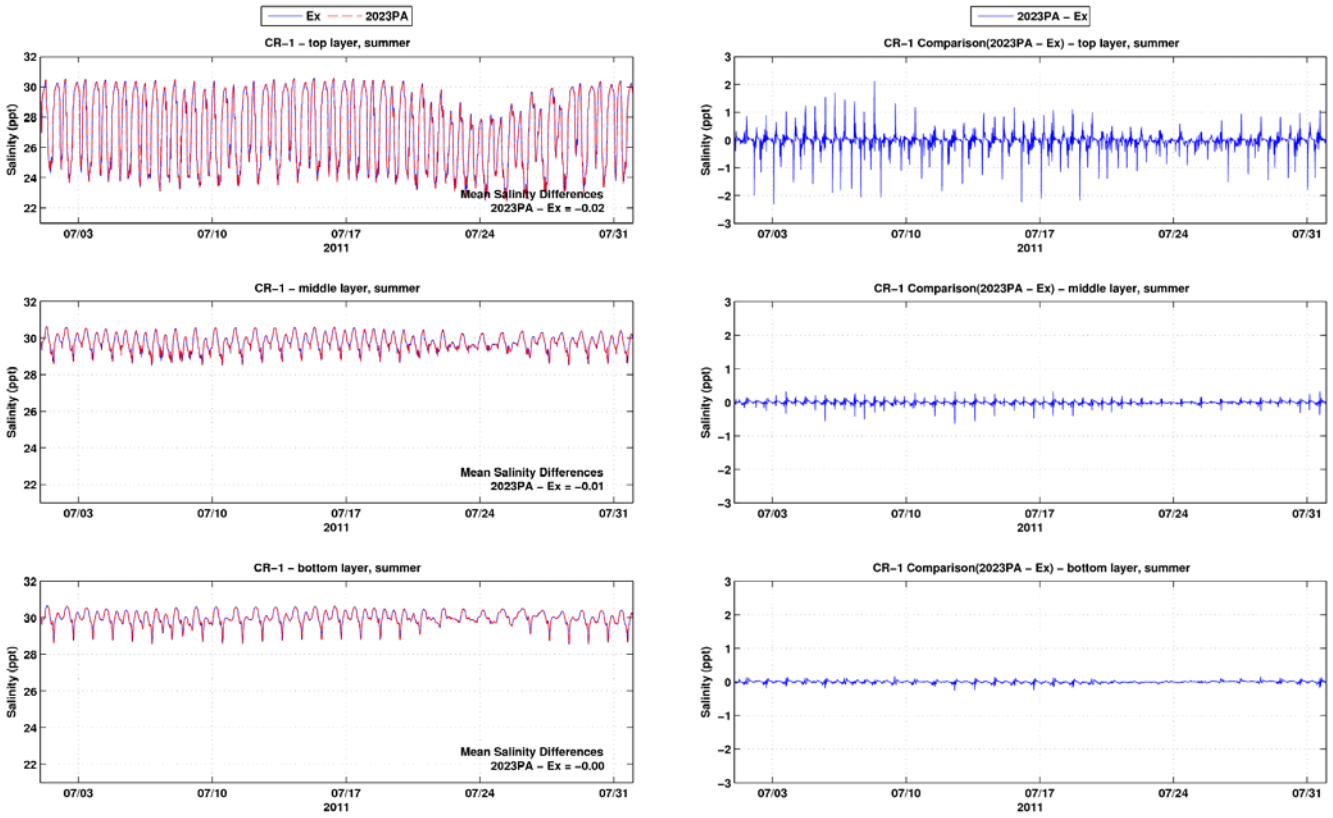

Figure A-1: Salinity time series and differences between the Existing Conditions and the 2023 PA at CR-1 during summer period

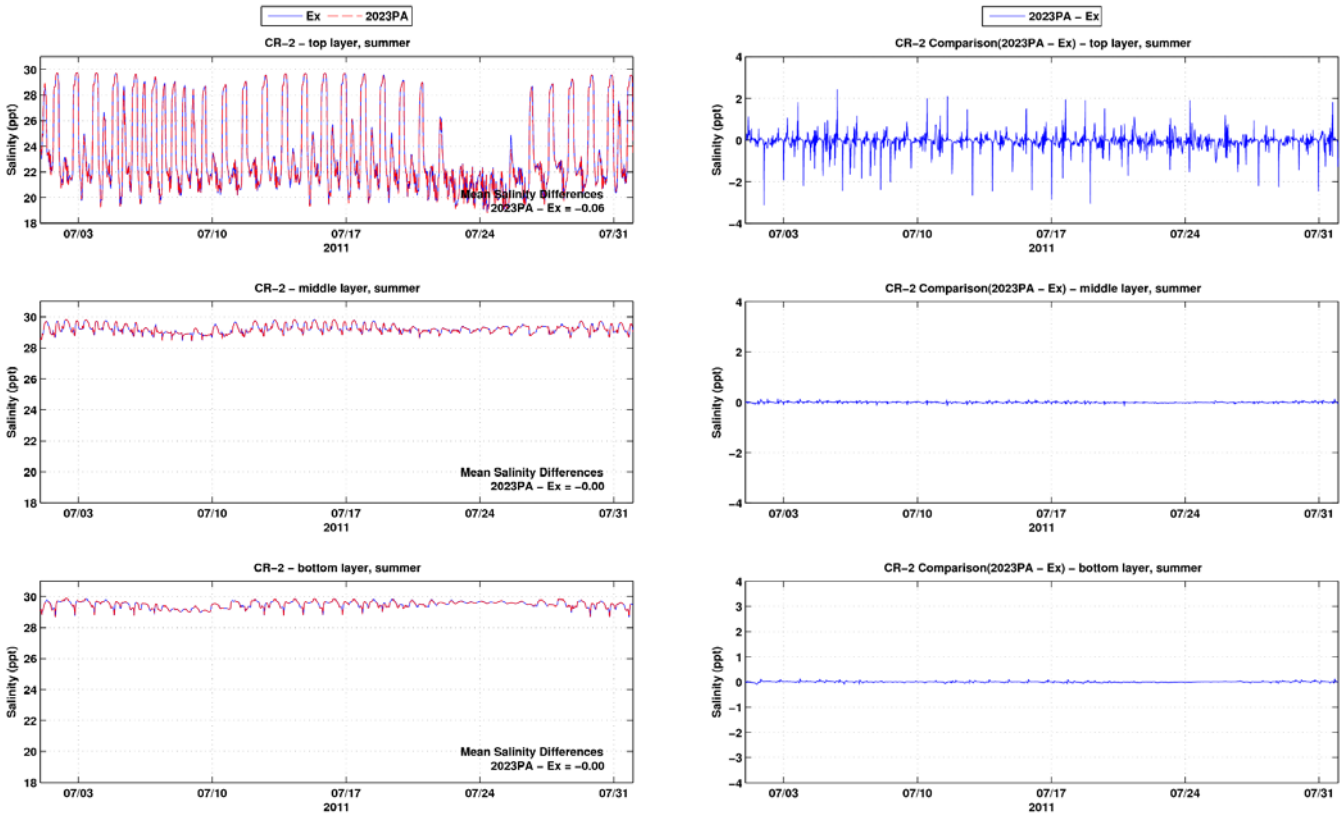

Figure A-2: Salinity time series and differences between the Existing Conditions and the 2023 PA at CR-2 during summer period

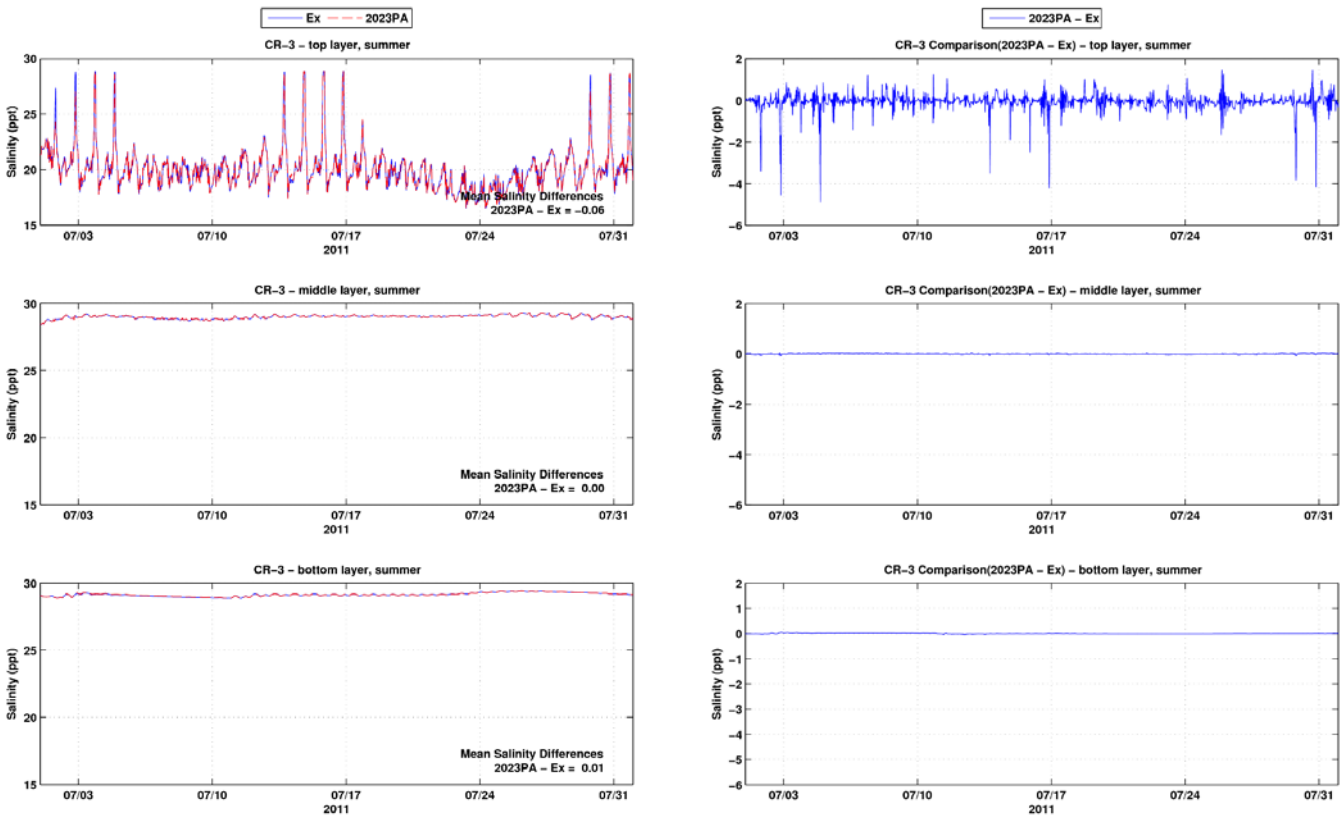

Figure A-3: Salinity time series and differences between the Existing Conditions and the 2023 PA at CR-3 during summer period

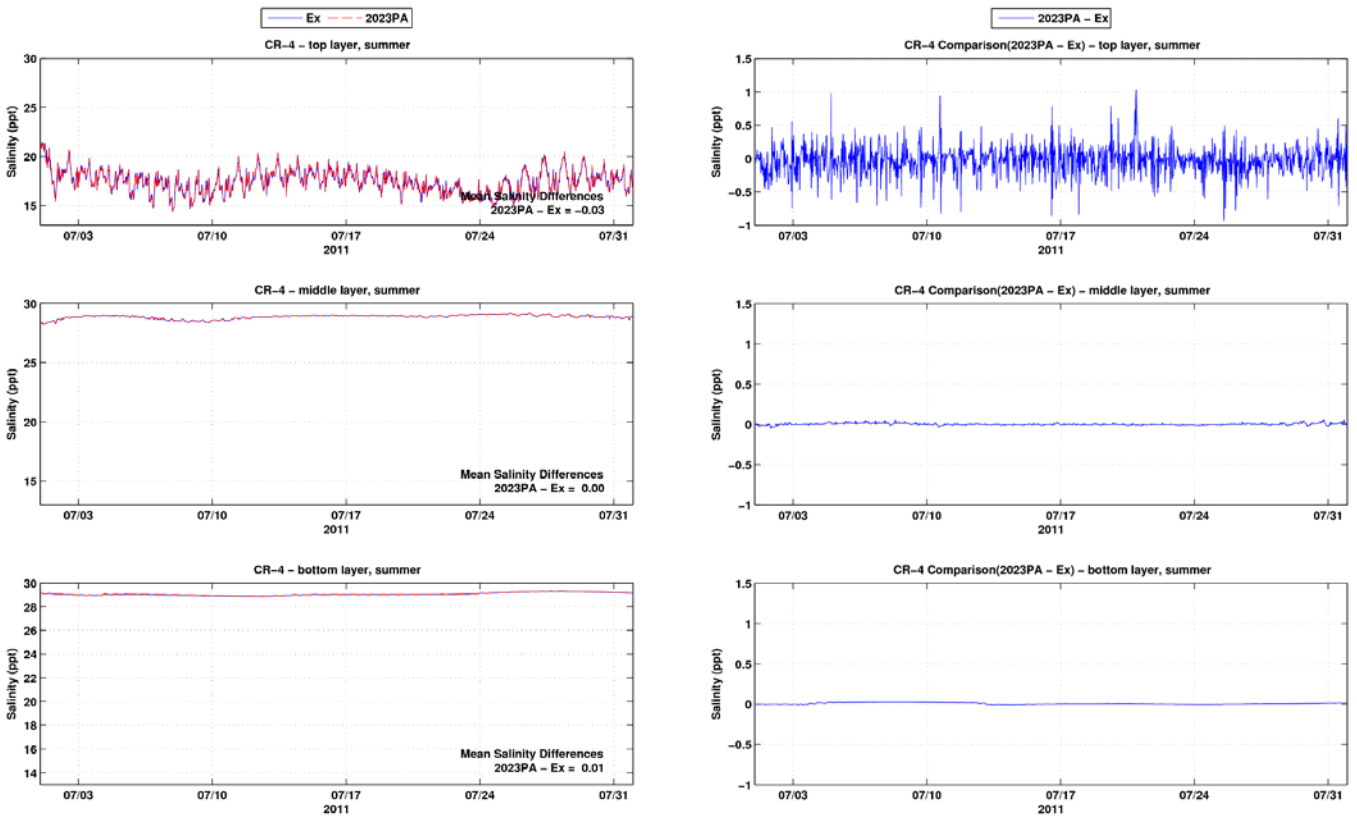

Figure A-4: Salinity time series and differences between the Existing Conditions and the 2023 PA at CR-4 during summer period

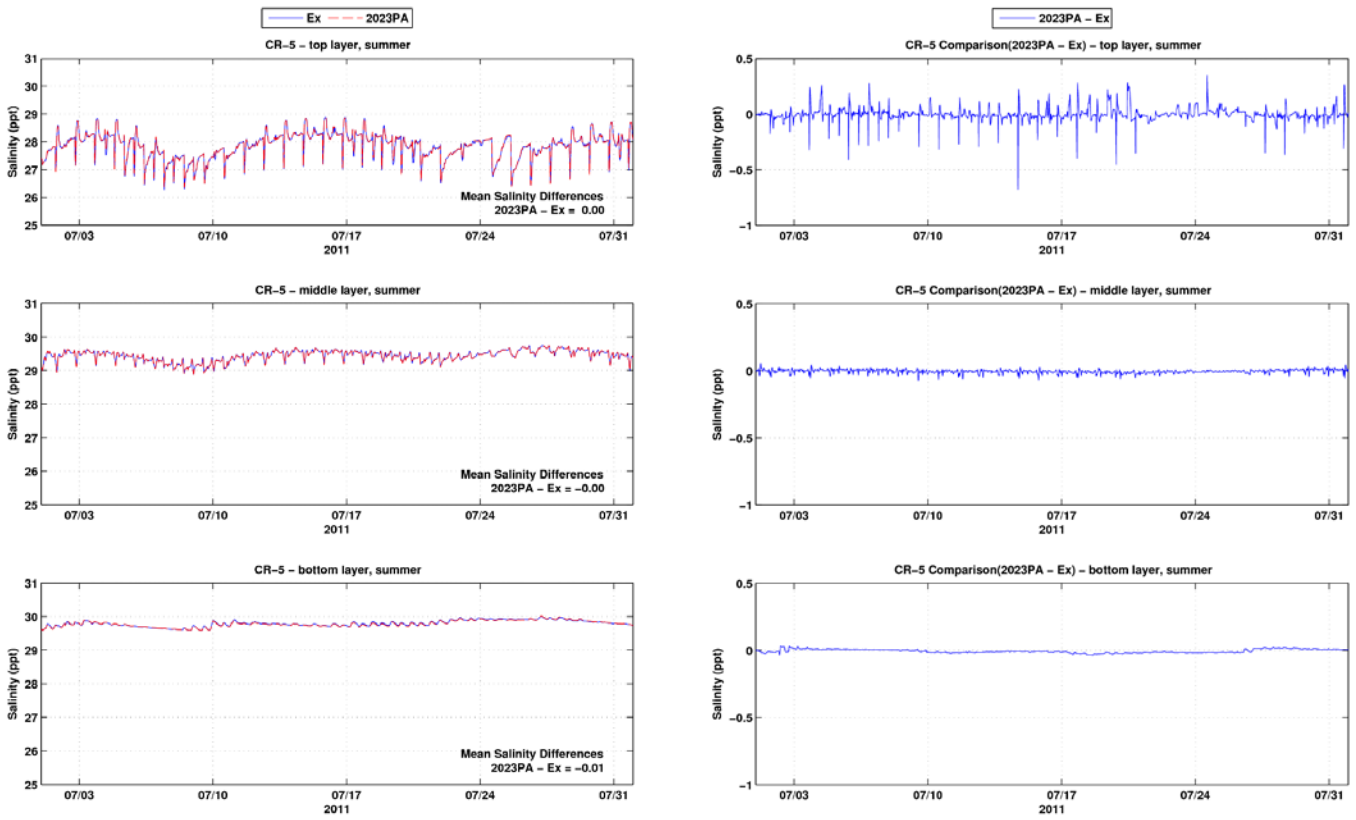

Figure A-5: Salinity time series and differences between the Existing Conditions and the 2023 PA at CR-5 during summer period

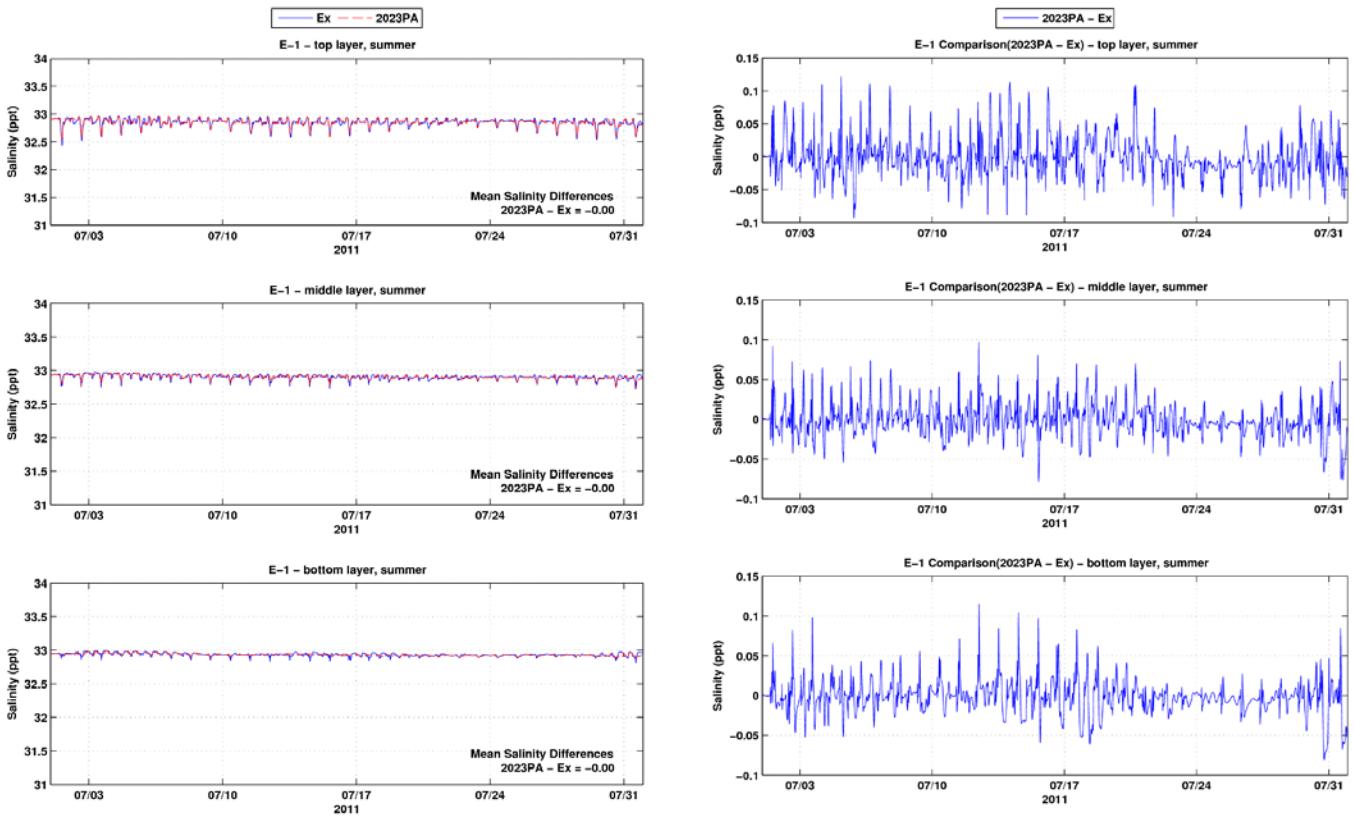

Figure A-6: Salinity time series and differences between the Existing Conditions and the 2023 PA at E-1 during summer period

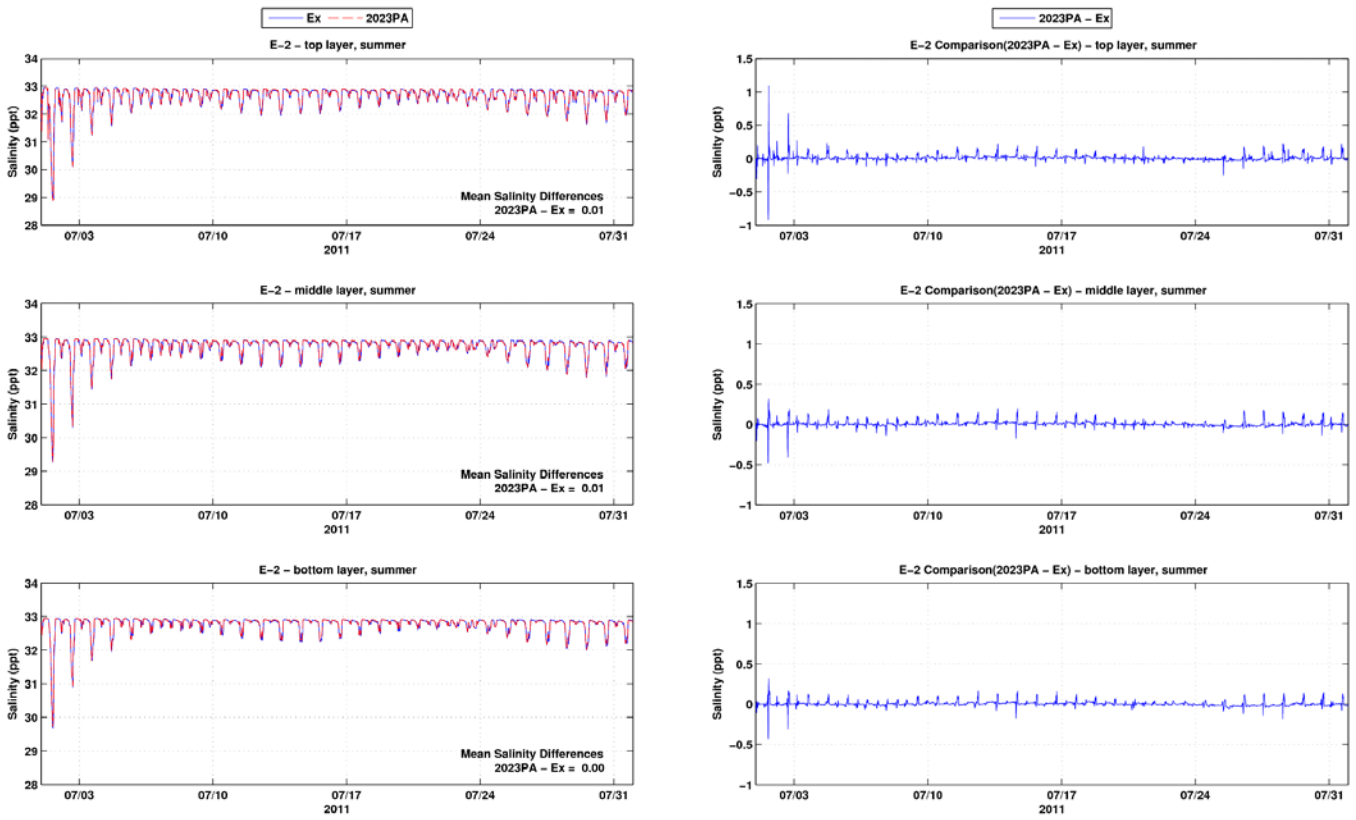

Figure A-7: Salinity time series and differences between the Existing Conditions and the 2023 PA at E-2 during summer period

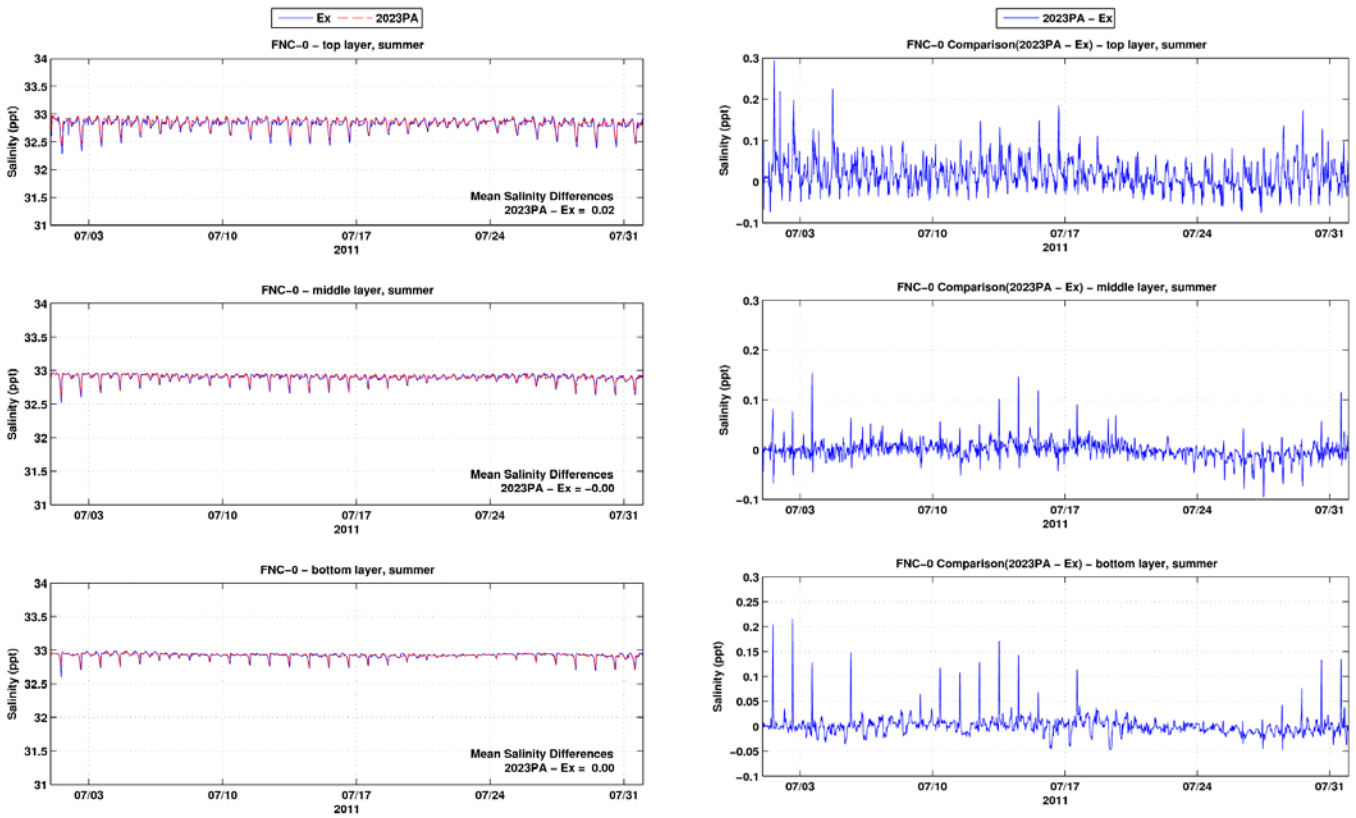

Figure A-8: Salinity time series and differences between the Existing Conditions and the 2023 PA at FNC-0 during summer period

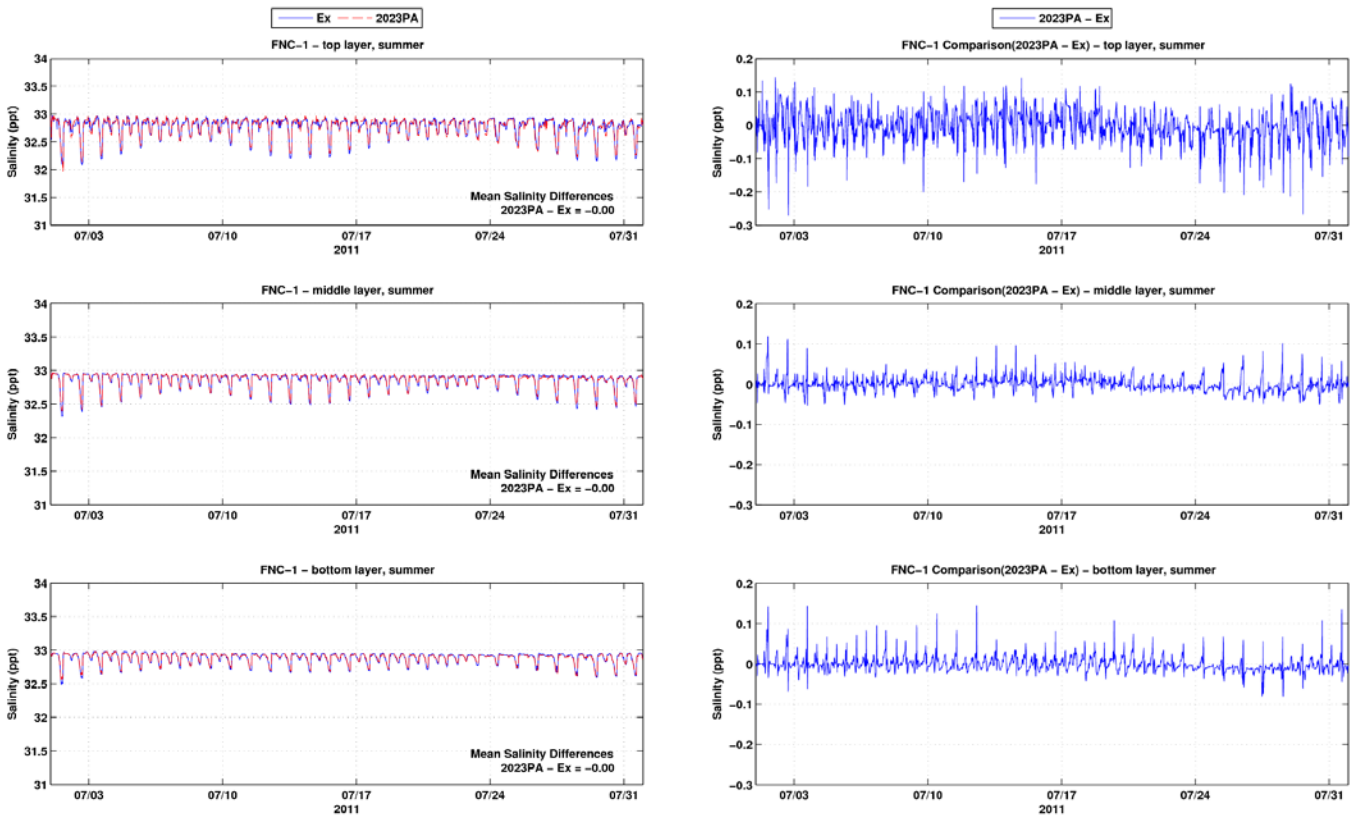

Figure A-9: Salinity time series and differences between the Existing Conditions and the 2023 PA at FNC-1 during summer period

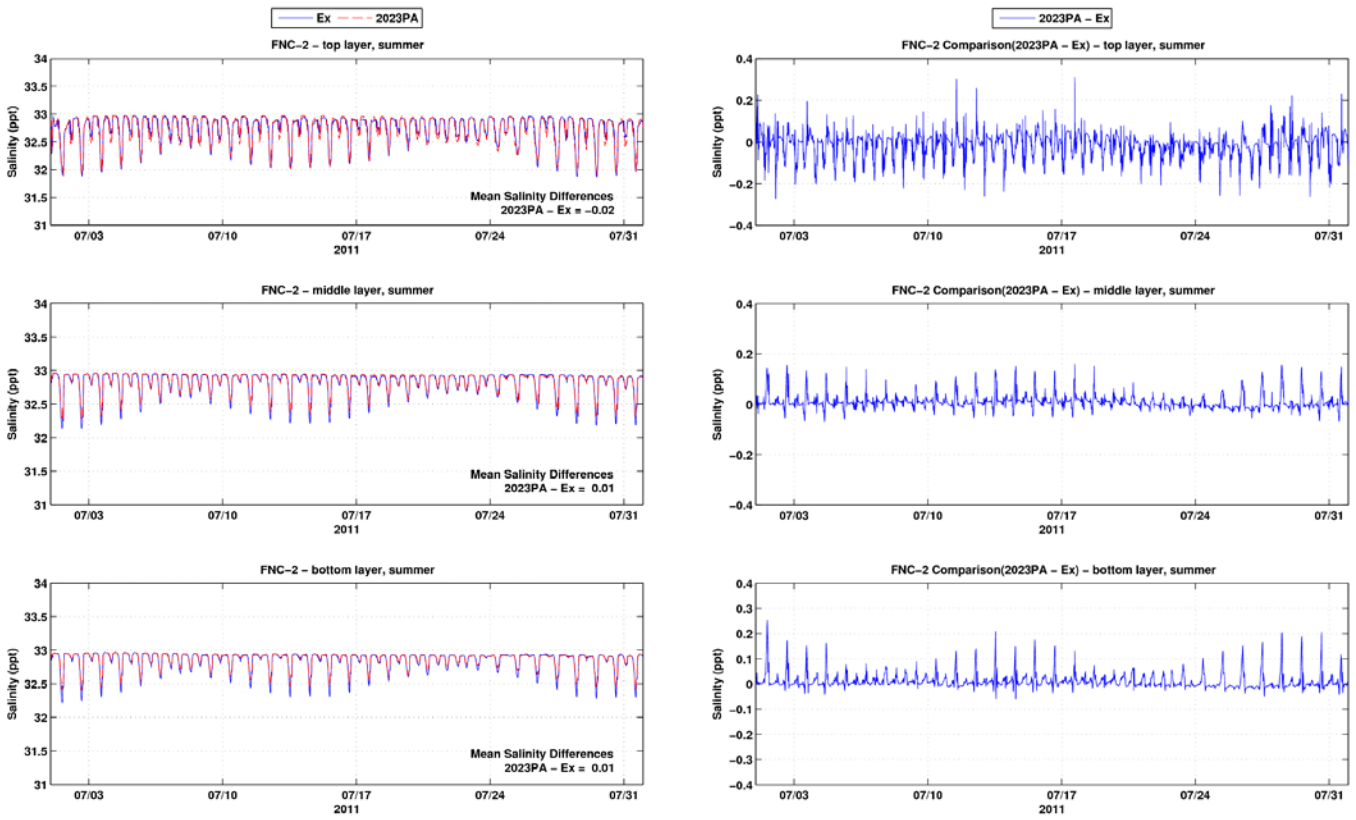

Figure A-10: Salinity time series and differences between the Existing Conditions and the 2023 PA at FNC-2 during summer period

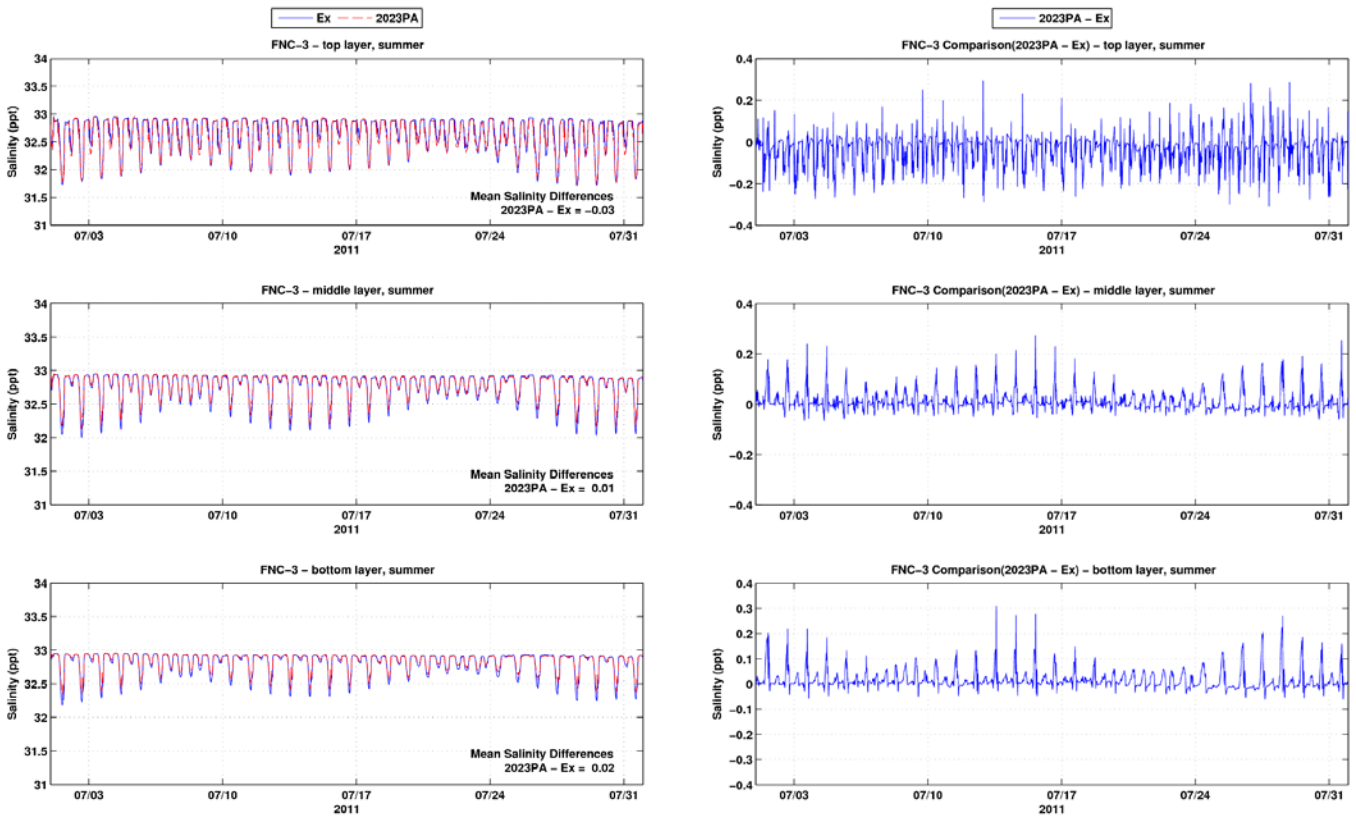

Figure A-11: Salinity time series and differences between the Existing Conditions and the 2023 PA at FNC-3 during summer period

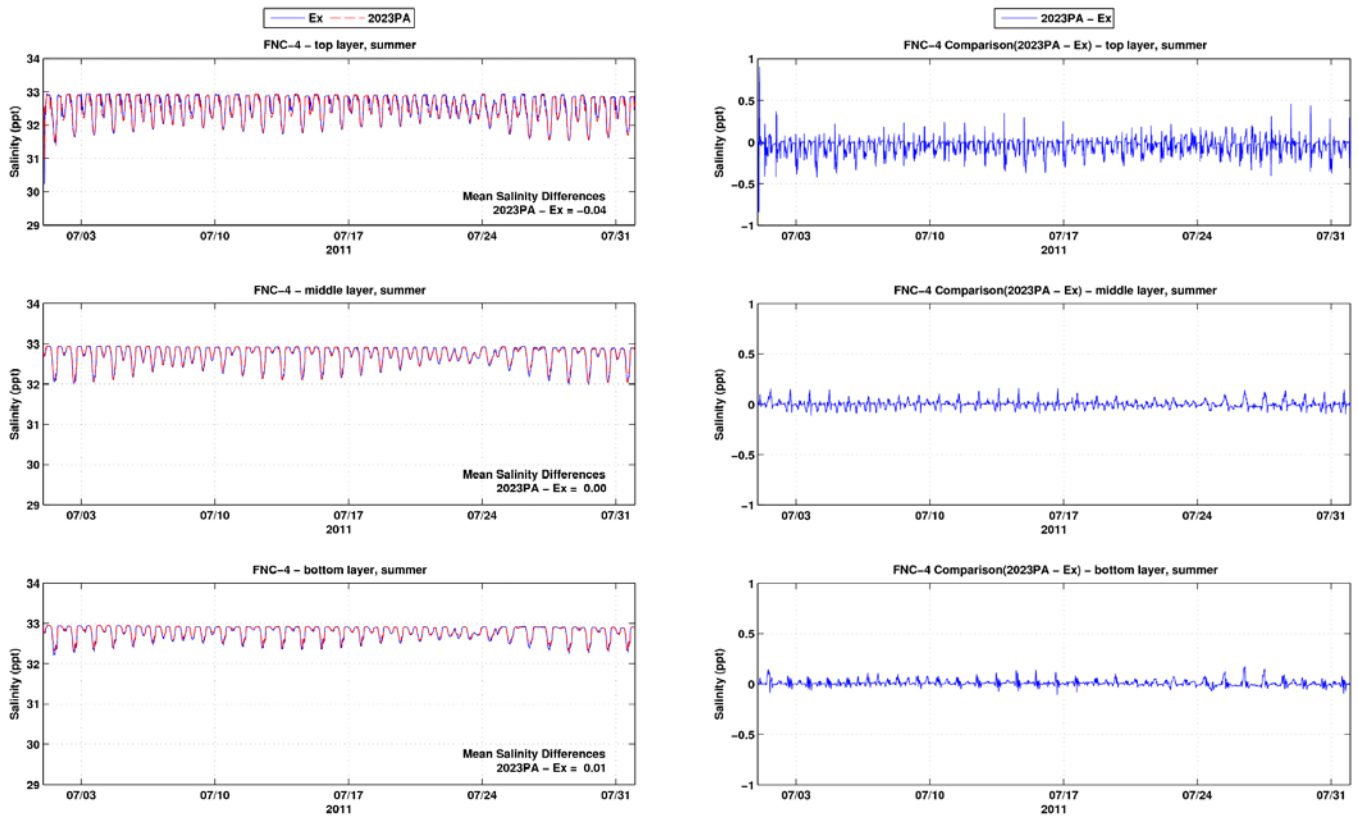

Figure A-12: Salinity time series and differences between the Existing Conditions and the 2023 PA at FNC-4 during summer period

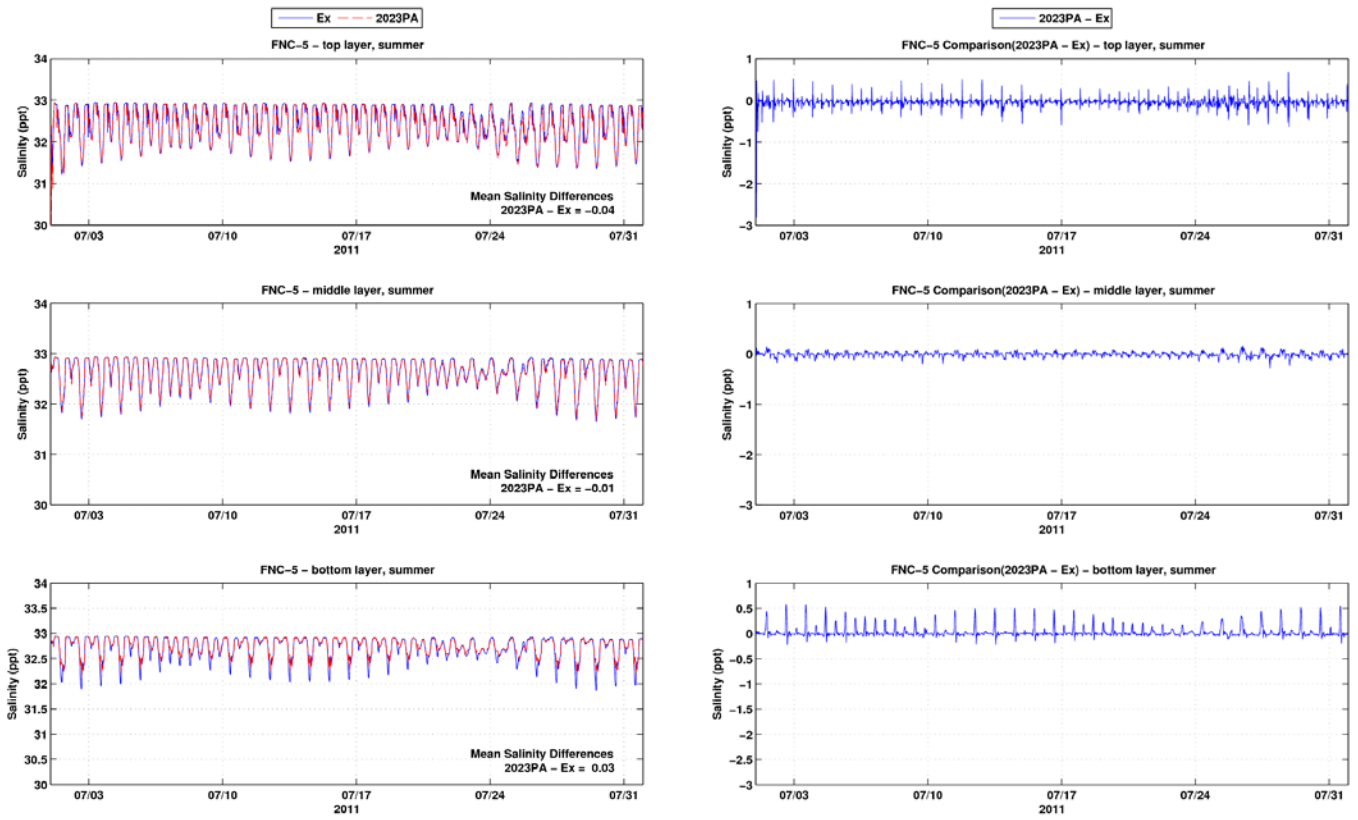

Figure A-13: Salinity time series and differences between the Existing Conditions and the 2023 PA at FNC-5 during summer period

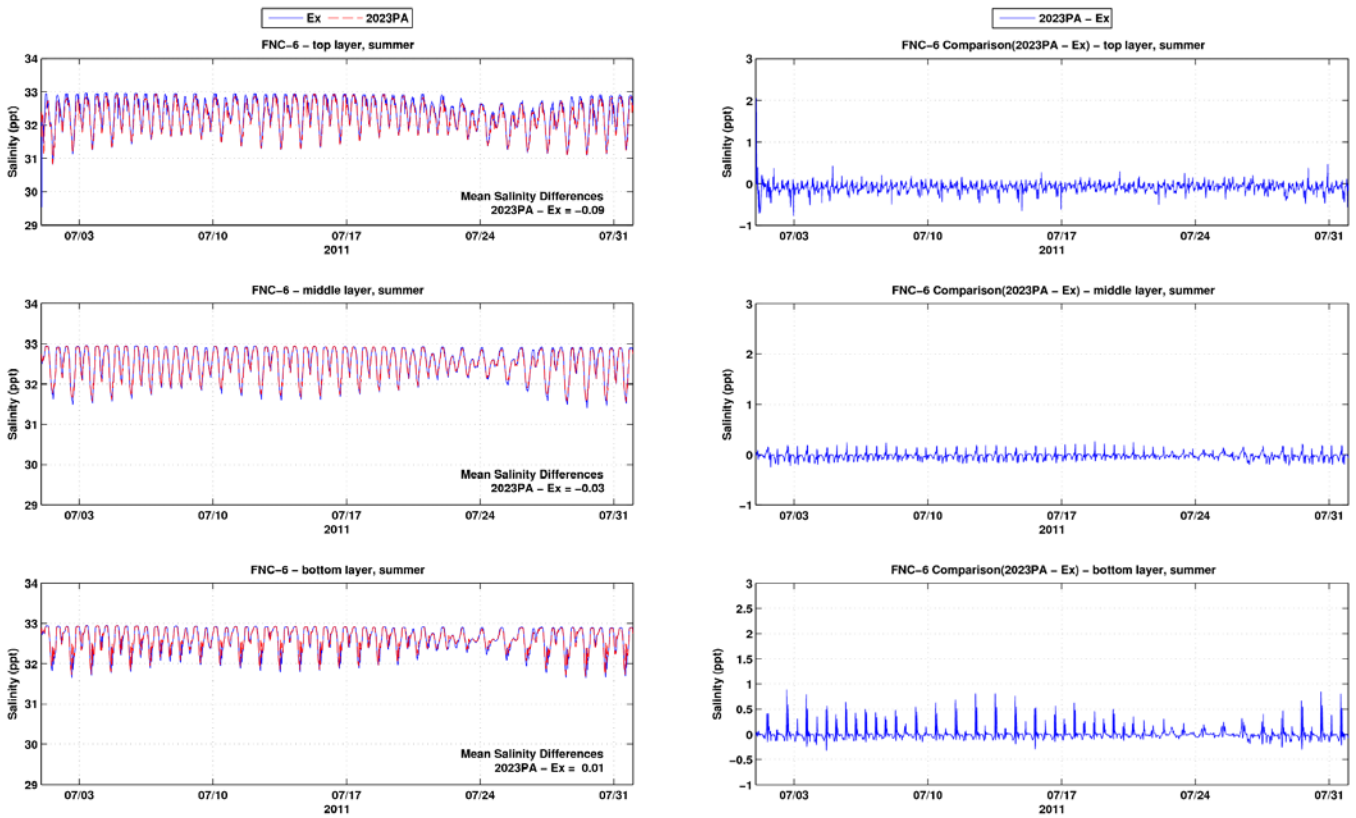

Figure A-14: Salinity time series and differences between the Existing Conditions and the 2023 PA at FNC-6 during summer period

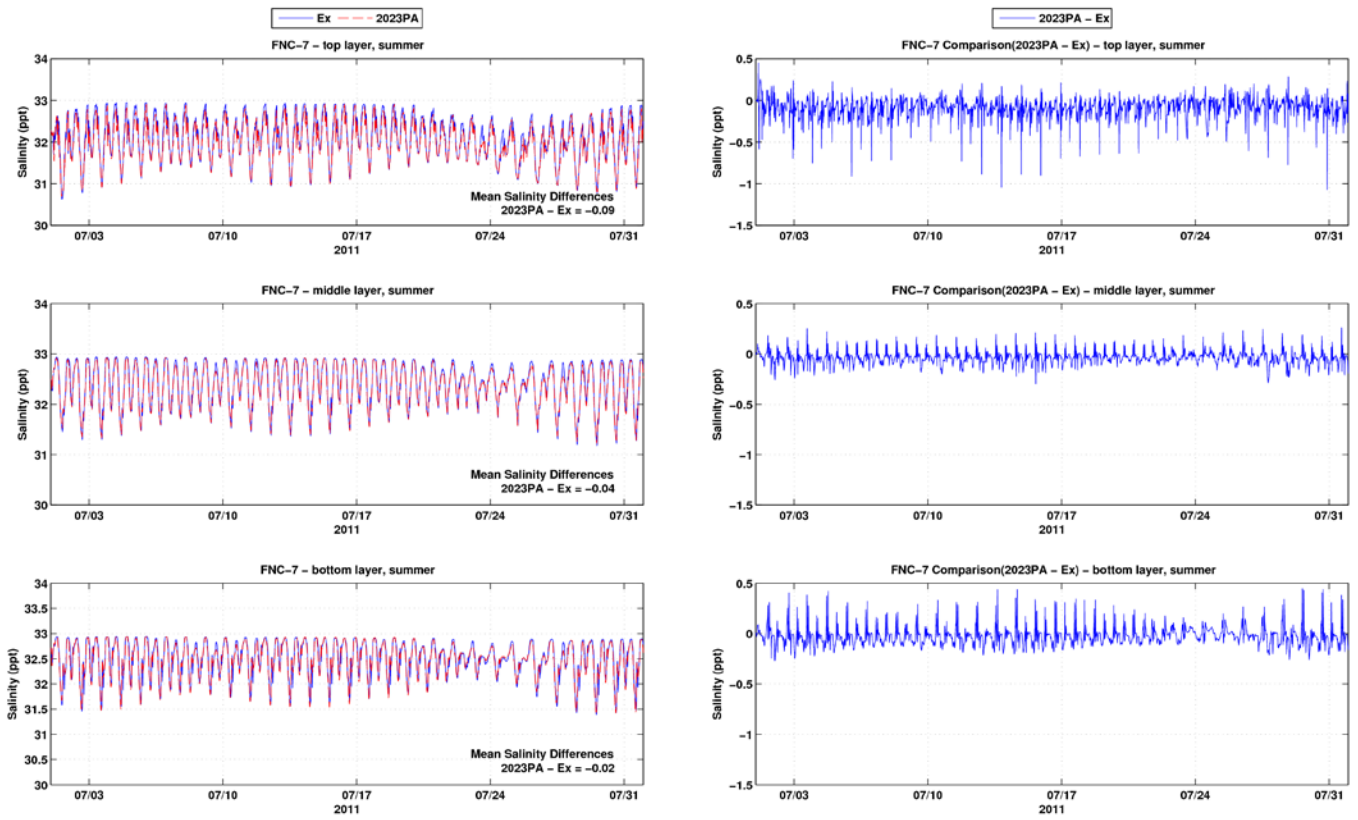

Figure A-15: Salinity time series and differences between the Existing Conditions and the 2023 PA at FNC-7 during summer period

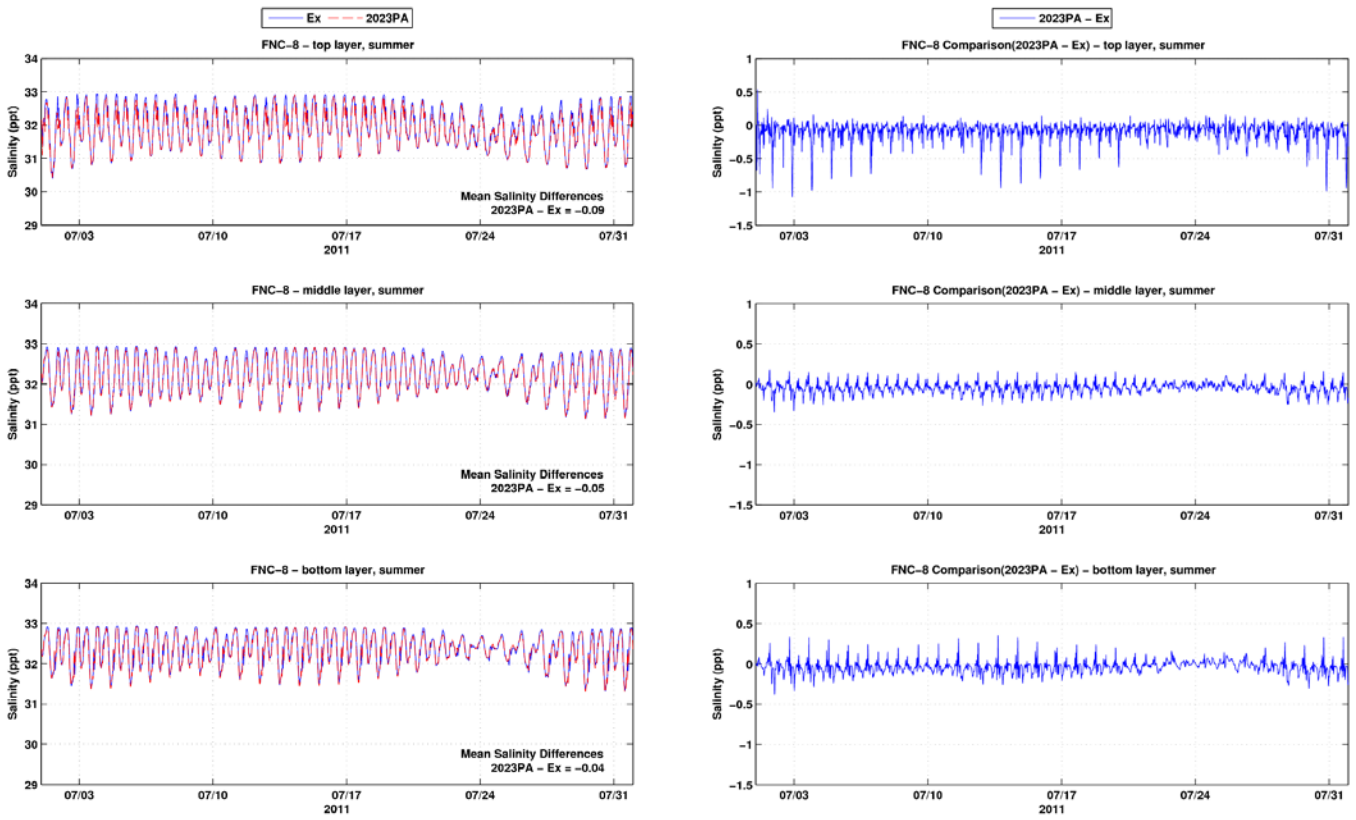

Figure A-16: Salinity time series and differences between the Existing Conditions and the 2023 PA at FNC-8 during summer period

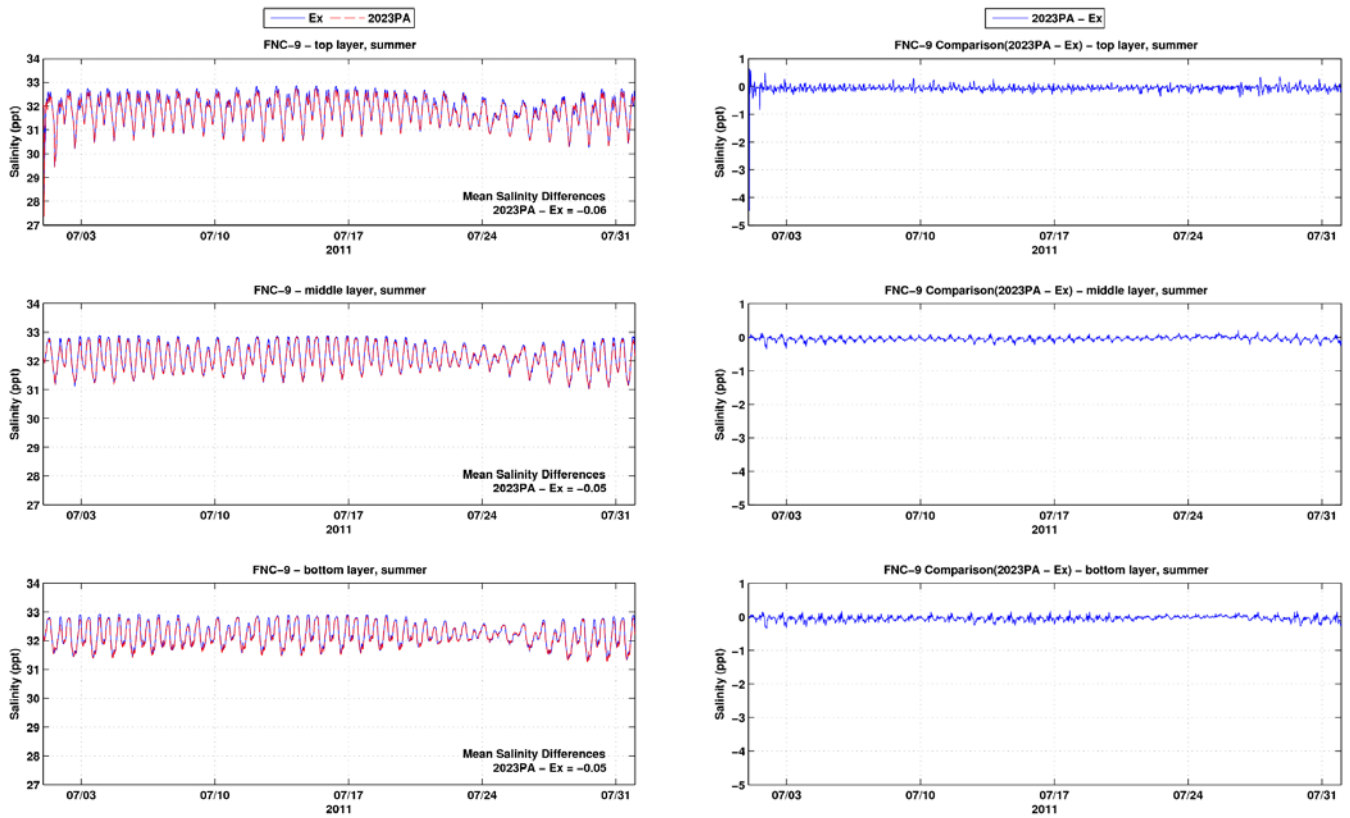

Figure A-17: Salinity time series and differences between the Existing Conditions and the 2023 PA at FNC-9 during summer period

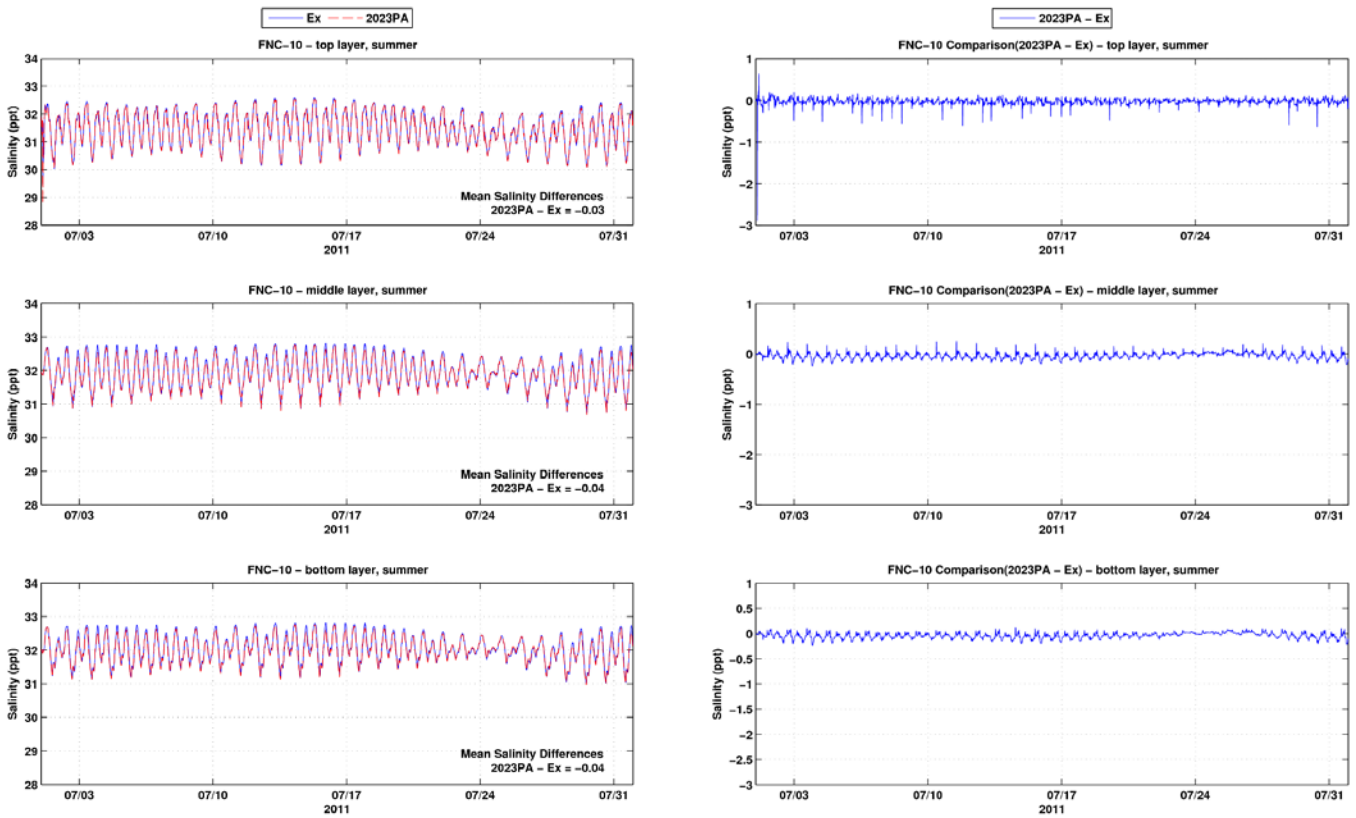

Figure A-18: Salinity time series and differences between the Existing Conditions and the 2023 PA at FNC-10 during summer period

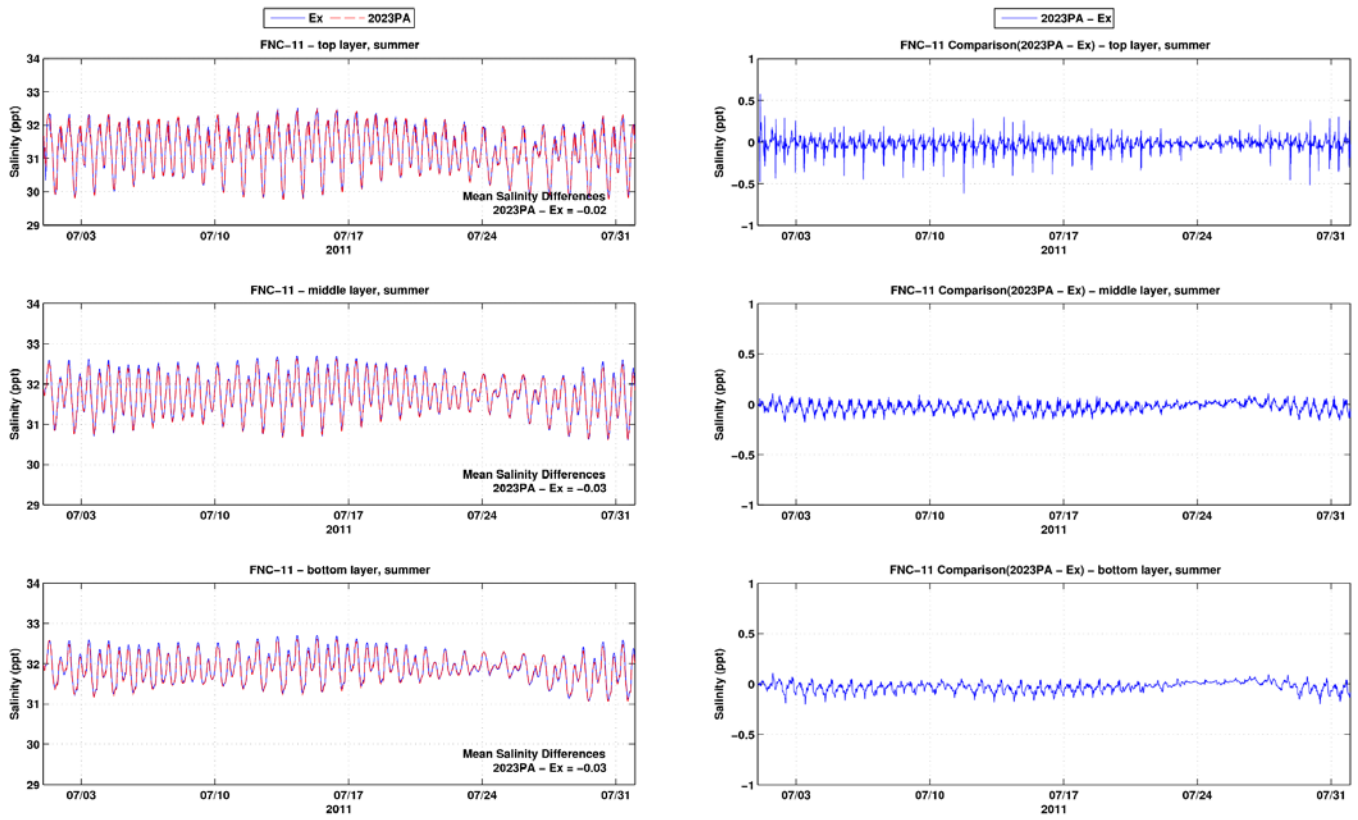

Figure A-19: Salinity time series and differences between the Existing Conditions and the 2023 PA at FNC-11 during summer period

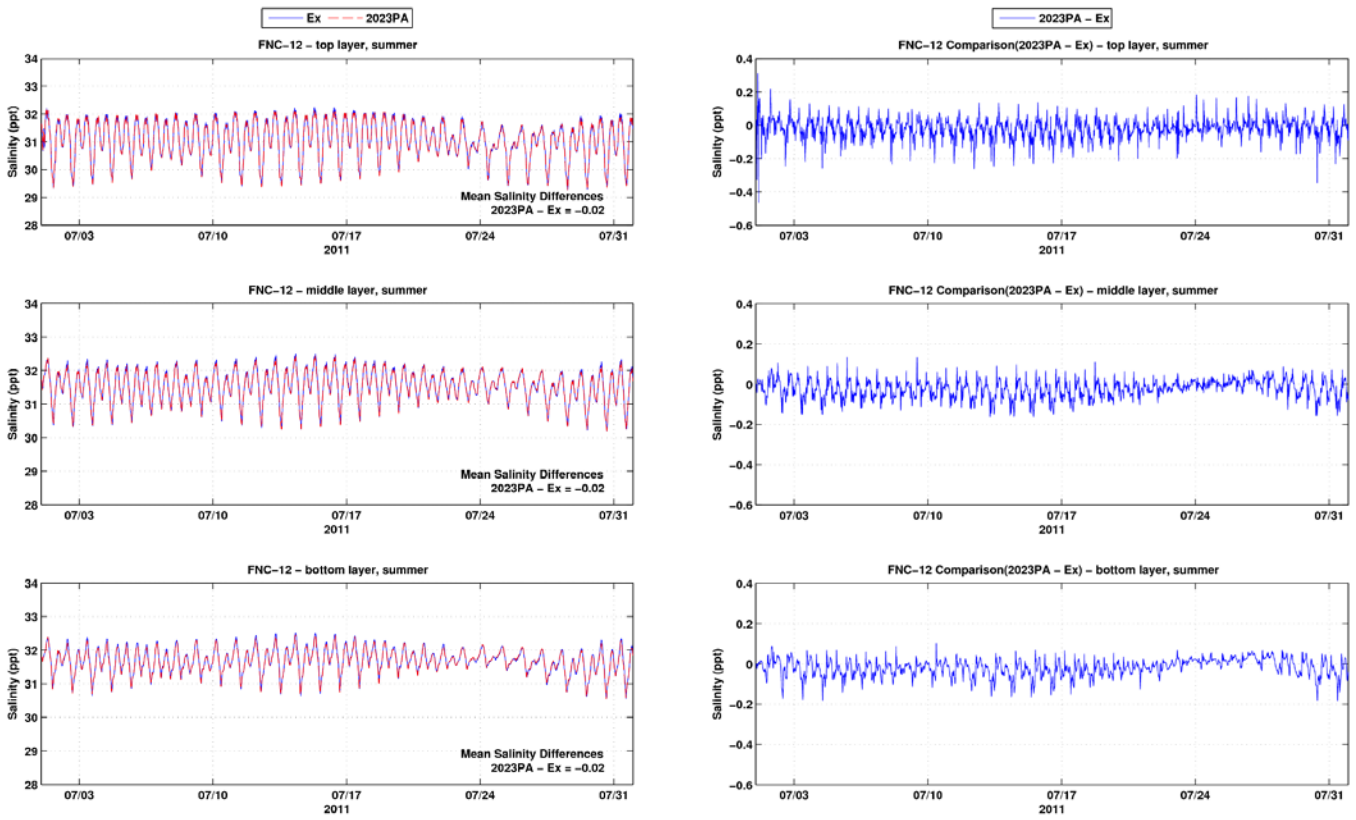

Figure A-20: Salinity time series and differences between the Existing Conditions and the 2023 PA at FNC-12 during summer period

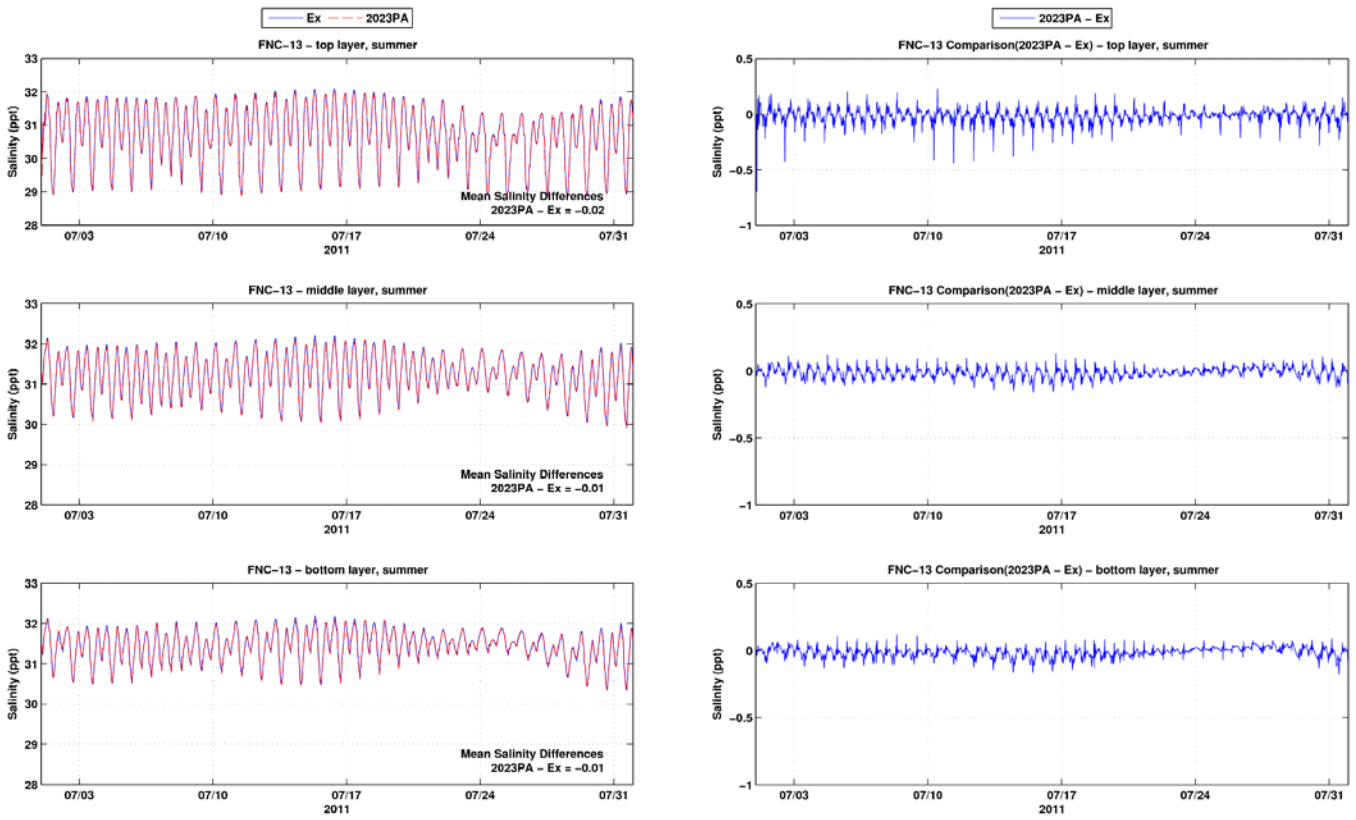

Figure A-21: Salinity time series and differences between the Existing Conditions and the 2023 PA at FNC-13 during summer period

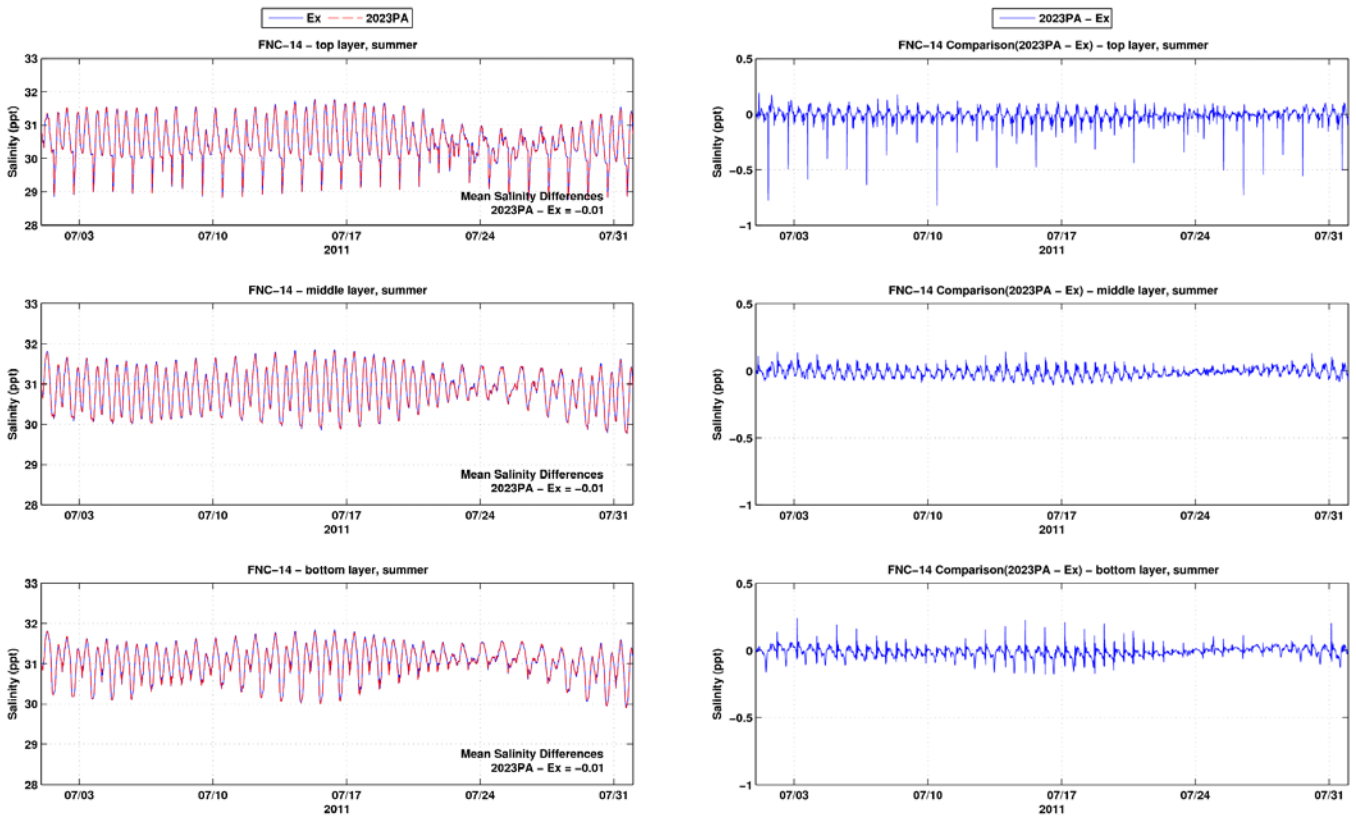

Figure A-22: Salinity time series and differences between the Existing Conditions and the 2023 PA at FNC-14 during summer period

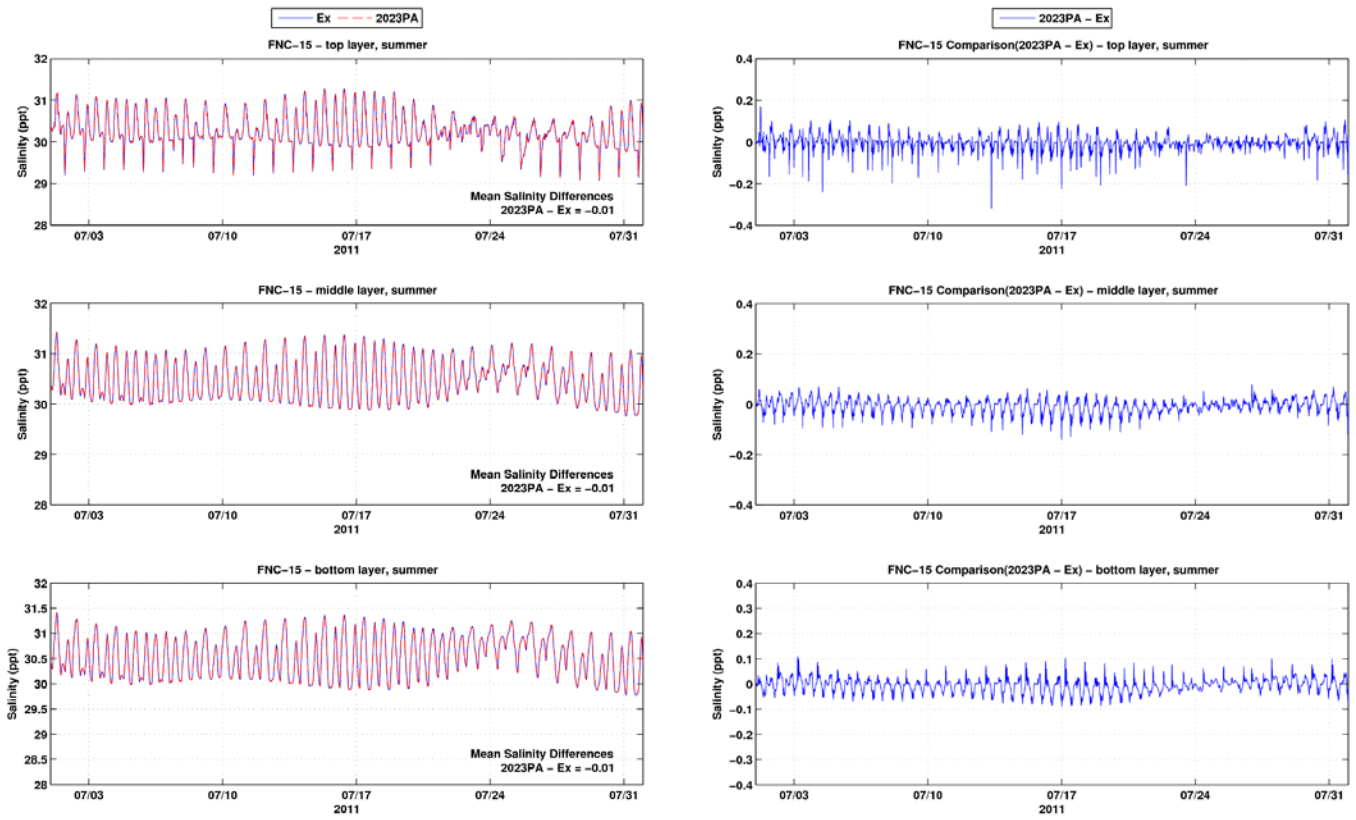

Figure A-23: Salinity time series and differences between the Existing Conditions and the 2023 PA at FNC-15 during summer period

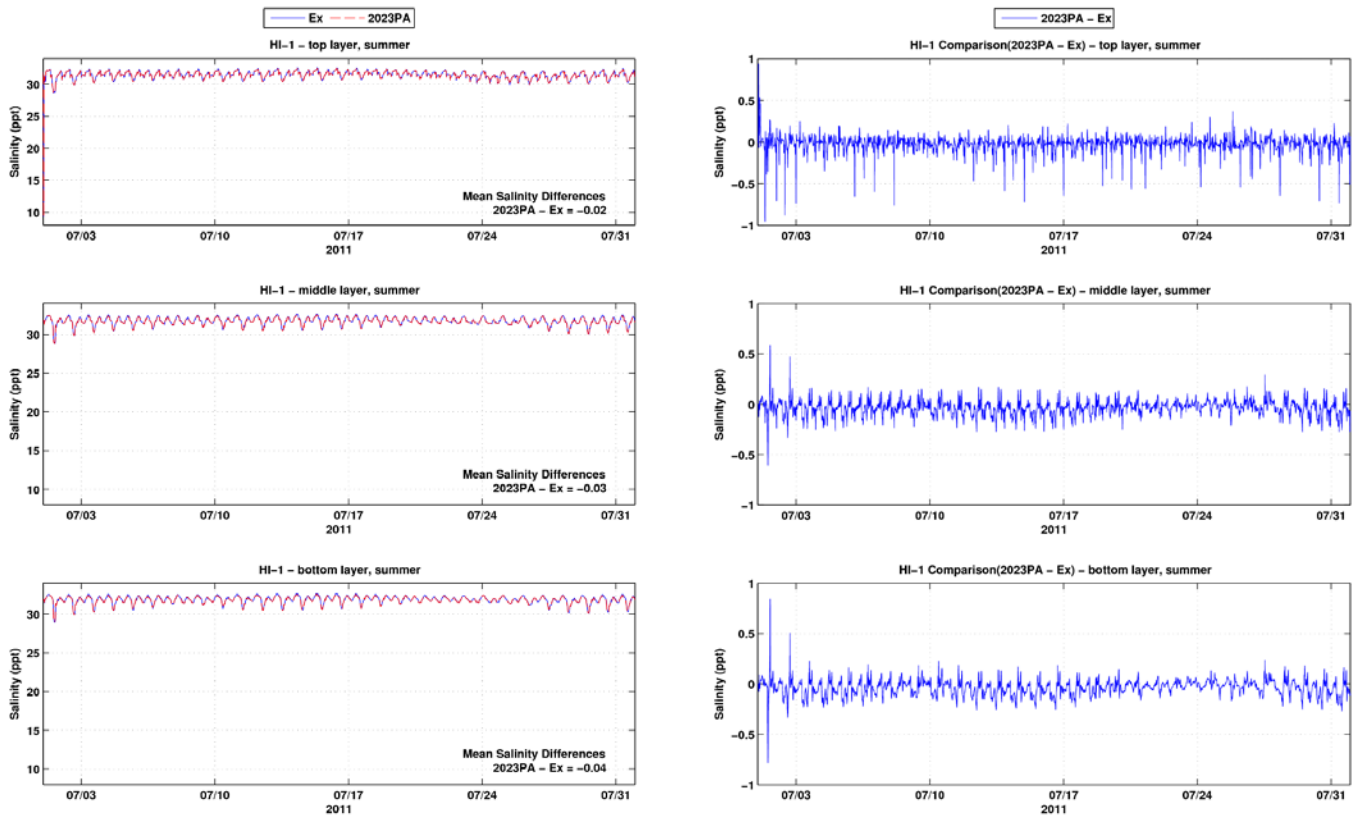

Figure A-24: Salinity time series and differences between the Existing Conditions and the 2023 PA at HI-1 during summer period

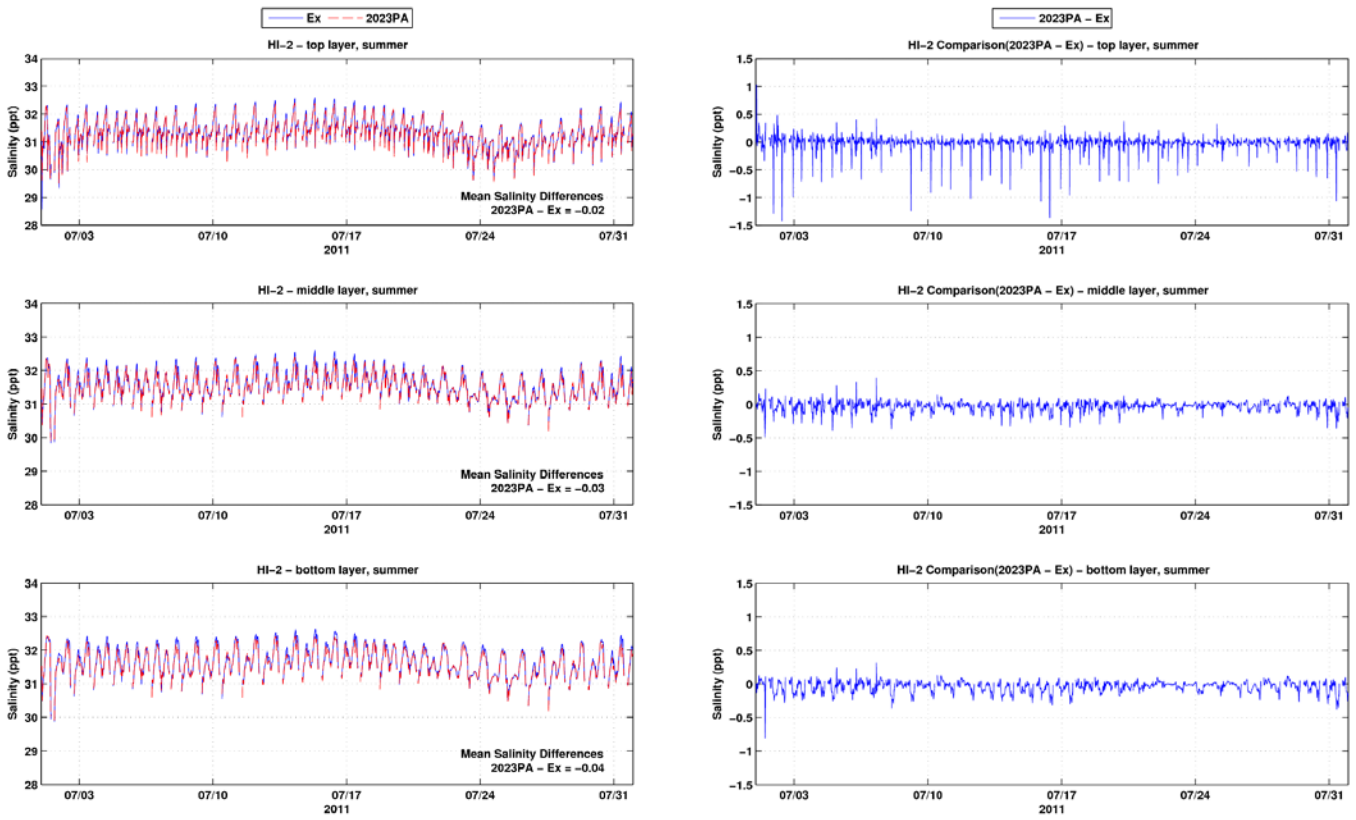

Figure A-25: Salinity time series and differences between the Existing Conditions and the 2023 PA at HI-2 during summer period

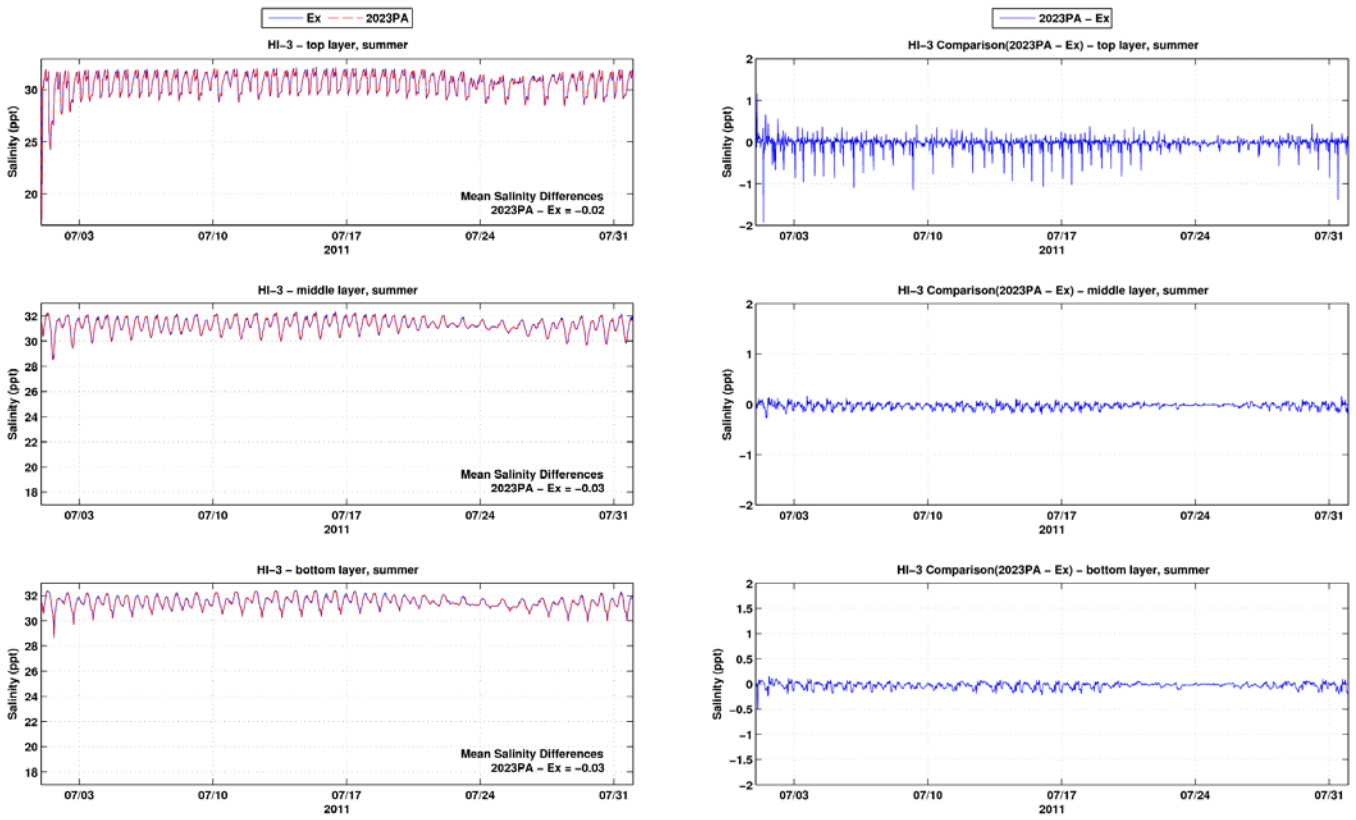

Figure A-26: Salinity time series and differences between the Existing Conditions and the 2023 PA at HI-3 during summer period

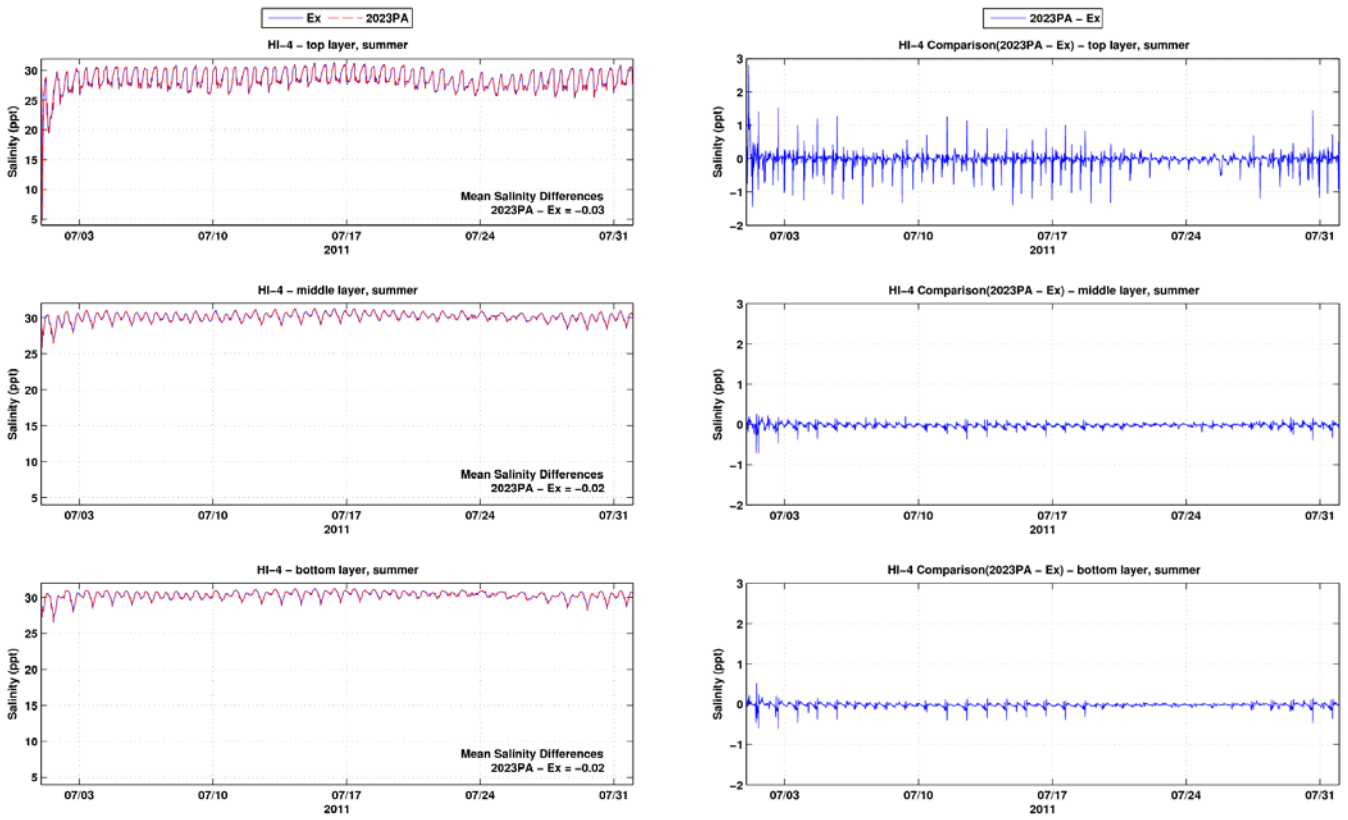

Figure A-27: Salinity time series and differences between the Existing Conditions and the 2023 PA at HI-4 during summer period

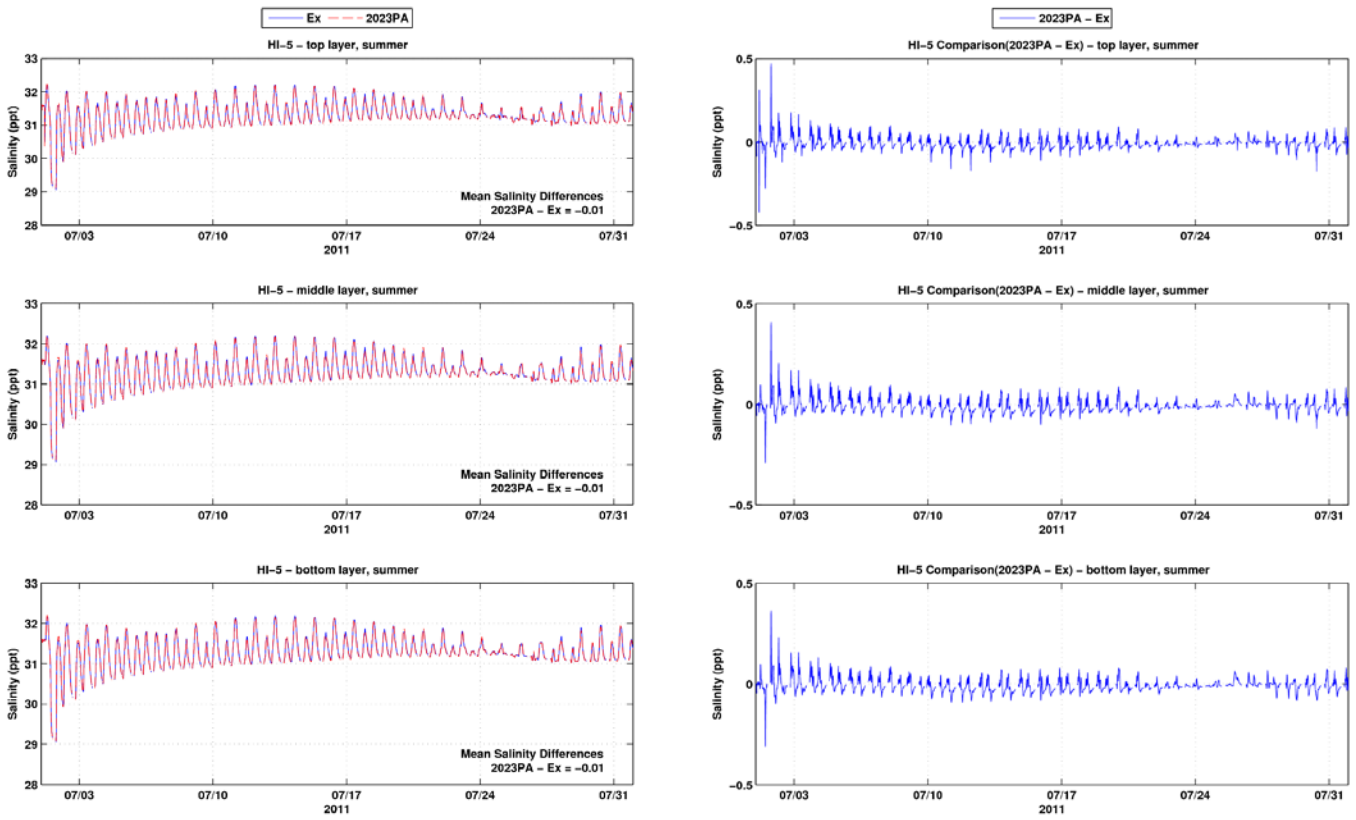

Figure A-28: Salinity time series and differences between the Existing Conditions and the 2023 PA at HI-5 during summer period

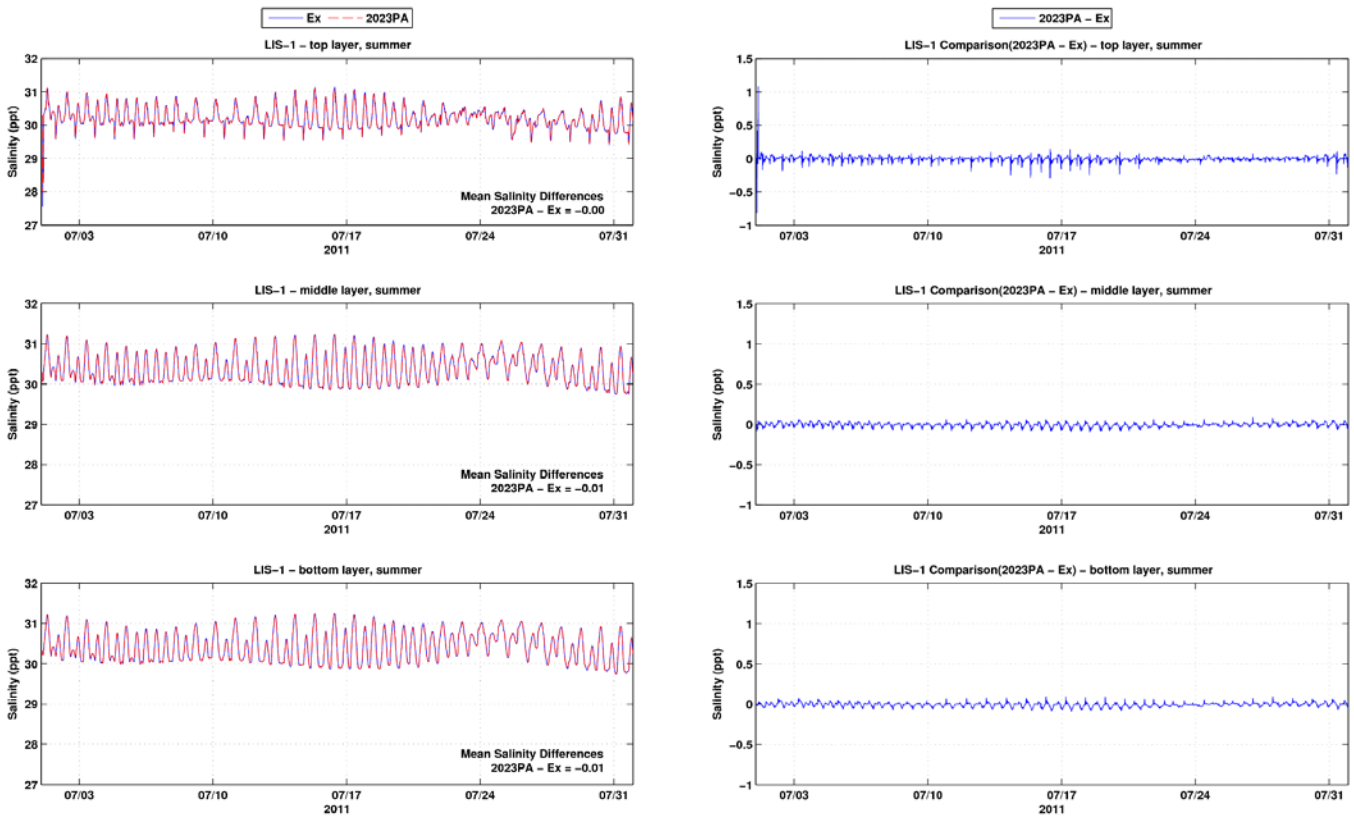

Figure A-29: Salinity time series and differences between the Existing Conditions and the 2023 PA at LIS-1 during summer period

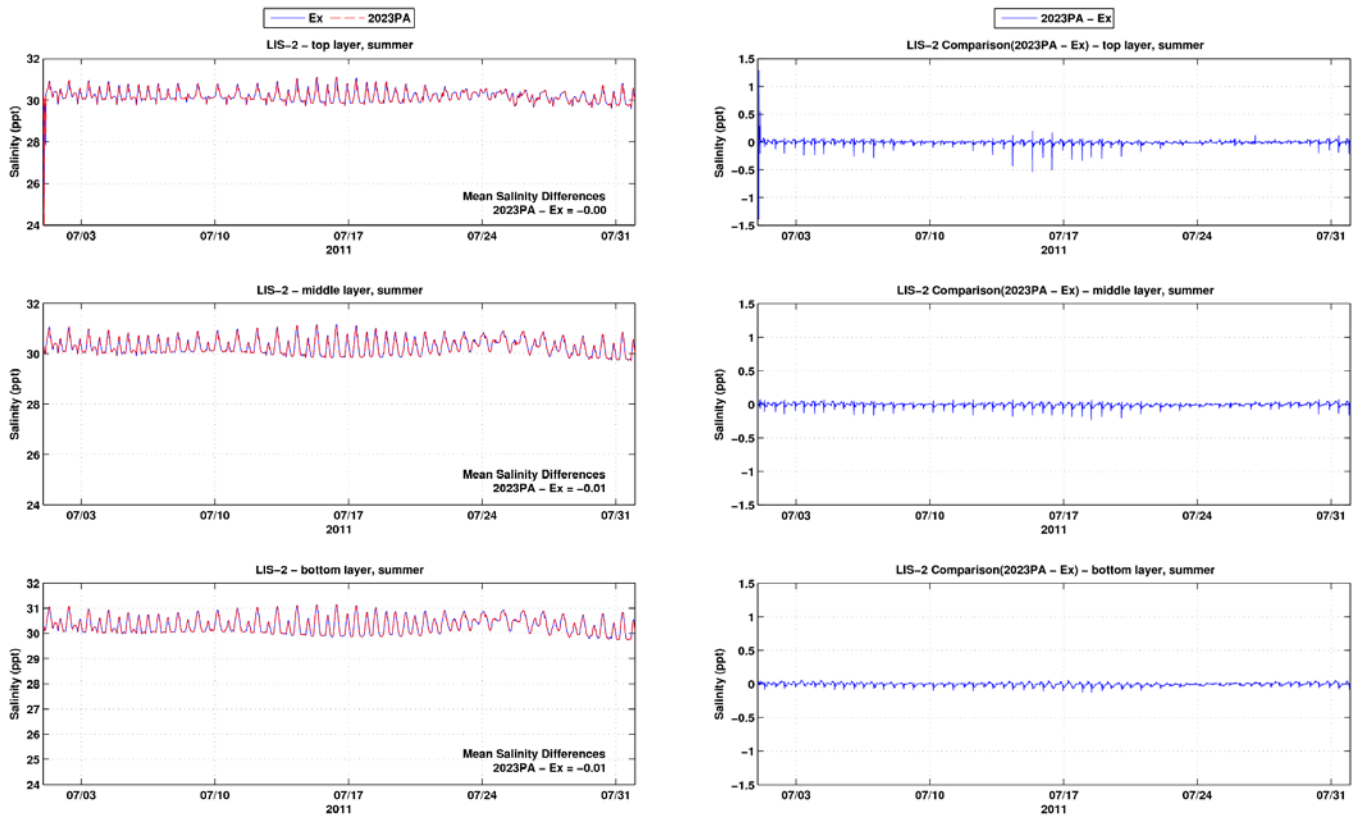

Figure A-30: Salinity time series and differences between the Existing Conditions and the 2023 PA at LIS-2 during summer period

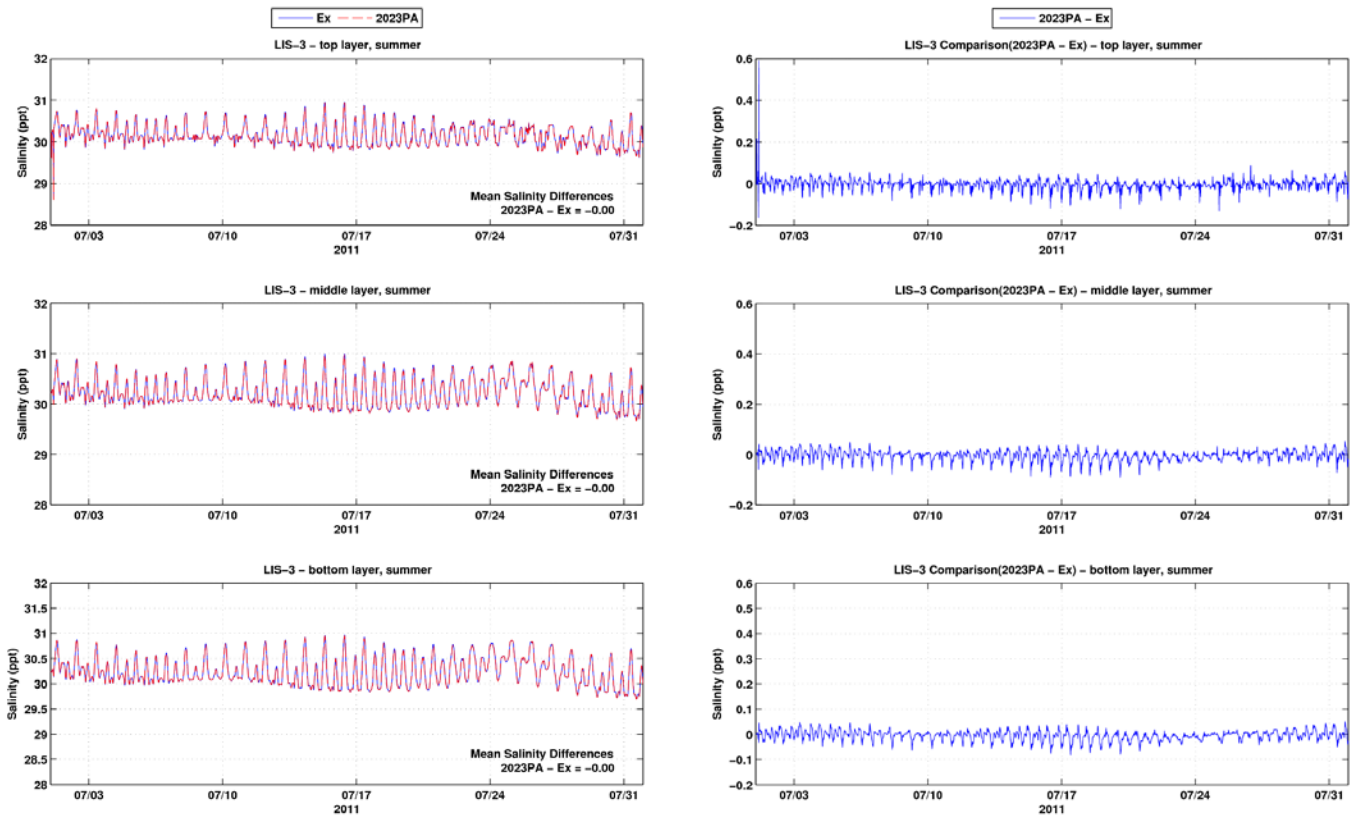

Figure A-31: Salinity time series and differences between the Existing Conditions and the 2023 PA at LIS-3 during summer period

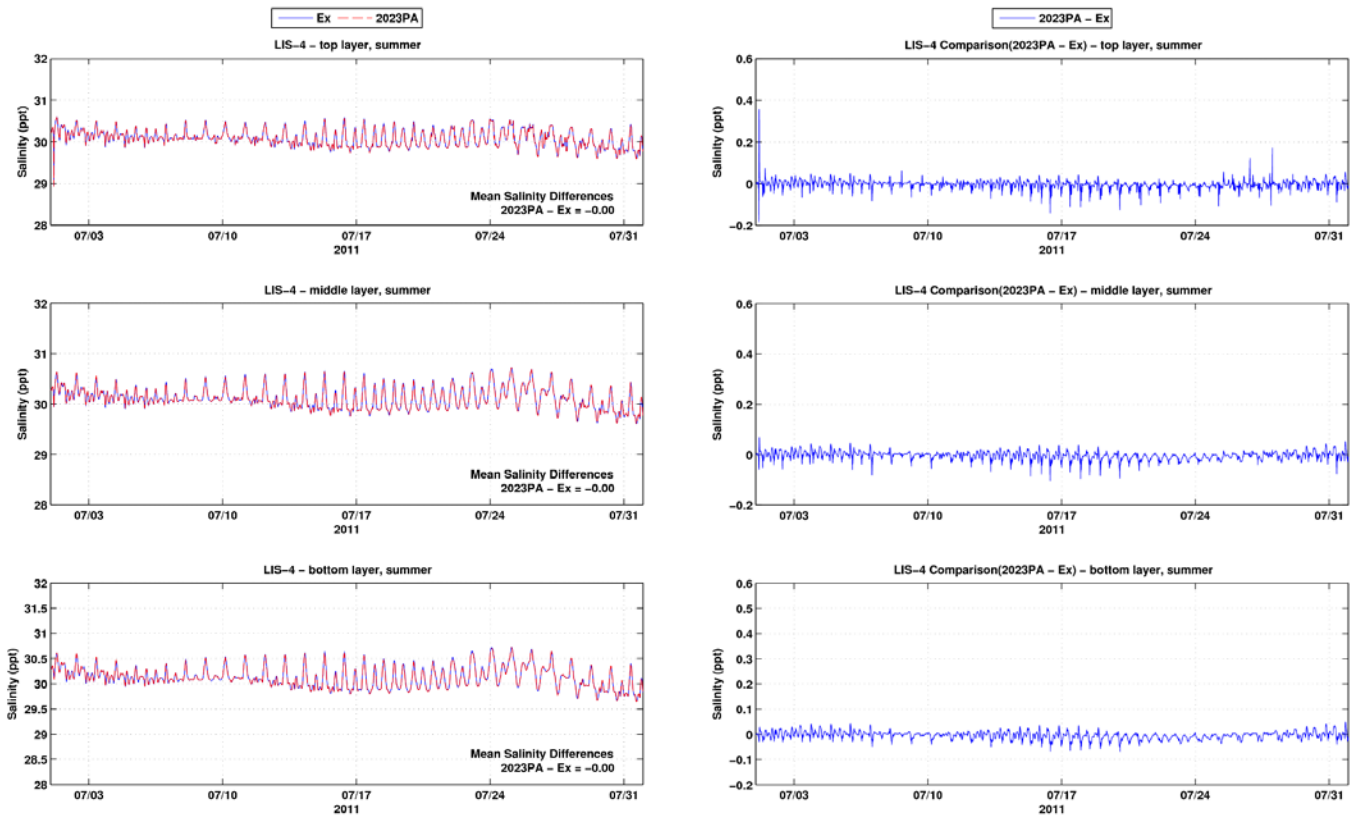

Figure A-32: Salinity time series and differences between the Existing Conditions and the 2023 PA at LIS-4 during summer period

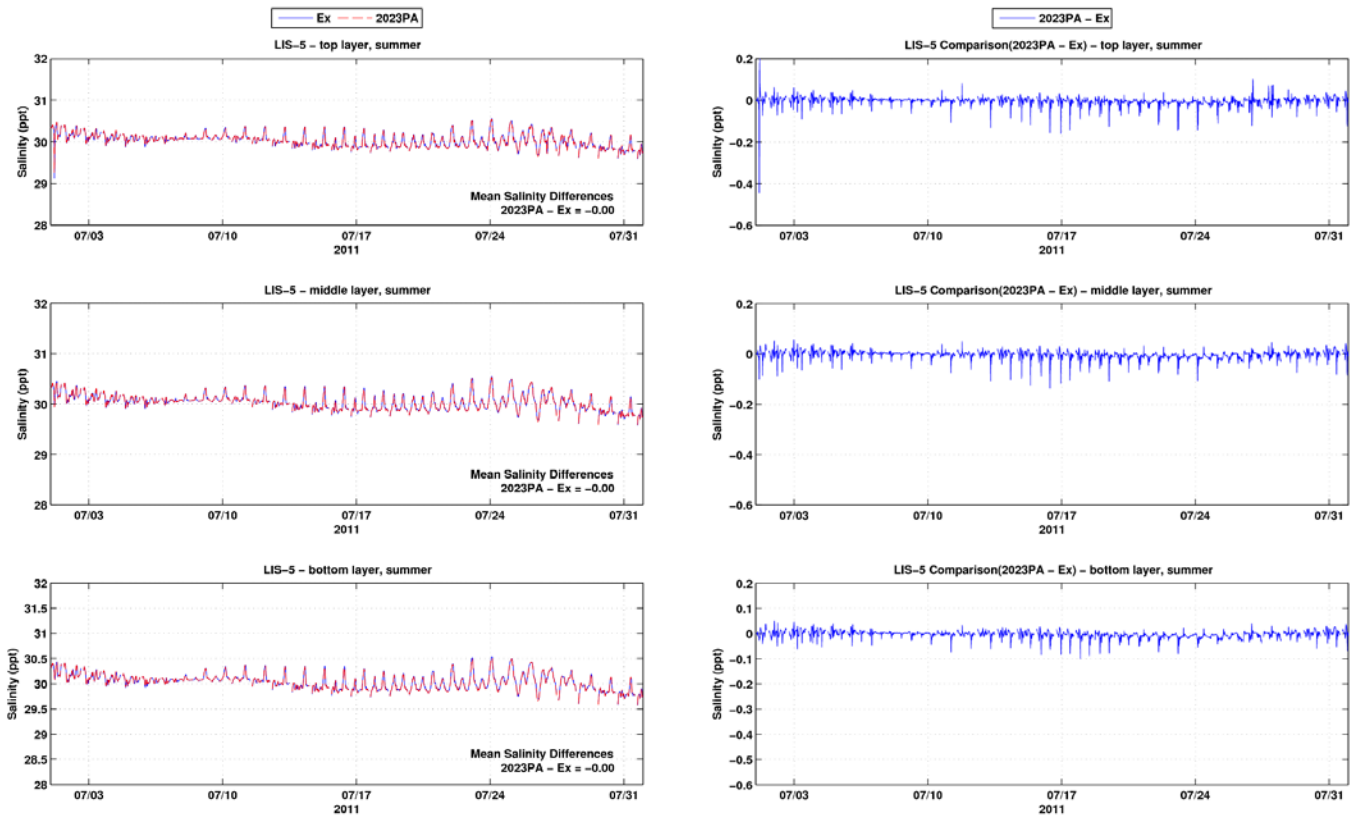

Figure A-33: Salinity time series and differences between the Existing Conditions and the 2023 PA at LIS-5 during summer period

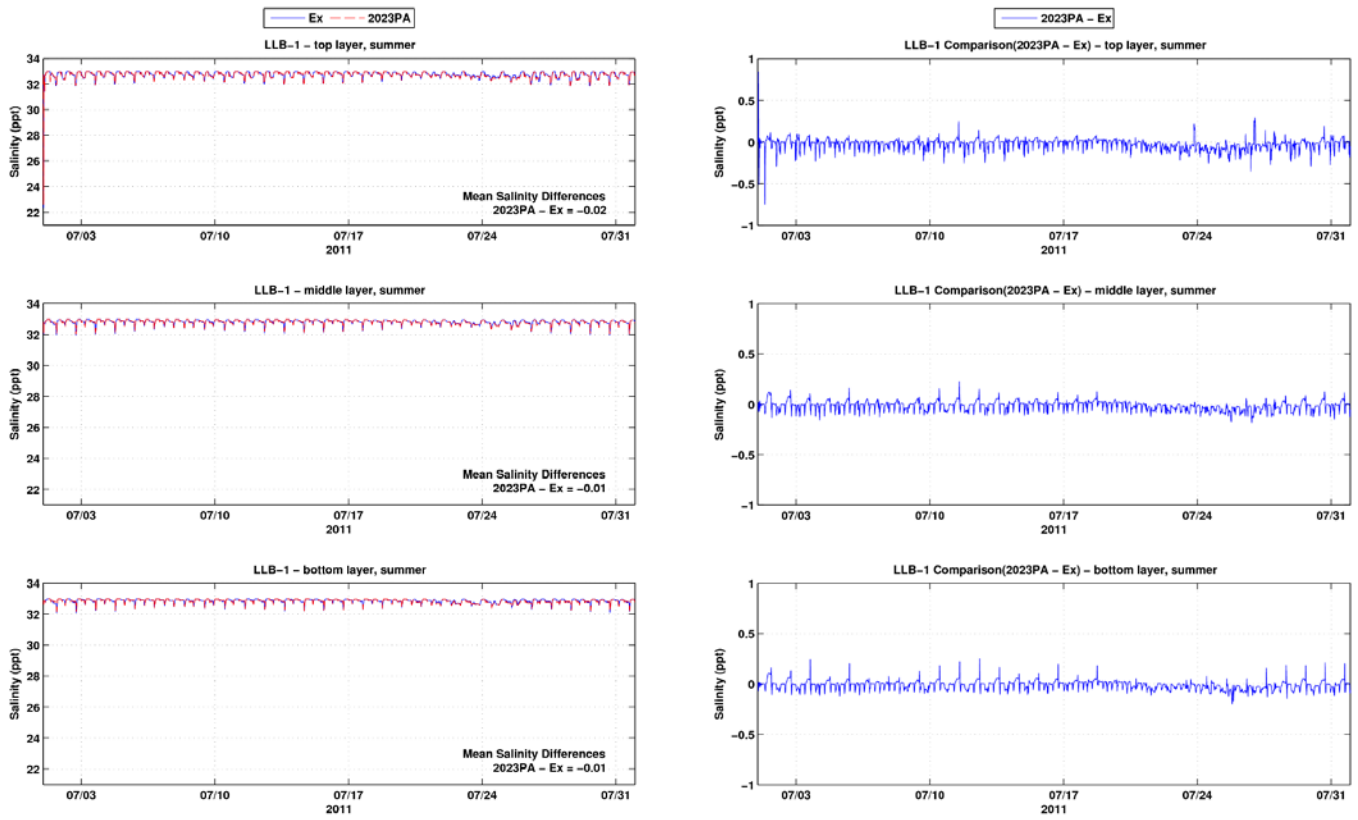

Figure A-34: Salinity time series and differences between the Existing Conditions and the 2023 PA at LLB-1 during summer period

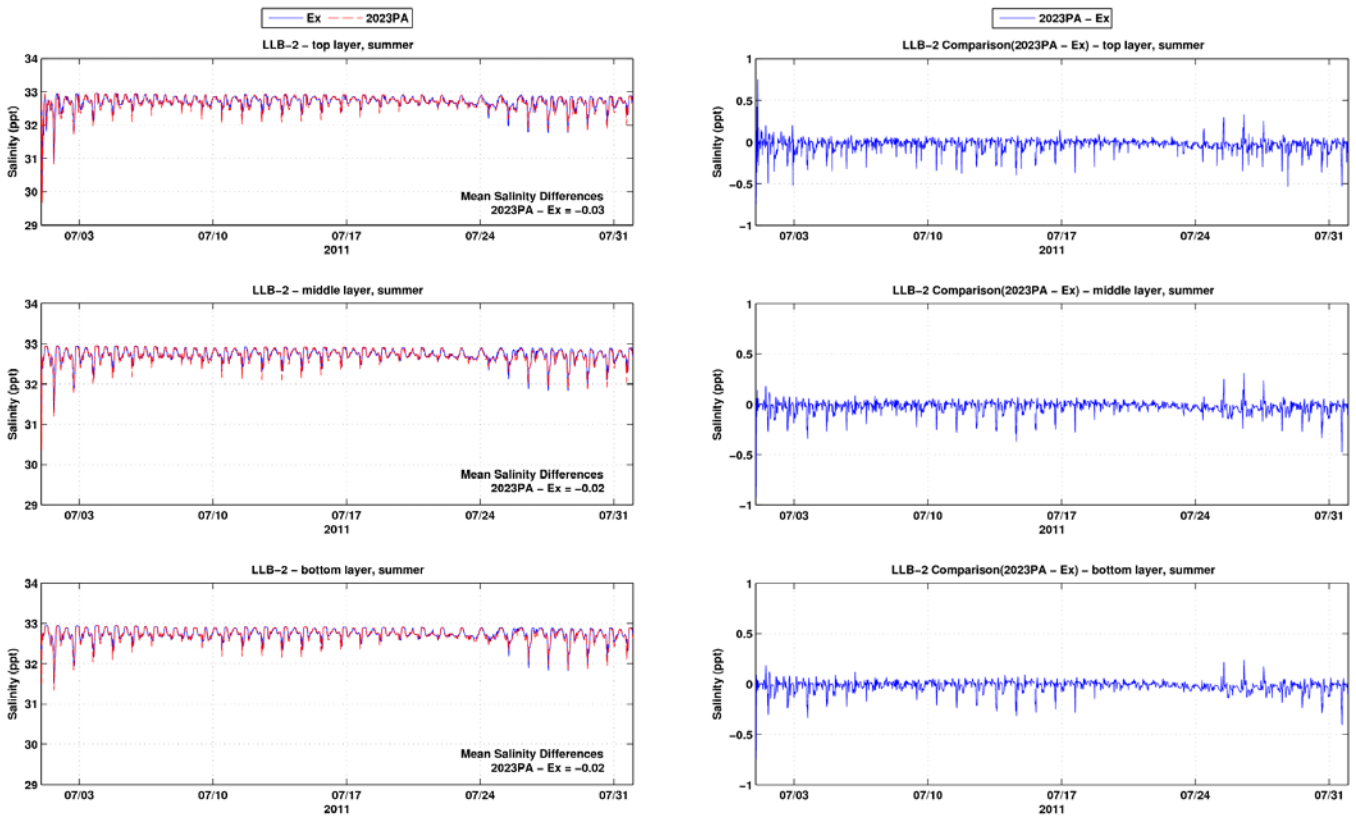

Figure A-35: Salinity time series and differences between the Existing Conditions and the 2023 PA at LLB-2 during summer period

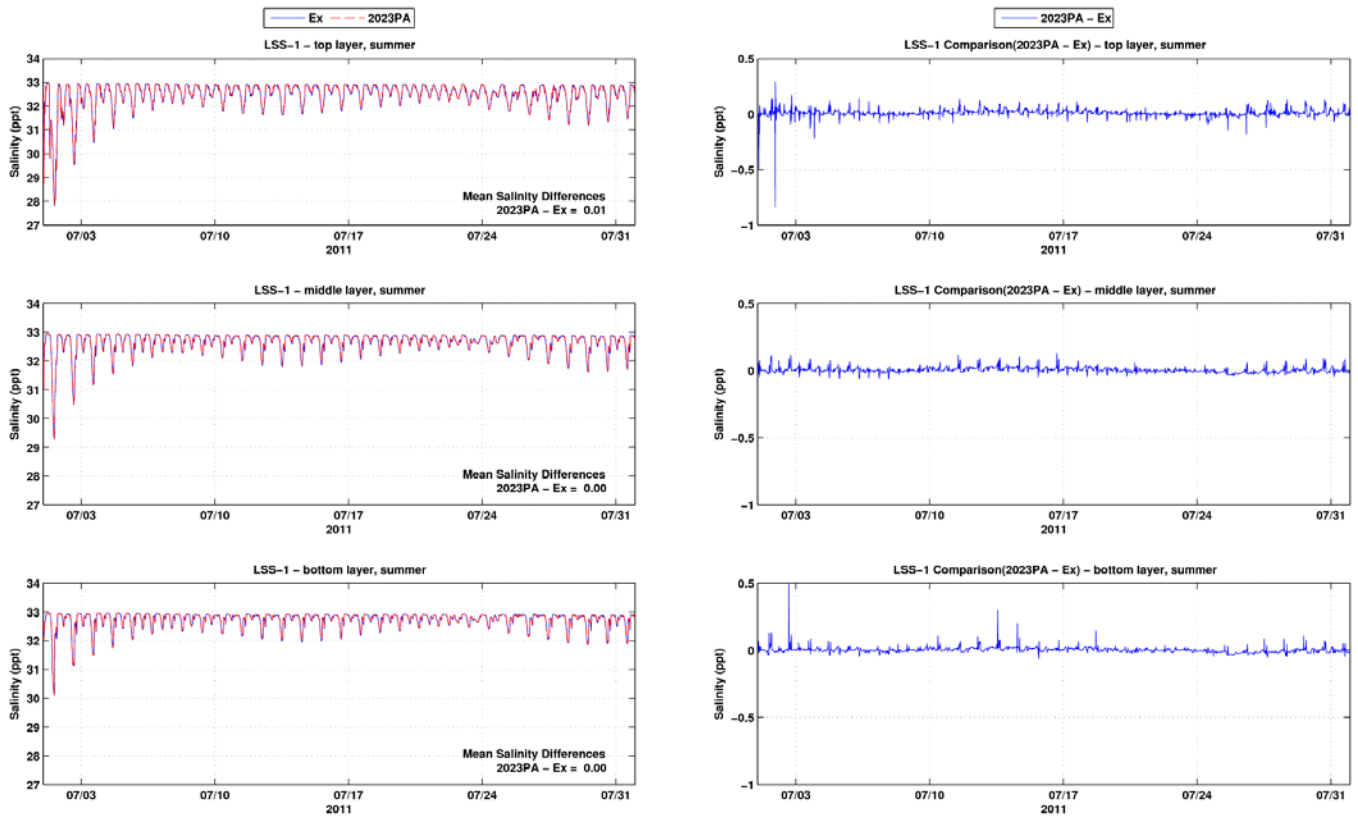

Figure A-36: Salinity time series and differences between the Existing Conditions and the 2023 PA at LSS-1 during summer period

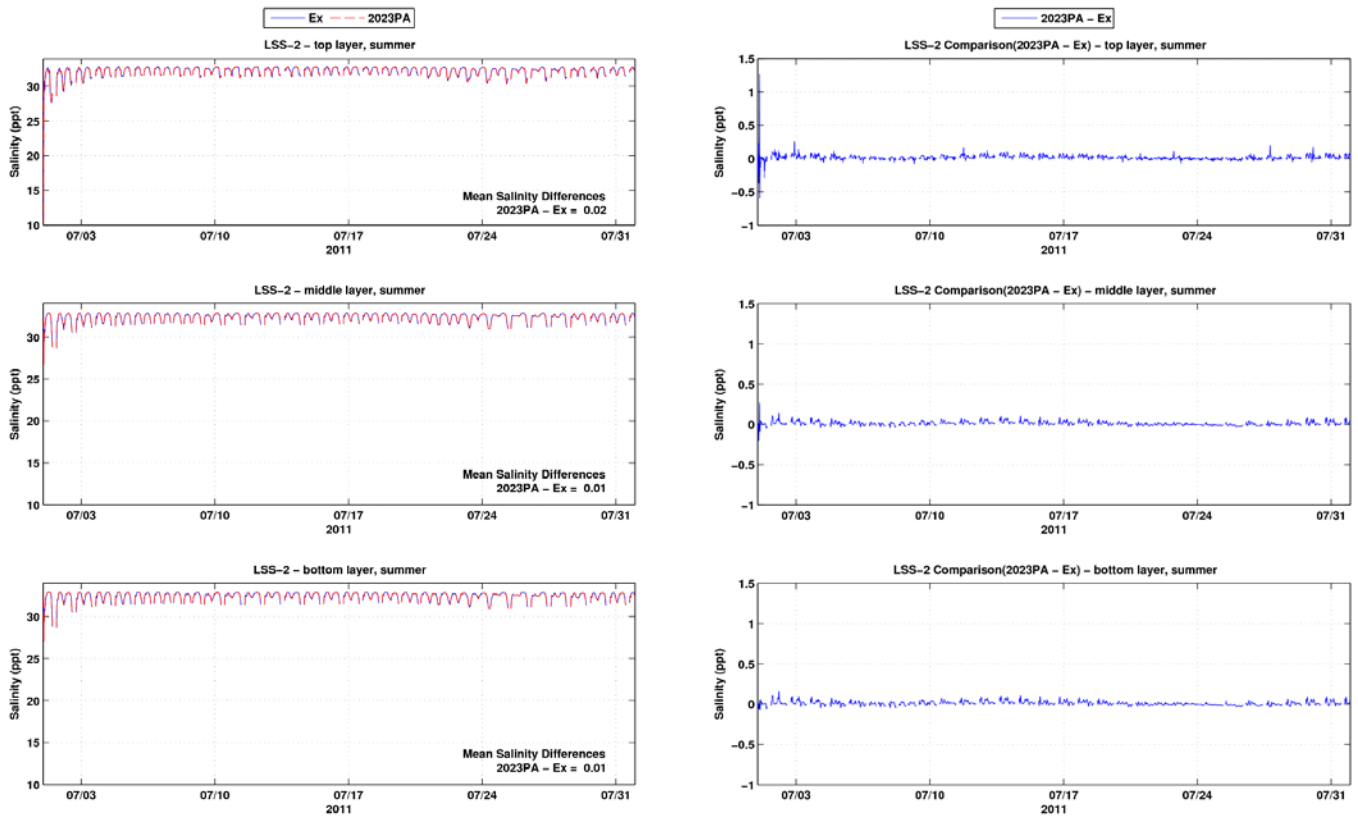

Figure A-37: Salinity time series and differences between the Existing Conditions and the 2023 PA at LSS-2 during summer period

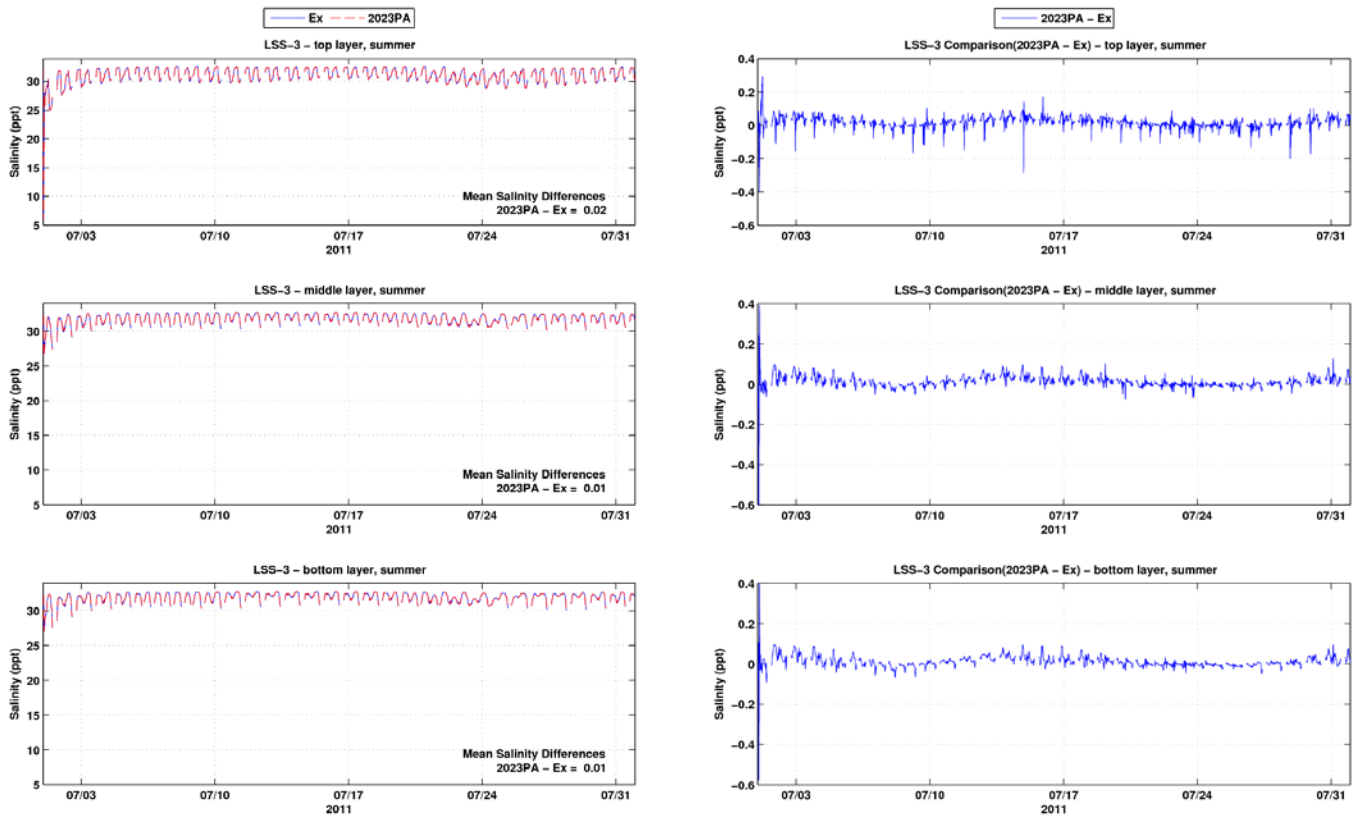

Figure A-38: Salinity time series and differences between the Existing Conditions and the 2023 PA at LSS-3 during summer period

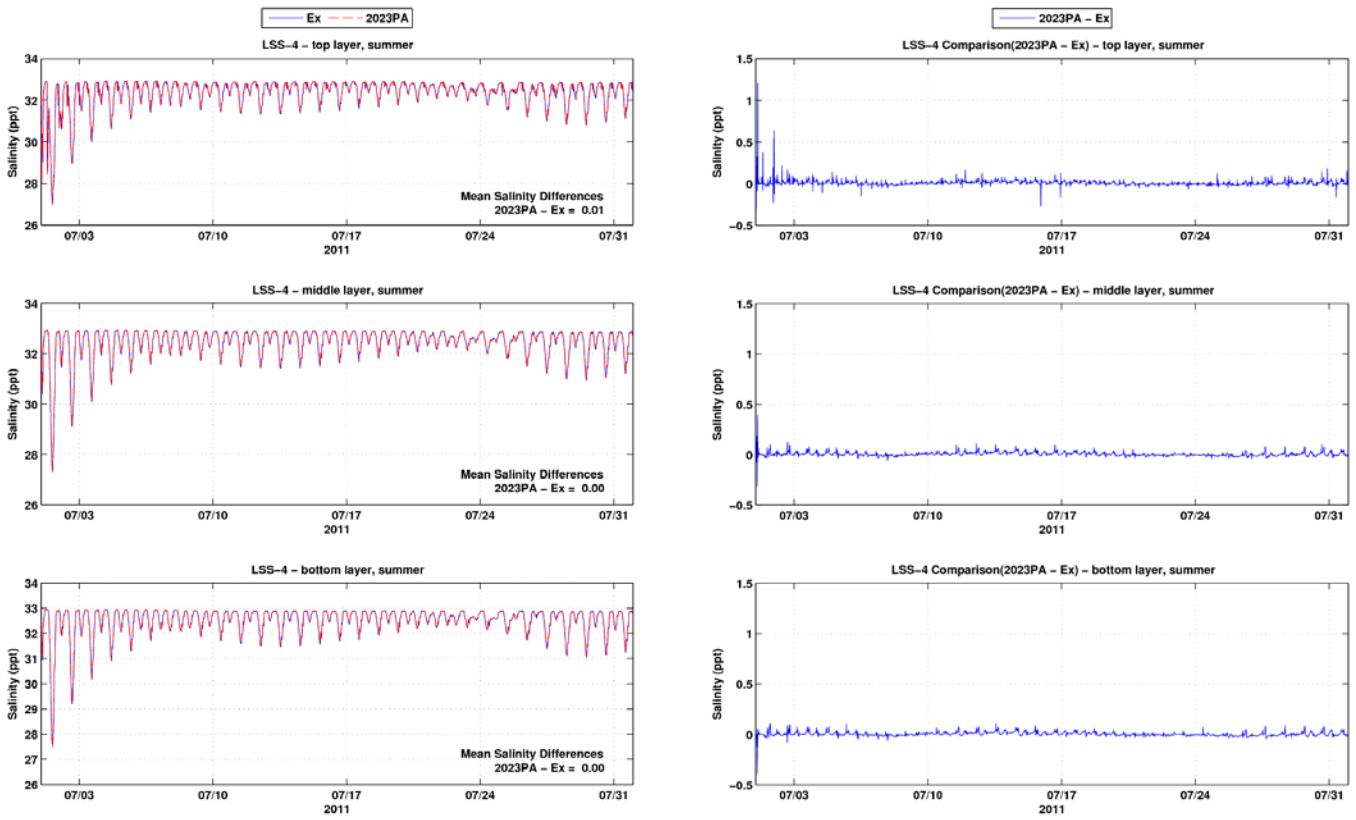

Figure A-39: Salinity time series and differences between the Existing Conditions and the 2023 PA at LSS-4 during summer period

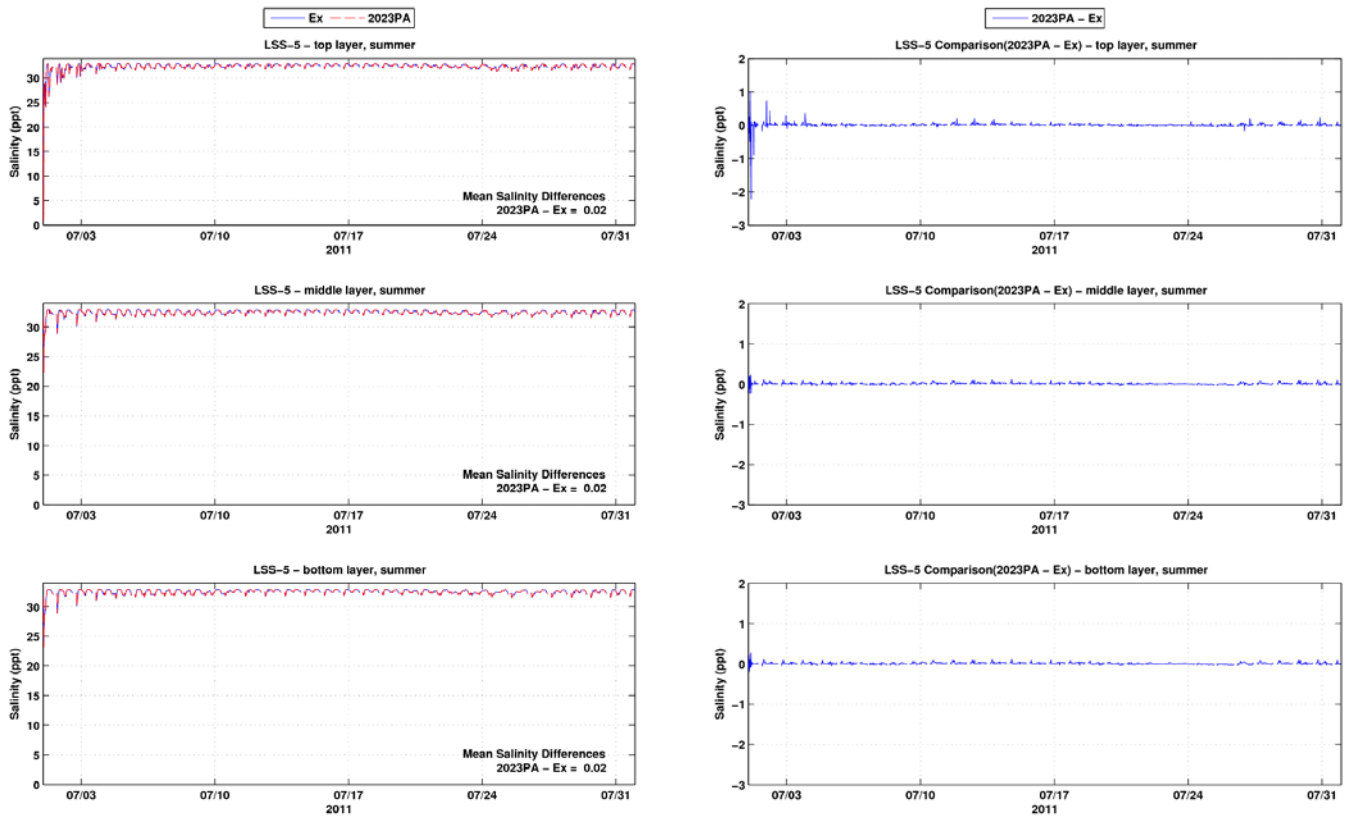

Figure A-40: Salinity time series and differences between the Existing Conditions and the 2023 PA at LSS-5 during summer period

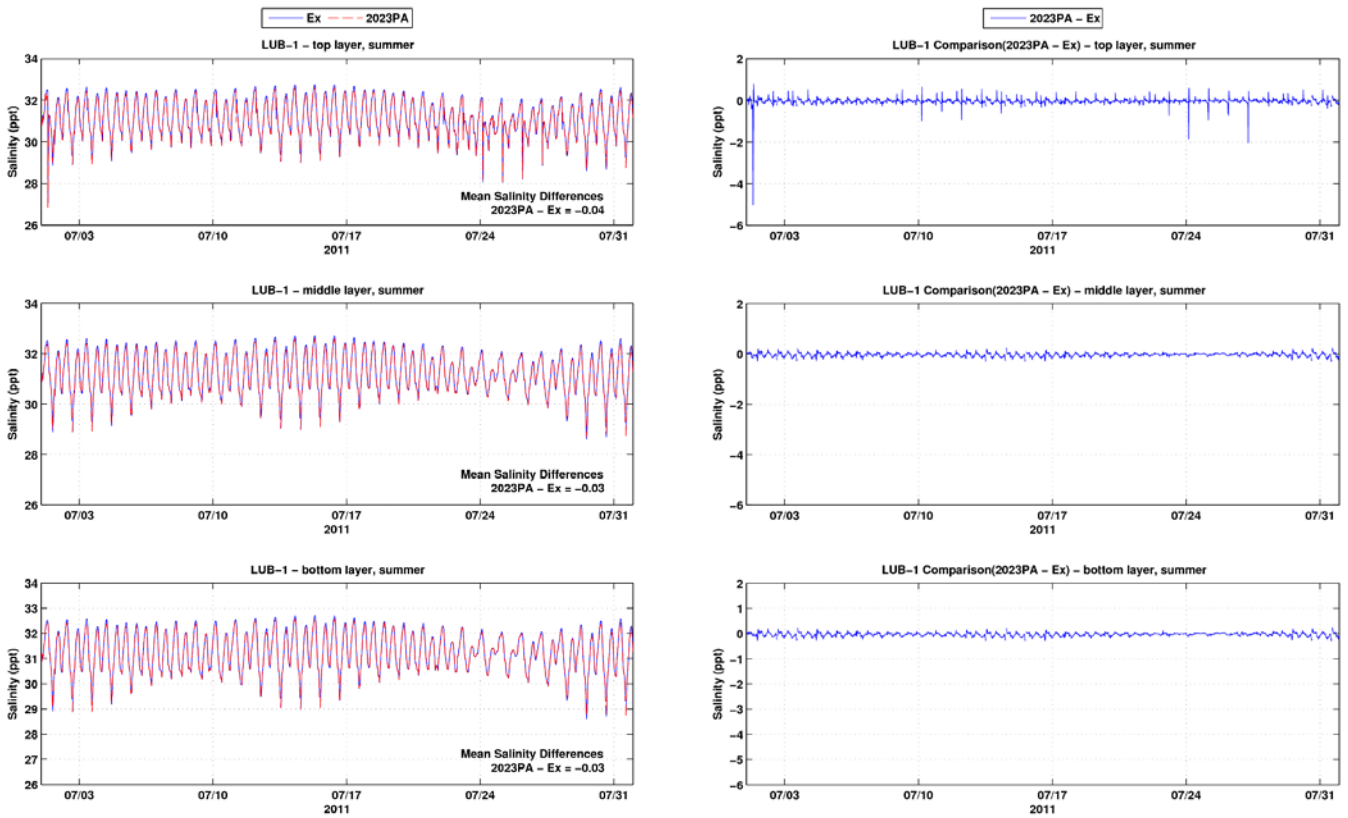

Figure A-41: Salinity time series and differences between the Existing Conditions and the 2023 PA at LUB-1 during summer period

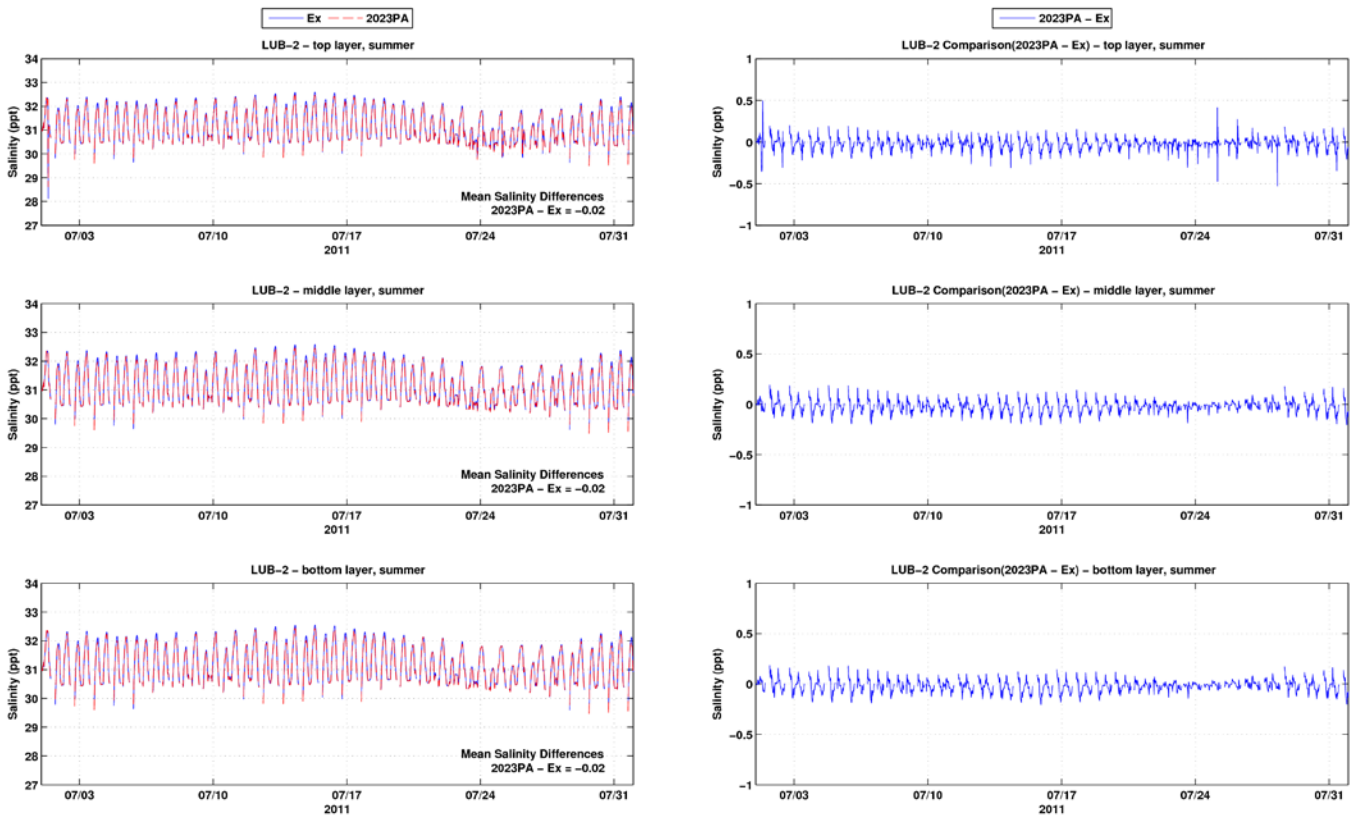

Figure A-42: Salinity time series and differences between the Existing Conditions and the 2023 PA at LUB-2 during summer period

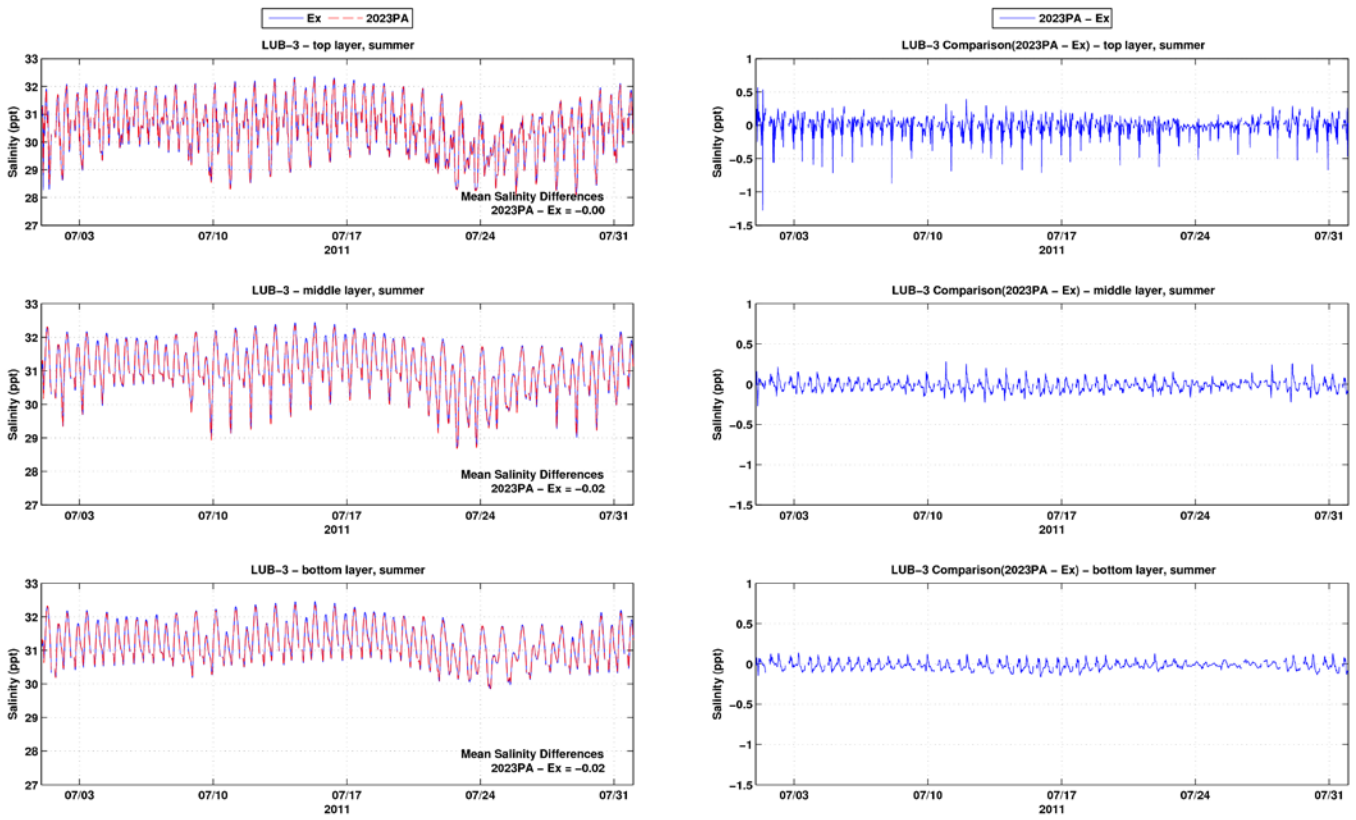

Figure A-43: Salinity time series and differences between the Existing Conditions and the 2023 PA at LUB-3 during summer period

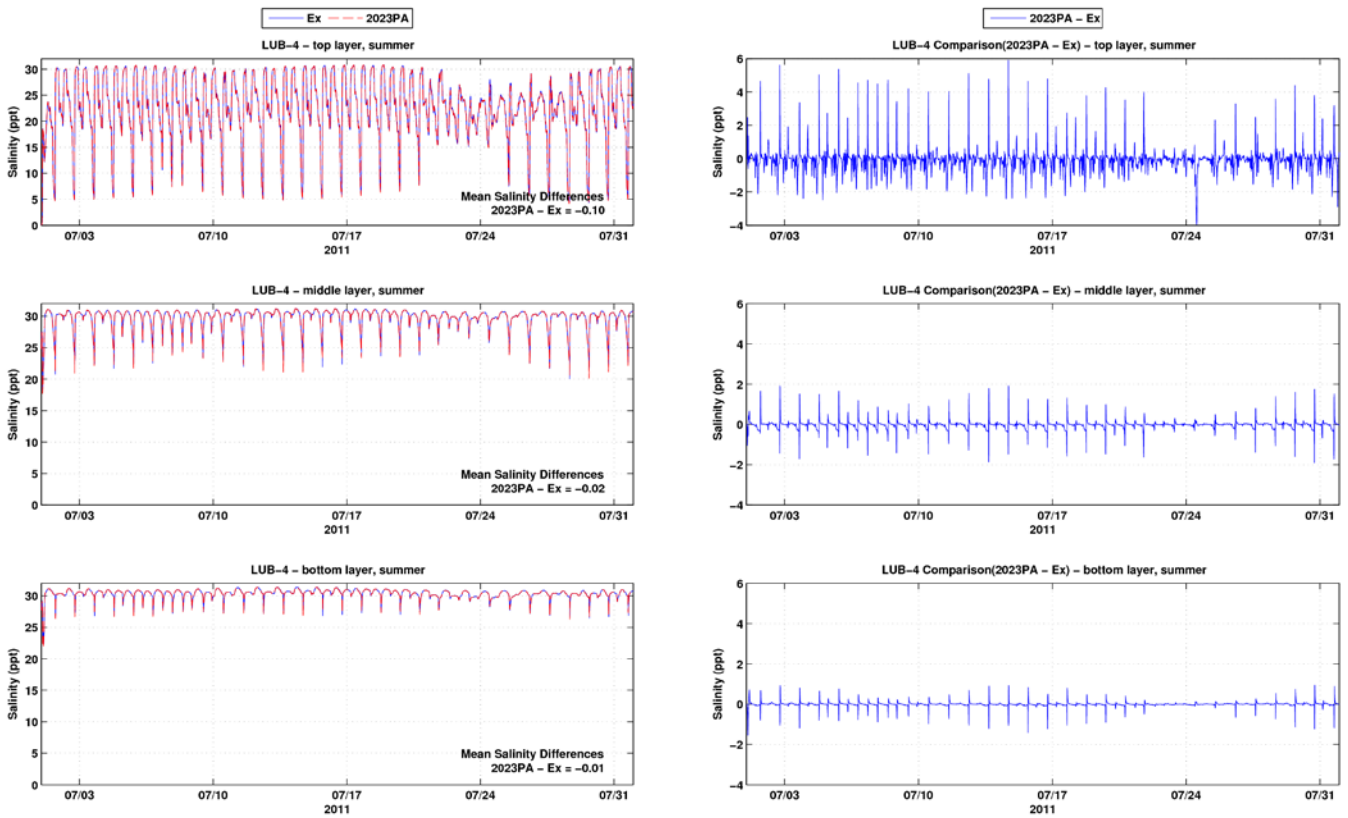

Figure A-44: Salinity time series and differences between the Existing Conditions and the 2023 PA at LUB-4 during summer period

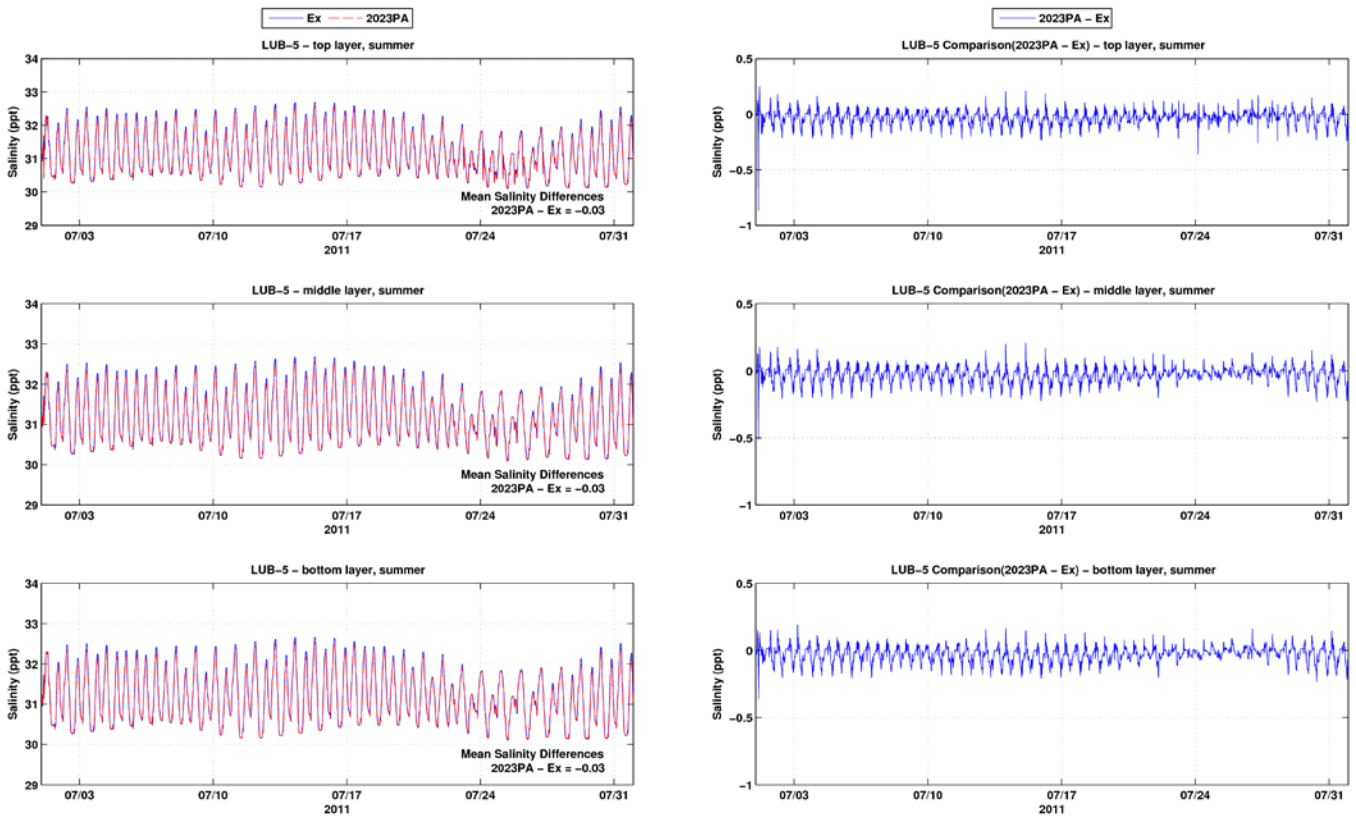

Figure A-45: Salinity time series and differences between the Existing Conditions and the 2023 PA at LUB-5 during summer period

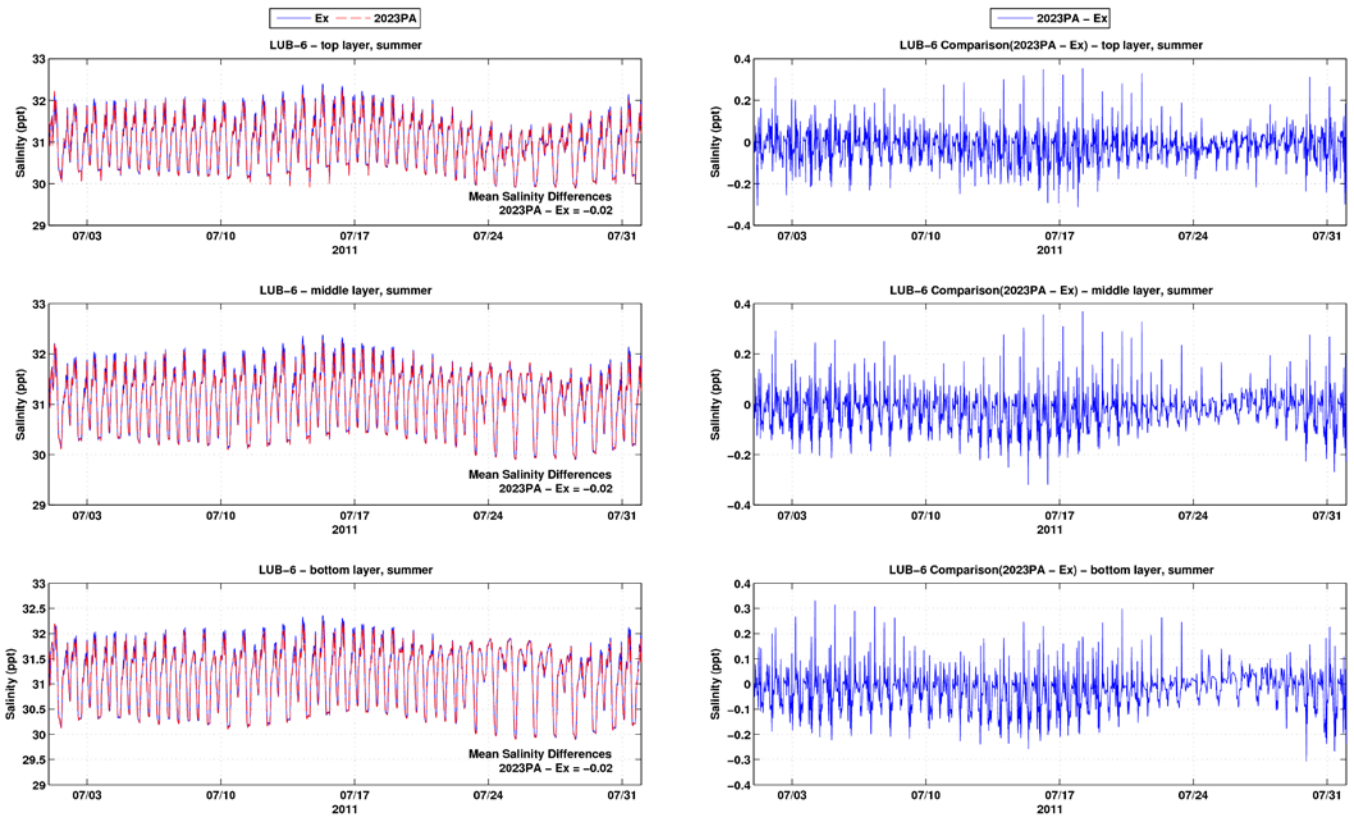

Figure A-46: Salinity time series and differences between the Existing Conditions and the 2023 PA at LUB-6 during summer period

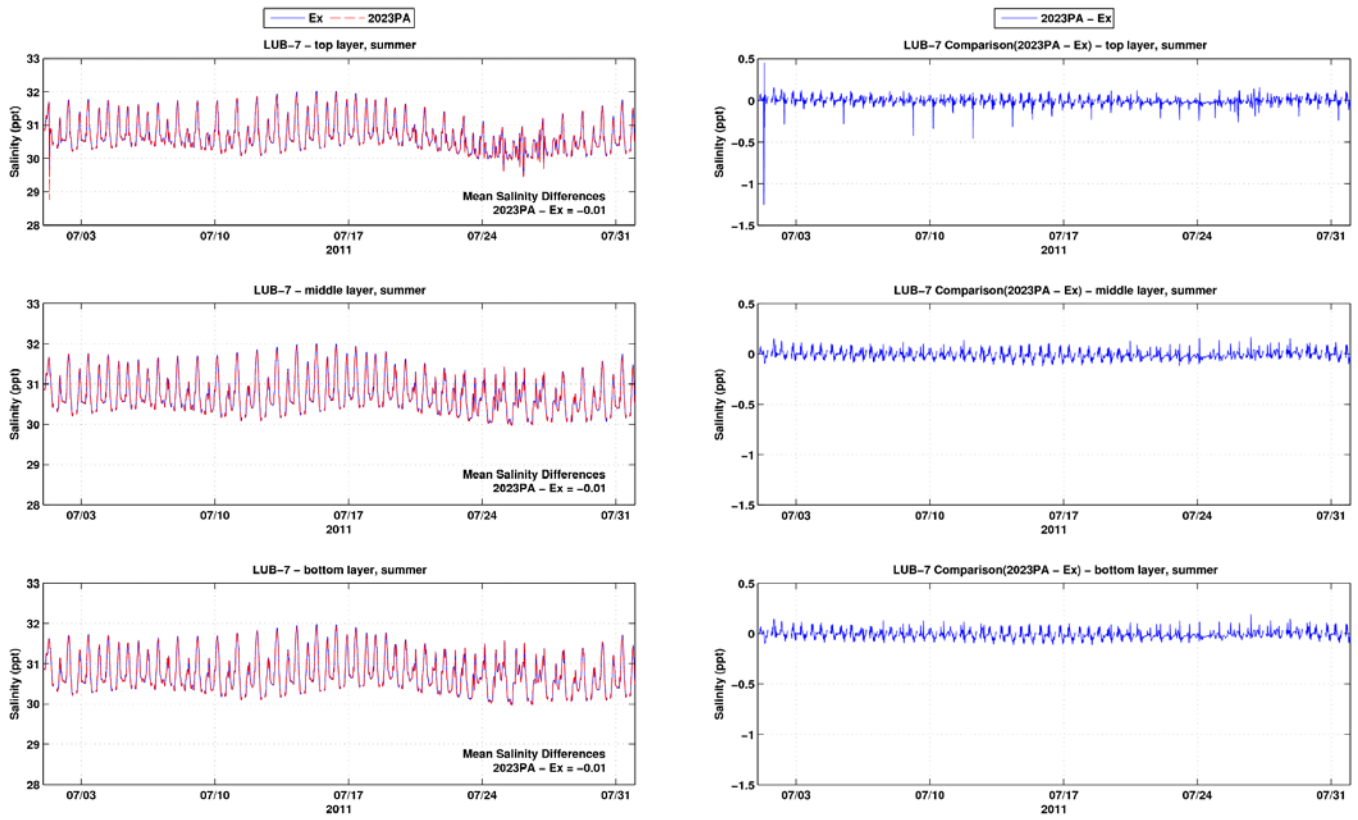

Figure A-47: Salinity time series and differences between the Existing Conditions and the 2023 PA at LUB-7 during summer period

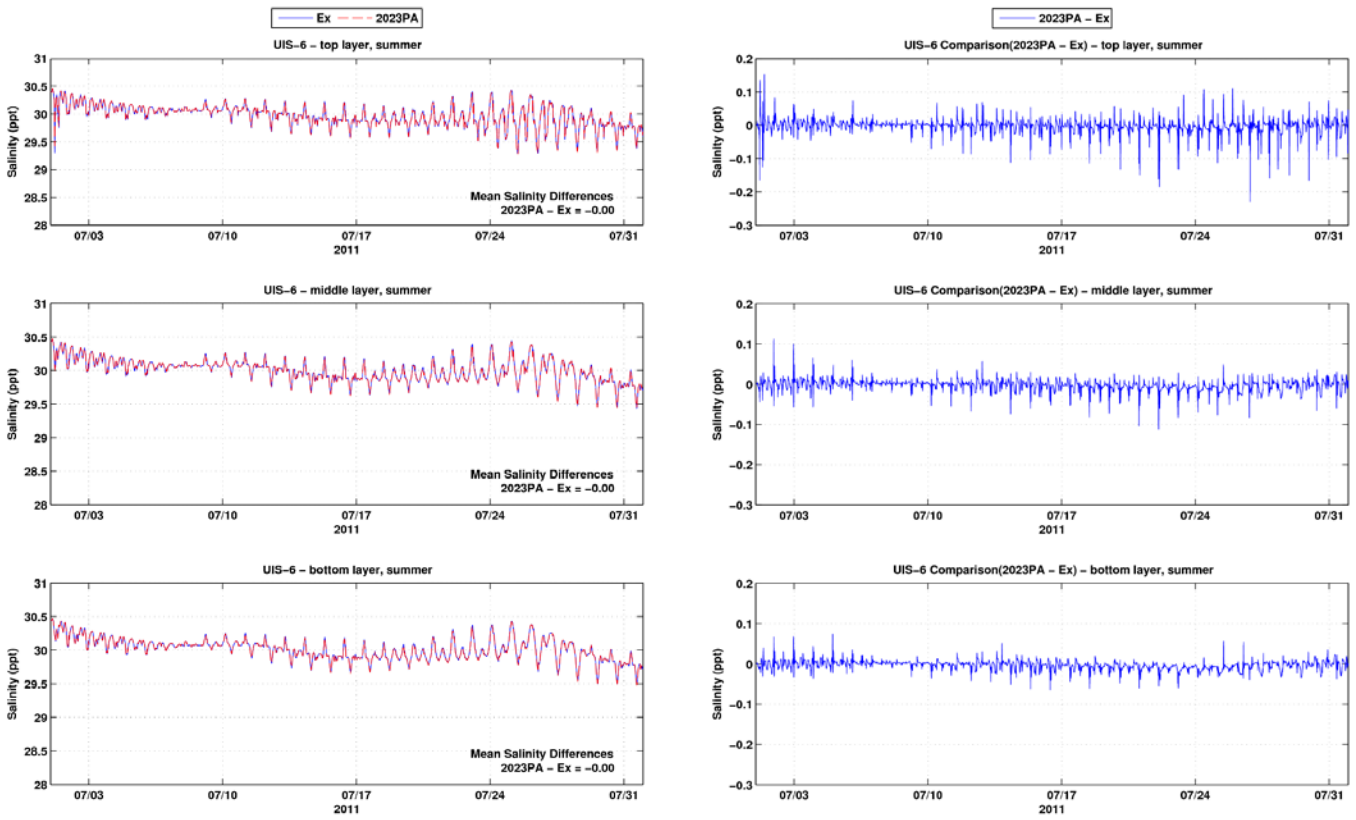

Figure A-48: Salinity time series and differences between the Existing Conditions and the 2023 PA at UIS-6 during summer period

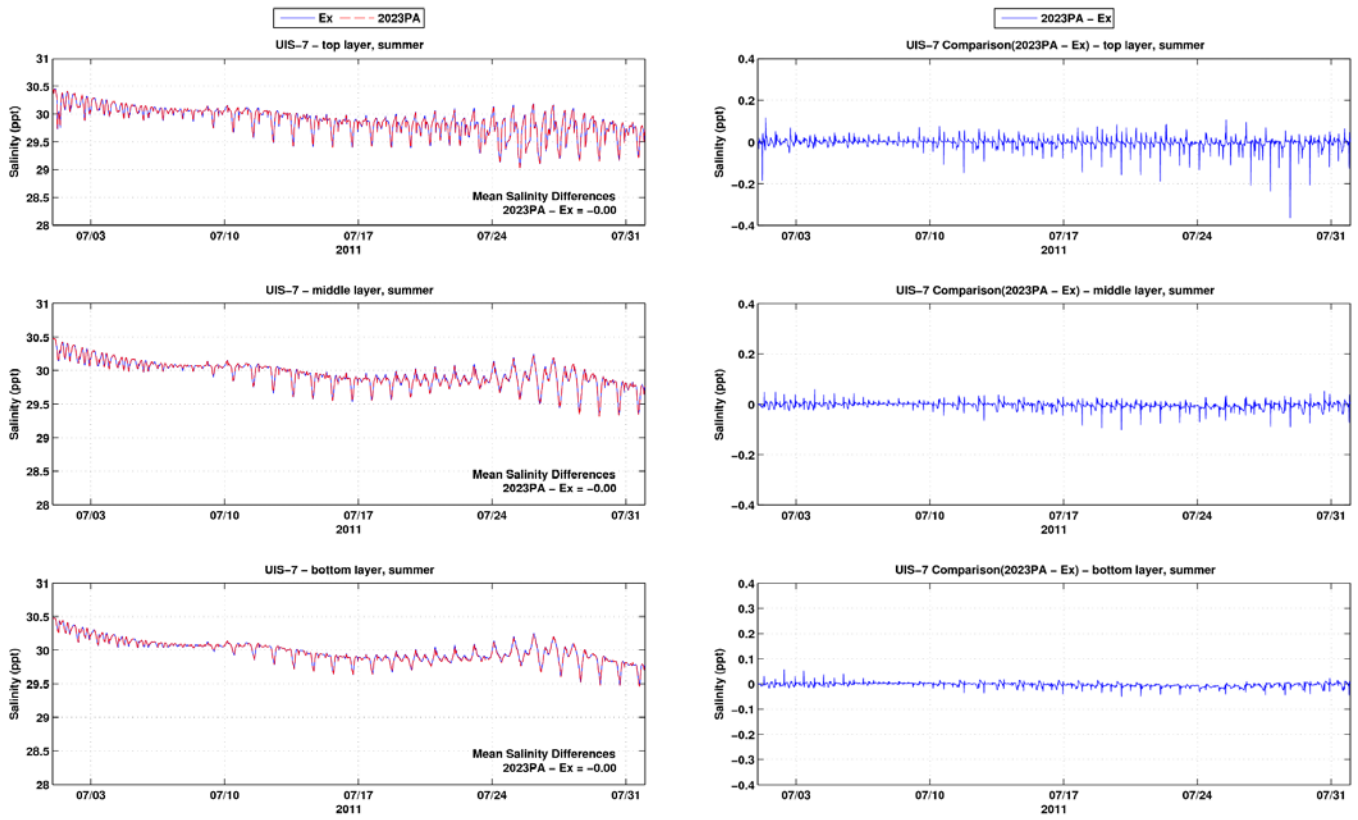

Figure A-49: Salinity time series and differences between the Existing Conditions and the 2023 PA at UIS-7 during summer period

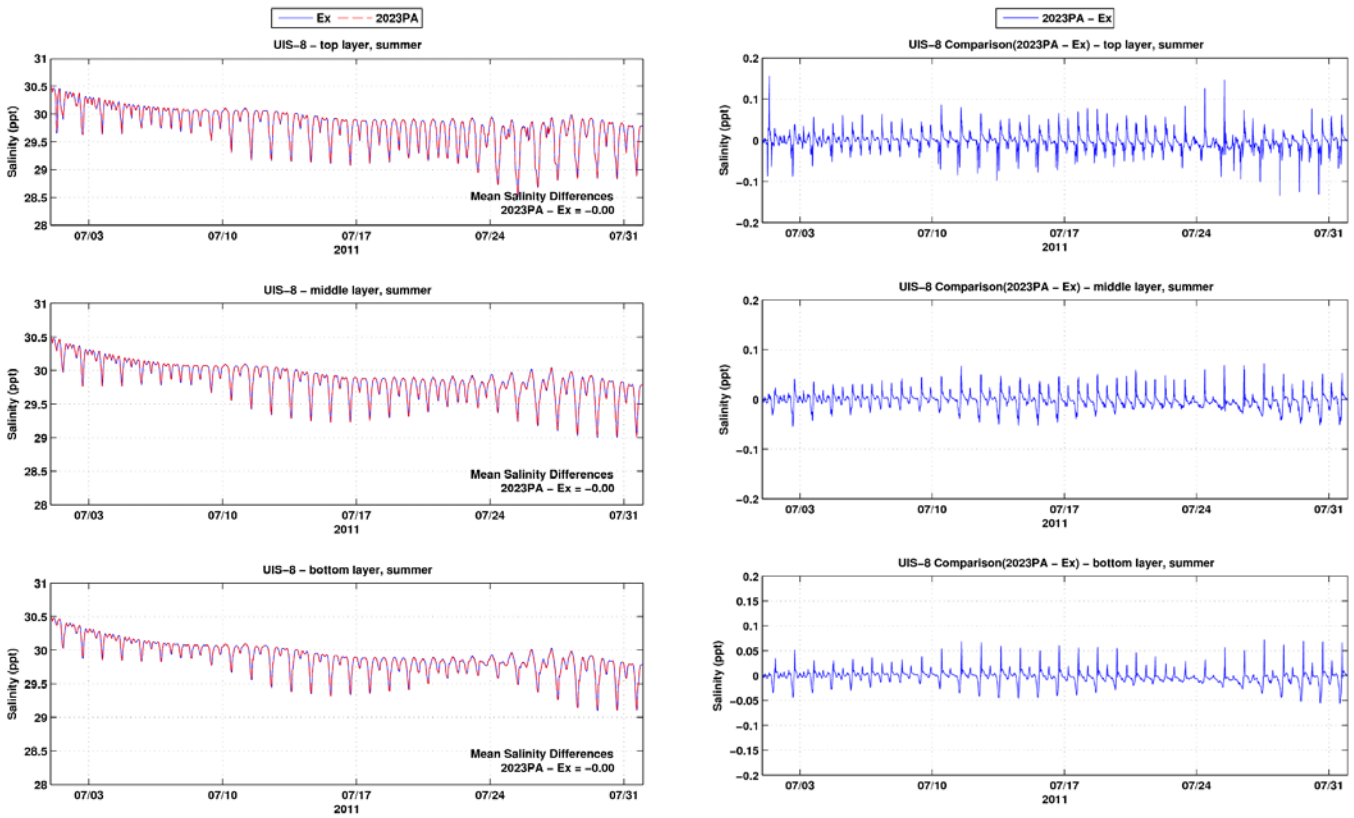

Figure A-50: Salinity time series and differences between the Existing Conditions and the 2023 PA at UIS-8 during summer period

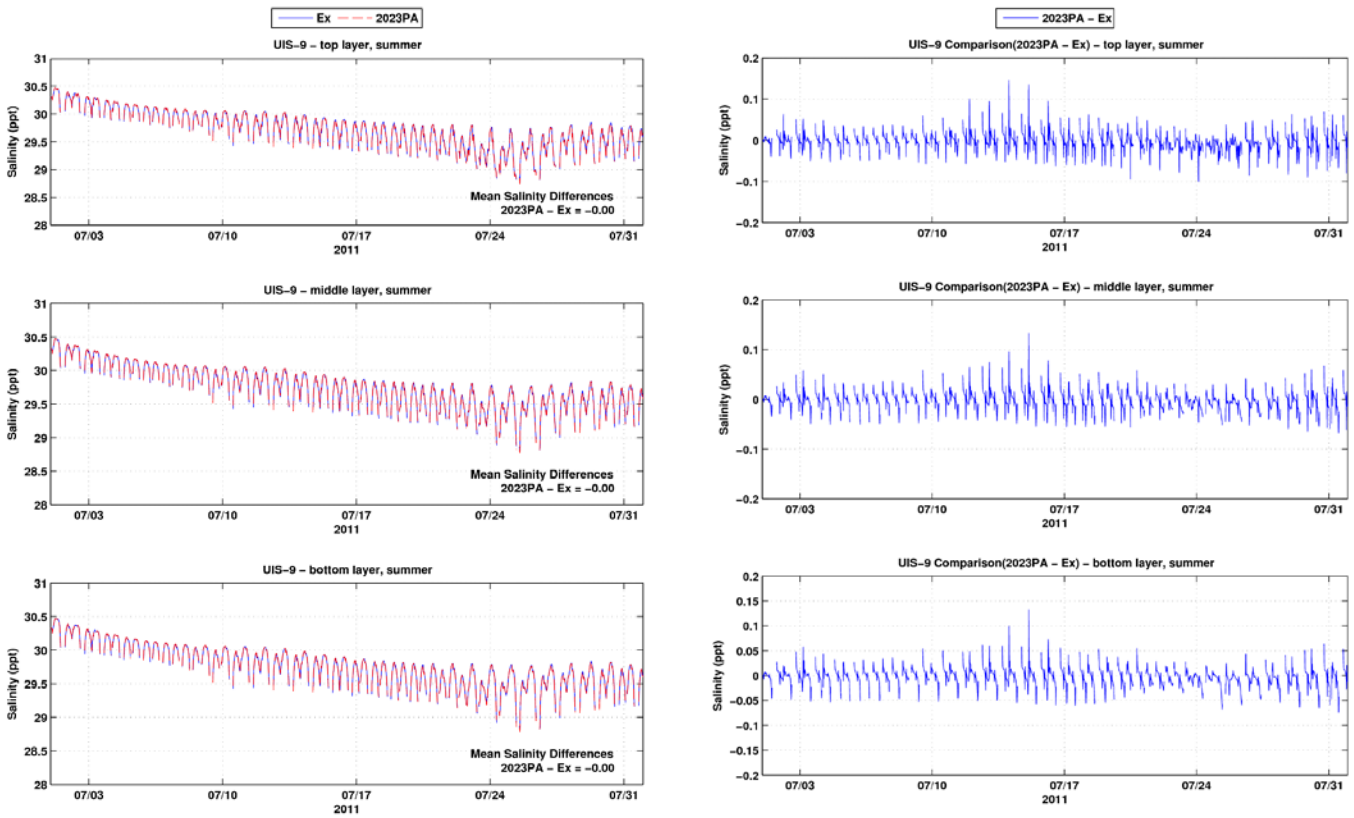

Figure A-51: Salinity time series and differences between the Existing Conditions and the 2023 PA at UIS-9 during summer period

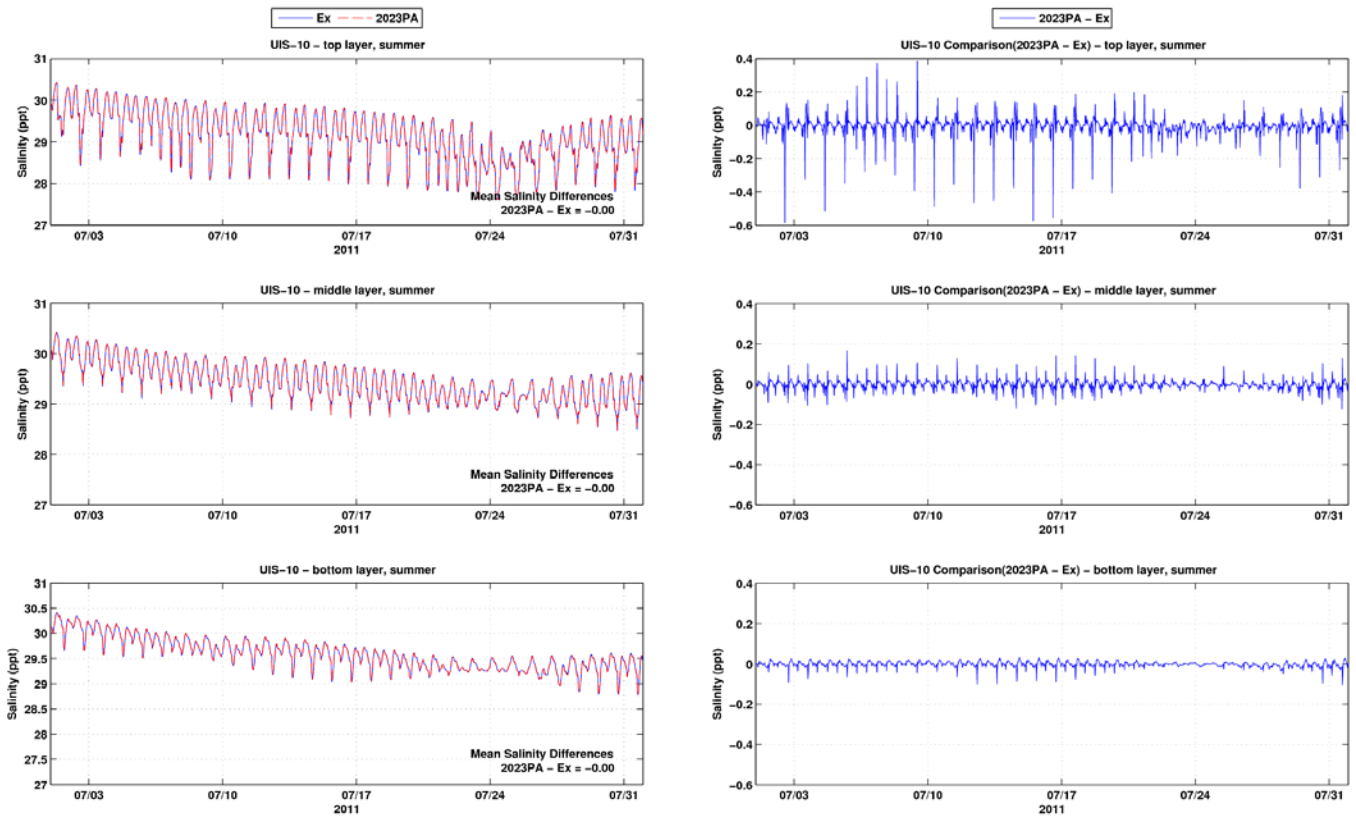

Figure A-52: Salinity time series and differences between the Existing Conditions and the 2023 PA at UIS-10 during summer period

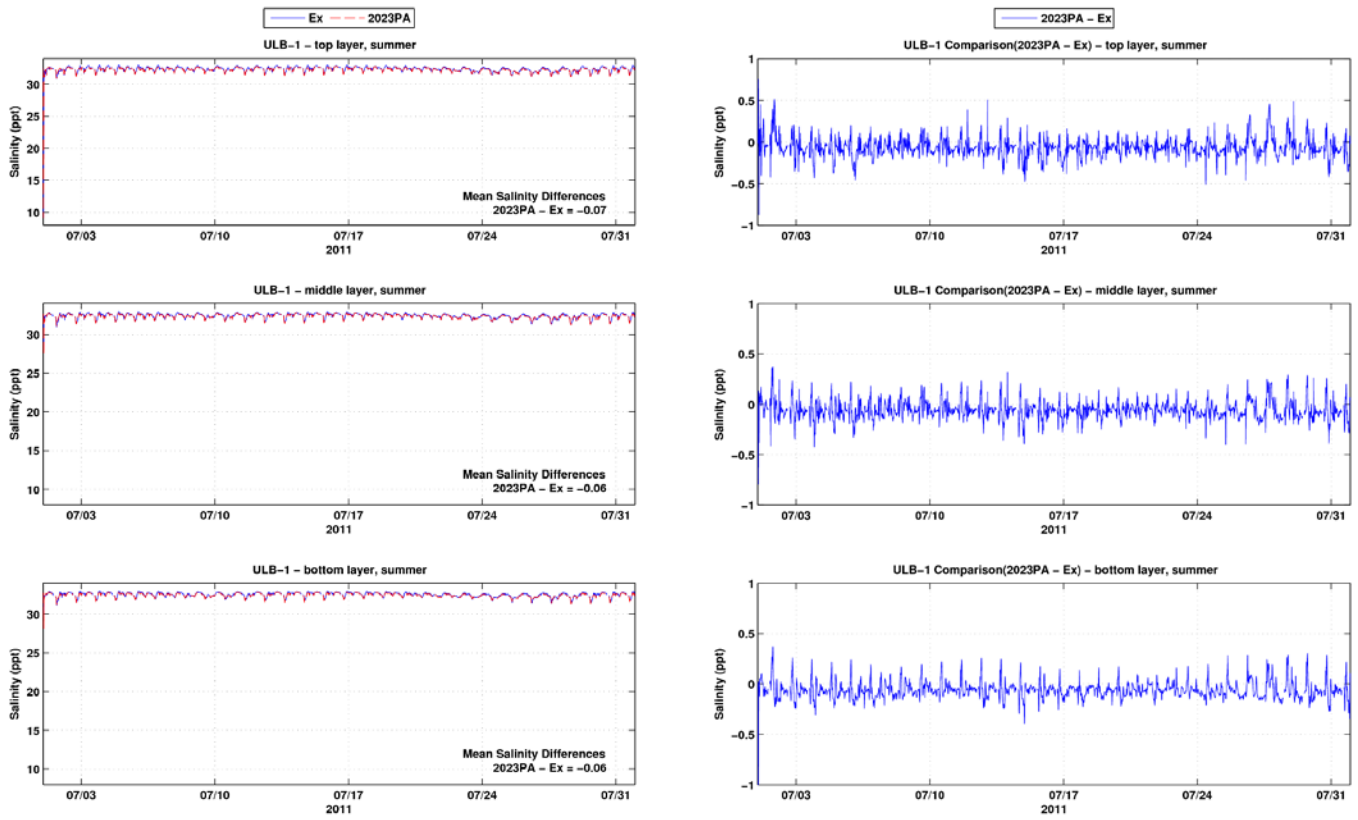

Figure A-53: Salinity time series and differences between the Existing Conditions and the 2023 PA at ULB-1 during summer period

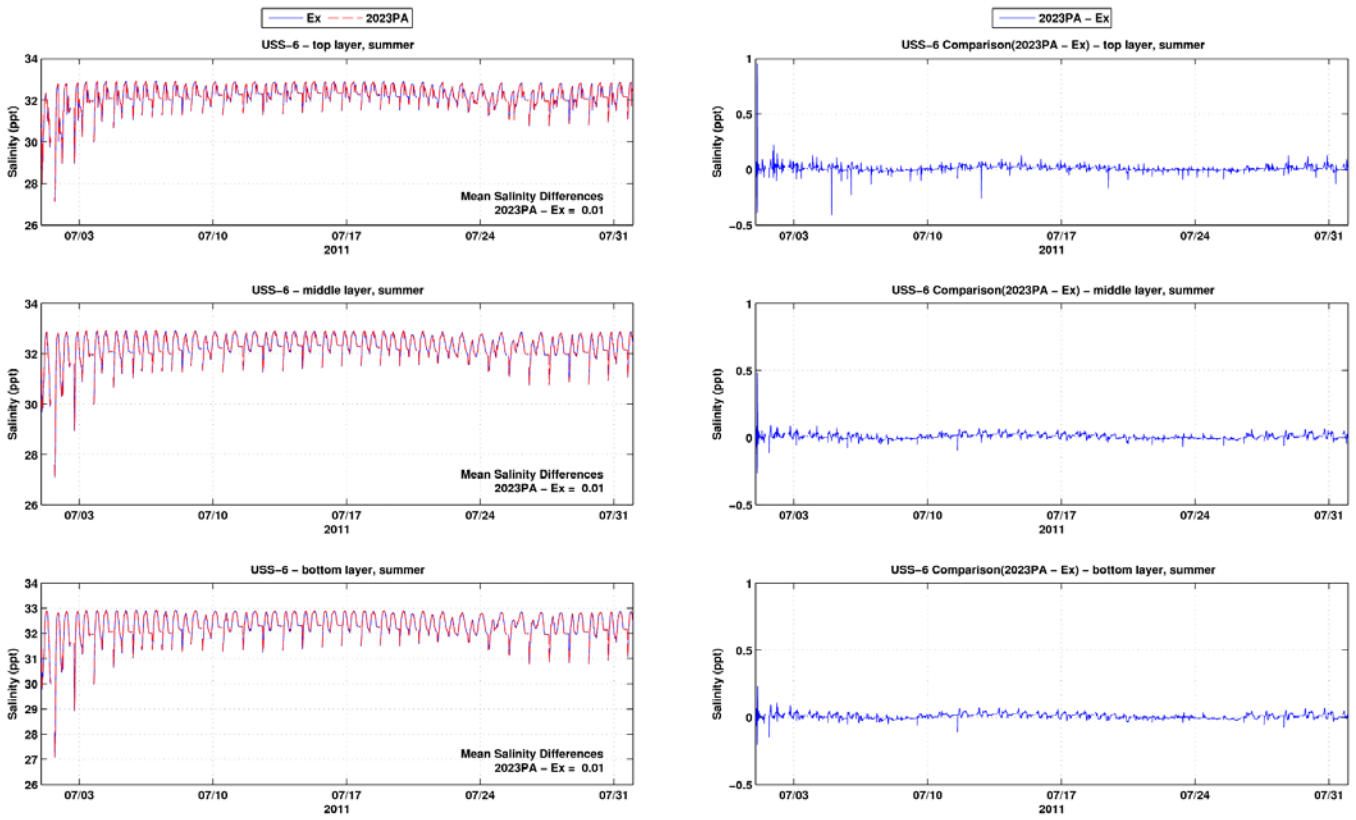

Figure A-54: Salinity time series and differences between the Existing Conditions and the 2023 PA at USS-6 during summer period

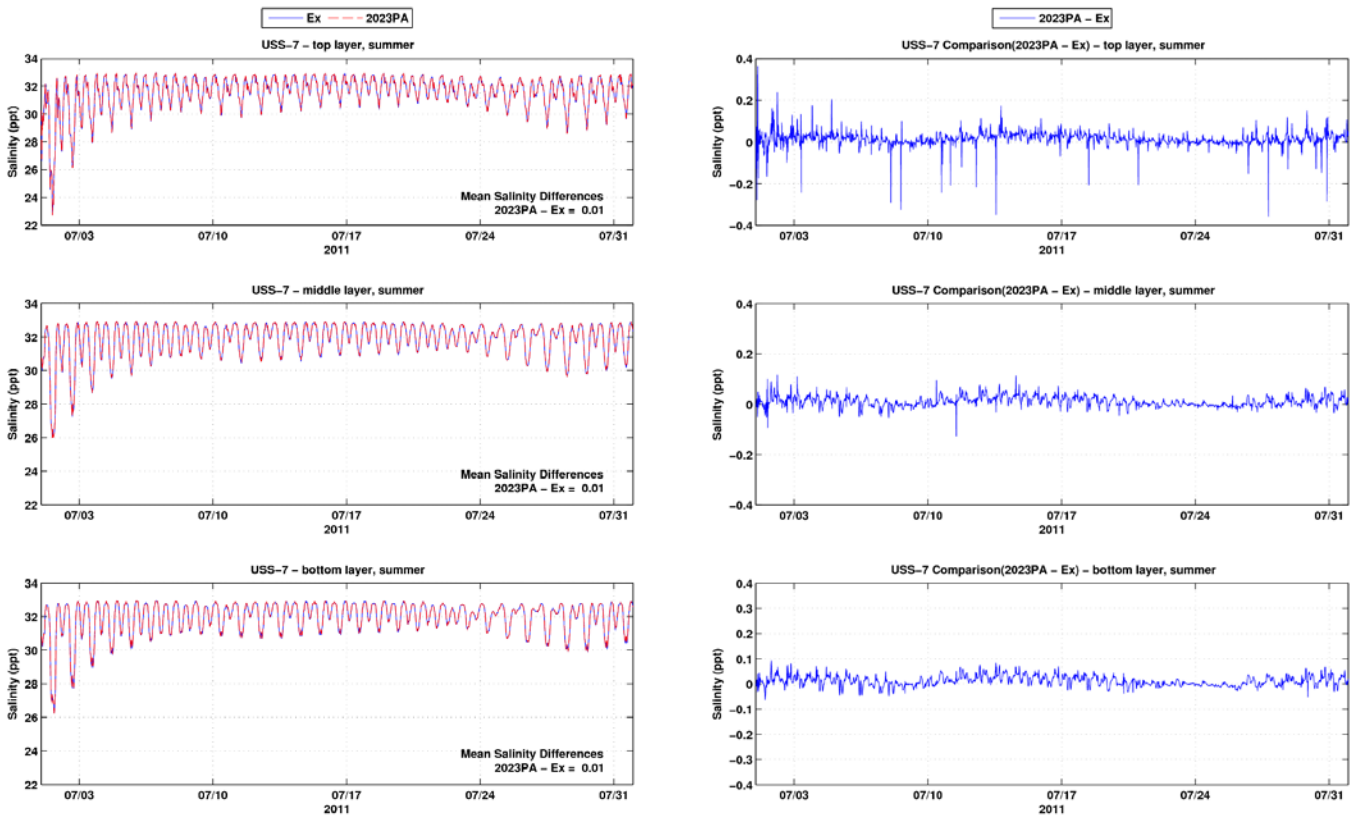

Figure A-55: Salinity time series and differences between the Existing Conditions and the 2023 PA at USS-7 during summer period

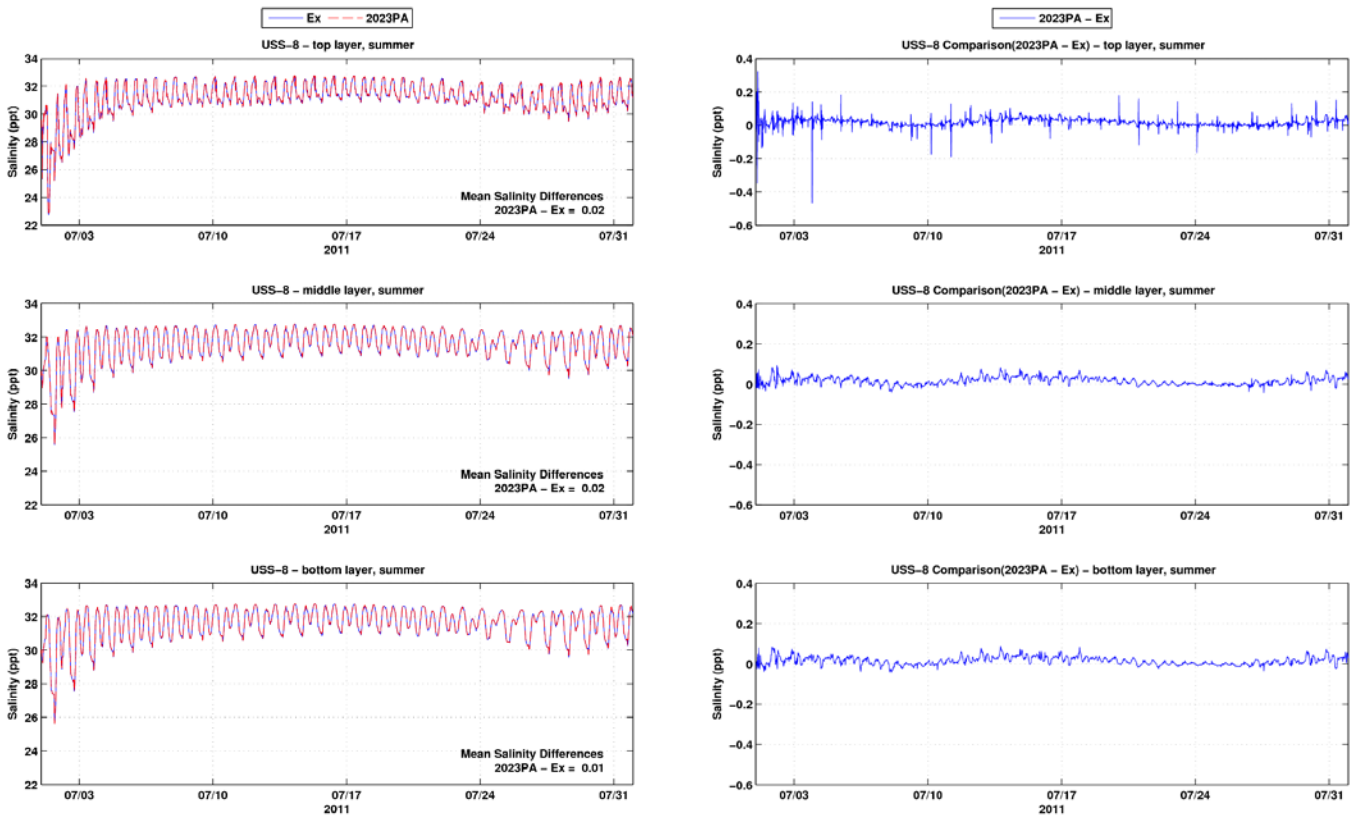

Figure A-56: Salinity time series and differences between the Existing Conditions and the 2023 PA at USS-8 during summer period

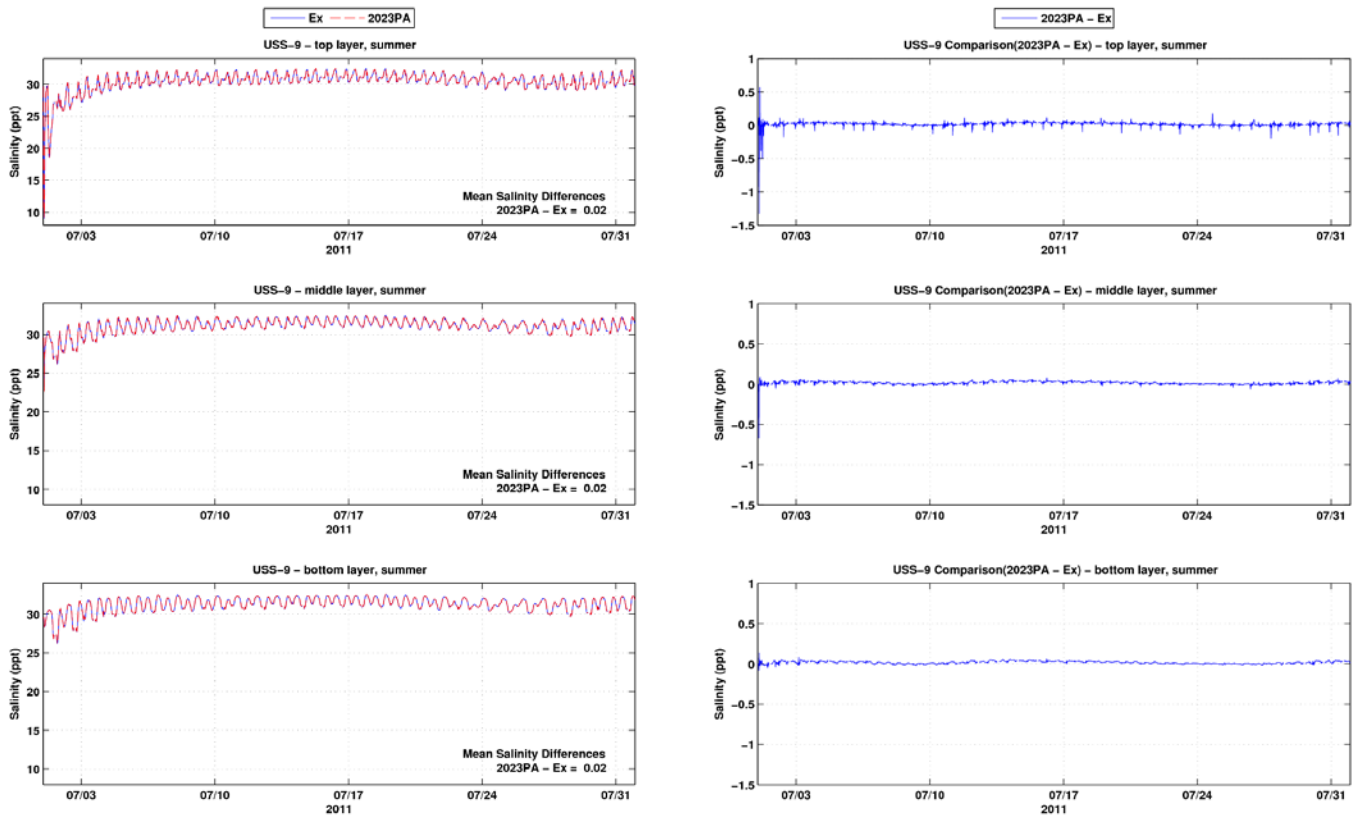

Figure A-57: Salinity time series and differences between the Existing Conditions and the 2023 PA at USS-9 during summer period

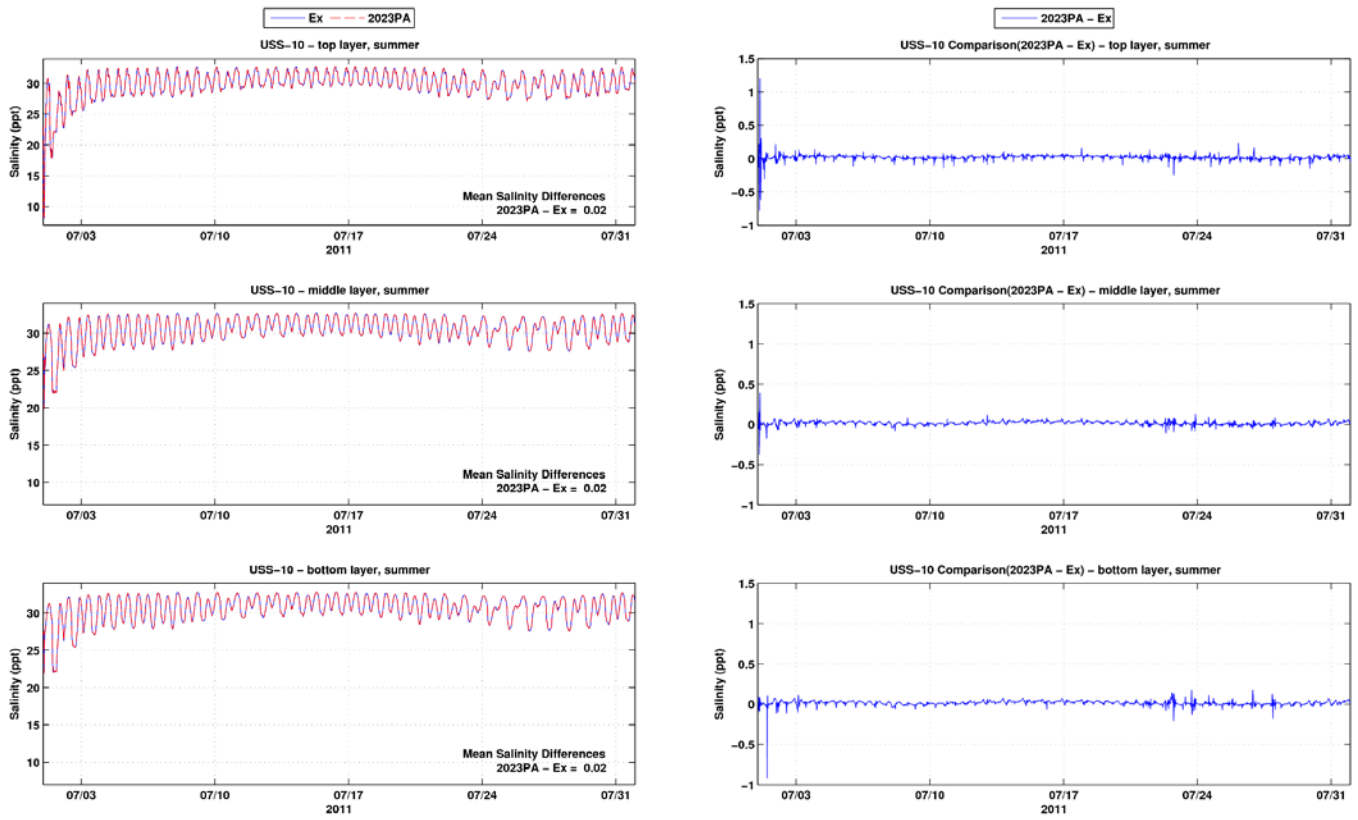

Figure A-58: Salinity time series and differences between the Existing Conditions and the 2023 PA at USS-10 during summer period

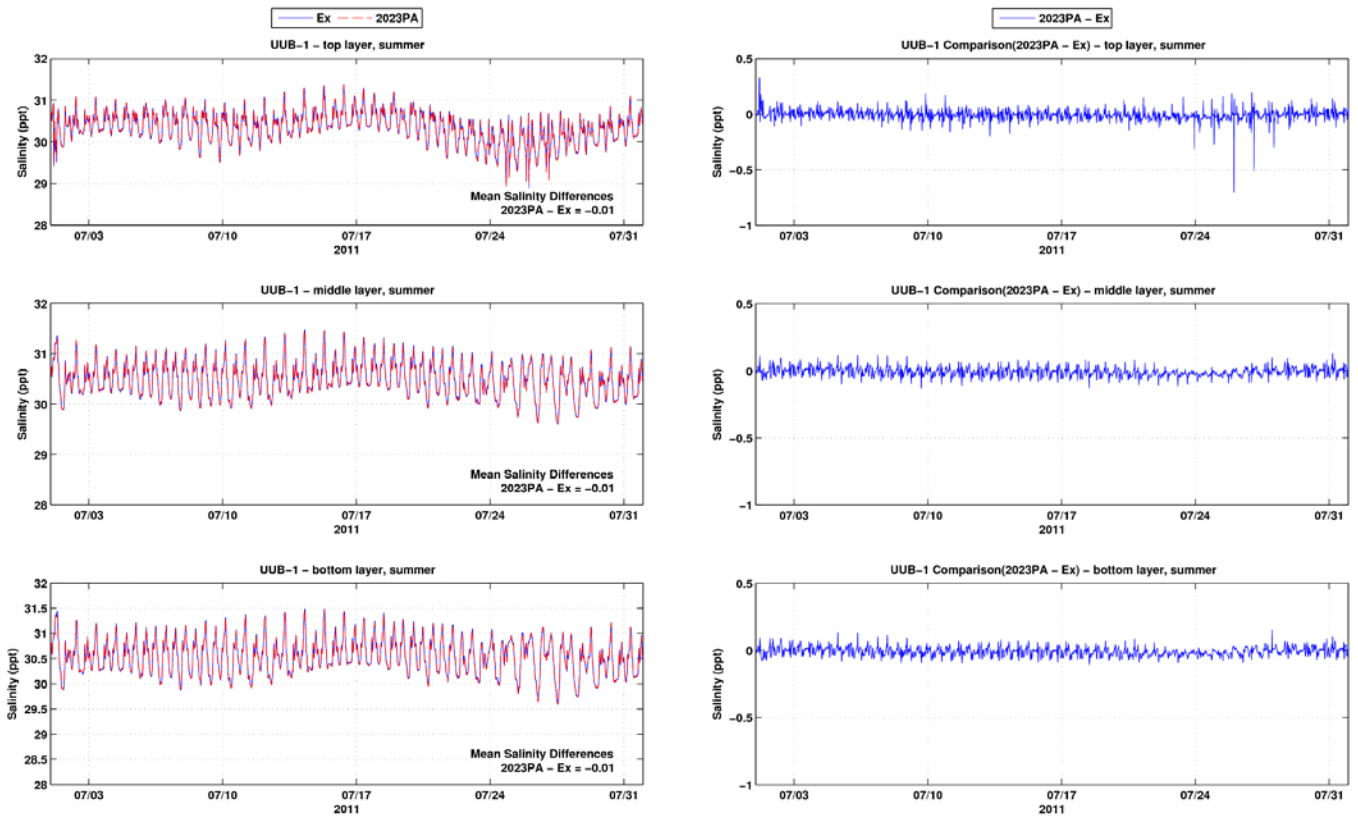

Figure A-59: Salinity time series and differences between the Existing Conditions and the 2023 PA at UUB-1 during summer period

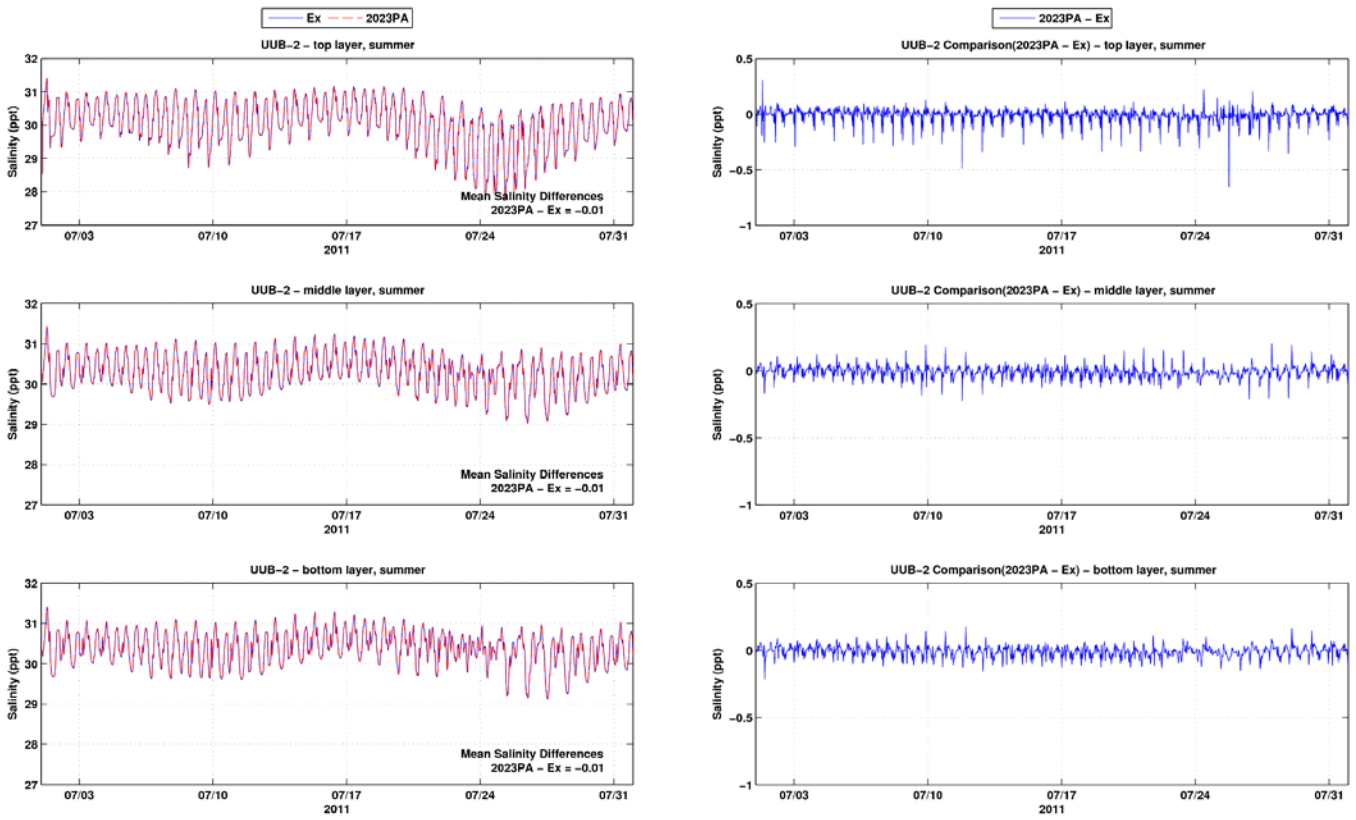

Figure A-60: Salinity time series and differences between the Existing Conditions and the 2023 PA at UUB-2 during summer period

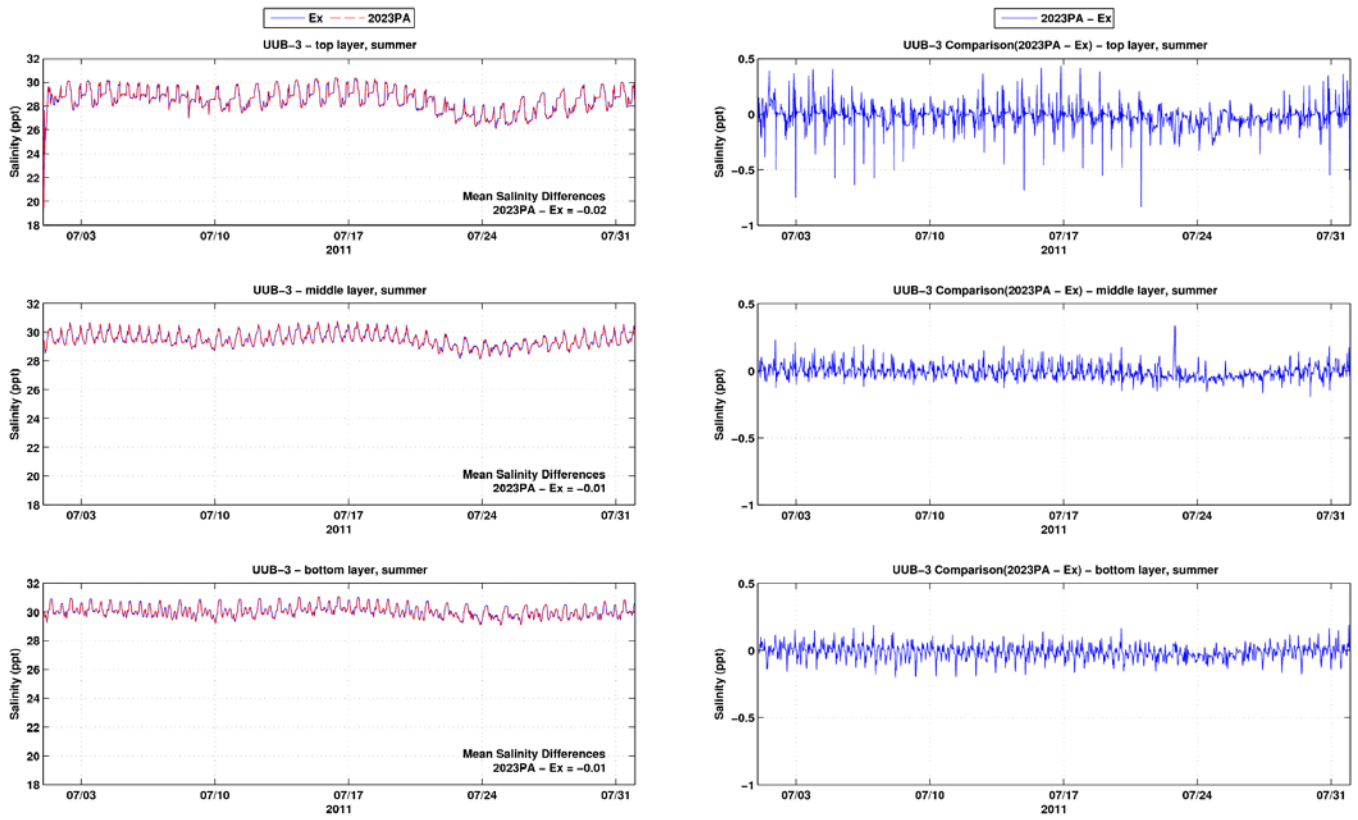

Figure A-61: Salinity time series and differences between the Existing Conditions and the 2023 PA at UUB-3 during summer period

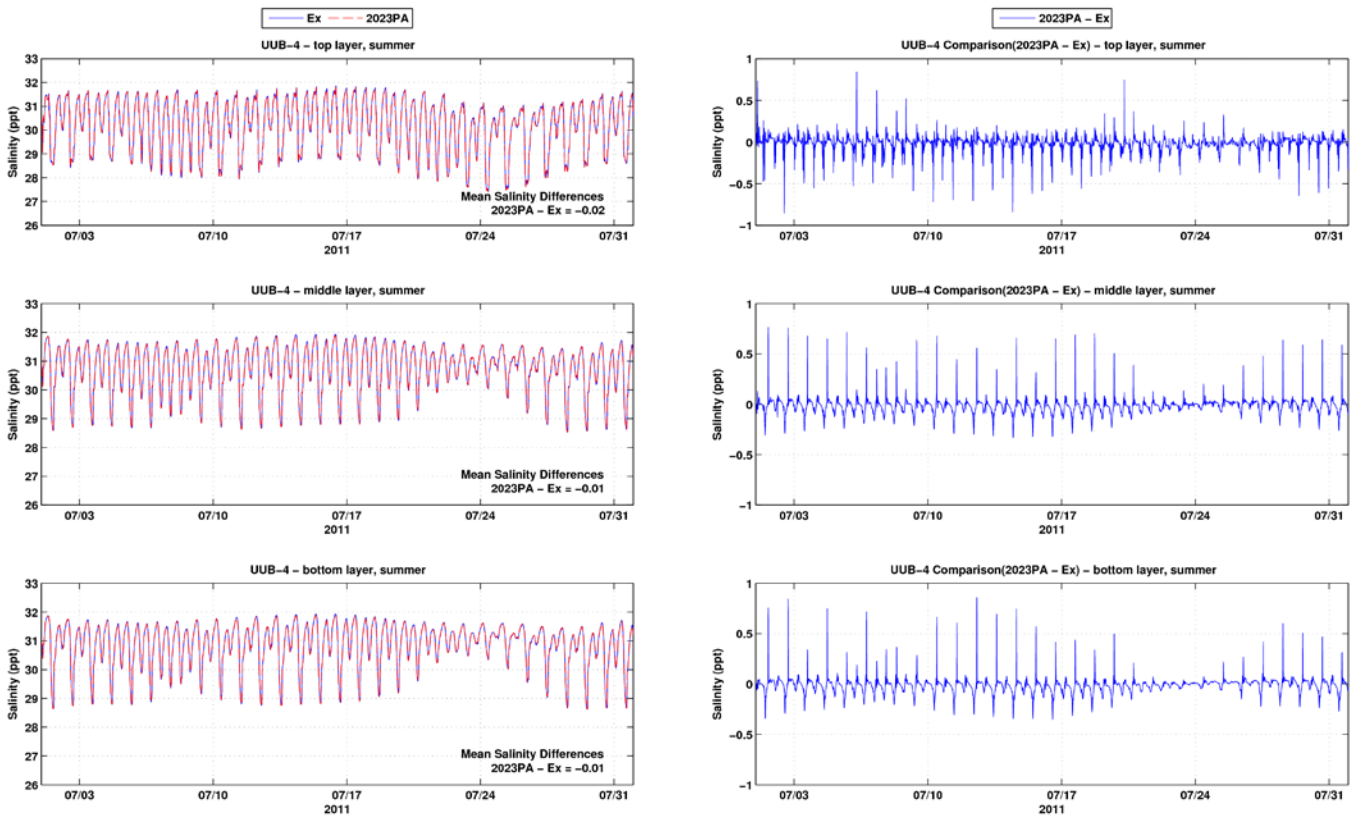

Figure A-62: Salinity time series and differences between the Existing Conditions and the 2023 PA at UUB-4 during summer period

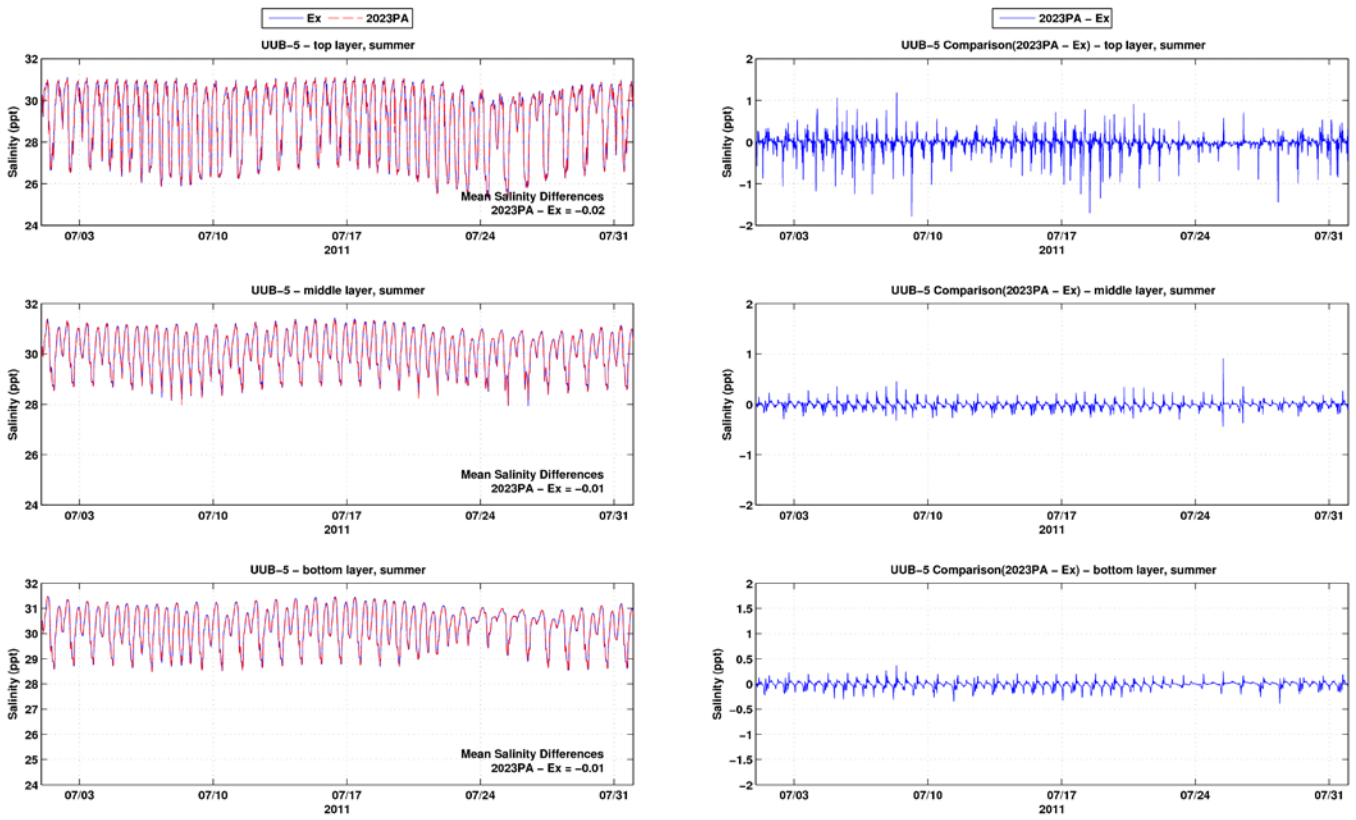

Figure A-63: Salinity time series and differences between the Existing Conditions and the 2023 PA at UUB-5 during summer period

Attachment B

Salinity Results for Winter/Spring Tide

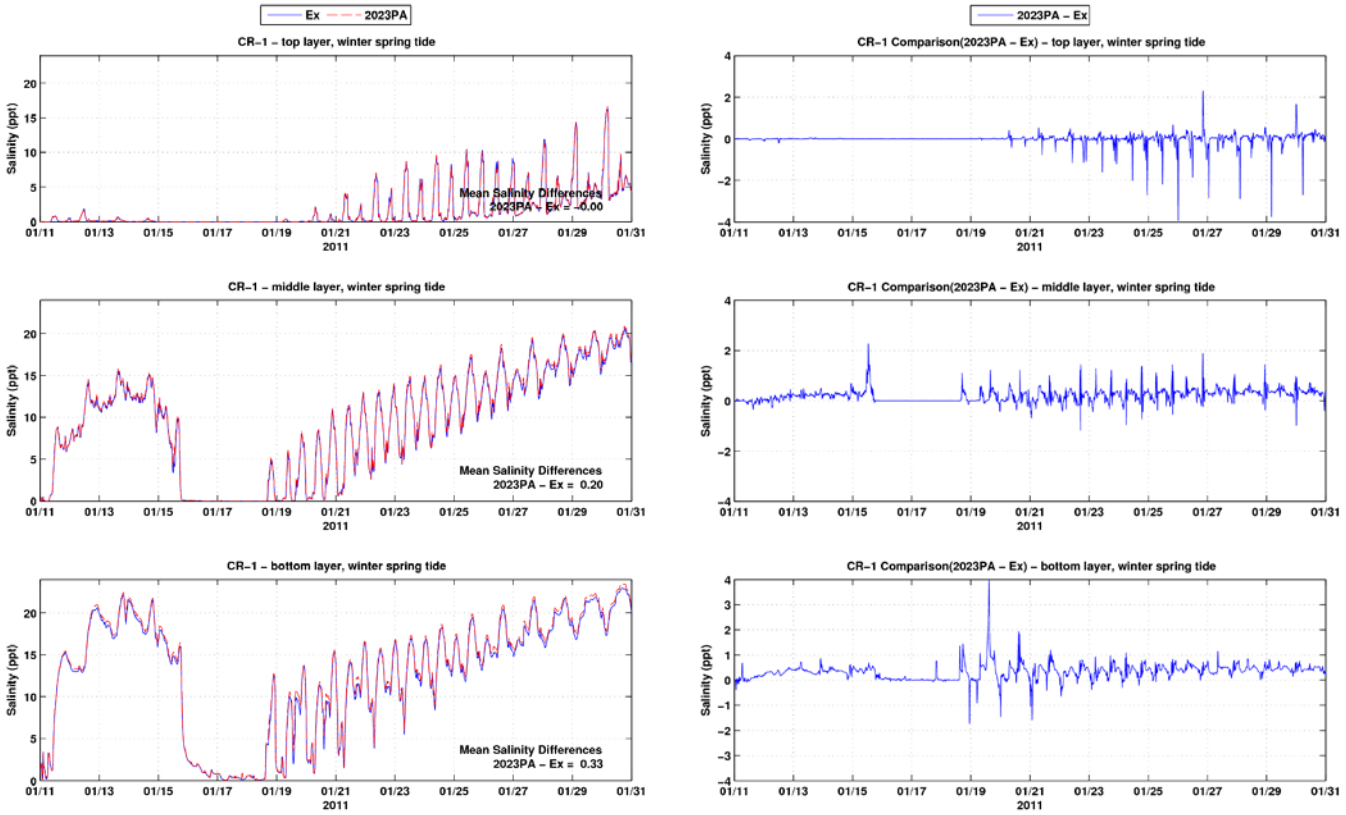

Figure B-1: Salinity time series and differences between the Existing Conditions and the 2023 PA at CR-1 during winter spring tide period

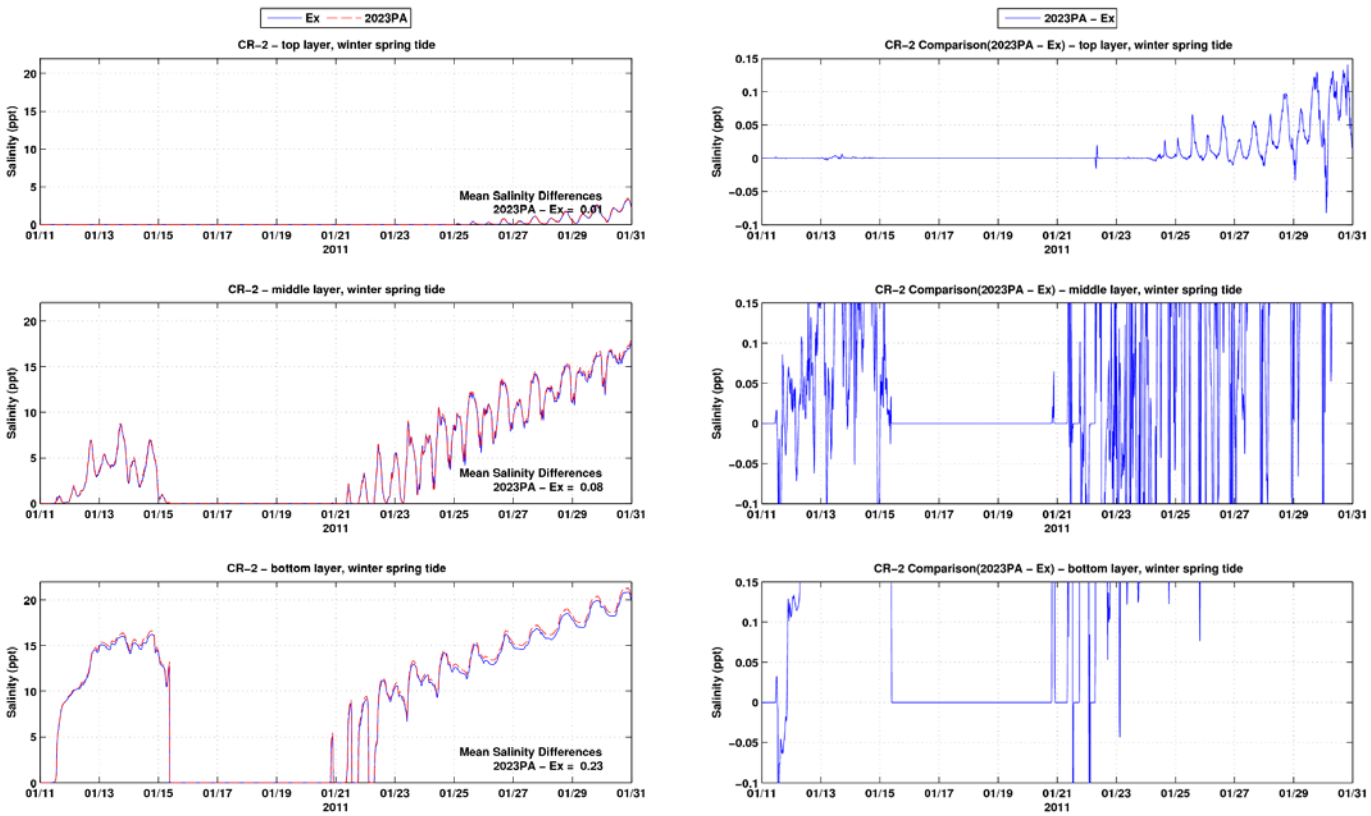

Figure B-2: Salinity time series and differences between the Existing Conditions and the 2023 PA at CR-2 during winter spring tide period

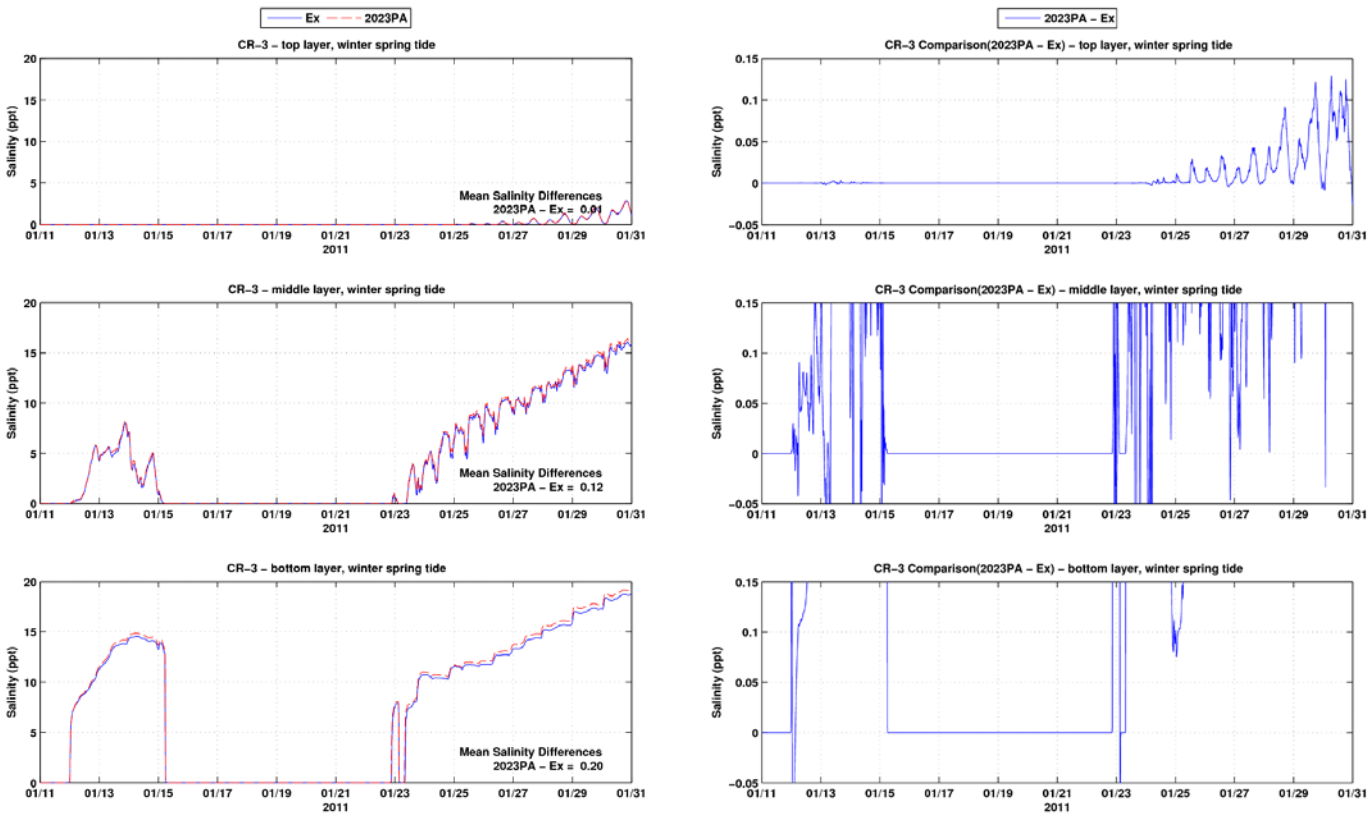

Figure B-3: Salinity time series and differences between the Existing Conditions and the 2023 PA at CR-3 during winter spring tide period

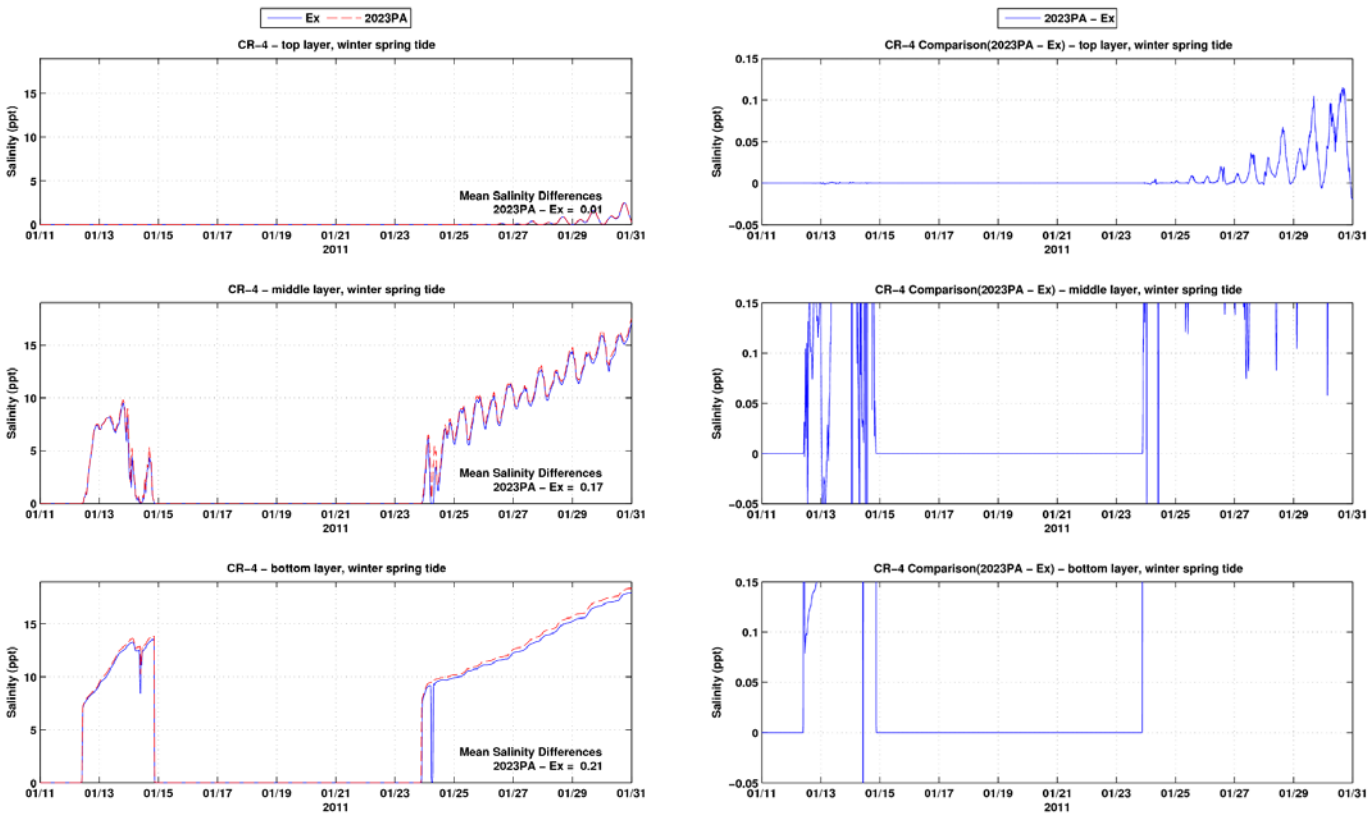

Figure B-4: Salinity time series and differences between the Existing Conditions and the 2023 PA at CR-4 during winter spring tide period

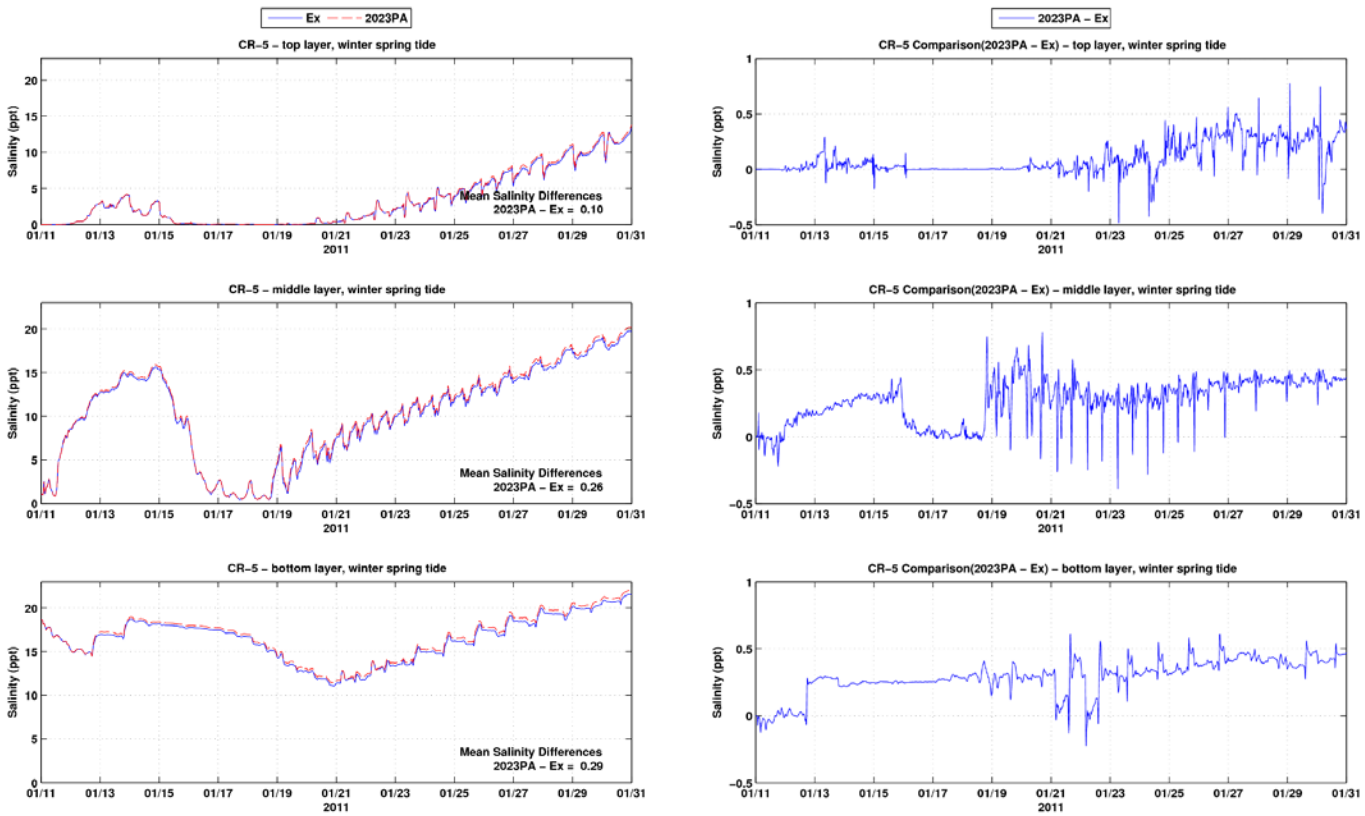

Figure B-5: Salinity time series and differences between the Existing Conditions and the 2023 PA at CR-5 during winter spring tide period

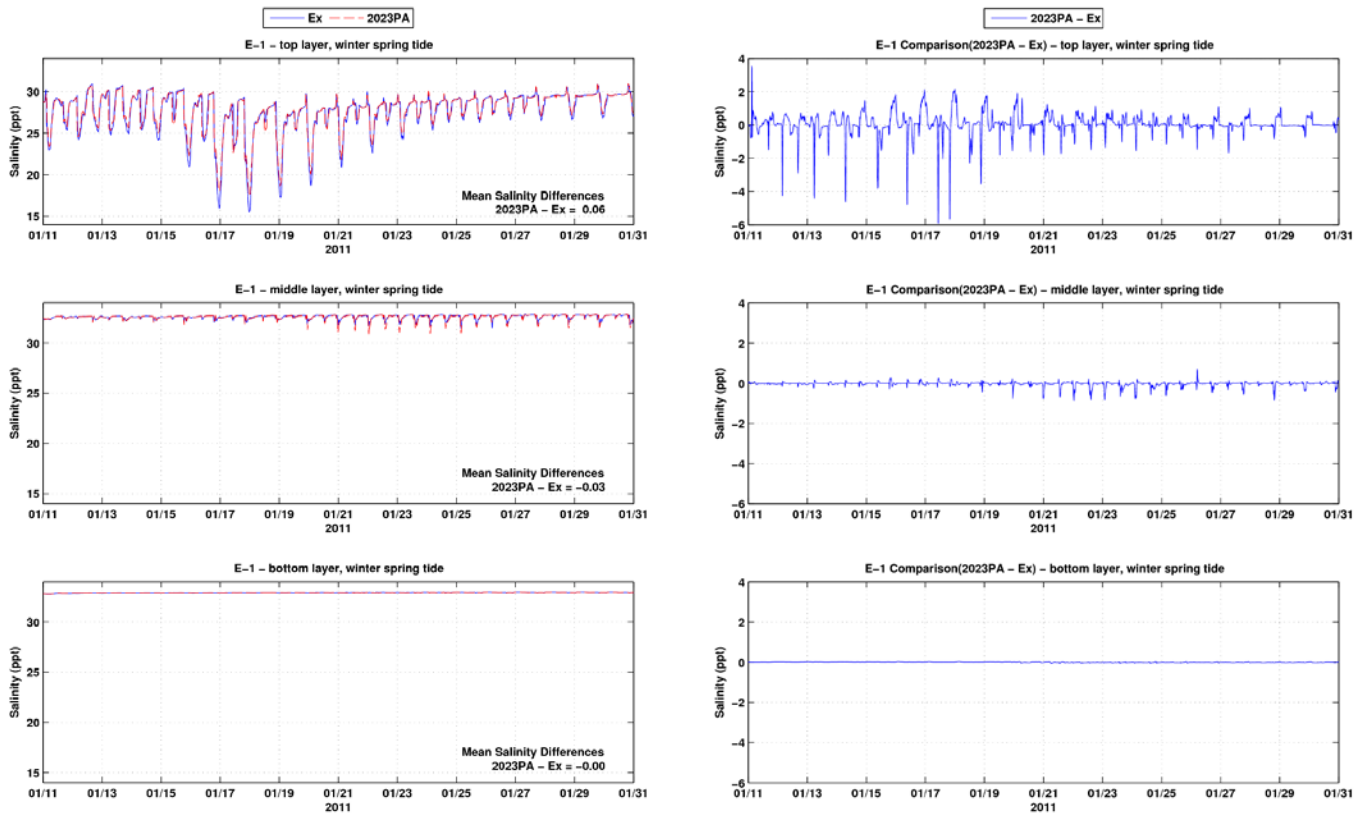

Figure B-6: Salinity time series and differences between the Existing Conditions and the 2023 PA at E-1 during winter spring tide period

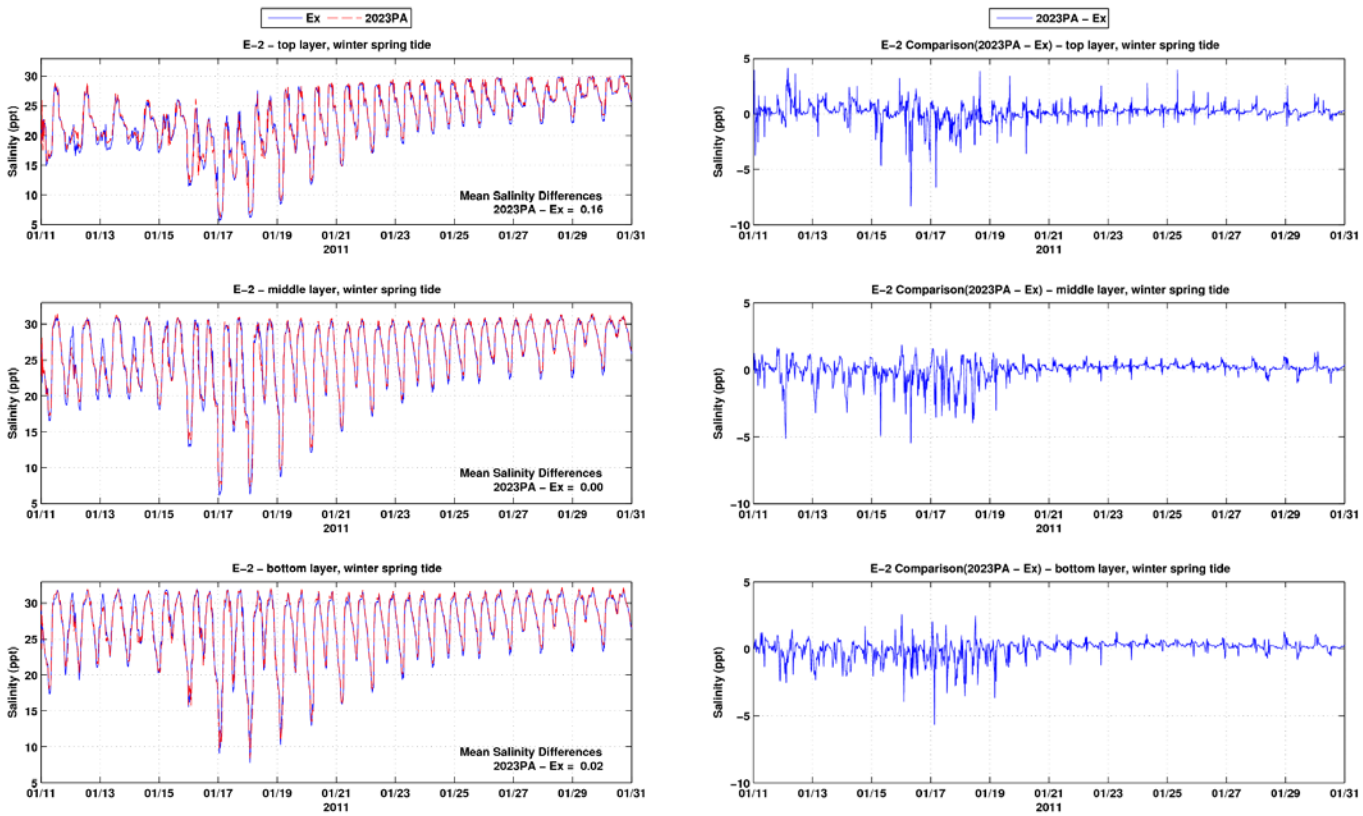

Figure B-7: Salinity time series and differences between the Existing Conditions and the 2023 PA at E-2 during winter spring tide period

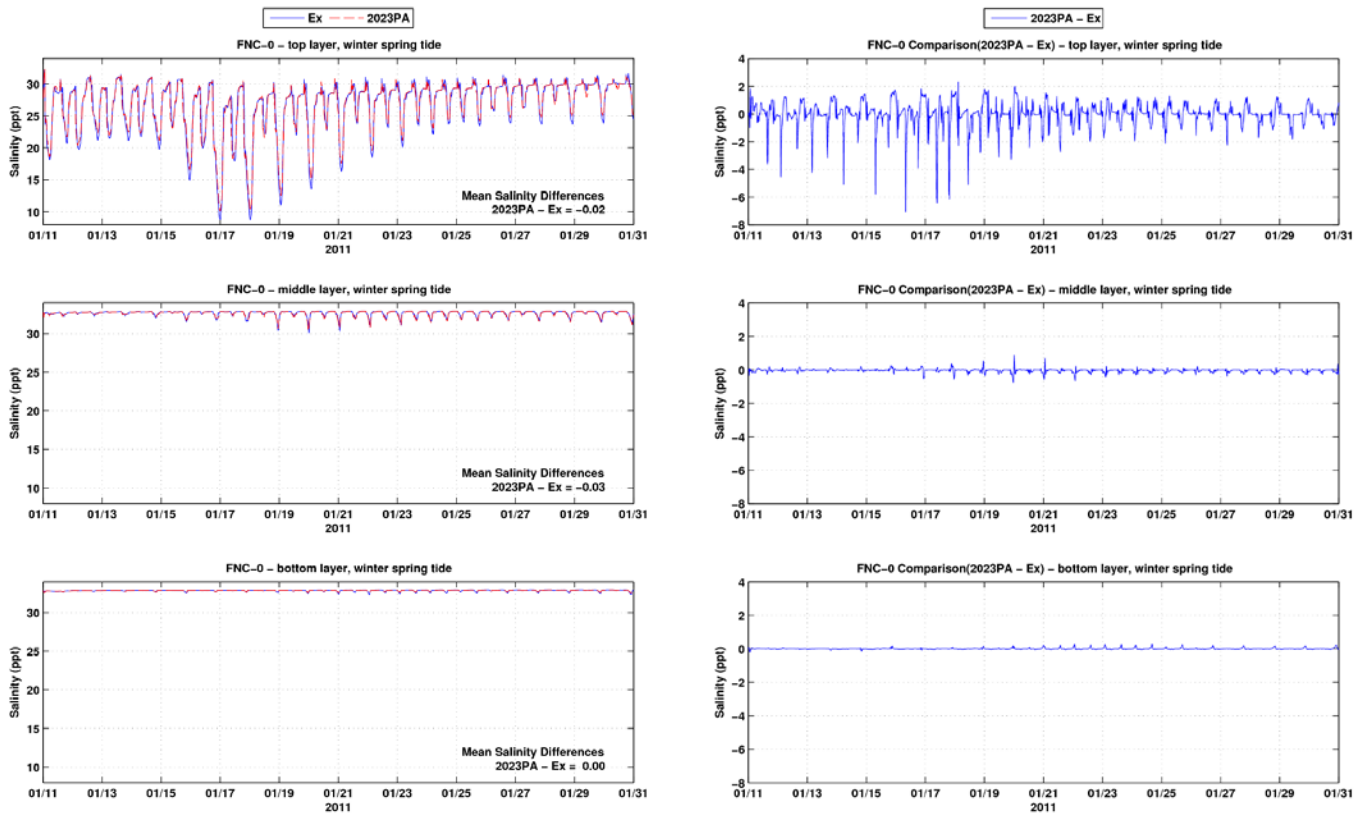

Figure B-8: Salinity time series and differences between the Existing Conditions and the 2023 PA at FNC-0 during winter spring tide period

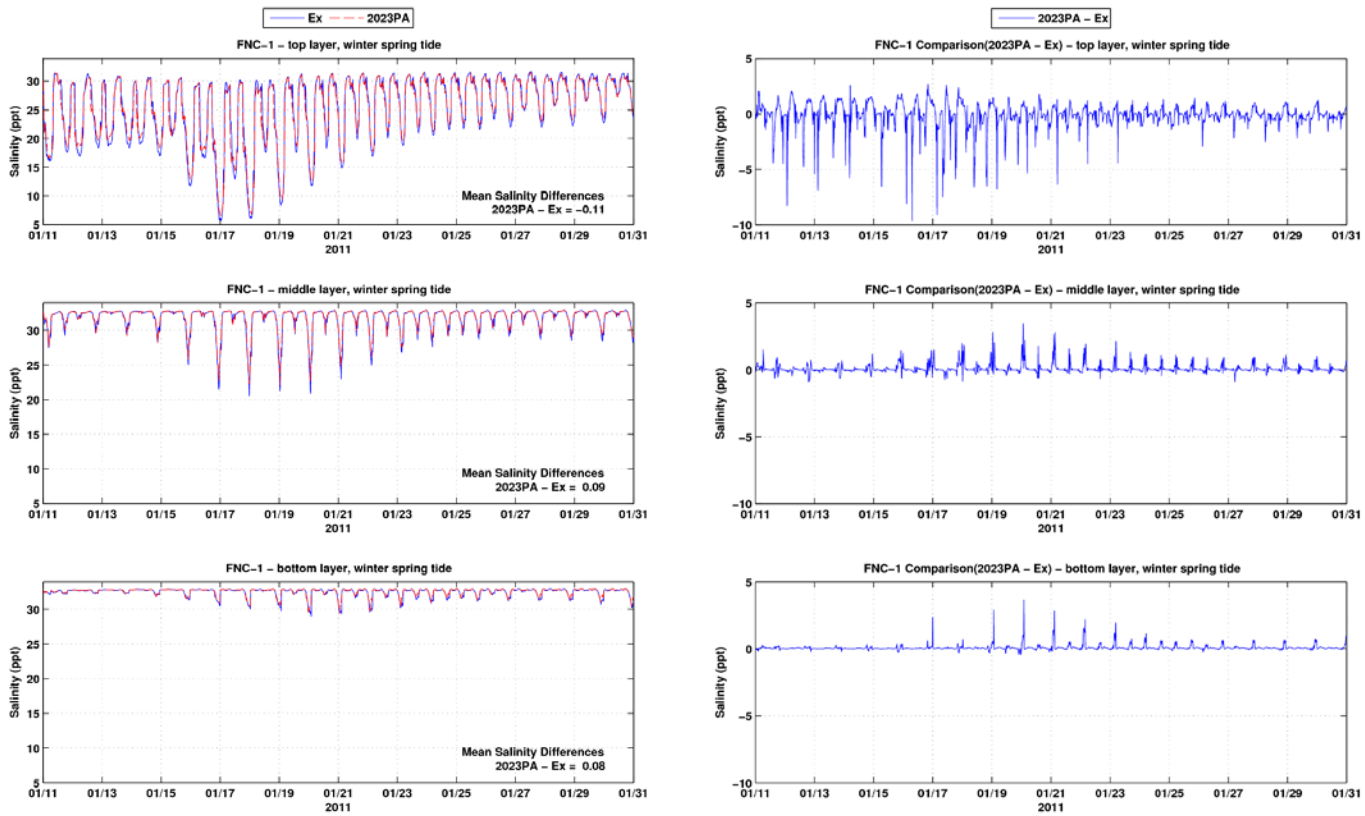

Figure B-9: Salinity time series and differences between the Existing Conditions and the 2023 PA at FNC-1 during winter spring tide period

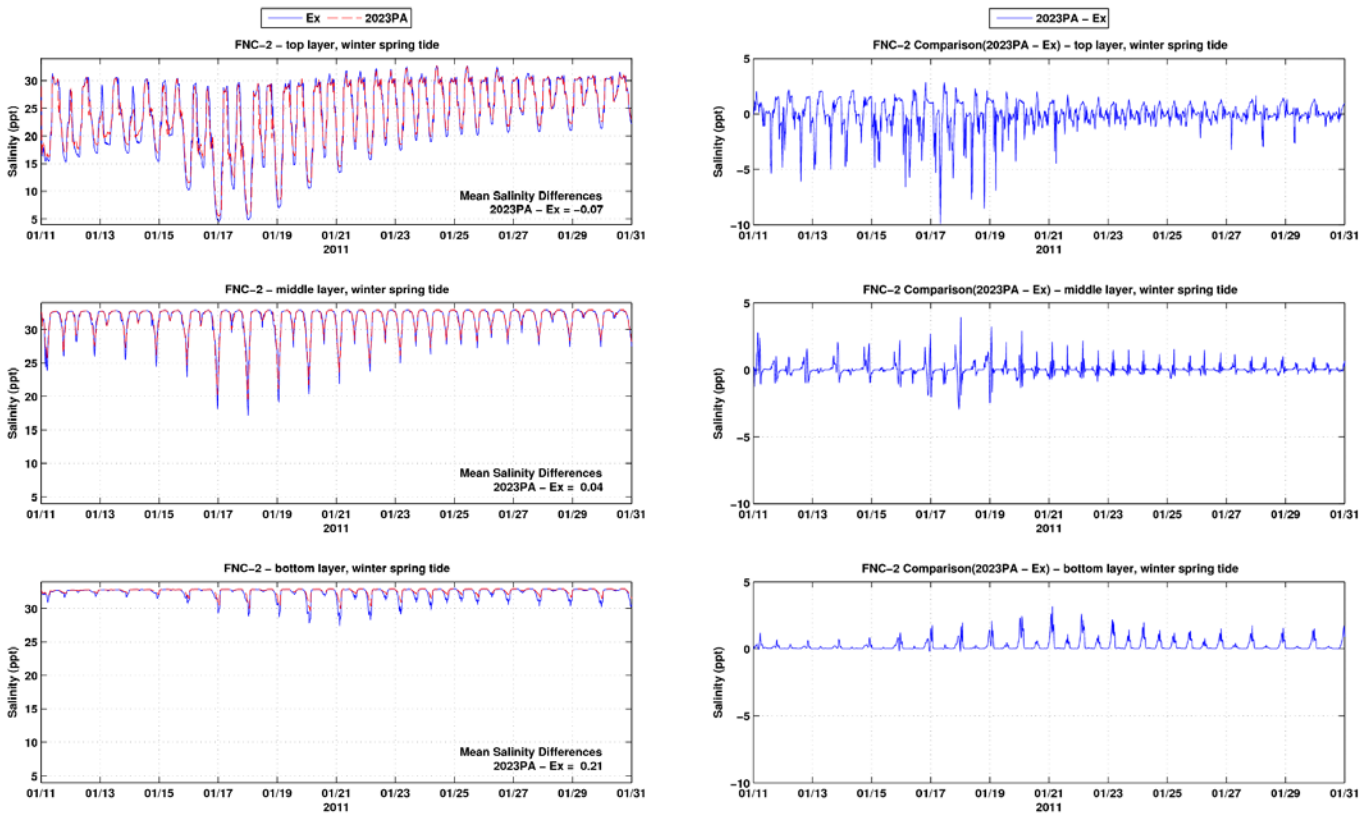

Figure B-10: Salinity time series and differences between the Existing Conditions and the 2023 PA at FNC-2 during winter spring tide period

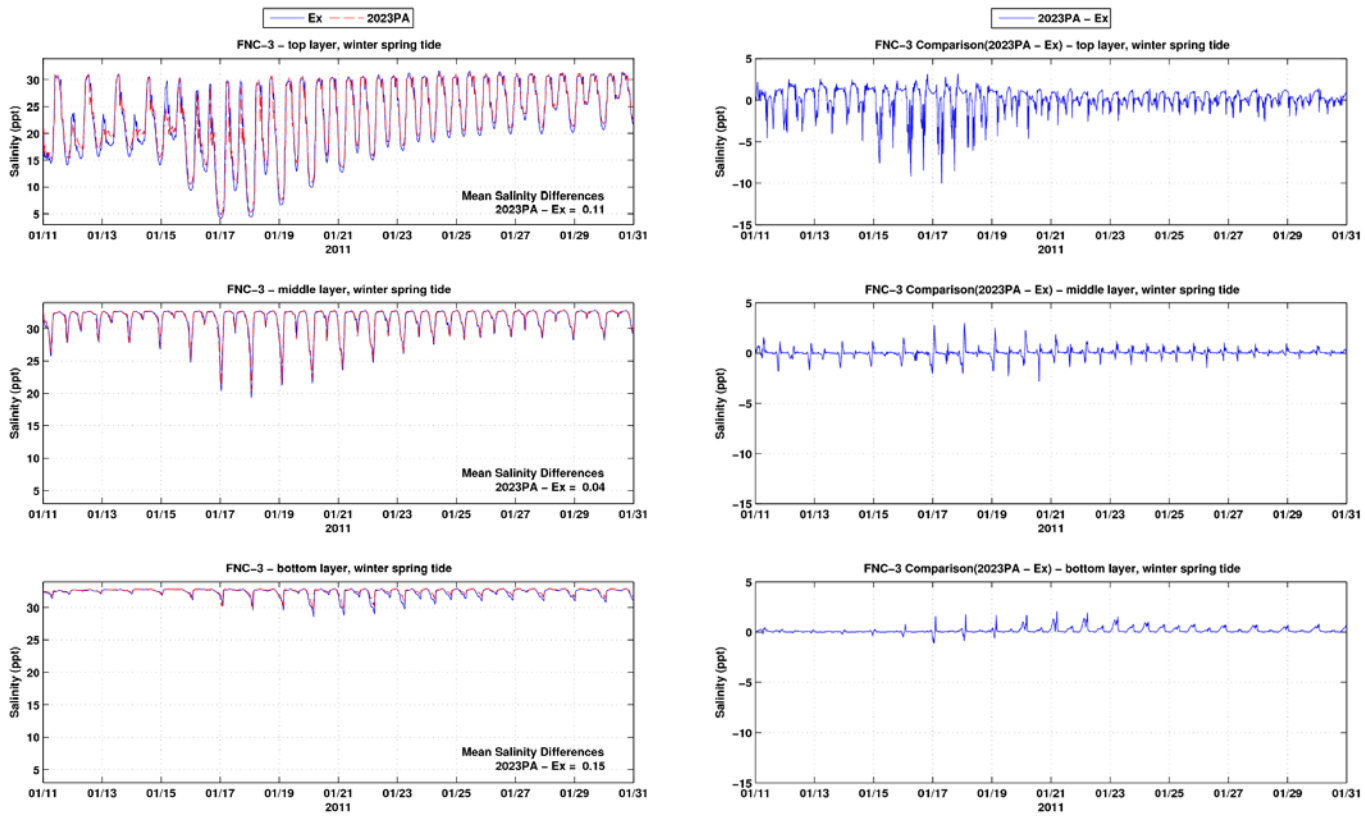

Figure B-11: Salinity time series and differences between the Existing Conditions and the 2023 PA at FNC-3 during winter spring tide period

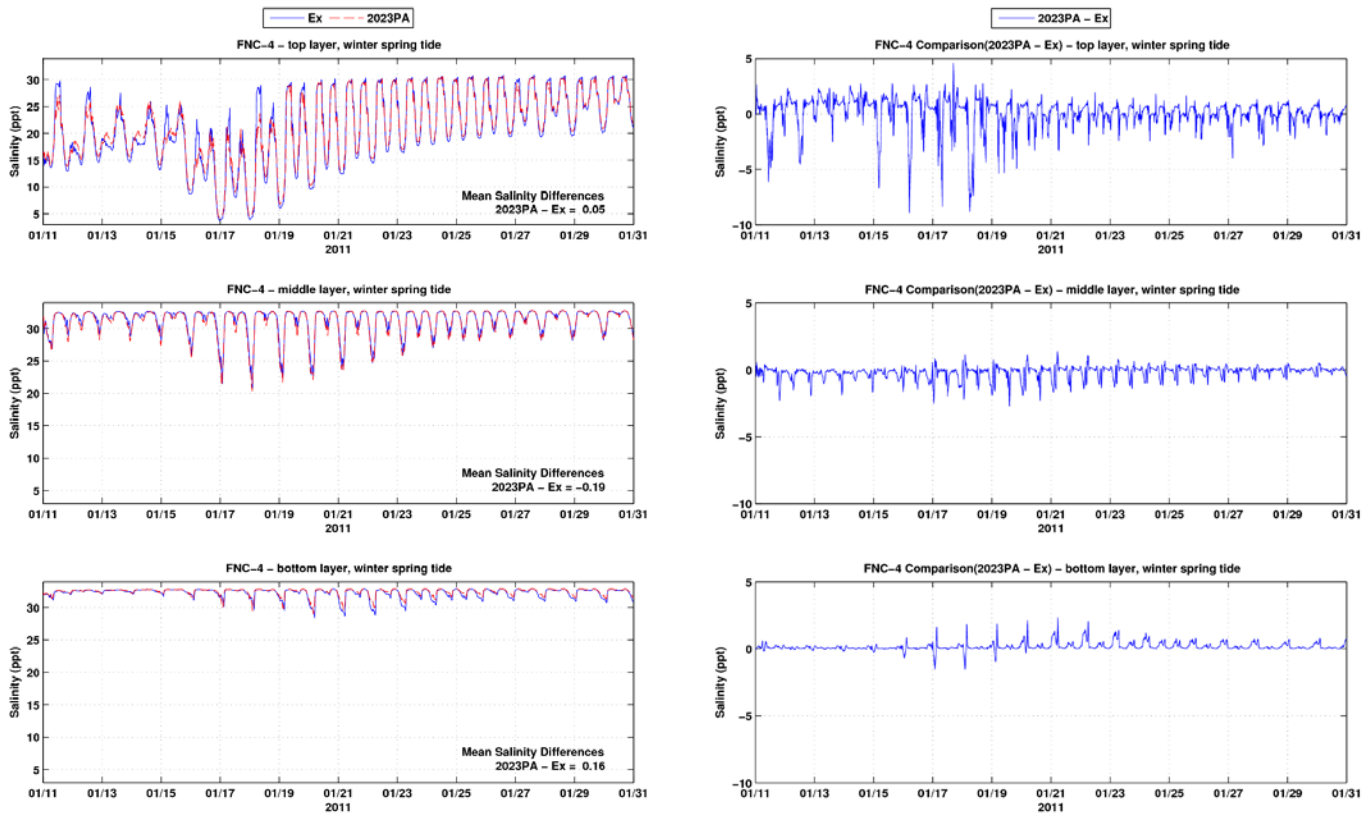

Figure B-12: Salinity time series and differences between the Existing Conditions and the 2023 PA at FNC-4 during winter spring tide period

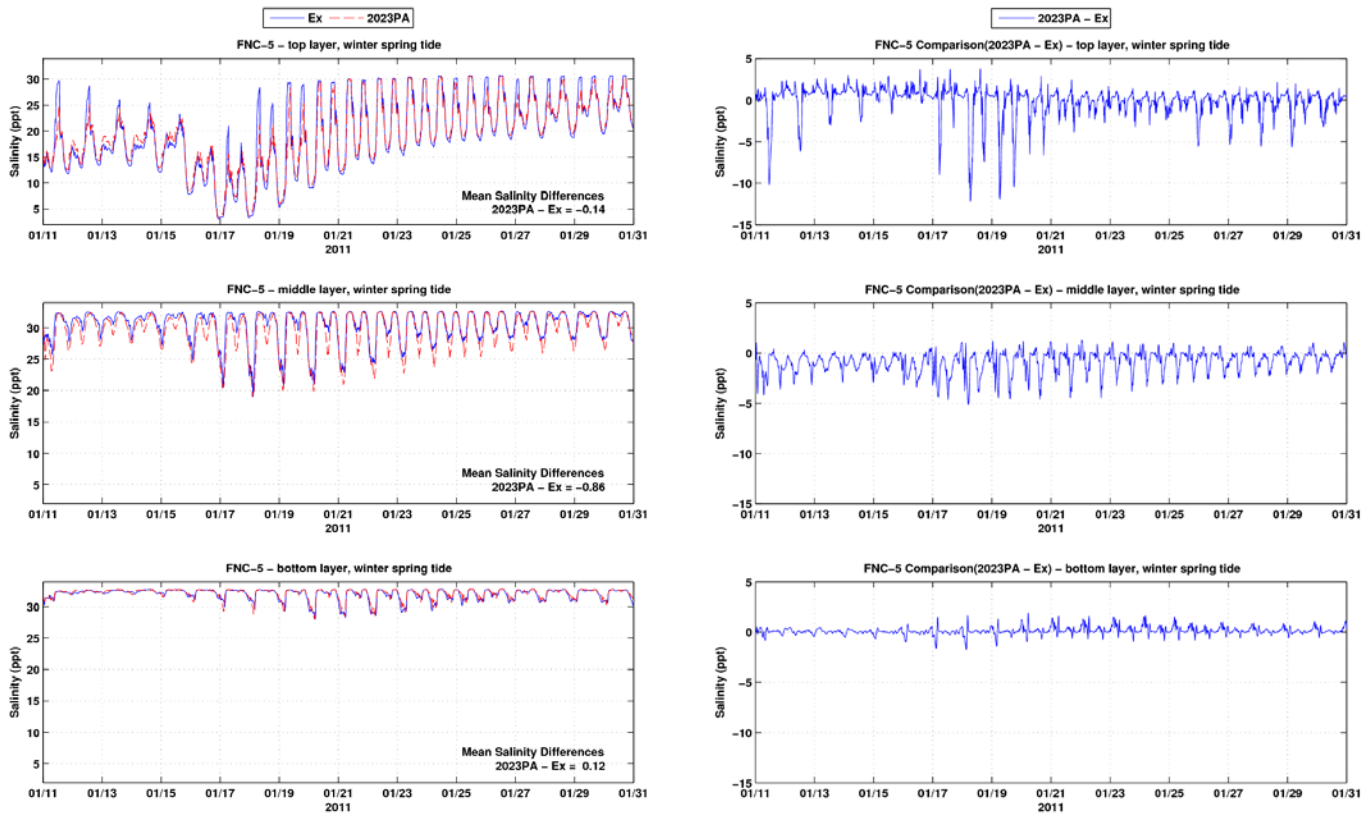

Figure B-13: Salinity time series and differences between the Existing Conditions and the 2023 PA at FNC5 during winter spring tide period

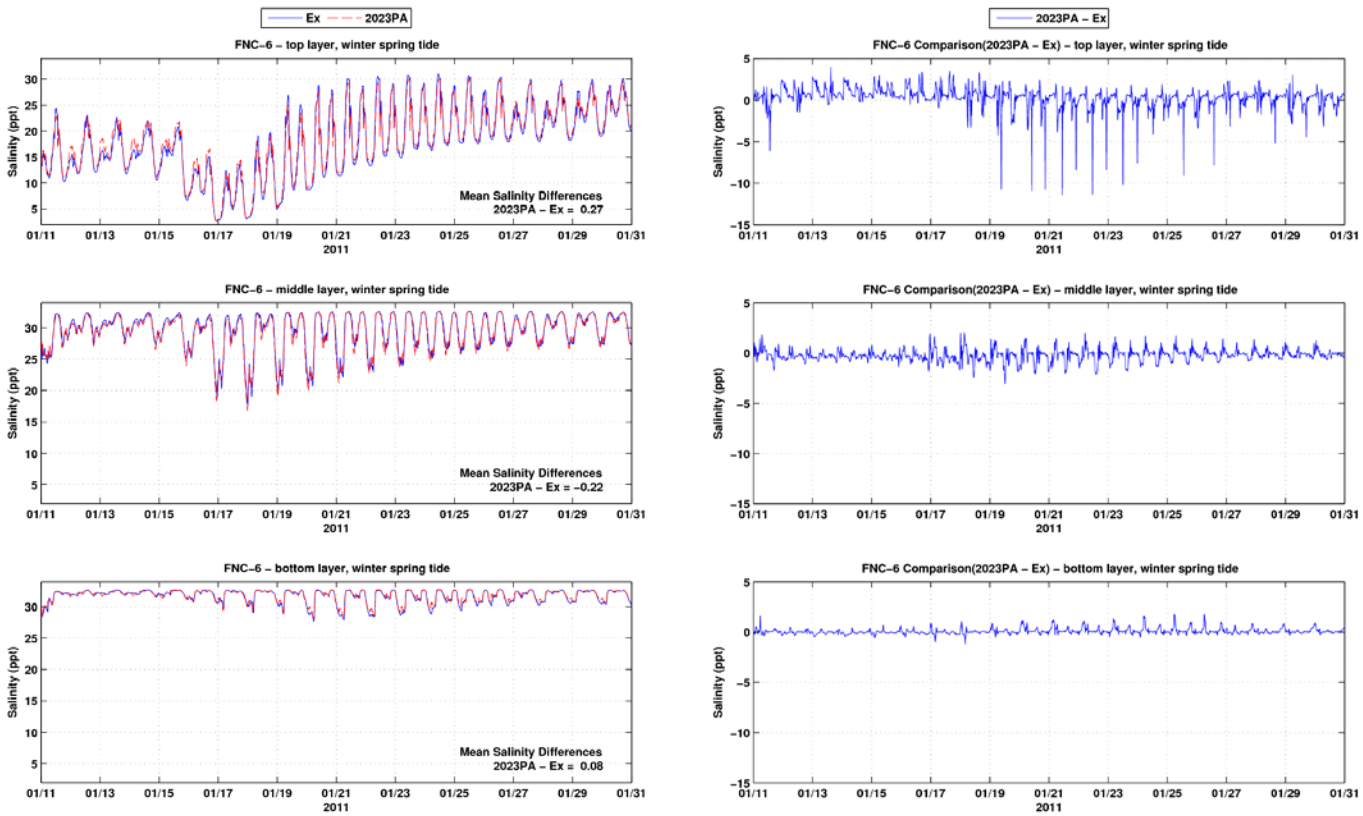

Figure B-14: Salinity time series and differences between the Existing Conditions and the 2023 PA at FNC-6 during winter spring tide period

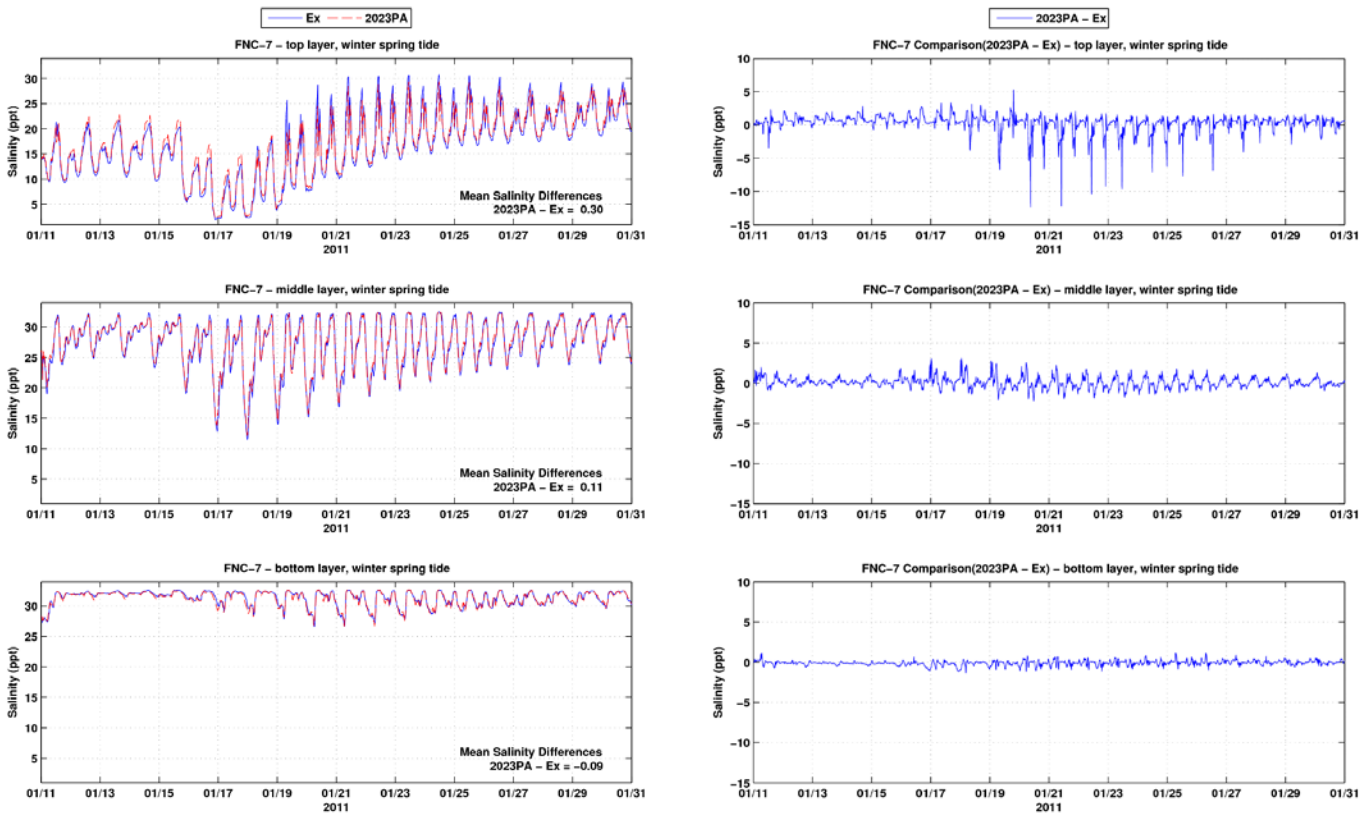

Figure B-15: Salinity time series and differences between the Existing Conditions and the 2023 PA at FNC-7 during winter spring tide period

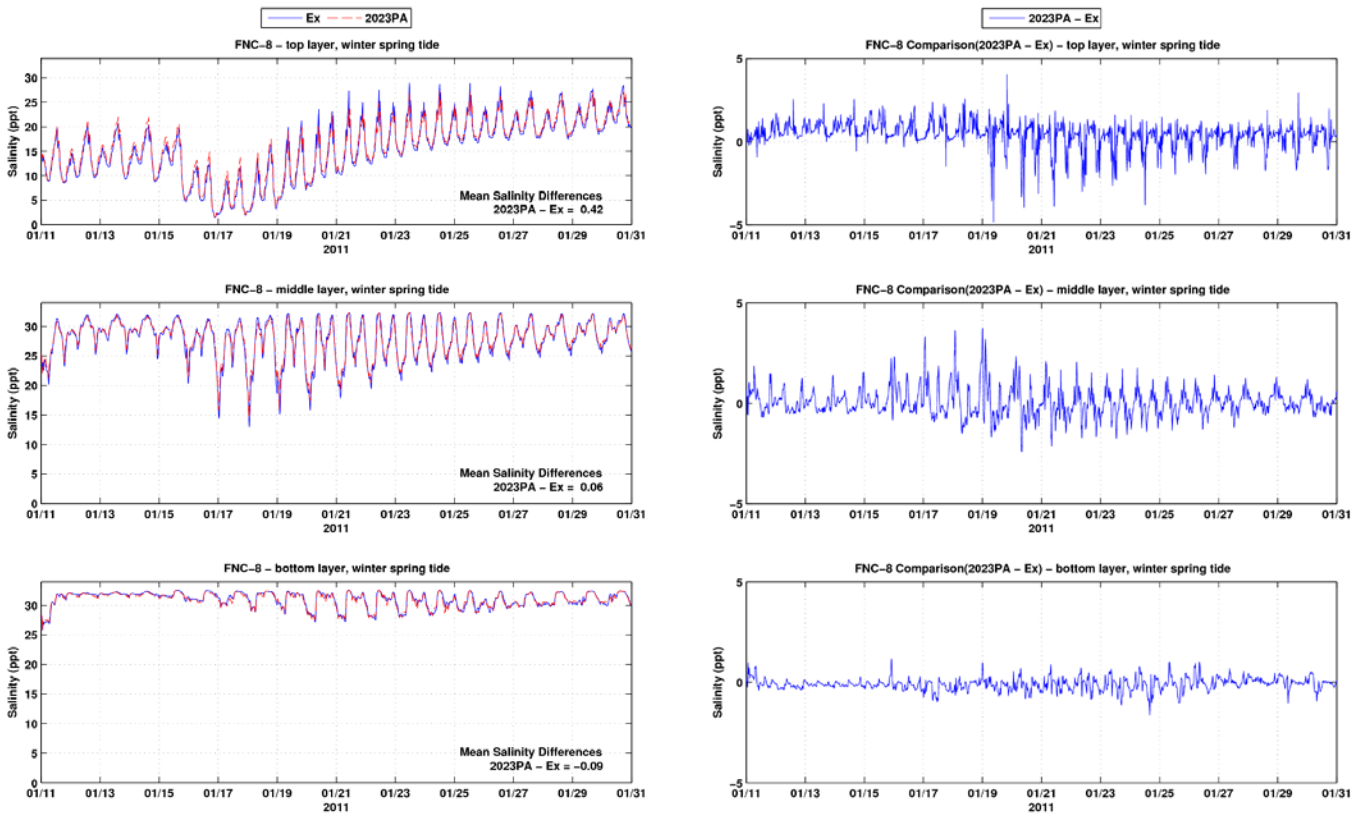

Figure B-16: Salinity time series and differences between the Existing Conditions and the 2023 PA at FNC-8 during winter spring tide period

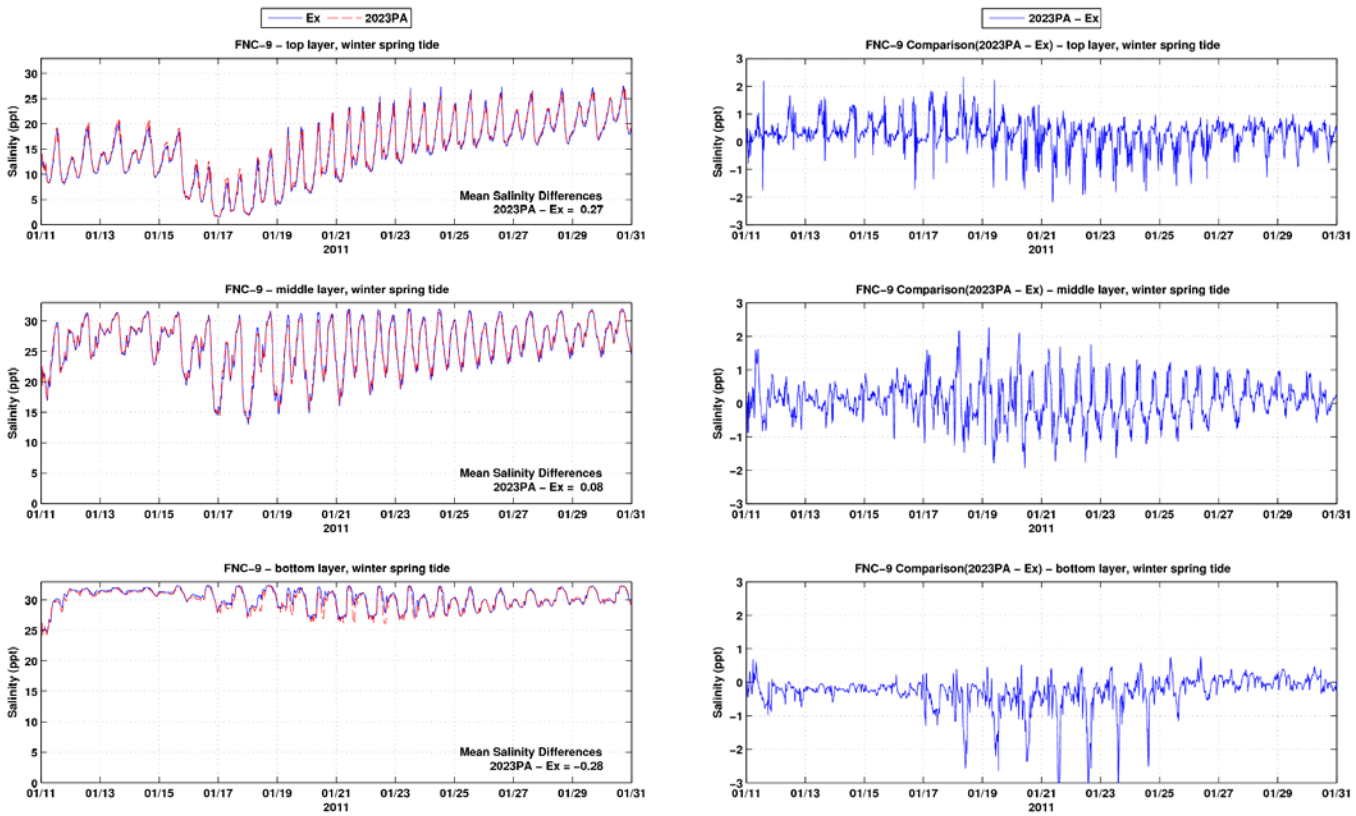

Figure B-17: Salinity time series and differences between the Existing Conditions and the 2023 PA at FNC-9 during winter spring tide period

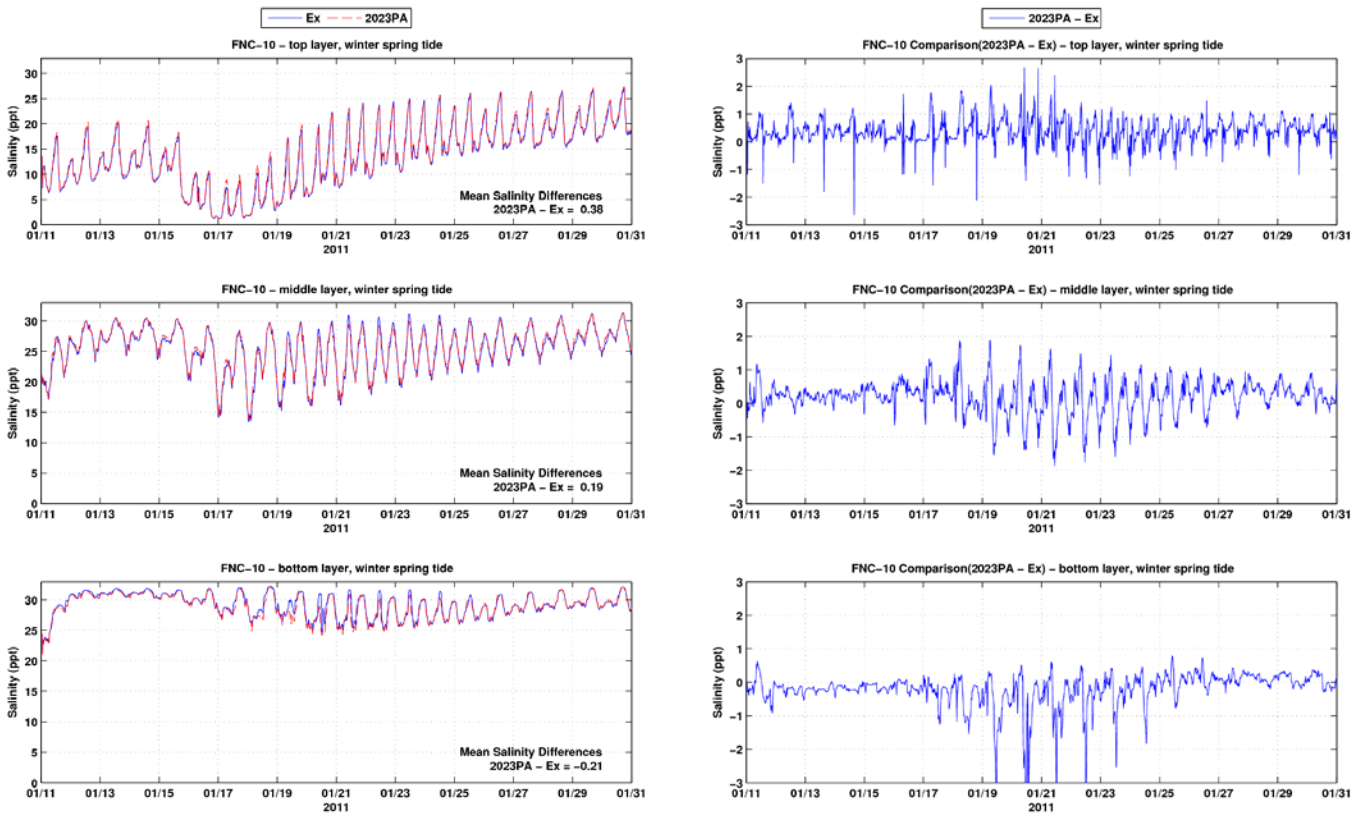

Figure B-18: Salinity time series and differences between the Existing Conditions and the 2023 PA at FNC-10 during winter spring tide period

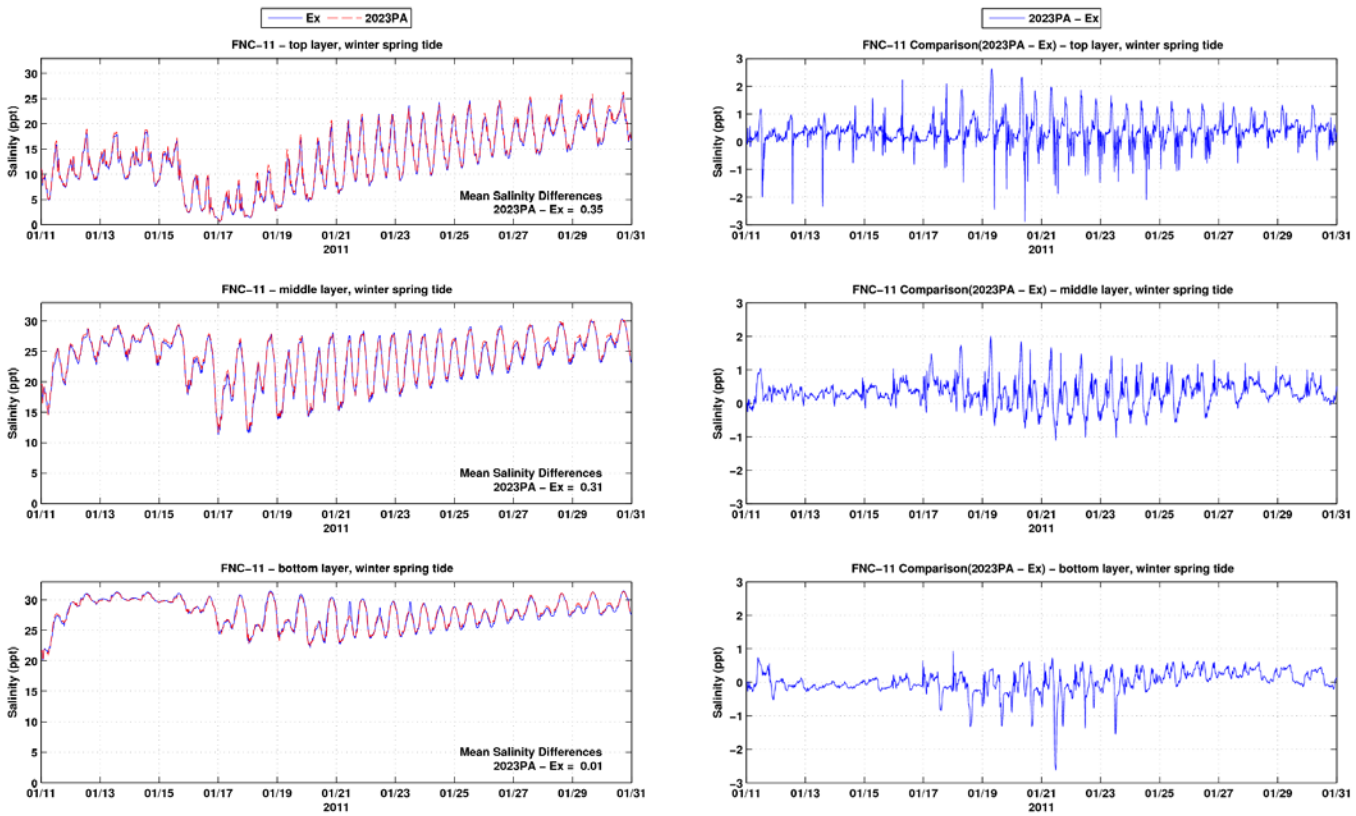

Figure B-19: Salinity time series and differences between the Existing Conditions and the 2023 PA at FNC-11 during winter spring tide period

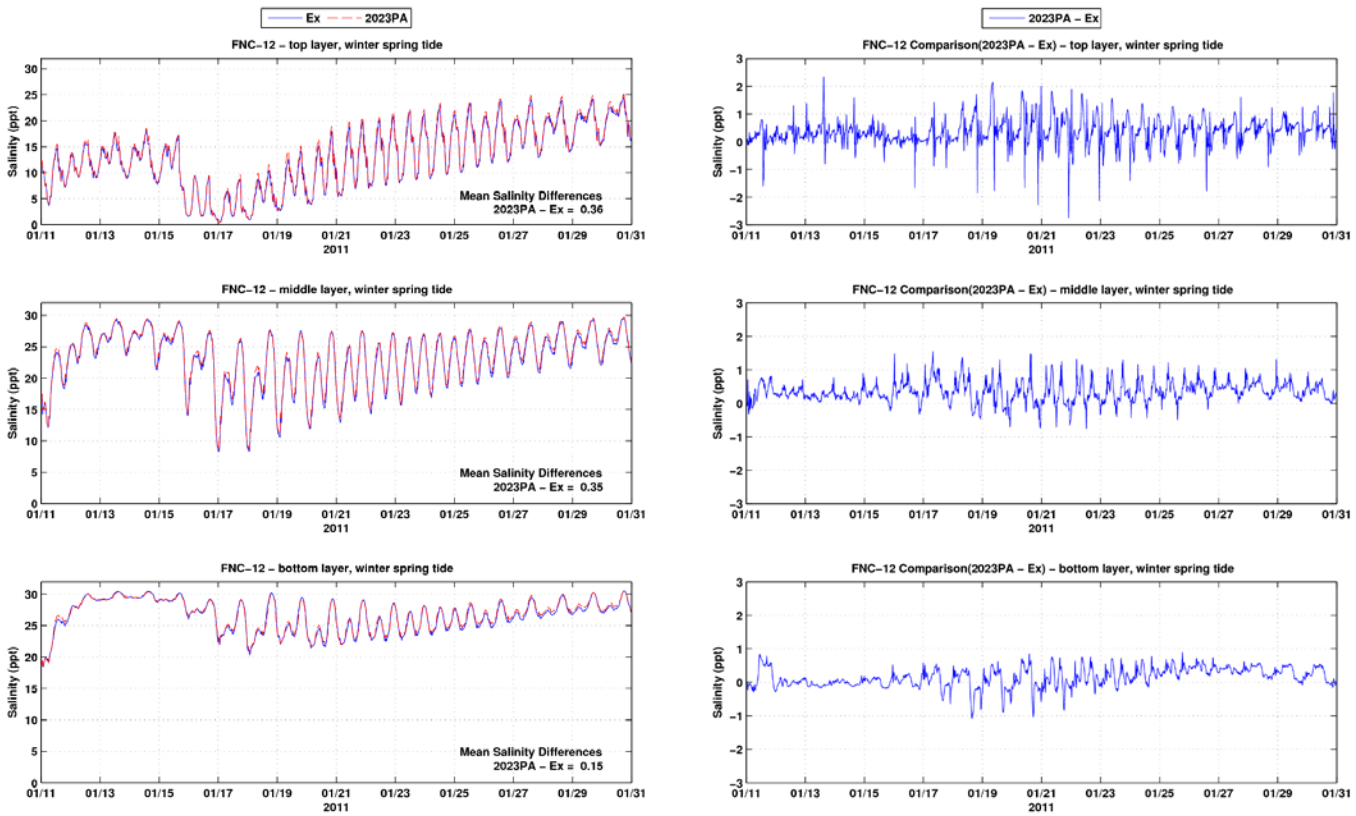

Figure B-20: Salinity time series and differences between the Existing Conditions and the 2023 PA at FNC-12 during winter spring tide period

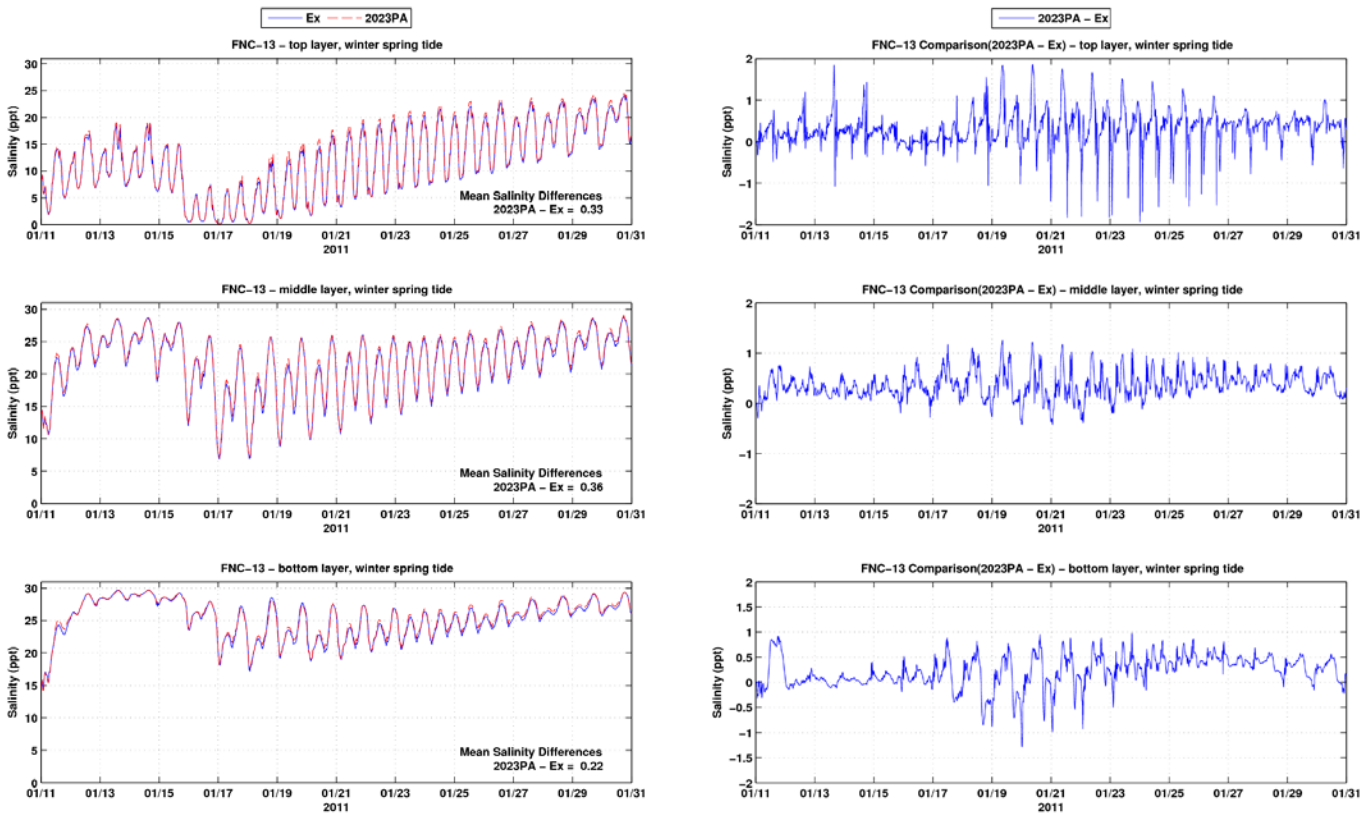

Figure B-21: Salinity time series and differences between the Existing Conditions and the 2023 PA at FNC-13 during winter spring tide period

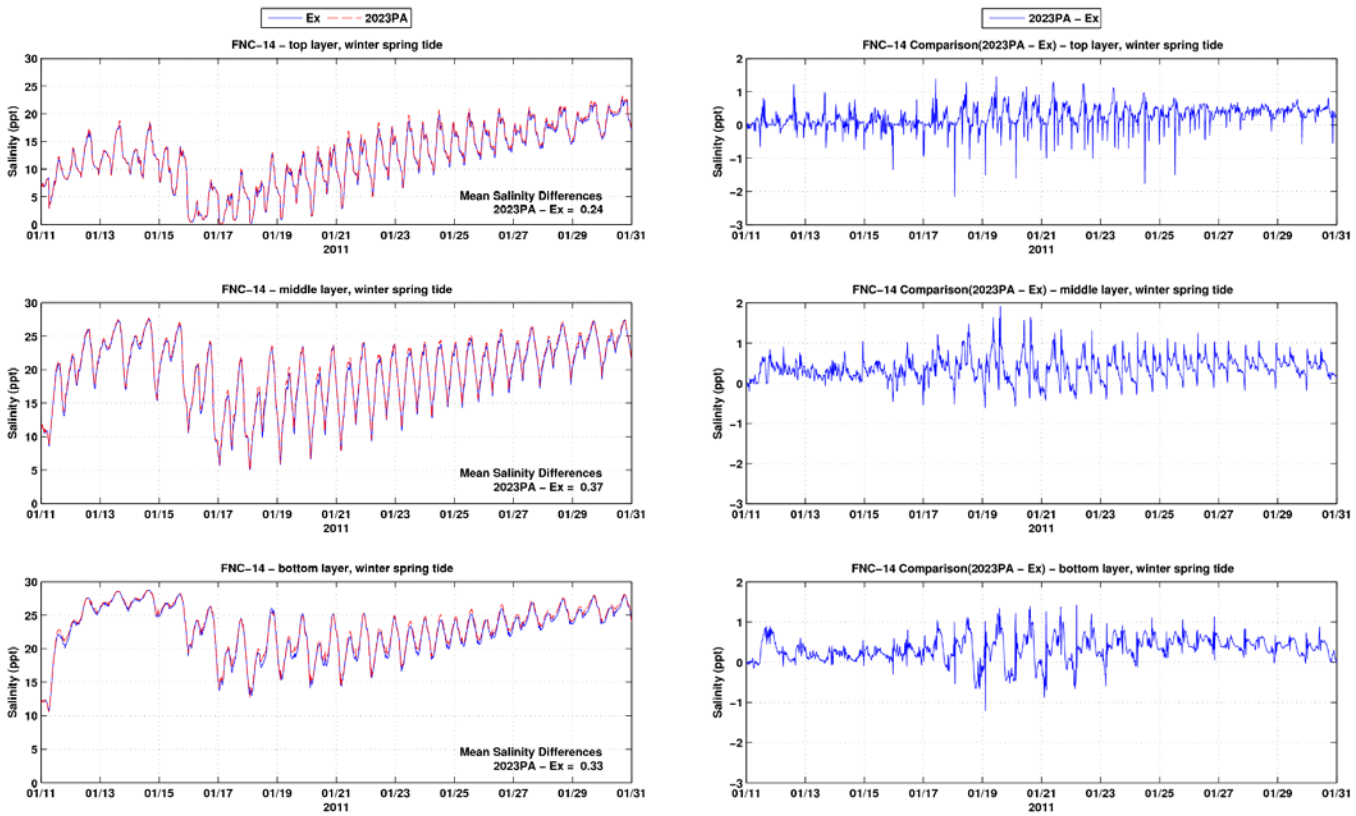

Figure B-22: Salinity time series and differences between the Existing Conditions and the 2023 PA at FNC-14 during winter spring tide period

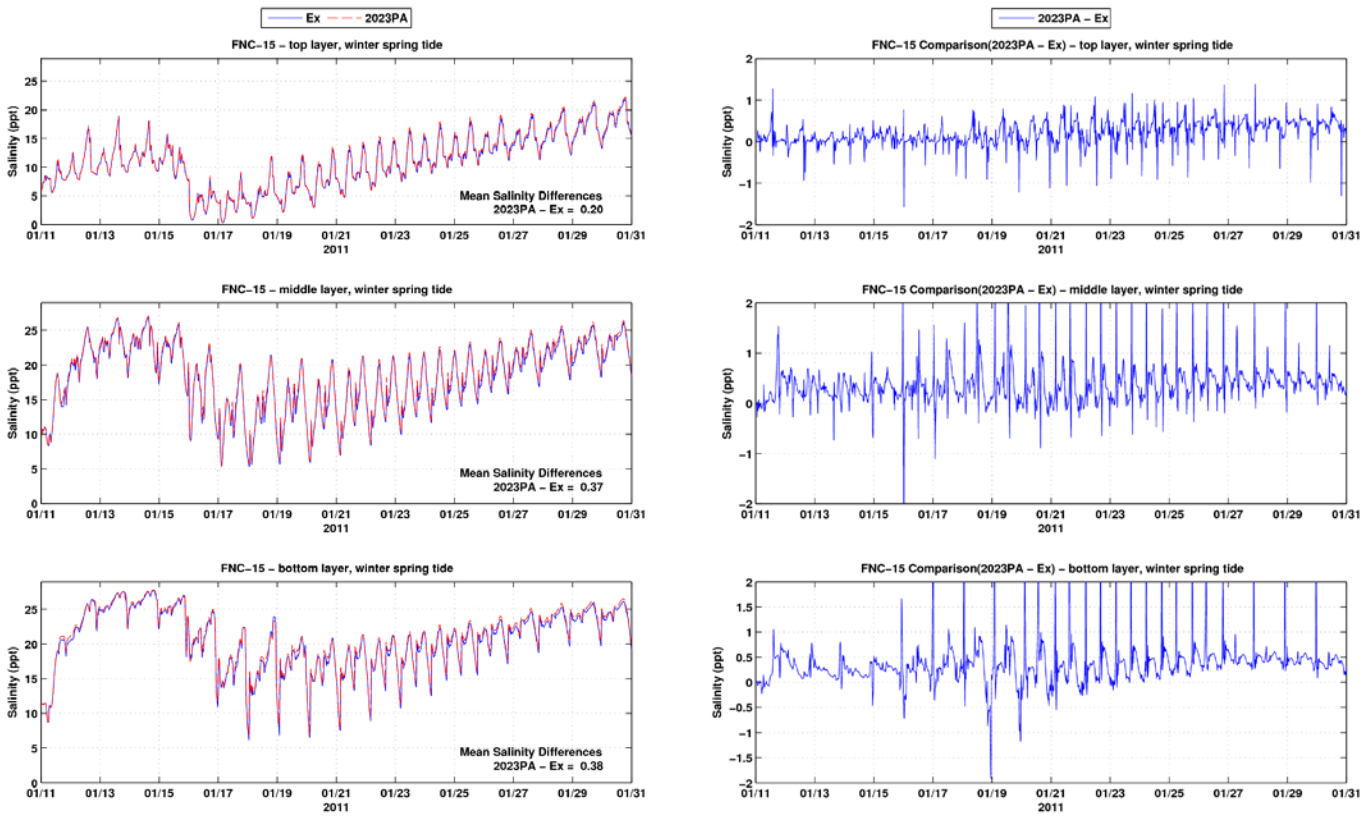

Figure B-23: Salinity time series and differences between the Existing Conditions and the 2023 PA at FNC-15 during winter spring tide period

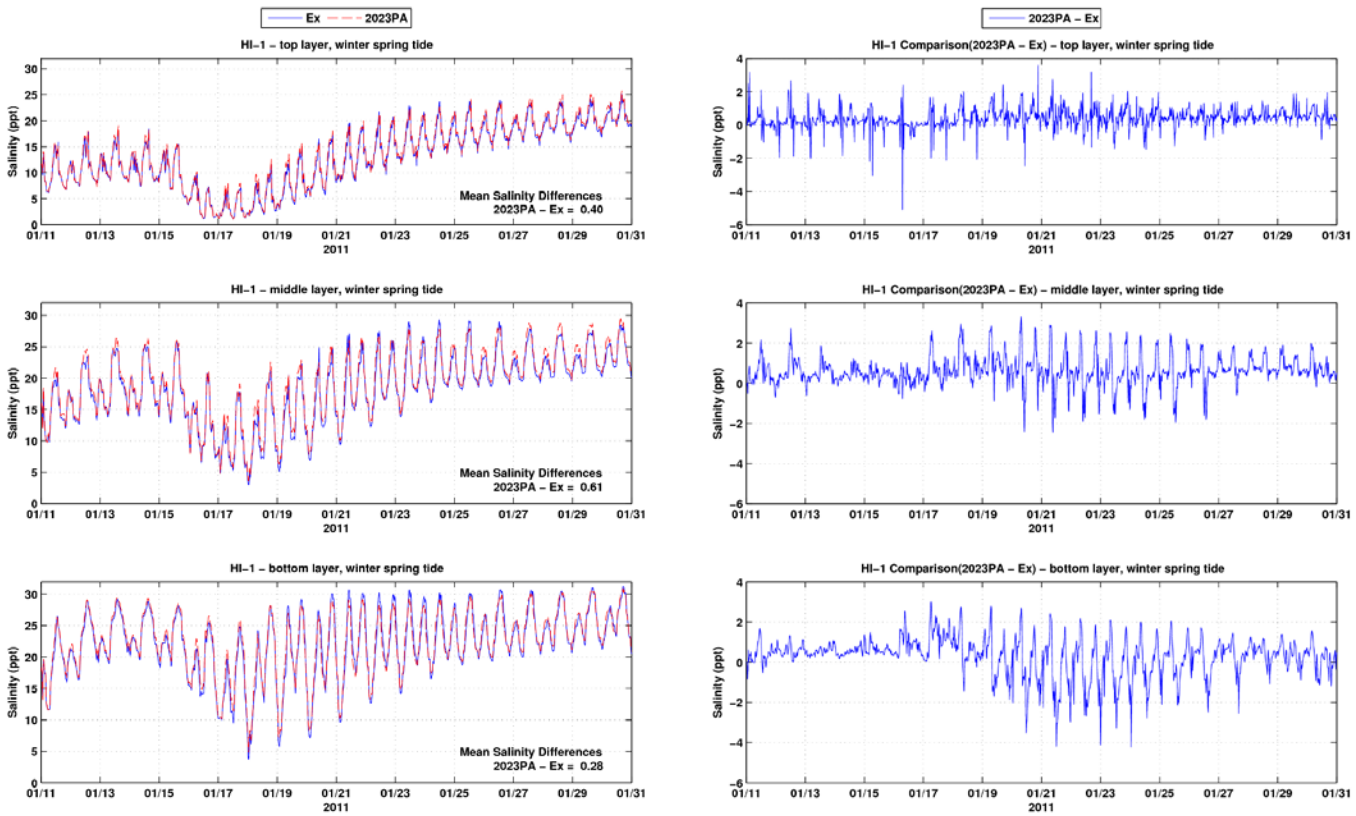

Figure B-24: Salinity time series and differences between the Existing Conditions and the 2023 PA at HI-1 during winter spring tide period

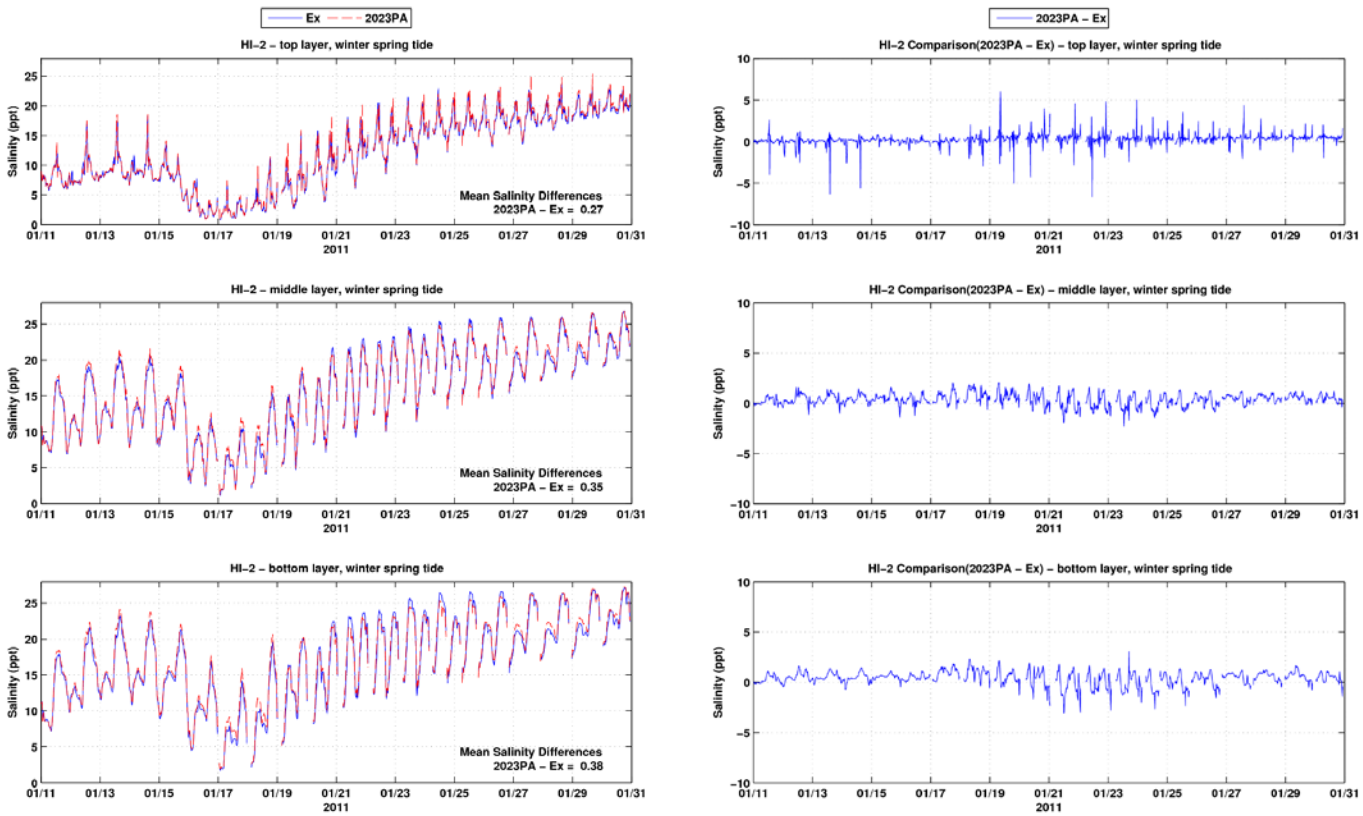

Figure B-25: Salinity time series and differences between the Existing Conditions and the 2023 PA at HI-2 during winter spring tide period

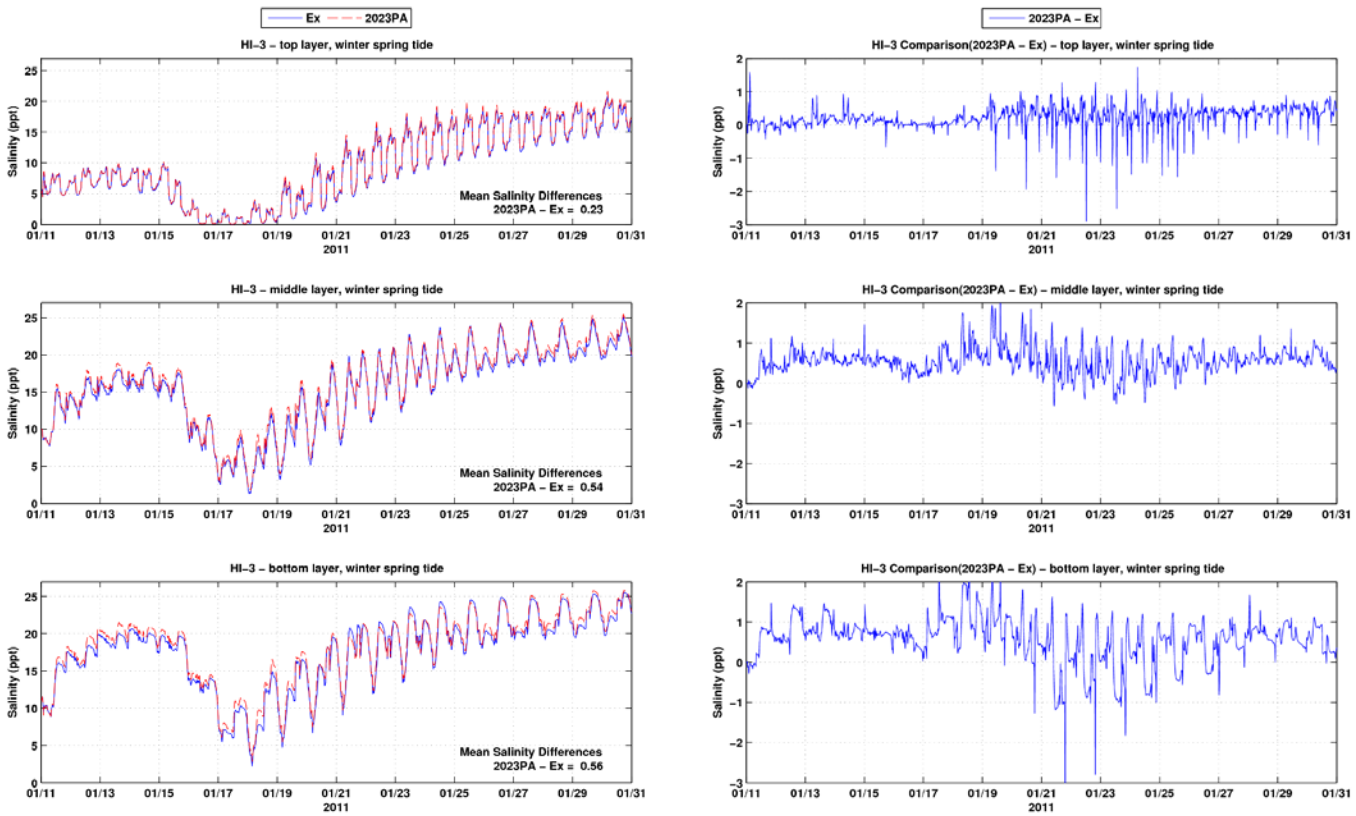

Figure B-26: Salinity time series and differences between the Existing Conditions and the 2023 PA at HI-3 during winter spring tide period

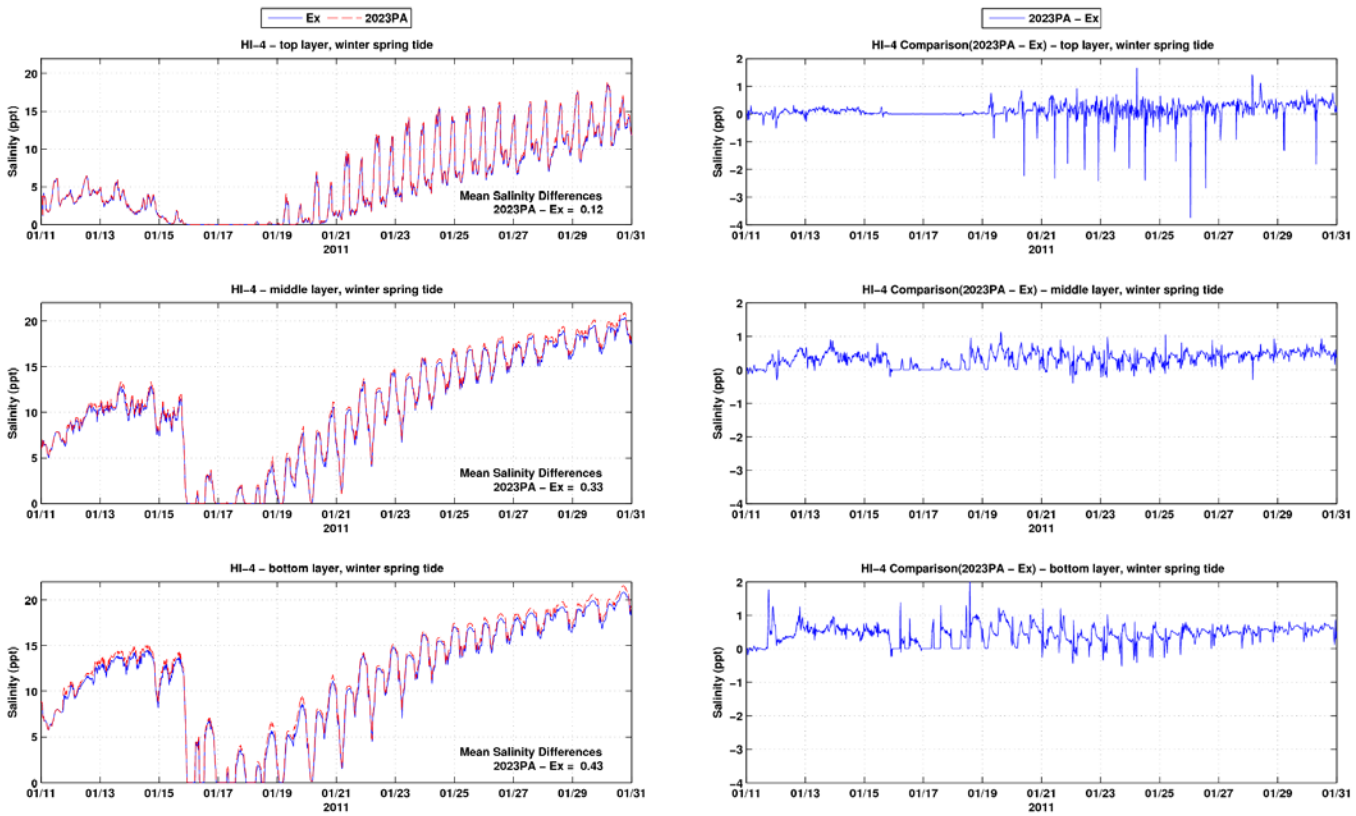

Figure B-27: Salinity time series and differences between the Existing Conditions and the 2023 PA at HI-4 during winter spring tide period

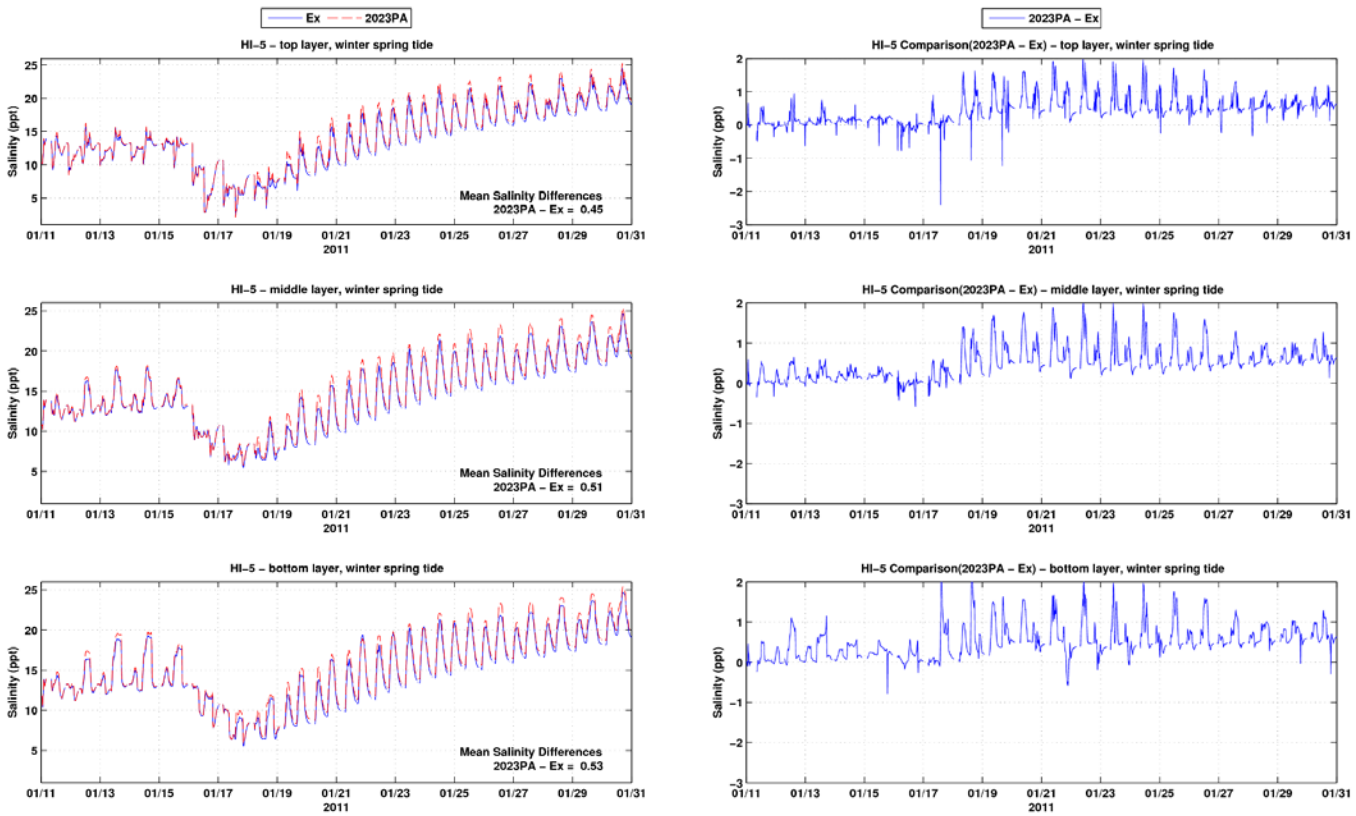

Figure B-28: Salinity time series and differences between the Existing Conditions and the 2023 PA at HI-5 during winter spring tide period

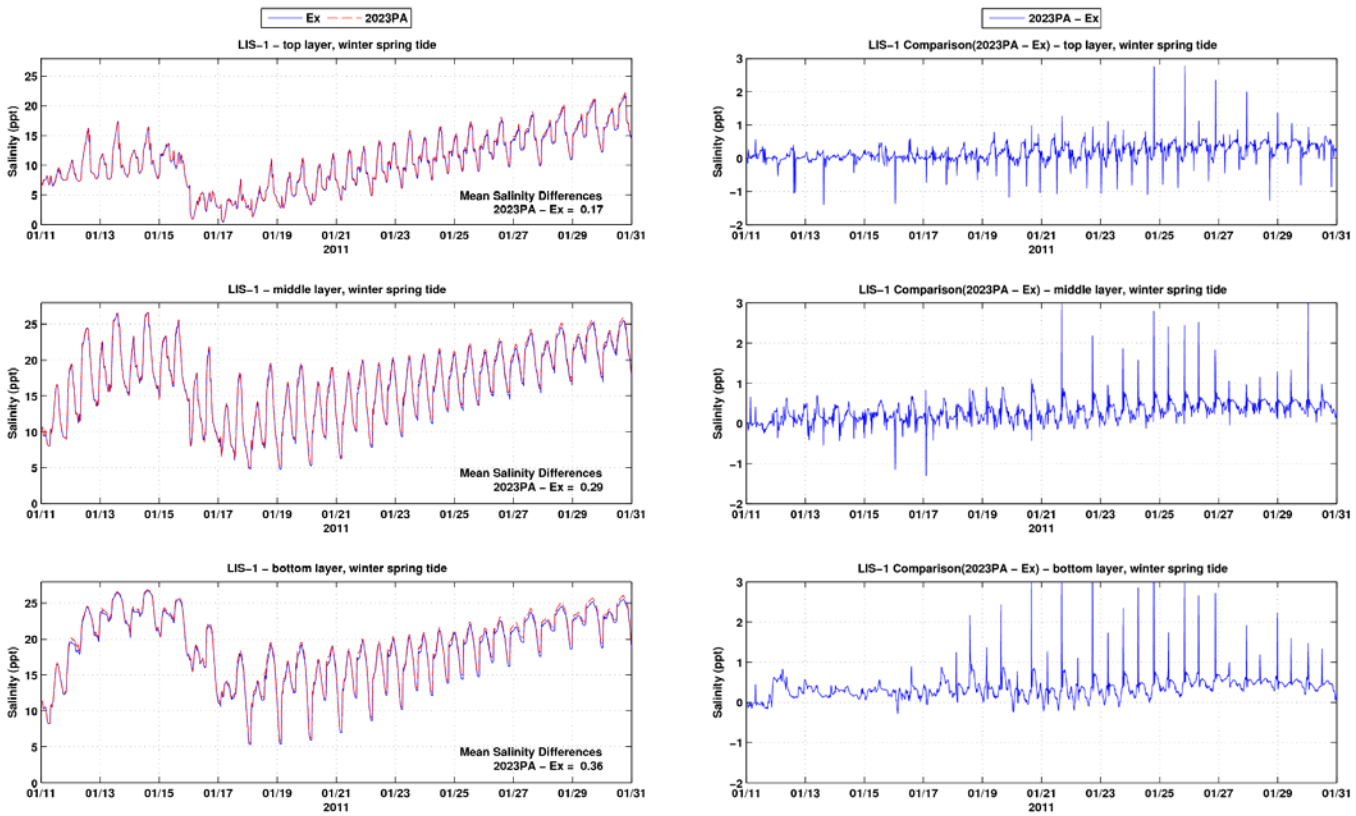

Figure B-29: Salinity time series and differences between the Existing Conditions and the 2023 PA at LIS-1 during winter spring tide period

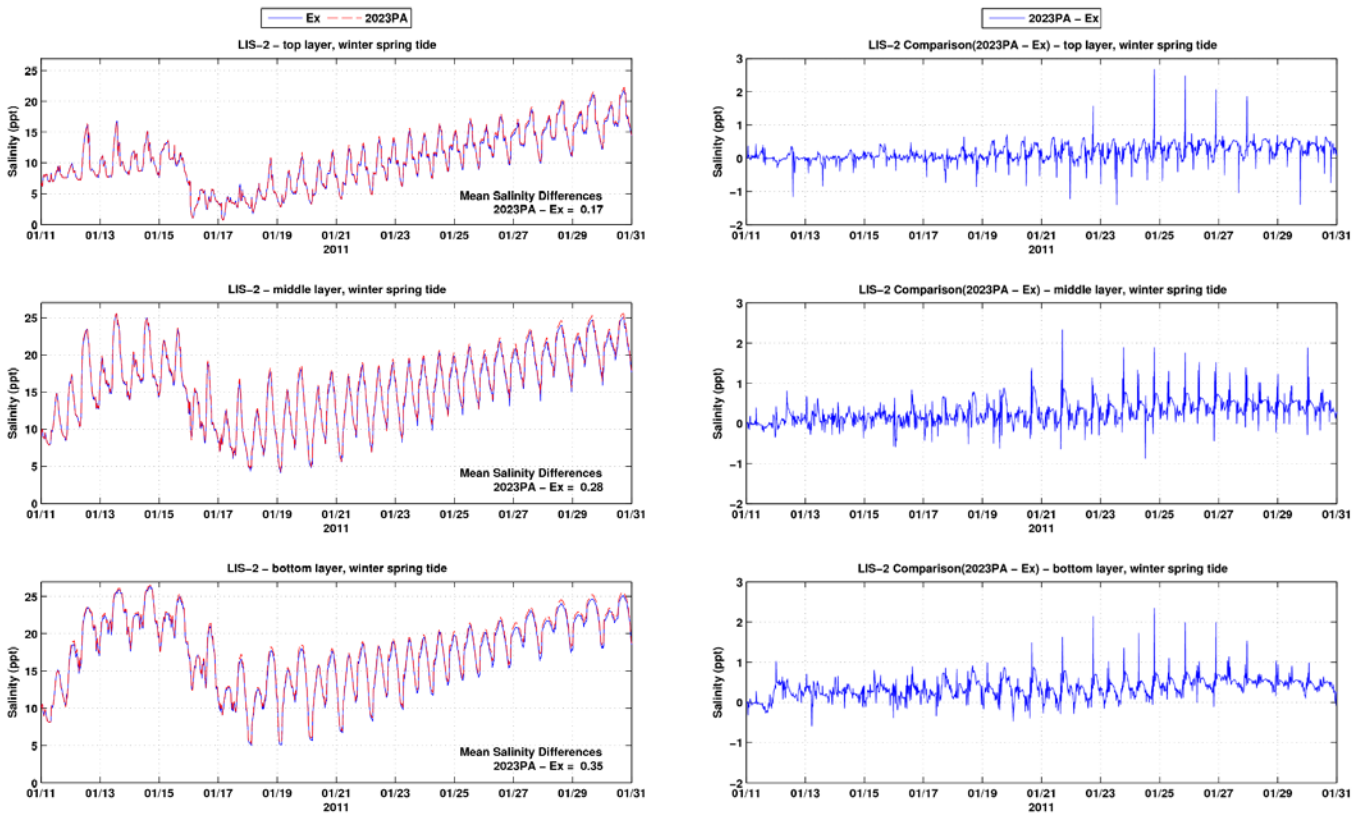

Figure B-30: Salinity time series and differences between the Existing Conditions and the 2023 PA at LIS-2 during winter spring tide period

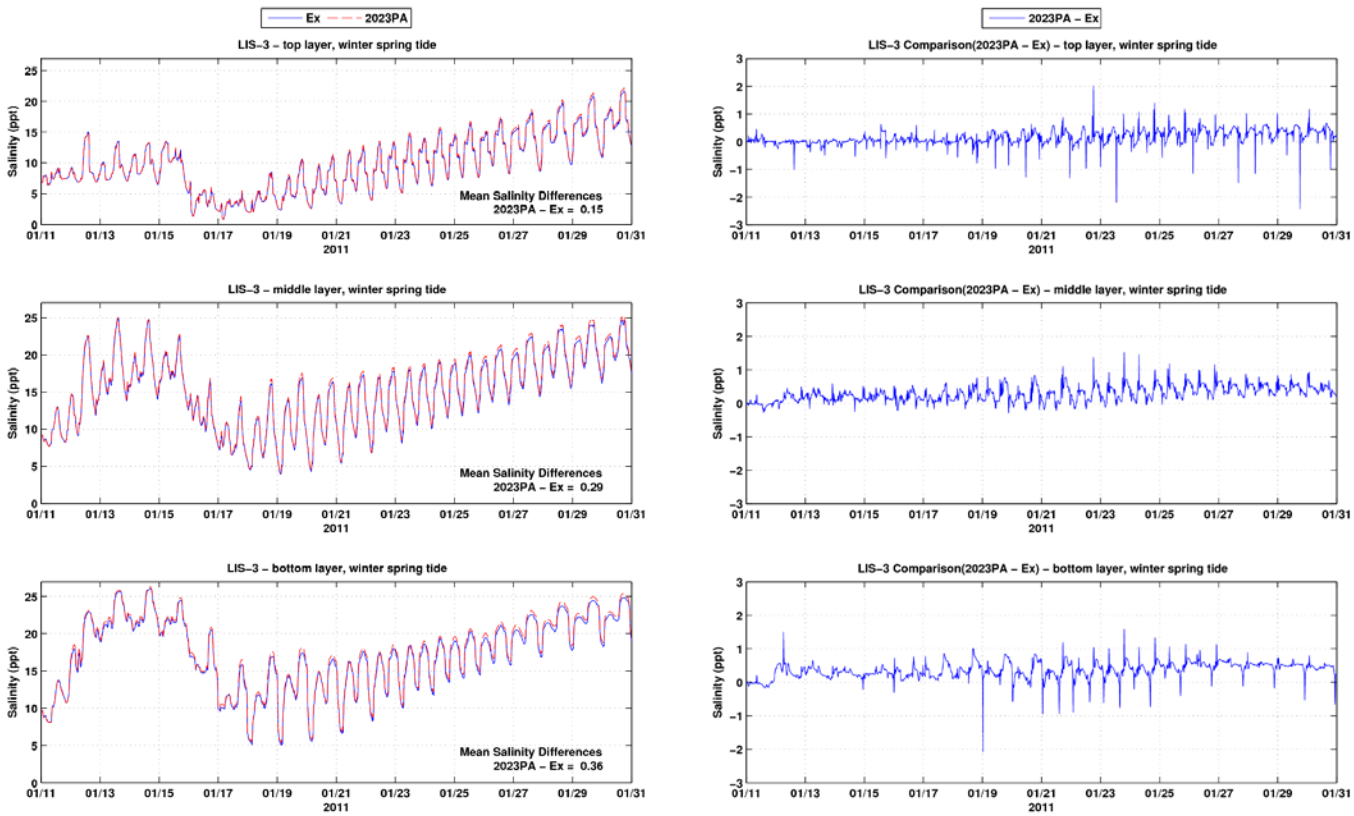

Figure B-31: Salinity time series and differences between the Existing Conditions and the 2023 PA at LIS-3 during winter spring tide period

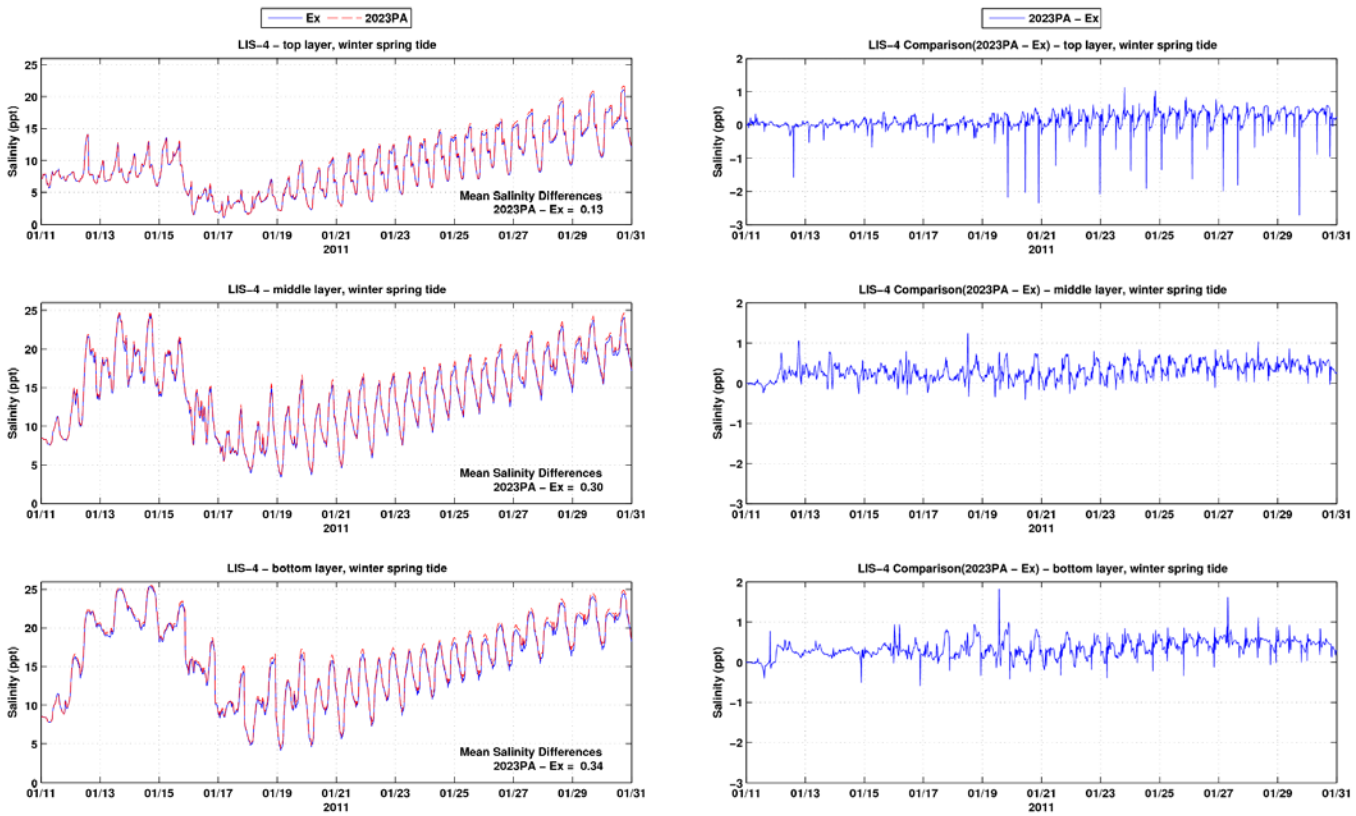

Figure B-32: Salinity time series and differences between the Existing Conditions and the 2023 PA at LIS-4 during winter spring tide period

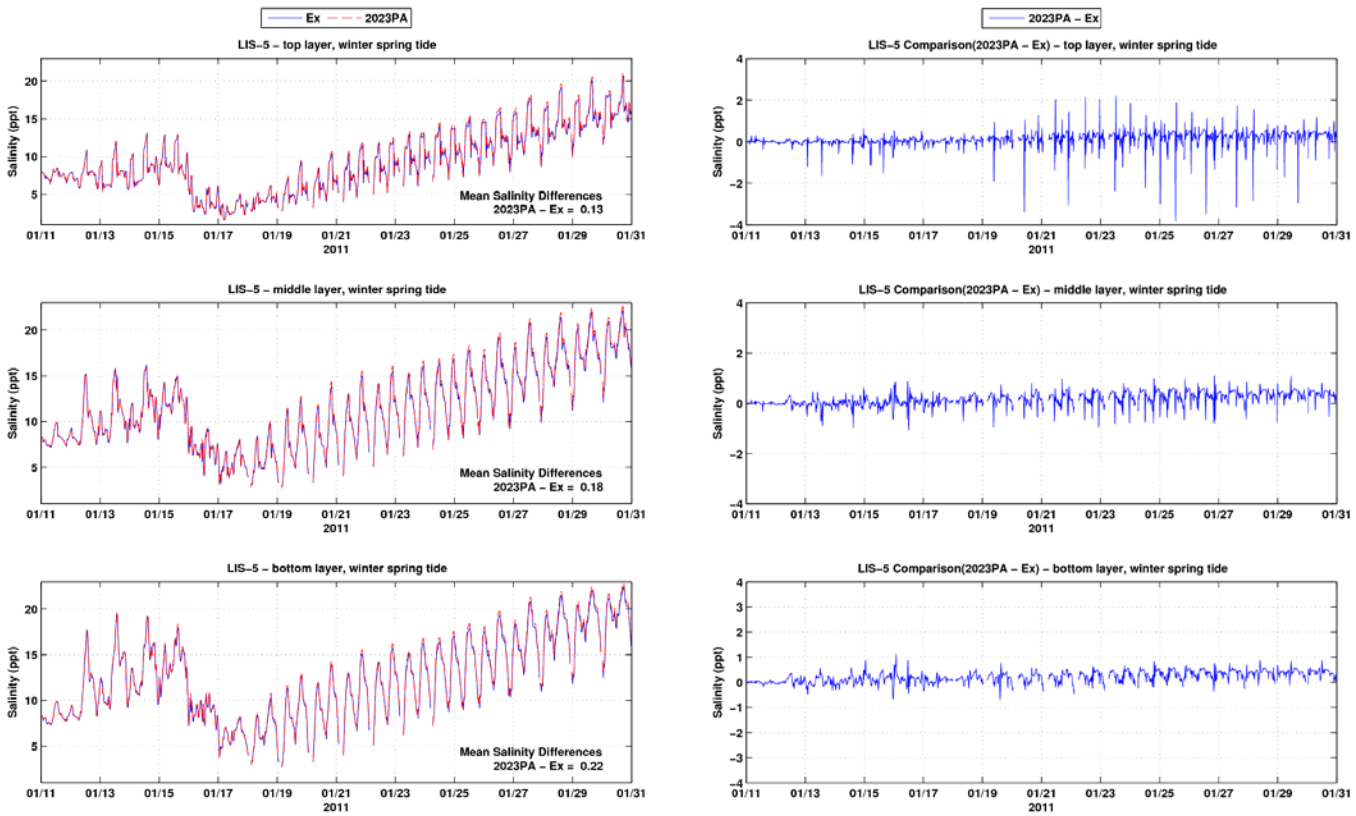

Figure B-33: Salinity time series and differences between the Existing Conditions and the 2023 PA at LIS-5 during winter spring tide period

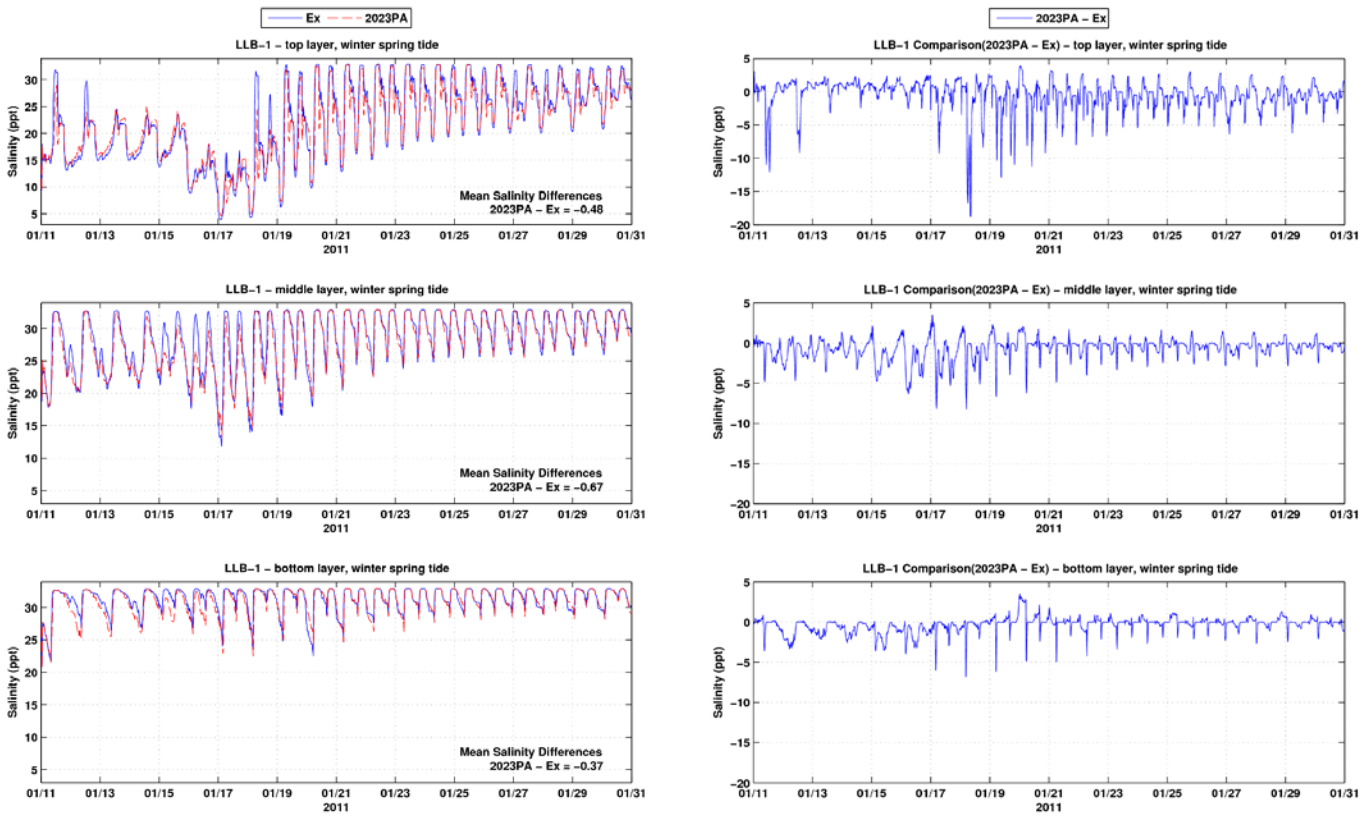

Figure B-34: Salinity time series and differences between the Existing Conditions and the 2023 PA at LLB-1 during winter spring tide period

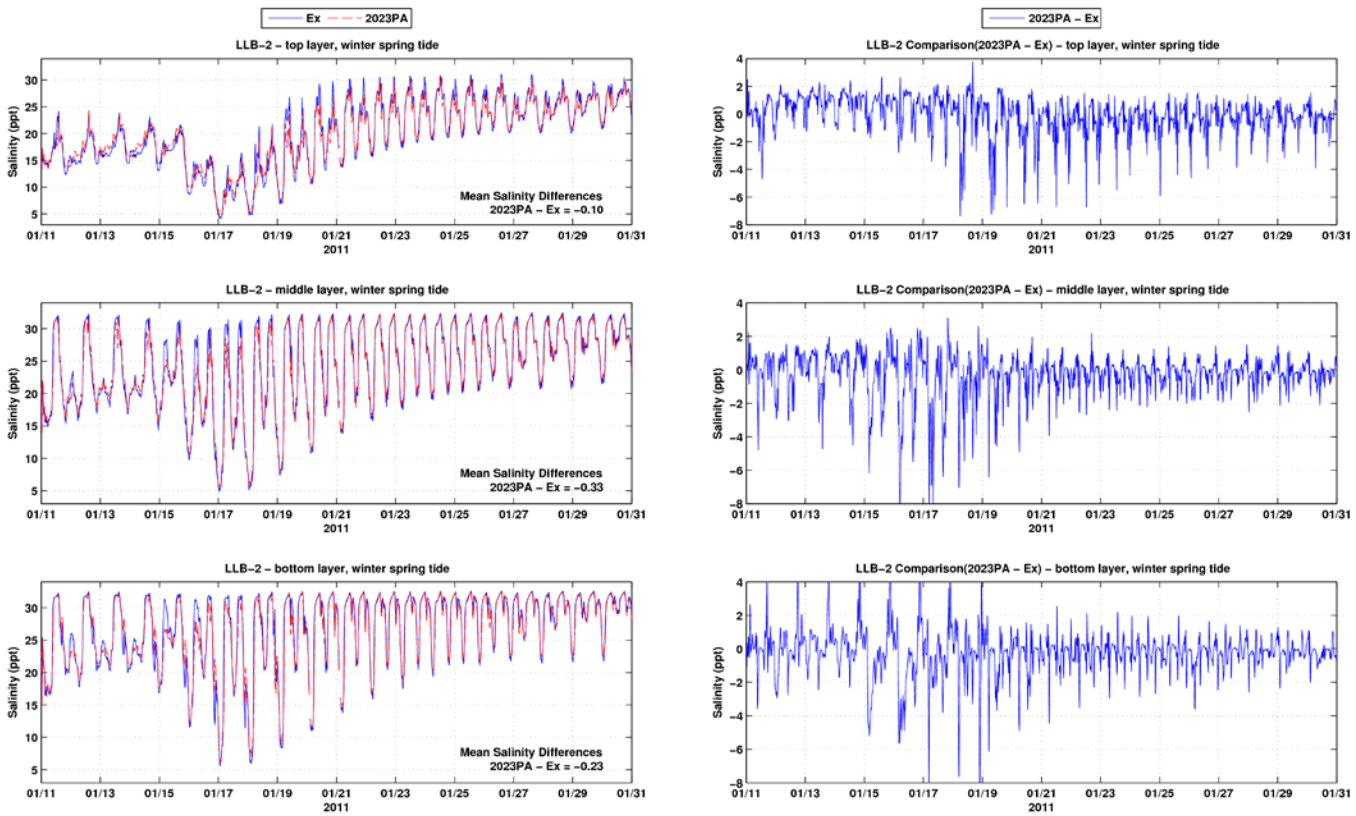

Figure B-35: Salinity time series and differences between the Existing Conditions and the 2023 PA at LLB-2 during winter spring tide period

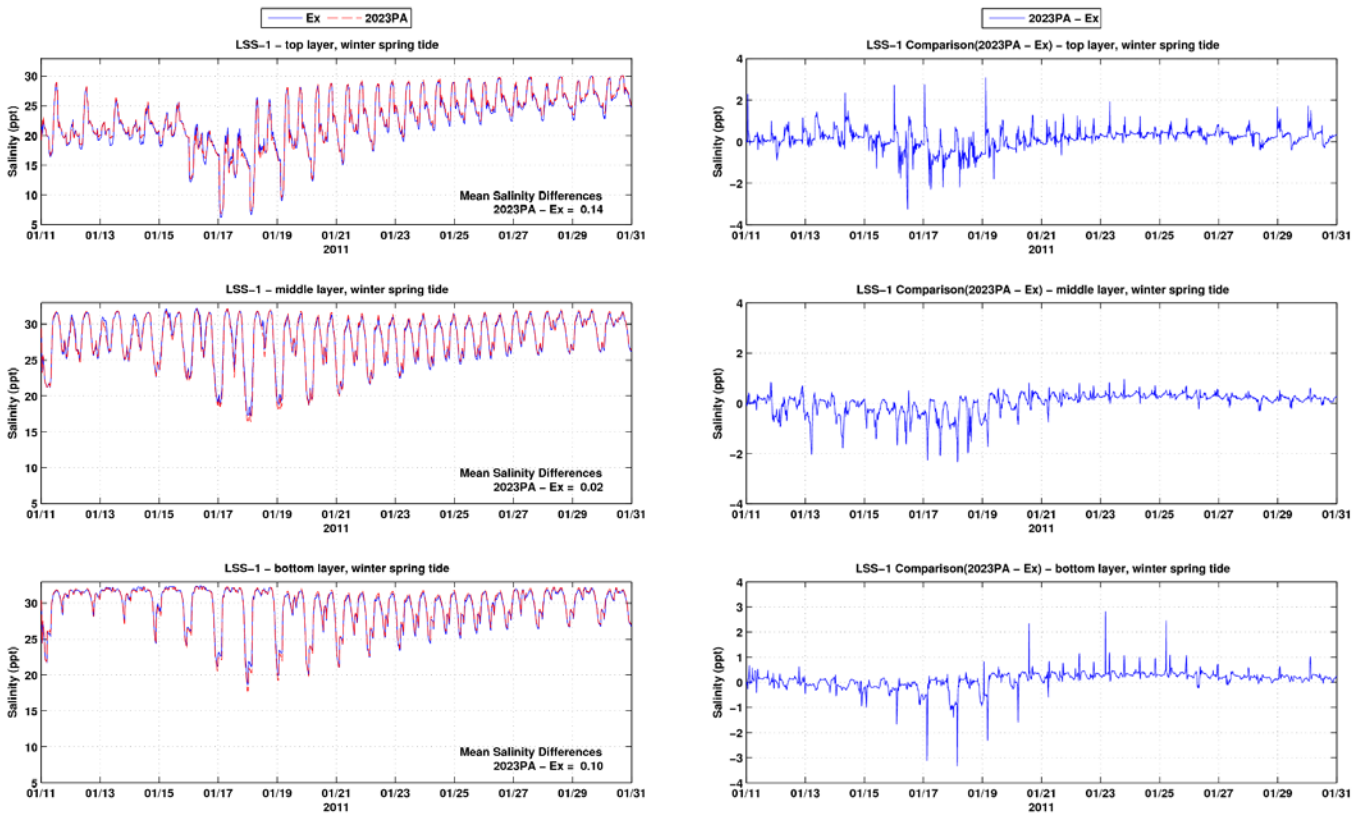

Figure B-36: Salinity time series and differences between the Existing Conditions and the 2023 PA at LSS-1 during winter spring tide period

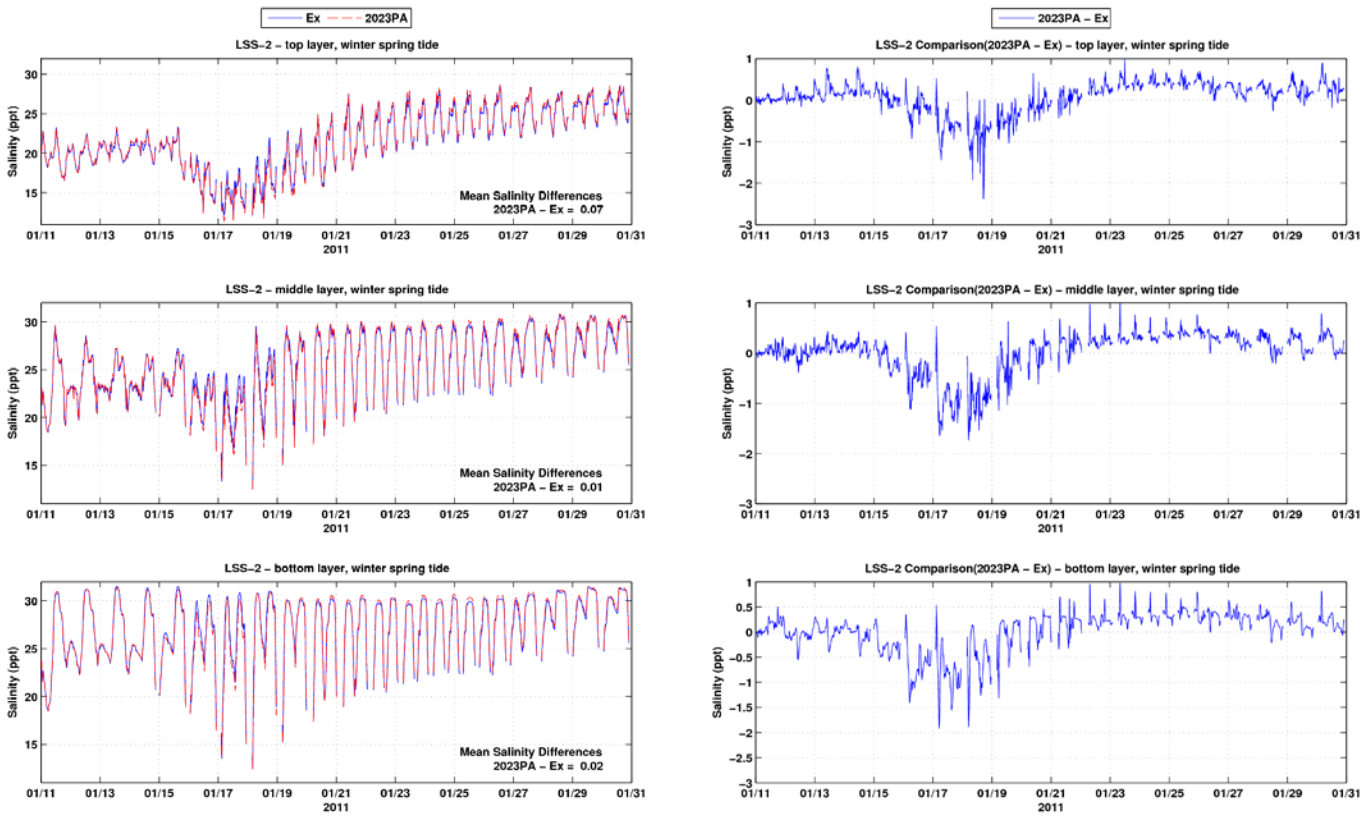

Figure B-37: Salinity time series and differences between the Existing Conditions and the 2023 PA at LSS-2 during winter spring tide period

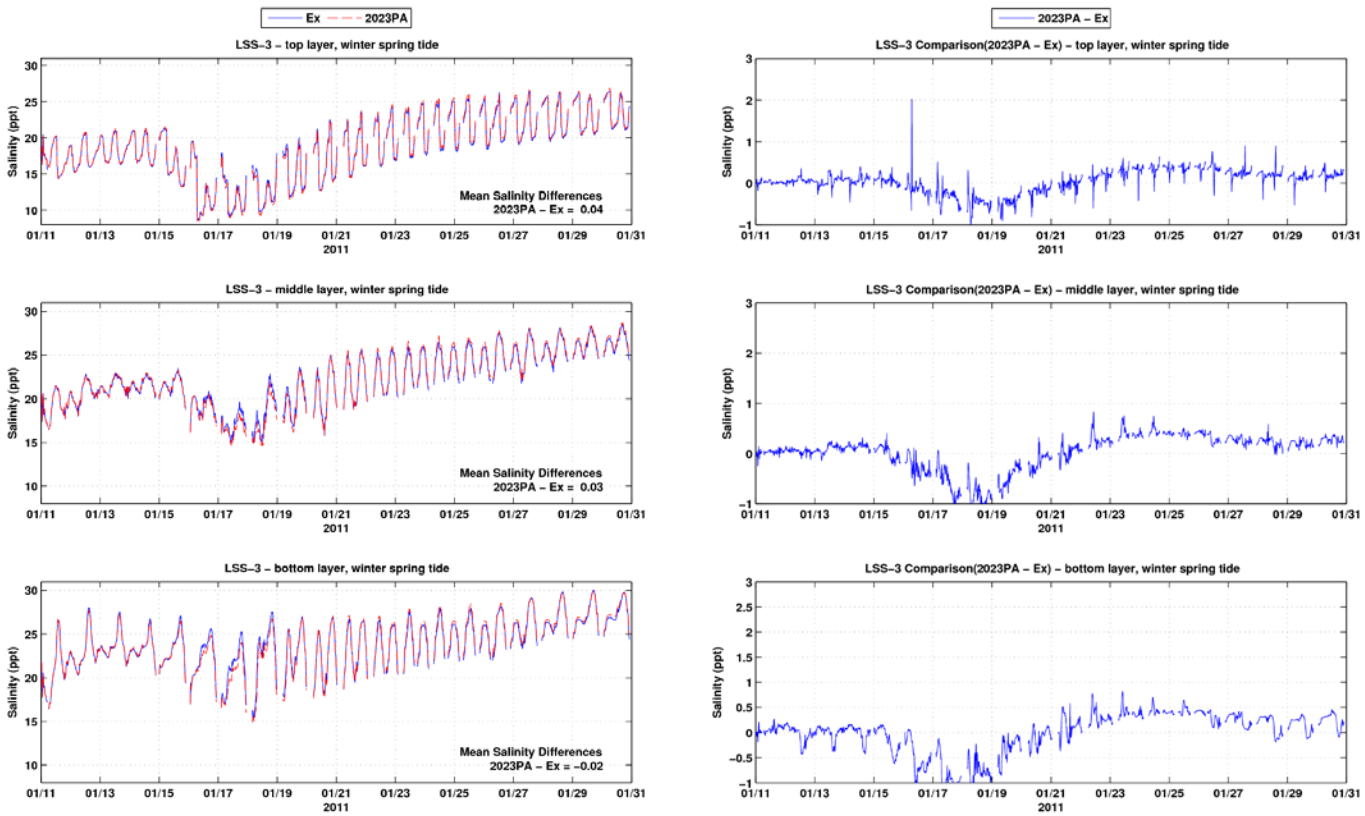

Figure B-38: Salinity time series and differences between the Existing Conditions and the 2023 PA at LSS-3 during winter spring tide period

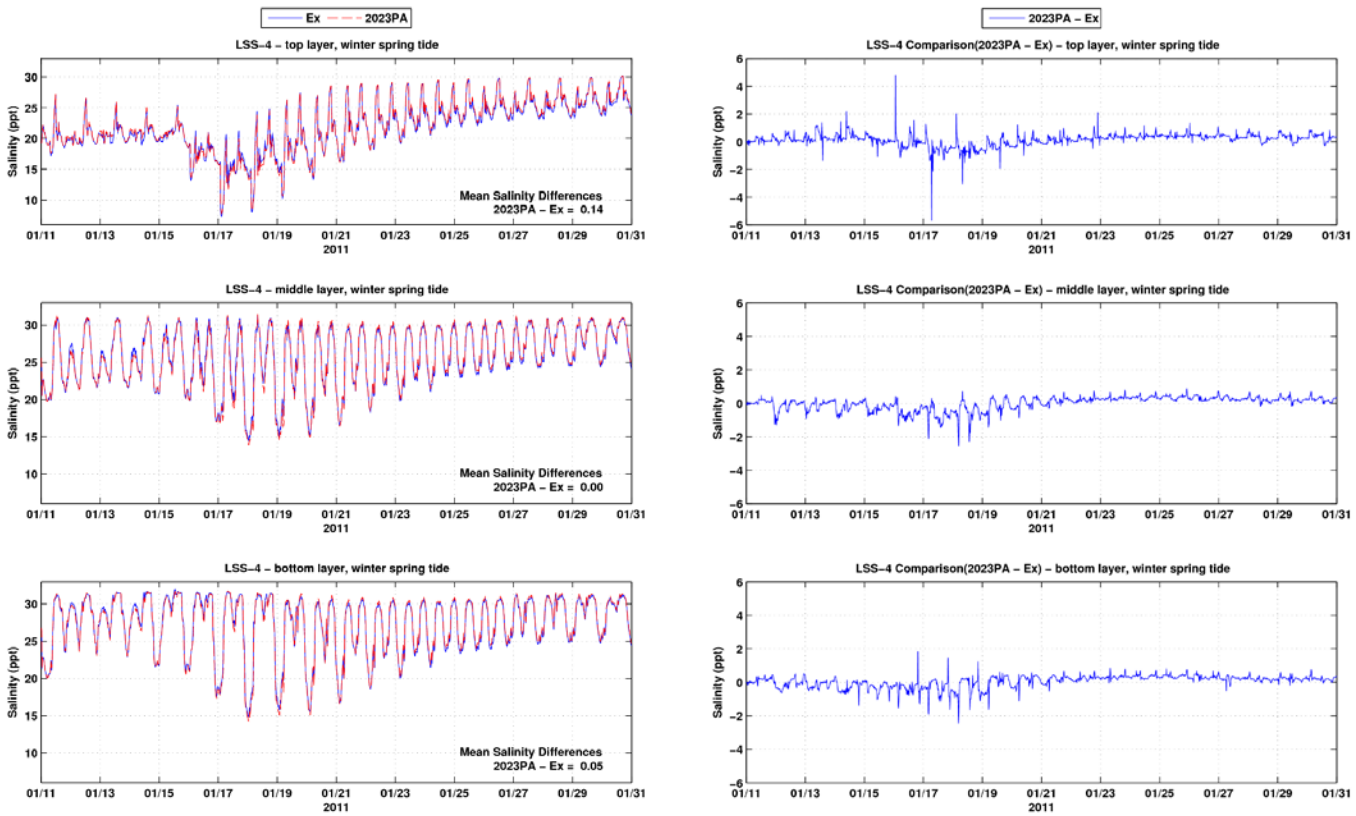

Figure B-39: Salinity time series and differences between the Existing Conditions and the 2023 PA at LSS-4 during winter spring tide period

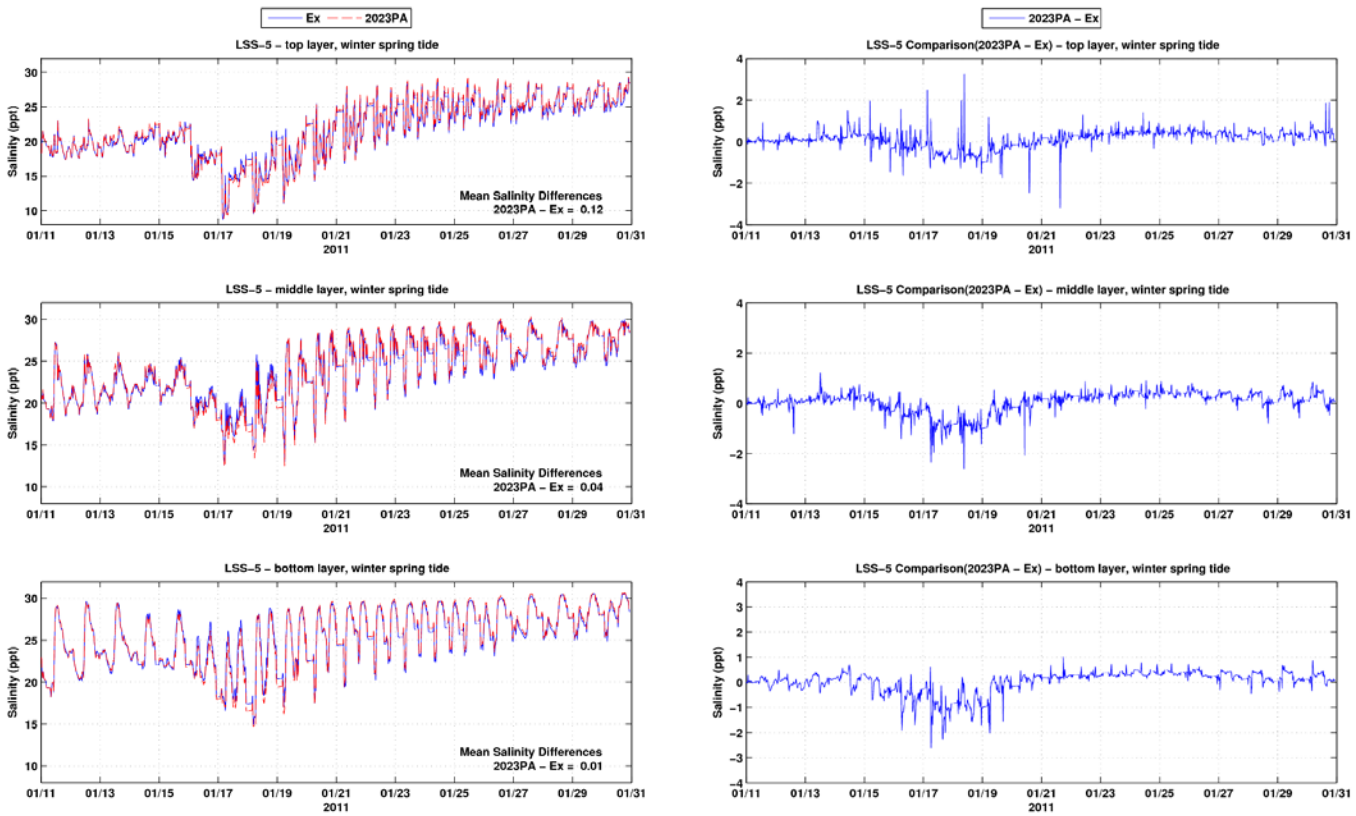

Figure B-40: Salinity time series and differences between the Existing Conditions and the 2023 PA at LSS-5 during winter spring tide period

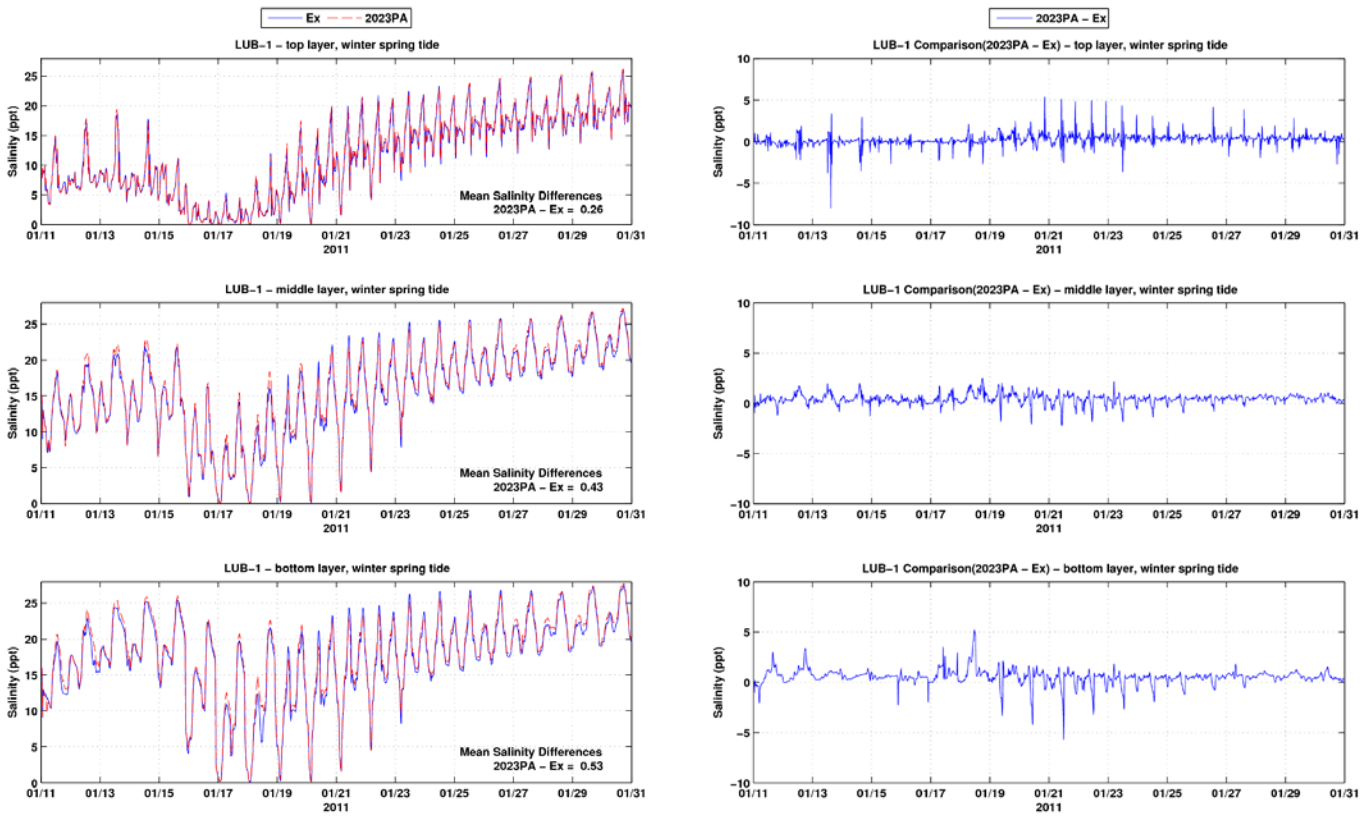

Figure B-41: Salinity time series and differences between the Existing Conditions and the 2023 PA at LUB-1 during winter spring tide period

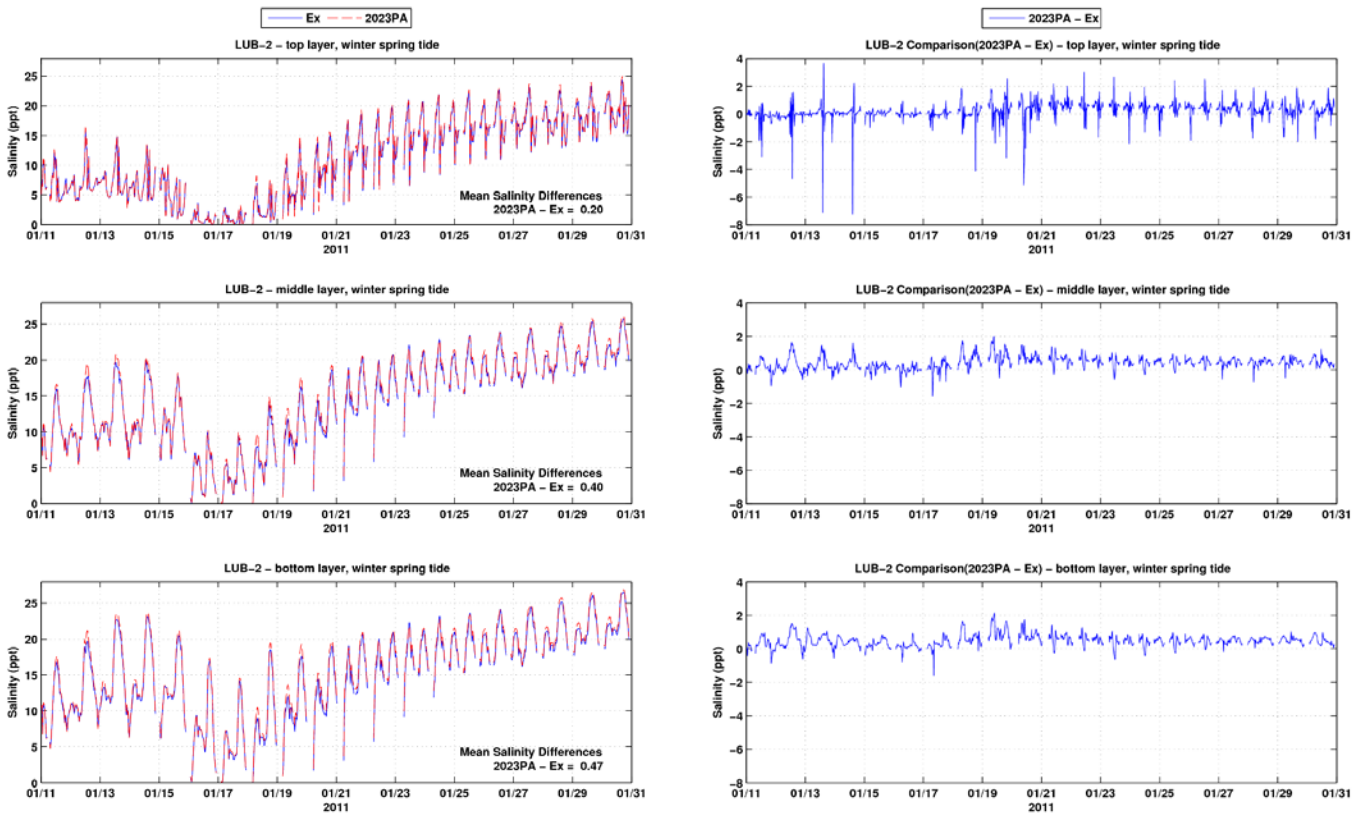

Figure B-42: Salinity time series and differences between the Existing Conditions and the 2023 PA at LUB-2 during winter spring tide period

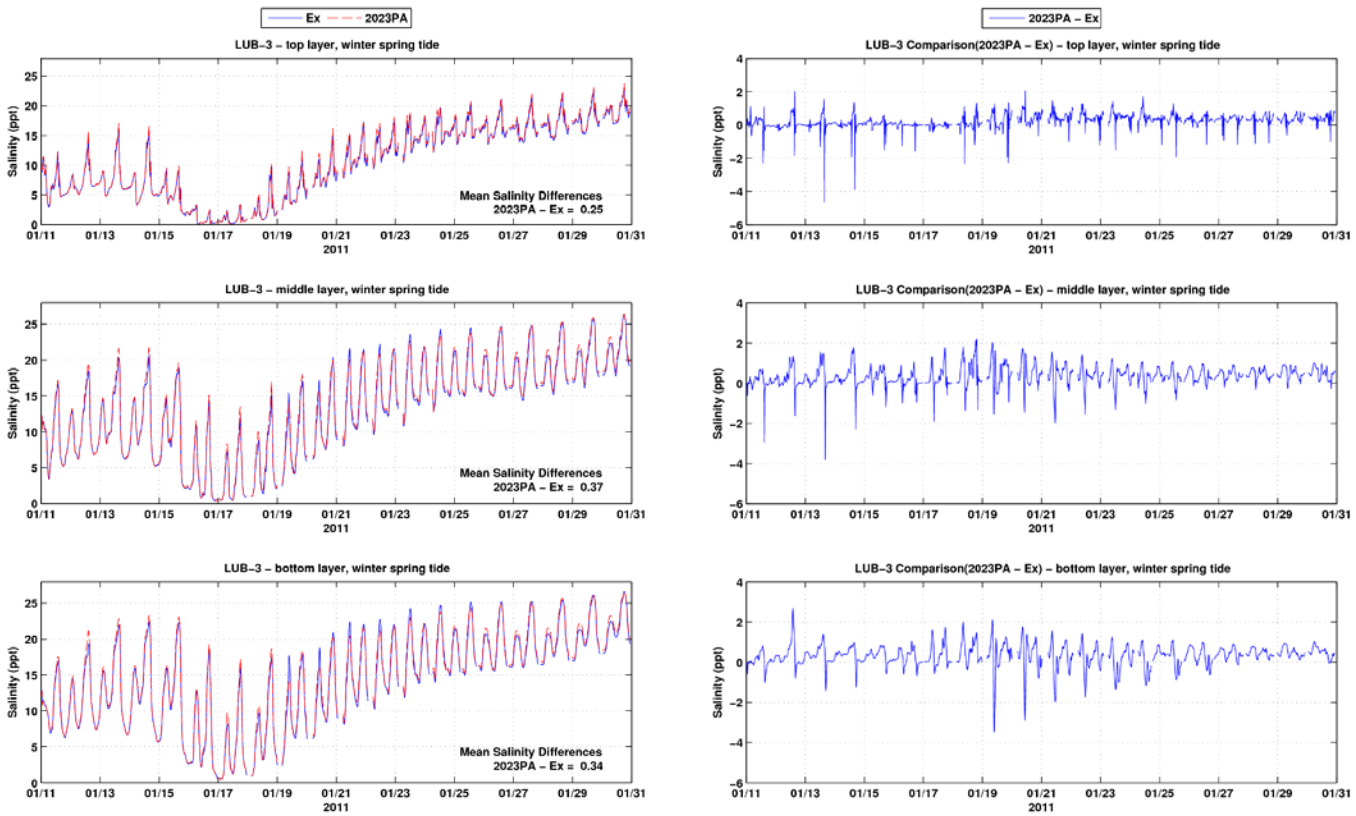

Figure B-43: Salinity time series and differences between the Existing Conditions and the 2023 PA at LUB-3 during winter spring tide period

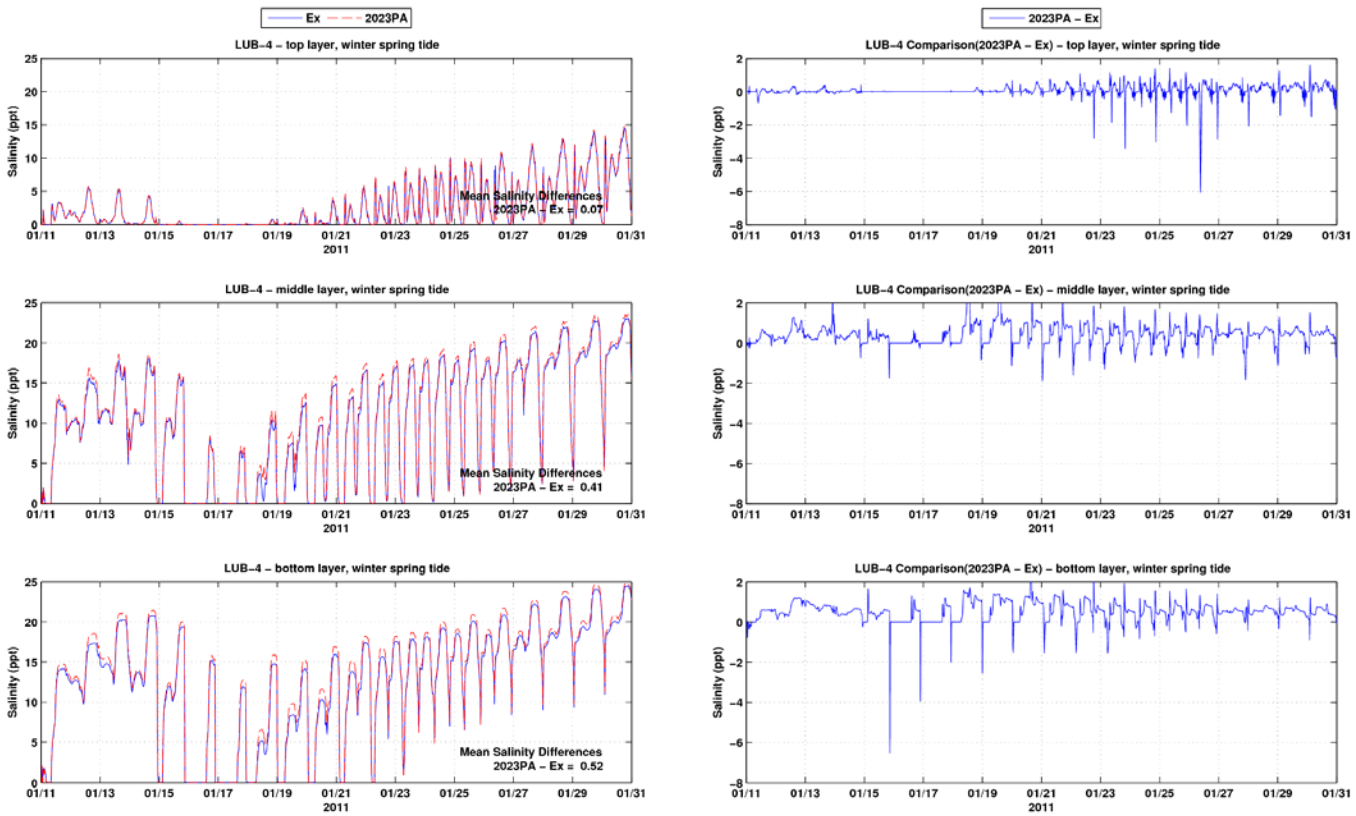

Figure B-44: Salinity time series and differences between the Existing Conditions and the 2023 PA at LUB-4 during winter spring tide period

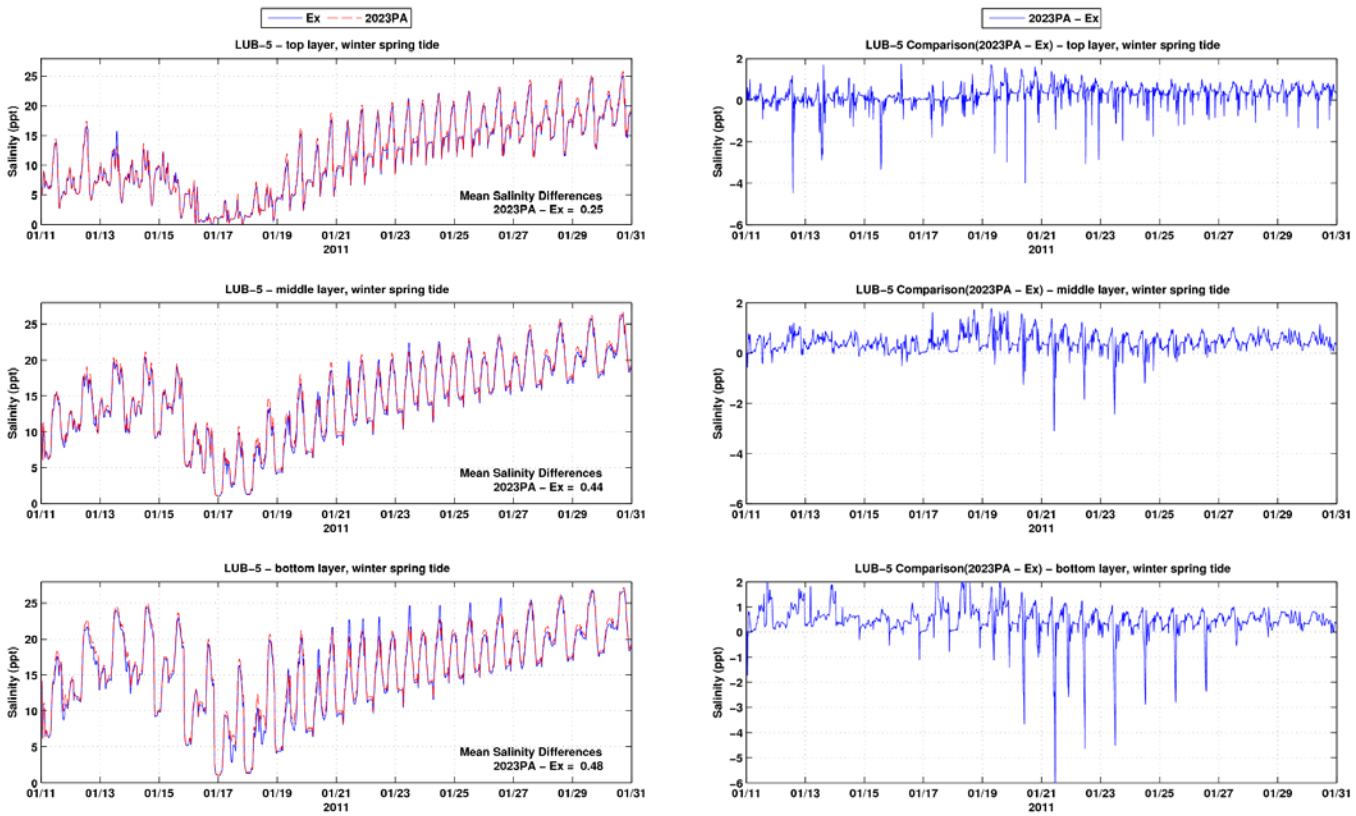

Figure B-45: Salinity time series and differences between the Existing Conditions and the 2023 PA at LUB-5 during winter spring tide period

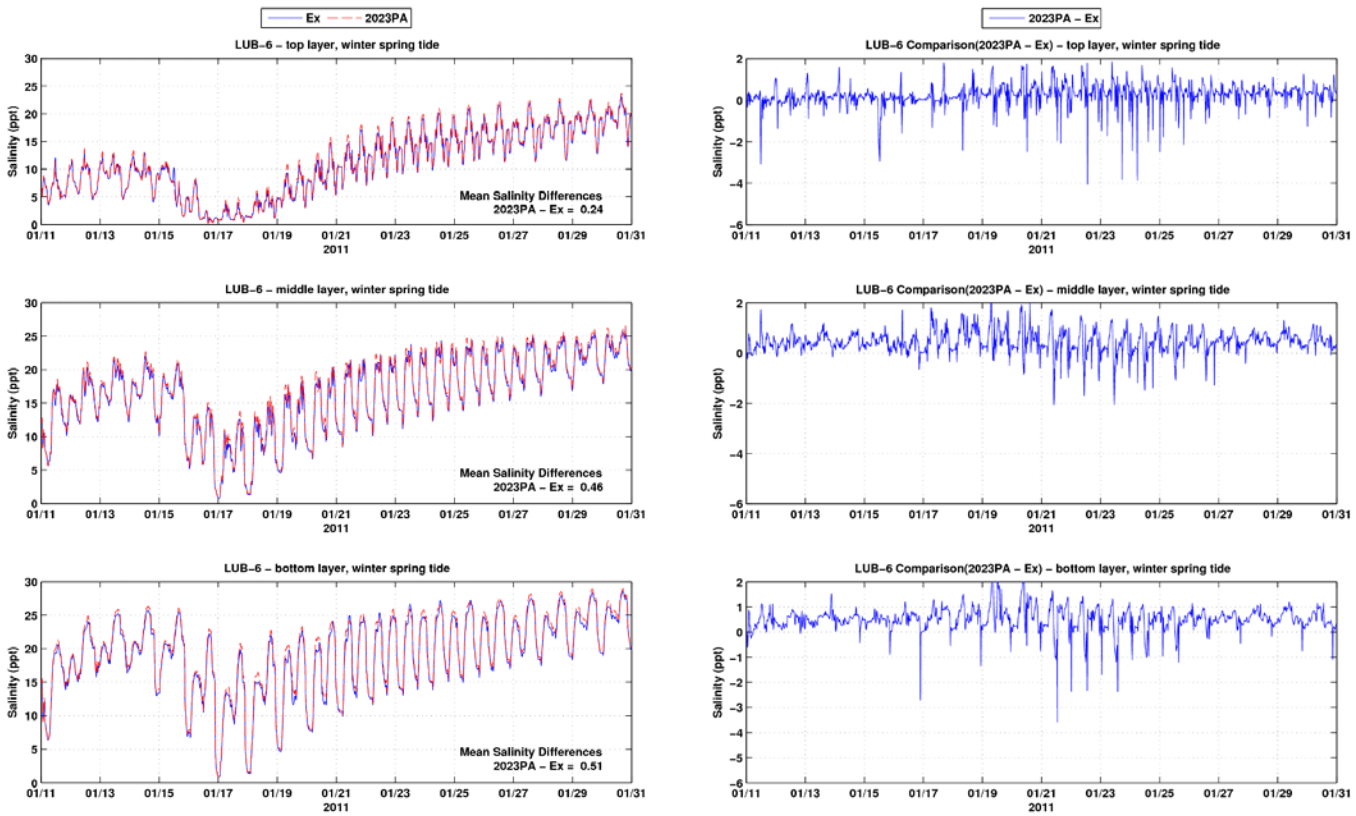

Figure B-46: Salinity time series and differences between the Existing Conditions and the 2023 PA at LUB-6 during winter spring tide period

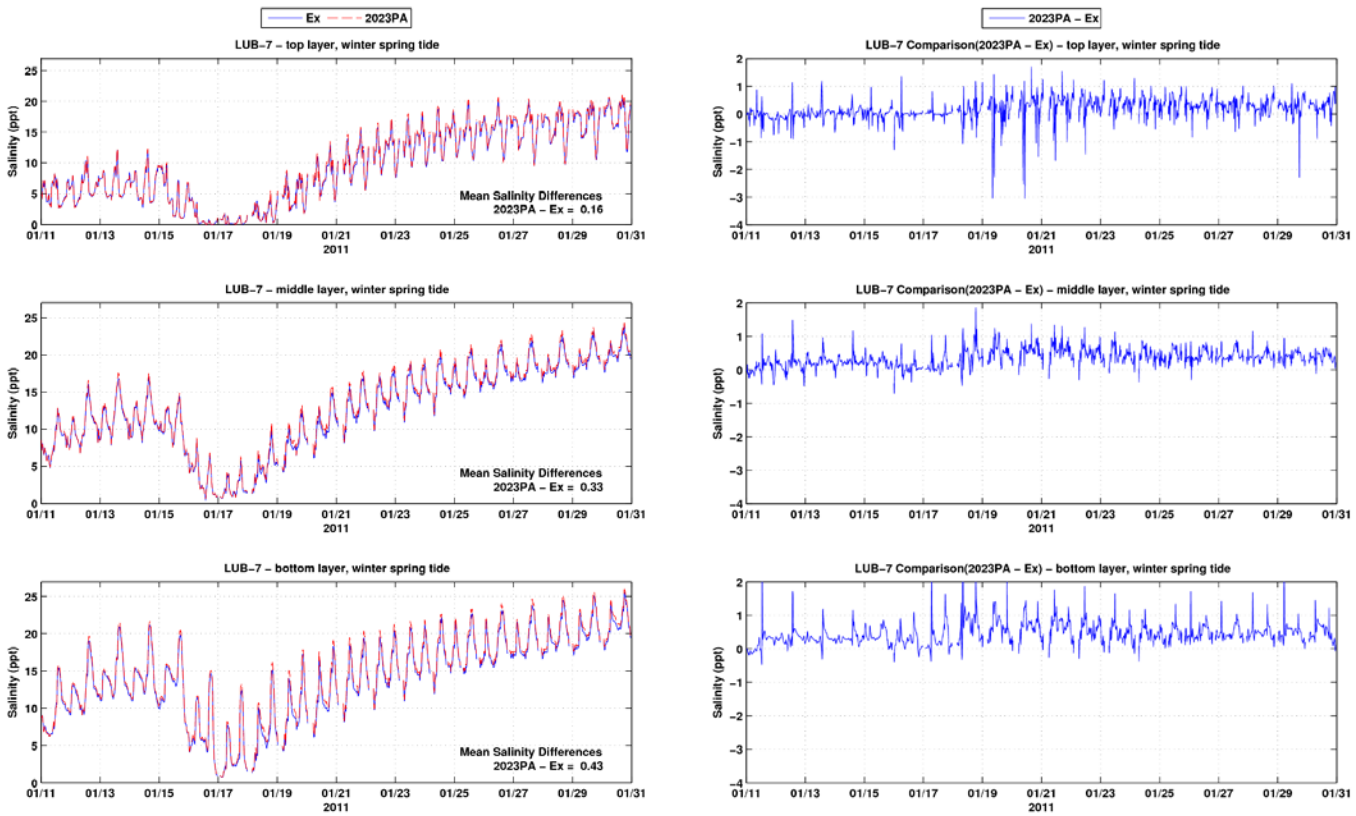

Figure B-47: Salinity time series and differences between the Existing Conditions and the 2023 PA at LUB-7 during winter spring tide period

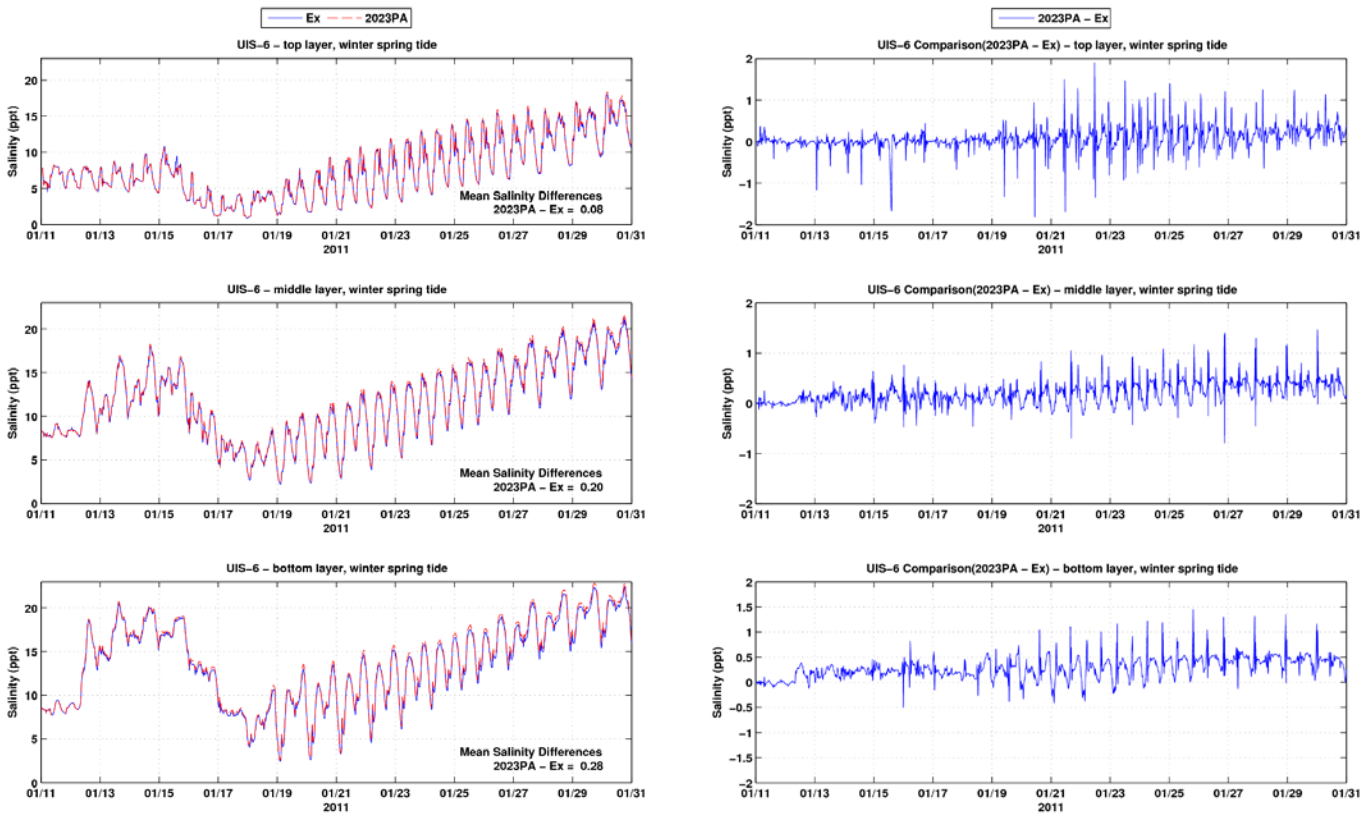

Figure B-48: Salinity time series and differences between the Existing Conditions and the 2023 PA at UIS-6 during winter spring tide period

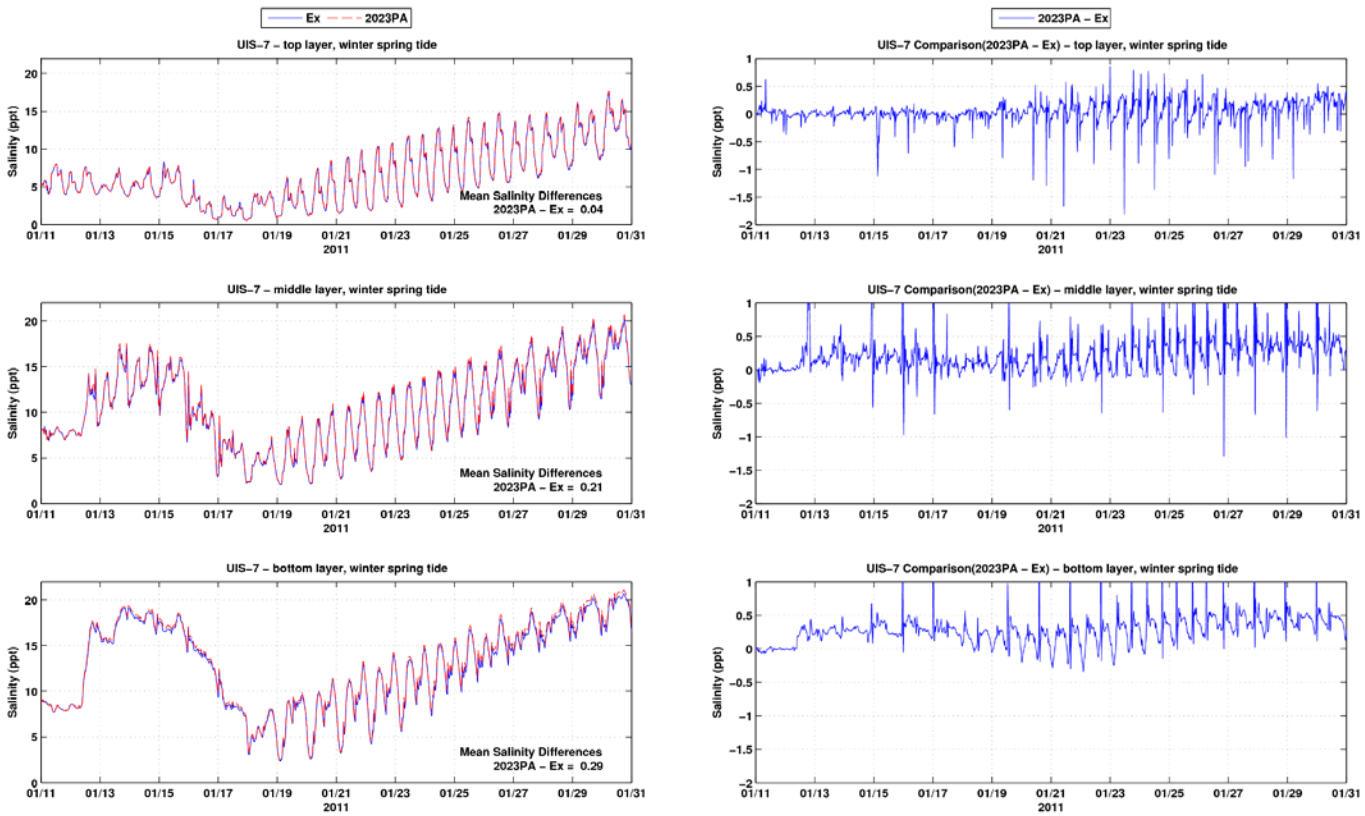

Figure B-49: Salinity time series and differences between the Existing Conditions and the 2023 PA at UIS-7 during winter spring tide period

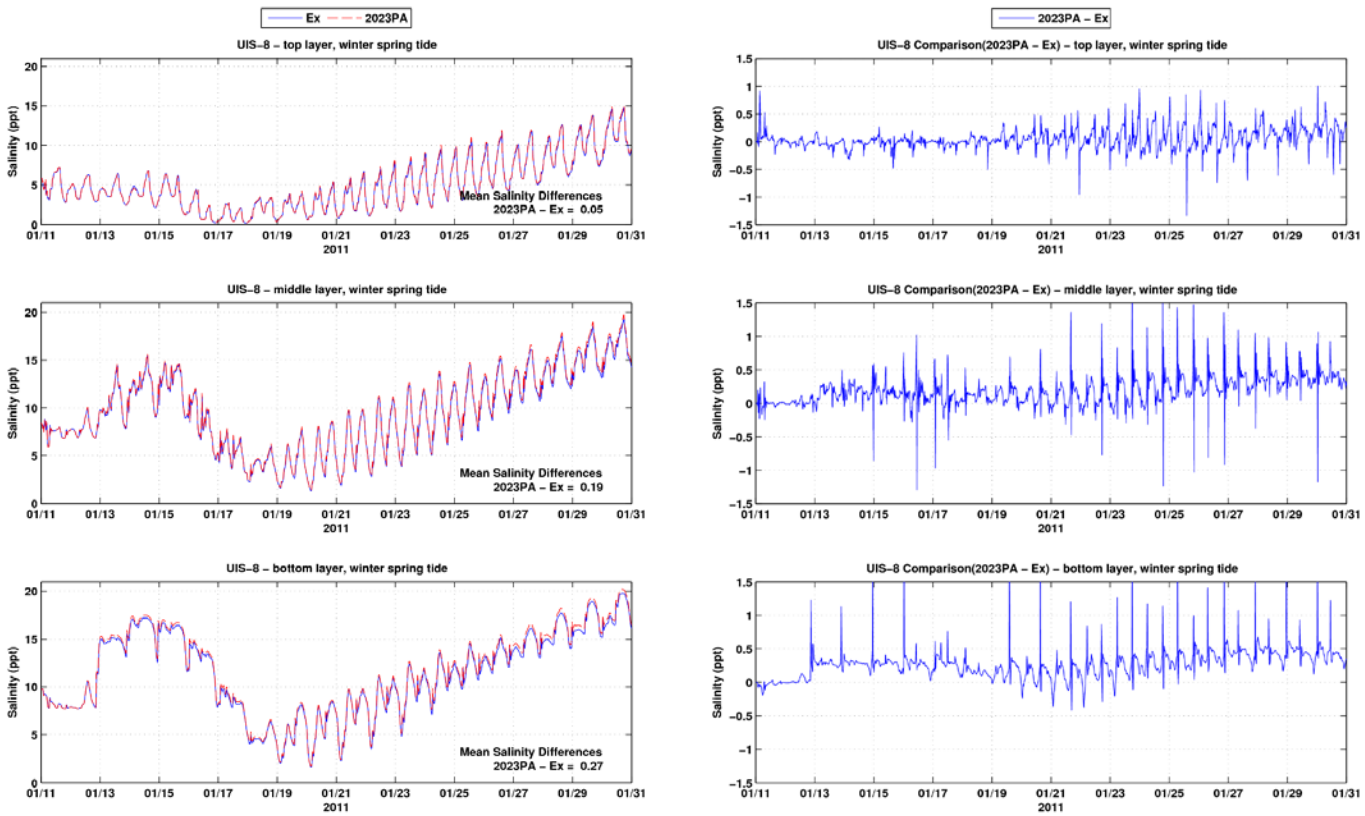

Figure B-50: Salinity time series and differences between the Existing Conditions and the 2023 PA at UIS-8 during winter spring tide period

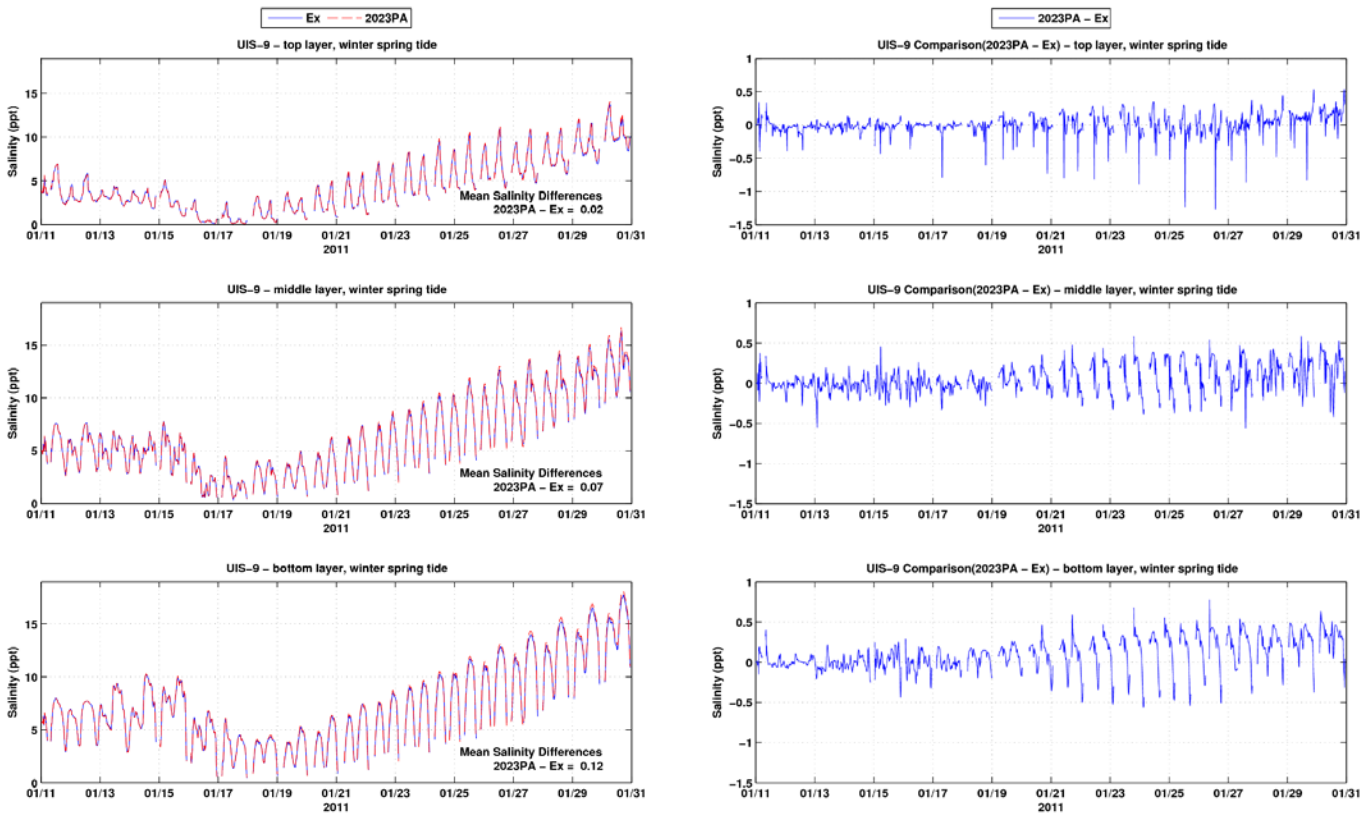

Figure B-51: Salinity time series and differences between the Existing Conditions and the 2023 PA at UIS-9 during winter spring tide period

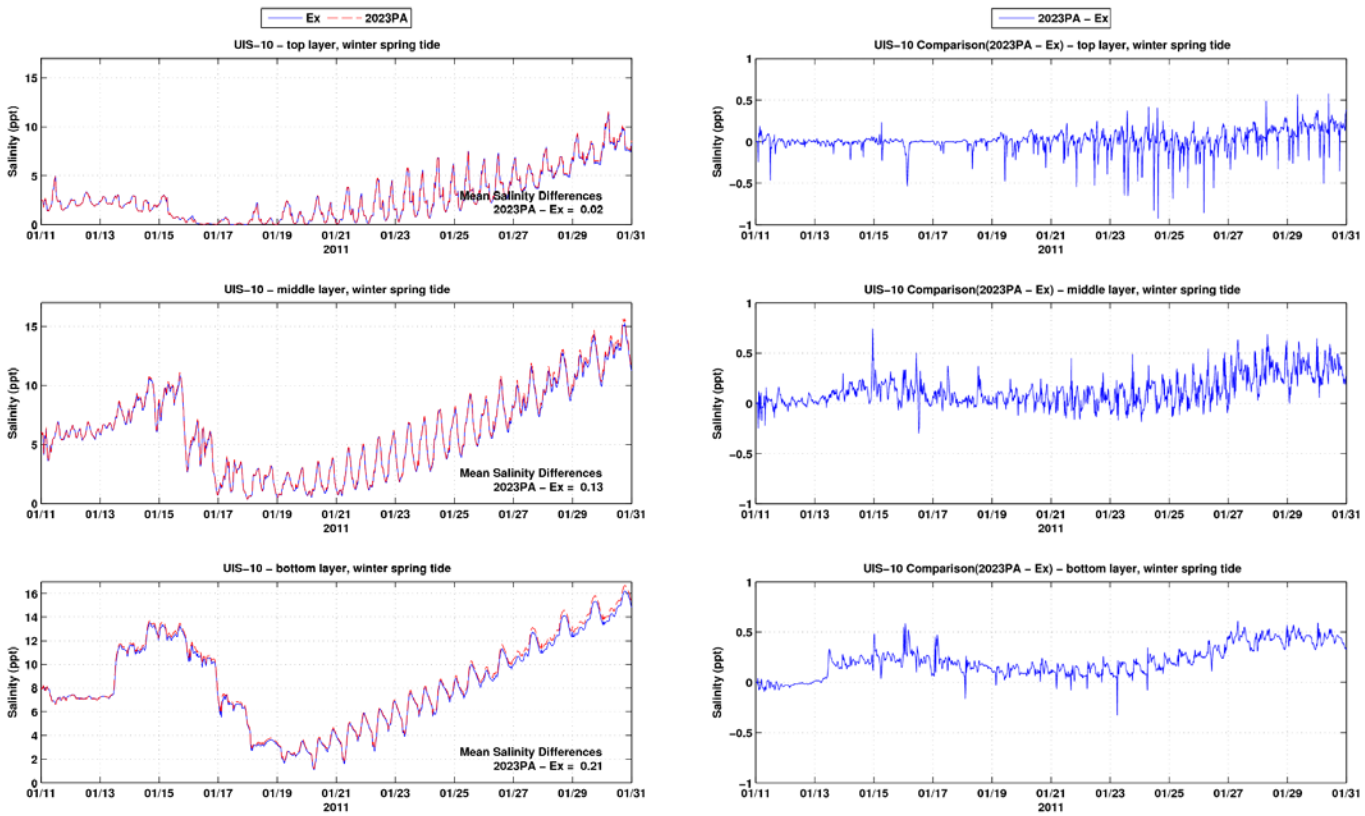

Figure B-52: Salinity time series and differences between the Existing Conditions and the 2023 PA at UIS-10 during winter spring tide period

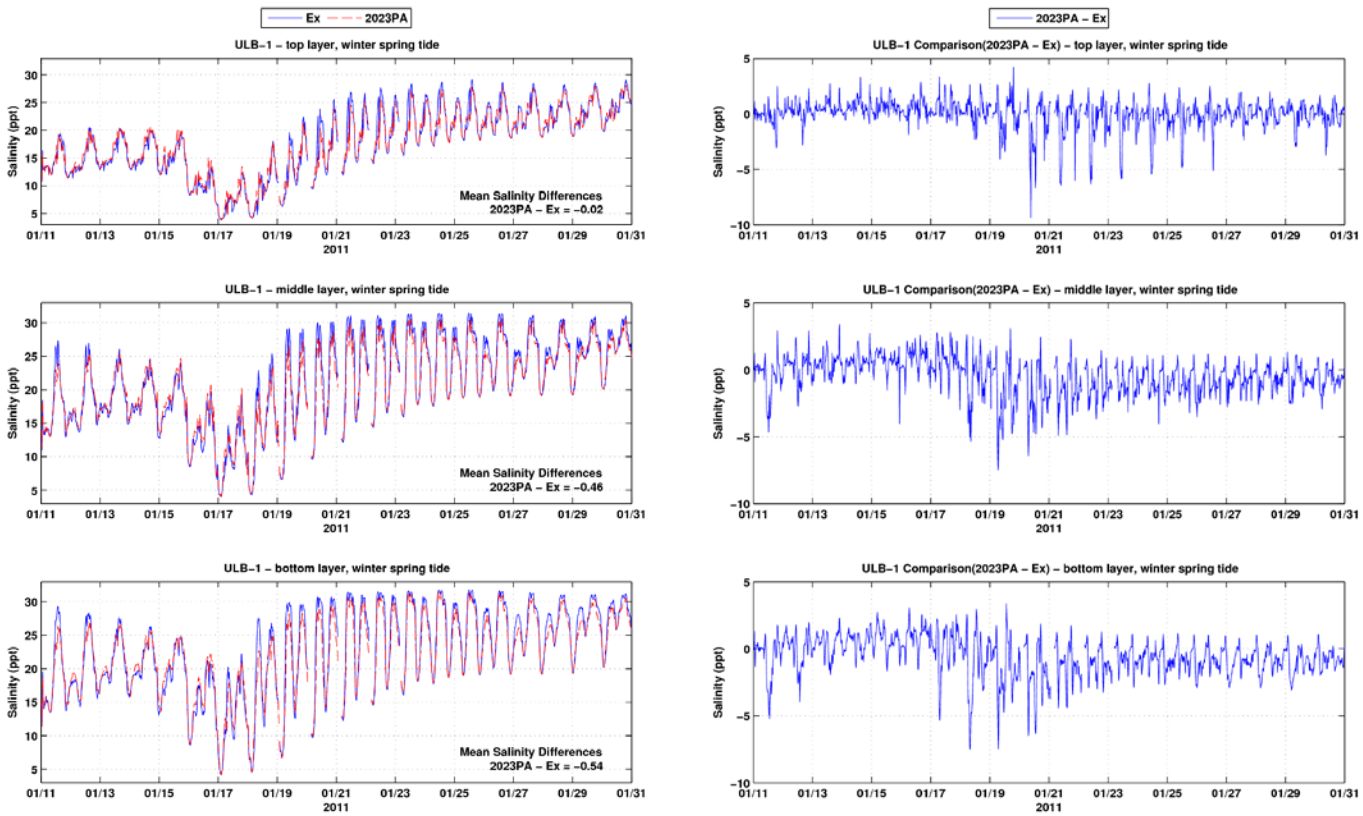

Figure B-53: Salinity time series and differences between the Existing Conditions and the 2023 PA at ULB-1 during winter spring tide period

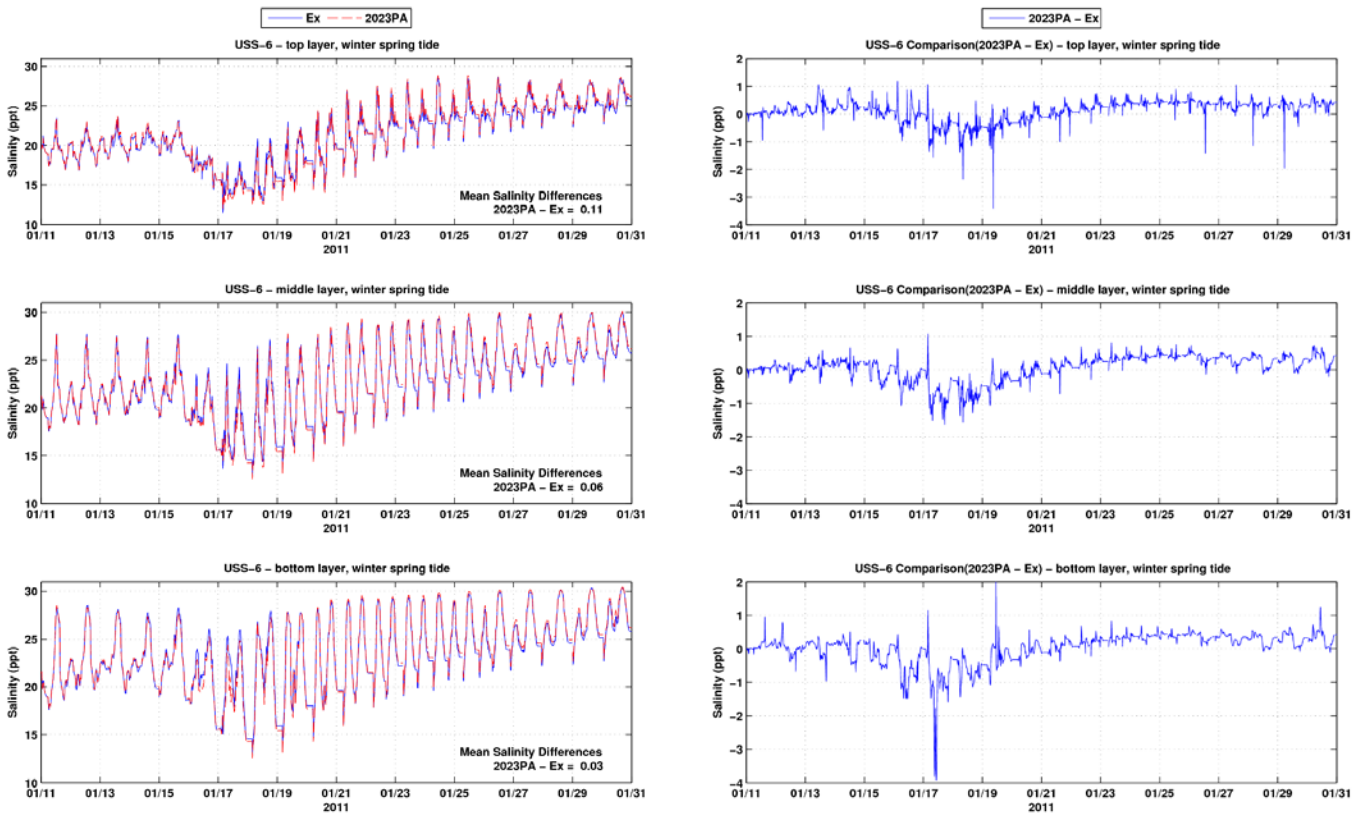

Figure B-54: Salinity time series and differences between the Existing Conditions and the 2023 PA at USS-6 during winter spring tide period

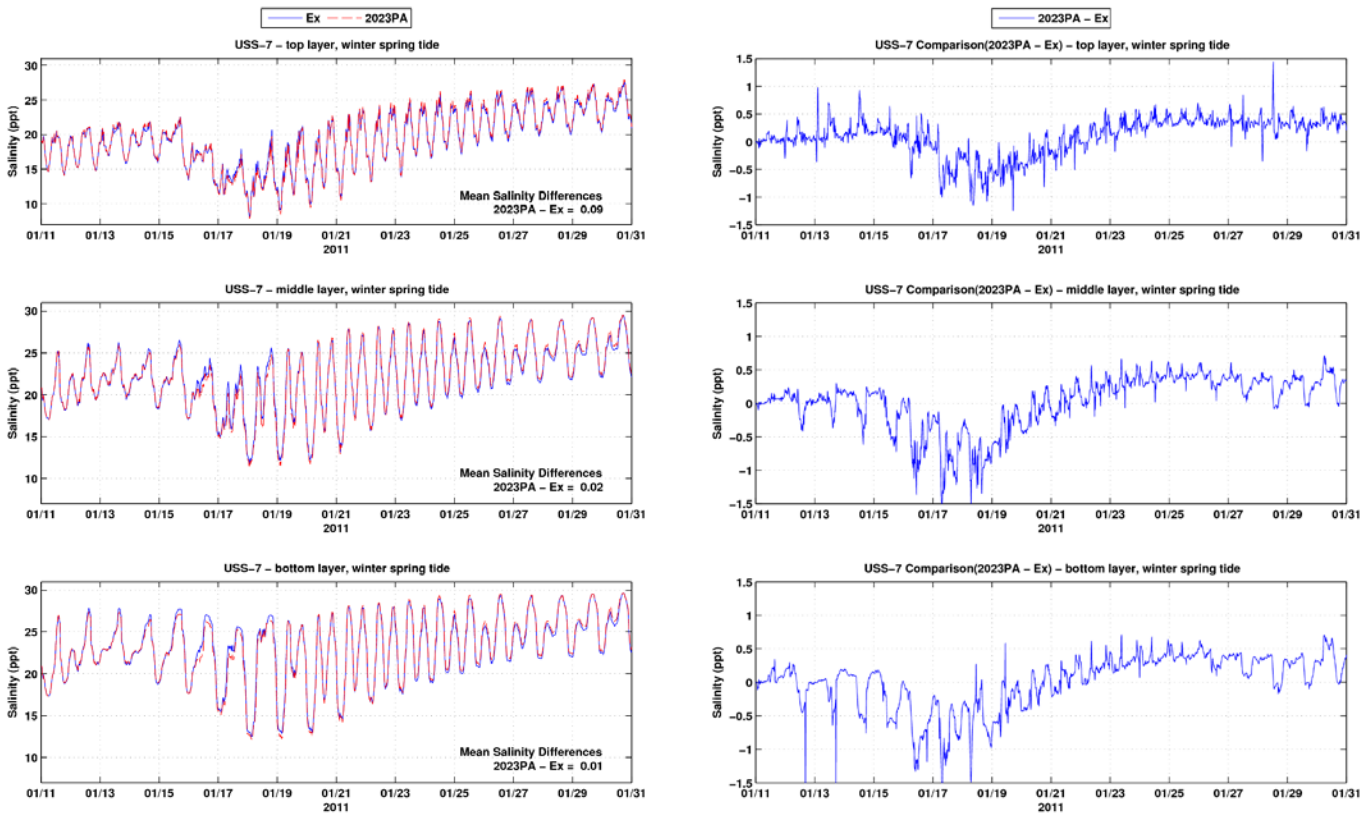

Figure B-55: Salinity time series and differences between the Existing Conditions and the 2023 PA at USS-7 during winter spring tide period

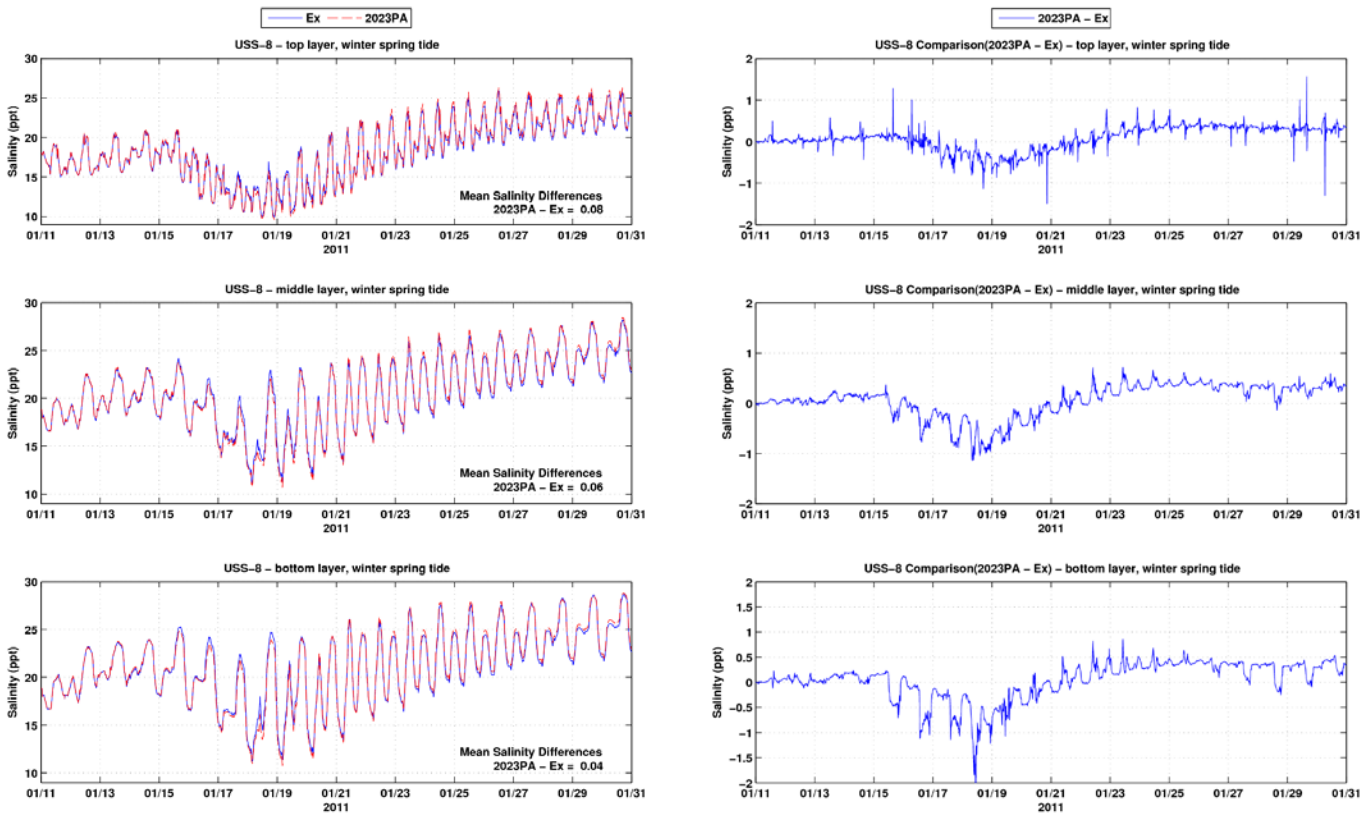

Figure B-56: Salinity time series and differences between the Existing Conditions and the 2023 PA at USS-8 during winter spring tide period

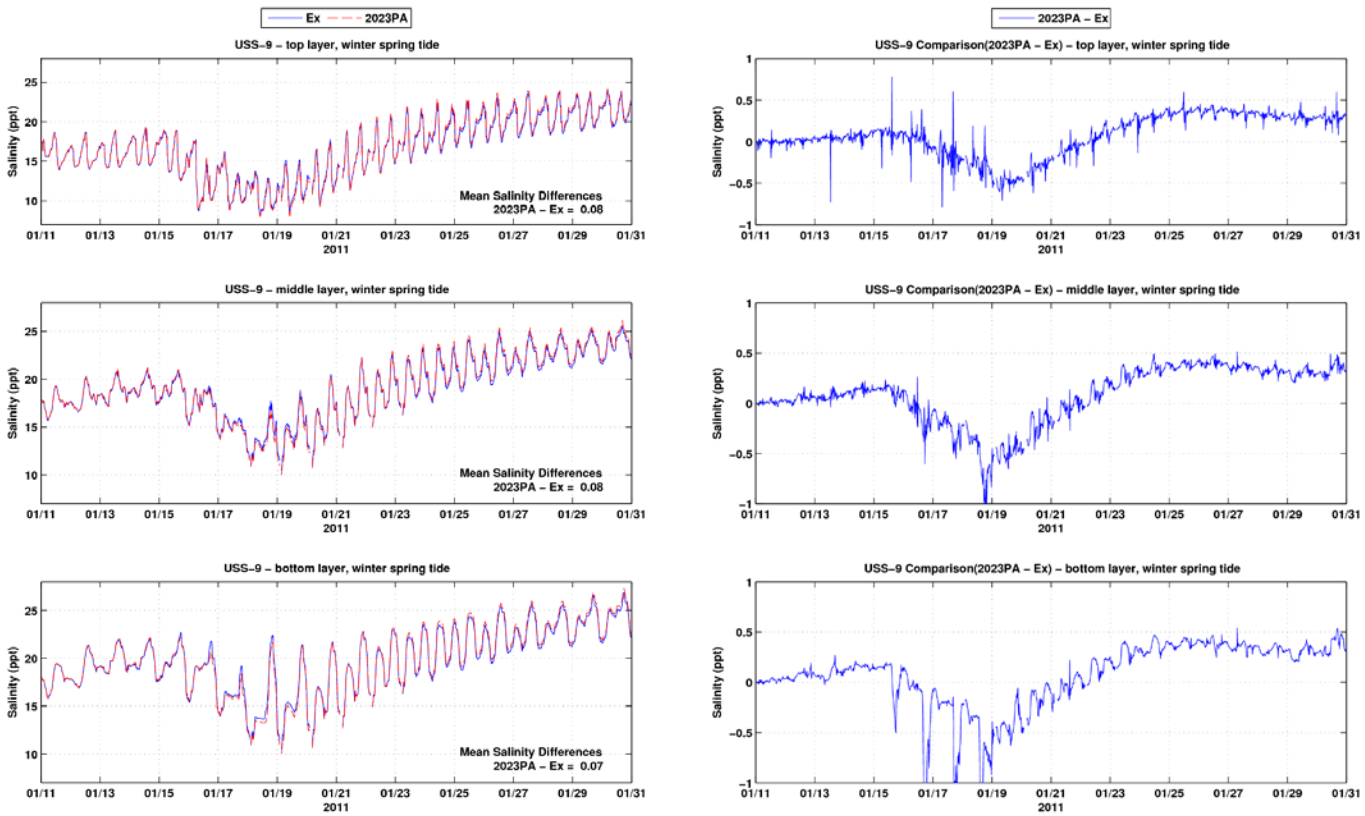

Figure B-57: Salinity time series and differences between the Existing Conditions and the 2023 PA at USS-9 during winter spring tide period

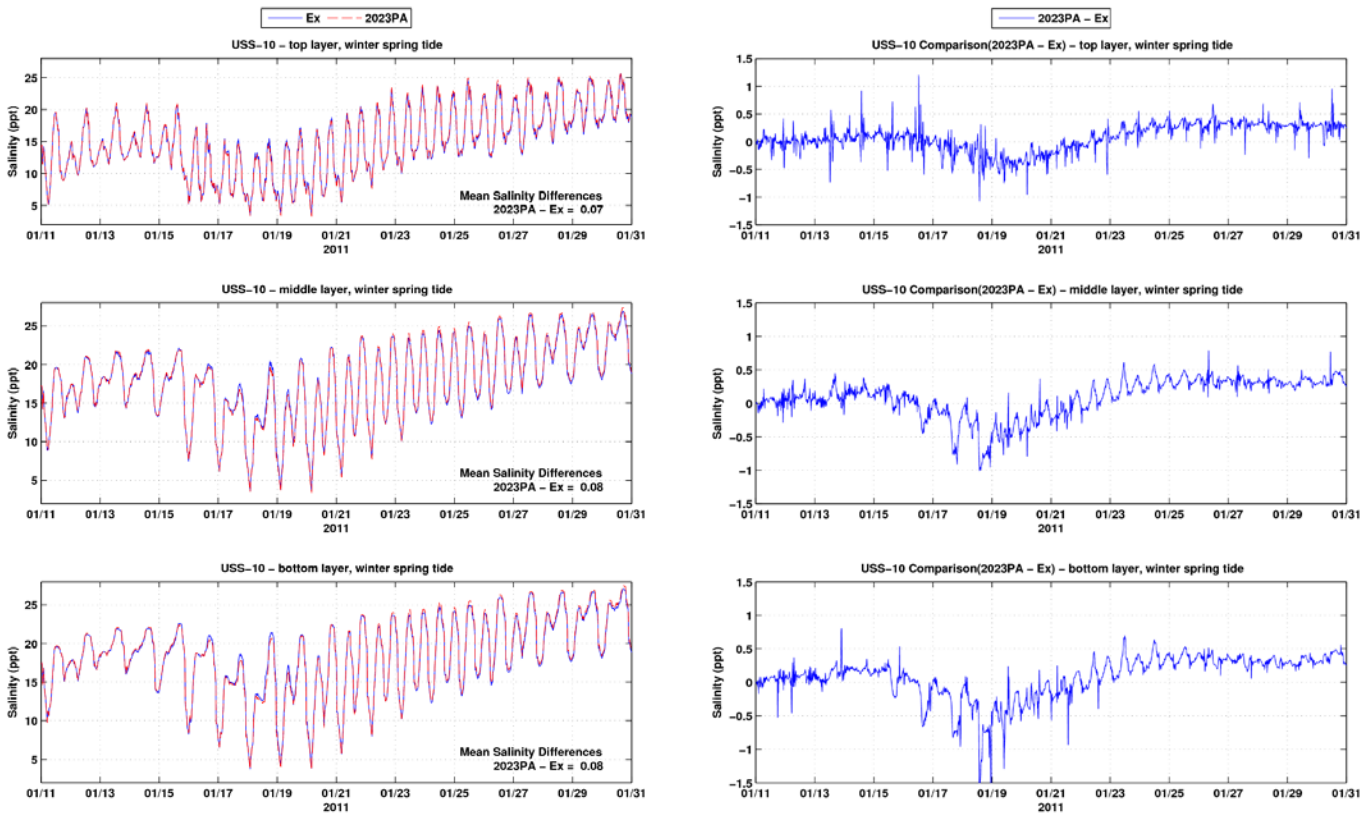

Figure B-58: Salinity time series and differences between the Existing Conditions and the 2023 PA at USS-10 during winter spring tide period

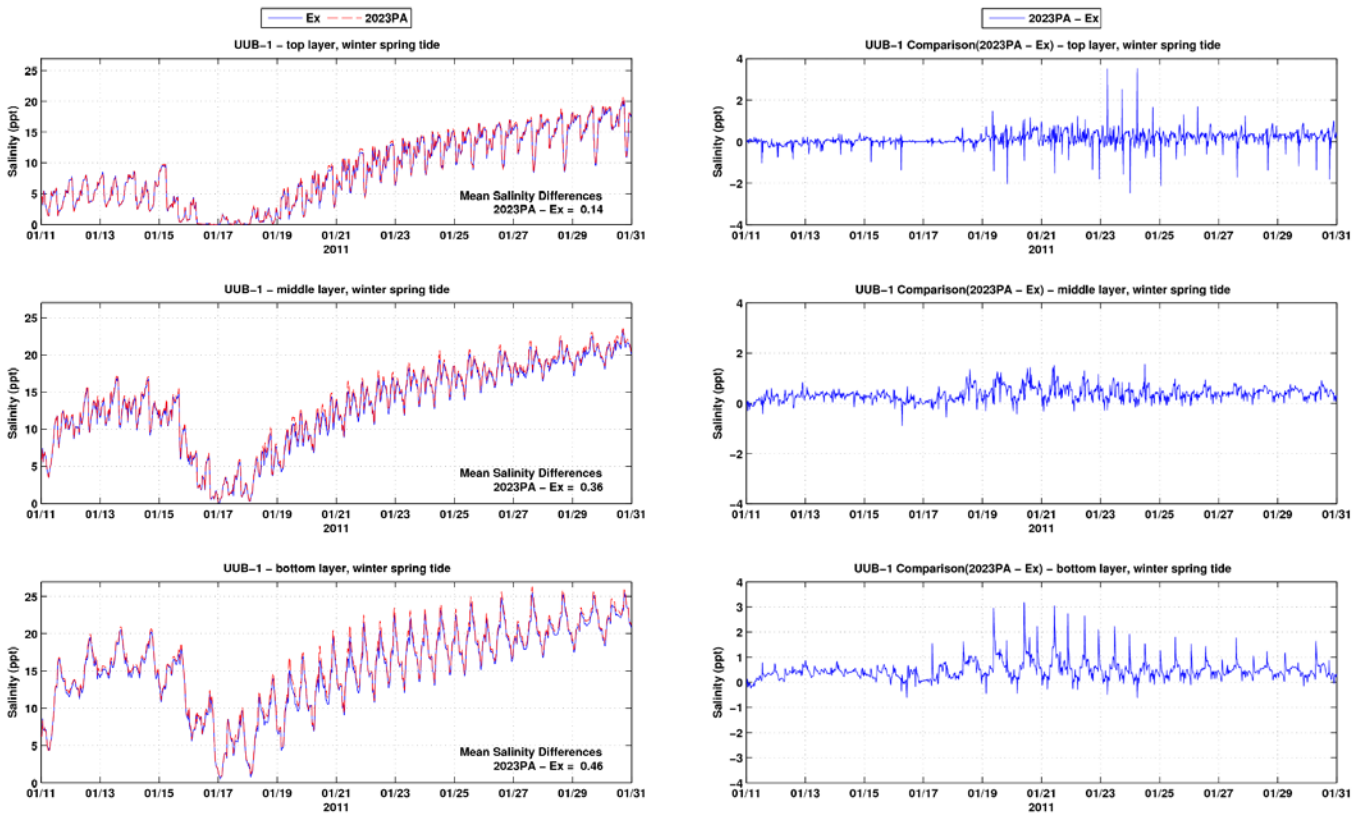

Figure B-59: Salinity time series and differences between the Existing Conditions and the 2023 PA at UUB-1 during winter spring tide period

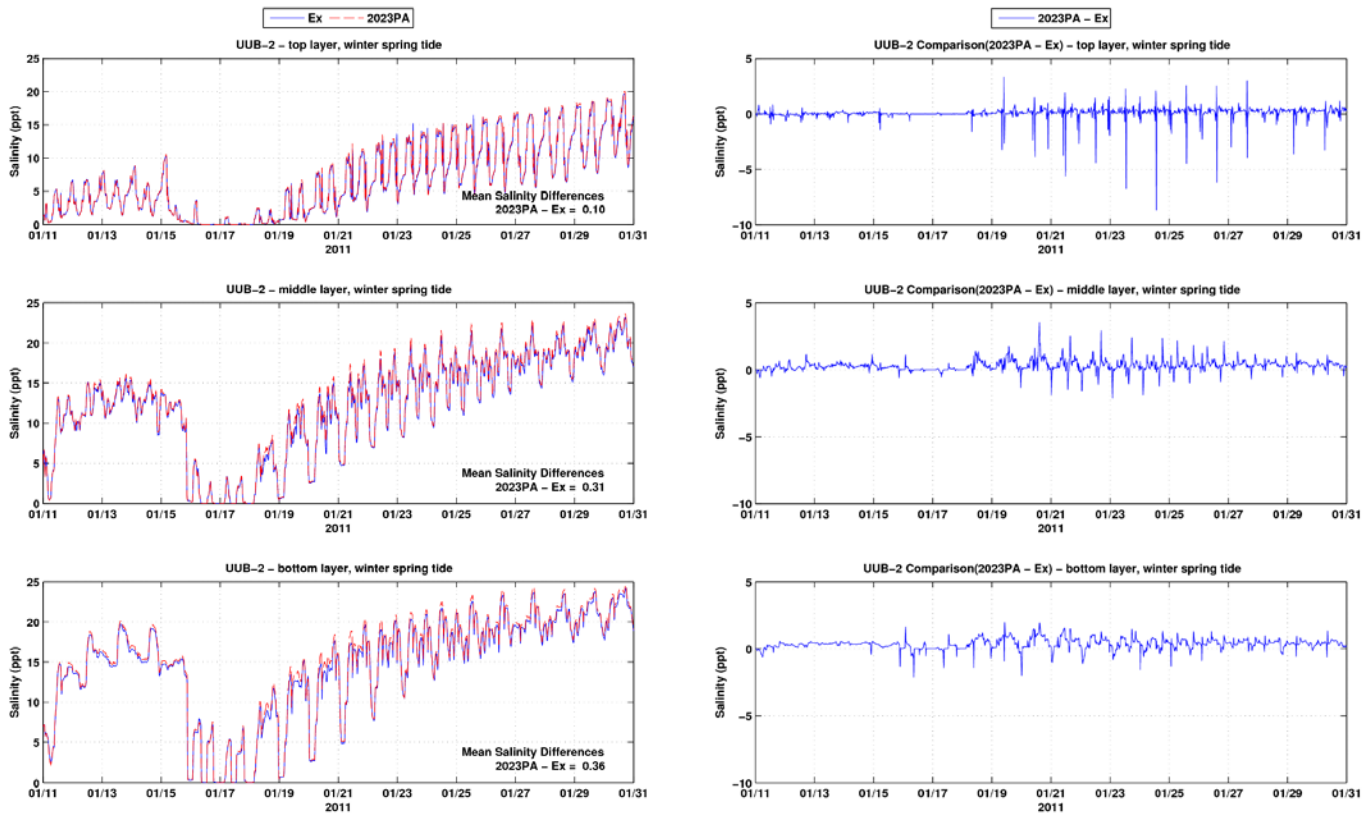

Figure B-60: Salinity time series and differences between the Existing Conditions and the 2023 PA at UUB-2 during winter spring tide period

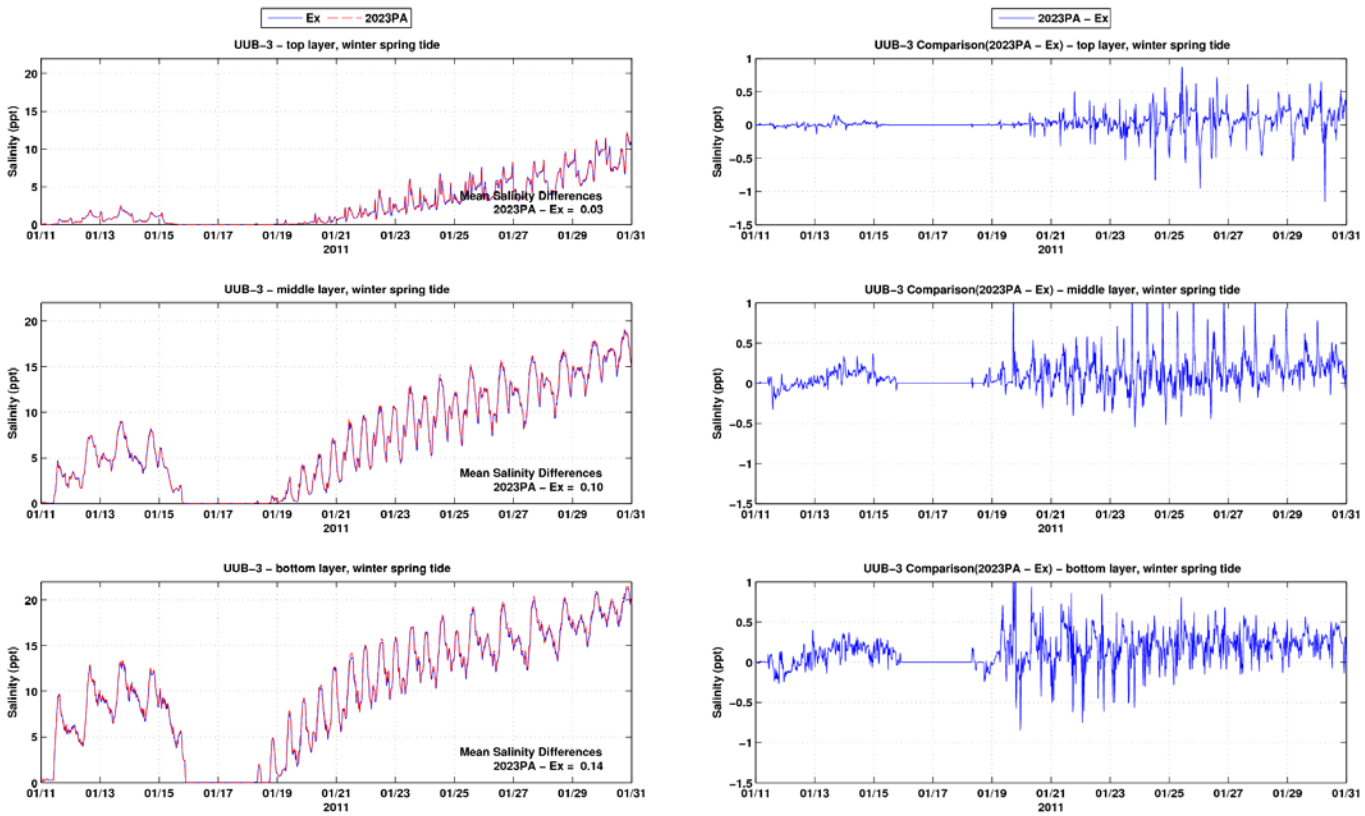

Figure B-61: Salinity time series and differences between the Existing Conditions and the 2023 PA at UUB-3 during winter spring tide period

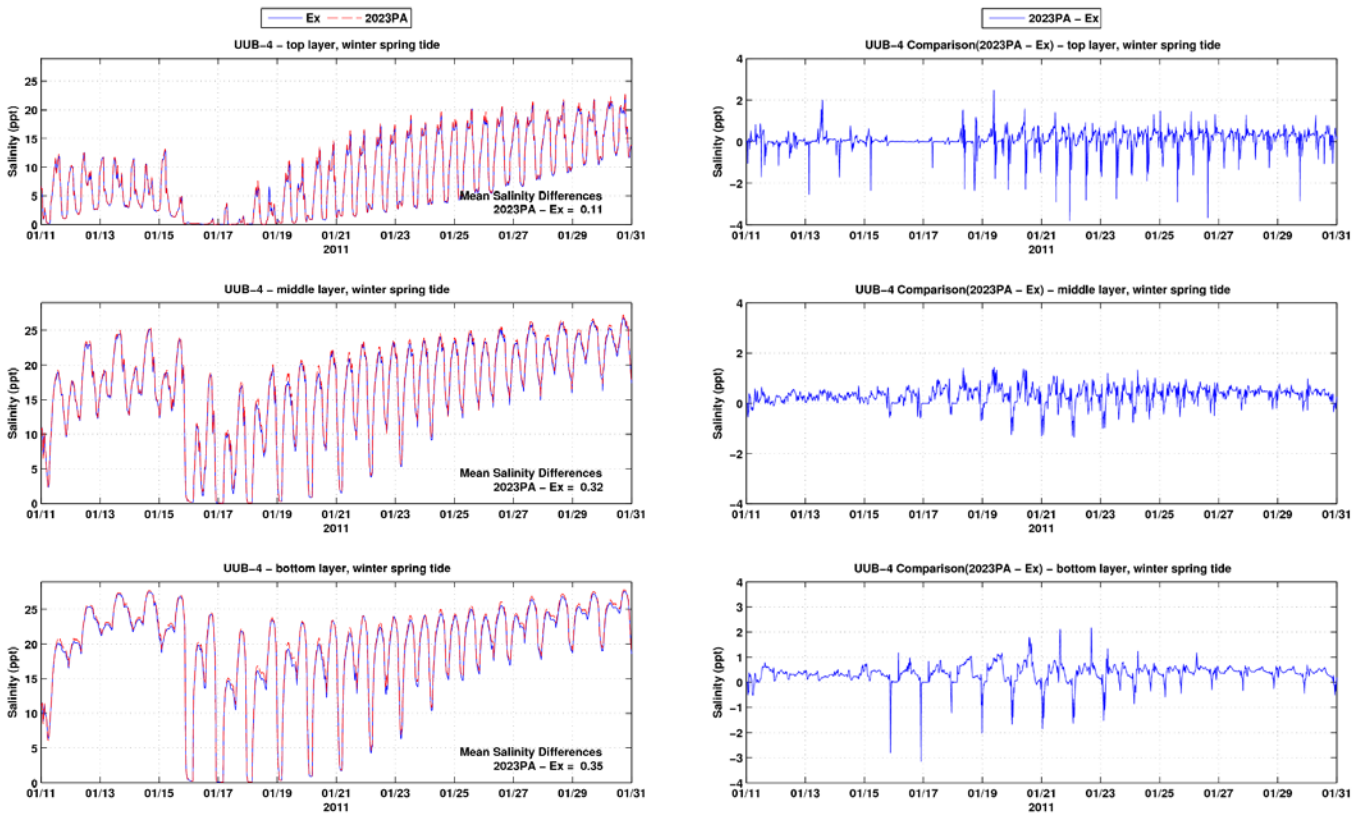

Figure B-62: Salinity time series and differences between the Existing Conditions and the 2023 PA at UUB-4 during winter spring tide period

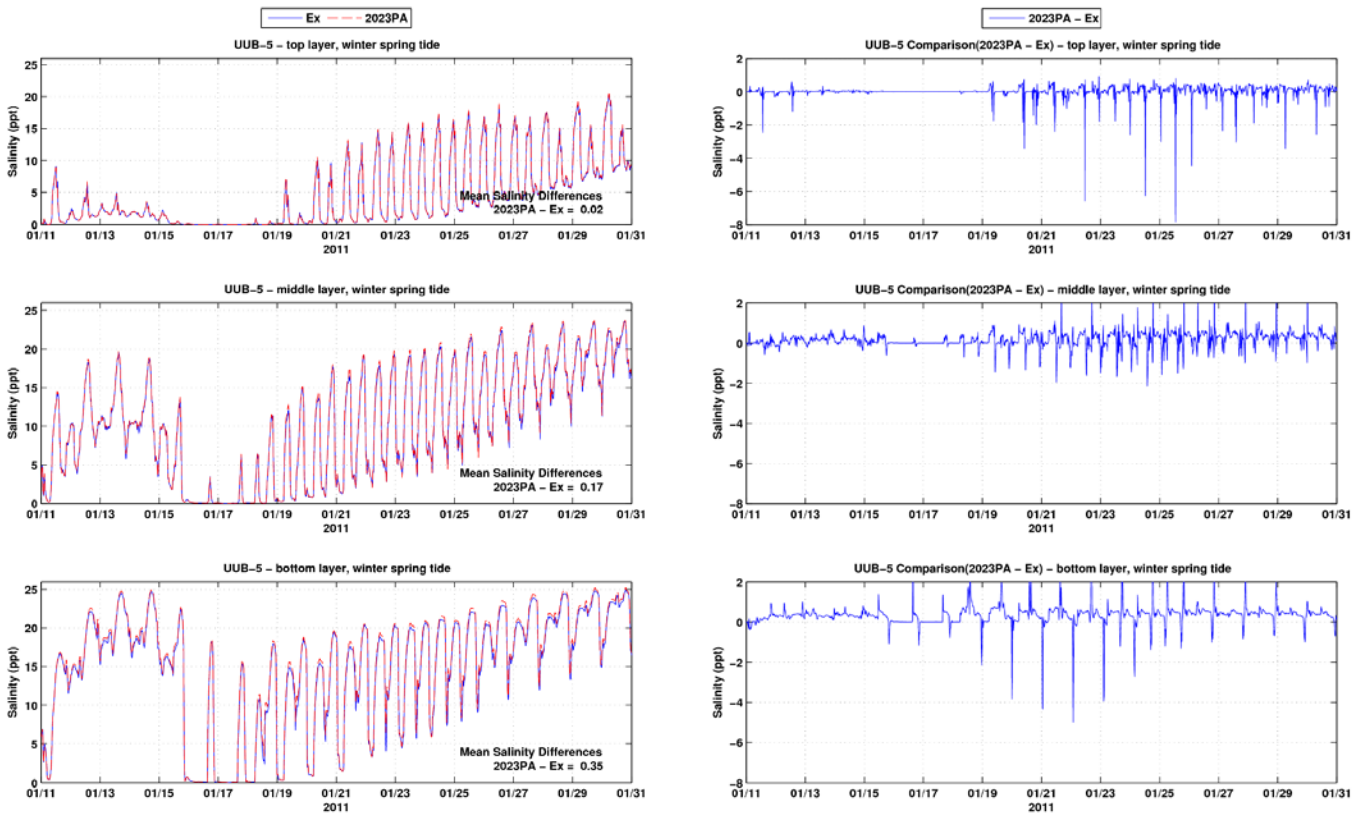

Figure B-63: Salinity time series and differences between the Existing Conditions and the 2023 PA at UUB-5 during winter spring tide period

Attachment C

Salinity Results for Winter Period with Neap Tide

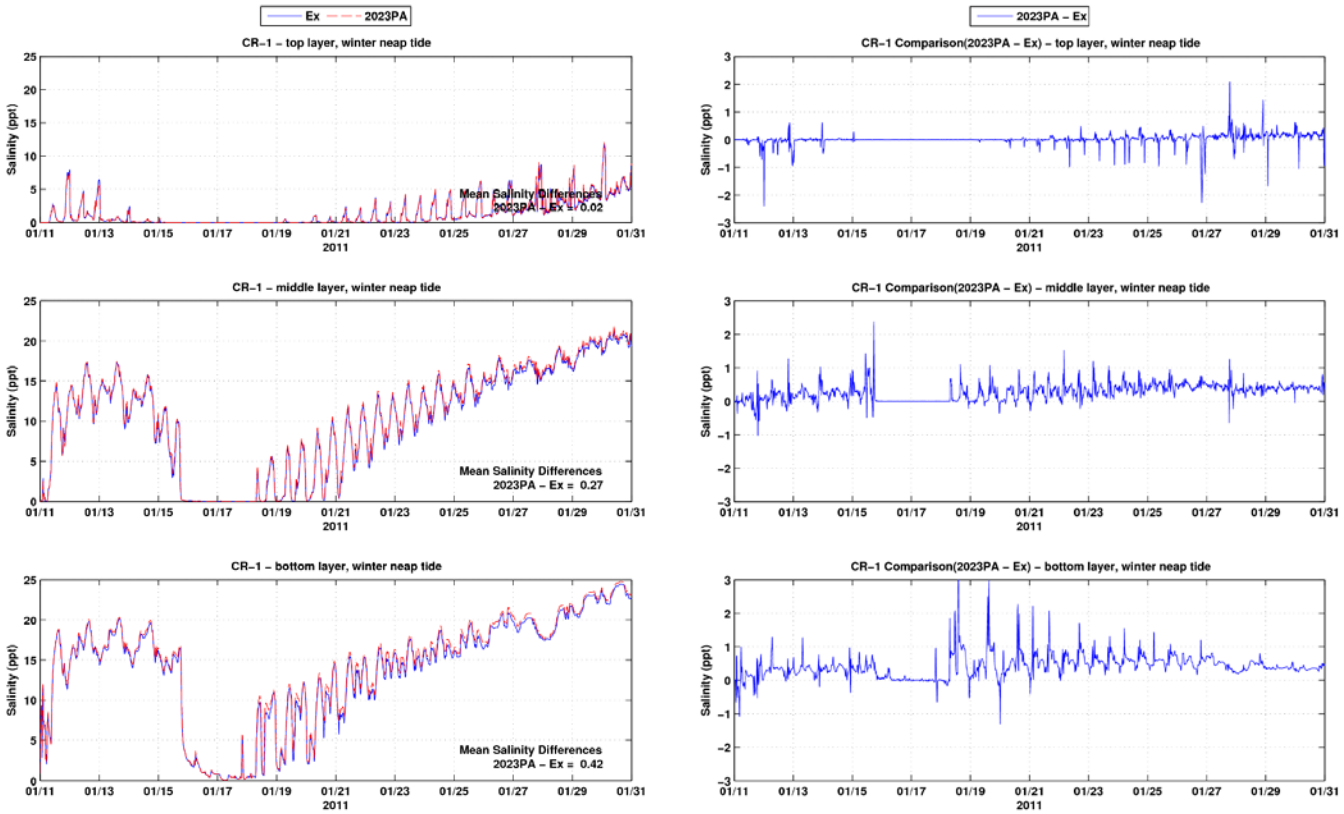

Figure C-1: Salinity time series and differences between the Existing Conditions and the 2023 PA at CR-1 during winter neap tide period

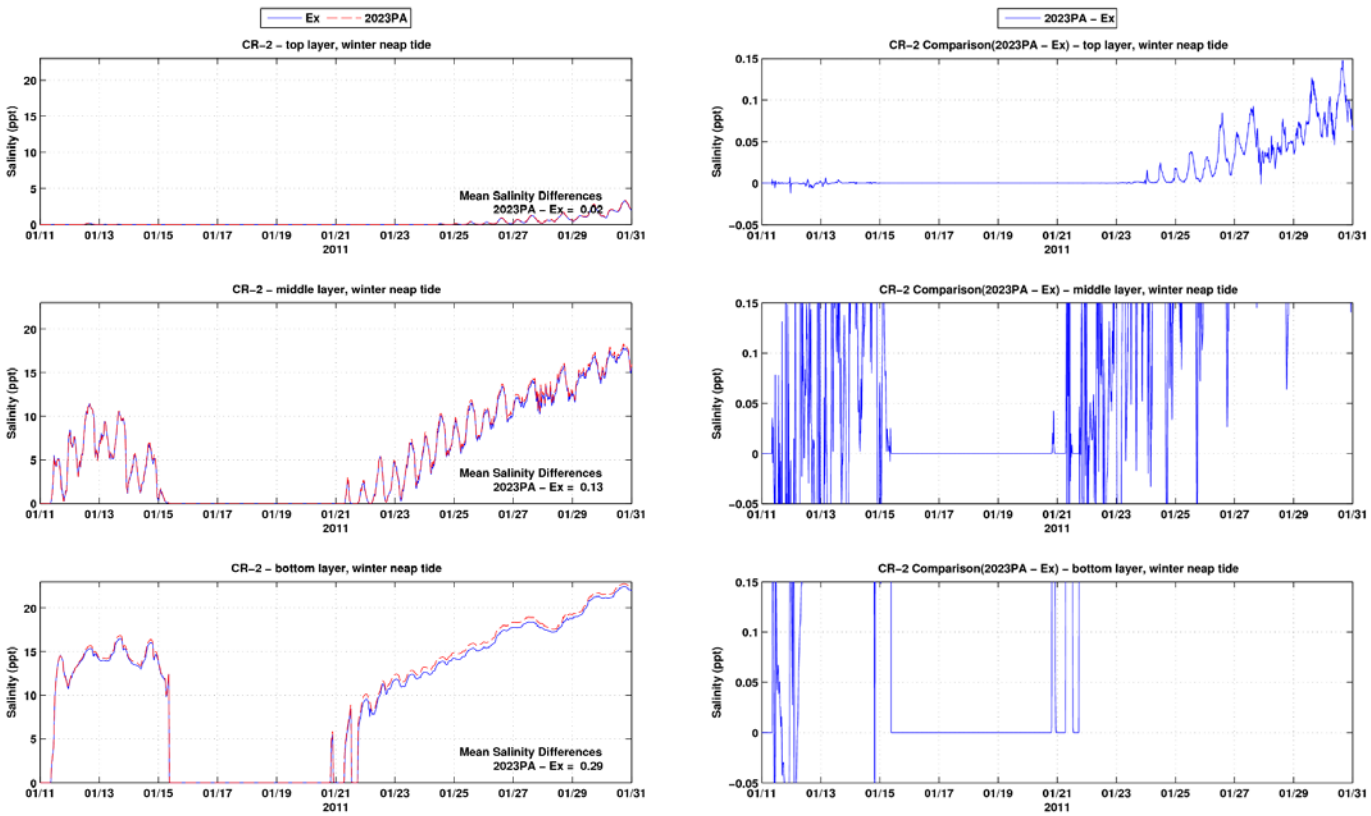

Figure C-2: Salinity time series and differences between the Existing Conditions and the 2023 PA at CR-2 during winter neap tide period

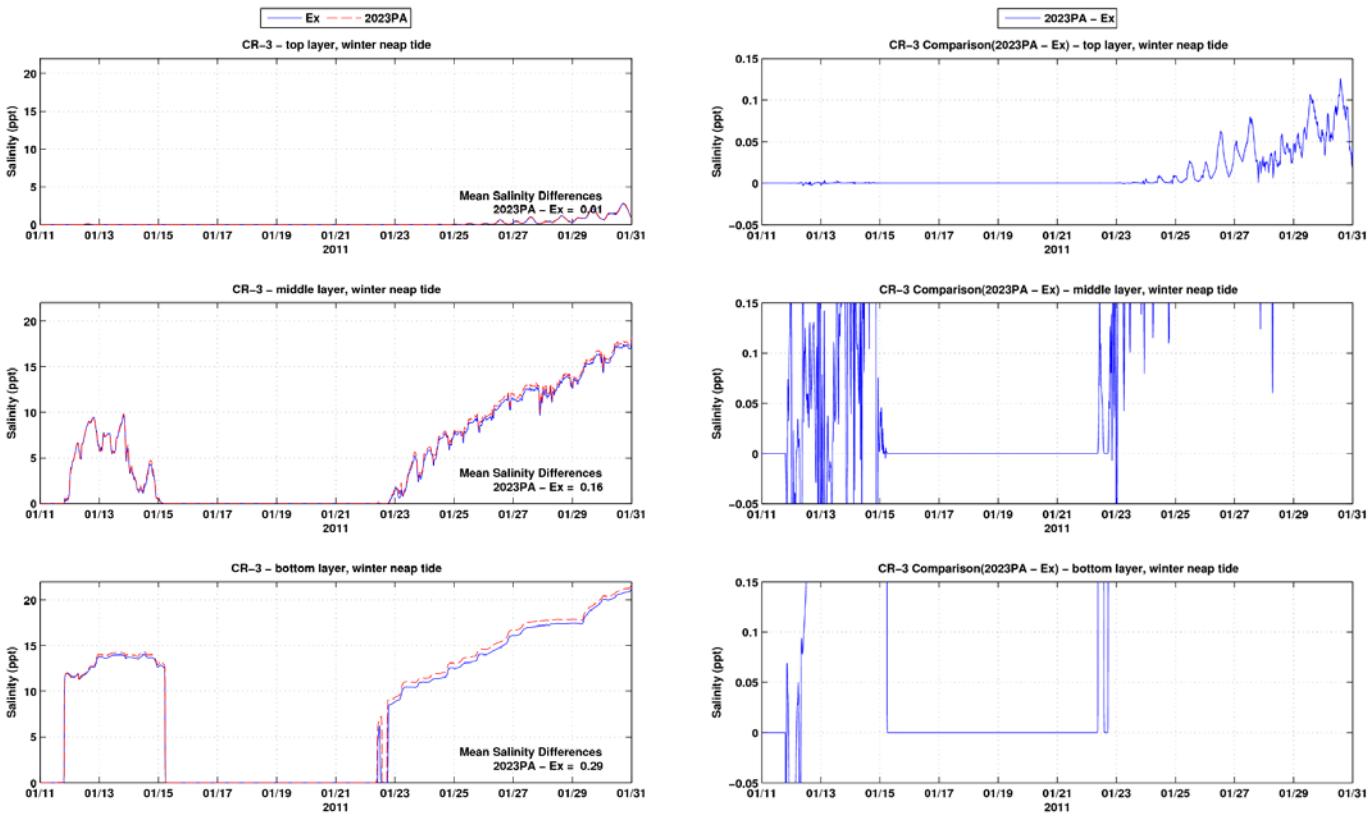

Figure C-3: Salinity time series and differences between the Existing Conditions and the 2023 PA at CR-3 during winter neap tide period

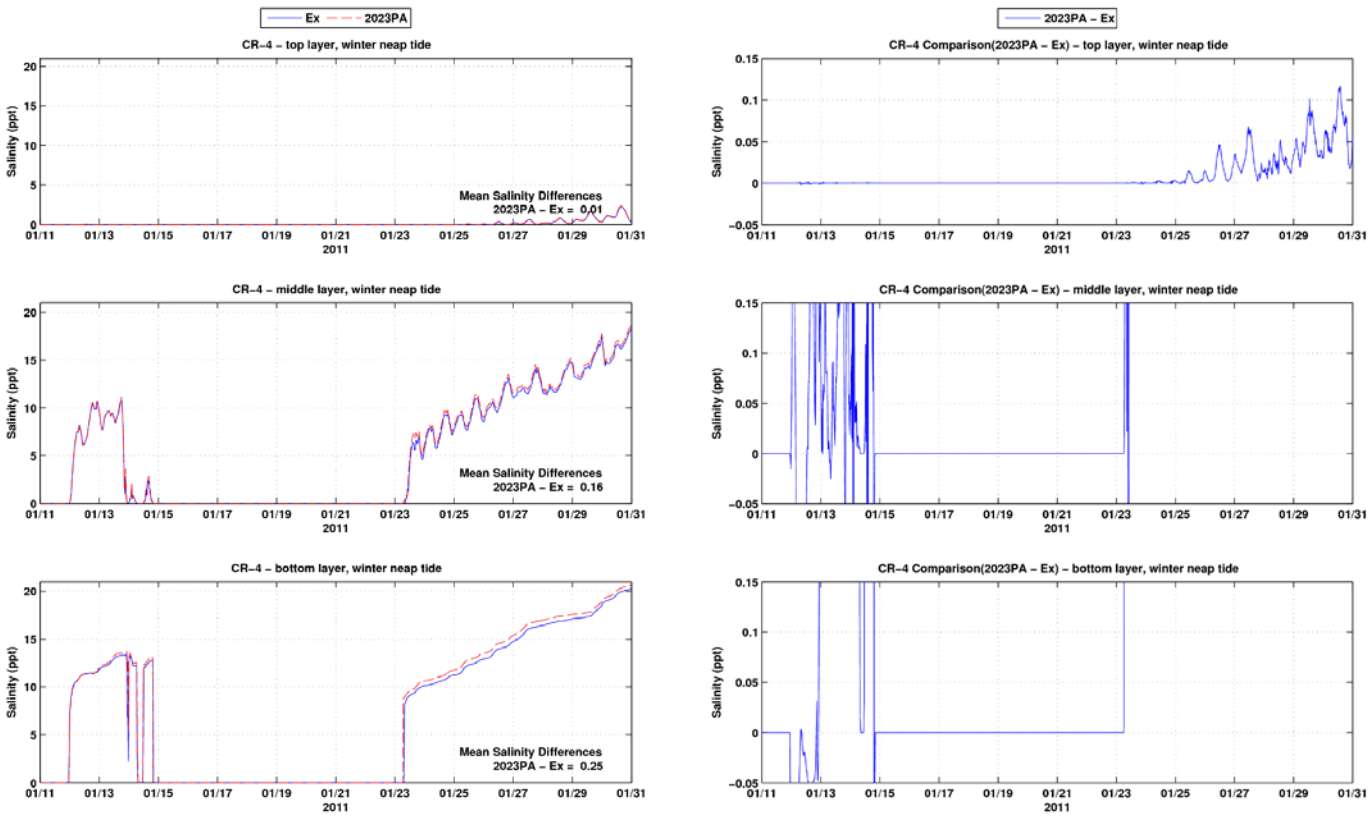

Figure C-4: Salinity time series and differences between the Existing Conditions and the 2023 PA at CR-4 during winter neap tide period

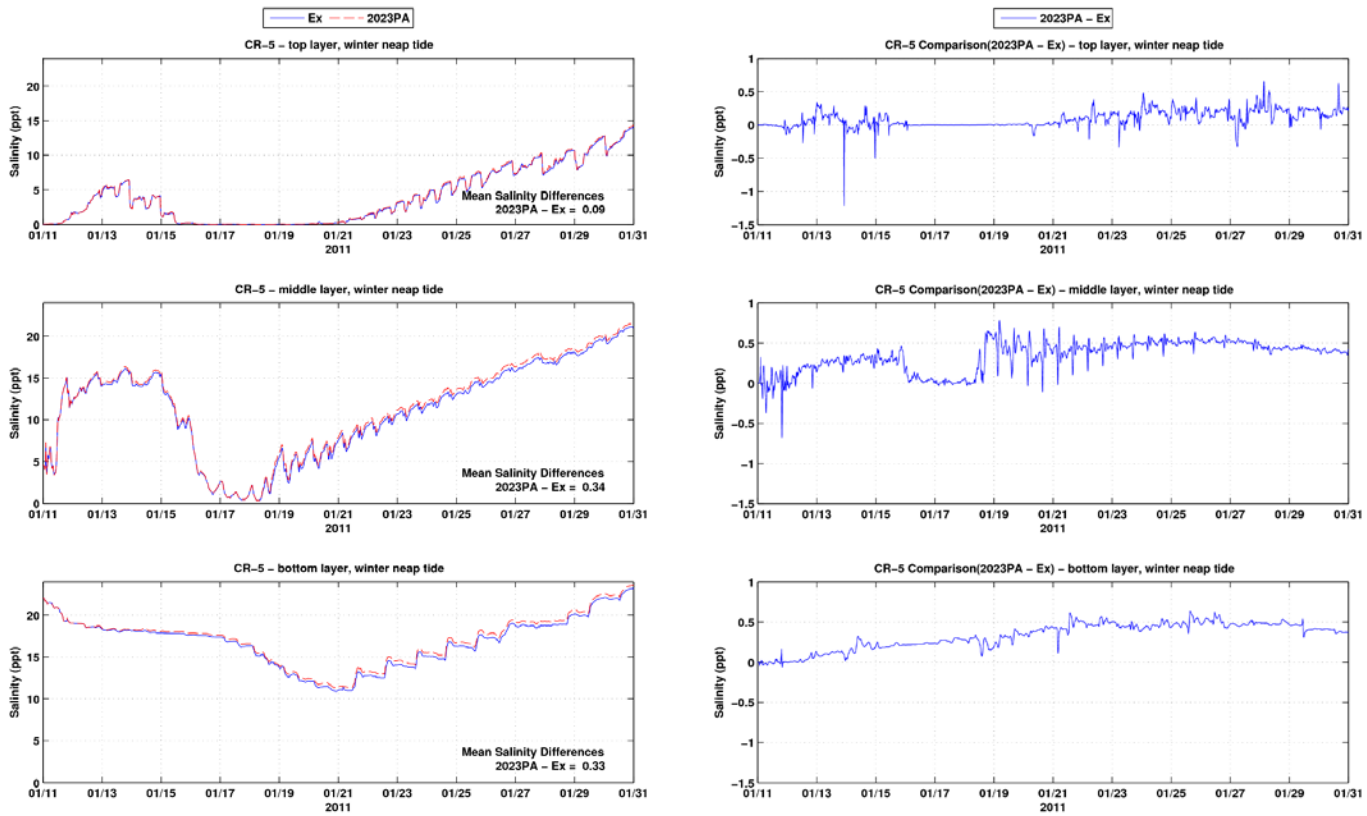

Figure C-5: Salinity time series and differences between the Existing Conditions and the 2023 PA at CR-5 during winter neap tide period

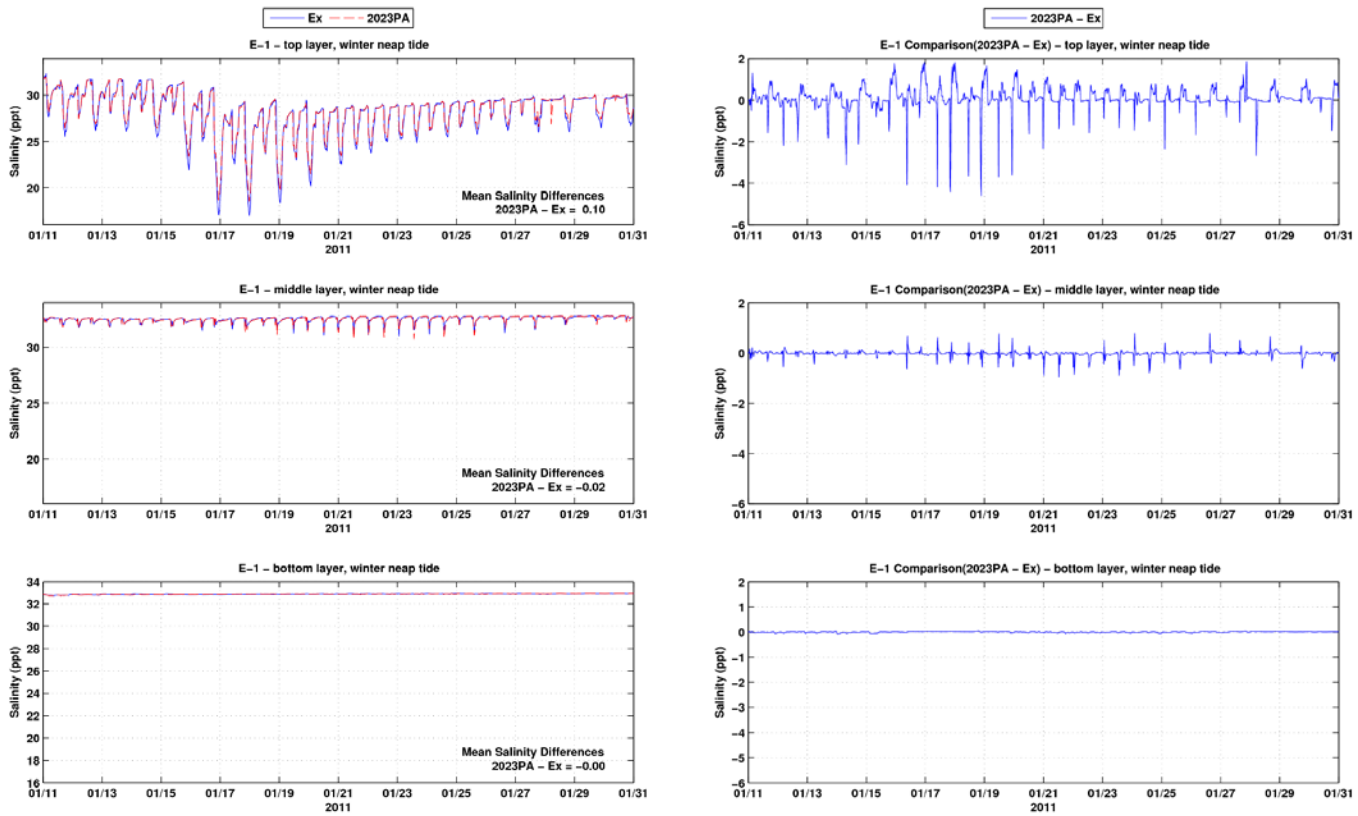

Figure C-6: Salinity time series and differences between the Existing Conditions and the 2023 PA at E-1 during winter neap tide period

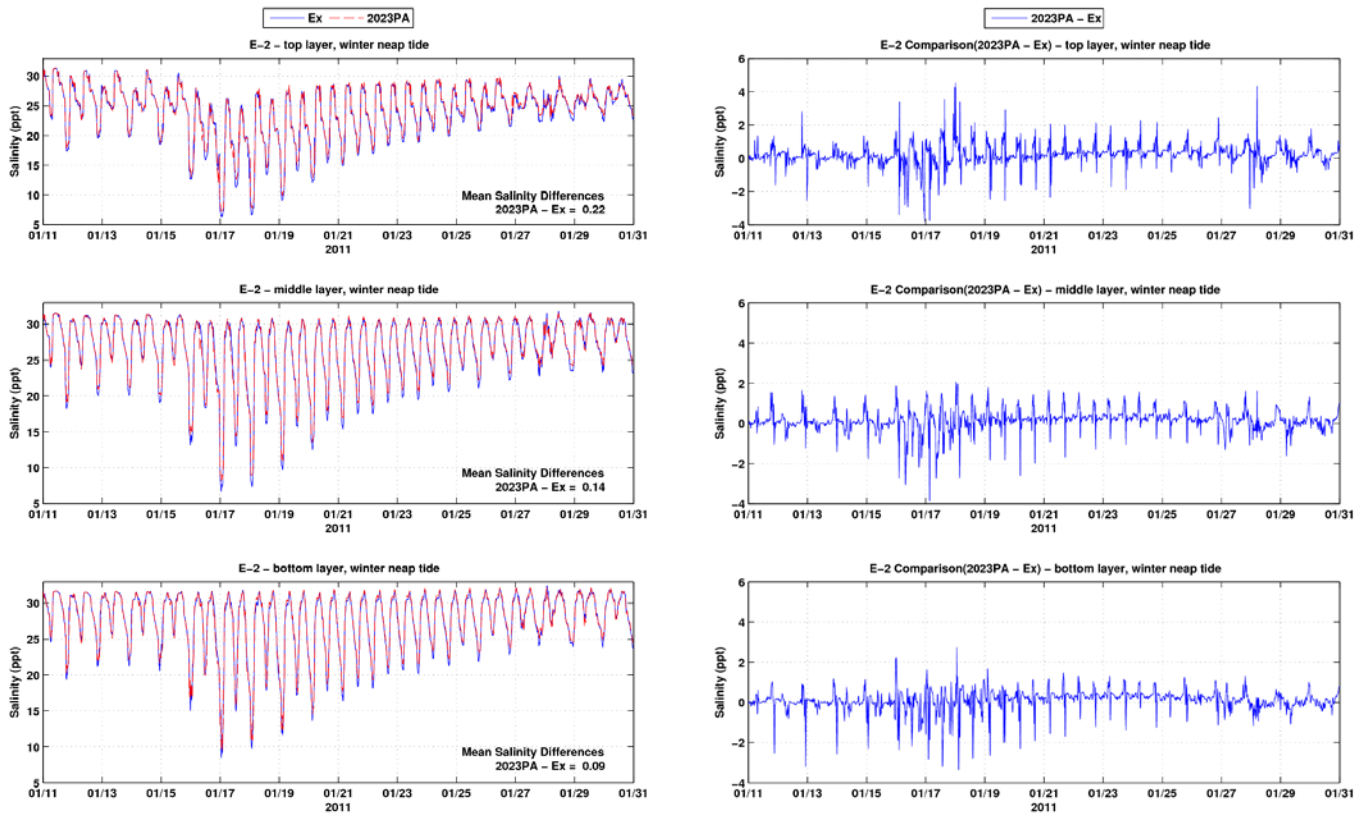

Figure C-7: Salinity time series and differences between the Existing Conditions and the 2023 PA at E-2 during winter neap tide period

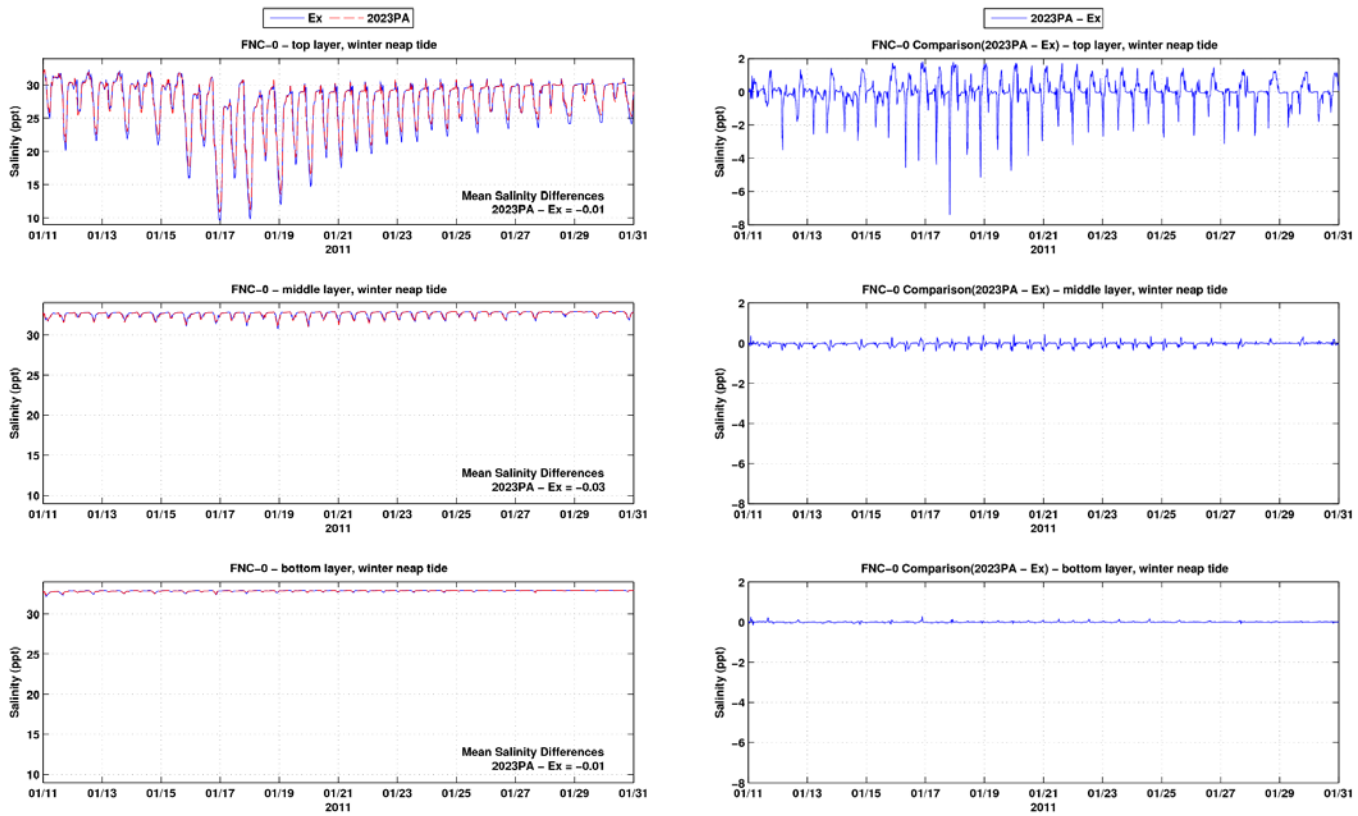

Figure C-8: Salinity time series and differences between the Existing Conditions and the 2023 PA at FNC-0 during winter neap tide period

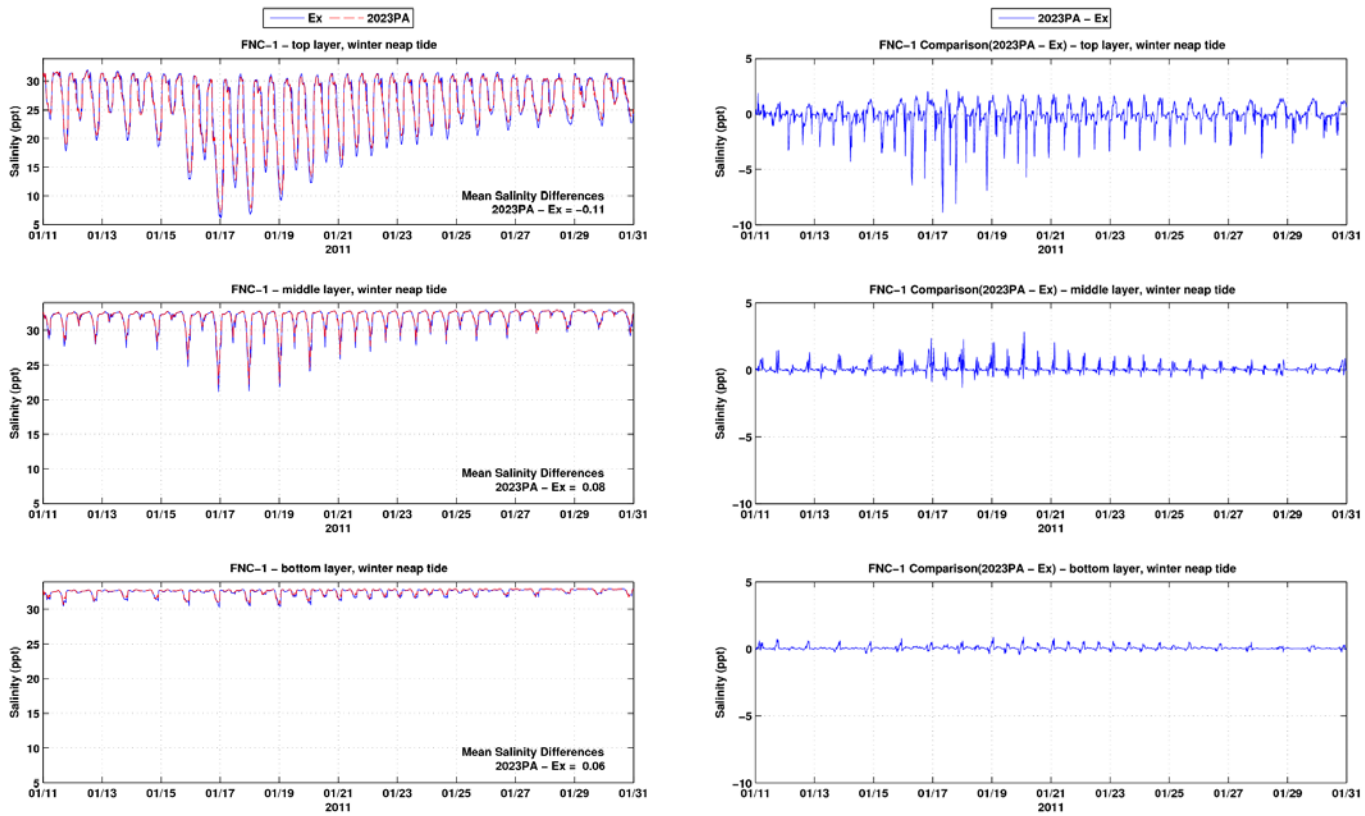

Figure C-9: Salinity time series and differences between the Existing Conditions and the 2023 PA at FNC-1 during winter neap tide period

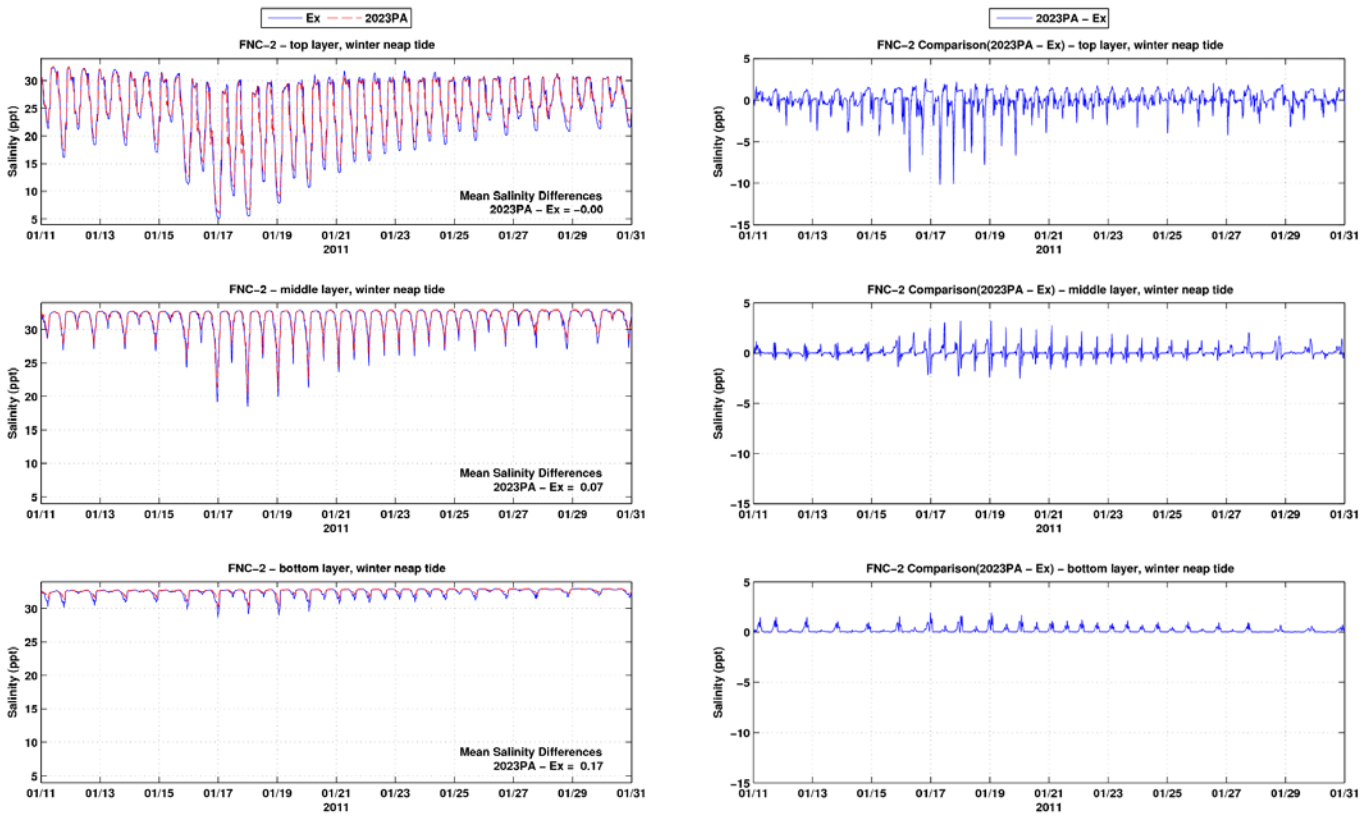

Figure C-10: Salinity time series and differences between the Existing Conditions and the 2023 PA at FNC-2 during winter neap tide period

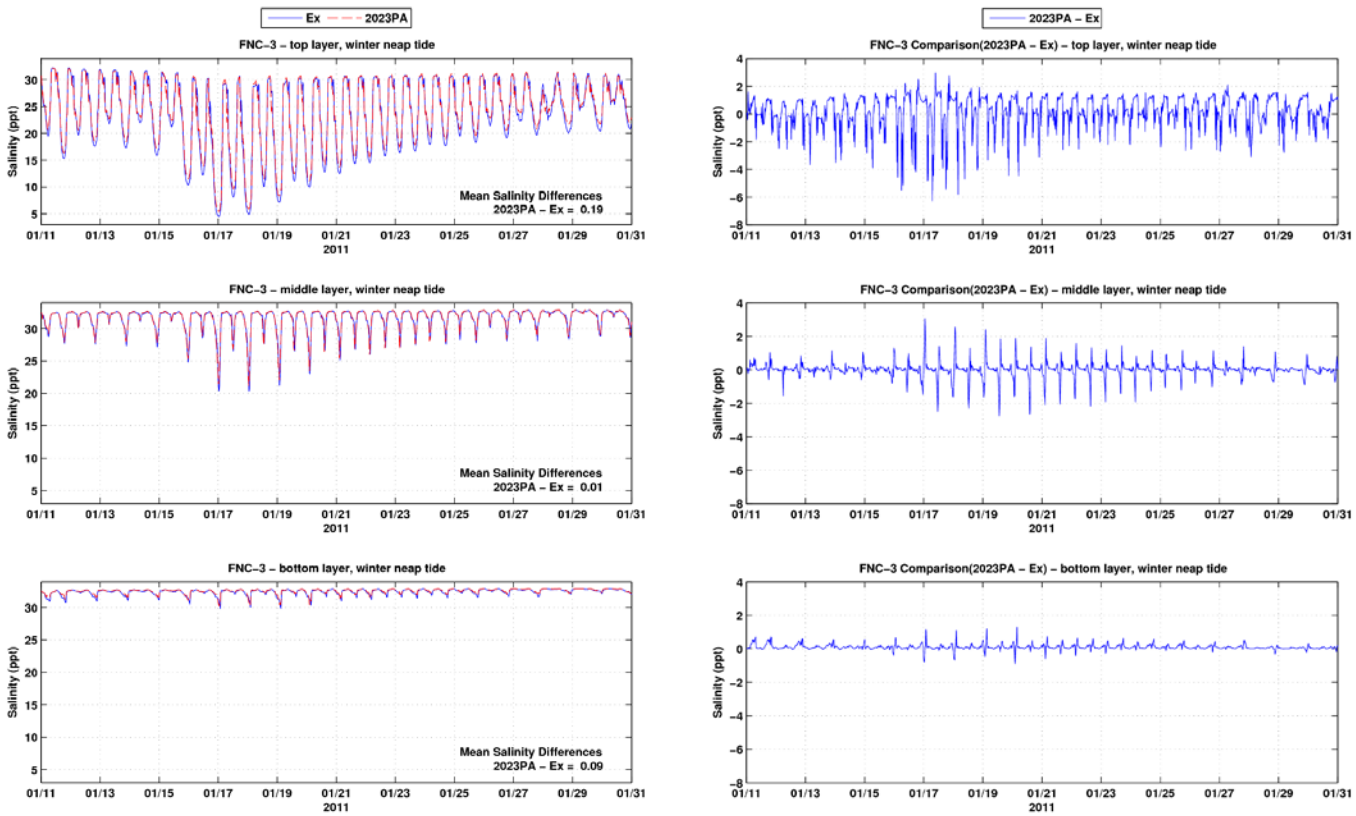

Figure C-11: Salinity time series and differences between the Existing Conditions and the 2023 PA at FNC-3 during winter neap tide period

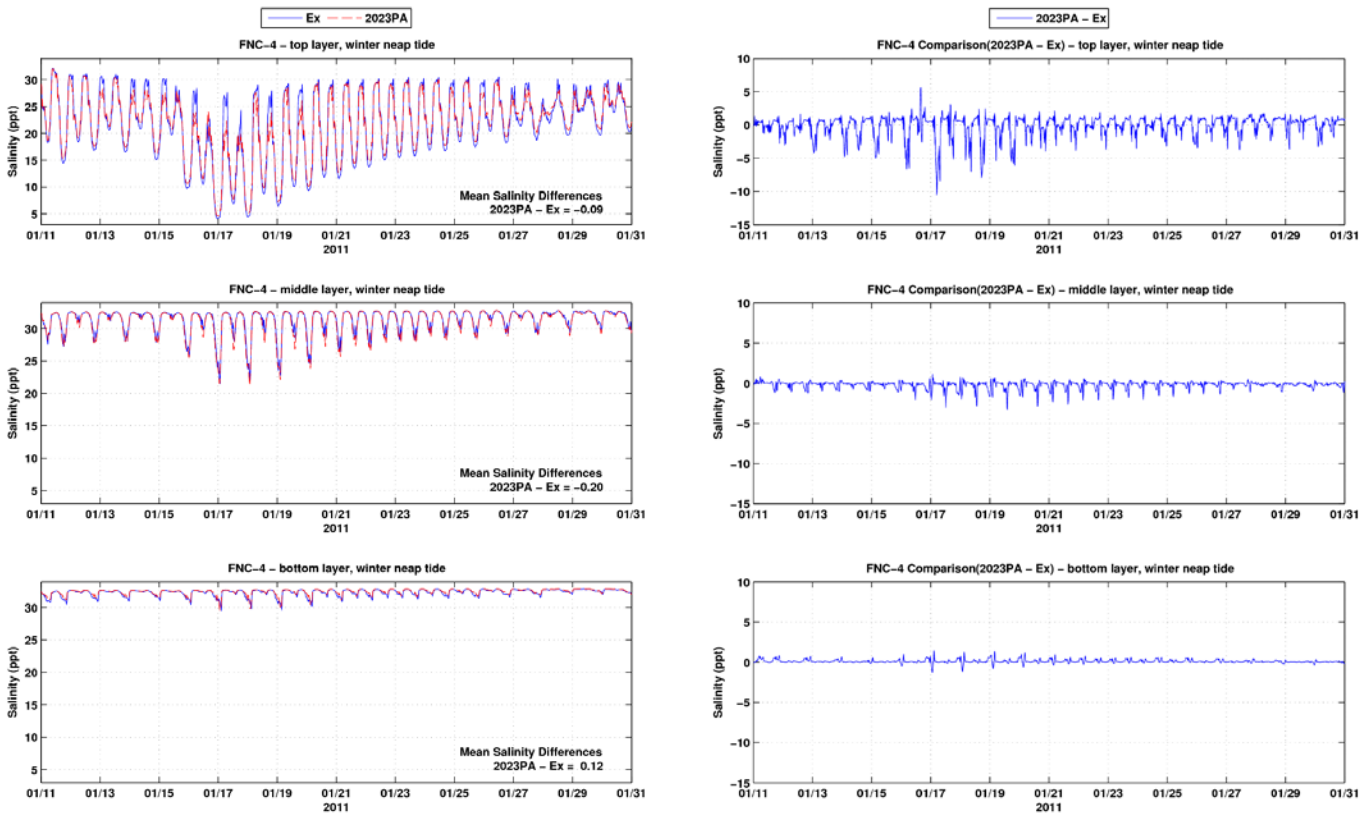

Figure C-12: Salinity time series and differences between the Existing Conditions and the 2023 PA at FNC-4 during winter neap tide period

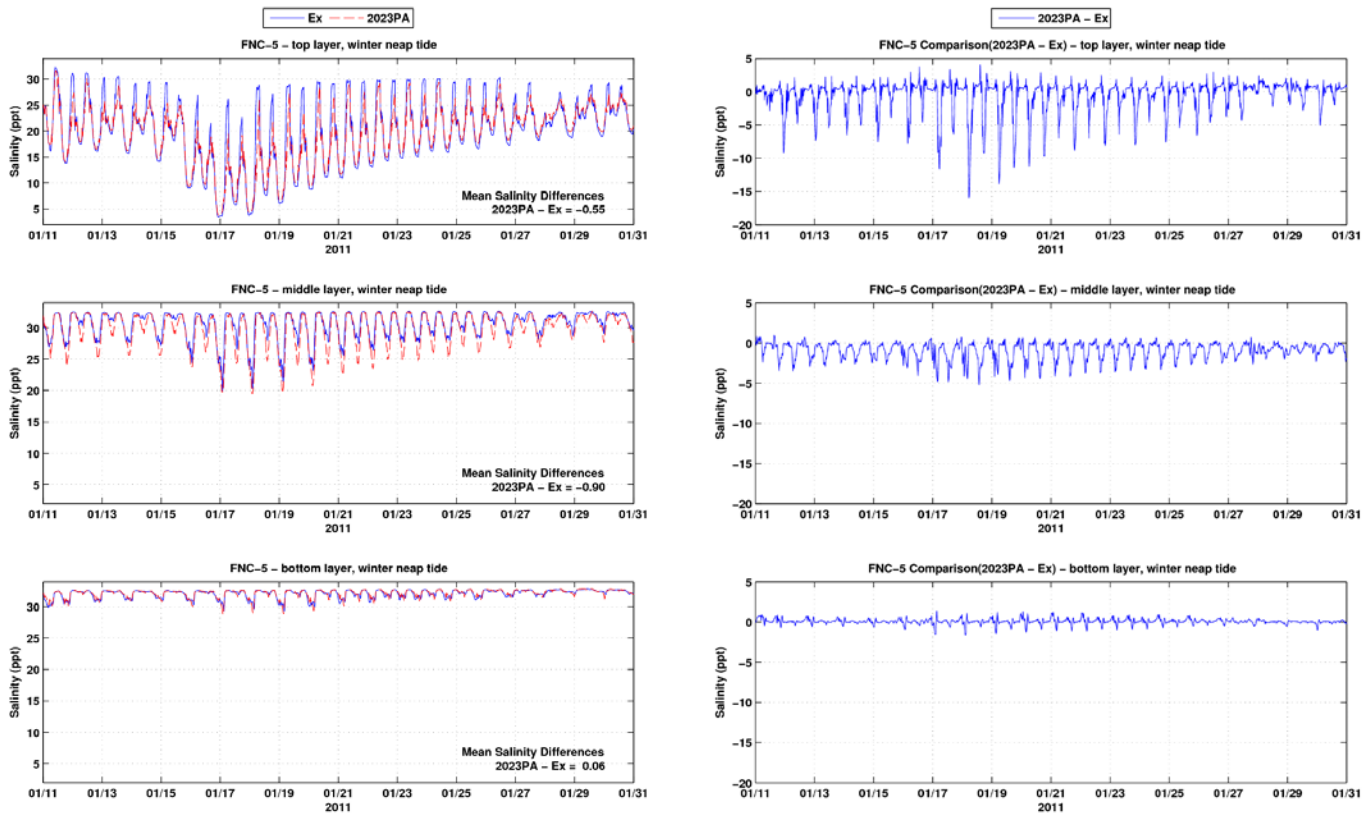

Figure C-13: Salinity time series and differences between the Existing Conditions and the 2023 PA at FNC-5 during winter neap tide period

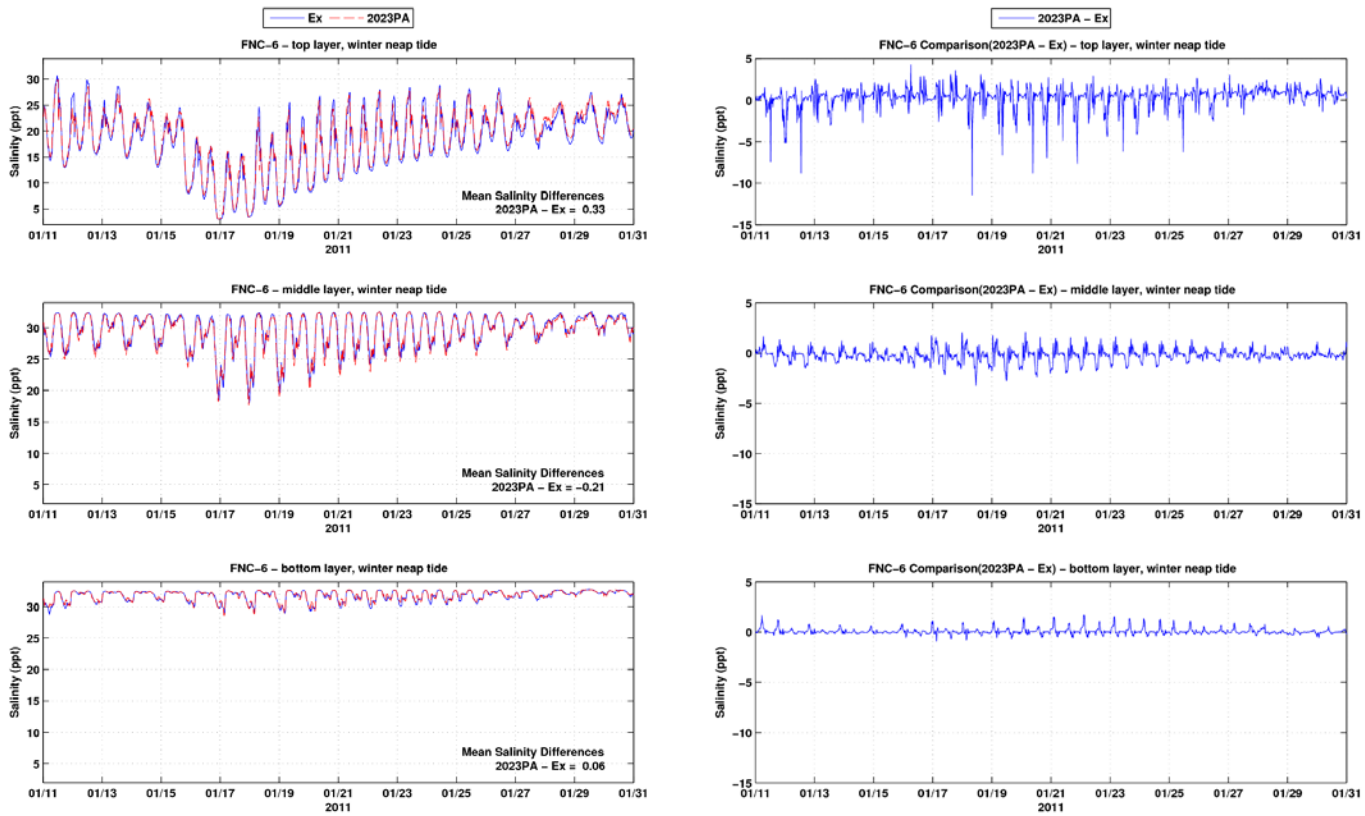

Figure C-14: Salinity time series and differences between the Existing Conditions and the 2023 PA at FNC-6 during winter neap tide period

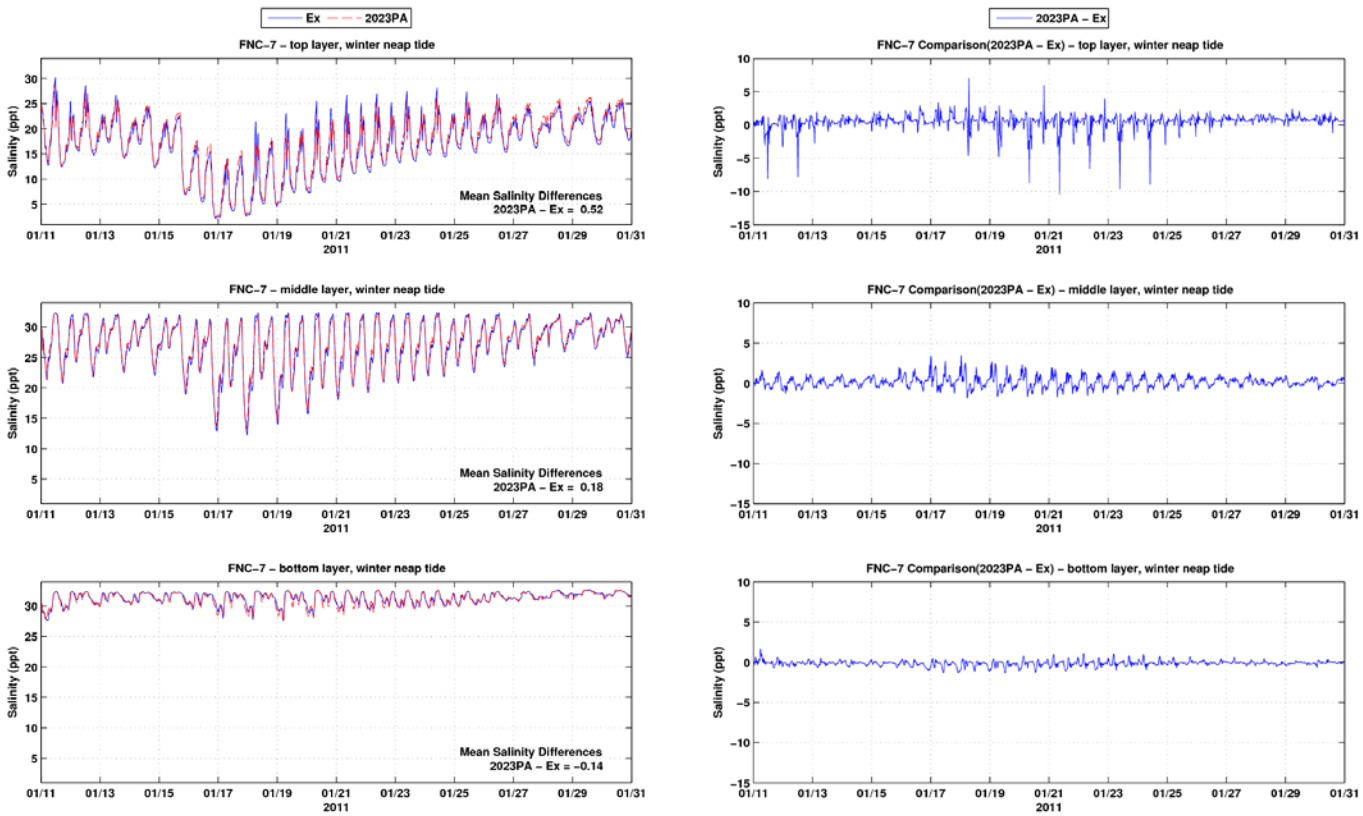

Figure C-15: Salinity time series and differences between the Existing Conditions and the 2023 PA at FNC-7 during winter neap tide period

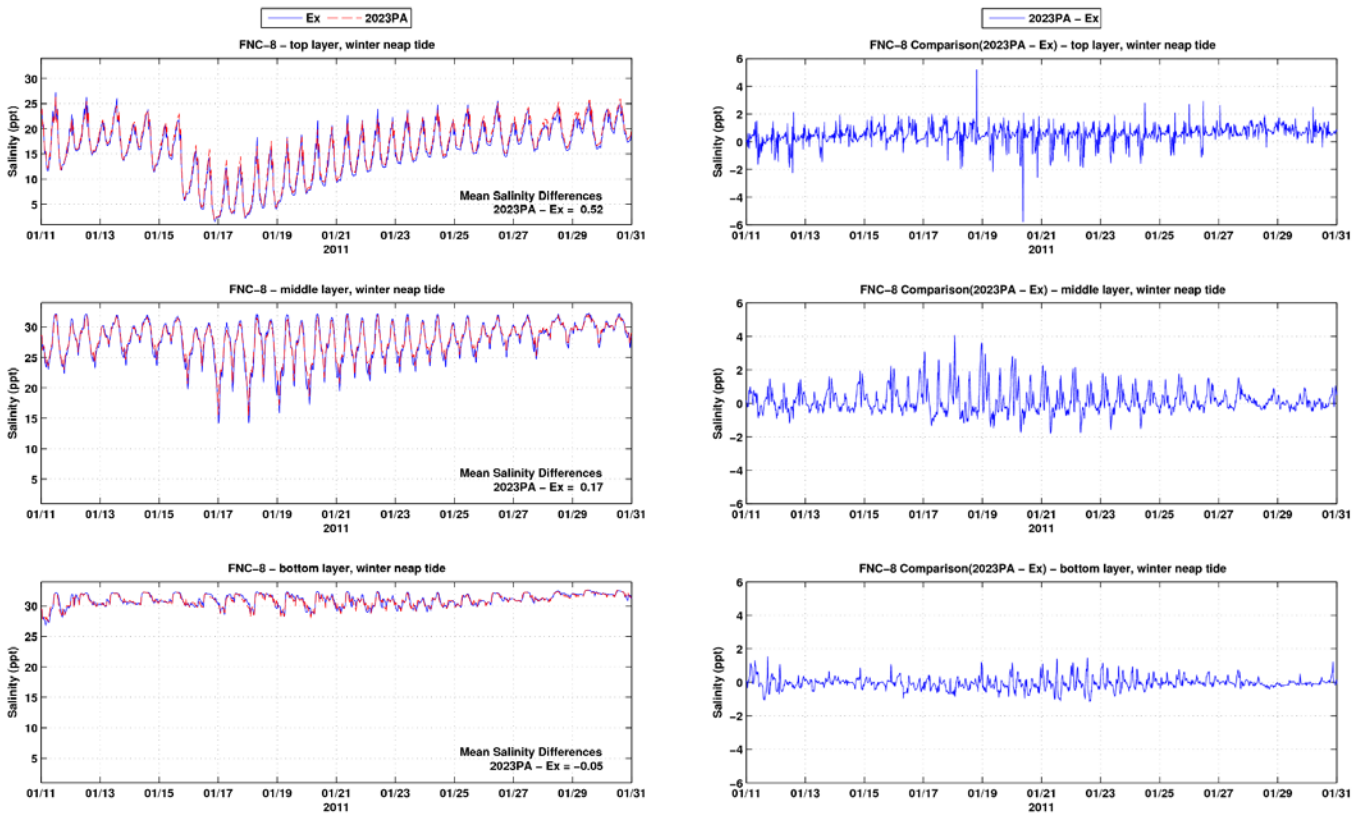

Figure C-16: Salinity time series and differences between the Existing Conditions and the 2023 PA at FNC-8 during winter neap tide period

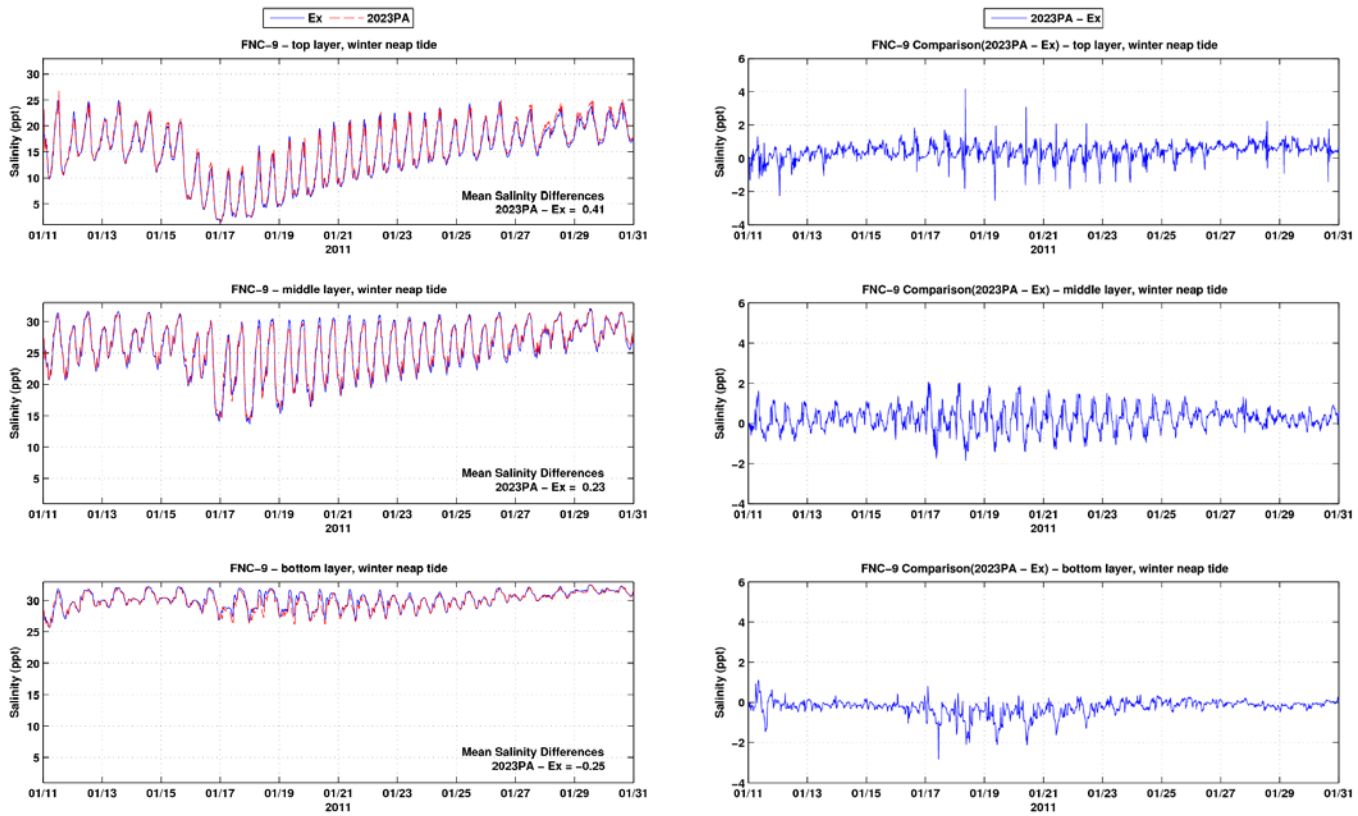

Figure C-17: Salinity time series and differences between the Existing Conditions and the 2023 PA at FNC-9 during winter neap tide period

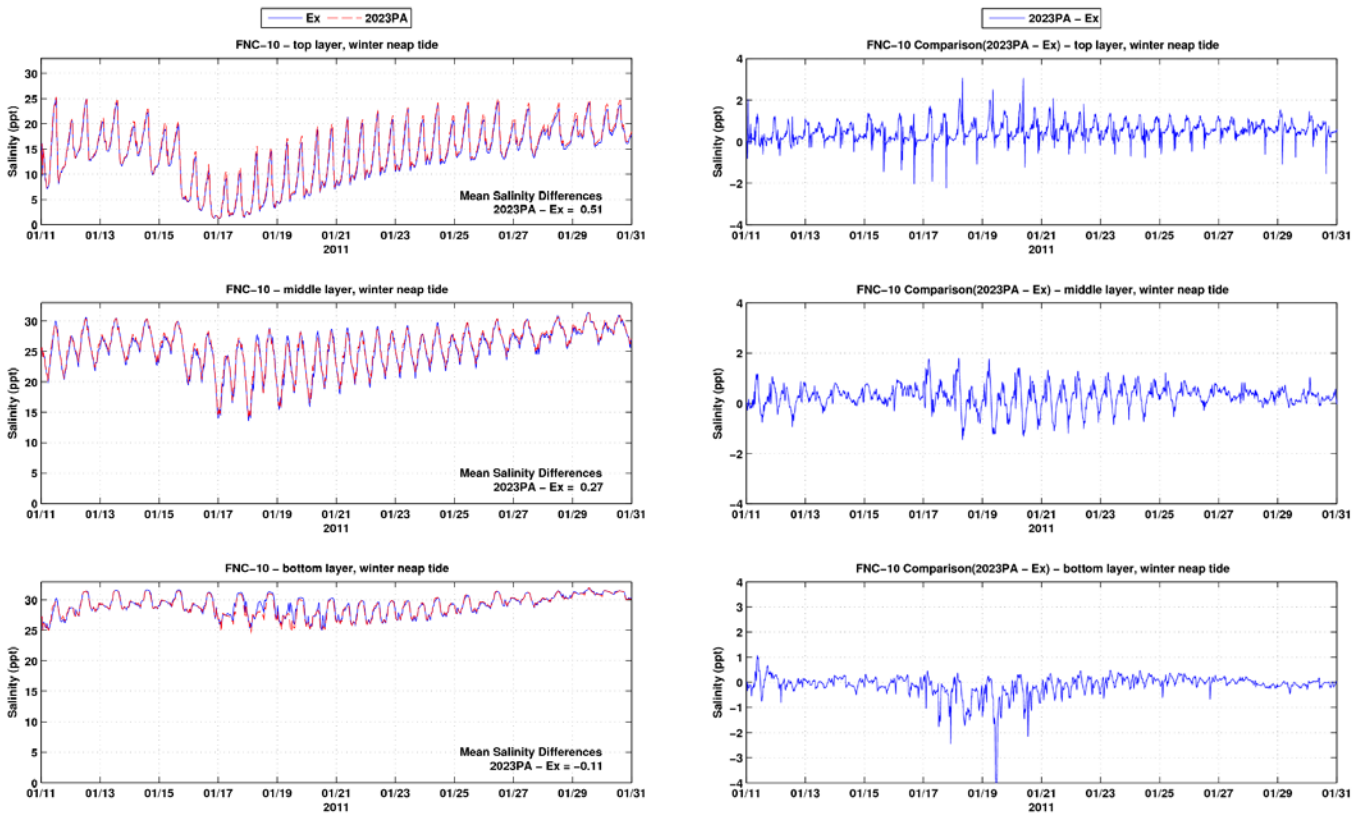

Figure C-18: Salinity time series and differences between the Existing Conditions and the 2023 PA at FNC-10 during winter neap tide period

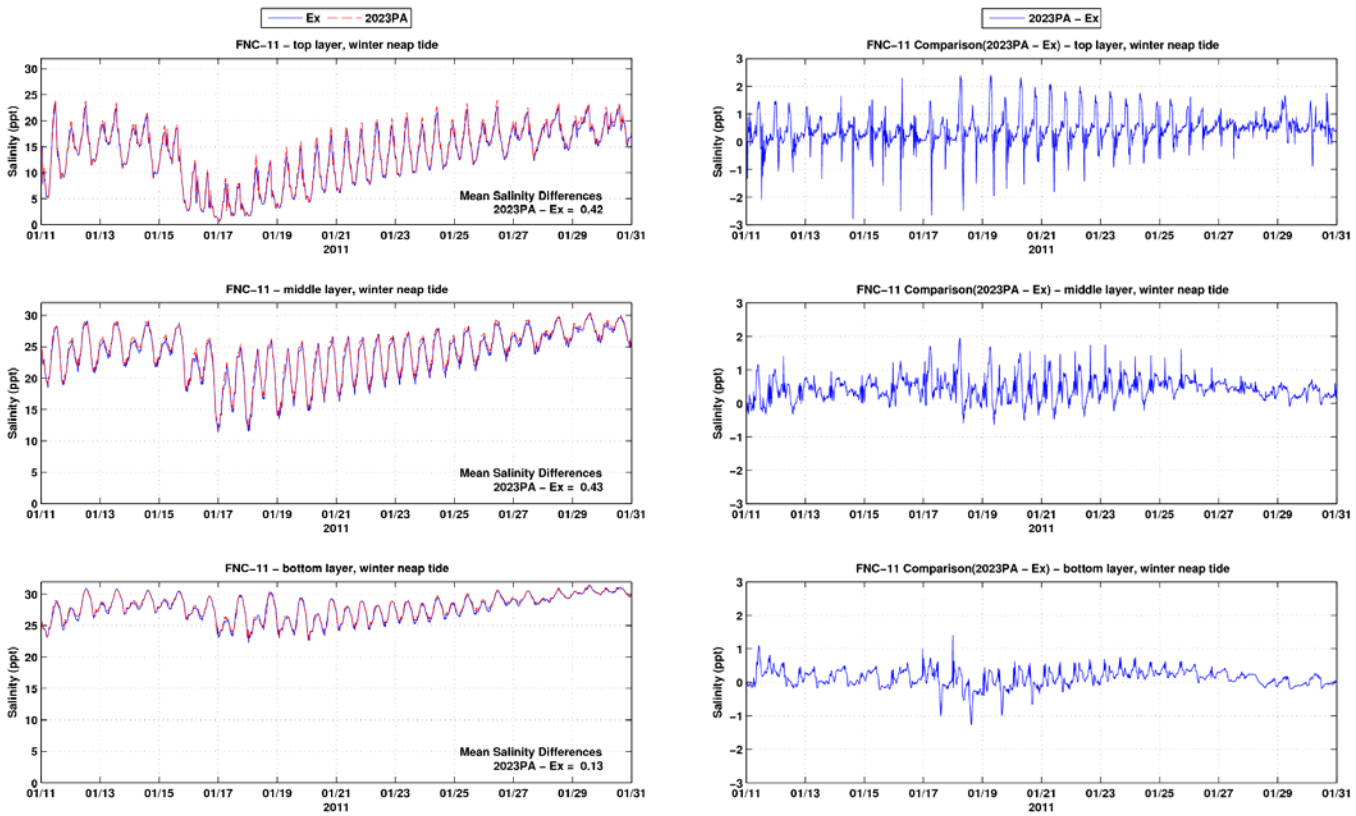

Figure C-19: Salinity time series and differences between the Existing Conditions and the 2023 PA at FNC-11 during winter neap tide period

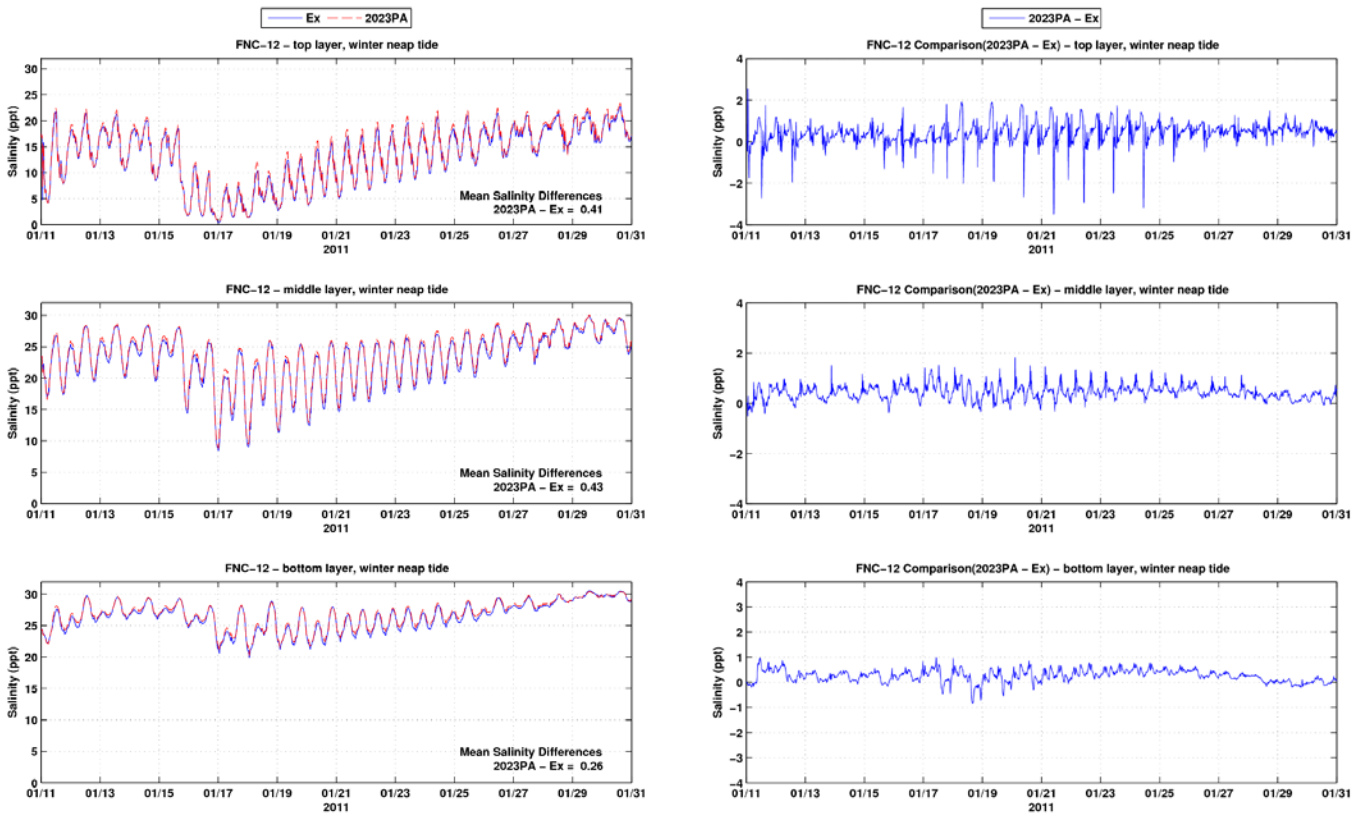

Figure C-20: Salinity time series and differences between the Existing Conditions and the 2023 PA at FNC-12 during winter neap tide period

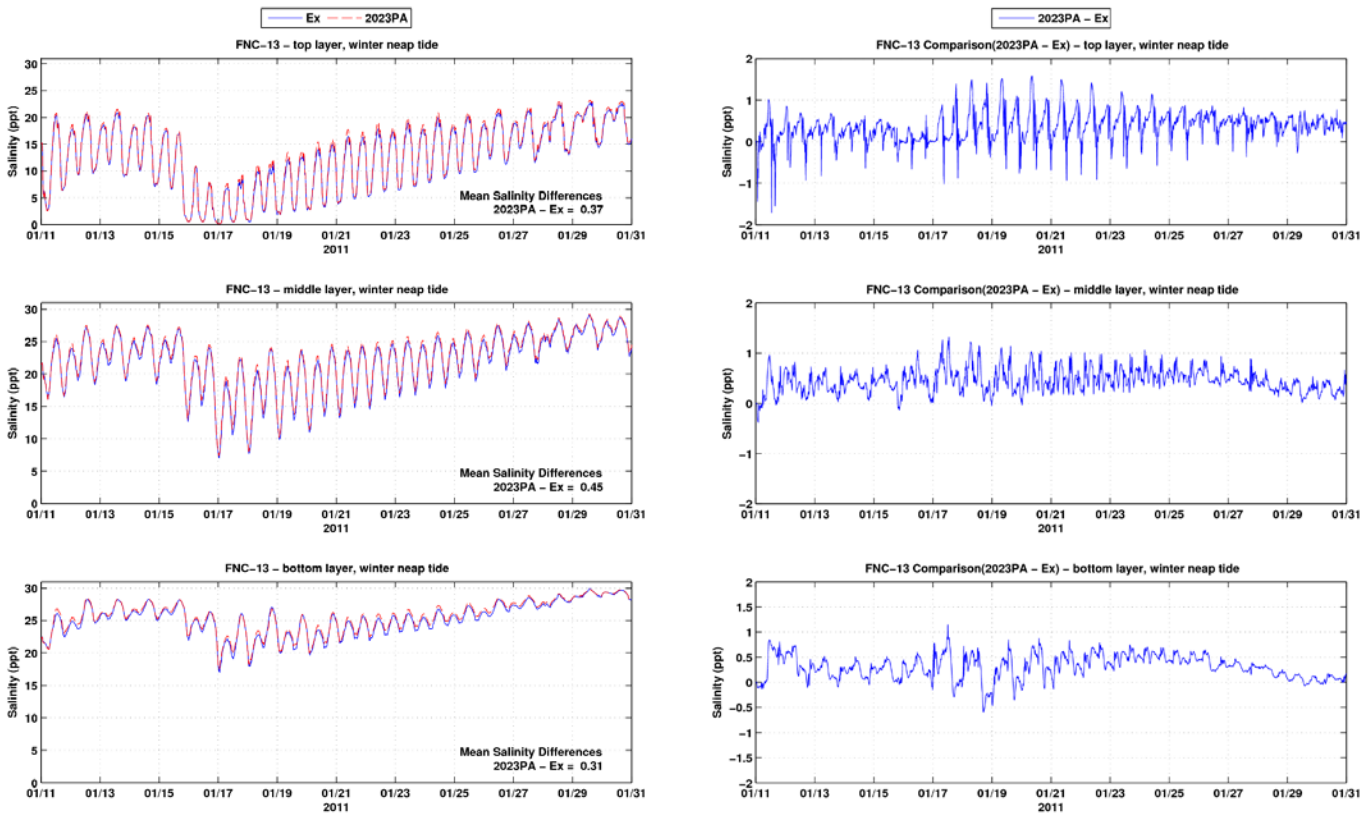

Figure C-21: Salinity time series and differences between the Existing Conditions and the 2023 PA at FNC-13 during winter neap tide period

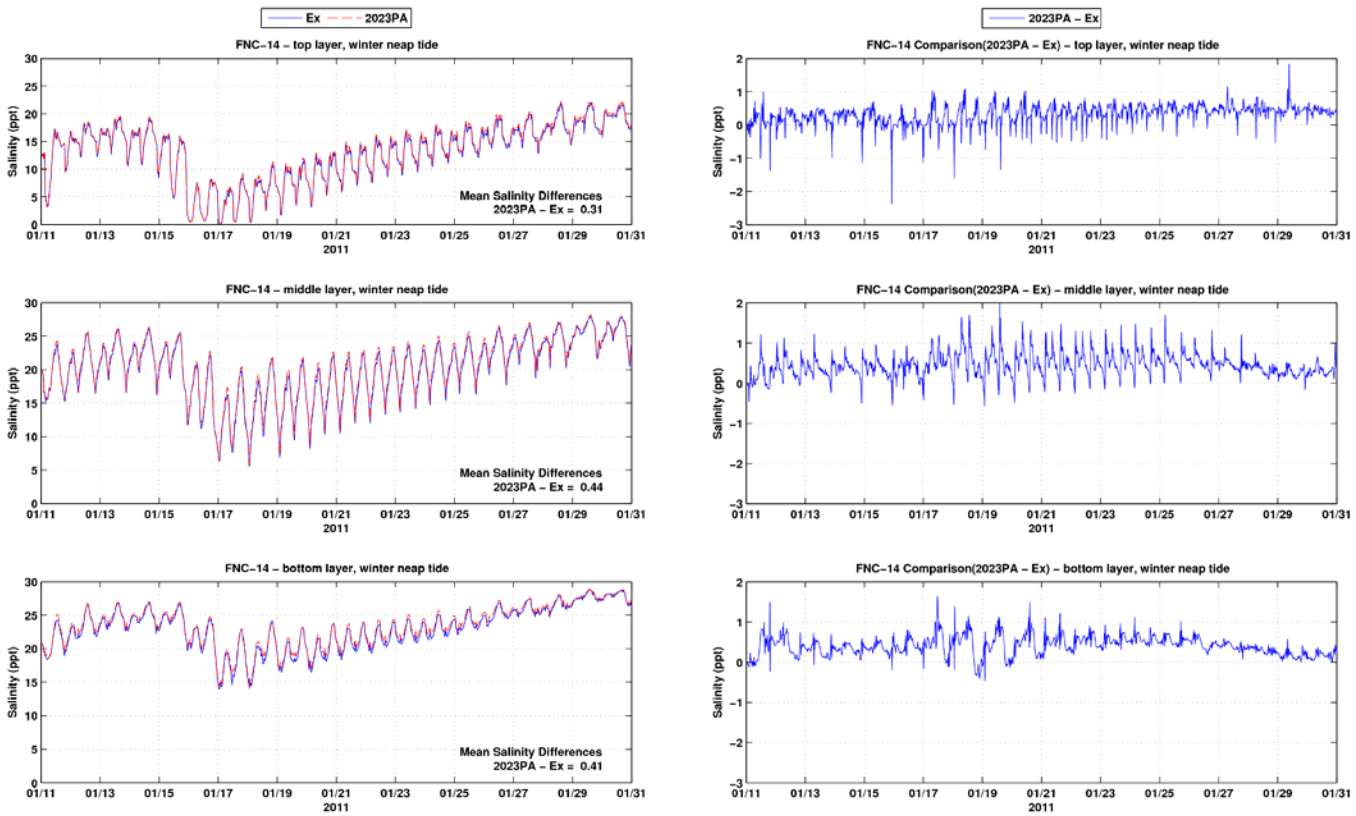

Figure C-22: Salinity time series and differences between the Existing Conditions and the 2023 PA at FNC-14 during winter neap tide period

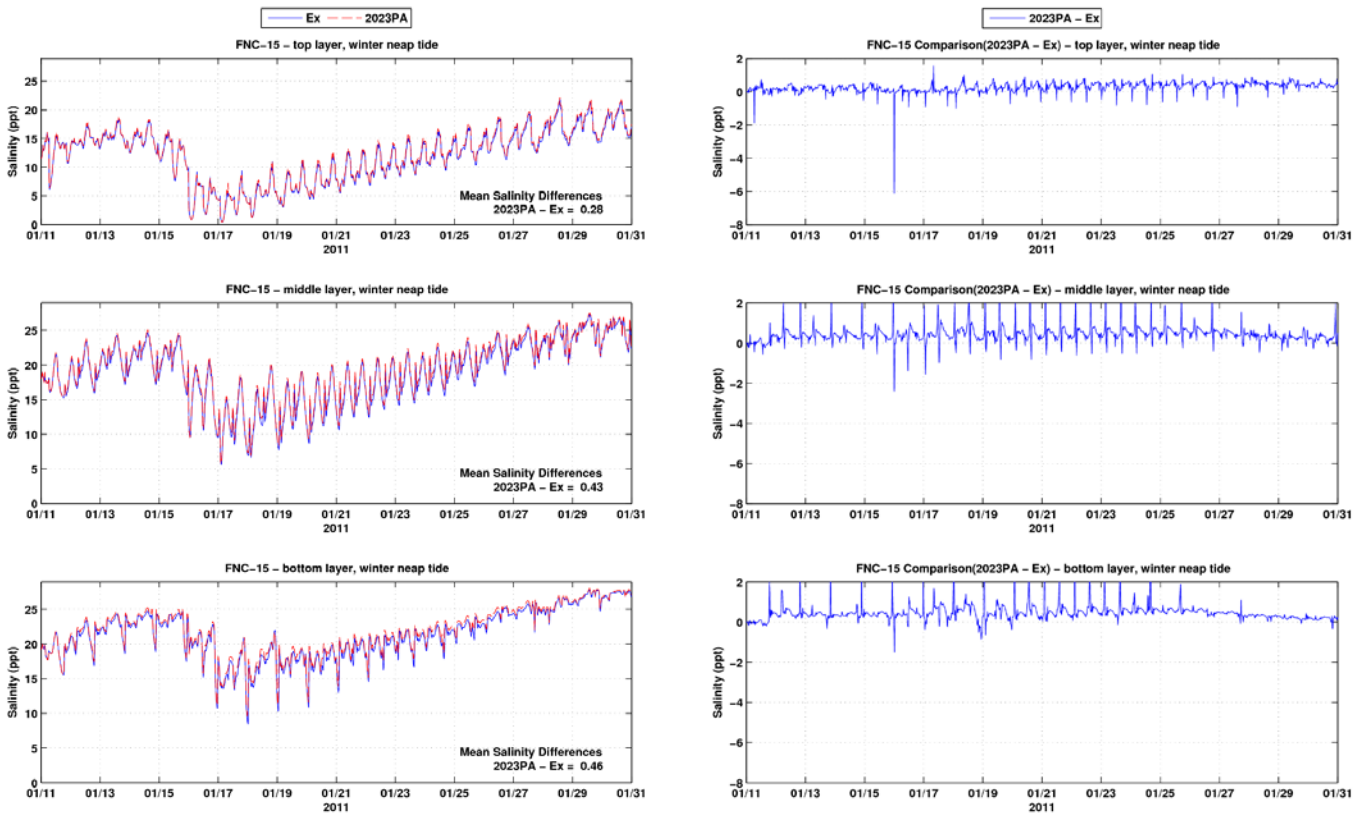

Figure C-23: Salinity time series and differences between the Existing Conditions and the 2023 PA at FNC-15 during winter neap tide period

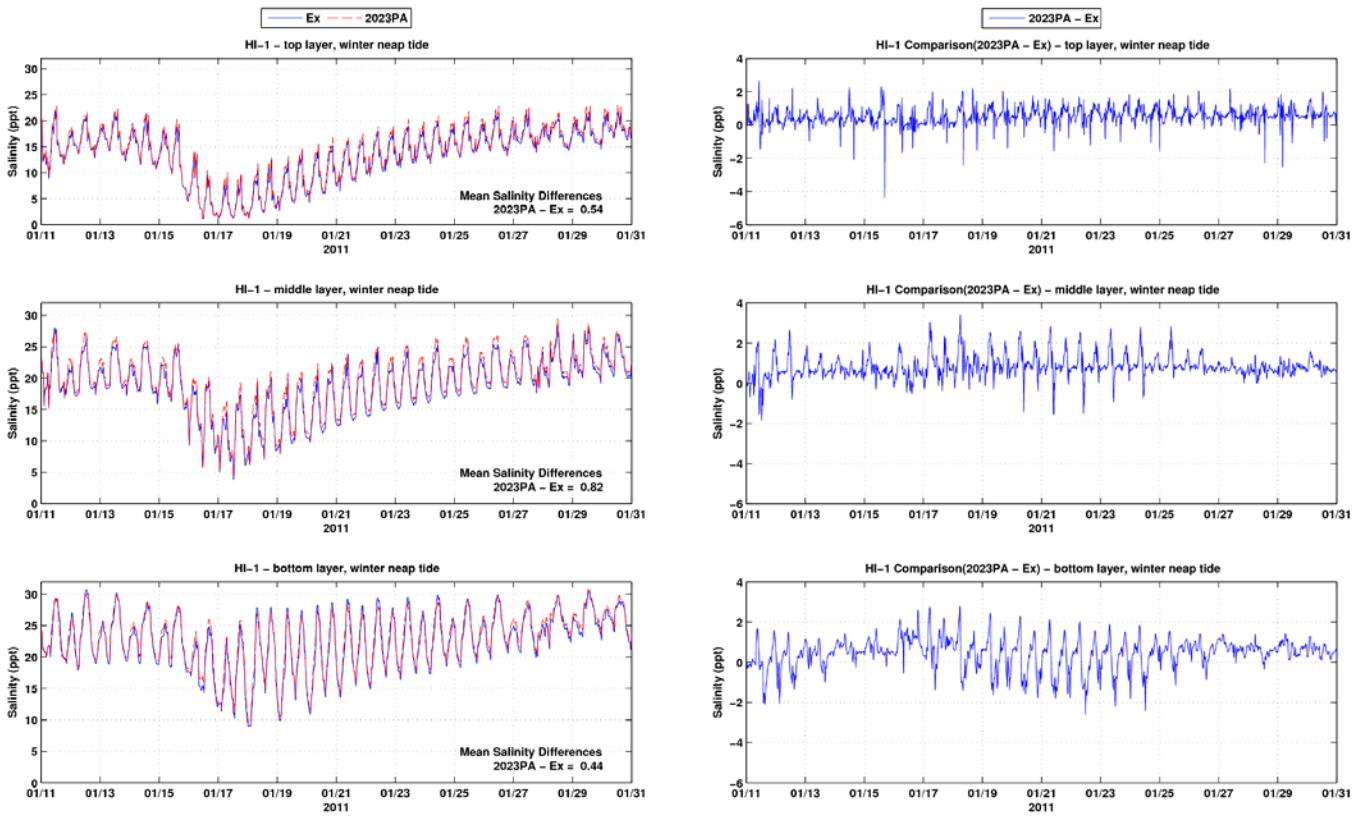

Figure C-24: Salinity time series and differences between the Existing Conditions and the 2023 PA at HI-1 during winter neap tide period

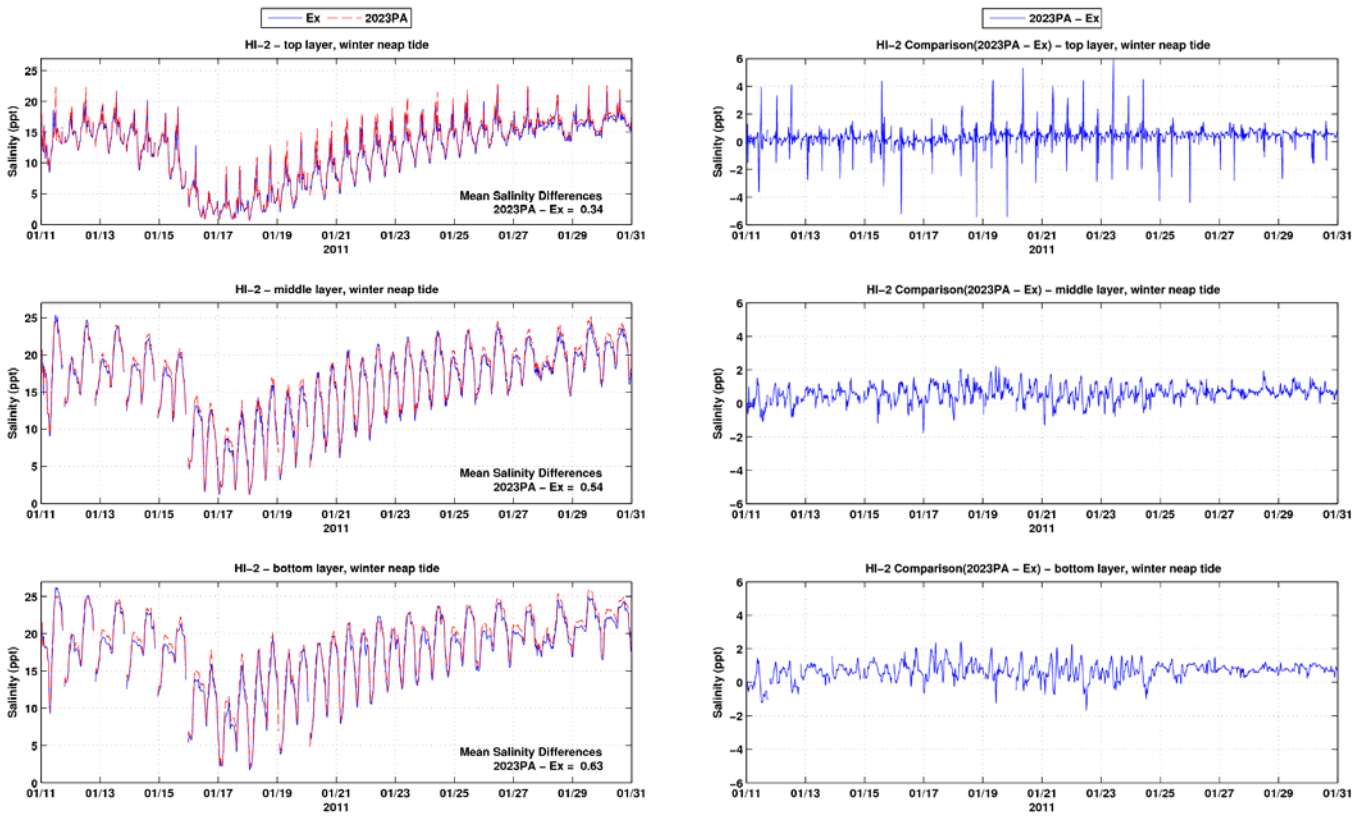

Figure C-25: Salinity time series and differences between the Existing Conditions and the 2023 PA at HI-2 during winter neap tide period

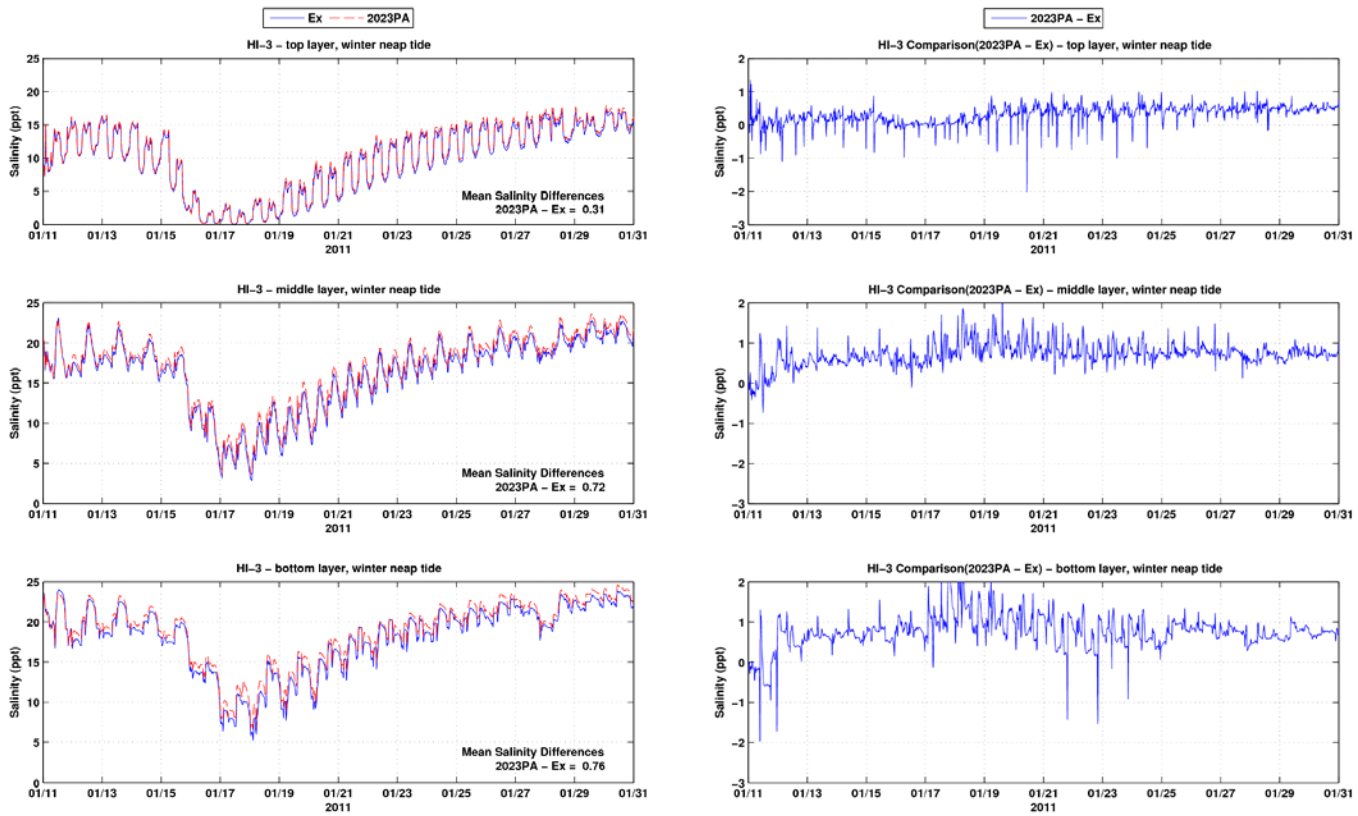

Figure C-26: Salinity time series and differences between the Existing Conditions and the 2023 PA at HI-3 during winter neap tide period

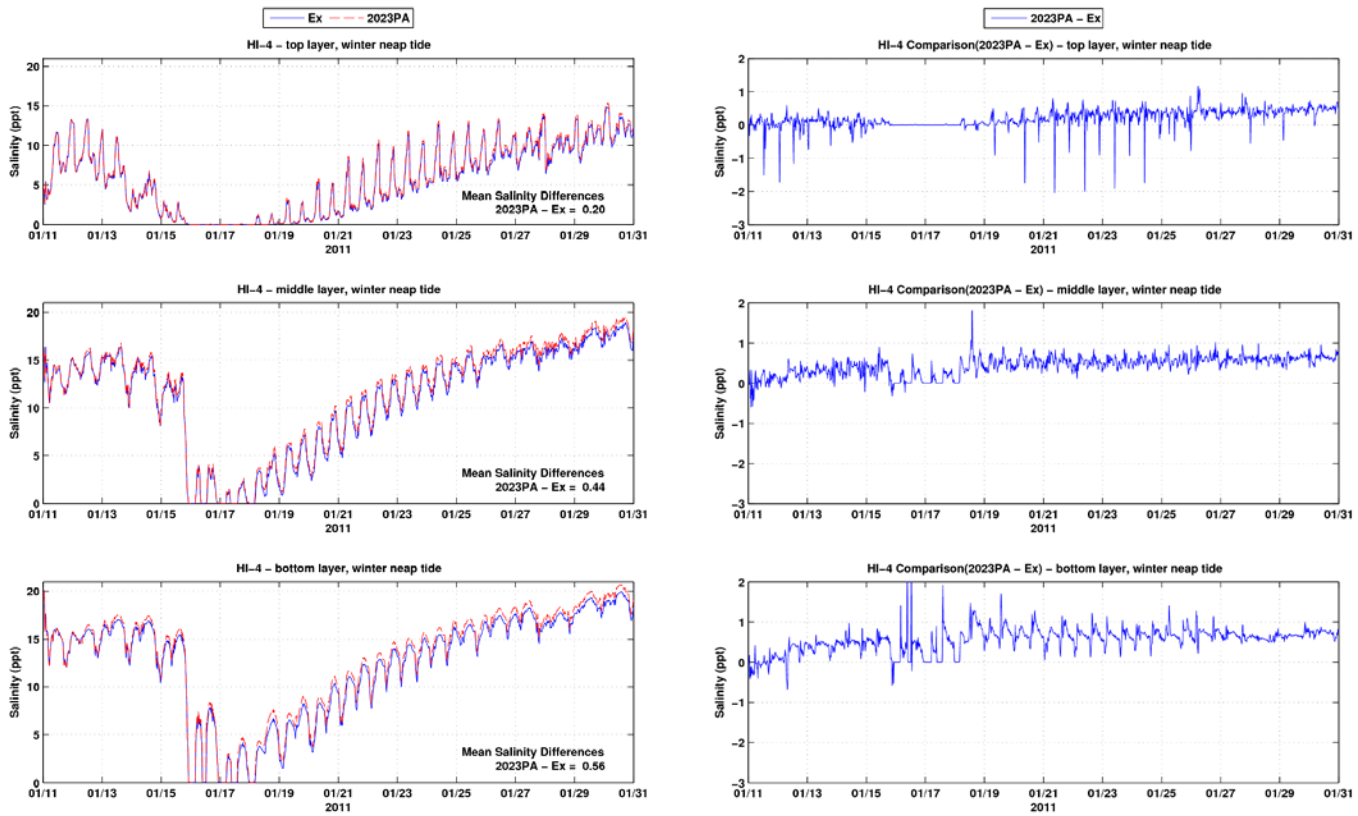

Figure C-27: Salinity time series and differences between the Existing Conditions and the 2023 PA at HI-4 during winter neap tide period

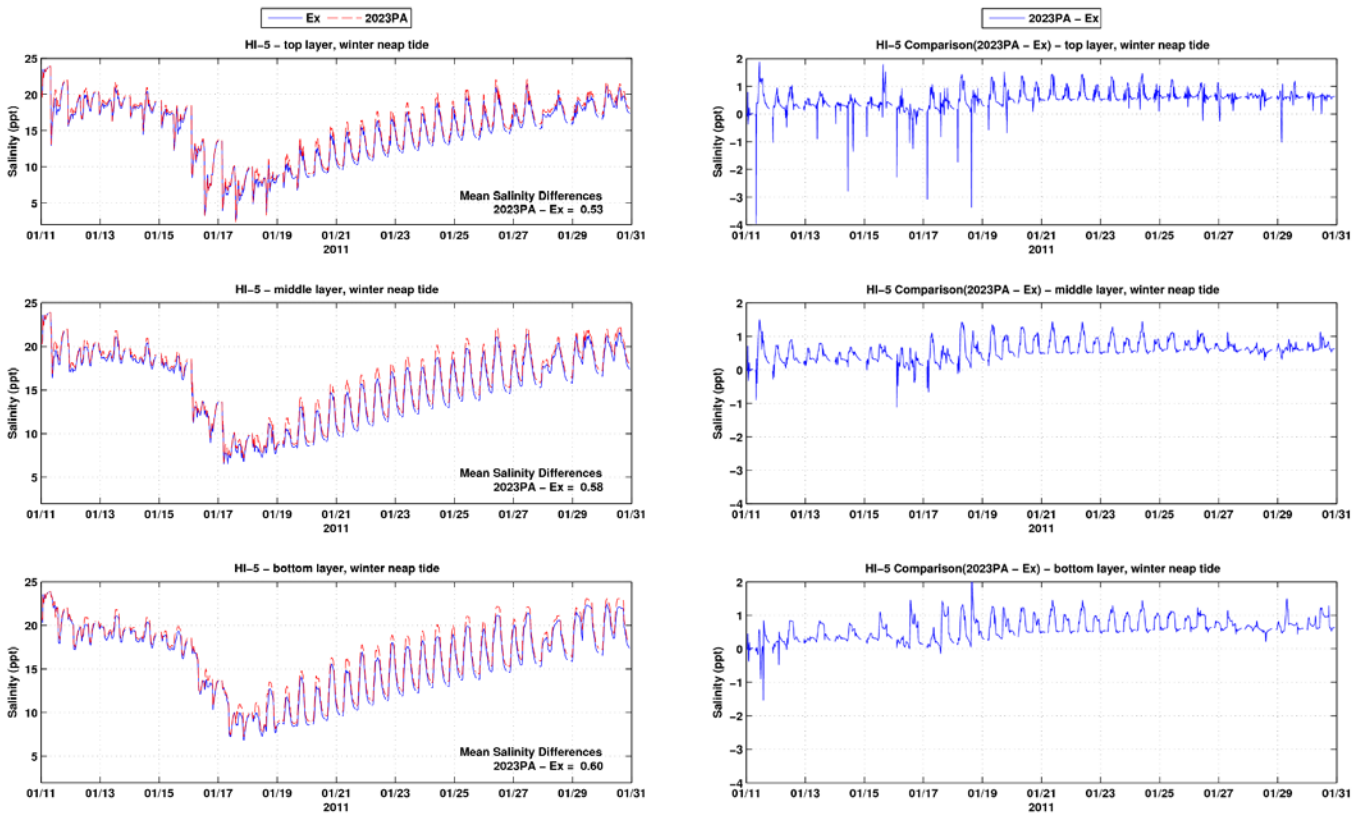

Figure C-28: Salinity time series and differences between the Existing Conditions and the 2023 PA at HI-5 during winter neap tide period

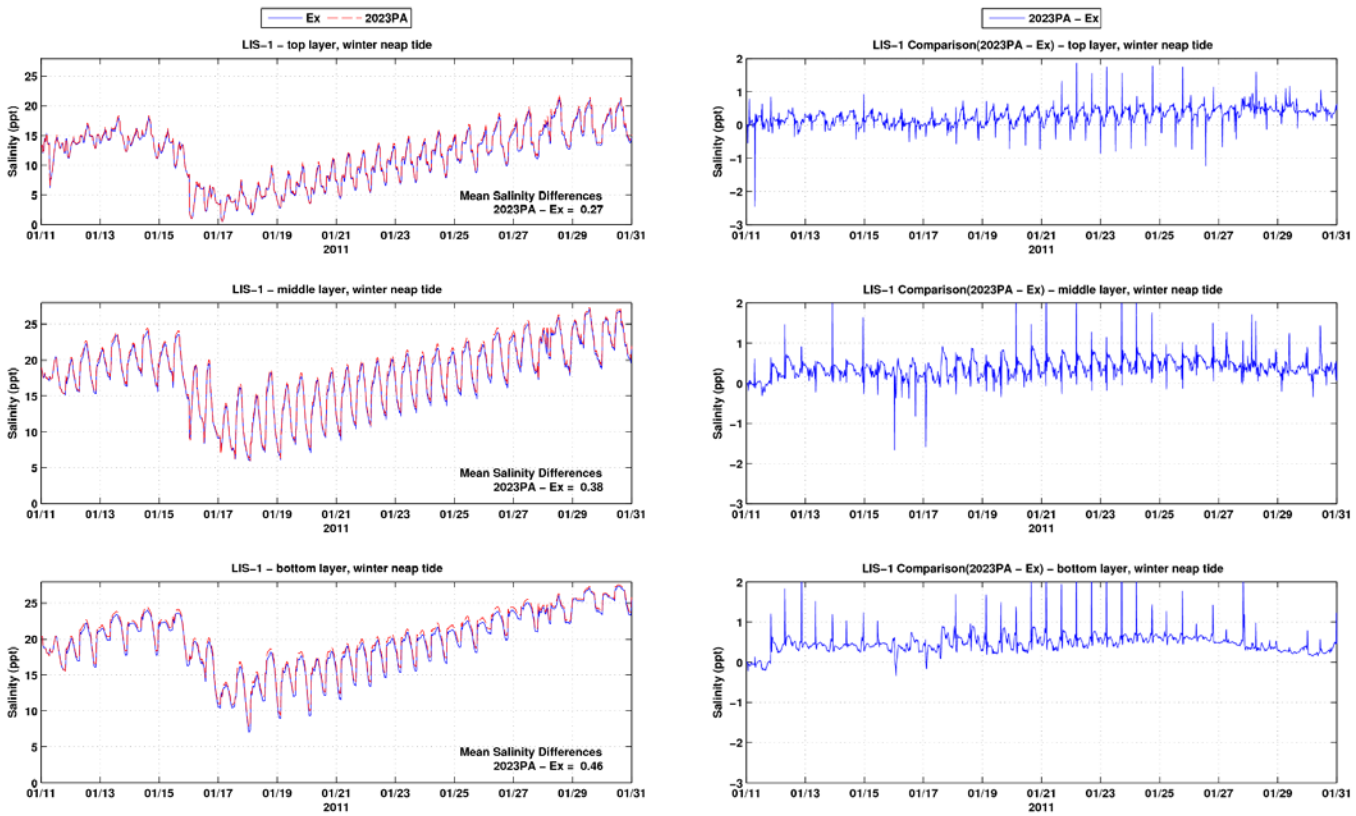

Figure C-29: Salinity time series and differences between the Existing Conditions and the 2023 PA at LIS-1 during winter neap tide period

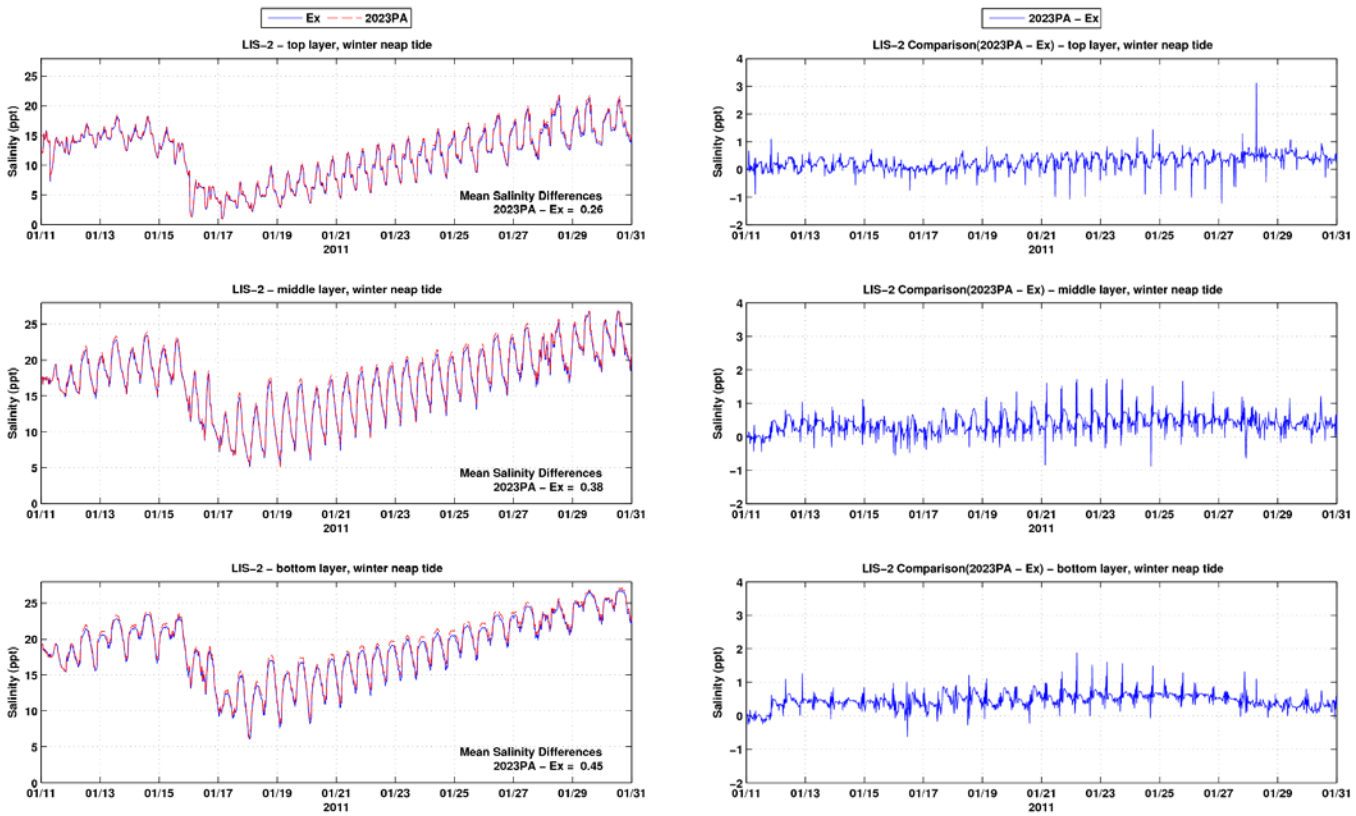

Figure C-30: Salinity time series and differences between the Existing Conditions and the 2023 PA at LIS-2 during winter neap tide period

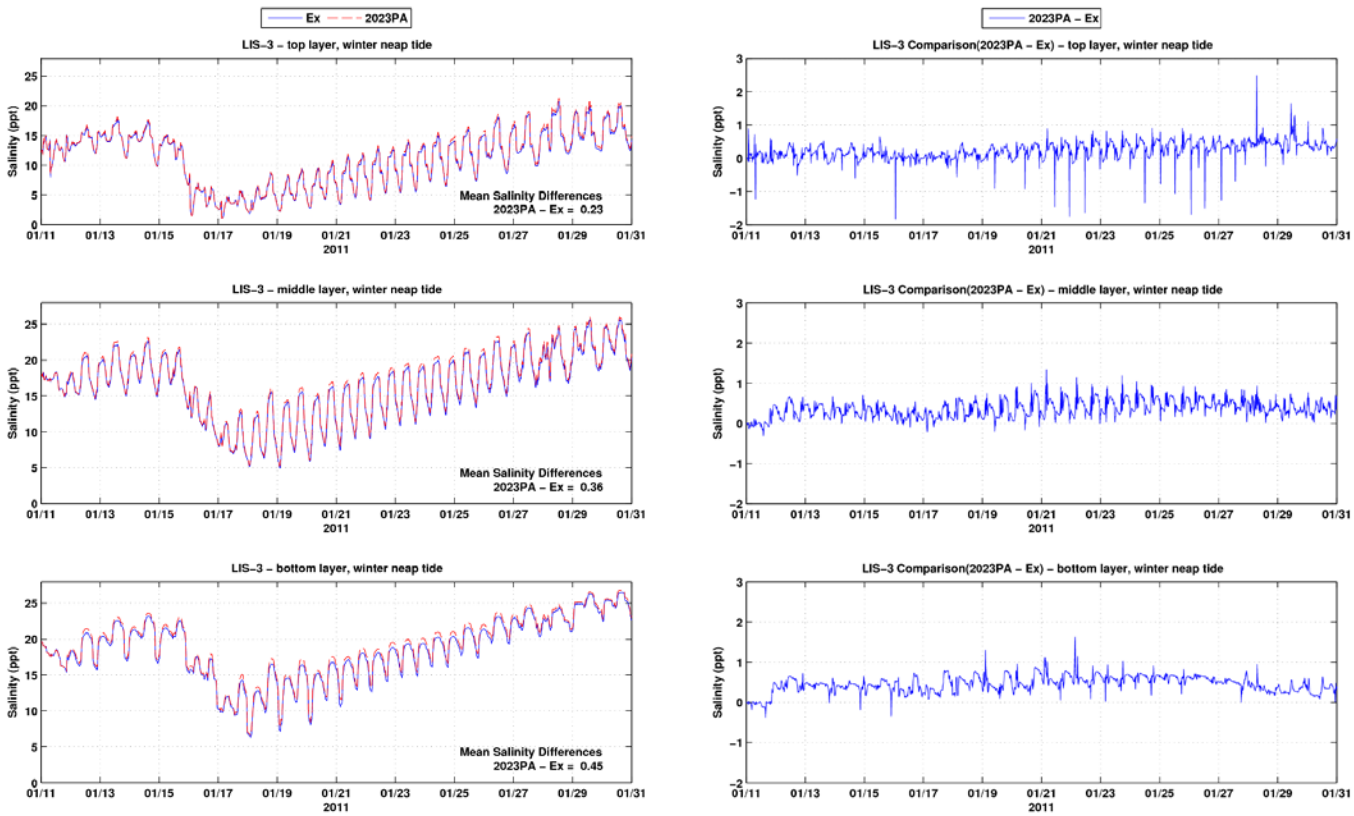

Figure C-31: Salinity time series and differences between the Existing Conditions and the 2023 PA at LIS-3 during winter neap tide period

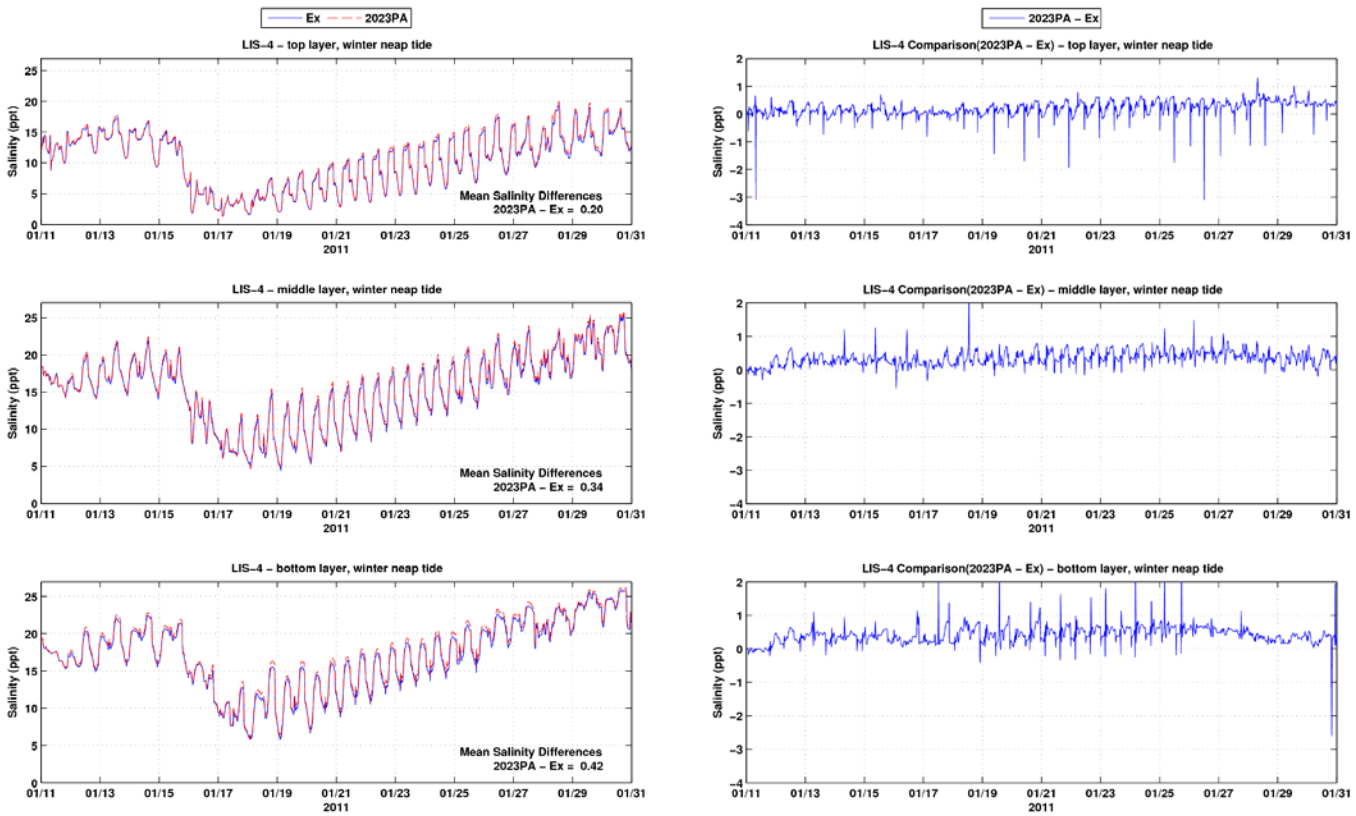

Figure C-32: Salinity time series and differences between the Existing Conditions and the 2023 PA at LIS-4 during winter neap tide period

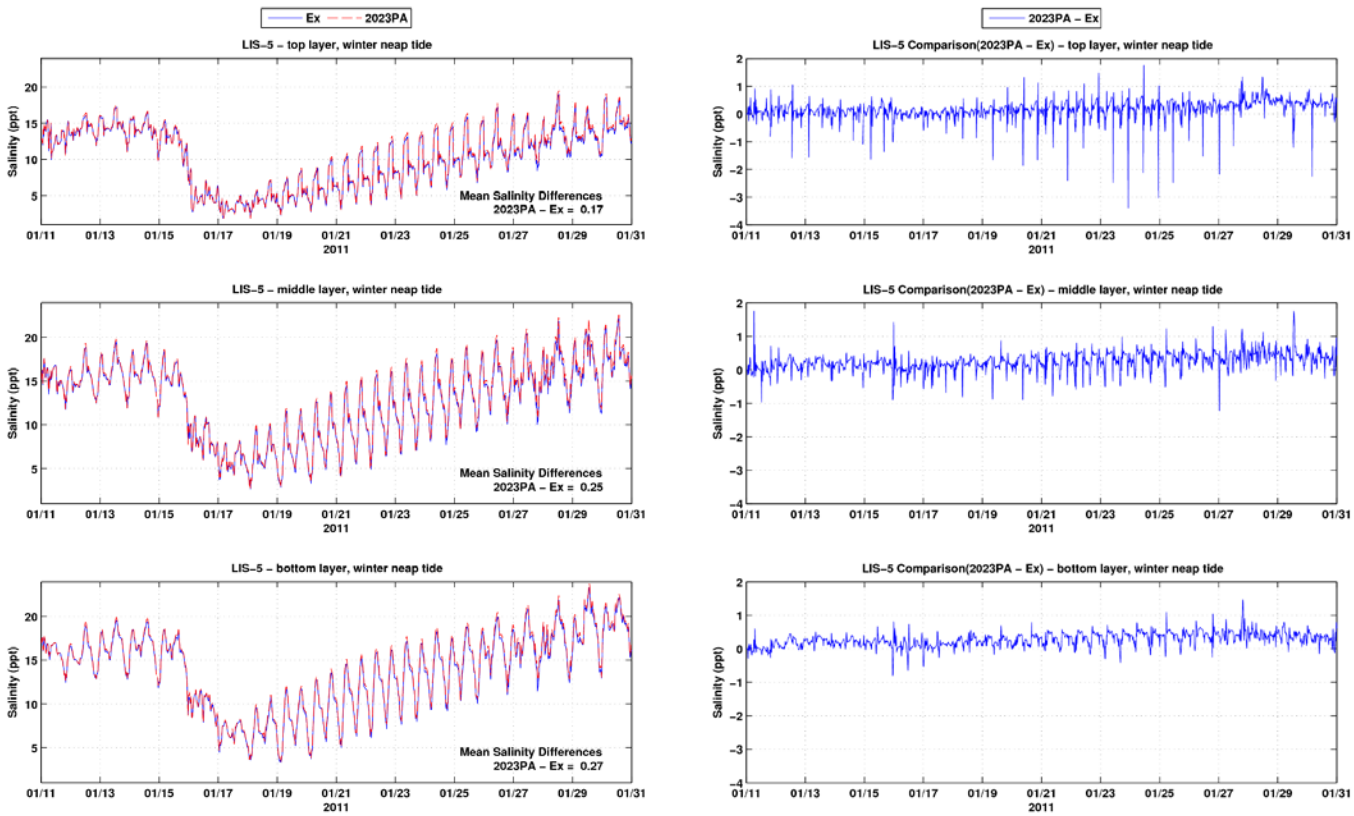

Figure C-33: Salinity time series and differences between the Existing Conditions and the 2023 PA at LIS-5 during winter neap tide period

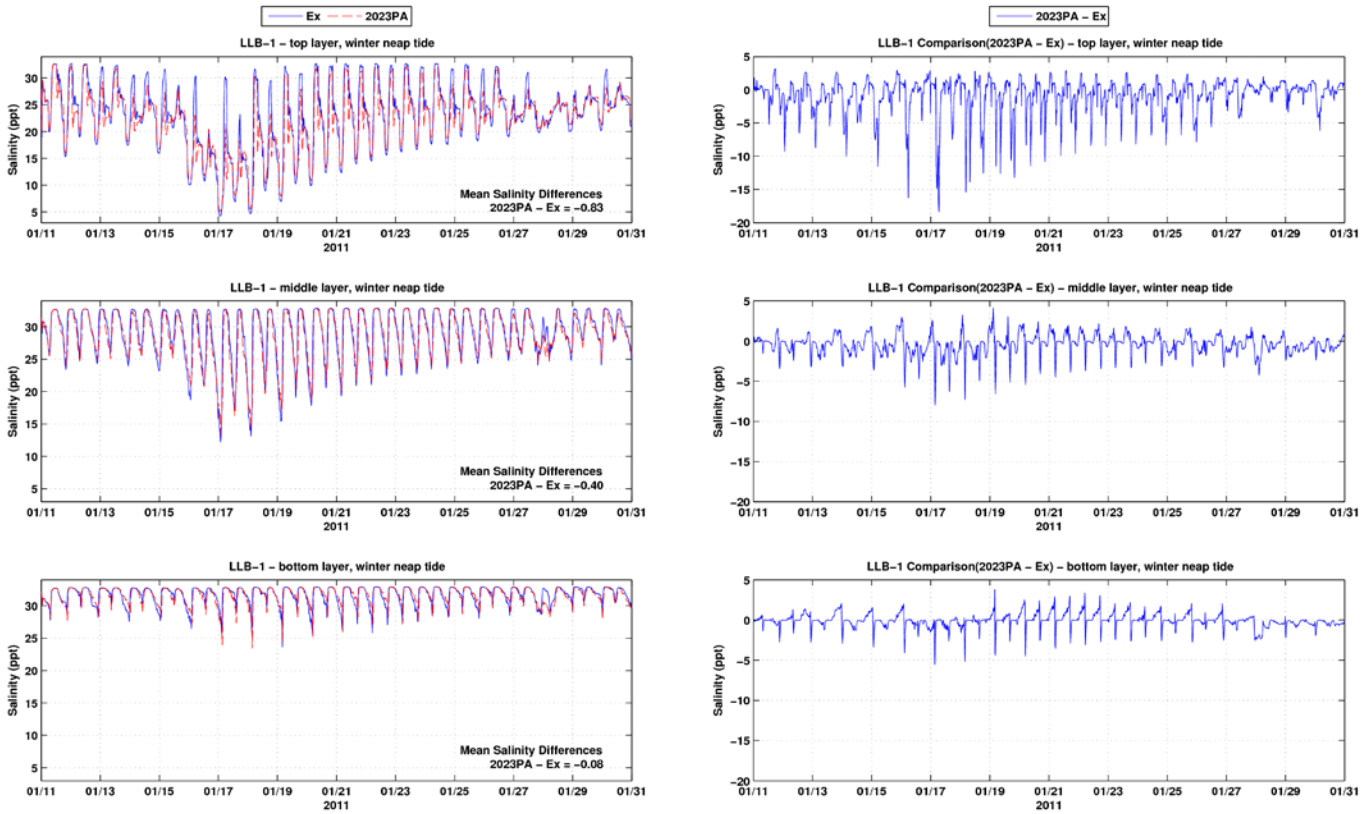

Figure C-34: Salinity time series and differences between the Existing Conditions and the 2023 PA at LLB-1 during winter neap tide period

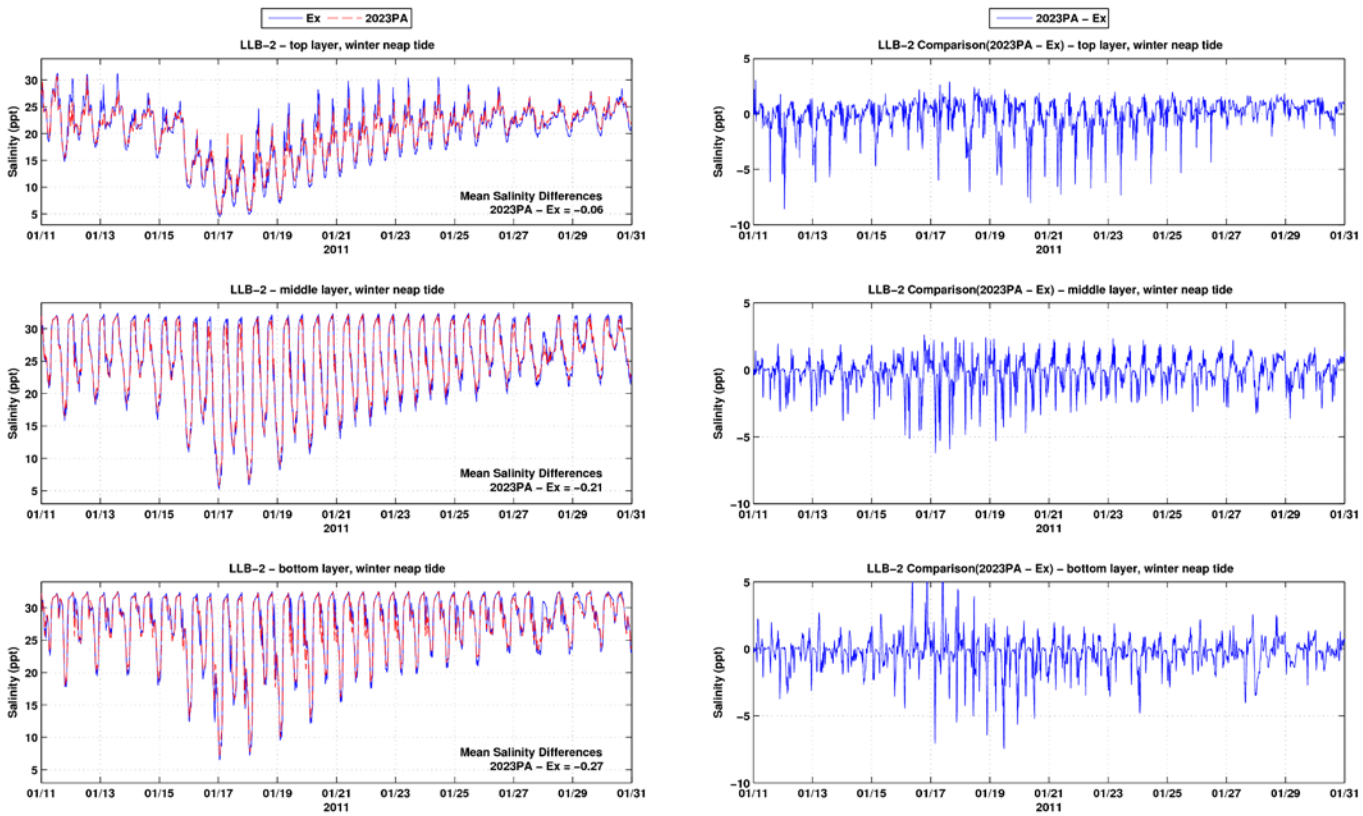

Figure C-35: Salinity time series and differences between the Existing Conditions and the 2023 PA at LLB-2 during winter neap tide period

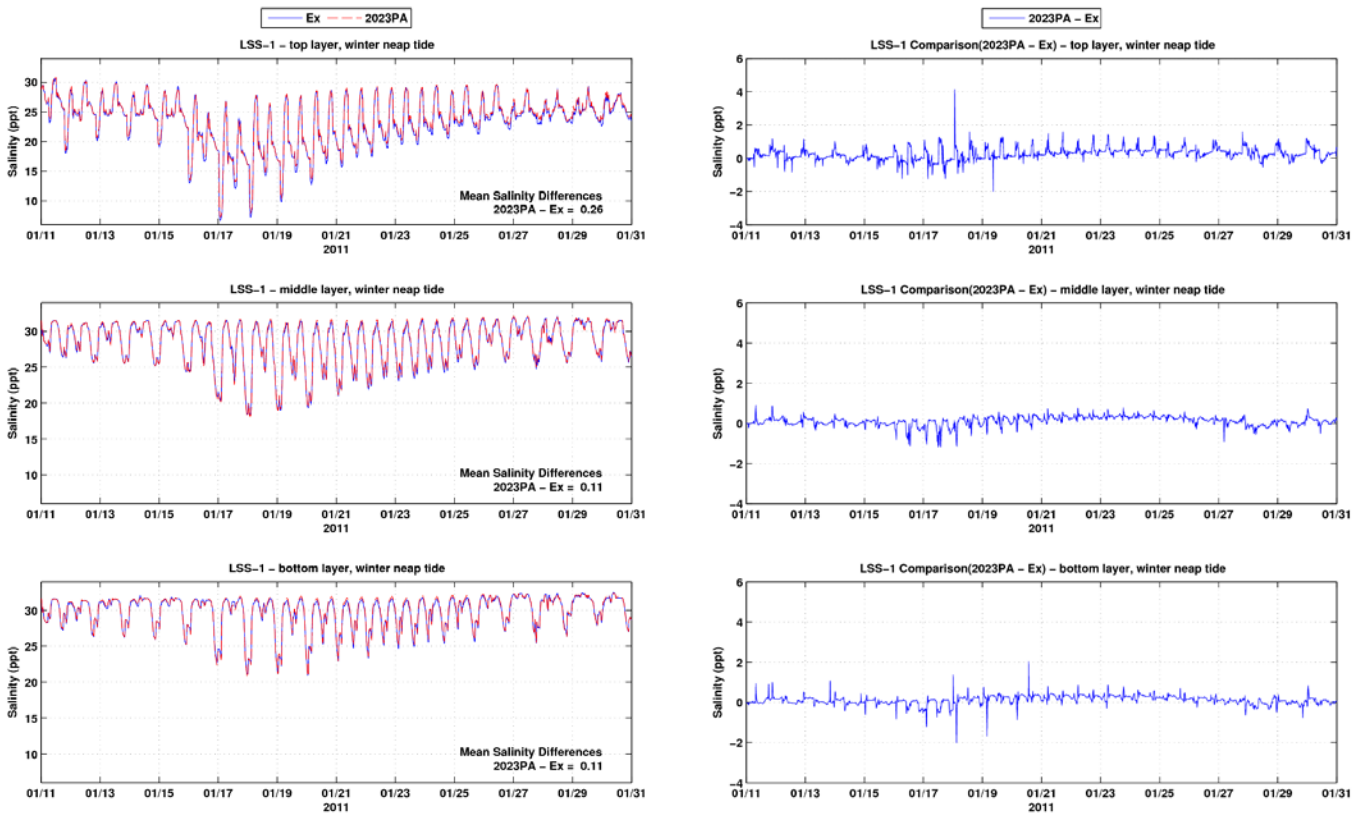

Figure C-36: Salinity time series and differences between the Existing Conditions and the 2023 PA at LSS-1 during winter neap tide period

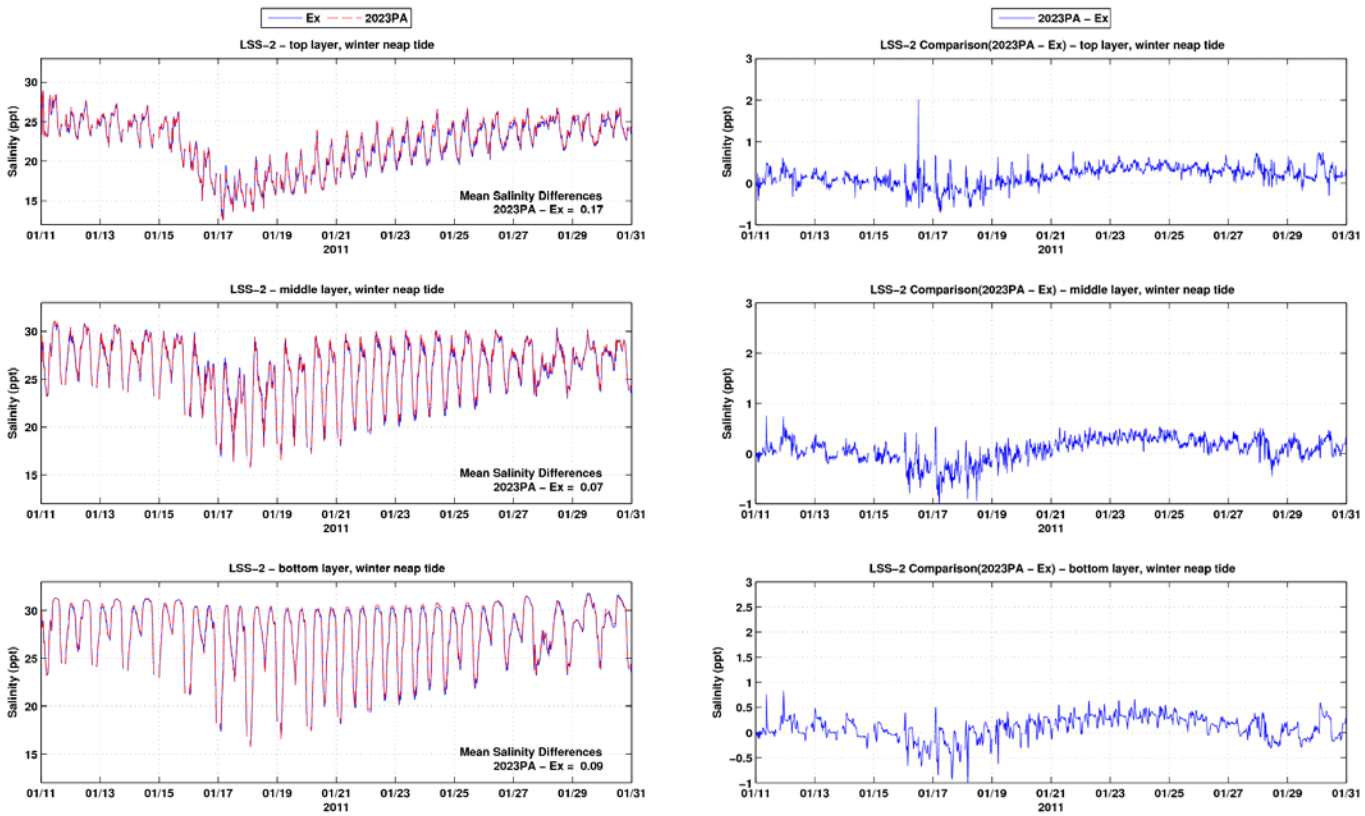

Figure C-37: Salinity time series and differences between the Existing Conditions and the 2023 PA at LSS-2 during winter neap tide period

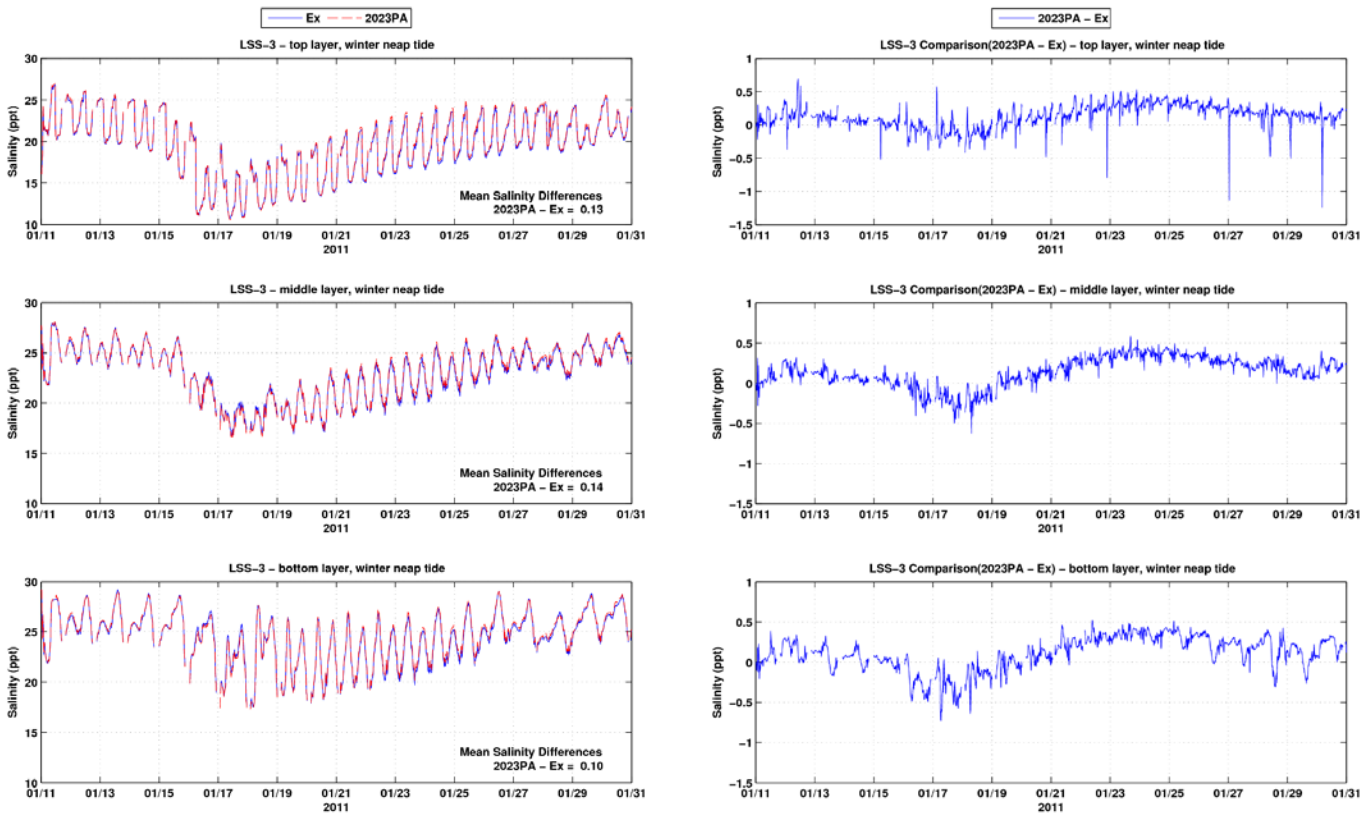

Figure C-38: Salinity time series and differences between the Existing Conditions and the 2023 PA at LSS-3 during winter neap tide period

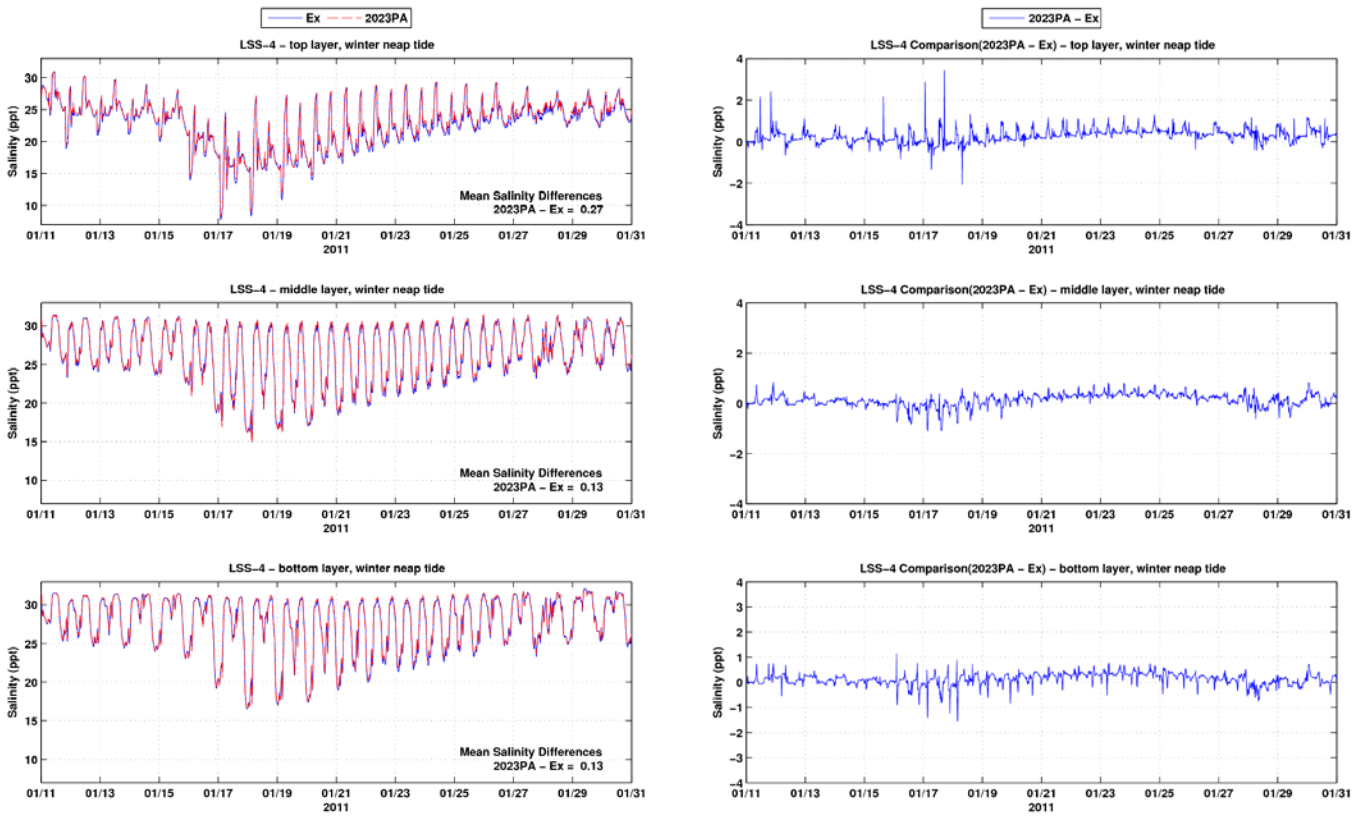

Figure C-39: Salinity time series and differences between the Existing Conditions and the 2023 PA at LSS-4 during winter neap tide period

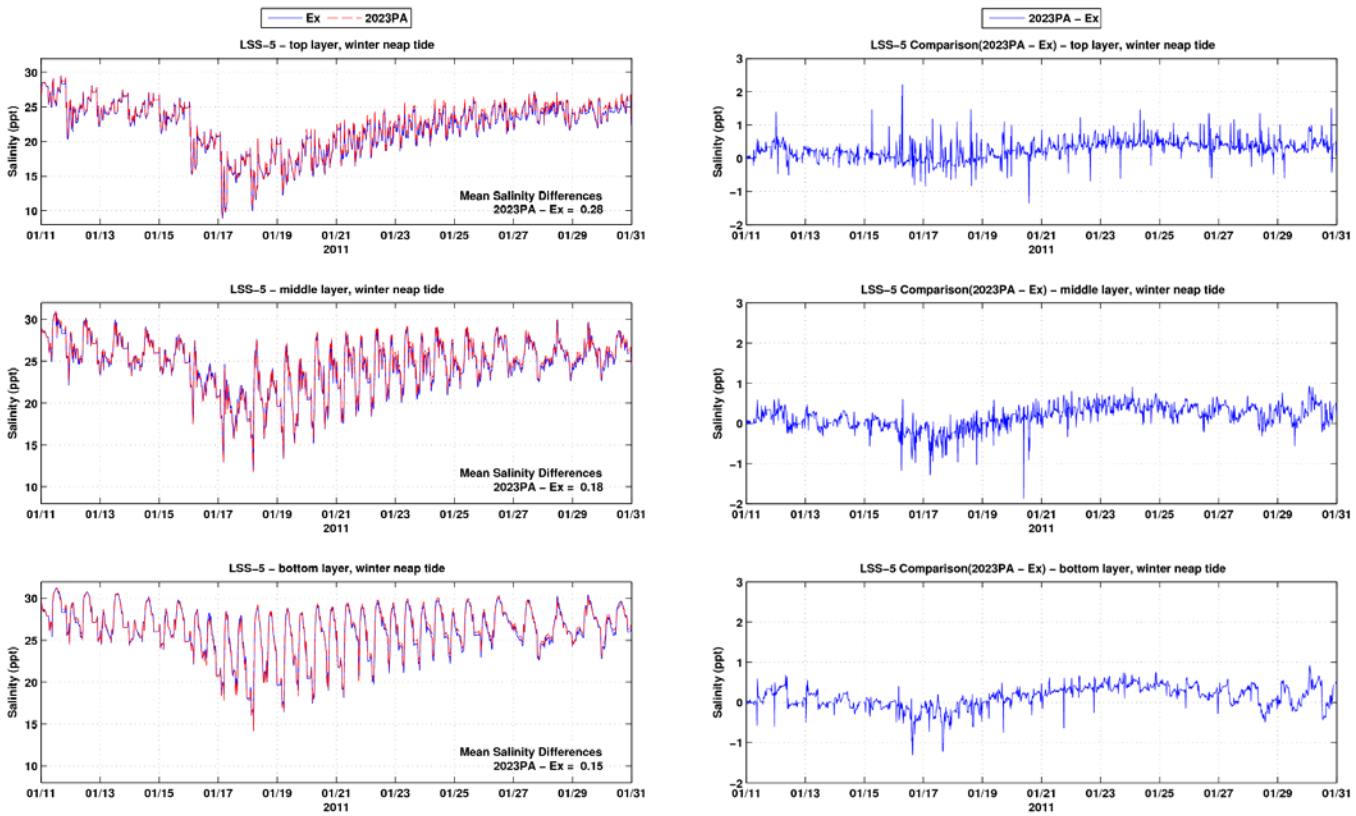

Figure C-40: Salinity time series and differences between the Existing Conditions and the 2023 PA at LSS-5 during winter neap tide period

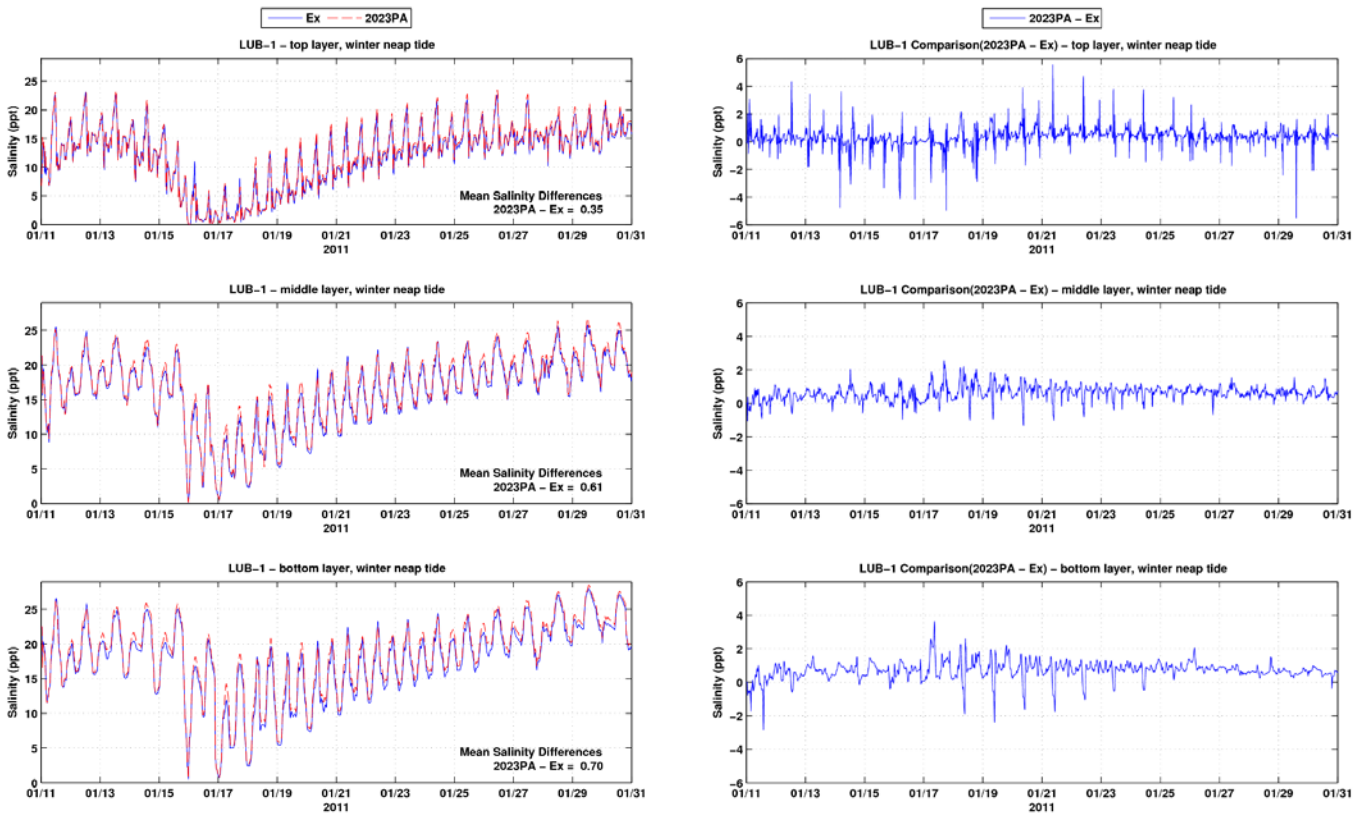

Figure C-41: Salinity time series and differences between the Existing Conditions and the 2023 PA at LUB-1 during winter neap tide period

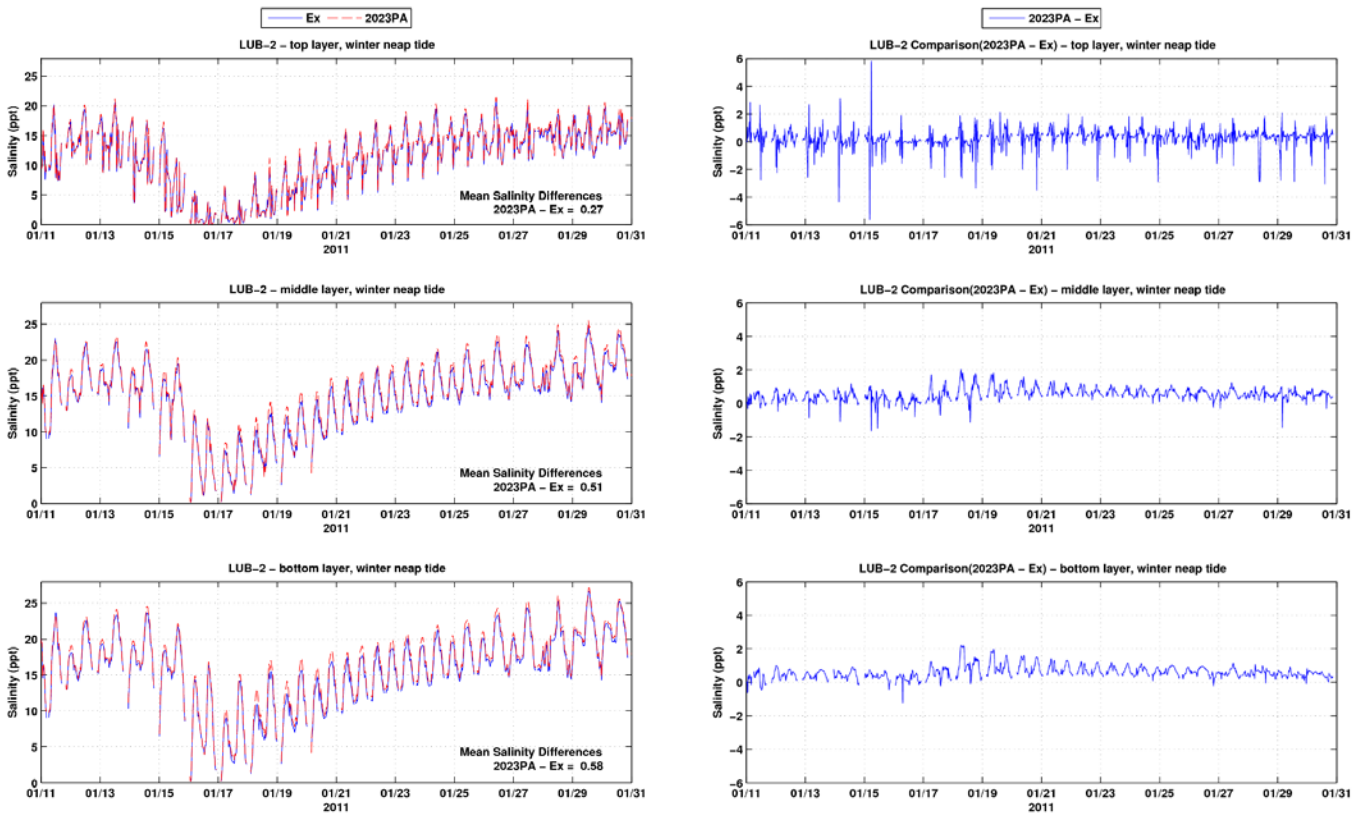

Figure C-42: Salinity time series and differences between the Existing Conditions and the 2023 PA at LUB-2 during winter neap tide period

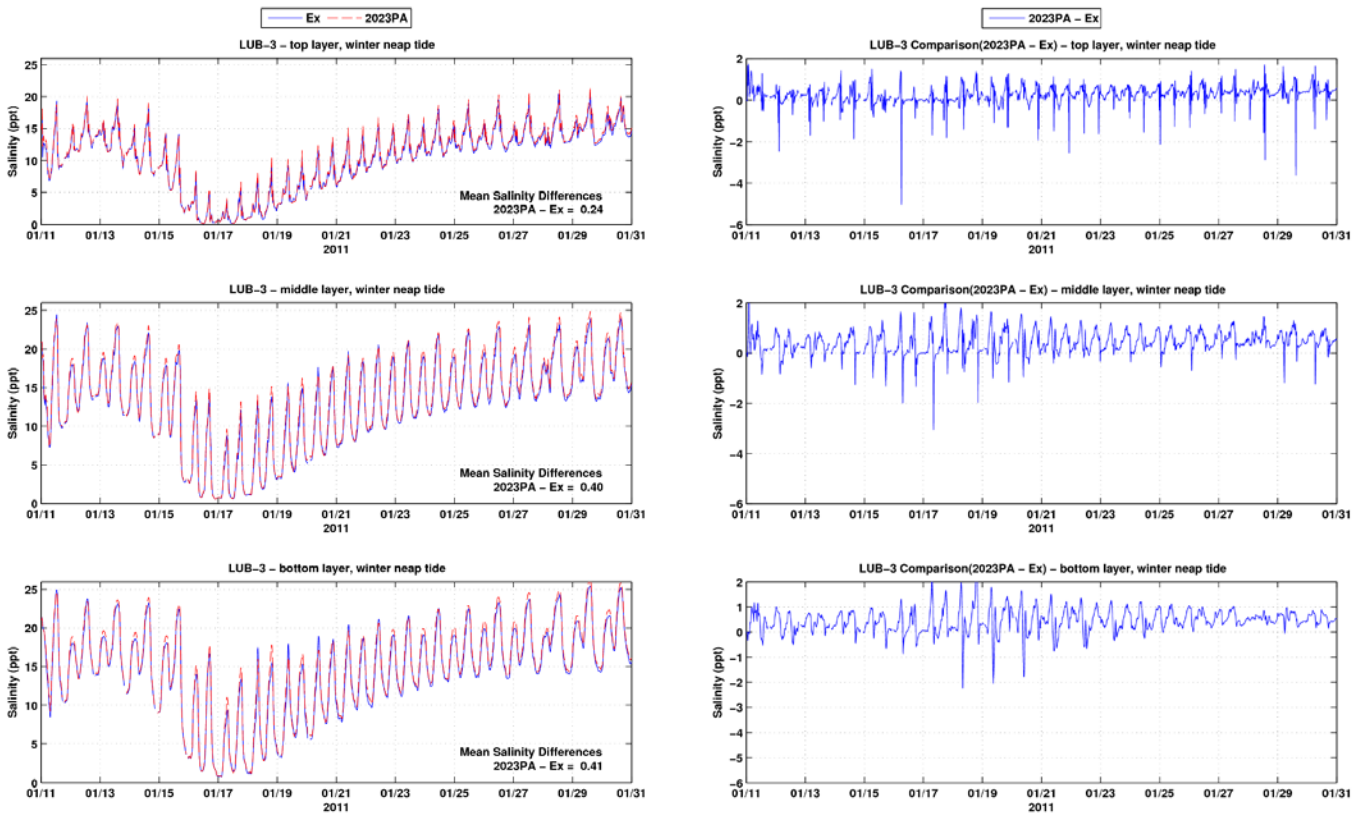

Figure C-43: Salinity time series and differences between the Existing Conditions and the 2023 PA at LUB-3 during winter neap tide period

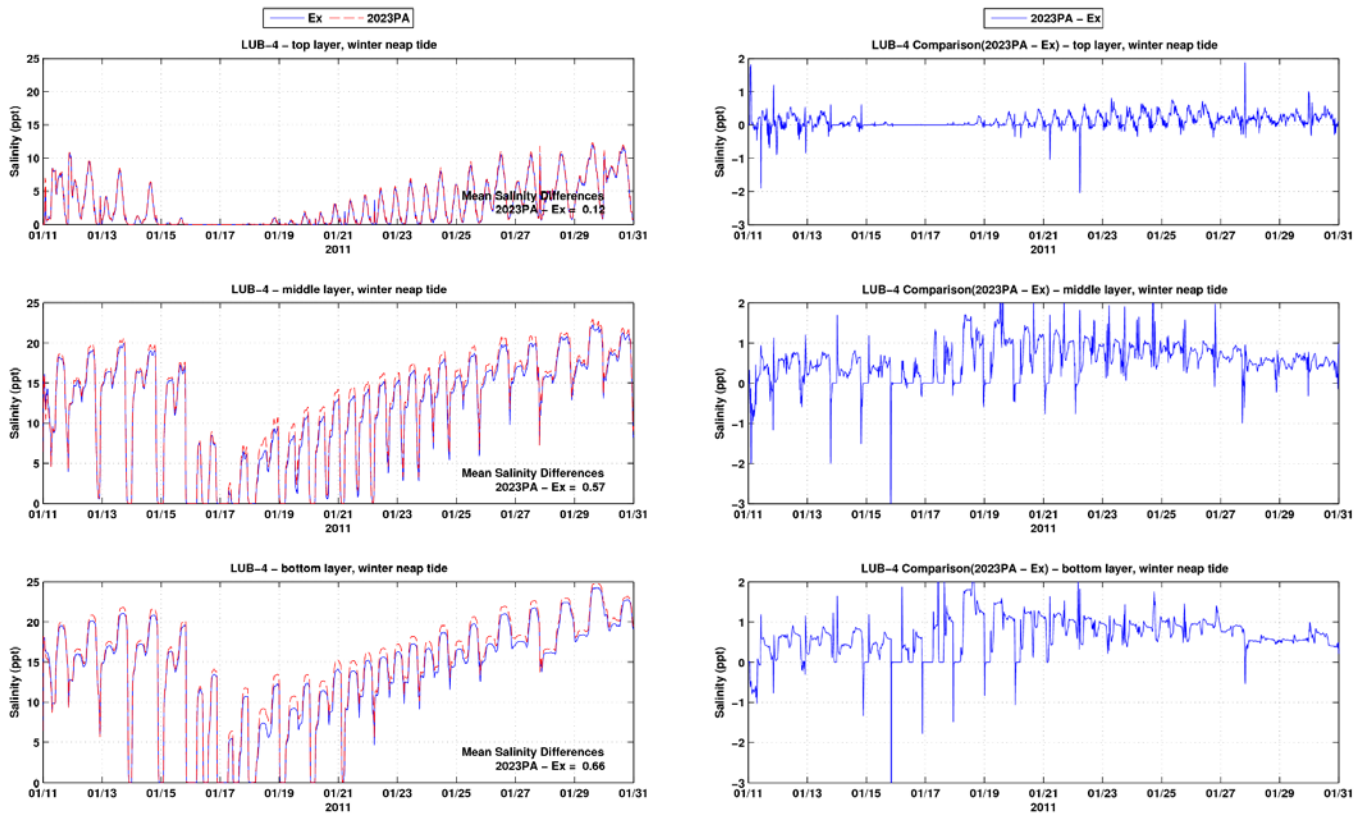

Figure C-44: Salinity time series and differences between the Existing Conditions and the 2023 PA at LUB-4 during winter neap tide period

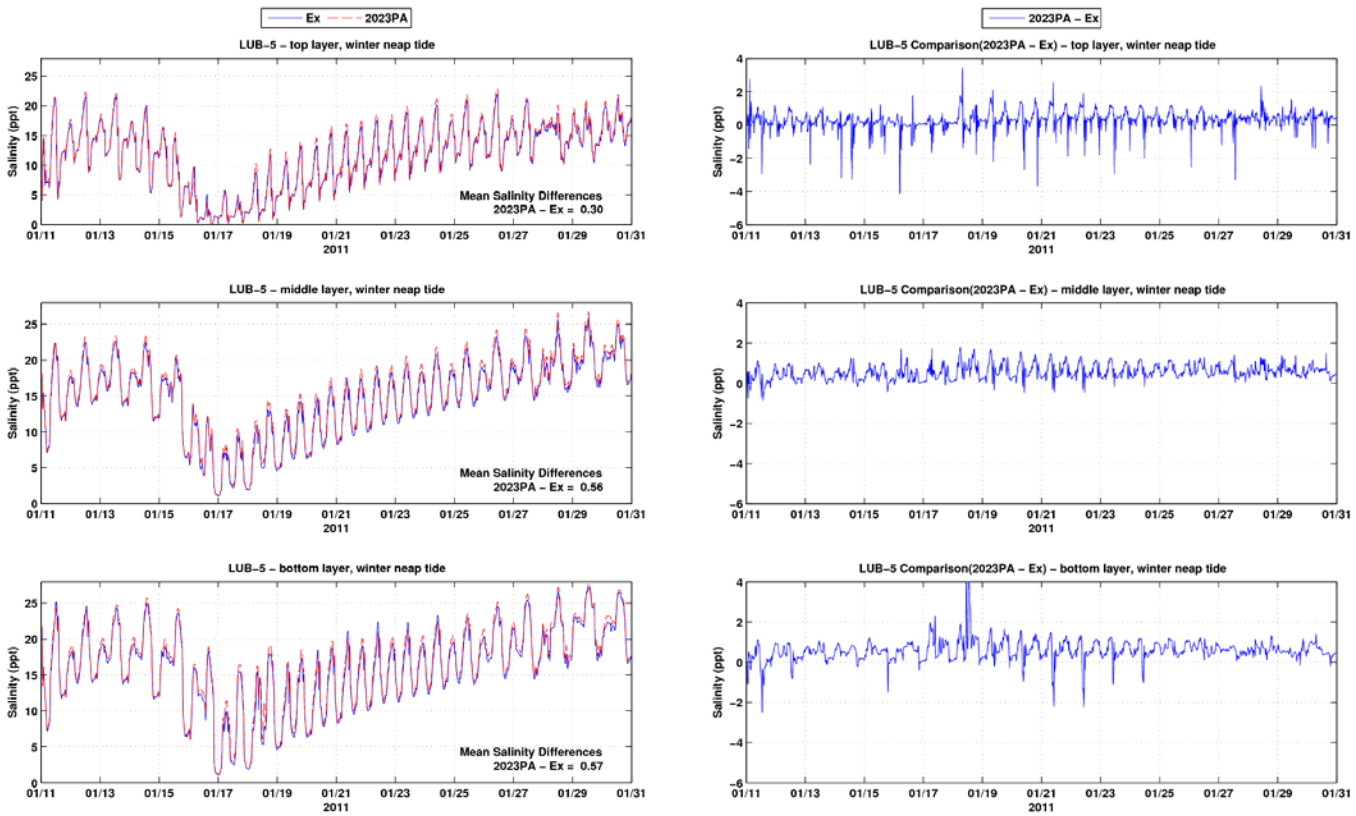

Figure C-45: Salinity time series and differences between the Existing Conditions and the 2023 PA at LUB-5 during winter neap tide period

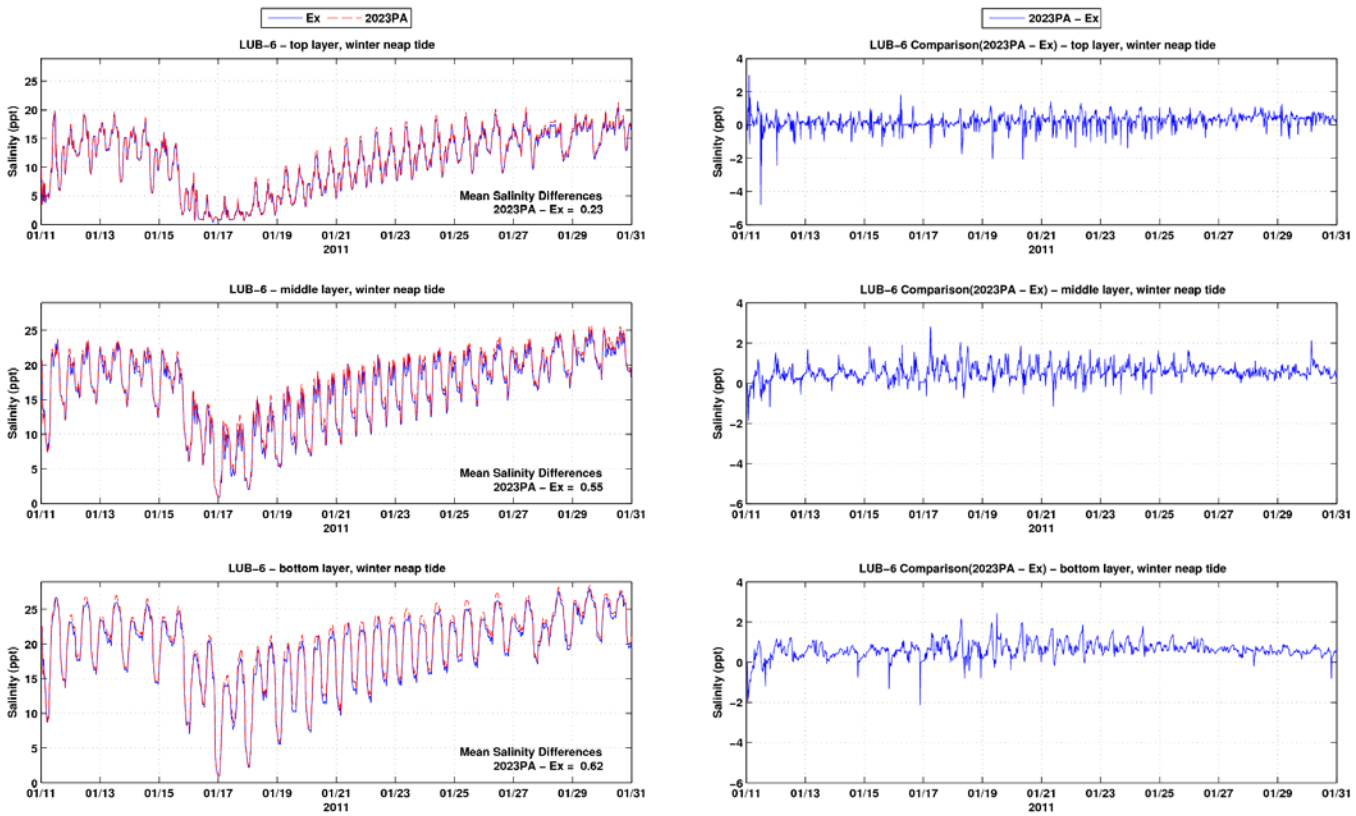

Figure C-46: Salinity time series and differences between the Existing Conditions and the 2023 PA at LUB-6 during winter neap tide period

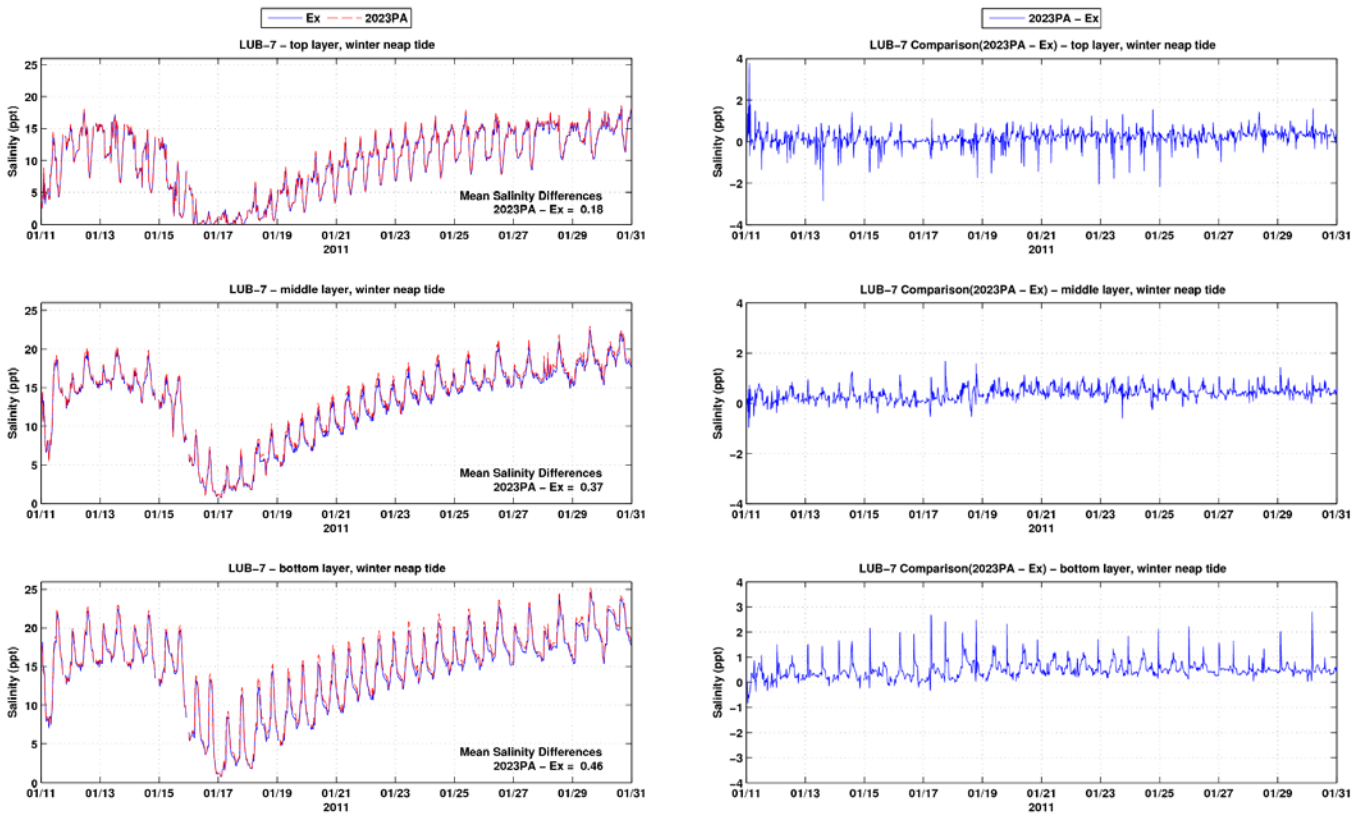

Figure C-47: Salinity time series and differences between the Existing Conditions and the 2023 PA at LUB-7 during winter neap tide period

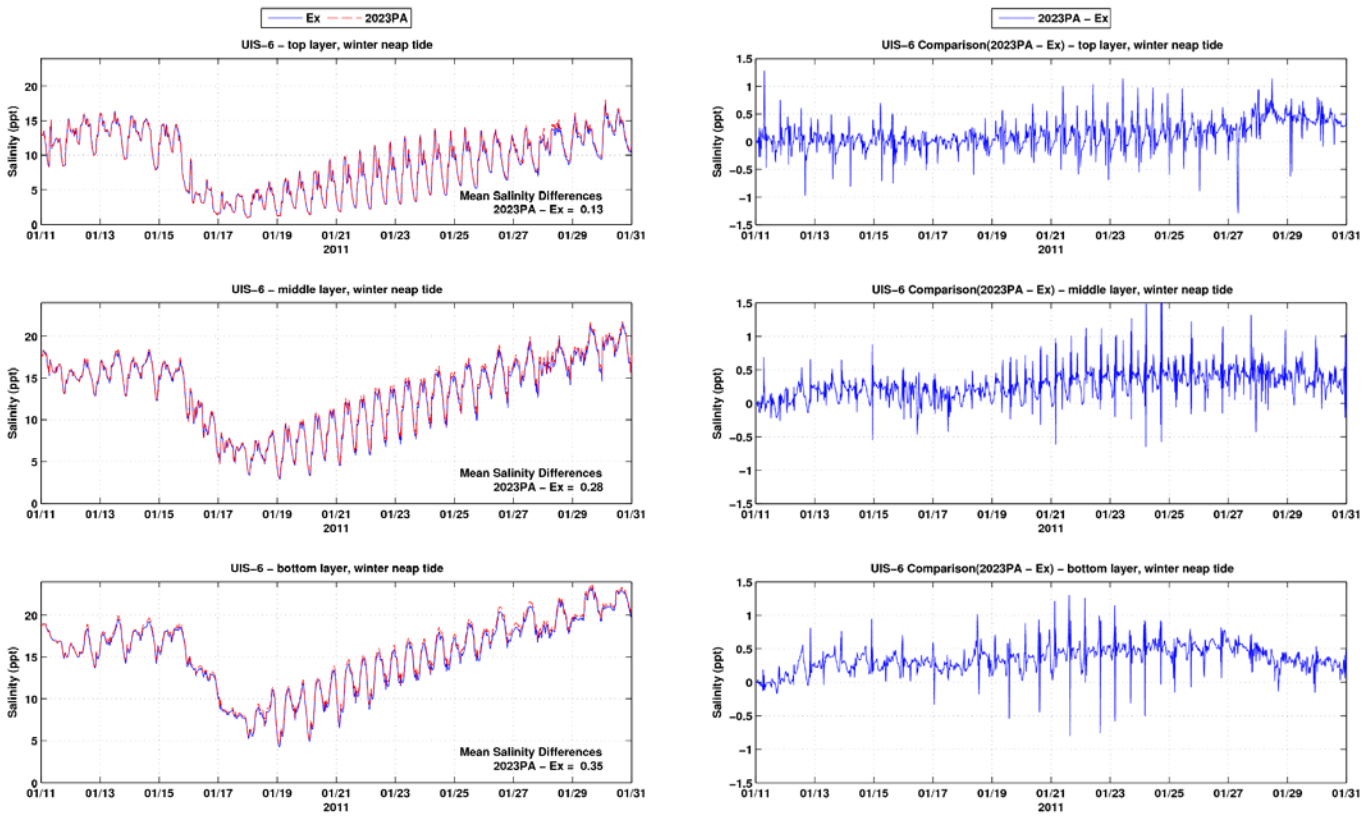

Figure C-48: Salinity time series and differences between the Existing Conditions and the 2023 PA at UIS-6 during winter neap tide period

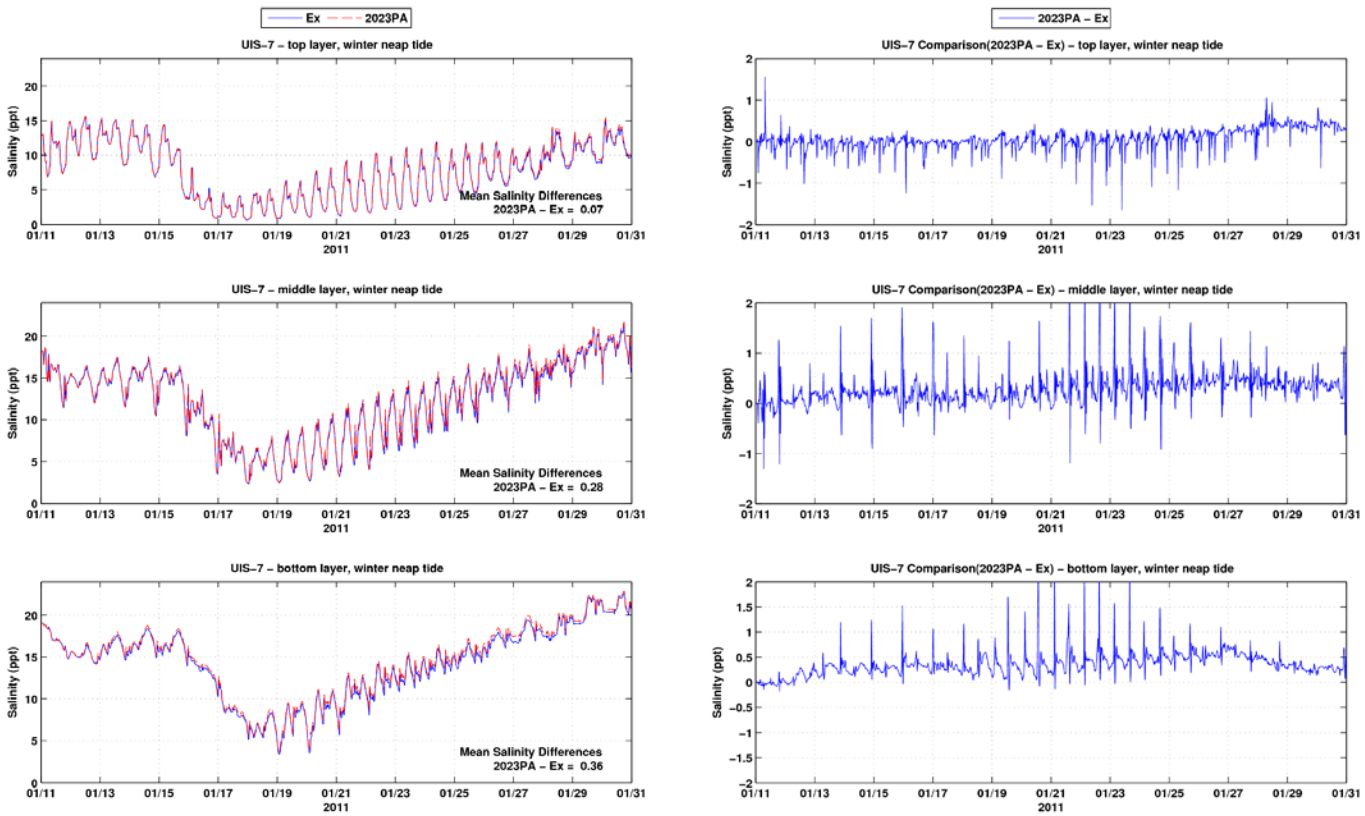

Figure C-49: Salinity time series and differences between the Existing Conditions and the 2023 PA at UIS-7 during winter neap tide period

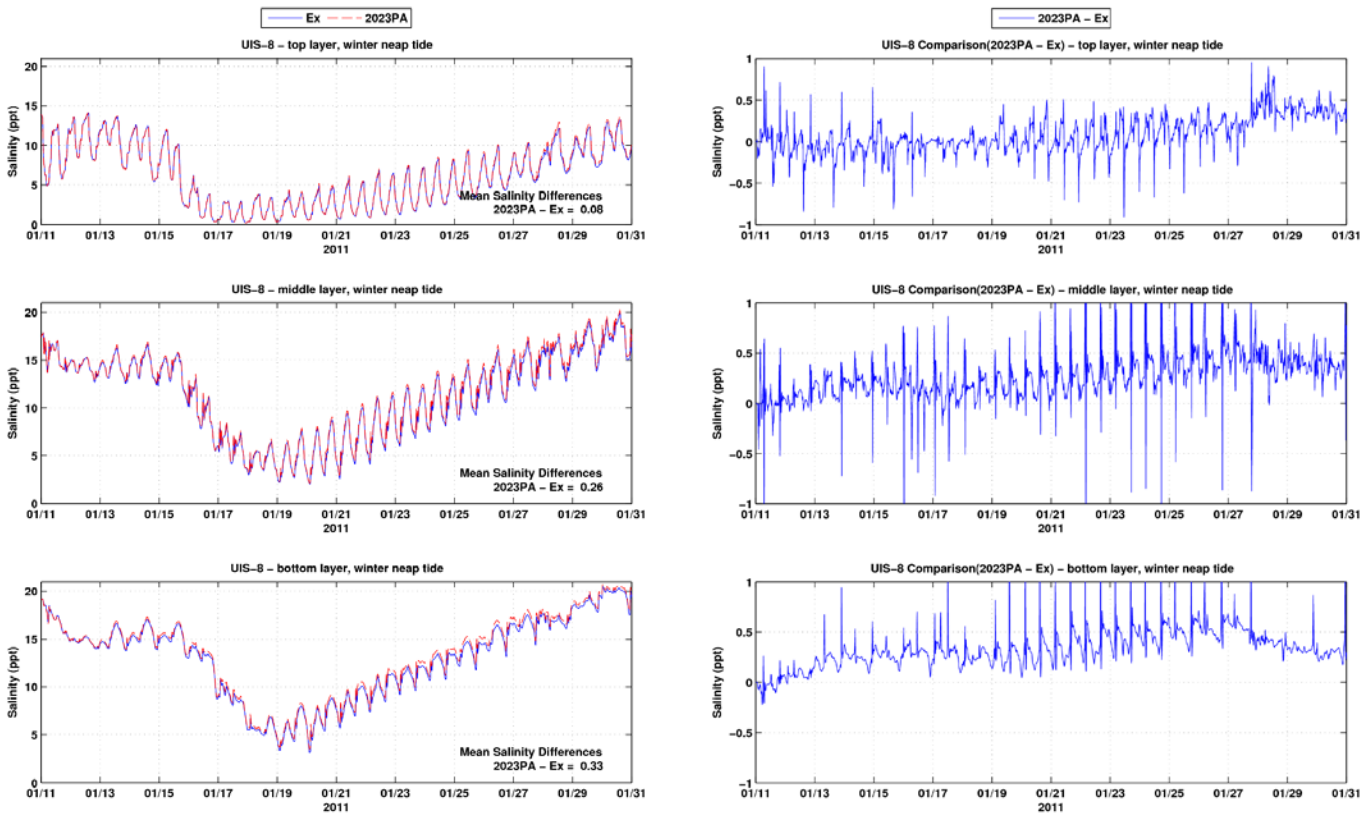

Figure C-50: Salinity time series and differences between the Existing Conditions and the 2023 PA at UIS-8 during winter neap tide period

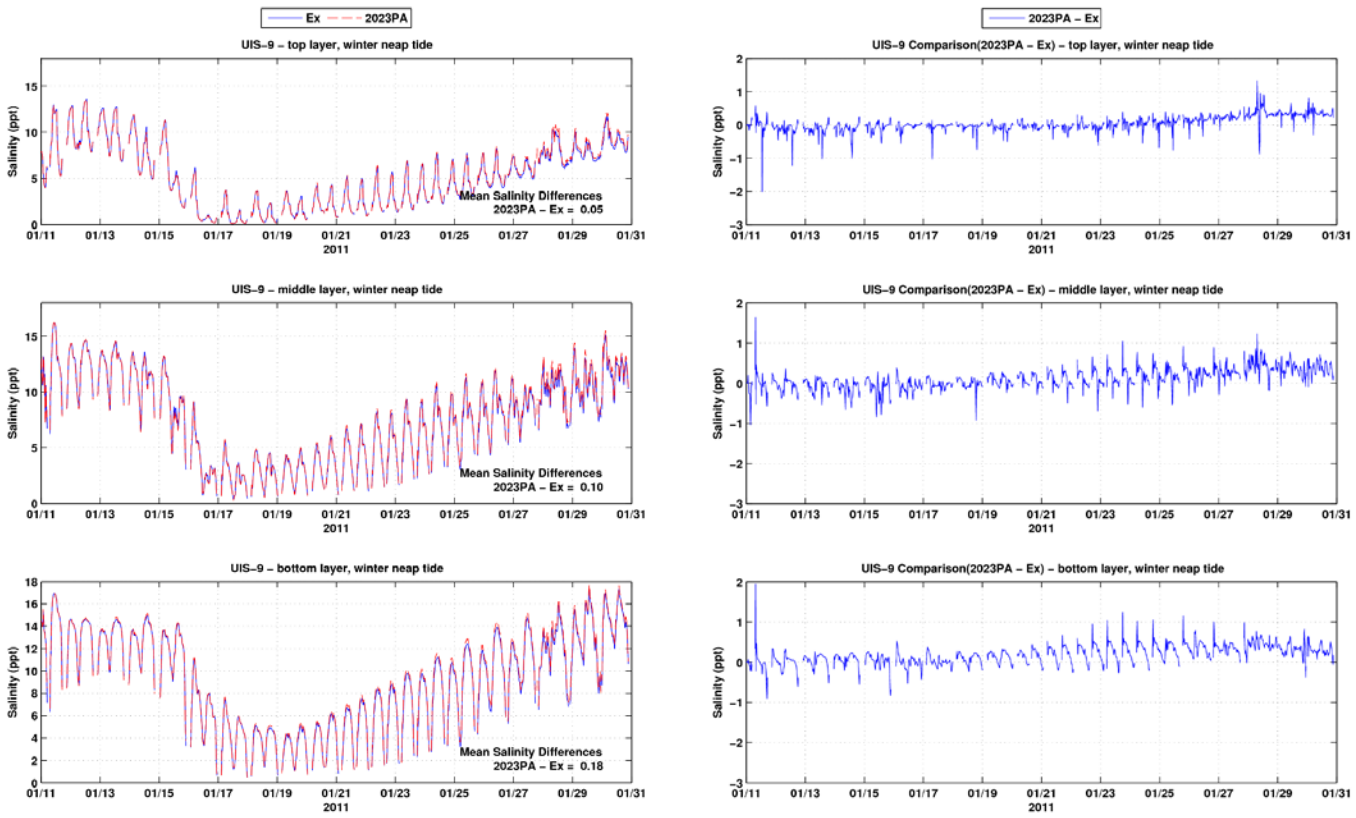

Figure C-51: Salinity time series and differences between the Existing Conditions and the 2023 PA at UIS-9 during winter neap tide period

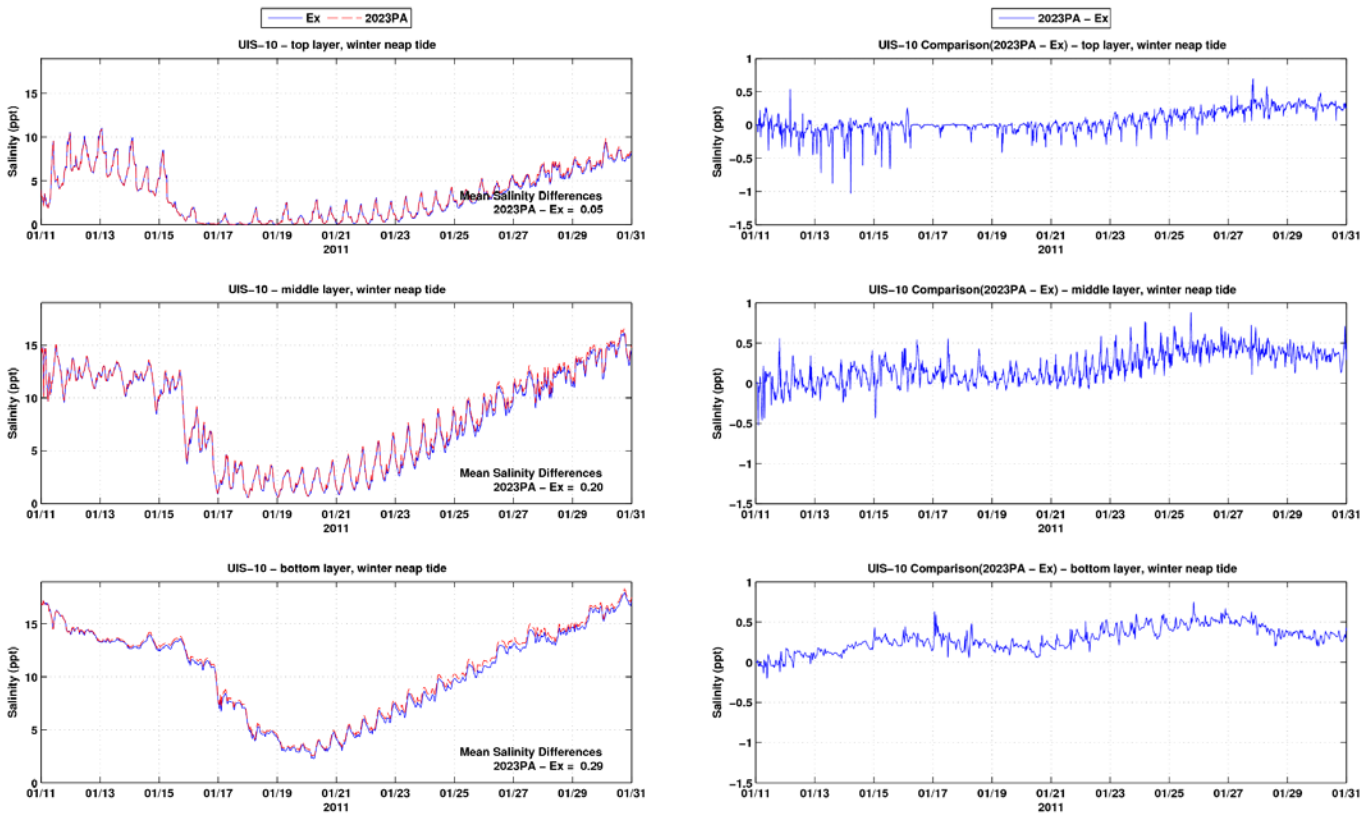

Figure C-52: Salinity time series and differences between the Existing Conditions and the 2023 PA at UIS-10 during winter neap tide period

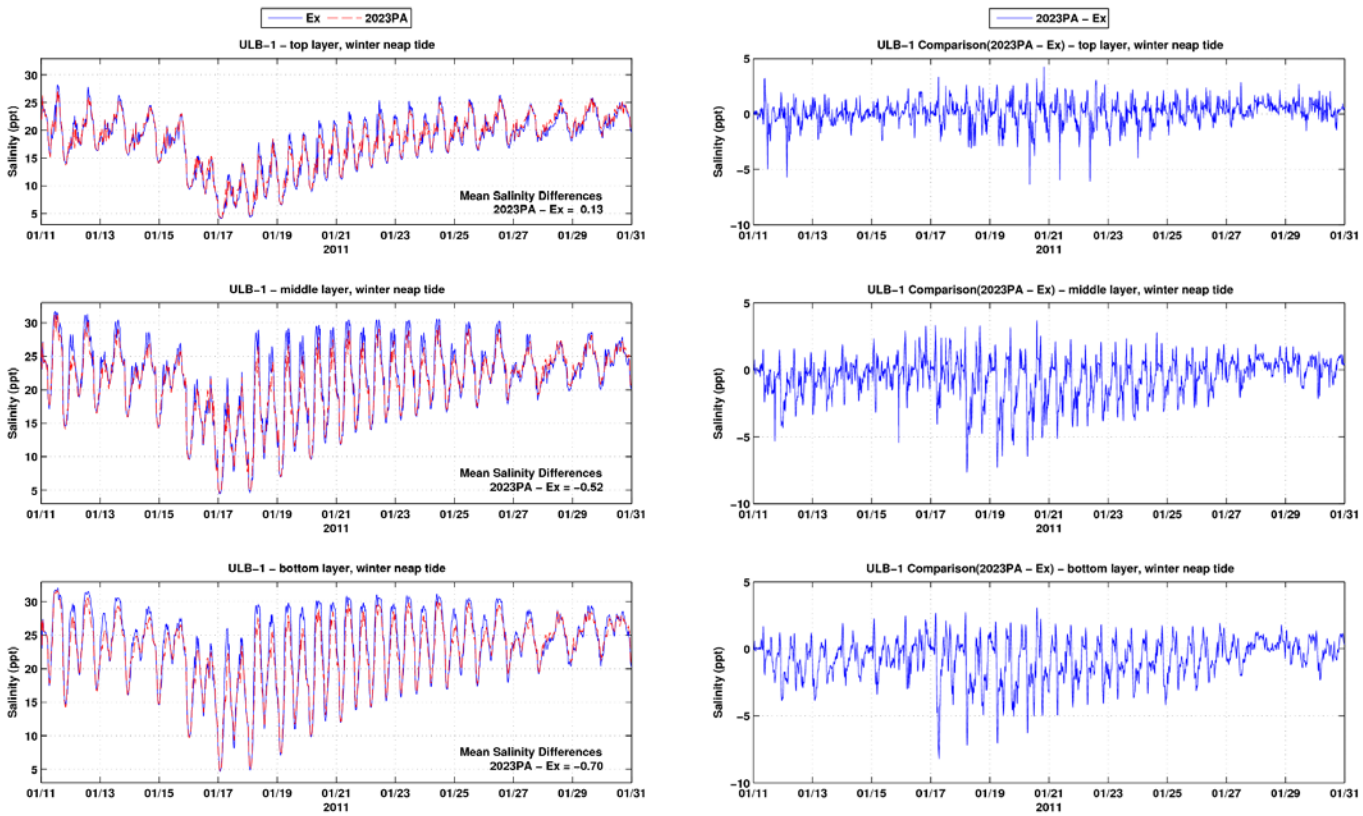

Figure C-53: Salinity time series and differences between the Existing Conditions and the 2023 PA at ULB-1 during winter neap tide period

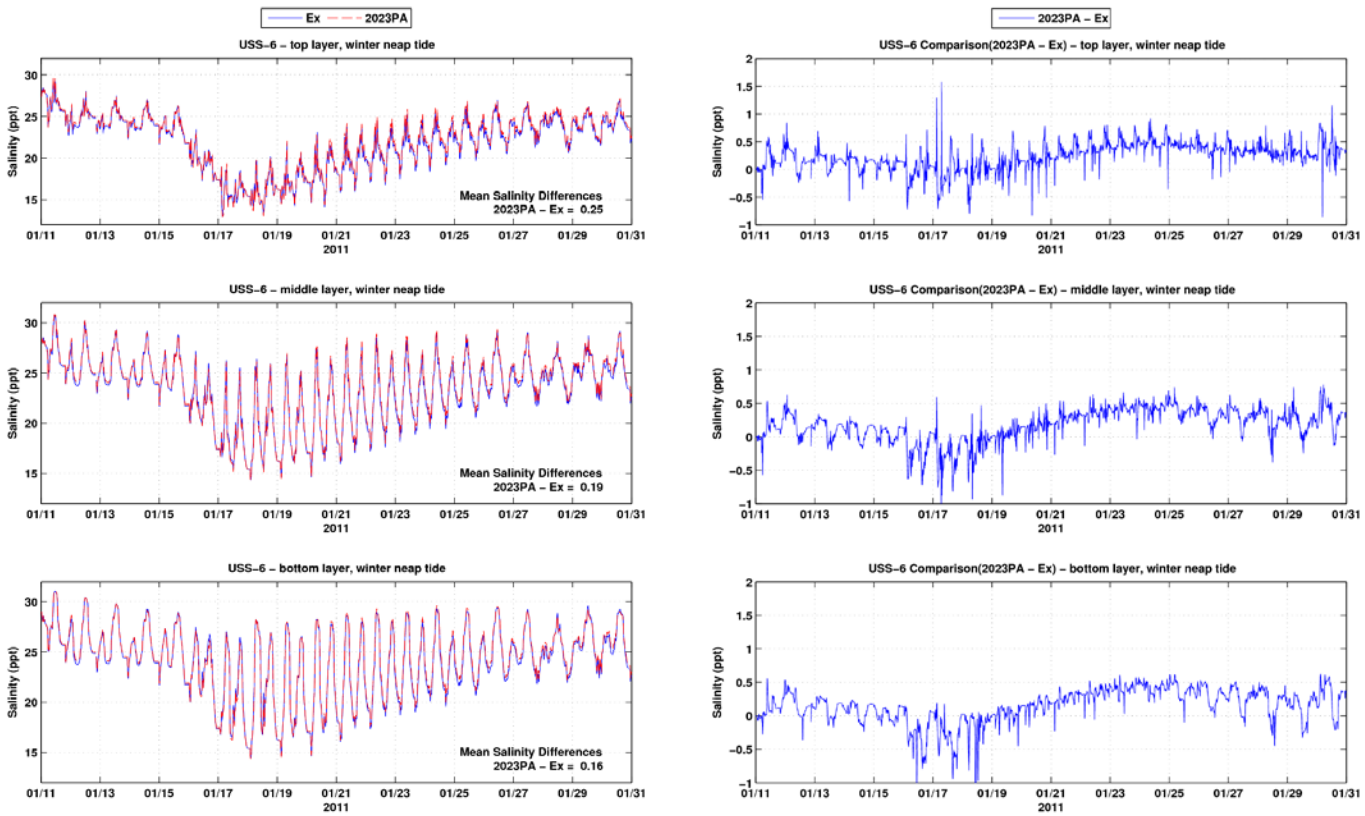

Figure C-54: Salinity time series and differences between the Existing Conditions and the 2023 PA at USS-6 during winter neap tide period

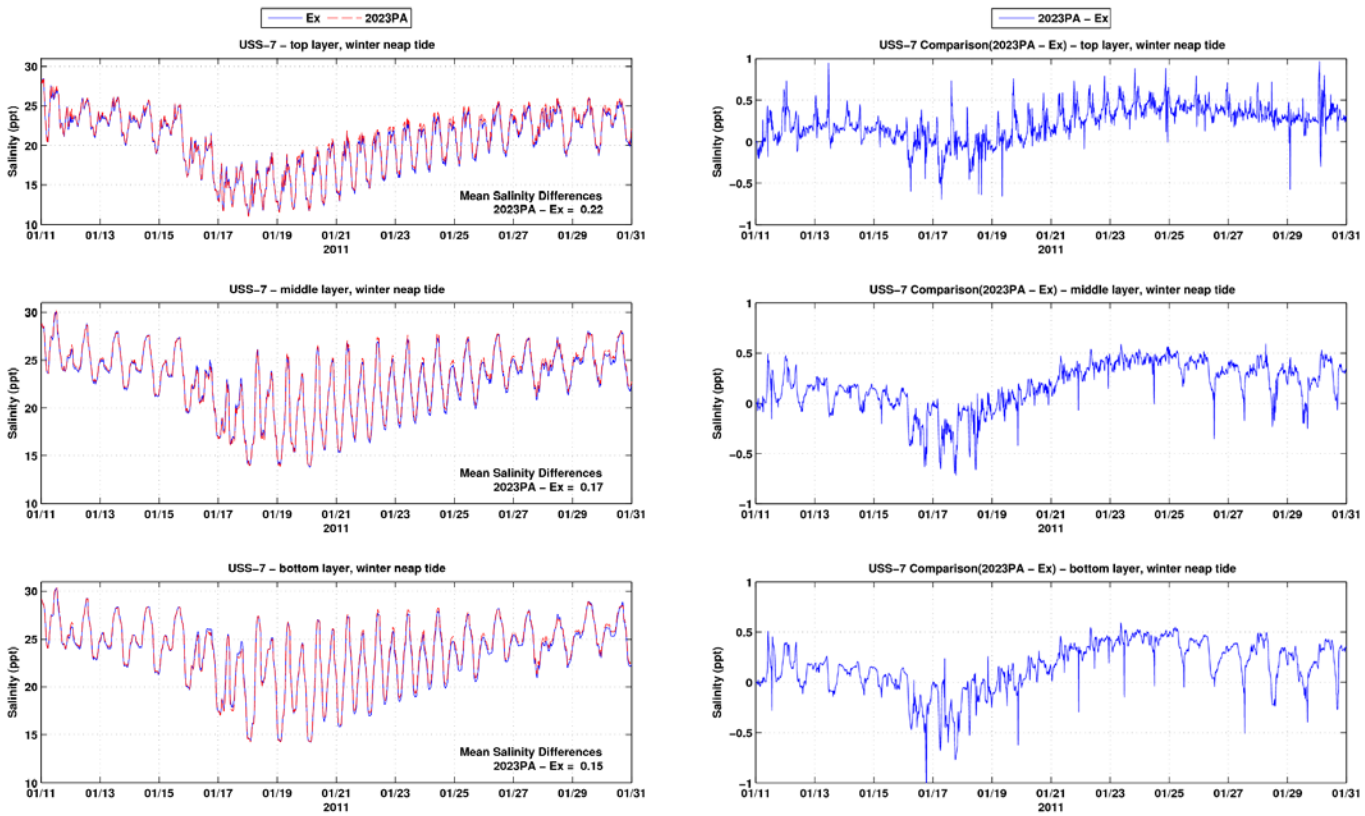

Figure C-55: Salinity time series and differences between the Existing Conditions and the 2023 PA at USS-7 during winter neap tide period

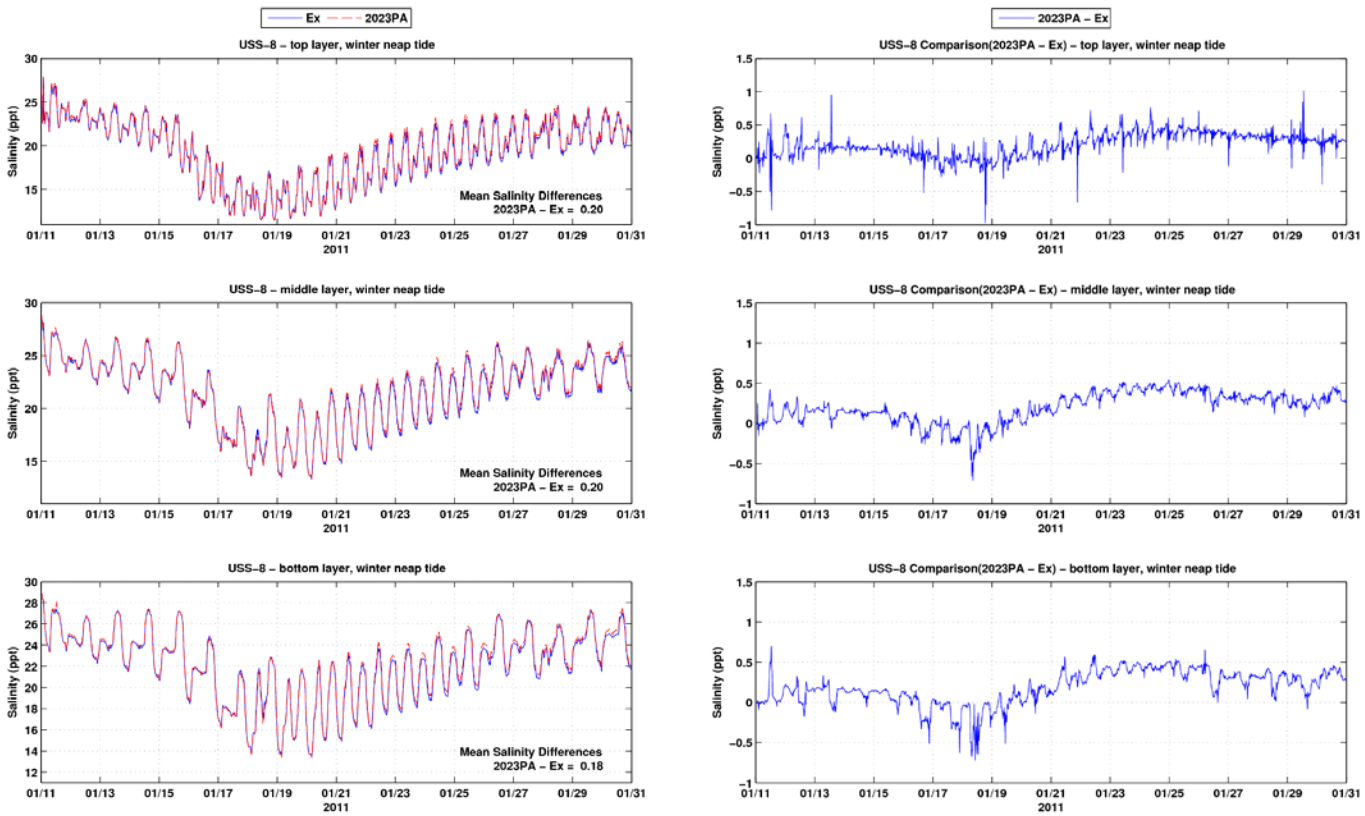

Figure C-56: Salinity time series and differences between the Existing Conditions and the 2023 PA at USS-8 during winter neap tide period

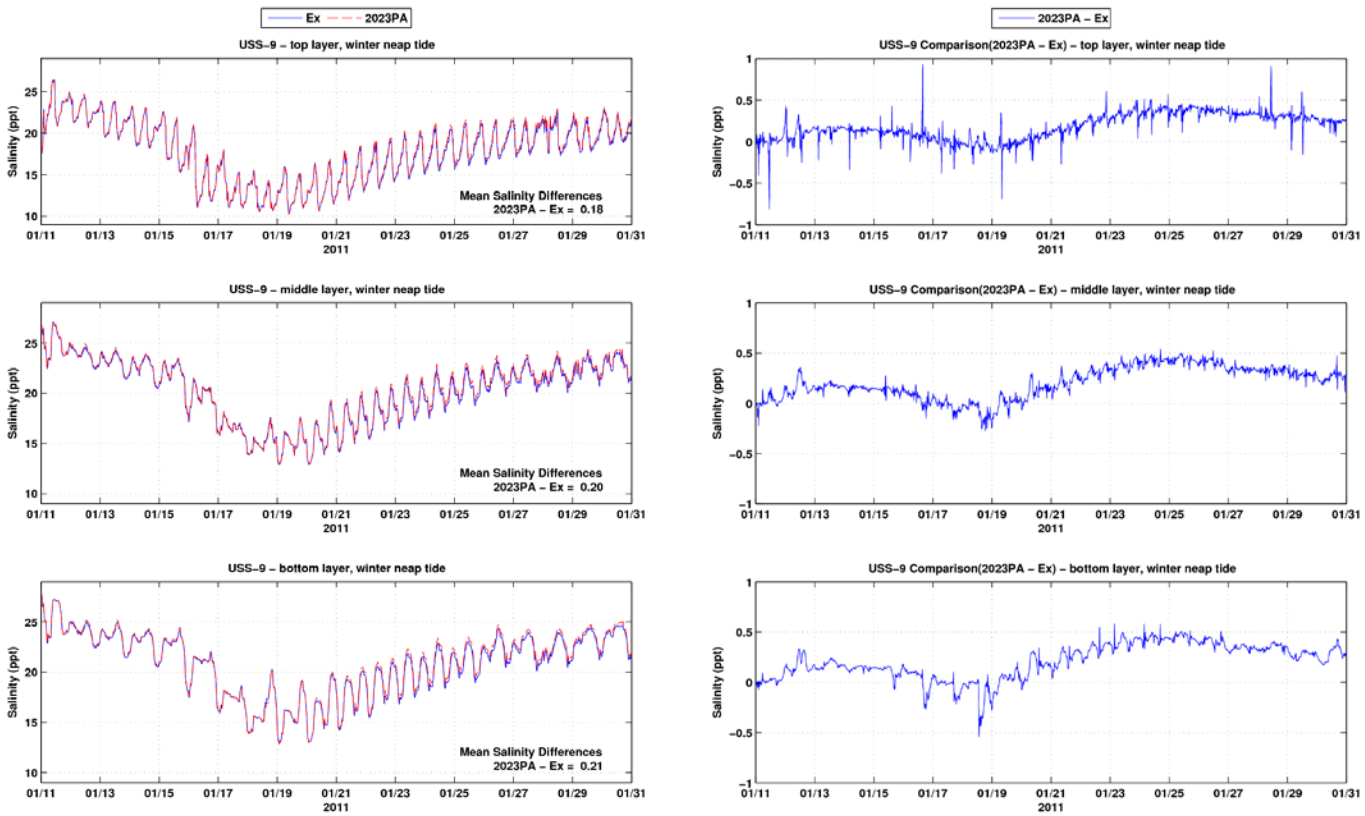

Figure C-57: Salinity time series and differences between the Existing Conditions and the 2023 PA at USS-9 during winter neap tide period

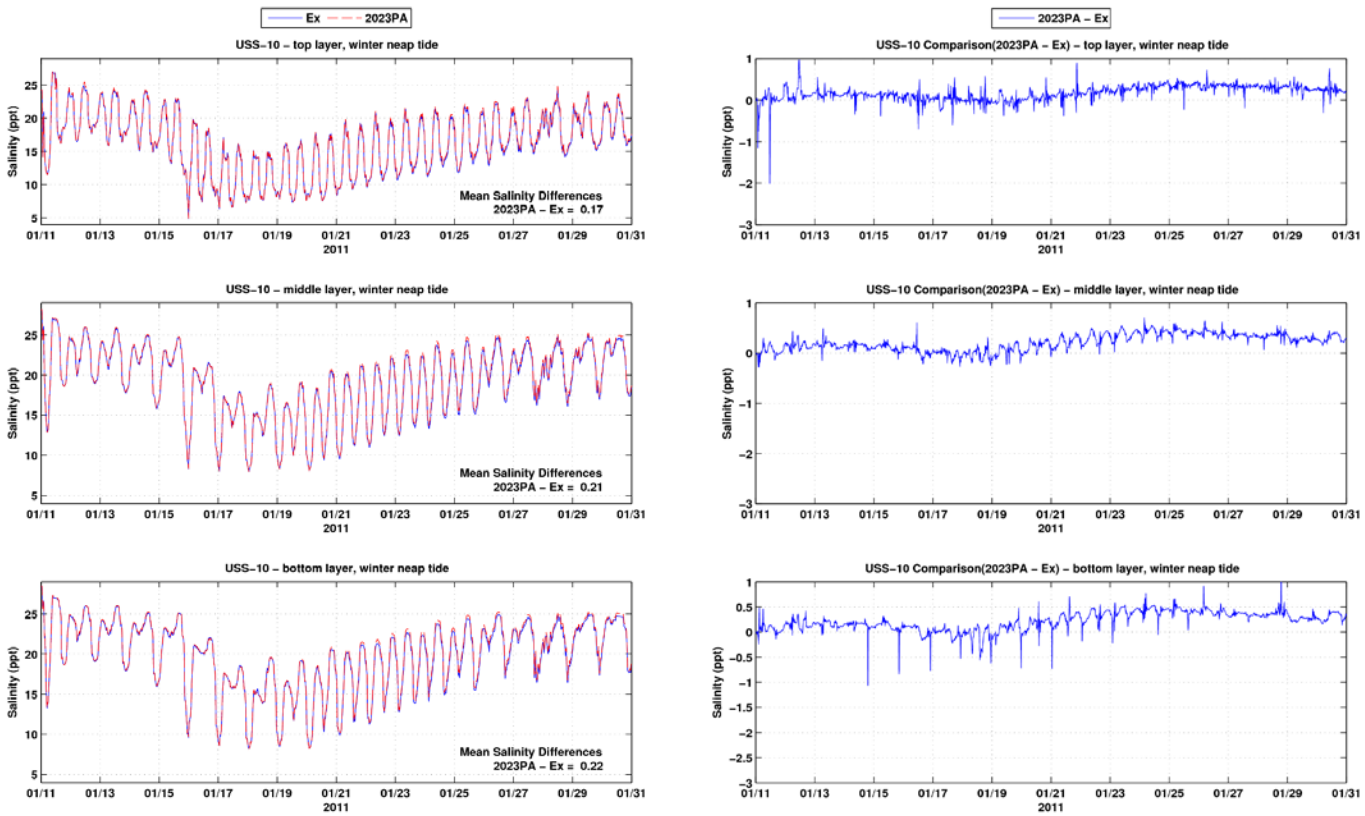

Figure C-58: Salinity time series and differences between the Existing Conditions and the 2023 PA at USS-10 during winter neap tide period

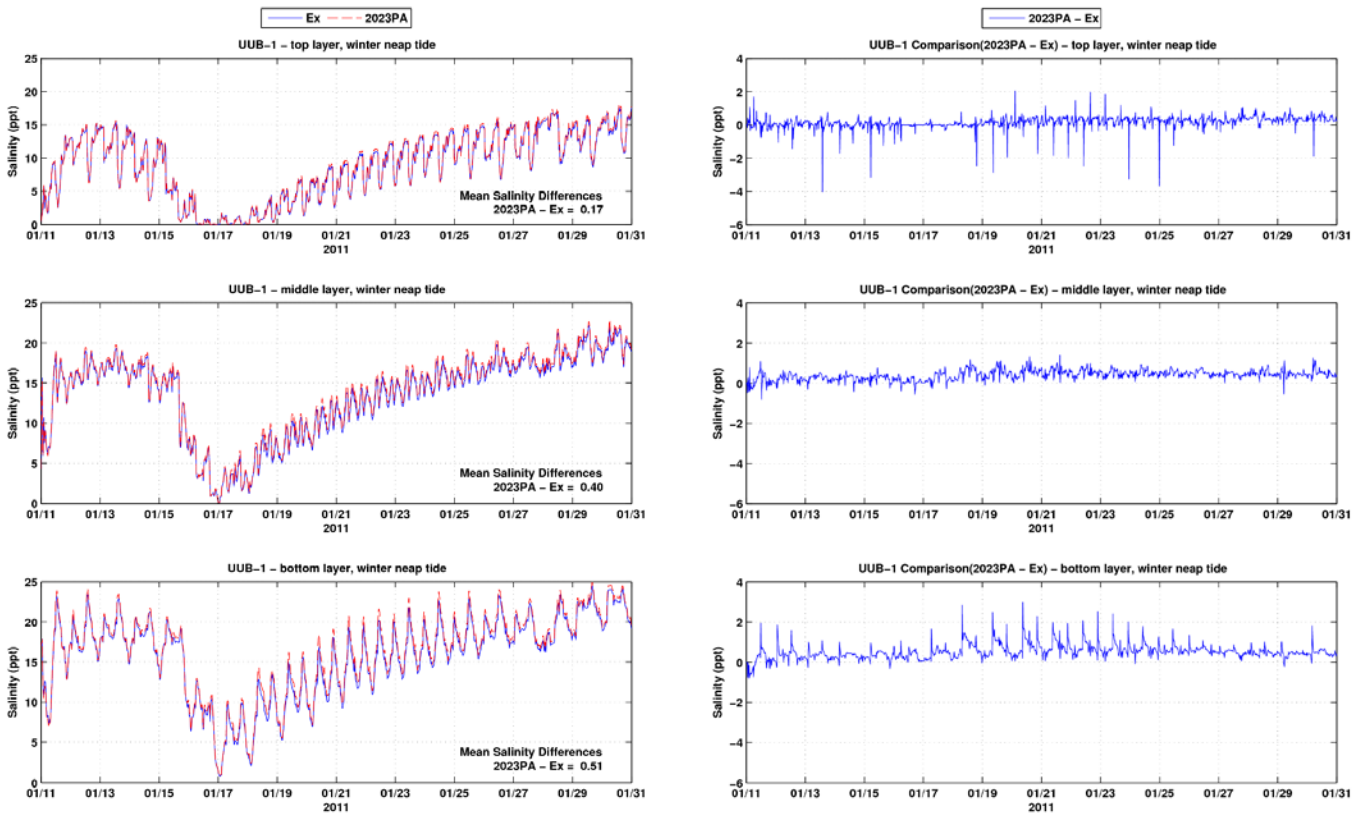

Figure C-59: Salinity time series and differences between the Existing Conditions and the 2023 PA at UUB-1 during winter neap tide period

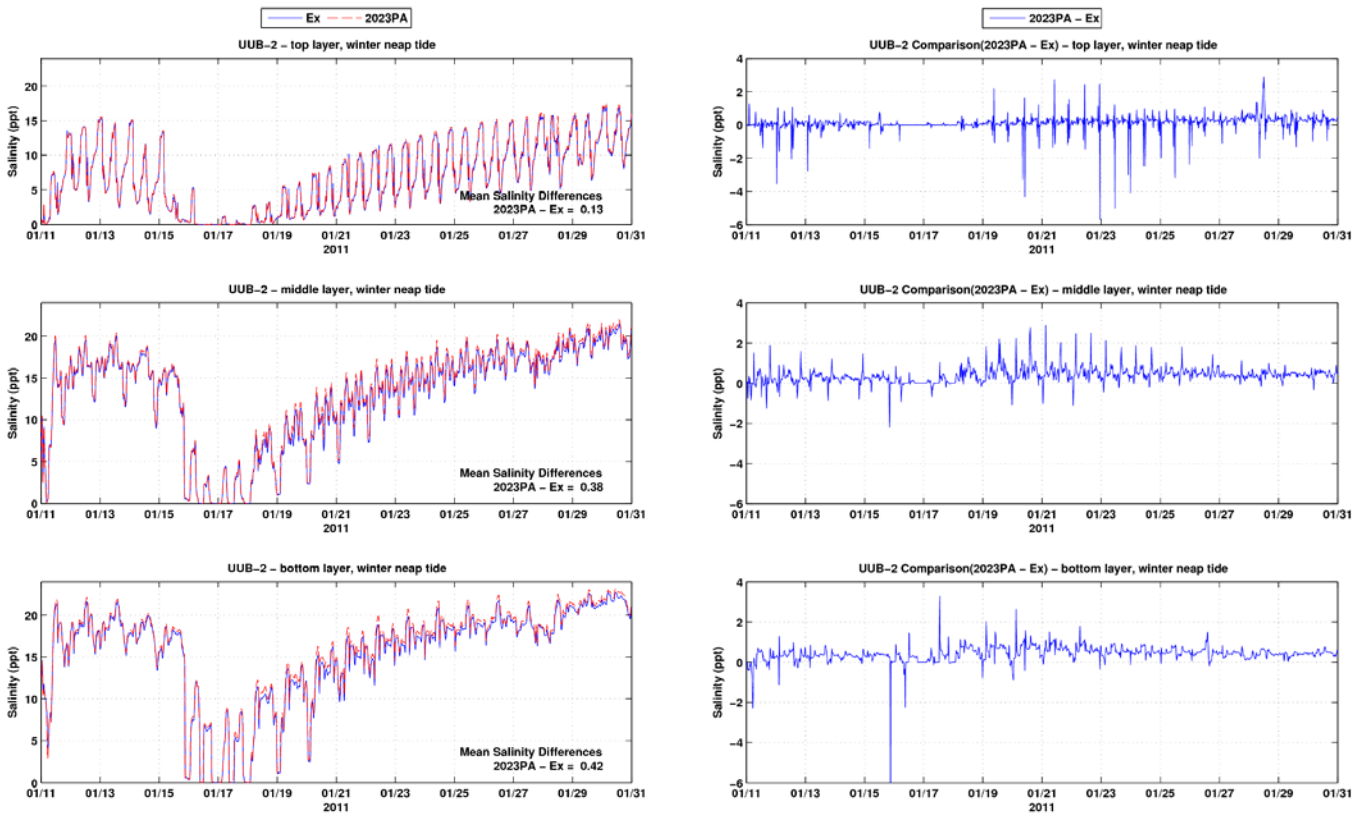

Figure C-60: Salinity time series and differences between the Existing Conditions and the 2023 PA at UUB-2 during winter neap tide period

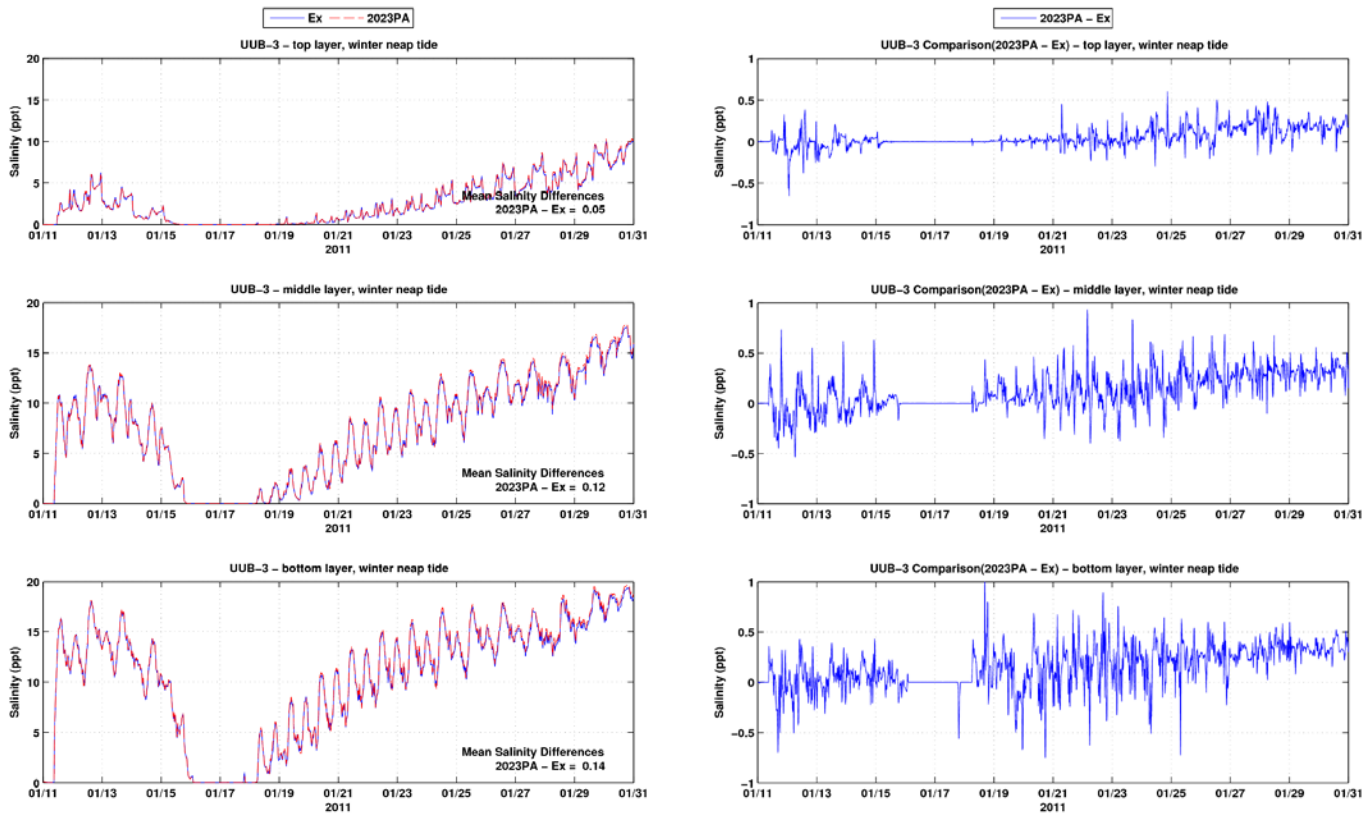

Figure C-61: Salinity time series and differences between the Existing Conditions and the 2023 PA at UUB-3 during winter neap tide period

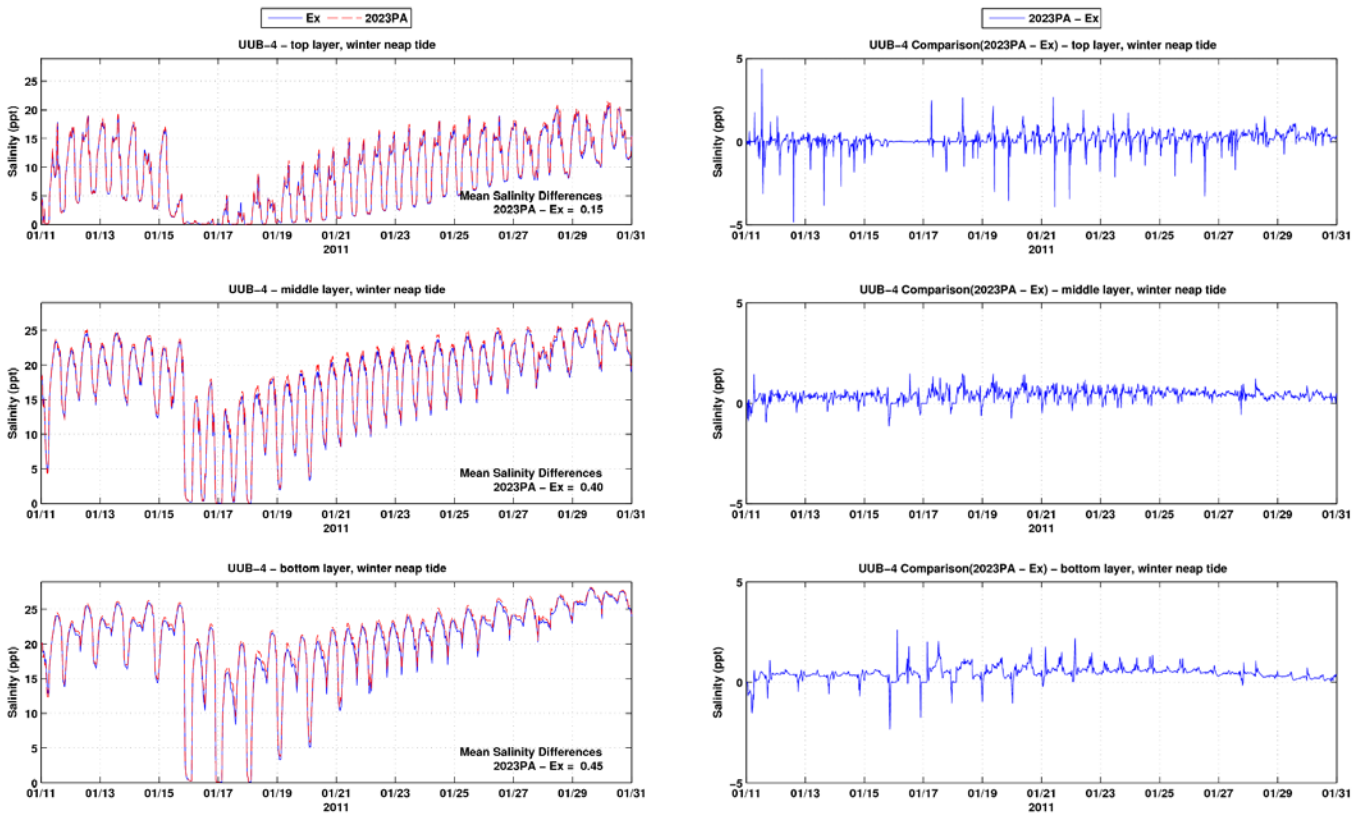

Figure C-62: Salinity time series and differences between the Existing Conditions and the 2023 PA at UUB-4 during winter neap tide period

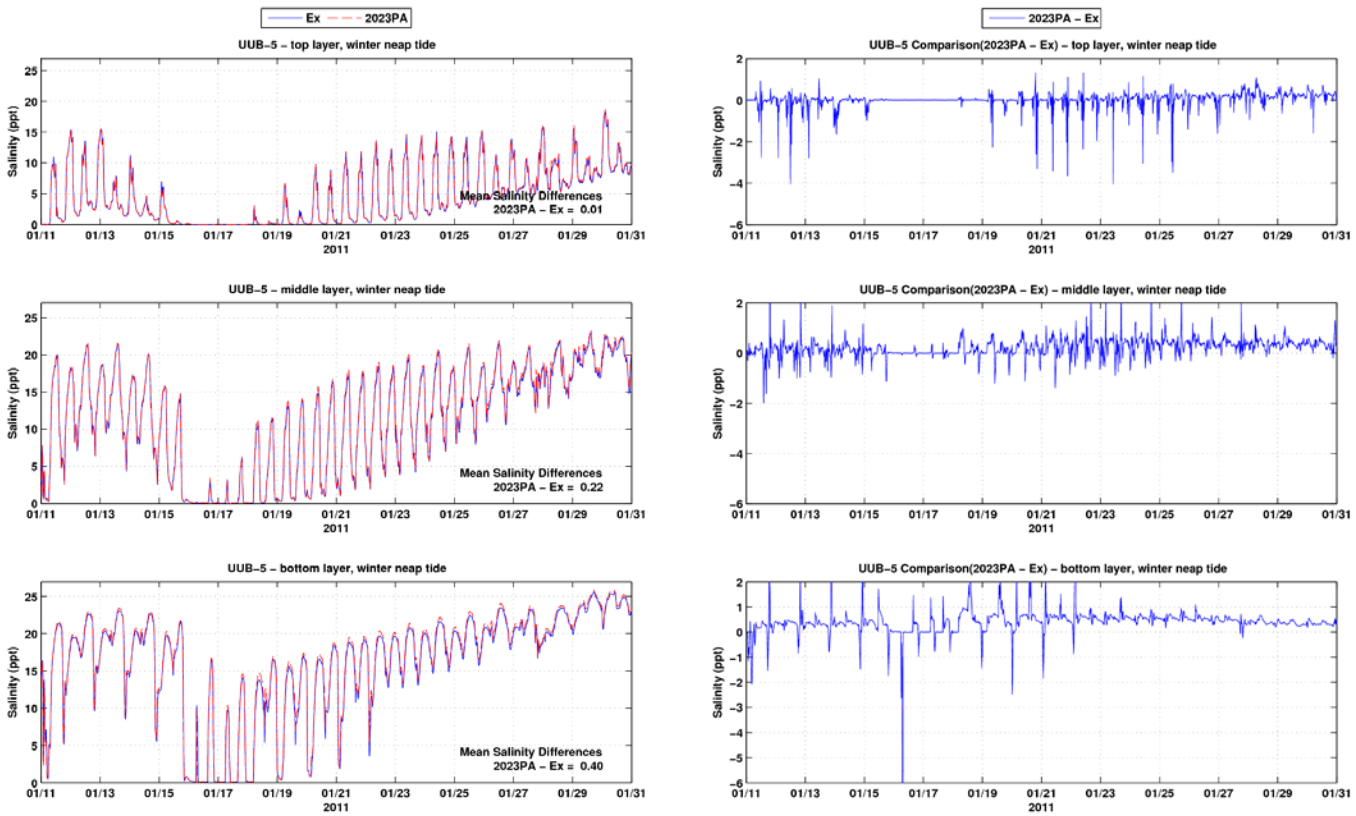

Figure C-63: Salinity time series and differences between the Existing Conditions and the 2023 PA at UUB-5 during winter neap tide period

Attachment D

Tidal Range Analytical Analysis

moffatt & nichol

Error! Unknown document property name.*, *Error! Unknown document property name.
Error! Unknown document property name.

Error! Unknown document property name. ❖ *Fax:* ***Error! Unknown document property name.***
www.moffattnichol.com

Memorandum

To:	USACE Portland District
From:	Moffatt & Nichol
Date:	Updated February 6, 2024
Subject:	Analysis of Tidal Amplitude in Coos Bay
Project:	Coos Bay Channel Modification Section 204(f)/408

This memorandum supports the Coos Bay, Oregon Section 204(f)/408 Channel Modification Project (the Project). From 2016 to 2019, the Port evaluated alternatives for modifications to the Coos Bay Federal Navigation Project in support of a previous proposal. In support of that effort, M&N prepared 19 substantial works of engineering and design, economics, modeling, and construction planning. The USACE, Portland District comprehensively reviewed and evaluated the entirety of the Port's proposals as reflected in their Main Report and all appendices (OIPCB 2019).

USACE reviewers expressed a concern that the modeling results appear to contradict general principles of estuarine hydraulics. Comment ID 7327343 remarked that, "*If hydraulic conveyance is increased through 2/3s of the estuary embayment, then tidal exchange within estuary would be affected resulting in non-trivial changes to estuary tidal datums, tidal prism, …*". The purpose of this memorandum focuses on the evaluation of potential changes to the tidal amplitude, collecting together supporting evidence to the findings presented in the prior work. The previous analysis was reviewed, two alternative methodologies were applied to assess the tidal amplitude, and the results of a similar study performed by USACE for a different federal project were reviewed and compared.

This memorandum reviews Existing Condition and the Proposed Alteration 2023 (PA).

1. PRIOR WORK PREDICTIONS

The tidal prism is the volume of water being exchanged between an estuary (enclosed bay) and the open sea over a complete tidal cycle. In other words, it is the storage volume of the estuary between high tide and low tide. In this analysis, the tidal prism is referred to as the mean tidal prism (estuary storage volume between mean high tide and mean low tide). The tidal prism volume can be expressed by the relationship: $Prism = h_b \cdot A_b$, where h_b is the average tidal range and A_b is the average surface area of the basin between high tide and low tide. For the current proposed project, the proposed deepening and widening are both subtidal. Hence, the area A_b does not change. Therefore, the review and analyses of changes focus on the tidal amplitude.

The prior work evaluated changes to the mean tidal range. The effects of the PA on mean tidal range, relative to the Existing Condition, can be seen in Table 1-1. The mean tidal range generally increases moving up the channel. The increase in tidal range under the PA relative to the Existing Condition is less than 0.1 ft throughout (rounding to 1 significant digit). This represents less than a two percent difference.

Table 1-1: Mean Tidal Range under Existing and PA Condition

Parameter	RM	Existing Condition	PA Condition	PA – Existing Condition
		Mean Tidal Range in feet		
Charleston Channel	1.7	5.4	5.5	< 0.1
Coos Bay Range	3.0	5.5	5.5	< 0.1
Empire Range	5.2	5.6	5.7	< 0.1
Upper Jarvis Range	8.0	5.8	5.9	< 0.1

2. ANALYTICAL CALCULATION OF CHANGE IN TIDAL AMPLITUDE

The tidal amplitude in an estuary is affected by the inlet channel dimensions (width, depth, and length), energy loss through the inlet channel due to friction, and inertia. Friction has the effect of restricting the conveyance of water through the channel, dampening the tides upstream. The effect of inertia causes water to move in the direction opposite to the slope of water surface (i.e., water moves from the ocean into the bay even though the bay has a higher water level elevation), effectively amplifying the tidal amplitude upstream and creating a system in which the currents lag the tides. Inertia is more pronounced in estuary systems with a relatively long and hydraulically efficient inlet channel such as Coos Bay. For small or narrow inlets, friction tends to dominate and the tide amplitude in an estuary is muted (tidal range in the bay is smaller than that in the ocean) relative to the offshore tidal amplitude. In a muted tidal estuary, an increase in the inlet channel geometry does efficiently reduce the friction loss, resulting in an increased tidal range and reduced phase lag between the ocean and bay. After the tidal range in the estuary reaches the full ocean tidal range, further increase in the channel geometry will no longer efficiently increase the tidal range in the estuary; however, it will continue to reduce the phase lag of tides in the bay. The relative importance of inertia will slightly increase with reduction in friction loss due to increase in the channel geometry. But the reduction in friction loss is very limited, hence, a significant change in tidal amplitude in the estuary is not expected.

The Coastal Engineering Manual (CEM), Part II-6-2-b, introduces a conceptual approach to estimate tidal amplitude in an enclosed bay. This approach is based on the one-dimensional equation of motion that incorporates inlet cross-sectional area, bay surface area, ocean tide amplitude and period, length of the connecting inlet channel, and head loss coefficients. Two solutions of the equation are presented in CEM, that developed by Keulegan (1967) and that improved by King (1974). This conceptual approach investigates the effects of both friction and inertia.

A schematic inlet bay system is shown in Figure 2-1. The system consists of a bay connected to sea through an inlet, with a defined inlet cross-sectional area; bay surface area and bay tidal amplitude; and sea tidal amplitude. The inlet cross-section is assumed to be constant over the length of the inlet channel.

The one-dimensional equation of motion and the continuity equation are used to develop the dimensionless King's coefficients, K_1 and K_2, and Keulegan's repletion coefficient, K, which are defined as:

$$K_1 = \frac{a_o A_b F}{2LA_c},\ K_2 = \frac{2\pi}{T}\sqrt{\frac{LA_b}{gA_c}},\ \text{and}\ K = \frac{1}{K_2}\sqrt{\frac{1}{K_1}}\ \text{with}\ F = k_{en} + k_{ex} + \frac{fL}{4R}$$

where T is the tidal period, A_c is the average area of the inlet cross-section, A_b is the surface area of the bay, g is the acceleration due to gravity, a_o is the ocean tide amplitude, k_{en} is the entrance energy loss coefficient, k_{ex} is the exit energy loss coefficient, f is the Darcy-Weisbach friction term, L is the inlet length, and R is the hydraulic radius of the inlet cross-section.

The hydraulic radius, *R*, and Darcy-Weisbach friction term, *f*, are defined as:

$R = \frac{A_c}{P_w}$ and $f = \frac{116n^2}{\sqrt[3]{R}}$

where P_w is the average wetted perimeter, and *n* is the Manning's coefficient.

These methods also include the calculation of a dimensionless velocity, defined as:

$V_m{}' = \frac{A_c T V_m}{2\pi a_o A_b}$,

where V_m is the maximum cross-section average velocity during a tidal cycle. Changes to the dimensionless velocity (V'_m) can be used to estimate changes to the maximum cross-section average velocity (V_m).

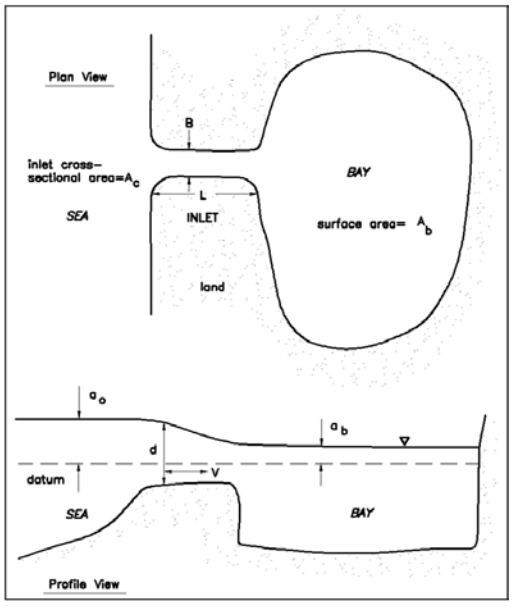

Figure 2-1: Inlet bay system (CEM Figure II-6-15)

Using King's coefficients K_1 and K_2, the ratio of bay tidal amplitude, a_b, and ocean/sea tidal amplitude, a_o or a_s, (the ratio is expressed as a_b/a_o) can be found from CEM Figure II-6-18 (Figure 2-2). Alternatively, using Keulegan's coefficient *K*, the ratio of amplitudes can be found from CEM Figure II-6-16 (Figure 2-3). The difference between the two methods is that the King's method (using Figure 2-4) includes the effect of inertia. The inertia effect can be seen in Figure when a_b/a_o is greater than one (i.e., tidal amplification within a bay). Comparing tidal measurements at Charleston (used as the offshore boundary) and at North Bend (located at approximately RM 11) show that the tidal range is 7% higher at North Bend than that at Charleston. This tidal amplification indicates that inertia does influence the hydrodynamics of Coos Bay. Keulegan's method, by contrast, does not

include inertia effects; therefore, it isolates the effect of friction due to change in the channel cross-section, and whether the modification project would make the channel more hydraulically efficient. A Keulegan's coefficient *K* equal to 1.0 means that the channel is perfectly efficient, after which friction reduction cannot change the tidal amplitude (as stated above).

The CEM also notes that tidal amplification may occur if the inlet system could have a natural frequency of oscillation (or pumping mode, where the basin oscillates uniformly) that is tuned to the forcing ocean tide (a classic example of this oscillation is Fundy Bay). However, these oscillation conditions are not present in Coos Bay.

Similar, using King's coefficients K_1 and K_2, the dimensionless maximum velocity, V'_m, can be estimated using CEM Figure II-6-19 (Figure 2-4) and used to estimate V_m.

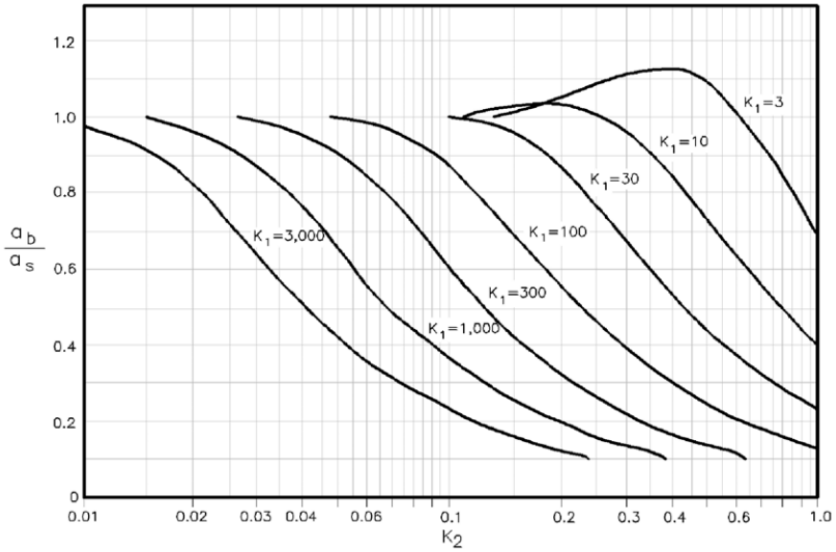

Figure 2-2: Ratio of bay to sea tidal amplitude versus King's K1 and K2 coefficients (CEM Figure II-6-18)

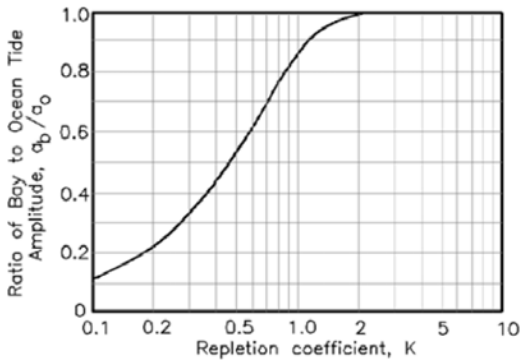

Figure 2-3: Variation of dimensionless parameters with Keulegan's repletion coefficient, K (CEM Figure II-6-16)

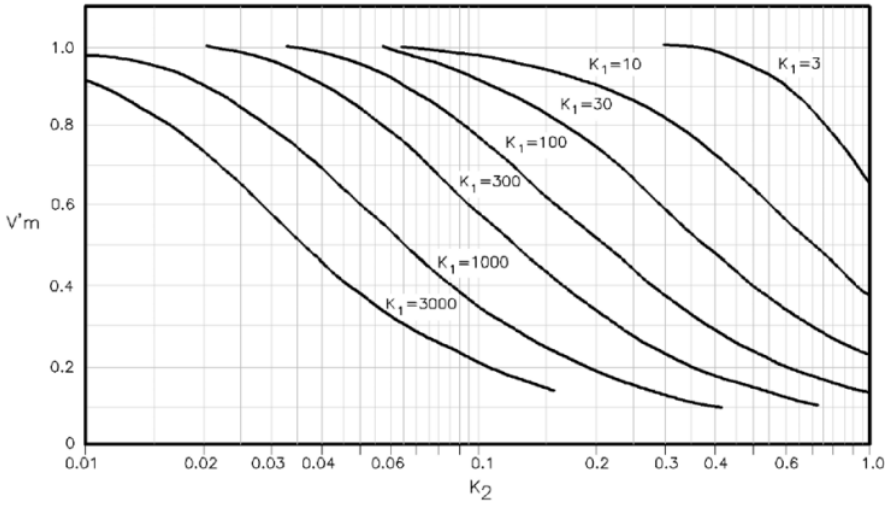

Figure 2-4: Dimensionless maximum velocity versus King's K_1 and K_2 coefficients (CEM Figure II-6-19)

The channel geometry is a critical variable in this assessment; the data used is presented in Table 2-1. It can be seen that the relative changes in the cross-section area, A_c, and hydraulic radius, R (a measure of efficiency of conveyance), are generally less than 30%. The relative change in the wetted perimeter, P_w, is less than 1%, indicating that the friction surface area remains consistent under the PA relative to the Existing Condition, although the average cross-section area increases by 14.5%. The small change in the wetted perimeter may be a result of comparing the rough Existing Condition bathymetry with the

smooth PA Condition dredge template. Over time, the wetted perimeter would increase, leading to a slight decrease in the hydraulic radius. Therefore, the hydraulic radius values presented in Table **2-**1 overstate the change between the PA and Existing Condition; This would cause the analytical method to overstate any change. The largest increase in cross-sectional area was 43.7%, at RM 5.5 in the location of the turning basin. The increase in cross-sectional area between the jetties is 29.2%.

Table 2-1: Comparison between selected cross-sections in Existing configuration and Proposed Alteration (PA)

RM	Existing			Proposed Alteration (PA)			% Change (PA vs. Existing)		
	A_c (m^2)	P_w (m)	R (m)	A_c (m^2)	P_w (m)	R (m)	A_c	P_w	R
0.5	6,777	611	11.1	8,753	611	14.3	29.2%	0.1%	29.1%
1.0	7,385	760	9.7	7,767	759	10.2	5.2%	-0.1%	5.2%
1.5	8,984	1,389	6.5	8,970	1,389	6.5	-0.2%	0.0%	-0.2%
2.0	7,205	1,284	5.6	7,760	1,284	6.0	7.7%	0.0%	7.8%
2.5	6,857	1,178	5.8	7,714	1,181	6.5	12.5%	0.3%	12.2%
3.0	6,916	1,675	4.1	7,547	1,679	4.5	9.1%	0.2%	8.9%
3.5	6,728	1,577	4.3	7,202	1,579	4.6	7.1%	0.2%	6.9%
4.0	6,202	1,080	5.7	6,770	1,084	6.2	9.2%	0.4%	8.8%
4.5	6,170	879	7.0	7,090	879	8.1	14.9%	0.1%	14.8%
5.0	5,578	963	5.8	7,287	967	7.5	30.6%	0.4%	30.1%
5.5	5,544	731	7.6	7,966	737	10.8	43.7%	0.8%	42.6%
6.0	7,625	1,278	6.0	8,373	1,278	6.6	9.8%	0.0%	9.8%
6.5	5,866	1,281	4.6	6,855	1,281	5.4	16.9%	0.0%	16.8%
7.0	5,263	746	7.1	6,200	746	8.3	17.8%	0.0%	17.8%
7.5	6,162	1,137	5.4	6,845	1,137	6.0	11.1%	0.0%	11.0%
8.0	5,923	884	6.7	7,293	885	8.2	23.1%	0.0%	23.1%
Ave	**6,574**	**1,091**	**6.0**	**7,525**	**1,092**	**6.9**	**14.5%**	**0.1%**	**14.3%**

Calculations of K_1, K_2, and K were performed with assumption of a 0.5- and 2.0-mile-long inlet channel. The 0.5-mile-long inlet channel was investigated because it maximized the increase in cross-sectional area. The 2.0-mile-long channel was used because it was more reflective of the actual length of the inlet. An example of computations is shown in the Attachment and the results are summarized in Table **2-**2. It should be noted that A_c for the 2.0-mile inlet is calculated as the average of cross-sectional areas from RM 0.5 to RM 2.0.

Table 2-2: Results of calculations

Parameter	Existing	PA	Existing	PA
	0.5-mile-long channel		2.0-mile-long channel	
A_b, mi^2	18.2	18.2	18.2	18.2
L, mi	0.5	0.5	2.0	2.0
A_c, m^2	6,777	8,753	7,588	8,313
P_w, m	611	611	1,011	1,011
K_1	6.758	4.748	4.282	3.568
K_2	0.106	0.093	0.201	0.192
K	3.623	4.913	2.408	2.762
King's a_b/a_o (CEM Figure II-6-18)	1.0	1.0	1.05	1.05
Keulegan's a_b/a_o (CEM Figure II-6-16)	1.0	1.0	1.0	1.0
King's V'_m (CEM Figure II-6-19)	1.0	1.0	1.0	1.0
V_m, m/s	0.831	0.643	0.742	0.677

The results for each method are presented in Table 2-2. For King's method, the ratio of tidal range in the bay to tidal amplitude in the ocean is 1.0 for 0.5-mile channel and 1.05 for 2.0-mile channel, under both the Existing and PA Conditions. These results are consistent with expectations, as the inertia effect increases with the channel length (which mainly effects K_2 coefficient). For 0.5-mile channel, despite the largest change in the cross-section area, there is insufficient distance to influence the tidal amplitude. For the 2.0-mile channel, this method predicts a tidal amplification of 5% (i.e., the amplitude in the bay is 5% higher than the amplitude in the ocean). This result is consistent with the 7% amplification between North Bend and Charleston based on observed tidal records.

Using Keulegan's method, the ratio between bay and ocean amplitudes is equal to 1.0 (i.e., the tidal amplitude is the same in the bay as it is in the sea) under both the Existing and PA Conditions. This indicates that the existing channel is already hydraulically efficient and does not dampen the tides (i.e., channel friction does not influence tidal amplitude). Further increase in the inlet channel dimensions under the PA condition does not provide additional benefit of increasing the tidal range in the bay. Neither King's nor Keulegan's methods predict that change to the tidal amplitude ratio will occur as a result of the PA.

Using King's method, the maximum cross-section average velocity, V_m, is calculated and presented in Table 2-2. V'_m is calculated to be equal to 1.0 for each configuration (and V_m is calculated from this value). This indicates that the increase in the channel cross-section area has no effect on channel resistance and that the total discharge (a product of the tidal velocity and the channel cross-section area) remains the same between the two configurations. The reduction in the maximum velocity in the PA configuration counteracts the increase in cross-section area, keeping the effect of inertia constant. As a result, the tidal prism (volume of water flowing through the inlet channel over a tidal cycle) is not

expected to change. The result of this analytical calculation provides further support to the conclusion that the amount of water flowing through the channel is not expected to increase.

3. ANALYSIS OF HISTORICAL WATER LEVELS

Section 2.0 provided calculations based on empirical formulae. In this section, an alternative method based on statistical analysis of measured historical water level data was used to investigate the changes in tidal ranges in response to channel dredging. Water level measurements at Charleston, OR (Station ID 9432780) were analyzed to evaluate the change in tidal range after previous deepening of the Federal Navigation Channel (FNC). The intent was to determine, using actual occurrences in Coos Bay, whether previous deepening projects resulted in a measurable change in tidal range.

Hourly water level measurements are available from 03/1970 until 05/1975 and then from 07/1978 until 02/2018 (as processed). There are significant gaps (over a month long) in the records in 1973, 1974, 1980, 1991, and 1992.

During the period of available observations, the FNC was dredged twice:

1. 1977 from 30 to 35 ft MLLW, and
2. 1996 from 35 to 37 ft MLLW.

In 1970, the Charleston Channel was extended to South Slough and dredged to the present depth.

The available hourly water level measurements were used to compute the tidal datums on a yearly and monthly basis using T_TIDE[8] Matlab code (Rich Pawlowicz, 2002). The mean tidal range was computed as the difference between MHW and MLW tidal levels.

Figure 3-1 shows the computed mean ranges based on monthly intervals and the corresponding statistics. The following statistics are shown: μ is the sample mean, σ is the sample standard deviation, Δ is the difference in means between post-dredge and pre-dredge, values in parentheses are the confidence intervals for the difference, and the text indicates whether the increase is statistically significant. The figure shows that during the 1970–1975 period, the mean tidal range was about 1.67 m. Later, in 1978–1996, the mean range increased by about 0.03 m to 1.70 m. This increase was statistically significant based on *t*-test with the confidence coefficient of 0.05. The mean tidal range after 1996 increased by less than 0.01 m. The increase was also statistically significant using the same test. The variability around the mean values is characterized by the sample standard deviation of about 0.015 m (0.05 ft).

Figure 3-2 shows changes in the mean tidal ranges computed based on the yearly intervals. The yearly intervals were taken as periods between January 1 and December 31 in each year. Due to the gaps in measurements, tidal datums for some years were not correctly computed and associated data points were removed. Statistics were computed using similar periods as with monthly data. This plot shows a similar result as Figure 3-1.

The period of observation for tidal measurements at Sitka Dock (Empire Range), North Bend (Upper Jarvis Range), and Isthmus Slough is September 1982; the period of the

[8] Available from https://www.eoas.ubc.ca/~rich/#T_Tide

observations and at DEA ADCP1 is March–April 2010. As can be seen, the measurements were not available concurrently, nor for the same channel depth. Numerical modeling was done for the period in 2010 to reflect the present channel depth (and hence the 2010 data was used to develop the model), but the results were compared to the observations performed in 1982.

Table 3-1 below presents tidal datums computed from the measurements at Charleston station during both March–April 2010 and September 1982. It can be seen that in September 1982 the tidal range was about 0.1 ft (0.03 m) higher than in March–April 2010. This indicates that the tidal amplitudes in 1982 at other stations should also be higher compared to the 2010 period used for modeling. This discrepancy affects the comparison between the model results and the measured tides at Sitka Dock, North Bend, and Isthmus Slough (described above) because the model was forced with smaller tidal amplitudes.

Table 3-1: Tidal datums at Station 9432780 Charleston, OR for two periods

Tidal Datums (ft, MLLW)	**Period 3/28/2010–4/18/2010**	**Period 9/1/1982–9/30/1982**	**Difference (ft)**
MHHW	3.25	3.38	0.13
MHW	2.79	2.78	0.01
MSL	0.00	0.00	0.00
MLW	−2.69	−2.78	−0.09
MLLW	−3.74	−3.78	−0.04
Mean Range of Tide (ft) (MHW – MLW)	5.48	5.57	0.09
Great Range of Tide (ft) (MHHW – MLLW)	7.02	7.16	0.14

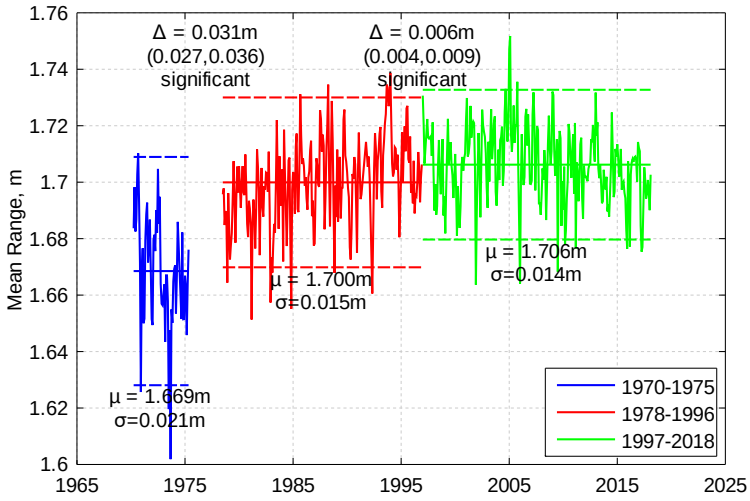

Figure 3-1: Mean tidal range based on monthly observations: solid line—sample mean, dashed line—95% confidence interval

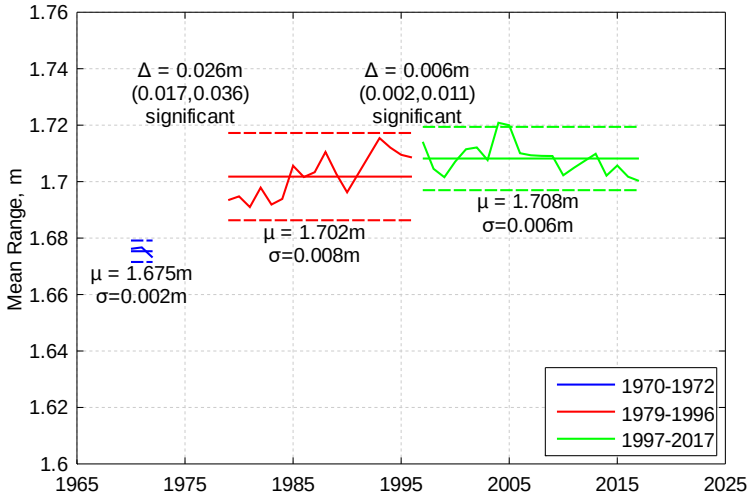

Figure 3-2: Mean tidal range based on yearly observations: solid line—sample mean, dashed line—95% confidence interval

The 0.1 ft (0.027 m) increase in the mean tidal range between 1975 and 1979 appears to correlate to the deepening of the FNC from 30 to 35 ft. While an increase in magnitude was also observed as a result of the deepening in 1996 from 35 to 37 ft, it was only 0.02 ft (0.006 m). The increase in the tidal range, proportional to the depth, was much lower for the 1996 dredging; this may indicate that the channel had already achieved hydraulic efficiency by this time.

A gradual increase in tidal range occurred from 1979–1996. There were no identified capital dredging projects or other channel enhancements to provide an explanation. In order to hypothesize potential causes of the changes in the mean tidal range from year to year, the tidal range was compared to maintenance dredging volumes. Table 2-6 in the Estuarine Dynamics Sub-Appendix presents the historical records of dredged quantities in the FNC. The PDT used this data to compare dredge volumes in the Entrance Range (the portion of the channel downstream of the Charleston gauge) to the computed annual mean tidal range at Charleston between 1998–2014 (see Figure 3-3). The two curves demonstrate a generally similar trend. The high dredging volume in 2003 corresponds to the increase in the tidal range in 2004. But the relative correlation does not exist for the two large dredging events in 1997 and 2006. Ultimately, observed tidal ranges in any given year are likely influenced by several factors not limited to dredging. The mean tidal ranges were also compared to the annual sea-level anomaly (the difference between the mean seal level and the average sea level for the year). There was no correlation found between the ranges and the sea levels.

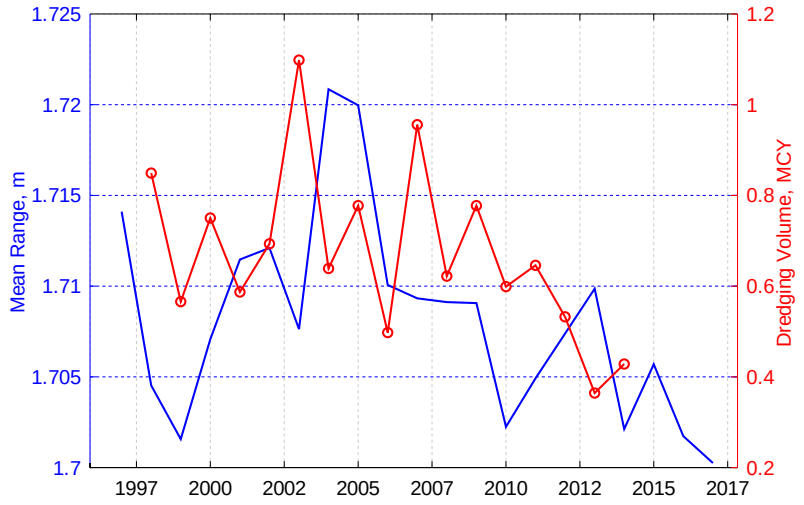

Figure 3-3: Variation of dredging volumes (red, right) and mean tidal range (blue, left)

4. CHANNEL IMPROVEMENT PROJECT IN CHARLESTON HARBOR

M&N reviewed information on other deepening projects in order to compare the methodology of evaluation of effects on water levels due to the project, and the predictions from those evaluations with the methodology used in the Coos Bay estuary. This section presents the information about the deepening of the Federal Navigation Channel in Charleston Harbor, South Carolina.

Improvements to the Federal Navigation Channel in Charleston Harbor, South Carolina included a 7 ft deepening of the channel from 45 to 52 ft MLLW in the main channel and from 47 to 54 ft MLLW in the entrance channel. This project was selected to be a valid comparison to Coos Bay for two reasons. Firstly, like Coos Bay, the channel is already relatively deep (meaning deep-draft vessels transit the channel), and therefore may be near its maximum hydraulic efficiency. Secondly, the deepening is roughly the same magnitude and resulted in a similar increase in cross-sectional area as calculated for Coos Bay.

A numerical modeling study for the channel deepening project was performed by the USACE using EFDC numerical model (USACE 2015). The purpose of this model was to predict effects on currents, salinity, DO and sedimentation of various channel modification alternatives. The model was approved by USACE and EPA for application to estuarine systems. The model included the entire estuary system, using water surface elevation gauges as far as 20 miles from the estuary. The gauge locations, which also represent the model output locations for tidal amplitude, are presented in Figure 4-1.

The model results showed that the changes in tidal amplitude between the 90^{th} percentile and 10^{th} percentile water level to be less than 0.2 ft at every location identified in Figure 4-1. This indicates that USACE accepts that the increase in the tidal prism as a result of the deepening would be less than 0.2 ft within the harbor and the rivers. Measurements collected post-dredging could be used to substantiate the results of the USACE modeling.

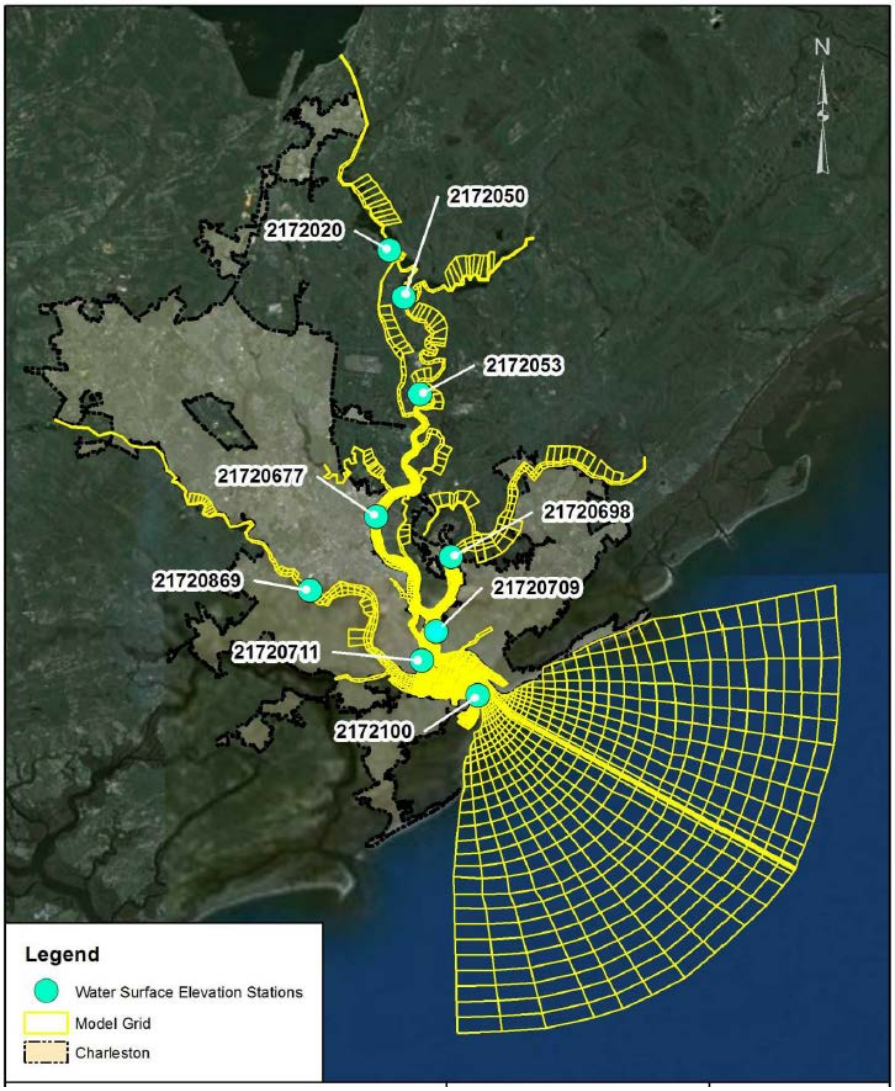

Figure 4-1: Water Surface Elevation Gauge Locations

5. DISCUSSION

This memorandum expands on the work presented previously by: 1) using a conceptual one-dimensional model to simulate the Coos Bay Channel Modification Project; 2) comparing measured water level data following previous deepening projects in Coos Bay; and 3) investigating the results of a USACE study for a similar channel deepening project. Discussions of the analyses are summarized below:

3. The 3D hydrodynamic model of the Coos Bay estuary predicted an increase of less than 0.1 ft in tidal range between the Existing Conditions and the PA. The actual predicted difference in mean tidal range by the numerical model is 0.05 ft (0.015 m) at the upper estuary area, which corresponds to an increase of less than 0.9%.

4. Differences in cross-sectional geometry (cross-section area, wetted perimeter, and hydraulic radius) along the Coos Bay Navigation Channel between Existing Condition and Proposed Alteration were computed. The average change is 14.5% in cross-section area, 0.1% in wetted perimeter and 14.3% in hydraulic radius. Although the cross-sectional area increases by 14.5%, but the entrance channel velocity is reduced by 9 to 23% based on the conceptual 1-D model calculation. Therefore, the average tidal range and overall tidal prism are not expected to change as increase in the cross-sectional area is compensated by the reduction in velocity.

5. The effect of inertia is important in the tidal hydraulics of Coos Bay and is the cause of tidal amplification within the bay. The hydrodynamic model, which was used to assess effects of the project, demonstrates this phenomenon by showing tidal amplification at RM 8.0. Results of the analysis presented herein indicate that the effect of inertia is similar between the two configurations (Existing Conditions and Proposed Alteration). The increased mass of water can be pushed through a larger cross-section is counteracted by a reduction in velocity, keeping the effect of inertia similar between the configurations.

6. According to calculations using the analytical method included in the CEM, the PA does not enhance the tidal amplitude relative to the Existing Condition.

7. Analyses of historical tidal records indicate that deepening the FNC from 30 to 35 ft in 1974 may have resulted in the tidal range increase of 0.1 ft (0.03 m). Similarly, deepening from 35 to 37 ft in 1996 may have resulted in a smaller increase in the tidal range of 0.02 ft (0.006 m). This latter increase is much smaller in proportion to magnitude of the deepening, indicating that the channel has been hydraulically efficient since achieving a depth of 35 ft.

8. The Charleston Harbor (South Carolina) Federal Navigation Channel project is similar to the PA in that it proposes to deepen a deep channel by a similar depth. A numerical modeling approach similar to that used for Coos Bay was performed by the USACE to evaluate changes to water levels. The results indicate that the expected changes in tidal amplitude between the proposed project and the future

without project conditions are less than 0.2 ft. Measurements collected post-dredging could be used to substantiate the results of the USACE modeling.

Overall, analyses of alternative methods of evaluating potential changes to the tidal amplitude support the conclusions presented previously, that tidal amplitude would be expected to change by less than 0.1 ft throughout the channel under the PA.

6. REFERENCES

Keulegan, G. H. (1967) “Tidal Flow in Entrances Water-Level Fluctuations of Basins in Communications with Seas,” Technical Bulletin No. 14, Committee on Tidal Hydraulics, U.S. Army Engineer Waterways Experiment Station, Vicksburg, MS.

King, D. B. (1974) “The Dynamics of Inlets and Bays,” Technical Report No. 2, Coastal and Oceanographic Engineering Laboratory, University of Florida, Gainesville.

Pawlowicz, R., B. Beardsley, and S. Lentz (2002) "Classical tidal harmonic analysis including error estimates in MATLAB using T_TIDE", Computers and Geosciences 28 (2002), 929-937.

U.S. Army Corps of Engineers (2006) Coastal Engineering Manual.

U.S. Army Corps of Engineers (2015) Final Integrated Feasibility Report and Environmental Impact Statement, Charleston Harbor Post 45, Charleston, South Carolina, June 2015.

Attachment

Example of Computation of Tidal Amplitude

Tidal Elevations in Inlet Bay System

Calculations follow CEM II-6-2-b

Tidal period	$T := 12.42hr$	$T = 4.471 \times 10^{4} \cdot s$
Ocean tidal amplitude	$a_o := \frac{1.7m}{2}$	$a_o = 0.85\,m$
Bay surface area	$A_b := 18.2mi^2$	$A_b = 4.714 \times 10^{7}\,m^2$
Channel length	$L := 2.0mi$	$L = 3.219 \times 10^{3}\,m$
Cross-section area	$A_c := 8313m^2$	
Wetted perimeter	$P := 1011m$	
Manning's number	$n := 0.025s \div \sqrt[3]{m}$	
Hydraulic radius	$R := \frac{A_c}{P}$	$R = 8.223\,m$
Darcy-Weisbach friction factor	$f := \frac{116n^2}{\sqrt[3]{R}} \cdot \frac{m}{s^2}$	$f = 0.036$
Entrance energy loss coefficient	$k_{en} := 0.25$	(0.005 to 0.25, 0.05 or less for natural inlets, 0.25 for inlets with jetties)
Exit energy loss coefficient	$k_{ex} := 1$	(<1 recommended for longer channels)
Inlet impedance	$F := k_{en} + k_{ex} + \frac{f \cdot L}{4 \cdot R}$	$F = 4.765$
King's coefficients	$K_1 := \frac{a_o \cdot A_b \cdot F}{2 \cdot L \cdot A_c}$	$K_1 = 3.568$
	$K_2 := \frac{2\pi}{T} \cdot \sqrt{\frac{L \cdot A_b}{g \cdot A_c}}$	$K_2 = 0.192$
Keulegan repletion coefficient	$K := \frac{1}{K_2} \cdot \sqrt{\frac{1}{K_1}}$	$K = 2.762$

Keulegan's method:

Change in bay amplitude	$r = 1$	(from Figure II-6-16)
Bay tidal amplitude	$a_b := r \cdot a_o$	$a_b = 0.85\,m$

King's method:

Change in bay amplitude	$r2 := 1.05$	(from Figure II-6-18)
Bay tidal amplitude	$a_b := r2 \cdot a_o$	$a_b = 0.892\,m$
Dimensionless maximum velocity	$V_m := 1.0$	(from Figure II-6-19)
Maximum velocity	$V_{max} := V_m \cdot \frac{2 \cdot \pi \cdot a_o \cdot A_b}{A_c \cdot T}$	$V_{max} = 0.677\,\frac{m}{s}$